Modelling the environmental transfers of radioactivity following the Fukushima accident

Kittisak Chaisan

The thesis is submitted in partial fulfilment of the requirements for the award of the degree of Doctor of Philosophy of the University of Portsmouth

June 2015

Abstract

After the massive tsunami on 11 March 2011, the explosions at 4 reactors of the Fukushima Dai-ichi (I) Nuclear Power Stations (Fukushima I NPSs) in Japan led to a large radioactive cloud being ejected into the atmosphere. Radionuclides released to the atmosphere were washed out in rain causing an area of remarkably high deposition in the area to the northwest of the Fukushima I NPSs. Activity remaining in the atmosphere was dispersed further to other areas of Japan. At various times during the accident, plumes of contamination were transported from Japan to the Pacific Ocean, the North American continent, crossing the Atlantic Ocean to Europe, and eventually to Asia. Due to the lack of measurements in three major ecosystem compartments i.e. air, soil and surface water, information on the highest impact early-phase after fallout and the interpretation of long-term impacts is limited and unclear.

The transfer of contaminated radionuclides to soil and air around the Fukushima I NPSs was studied using ratios of various radioisotopes to the long-lived nuclide ^{137}Cs. It was found that ratios of three radionuclides i.e. ^{134,136}Cs and ^{132}Te were consistent with direction and distance in air and soil while the ratio ^{131}I/^{137}Cs was not. It was shown that, deposited ^{131}I/^{137}Cs had an inverse correlation with ^{137}Cs activity in soil.

These nuclides were key in forming the high-gamma dose rates in the early phase, particularly the high gamma energy of ^{132}I from the ^{132}Te/^{132}I decay. The derived ratios of these key radionuclides in soil were used together with available measured gamma dose rates in the early phase (<30 days) to develop a model to reconstruct and predict external gamma dose rate. Model "blind" tests showed that more than 95% of predictions were within a factor of two of measurements from 15 sites to the north, northwest and west of the power station. It is demonstrated that generic isotope ratios provide a sound basis for reconstruction of early-phase external dose rates in these most contaminated areas.

For contamination in surface runoff water, lake water and fish, a previous model developed following the Chernobyl accident (AQUASCOPE) was applied to the Fukushima situation. It was shown that by adjusting for the stronger absorption of radiocaesium in soils in Japan (compared with European countries) the model could be used successfully to predict long-term contamination in aquatic systems affected by Fukushima fall out. The results of the model showed good agreement with measured data, in particular in the long-term period (around 0.5-2 years) after the accident.

Table of contents

Declaration

Whilst registered as a candidate for the above degree, I have not been registered for any other research award. The results and conclusions embodied in this thesis are the work of the named candidate and have not been submitted for any other academic award.

Word count: 39,296 words

List of tables

List of figures

Abbreviations

<; less than

>; more than

^{7}Be; Beryllium-7

^{59}Fe; Iron-59

^{90}Sr; Strontium-90

^{95}Nb; Niobium-95

^{95}Zr; Zirconium-95

^{99}Mo; Molybdenum--99

^{103}Ru; Ruthenium-103

^{106}Ru; Ruthenium-106

^{127}Sb; Antimony-127

^{129}Te; Tellurium-129

^{129m}Te; Tellurium-129 Isomer

^{131}I; Iodine 131

^{132}I; Iodine 132

^{132}Te; Tellurium-132

^{131m}Xe; Xenon-131 Isomer

^{133}Xe; Xenon-133

^{133m}Xe; Xenon-133 Isomer

^{134}Cs; Caesium-134

^{136}Cs; Caesium-136

^{137}Cs; Caesium-137

^{140}Ba; Barium-140

^{140}La; Lanthanum-140

^{239}Np; Neptunium-239

^{239}Pu; Plutonium-239

^{240}PuPlutonium-240

μ; micro

η; nano

a; anual

Bq; Becquerels

c; centi

C; carbon

CF; concentration factor

C.V.; coefficient of variation

d; day

DOE; the United States Department of Energy

EPA; the United States United Environmental Protection Agency

EU; European Unionarcgis

g; gram

GRANIS; gamma radiation aboe nuclides in soil

Gy; gray

h; hour

HPA; Health Protection Agency

IAEA; International Atomic Energy Agency

ICRP; International Commission on Radiological Protection

IRSN; Institut de radioprotection et de sûreté nucléaire

ISIS; Institute for Science and International Security

J; Joule

JAEA; Japan Atomic Energy Agency

JMA; Japan Meteorology Agency

JST; Japan Science and Technology Agency

k; kilo

KEK; High Energy Accelerator Research Organization

L; litre

m; metre

M; mega

m^2; Becquerels per square meter

m^3; Becquerels per cubic meter

MEXT; Ministry of Education, Culture, Sports, Science and Technology

MHLW; Ministry of Health, Labour and Welfare

min; minute

mol; mole

ev; electron volt

N; number

NIES; National Institute for Environmental Studies

NISA; Nuclear and Industrial Safety Agency

nt.; nuclear transformation

O; Oxygen

p; probability

P; pico

RIKEN; Rikagaku Kenkyūsho

s; second

S.E.; standard error

S.D.; standard deviation

Si; silicon

Sv; Sieverts

UCB; University of California, Berkeley

UNEP; the United Nations Environment Programme

UNSCEAR; United Nations Scientific Committee on the Effects of Atomic Radiation

US; United States

USSR; Soviet Union

WHO; World Health Organization

y; year

Acknowledgments

I would like to express my deepest gratitude to my supervisors Prof. Jim Smith for his guidance, supervision, encouragement, and support throughout the duration of this project. Without him completing this thesis would not have been possible (and I wouldn't have the experience of visiting Iitate Lake near the Fukushima Dai-ichi Nuclear Power Stations). Also, thanks for his patience when reading over parts of my thesis, and struggling with my English.

This thesis would not have been completed without the help of Dr. Peter Bossew and Dr. Gerald Kirchnerand from German Federal Office for Radiation Protection, and Dr. Gennady Laptev from Ukrainian Institute of Hydrometeorology. I would like to send my appreciation to them for their collaboration to provide measurement data during this research.

The special thank is extended to Prof. Yutaka Kameda at Chiba Institute of Technology (Japan) for his worthy help when I visited Iitate Lake and valuable information about lakes and catchments in Japan. Namphone Khampilang from the Department of Mineral Resources (Thailand) must be thanked for her help to make catchment of all surface water ecology.

I would like to thank the Thai Government for their financial support and for providing me with a wonderful opportunity to extend my education and gain valuable experience in England.

Finally, I would like to express my deepest gratitude to my lovely family for their love, full support, and encouragement throughout these years particularly from my wife and my new-born son.

Dissemination

Journal Publication

Chaisan, K., Smith, J. T., Bossew, P., Kirchner, G., & Laptev, G. V. (2013). Worldwide isotope ratios of the Fukushima release and early-phase external dose reconstruction. *Scientific reports, 3*.

Chapter 1 Contamination following Fukushima accident

1.1 Introduction

Following the accident at the Fukushima Dai-ichi (I) Nuclear Power Station (Fukushima I NPS) on 11 March 2011 (NISA, 2011a), various artificial nuclides were released to environmental systems in Japan and around the world. Radionuclides released to the atmosphere were washed out in rain causing an area of remarkably high deposition to the northwest of Fukushima I NPSs (S. Endo et al., 2012; Kinoshita et al., 2011). Activity remaining in the atmosphere was dispersed further to others areas of Japan, the Pacific Ocean, northern America, the Atlantic Ocean, Europe (Lujaniene et al., 2011; Masson et al., 2011; Piñero García & Ferro García, 2012) and, finally, back into Asia in the beginning of April (Kim et al., 2012; Qiao et al., 2011; Takemura et al., 2011).

There was also radioactive material released directly from the NPSs into the sea (Kawamura et al., 2011; Tsumune, Tsubono, Aoyama, & Hirose, 2012), however, this research focuses on the evaluation of the transfers of radionuclides in air around the World, the deposition into soil, the contamination in water and fish in freshwater systems, and external gamma dose rate in the early and long-term phase.

1.2 Consequence of the accident at NPSs

At 14:46 on 11 March 2011, the Great East Japan Earthquake occurred (JST, 2011; NISA, 2011a). The 9.0 magnitude earthquake was the biggest ever recorded in Japan. The epicenter was approximately 70 km to the east of the Japanese coast (38°6”N and 142°51”E) at a water depth of 24-km. The earthquake caused the immediate shutdown of the reactors at the Fukushima Dai-ichi (I) Nuclear Power Station (Fukushima I NPS), a six-unit Boiling Water Reactor (BWR), and automatic operation of the electricity generator and cooling systems of Fukushima I NPS. The massive tsunami (> 14 m) triggered by the earthquake subsequently reached the east coast of the northern area of the main island of Japan and destroyed houses, farms, cars and buildings including overwhelming the flood defences of the Fukushima I NPS. This caused the emergency diesel power generators and seawater pumps for the cooling systems to fail at 15.41, less than an hour after the earthquake. The failure of the cooling systems led to overheating of the cores of three reactor units and the production of hydrogen gas from the high-

temperature reaction between water and zirconium fuel cladding. A hydrogen explosion in the operational floor of reactor building of Unit 1 occurred at 15.36 on 12 March. During the next two days, there was an increase of the pressure in the primary containment vessel of Unit 3 resulting in an explosion in the reactor building at 11.01. On 15 March, explosions took a place at Unit 4 and 2 at 6:00 and 6:10 respectively. There was no nuclear fuel assembly in Unit 4 for preparation of new fuel replacement (Povinec, Hirose, & Aoyama, 2013), the explosion at this unit was consequence from released hydrogen of Unit 3. Then, in Unit 4, a part of the wall of the operation floor was destroyed at 6.14 and a fire occurred from 9.38 to 11.00. There was white smoke released from unit 4 on 15 March.

After the initial explosions, a significant amount of radioactive material was released on 21 March (Povinec, et al., 2013) which corresponded to the white smoke venting from Unit 2 resulting in the high contamination in Kanto and Tohoku regions (region in the south direction of Fukushima within the region of Fukushima respectively) during 21-24 March. Finally, the releases of white smoke occurred in all destroyed Units of Fukushima I NPSs on 30 March for Unit 4 and 31 March for Unit 1, 2 and 3. There was no official report about the white smoke following the initial explosions, particularly the high contamination event on 21 March. However, it has been suggested that the of white smoke was a remelting of Unit 2 nuclear fuel (Povinec, et al., 2013)

Table 1-1 Summary of accidental consequences of Fukushima I NPSs

Date and Time	Event	Reference
11/03/2011 14:46	Date of earthquake	NISA (2011a) and JST (2011)
11/03/2011 15:41	The emergency diesel power generators and the pumps supplying seawater to the cooling system were stopped due to the Tsunami	JST (2011)
12/03/2011 15:36	Explosion at Unit 1	NISA (2011a), ISIS (2011) and JST (2011)
14/03/2011 11:01	Explosion at Unit 3	NISA (2011a), ISIS (2011) and JST (2011)
15/03/2011 06:00	Explosion at Unit 4	ISIS (2011)
15/03/2011 06:10	Explosion at Unit 2	NISA (2011a), ISIS (2011) and JST (2011)
15/03/2011 06:14	Collapsion of building wall at Unit 4	JST (2011)
15/03/2011 09:38	Fire occurred at Unit 4	NISA (2011a) and JST (2011)
16/03/2011 N/A	White smoke released from Unit 4	NISA (2011a)
21/03/2011 N/A	White smoke released from Unit 2	NISA (2011a) and Povinec et al. (2013)
30/03/2011 N/A	White smoke released from Unit 4	NISA (2011a)
31/03/2011 N/A	White smoke released from Unit 1, 2 and 3	NISA (2011a)

Note that N/A means time of event was not available

1.3 Release amounts of radioactive materials

Numerous radioactive materials were released to air during this period (JAEA, 2012). The isotopes which were most commonly measured were ^{131}I and ^{134,137}Cs, with fewer measurements of ^{132}Te/^{132}I and ^{136}Cs (JAEA, 2012; Kanai, 2012; MEXT, 2011a, 2011b; Momoshima, Sugihara, Ichikawa, & Yokoyama, 2012; RIKEN, 2011; Stoehlker, Nikkinen, & Gheddou, 2011) while ^{95}Nb, ^{99}Mo/^{99m}Tc, ^{110m}Ag, ^{129m}Te/^{129}Te, ^{133}I, ^{133}Xe, ^{140}Ba/^{140}La were also released but were more rarely measured (JAEA, 2012; Kanai, 2012; Stoehlker, et al., 2011). The total amount of two radionuclides of key importance, ^{131}I and ^{137}Cs released to the atmosphere have been estimated to be approximately 0.9-1.6×10^{17} and 1.0-1.5×10^{16} Bq respectively (Chino et al., 2011; IRSN, 2011a; Kantei, 2011; NISA, 2011b). These releases are lower than Chernobyl (UNSCEAR, 2000b) by factors of 13 and 7 respectively. A compilation of literature estimates of ^{131}I and ^{137}Cs releases and comparison with Chernobyl is shown in Table 1.2. From measurement data (and see Section 3.3.1 below), the ratio of ^{134}Cs to ^{137}Cs was almost ~1 (Kinoshita, et al., 2011; Masson, et al., 2011) so that the total amount of ^{134}Cs was close to that of ^{137}Cs. In addition, there was a discharge to the Pacific ocean (not from fallout), with total amount of ^{131}I and ^{137}Cs, approximately 11×10^{5} and 4×10^{5} Bq released directly from NPSs during 21 March to 30 April 2011 estimated by Kawamura et al. (2011) and 11.1×10^{5} and 3.55×10^{5} Bq of ^{131}I and ^{137}Cs respectively released directly during 26 March 2011 to the end of February 2012 2011 as was estimated by Tsumune et al. (2012).

Table 1-2 Comparison of the estimation of total amount of ^{131}I and ^{137}Cs released during the accidents at Chernobyl NPP and Fukushima I NPSs.

Radioactive material		Total Amount (Bq)	Refference
Chernobyl			
^{131}I		1.8×10^{18}	UNSCEAR (2000b)
^{137}Cs		8.5×10^{16}	UNSCEAR (2000b)
Fukushima			
^{131}I		1.6×10^{17}	Kantei (2011)
		1.5×10^{17}	Chino (2011)
		1.5×10^{17}	NISA (2011b)
		9.0×10^{16}	IRSN (2011a)
	Mean	*1.4×10^{17}*	
^{137}Cs		1.5×10^{16}	Kantei (2011)
		1.2×10^{16}	Chino (2011)
		1.2×10^{16}	NISA (2011b)
		1.0×10^{16}	IRSN (2011a)
	Mean	*1.2×10^{16}*	

1.4 Air transport of radionuclides

1.4.1 The pattern and composition of release plumes during the accident

In the area around Fukushima I NPSs, the first detection of unusual gamma dose rate (0.18 μSv/h, factor of 3 times higher than background) and the first detection of ^{131}I (4.30 Bq m^{-3}) in air samples were observed on 12 March 2011 at around 8.30 in a site located in Shinyonomori, Motooka, Tomioka town approximately 7 km to the southwest of Fukushima I NPSs (NISA, 2011c). However, it is clear that the major transport to terrestrial systems (Kinoshita, et al., 2011) occurred on 15 March 2011 to the northwest of Fukushima I NPSs. At distance of approximately 50 km from Fukushima I NPSs, the wind changed direction, moving the plume to the southwest. Following the 15th March plume, a smaller release occurred on 21 March. This second plume moved to the South for approximately 200-300 km, then change direction away from Japanese soil to the Pacific Ocean.

During the first plume significantly affecting terrestrial systems, there was approximately 10 mm of rainfall from 17.00 on 15 March to 4.00 on 16 March 2011 (7 hours) in the northern area of Fukushima prefecture to about 50 km in north and northwest of Fukushima I NPSs. During the second plume, rainfall occurred between 8.00 on 21 March

and 6.00 on 23 March (almost 3 days) in southern areas, estimated rainfall being 10-20 mm within 100-km and heavier rain (approx. 30 mm) 100-200-km (Kinoshita, et al., 2011). The reconstruction of the plume release from Fukushima I NPSs and amount of precipitation around the NPPs are shown in Figure 1-1 produced by Kinoshita and co-workers (2011).

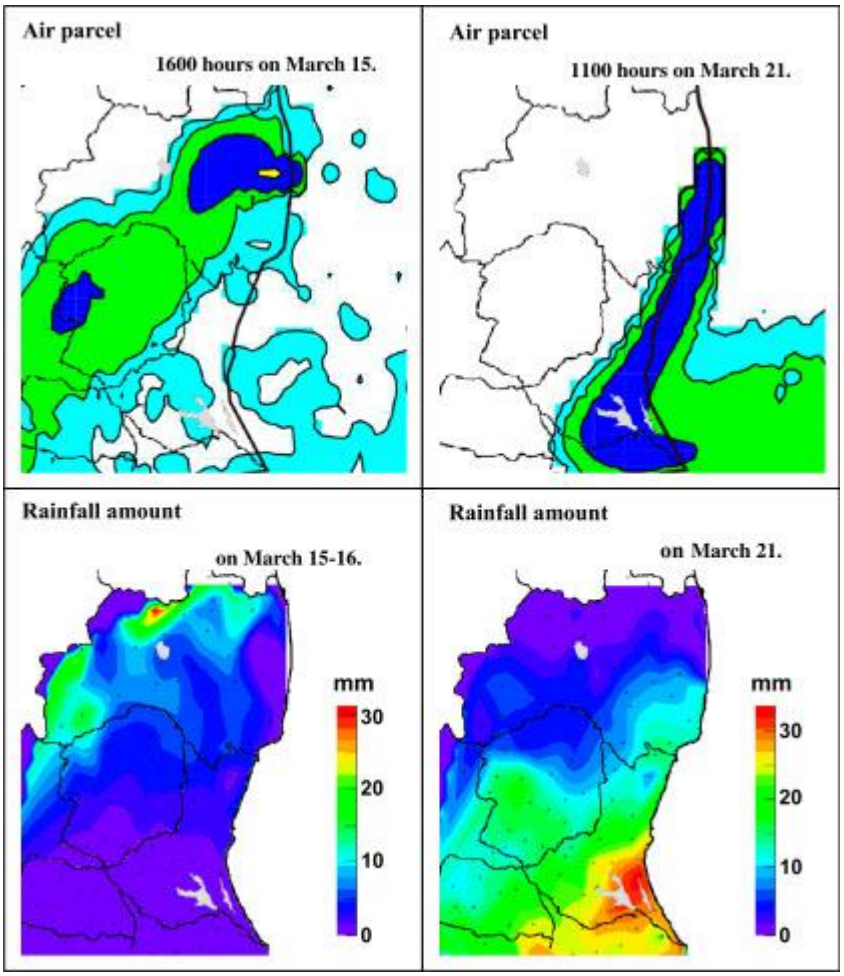

Figure 1-1 Illustration of the passage of air parcel that passed through the Fukushima I NPSs and amount of rainfall (Kinoshita, et al., 2011).

Figure 1-2 shows the nearest continuous gamma dose rate data from the Japan Atomic Energy Agency (JAEA), Tokai-mura, Ibaraki prefecture located approximately 120 km to the South of Fukushima I NPSs (JAEA, 2012). This shows various peaks in dose rate during the weeks after the accident, but these cannot necessarily be linked directly with events at the site since the measured data at JAEA are dependent on wind direction. The

first peak event coincides with the highest gamma dose rate (12,000 μSv/h) observed inside the 20-km evacuated area at the Front Gate of Fukushima I NPSs on 15 March between 6.00 and 12.00. Monitoring at this site had been continuous since the earthquake on 11 March (NISA, 2011a). The continuous monitoring of gamma dose at the Japan Atomic Energy Agency (JAEA, 2012) showed five peaks of gamma dose rate (Figure 3.2). The first peak was the highest by factor of 100 comparing with background level, and was the consequence of the first major release plume (north-western plume on 15 March) occurred at the time of explosion at Unit 4 and 2 (15 March 6:01-6:00). Then, there was a slightly lower peak on the day after, when white smoke was released from Unit 4. The third peak occurred three days after the first peak, this peak was significantly lower than the first peak (no visual sight from NPSs). Then, the gamma dose reached almost its highest point in six days after the first peak when the second plume (southern plume on 21 March) dominated, this event occurred around the time of white smoke release from Unit 2. On 22 March, the last peak, which also was a consequence of the second plume, occurred to the same degree as the previous peak ((no visual evidence of release).

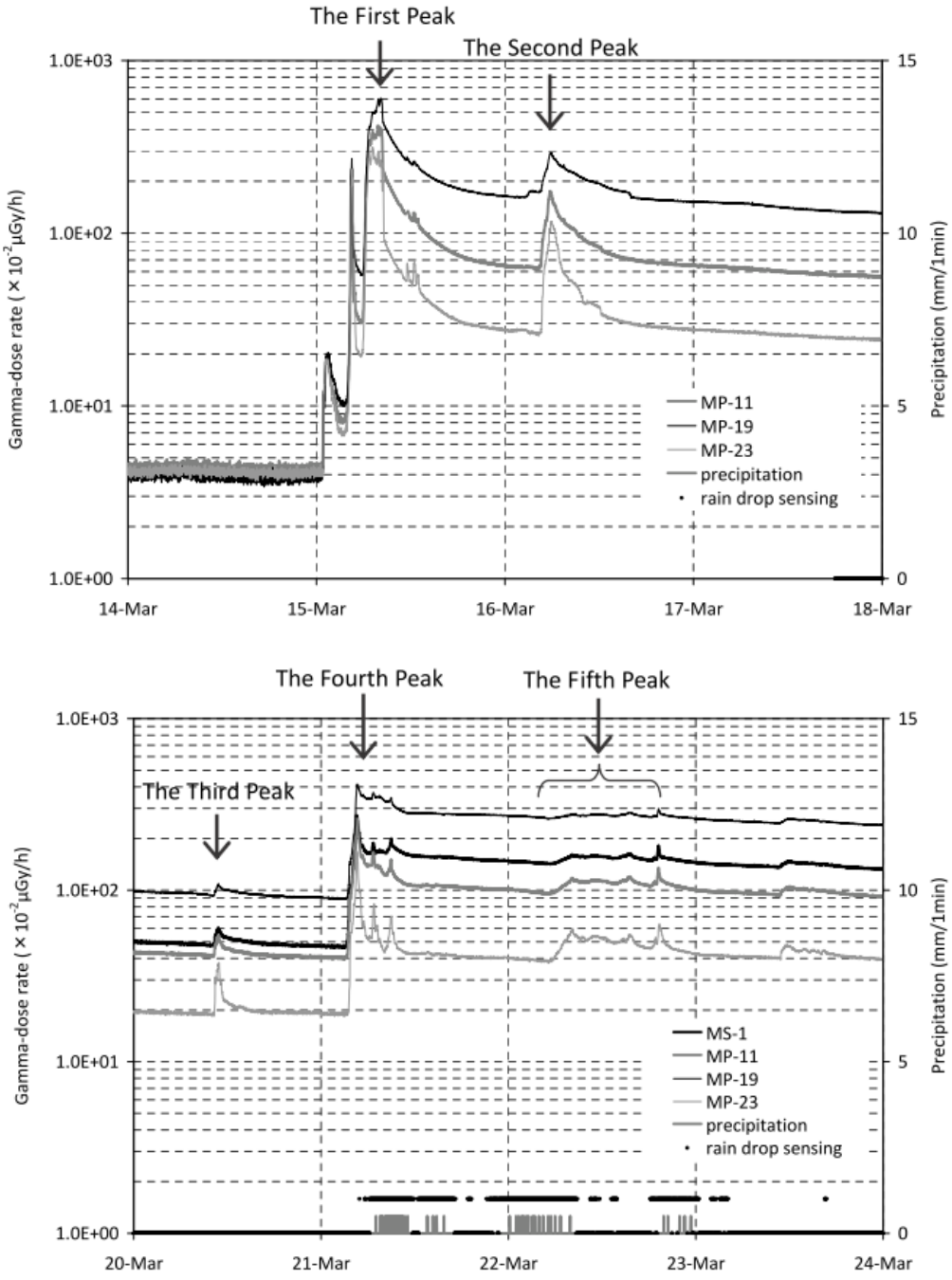

Figure 1-2 Illustration of the continuous gamma dose rate and precipitation at 4 sites (MS-1, MP-11, MP-19 and MP-23) within the Japan Atomic Energy Agency (JAEA), Tokai-mura, Ibaraki prefecture located approximately 120 km to the South of Fukushima I NPSs (JAEA, 2012).

1.4.2 The atmospheric radionuclides in areas around Fukushima I NPSs

Beginning on 17th March, two days after the major 15th March release, , the Japanese Ministry of Education, Culture, Sports, Science and Technology (MEXT) established daily measurements of gamma dose rate and the ambient concentration of contaminated radioactivity (mainly only ^{131}I, ^{134}Cs and ^{137}Cs) at seven sites (MEXT, 2011a) around the Fukushima I NPSs. The measurements began 8-9 days after the earthquake (around 5 days after the highest peak from the first release plume and almost the same day as the second high peak). This initial monitoring primarily focused on the area between 24 and 62 km in all directions from Fukushima I NPSs. The area was subsequently expanded at the beginning of April to cover about 60 km in all directions from the NPSs, except in the southern direction where monitoring reached to approximately 80 km.

The radioactivity in air resulting from the first plume was observed at Yagisawa, Iitate village, Soma county (site 2-1, 36 km in northwest of Fukushima I NPSs) ^{131}I, ^{134}Cs and ^{137}Cs were 270, 39 and 42 Bq kg^{-1} of air respectively (MEXT, 2011a) but these measurements were found in 5 days after the release of first plume (Figure 1-3). Following the second plume, 530, 65, and 66 Bq kg^{-1} of air was found at Shimokitaba, Hirono town, Futaba county (site 1-5, 23 km in south direction) 2 days after second plume release (Figure 1-4).

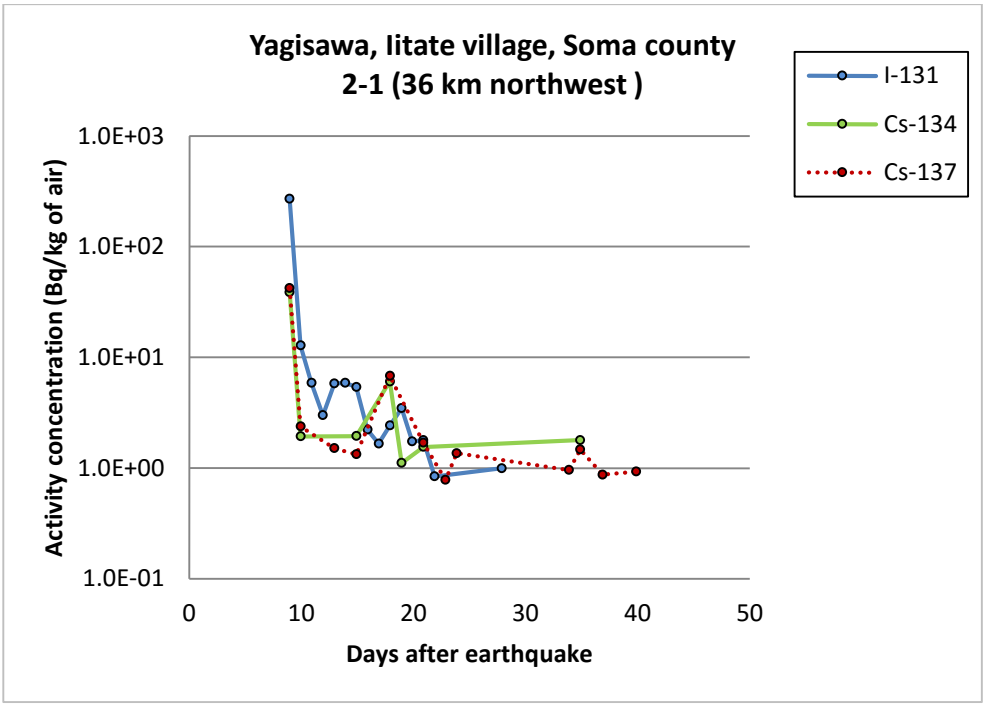

Figure 1-3 Illustration of the daily continuous concentration of ^{131}I, ^{134}Cs and ^{137}Cs in air (Bq kg^{-1} of air) at Yagisawa, Iitate village, Soma county located approximately 36 km to the Northwest of Fukushima I NPSs (MEXT, 2011a).

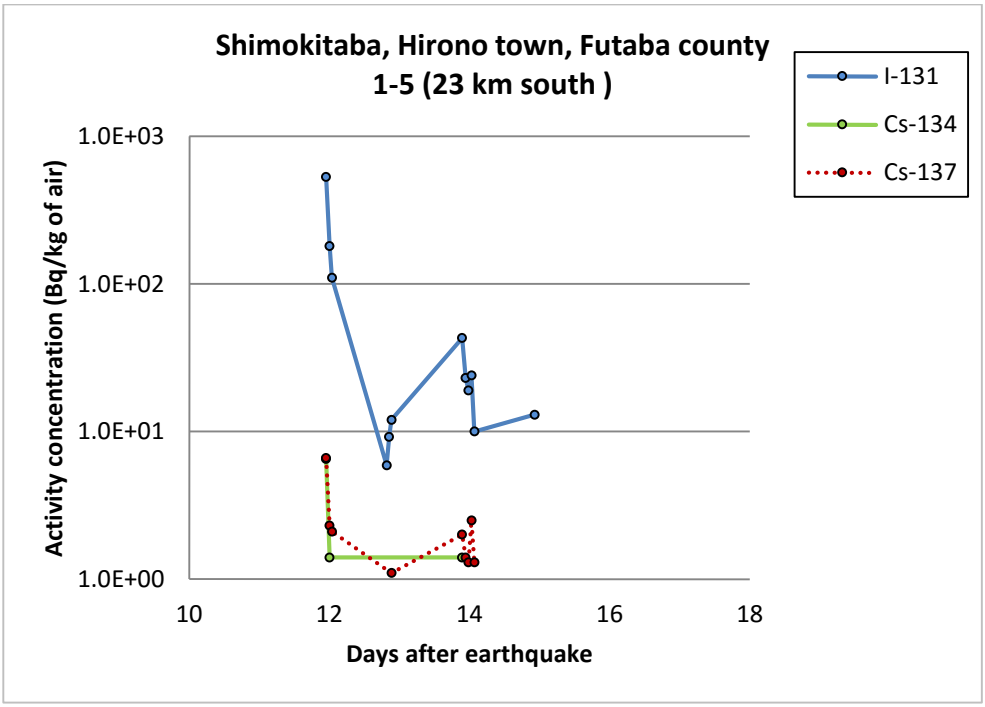

Figure 1-4 Illustration of the daily continuous concentration of ^{131}I, ^{134}Cs and ^{137}Cs in air (Bq kg^{-1} of air) at Shimokitaba, Hirono town, Futaba county located approximately 23 km to the South of Fukushima I NPSs (MEXT, 2011a).

Closer to Fukushima 1 NPSs, there were four daily monitoring sites where the high peaks from both the first and the second plume (~4 and ~10 days after earthquake respectively) could be detected in air. One site is to the South and the other three site are located to the southwest of Fukushima I NPSs. Both plumes passed all of these sites (Kinoshita, et al., 2011) and measurements were made before the arrival of these plumes. The JAEA (2012) site at Tokai-mura, Ibaraki prefecture measured both atmospheric aerosol and gaseous phases of ^{95}Nb, ^{129m}Te/^{129}Te, ^{131}I, ^{132}Te/^{132}I, ^{134,136,137}Cs but only particulate ^{99m}Tc were monitored in this site. These data are shown in Figures 1-5 to 1-8. The highest concentration of ^{131}I, ^{134}Cs and ^{137}Cs from the first plume were 1.4×10^{3}, 3.7×10^{2} and 3.7×10^{2} Bq m^{-3} respectively for particulate form and 1.4×10^{3}, 7.2 and 1.1 for gaseous form, while the highest values from the second were 1.1×10^{3}, 4.3×10^{2} and 4.3×10^{2} for particulate form and 9.9×10^{2}, 9.6 and 1.2×10 for gaseous form.

Other key measurements (Stoehlker, et al., 2011) were conducted by the Comprehensive Nuclear-Test-Ban Treaty (CTBT) at Gunma prefecture approximately 220 km in Southwest direction. Most particulate nuclides from the two plumes, ^{95}Nb, ^{99m}Tc, ^{129m}Te/^{129}Te, ^{131}I, ^{132}Te/^{132}I, ^{134,136,137}Cs, ^{140}Ba/^{140}La and the noble gas ^{133}Xe were detected at this site. However, the noble gas ^{133}Xe was the total amount which consisted of the contamination from the Fukushima accident and typical background about 1×10^{-3} Bq m^{-3}. ^{131}I, ^{134}Cs and ^{137}Cs (particulate) from the first plume were highest at 1.5×10^{1}, 6.9 and 5.6 Bq m^{-3} respectively, and from the second plume were up to 5.2, 3.3 and 3.8 Bq m^{-3} respectively (Figure A-1 and A-2 in Appendix A)

The key atmospheric radionuclides (see Section 3.2.2 below) ^{131}I, ^{132}Te and ^{134,136,137}Cs were also observed at the Japan Chemical Analysis Center (JCAC), Chiba prefecture (Amano et al., 2012) and at another site at Waku Institute, Saitama prefecture (RIKEN, 2011) where measurements also included ^{140}Ba/^{140}La . Both sites are to the southwest, the distances from NPSs being similar at about 220 km. At JCAC (Figure A-3 in Appendix A), the highest point of ^{131}I, ^{134}Cs and ^{137}Cs resulting from the second plume were 4.7×10^{1}, 6.1 and 7.5 Bq m^{-3} respectively, and 3.3×10^{1}, 7.0×10^{-1} and 8.7×10^{-1} Bq m^{-3} for the first plume. As shown in Figure A-4 in Appendix A, the highest concentrations at Waku Institute during the first plume were 3.6×10^{1}, 7.0 and 9.5 Bq m^{-3} for ^{132}I, ^{134}Cs and ^{137}Cs respectively, compared with 7.8, 1.8 and 2.4 Bq m^{-3} contributed by the second plume.

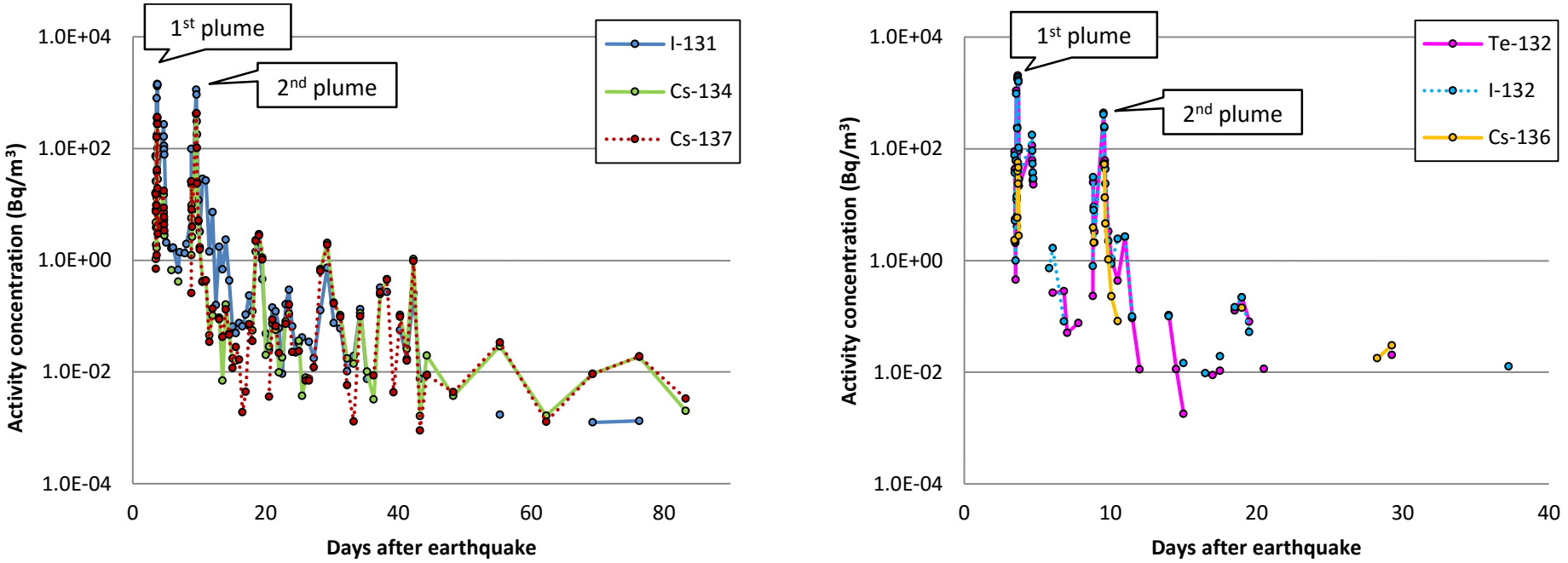

Figure 1-5 Illustration of the contaminated concentration in air of ^{131}I, ^{134}Cs and ^{137}Cs in particulate form. From measurements at JAEA, Tokai-mura, Ibaraki prefecture located approximately 120 km in south direction of Fukushima I NPSs (JAEA, 2012).

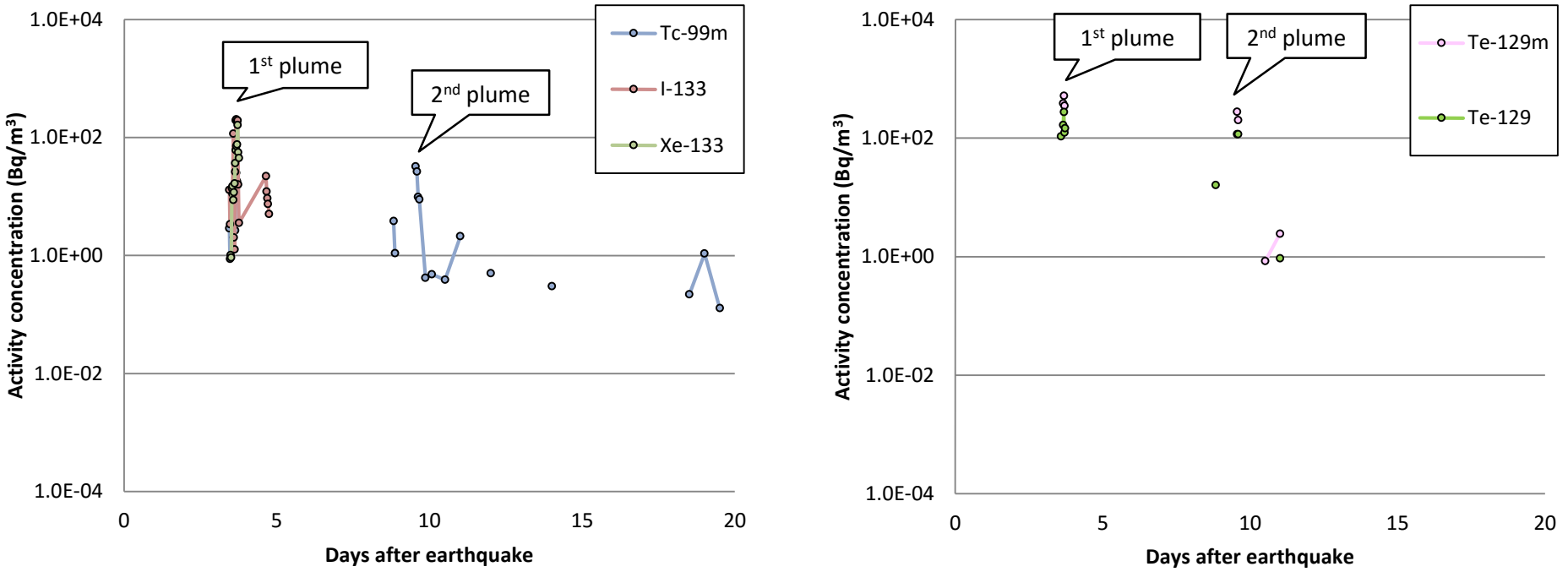

Figure 1-6 Illustration of the contaminated concentration in air of other radionuclides in particulate form at JAEA, Tokai-mura, Ibaraki prefecture located approximately 120 km in south direction of Fukushima I NPSs (JAEA, 2012).

From all of these data, it is clear that there were two high peaks in atmospheric contamination: the first plume around 4 days and the second plume about 10 days after earthquake. It can be concluded that meteorological information presented in Kinoshita et al. (2011) shows that all of these four sites were in the pathway of air transfers explaining why both plumes are clearly observable at all sites.

The decrease process of radionuclide concentrations in air is not only due to radioactive decay but also from dispersion by wind, washout by rainfall and dry deposition to the ground surface.

For very short-lived nuclides such as ^{129}Te (69.6 m), ^{132}I (2.295 h) and ^{140}La (1.68 d), the measurements in air consist of the amount directly released from the reactor fuels plus their production from decay of their parent radionuclide (^{129m}Te, ^{132}Te, and ^{140}Ba respectively). Due to their short half-life, and the significant time period between reactor shut down and the first major release, The amount directly discharged from fuel must have been very low so that the vast majority in air measurements were due to ingrowth. This is supported by the observation that the concentrations and trend of the decreases were almost the same as those of their parent providing evidence that they were in secular equilibrium (Section 4.2.2).

1.4.3 The patterns of worldwide plumes

Since the Fukushima accident, numerous plume transport models have evaluated the trajectories of radionuclides transported around the world. Both two plumes (Section 3.3.6) were transported from Japan to the Pacific Ocean. As radioactivity travelled across the Pacific Ocean it was dispersed and deposited. The plume travelled across the North American continent, eventually crossing the Atlantic Ocean to Europe (Kim, et al., 2012; Lujaniene, et al., 2011; Masson, et al., 2011; Piñero García & Ferro García, 2012; Qiao, et al., 2011; Takemura, et al., 2011), and Asia (Kim, et al., 2012; Qiao, et al., 2011). A small amount of radioactivity, however was in a parcel of air which changed direction as it crossed the Pacific Ocean and moved backwards to Southeast Asia (Kim, et al., 2012; Piñero García & Ferro García, 2012).

Piñero García and Ferro García (2012) calculated that approximately 96% of air masses from Fukushima crossed the Pacific to North America (Figure 1-7). Sixty-one percent of the air mass transported radionuclides to the northern part of North America, 33% to the

middle part of North America (US territory), only 2% of radioactivity crossed the Atlantic Ocean to Europe (arriving at the beginning of April 2011). Some of the radioactivity reaching Europe, continued on to Asia where radioactivity could be detected in air samples (Kim, et al., 2012; Qiao, et al., 2011). Radioactivity therefore reached Asia from both directions. Around 4% of total air masses from Fukushima (Piñero García & Ferro García, 2012) moved out from Japan to the Pacific Ocean, and was subsequently transported backward to Southeast Asia. Kim and coworkers (2012) also found evidence of these forward and backward clouds. The forward cloud could be observed by the detection of contamination in air in the north and western parts of Korea on 28 March, whereas the backward reached to the southeast part of Korea later on 5-7 April 2011.

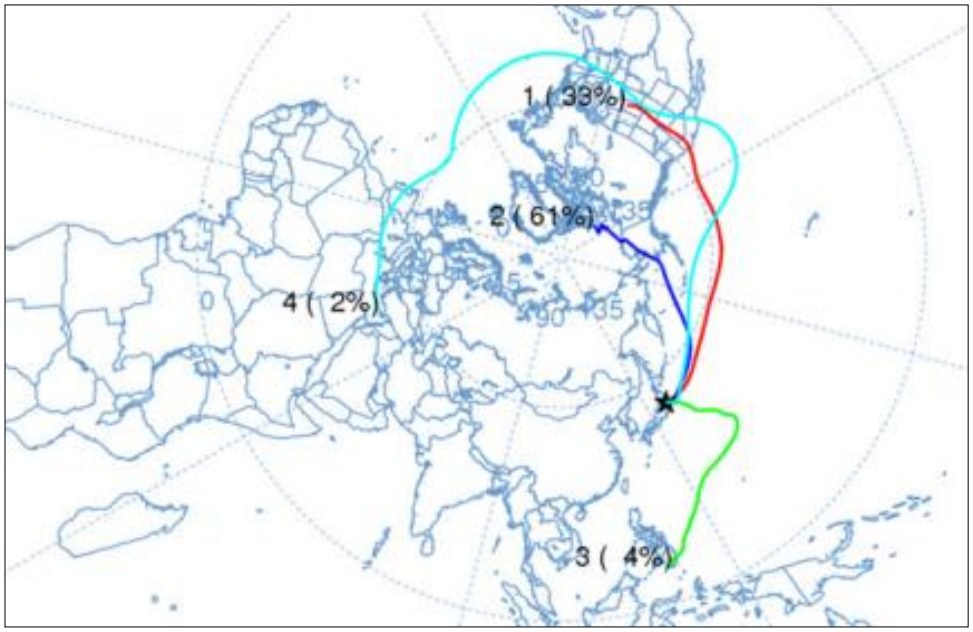

Figure 1-7 Illustration of the movement of air masses (as a percentage) from Fukushima to others areas around the world (Piñero García & Ferro García, 2012)

1.4.4 Atmospheric radionuclides around the world.

Radionuclides releasing from Fukushima I NPSs were observed at many sites around the world. The main radionuclides measured were, as in Japan, ^{131}I, ^{132}Te/^{132}I and ^{134,137}Cs; ^{136}Cs was also detected at some sites. Another high nuclide expected to be at high concentrations, ^{129m}Te/^{129}Te, was not reported in the literature, but it can be ignored since the emitted gamma energies from ^{129m}Te and ^{129}Te are very low at 0.0376 and 0.0625 MeV respectively (ICRP, 2008).

The two peaks observed in Japanese monitoring data were also detected in the Pacific Ocean, North America and Europe but their magnitude were significantly lower than that in Japan. As discussed above, a small proportion of the plume which travelled over the Pacific Ocean was transferred backward to Southeast Asia. (Piñero García & Ferro García, 2012). Once site in Guam (about 2,700 from Fukushima prefecture) could detect the backward radionuclide cloud starting from about 9 days after the earthquake and showing two peaks on days 10 and 14 (Figure A-5 in Appendix A). The concentrations of ^{131}I at two peaks were 8.5×10^{-3} and 2.3×10^{-3} Bq m^{-3} (Biegalski et al., 2011), lower than the concentration at JAEA (the nearest sites in Japan) by factor of 16,000 and 480,000 respectively. This site confirms the existence of the backward radionuclide cloud which is not a consequence of the cloud from Japan crossing Europe and moving to Asia. The measurements were made about 10 days after the earthquake whilst the cloud which crossed Europe to Asia took significantly longer to arrive (about 20 days). A second reason is that the concentration of radionuclides were similar to those in the forward cloud. For the forward radionuclide cloud, for example, Midway Islands (approximately 4,000 km from NPSs) had two peaks of ^{131}I at 1.7×10^{-4} and 9.4×10^{-5} Bq m^{-3} on days 11 and 16 (Figure A-6 in Appendix A). These were less than those measured at JCAC by factors of 8×10^{6} and 12×10^{6} respectively (Biegalski, et al., 2011) demonstrating the large dispersion of the plume as it crossed the Pacific. By the time radioactivity had reached North America, (Figure A-7 in Appendix A) the highest measured value of ^{131}I of 4.3×10^{-9} Bq m^{-3} occurred around 14 days after the earthquake at University of California, United States located approximately 8,000 km from Fukushima I NPSs (UCB, 2011). The concentration of ^{131}I from this site was less than the first peak at JAEA by a factor of 3×10^{11}.

The air dispersion model of Piñero García and Ferro García (2012) shows (Figure 1-7) that the radionuclide cloud entered the southern part of Europe (Portugal and Spain) then spread out to other countries. For example, Bossew and co-workers (2012) observed radionuclides in air at Offenbach, Germany beginning approximately 14 days after the earthquake. At this site about (~21,000 km from the NPSs), the highest particulate ^{131}I was 1.8×10^{-3} Bq m^{-3} which less than JAEA's peak around factor of 8×10^{5} (Figure A-8 in Appendix A) Data provided for this thesis bythe Ukrainian Institute of Hydrometeorology at Rivnenska Nuclear Power Plant in Kiev, Ukraine (see Appendix A-9 in Appendix A) located approximately 22,600 km from Fukushima I NPSs. As shown in Figure A-9 in

Appendix A, this site observed contamination in air approximately13 days after the earthquake, the highest concentration of ^{131}I (about 6 days after first detection) being 6.3×10^{-3} Bq m^{-3}, 2×10^{5} times lower than the highest concentration in first peak at JAEA. The Health Protection Agency (2011), conducted continuous monitoring in the centre at Oxford, United Kingdom located about 22,000 km from NPSs. The wind blew radionuclides cloud to this site at around 20 days after the earthquake; ^{131}I reached to the peak at 6.7×10^{-4} Bq m^{-3} about four days later (Figure A-10 in Appendix A).

After crossing Europe, radioactivity was transported to Asia with the arrival of the contamination plume in South Korea on 28 March 2011 or seventeen days after the earthquake (Kim, et al., 2012). The highest ^{131}I measurement of 3.1×10^{-3} Bq m^{-3} was detected at Gunsan, South Korea (lower than JAEA'peak by factor of 5×10^{5}).

Table 1-3 shows a summary of examples of the highest radioactivity concentration of ^{131}I, ^{132}Te and $^{134,136,137}Cs$ for sites at different distances from the Fukushima I NPSs, The pattern of two peaks corresponding to the two plumes occurred from sites in Japan and the Pacific Ocean, and mostly the highest peak caused by the first plume except a site at JCAC in Japan. The two peak pattern disappeared when radioactivity reached the US territory, after that, one plume pattern still dominated at sites in Europe. The highest values of radioactivity concentration of all nuclides from each station was shown in Figure 1-8, as expected, the concentration in Japan was significantly higher than sites in the Pacific Ocean, US and EU approximately by two or more orders of magnitude for ^{131}I and three or more for ^{137}Cs (there was no significant difference between Pacific Ocean, US and EU). The highest ^{131}I in Asia was still not different to sites in the Pacific Ocean, US and EU, however, ^{137}Cs was slightly higher which might be a result of a combination of forward and backward plumes.

Note that distances of all site were estimated by using the air mass trajectory from the study of the passage of releases from Fukushima I NPSs by Piñero García and Ferro García (2012). Therefore, the plume travelled from Japan to the Pacific Ocean, North America, the Atlantic Ocean, and then entered southern Europe.

Table 1-3 Summary of the highest radioactivity concentration (Bq m^{-3}) of ^{131}I, ^{132}Te and $^{134,136,137}Cs$ of each plume for the sites at different distances from Fukushima I NPSs.

Site	Distance	First plume					Second plume				
	(km)	I-131	Te-132	Cs-134	Cs-136	Cs-137	I-131	Te-132	Cs-134	Cs-136	Cs-137
In Japan											
JAEA, Tokai-mura, Ibaraki, Japan	115	1.4E+03	2.1E+03	3.7E+02	5.7E+01	3.7E+02	1.1E+03	4.4E+02	4.2E+02	5.5E+01	4.2E+02
Takasaki, Gunma, Japan	219	1.5E+01	2.7E+01	6.9E+00	8.6E-01	5.6E+00	5.2E+00	4.6E+00	3.3E+00	5.2E-01	3.8E+00
JCAC, Chiba, Japan*	220	3.3E+01	5.7E+00	7.0E-01	1.3E-01	8.7E-01	4.7E+01	2.6E+00	6.1E+00	3.6E-02	7.5E+00
RIKEN Wako Institute, Saitama, Japan	223	3.6E+01	6.1E+01	7.0E+00	1.3E+00	9.5E+00	7.8E+00	7.4E-01	1.8E+00	9.7E-03	2.4E+00
Pacific Ocean											
Guam, US	2,687	8.5E-03	1.9E-03	9.2E-04	1.4E-04	1.1E-03	2.3E-03	3.3E-05	3.7E-05	5.8E-06	4.5E-05
Midway Islands, US	4,028	1.7E-04	2.6E-05	9.6E-06	2.4E-06	9.4E-06	9.4E-05	2.2E-05	1.1E-05	2.1E-06	1.0E-05
US											
University of Washington, Washington, US	7,475	4.4E-03	7.8E-04	1.1E-04	-	1.4E-04					
University of California, California, US	8,067	4.7E-06	8.8E-07	1.1E-06	-	1.2E-06					
Melbourne, FL, US	11,520	3.1E-02	3.9E-03	1.9E-03	2.7E-04	2.3E-03					
EU											
Offenbach, Germany	21,040	1.8E-03	1.2E-04	1.1E-04	-	1.3E-04					
Sacavém, Lisbon, Portugal	21,859	1.4E-03	6.2E-05	1.5E-04	-	1.4E-04					
HPA, Oxon, UK	21,928	6.7E-04	-	9.6E-05	-	9.4E-05					
Kiev	22,581	6.3E-03	1.1E-04	5.4E-04	-	4.2E-04					
Asia											
Gunsan, South Korea$^{\Delta}$	28,476	3.1E-03	-	1.9E-03	-	1.3E-03					

Note that: * Highest peak occurred in second plume.

$^{\Delta}$ The pattern of two plumes was disappeared.

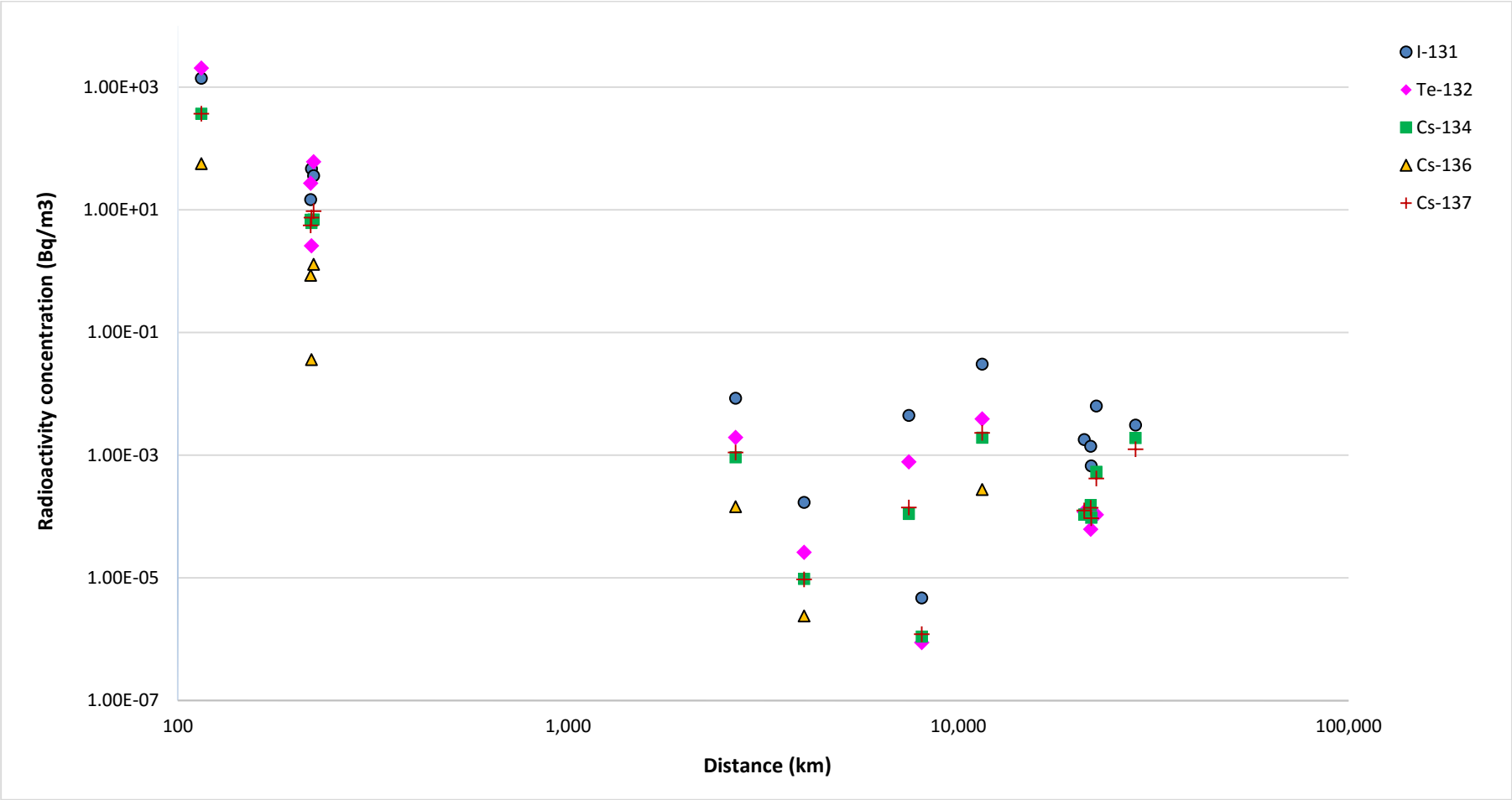

Figure 1-8 the highest radioactivity concentration (Bq m^{-3}) of ^{131}I, ^{132}Te and $^{134,136,137}Cs$ for sites at different distance from Fukushima I NPSs.

1.5 The deposition of radionuclides

This study focuses primarily on the area outside the exclusion zone at Fukushima I NPSs (>20 km) to determine external gamma dose rates in the early period after the accident. This is because measurements of soil radionuclide concentration and gamma dose rate were available at the same sites (used for estimating gamma dose in Chapter 4) between 24 and 62 km from NPSs. In addition, soil is an important pathway for the transfer of radionuclides to humans and biota. Therefore, understanding the contamination of different radionuclides in soil in high fallout areas is very useful for dose reconstruction.

During atmospheric transport, radionuclides are deposited to the ground either by wet (being washed out by precipitation or snow) or dry (attachment or absorption on surfaces) deposition. Following the Fukushima accident, numerous radionuclides, including ^{95}Nb, ^{99}Mo/^{99m}Tc, ^{110m}Ag, ^{129m}Te/^{129}Te, ^{131}I, ^{132}Te/^{132}I, ^{133}I, ^{133}Xe, ^{134}Cs, ^{136}Cs, ^{137}Cs, ^{140}Ba/^{140}La, could have potentially deposited on the Earth's surface. However, only a few of these were in sufficient quantity to be readily detected in soil. In the area from outside the 20 km exclusion zone to 80 km distance, ^{129m}Te/^{129}Te, ^{131}I, ^{132}Te/^{132}I, ^{134}Cs, ^{136}Cs and ^{137}Cs were observed in significantly high concentrations in soil, while ^{95}Nb, ^{110m}Ag, ^{140}La (directly released from reactor cores) and ^{140}Ba/^{140}La were detected in small amounts [^{140}Ba/^{140}La was not found and amounts of ^{95}Nb, ^{110m}Ag, ^{140}La at two sites located in the southern area around 20 and 220 km respectively from NPSs were lower than the lower limit of detection (<50 Bq kg^{-1}) while ^{137}Cs in the upper 2 cm of soil were 1.2×10^{4} Bq kg^{-1} and 1.1×10^{3} Bq kg^{-1} respectively (Tagami et al., 2011)] which did not allow for accurate evaluation of the concentration. ^{99}Mo/^{99m}Tc, ^{129}Te, ^{132}I and ^{133}I have very short half-lives (65.94 h, 69.6 m, 2.3 h, and 20.8 h respectively) and so would have decayed rapidly meaning that accurate measurement was not possible. In case of noble gases such as ^{133}Xe, there was no evidence of any deposition to the ground surface because of their gaseous nature and low reactivity with surfaces (S. Endo, et al., 2012; Imanaka et al., 2012; MEXT, 2011b, 2011c; Tagami, et al., 2011; Yamamoto et al., 2012).

The most highly contaminated area in the near-zone to Fukushima I NPSs was to the northwest where most of the aerosol monitoring was conducted (S. Endo, et al., 2012; Imanaka, et al., 2012; Kinoshita, et al., 2011; MEXT, 2011b, 2011c, 2011d). As shown inn Figure 1-9, the highest radiocaesium activity concentrations (consisting of ^{134}Cs and ^{137}Cs only, in the range 3-30 MBq/m^{2}) extended to about 36 km.

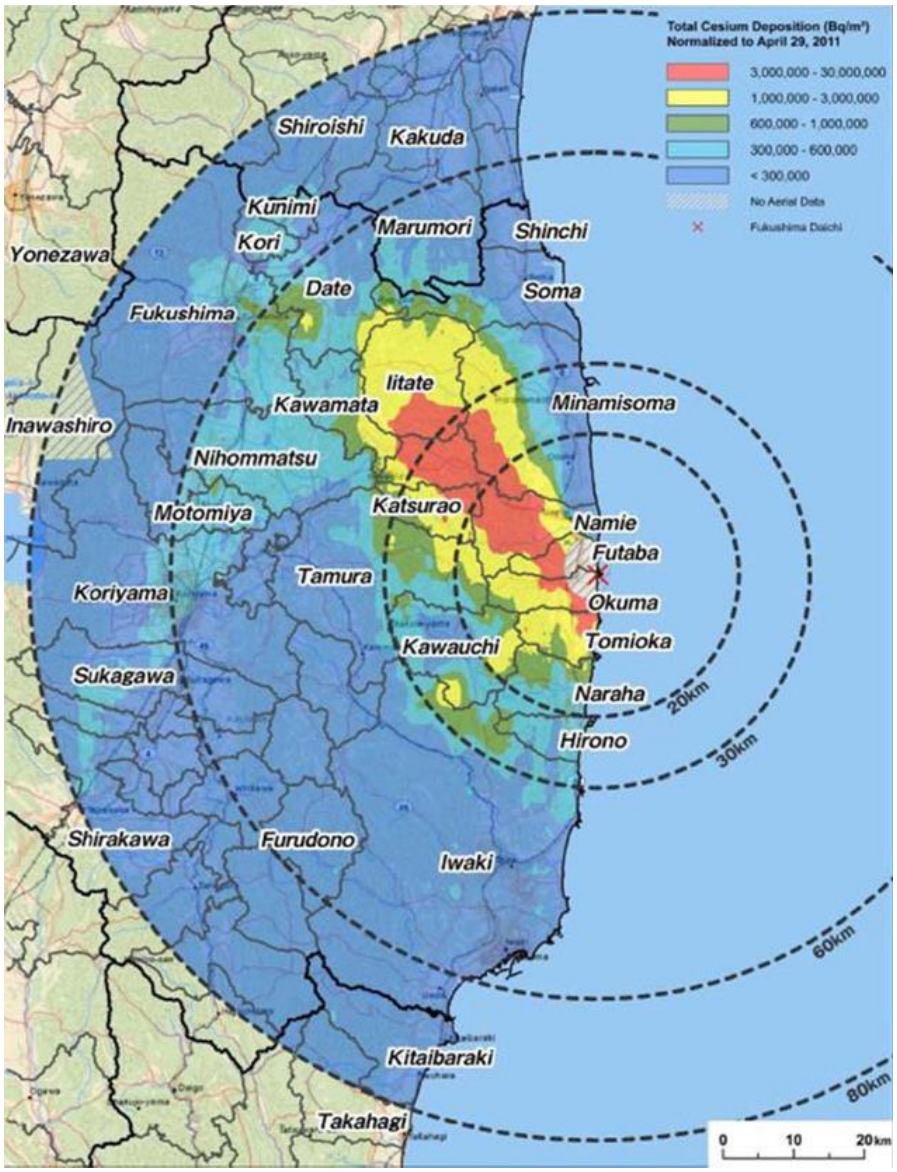

Figure 1-9 Map of the deposited radiocaesium (summation of ^{134,137}Cs) in the near-zone area (<80 km) of Fukushima I NPSs (MEXT, 2011d).

In the northwest direction, high deposition densities could be observed at distances from 20 to 62 km, range 0.04-31 MBq/m^2 for ^{137}Cs, sites=91 as shown in Table 1-4, the highest observation in this direction occurred at 22 km distance at Kurabeishi, Hirusone, Namie town, Futaba county (MEXT, 2011c) with mean 25 and 31 MBq/m^2 for ^{134}Cs and ^{137}Cs respectively (mean and S.E. of deposition density (Bq/m^2) in near-zone of Fukushima I NPSs was shown in Table A-1 in Appendix A). For ^{131}I in Kurabeishi, after correction back to the time of maximum deposition on 15 March (Kinoshita, et al., 2011), the estimation of deposition density of ^{131}I was 196 MBq/m^2.

To contrast with Chernobyl accident, there were few measurements of the full range of radionuclides during the first few weeks. Maps of radionuclide deposition were therefore reconstructed based on later measurements of long-lived ^{137}Cs. UNSCEAR (2000b) reported the average deposited concentration of ^{137}Cs at contaminated area (Belarus, the Former Russian Federation and Ukraine) around Chernobyl was greater than 0.037 MBq/m^2. The highest deposition density was greater than 3.7 MBq/m^2 in the area within 5-km radius around Chernobyl NPP, and in some areas between NPP and 30-km area in the north and between 30-km and 60-km areas in the west direction of NPP as shown in Figure 1-10.

For ^{131}I, there was the lack of measurement at deposition time so that the deposition of ^{131}I was approximately >37 MBq/m^2 at closed area of NPP (estimated by using relative ratio to ^{137}Cs varied between 5 and 60 as the resulted this estimation provided not accurate deposition density). Other study, Kryshev and Ryazantsev (2000) reported same value (>1.5 MBq/m^2) at the areas far from NPP up to hundreds kilometre in west, northwest and northeast direction, and IAEA (1991) reported the estimation of 0.6-1.5 and 1.3 MBq/m^2 for range and average of deposited ^{137}Cs in Polesskoe, Ukraine located about 290 km in northwest and 0.004-1.5 and 0.8 MBq/m^2 in Bragin, Belarus located around 46 km in northern area

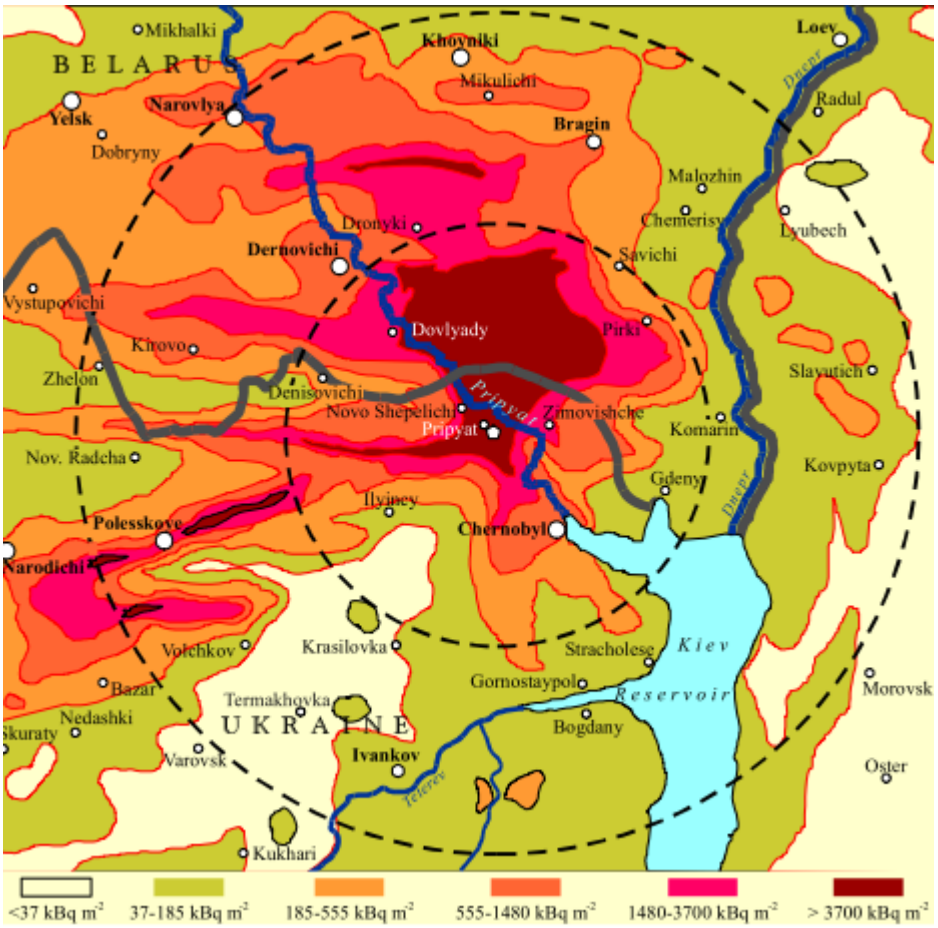

Figure 1-10 Map of the deposited ^{137}Cs (kBq/m^2) within 30-km and 60-km areas of Chernobyl NPP produced by UNSCEAR (2000b).

Table 1-4 Deposition density of ^{134}Cs and ^{137}Cs (Bq/m^2) in the near-zone (20-80 km) of Fukushima I NPSs (S. Endo, et al., 2012; Imanaka, et al., 2012; MEXT, 2011b, 2011c).

Direction	Mean	± S.E.	Max.	Min.	Sites	Samples	Distance covered (km)
^{134}Cs							
N	1.8E+05	2.2E+04	3.1E+05	1.5E+04	12	243	50
NW	2.2E+06	3.8E+05	2.5E+07	1.7E+04	91	821	62
W	8.1E+05	4.3E+05	9.8E+06	7.3E+03	22	420	60
SW	1.4E+05	3.4E+04	3.9E+05	4.4E+04	10	184	80
S	7.4E+04	1.4E+04	1.7E+05	1.6E+03	12	197	44
^{137}Cs							
N	2.0E+05	2.6E+04	3.4E+05	1.6E+04	12	243	50
NW	2.7E+06	4.6E+05	3.1E+07	2.1E+04	91	821	62
W	8.9E+05	4.5E+05	1.0E+07	1.2E+04	22	420	60
SW	1.5E+05	4.0E+04	4.7E+05	5.2E+04	10	184	80
S	8.7E+04	1.7E+04	2.0E+05	2.3E+03	12	197	44

In the near-zone area (20-80 km), soil monitoring was conducted by MEXT (2011b): 6 sites of continuous monitoring were established on 18 March (3 days after the high deposition phase on 15 March) which could detect the second plume on 21 March. The continuous monitoring sites were subsequently extended to more than 50 sites in the beginning of April, plus single sampling of 71 sites by MEXT at the end of May (2011b, 2011c), 15 sites by Endo at al. (2012) were sampled on 15 March, and 5 sites were studied on 31 March (Imanaka, et al., 2012). Table 1-4 shows a summary of the contamination in each direction from Fukushima I NPSs in the near-zone area. Deposition density in the north-western area was highest with mean 2.7×10^6 Bq/m^2, the second most contaminated area was the western part in which contamination was lower than the NW by a factor of three. These were followed by the northern and south-western areas which had one order of magnitude lower fallout and in the south, fallout was thirty times lower. Therefore, (Figure 1-9 and Table 1-4) the north-western area around 0-36 km from NPSs was affected by the highest gamma dose rate emitted from soil as the contamination was influenced by first plume so this is a key region to carry out an estimation of external gamma dose rate.

1.6 The contamination of aquatic systems

There were a lack of measurements in aquatic systems affected by the high fallout from Fukushima, particularly in the near-zone during the initial phase. However, one lake located around 50 km from the NPSs in the high contamination area in the northwest region was monitored for ^{131}I and $^{134, 137}Cs$ by MEXT (2011b). Daily monitoring of total phase (particulate and dissolved) of these three nuclides was conducted from 18 March until the end of August 2011. The radioactivity concentration in lake water during the first monitoring were 2.1×10^{6}, 4.6×10^{5} and 5.11×10^{5} Bq m^{-3} for ^{131}I and $^{134,137}Cs$ respectively.

Around four months after the accident, Ueda et al. (2013) collected particulate and dissolved phase ^{137}Cs in two rivers, Wariki and Hiso River during August – November 2011. The total radioactivity of ^{137}Cs on 20 July 2011 were 7.6×10^{3} and 1.1×10^{4} Bq m^{-3} for each river respectively. In the northwest direction, approximately 60 km from the NPSs, $^{134,137}Cs$ concentration (total phase) in a single sample at the Matsu River on 14 September 2012 contained 5.1×10^{-2} and 9.6×10^{-2} Bq m^{-3} respectively (Yasutaka et al. (2014)). Figure 1-9 shows that this river was outside the highest contamination area. On 14 September 2012, Yasutaka and co-workers (2014) also collected samples from two rivers in the western area: the Sugita and Gohyaku Rivers (both were about 55 km from the NPSs) and one other river, the Yashiro River in the Southwest (~60 km). Since all three rivers were outside the high contamination area, $^{134,137}Cs$ concentrations were 5.3×10^{-2} and 9.6×10^{-2} Bq m^{-3} for Sugita, 1.0×10^{-1} and 1.7×10^{-1} Bq m^{-3} for Gohyaku and 1.4×10^{-2} and 2.9×10^{-2} Bq m^{-3} for Yashiro River.

Within the near-zone, Nagao et al. (2013) collected six samples (total phase) during 12 July – 06 December 2011 from each of the Natsui and Same Rivers which were both in the southern area and around 45 and 60 km respectively from the NPSs. $^{134,137}Cs$ concentration in runoff on 12 July were 49 and 52 Bq m^{-3} for the Natsui River and 75 and 81 Bq m^{-3} for the Same River.

Note that locations of all rivers and lakes studied in this thesis are shown in Figures 5-1 and Figure 5-2 and summaries of measured data are available in Section 5.2.1 together with other information such as catchment area, and water residence time.

1.7 Modelling of environmental systems following the Fukushima accident

There was significant contamination of the environment following the release of high amounts of radionuclides from the Fukushima I NPSs. Measurements around the world detected long range transport of radioactivity. This research will carry out an assessment of the worldwide transfers of radionuclide cloud by studying the decay corrected ratio of various radionuclides to long-lived ^{137}Cs and how these change with time and distance from Fukushima.

For analysis of deposition and external gamma dose rate, this research will focus on the highly contaminated area within the near-zone (<80 km) of the Fukushima I NPSs particularly in the northwest area where most contamination was found (Chino, et al., 2011; Katata, Ota, Terada, Chino, & Nagai, 2012; Katata, Terada, Nagai, & Chino, 2012; Kinoshita, et al., 2011; Morino, Ohara, & Nishizawa, 2011). that the focus on the highly contaminated northwest area allows the use of empirical measurements of external gamma dose rate to calibrate and test a model based on the emission of gamma energy from the range of short and long-lived radionuclides in soil Since both data on dose rate and radionuclide contamination in soil were available only in the near-zone the research on this topic focused on this area.

The aim of modelling in aquatic systems is the early phase reconstruction and long-term prediction of contamination in water and fish (both predatory and non-predatory) in any freshwater systems in Japan which were affected by fallout from Fukushima This research will use measurements from a range of rivers and lakes discussed above, including eight rivers and one lake within the near-zone. From a collaboration with the Chiba Institute of Technology, further field-measurements were made to support this research. This compilation of data allowed the testing and further development of a model for radionuclides in Japanese aquatic systems.

Chapter 2 Modelling radionuclide transfers and external dose following a nuclear accident

2.1 Introduction

In order to implement radiological countermeasures and evaluate and reduce human exposures from a contaminated environment, it is necessary to develop effective methods of estimating radiological impacts. This study will focus on the evaluation of the external gamma dose in the near-zone of Fukushima in the early and long-term phases after deposition, and long-term transfer of radionuclides in terrestrial and aquatic systems.

The environment and human food chain have been significantly affected by past releases of contaminated radioactive materials. These include artificial releases of radionuclides from Nuclear Weapons Testing and the Chernobyl accident. Following these past releases, there have been many studies evaluating the radiological impact of these events which give a strong methodological basis for evaluating the impact of the recent nuclear accident at Fukushima. This chapter reviews modelling methods for evaluating radionuclide transfers in the ecosystem and external doses, and develops them for application to the Fukushima accident.

2.2 Air transport and deposition of radionuclides following Chernobyl

After the nuclear accident at the Chernobyl Nuclear Power Plant (NPP), large amounts of various radionuclides were released from the severely damaged Unit 4 reactor into the atmosphere. Radioactive material spread out over the former Soviet Union territories and in lesser quantities in many other part of the World including Europe, Asia, North Africa and North America (Yablokov, Nesterenko, Nesterenko, & Sherman-Nevinger, 2010). The release occurred over 10 days (UNSCEAR, 2000a) and included nuclides of key importance to public dose, particularly ^{131}I and ^{137}Cs (approximately 1.76×10^{18} and 8.5×10^{15} Bq respectively) Other radionuclides including ^{7}Be, ^{59}Fe, ^{90}Sr, ^{95}Nb, ^{95}Zr, ^{99}Mo, ^{103}Ru, ^{106}Ru, ^{127}Sb, ^{129m}Te/^{129}Te, ^{131m}Te, ^{132}Te/^{132}I, ^{133}I, ^{134}Cs, ^{136}Cs, ^{140}Ba/^{140}La, ^{239}Np, ^{239}Pu, ^{240}Pu were also released from this catastrophe accident. The widespread atmospheric dispersal resulted in major transfers of radioactive elements to terrestrial, freshwater and marine ecosystems. During the period in which radioactive materials were dispersed throughout the atmosphere, two key deposition processes caused contamination

of the surface environment. Some radionuclides were primarily washed out by rain or snow and deposited to the ground (wet deposition) whilst others also showed a significant deposition velocity under conditions of no deposition (dry deposition) (Mück et al., 2002; F. B. Smith & Clark, 1989; J. T. Smith & Beresford, 2005a).

Following a release of radioactivity to the environment, very short-lived radionuclides decay before full mapping of their deposition can be made. By estimating their ratios to relatively long-lived ^{137}Cs (half-life 30.2 years), the distribution of short-lived radionuclides can be mapped and early-phase external doses reconstructed. There have therefore been many studies on the air transport and deposition of radionuclides to define the levels and characteristics of contamination, and estimate the external gamma dose to humans and wildlife. In the 30-km exclusion zone around reactor Unit 4 of Chernobyl NPP, a key study of radionuclide transfer as a ratio to ^{137}Cs was carried out by Mück and co-workers (2002). The research focused on the radionuclide (RN): ^{137}Cs ratios as a function of direction and distance from Chernobyl NPP. The ratios were determined by analysing literature data of measurements of radioactivity concentration in air and ground deposits, in comparison with estimates of ratios within the reactor core using burn-up data. Empirical relationships of ratios to direction and distance were determined. In terms of radionuclide transfer, Mück and co-workers (2002) found that different isotopes of the same element (such as the ratio of the relatively volatile nuclide ^{134,136}Cs to ^{137}Cs) were transported and deposited in the same pattern. For radiocesium released from Chernobyl, the average ratio of ^{134}Cs: ^{137}Cs in air was constant with distance and direction, with range between 0.55 and 0.59, while the deposited ratio was also constant with value in the range 0.54-0.57. The other main radioactive isotope of caesium, ^{136}Cs also showed a ratio to ^{137}Cs which was constant with distance and direction with range approximately 0.15-0.27 and 0.22-0.27 for ratio in air and deposition respectively. Other relatively volatile radionuclides, ^{103}Ru and ^{132}Te were also observed (Muck et al. 2002) to be constant with distance.

The non-volatile radionuclides, however, showed a different distribution in air. The ratios of ^{99}Mo, ^{90}Sr, ^{95}Zr, ^{140}Sr and ^{144}Ce to ^{137}Cs in the near zone were much higher than at long distances (200-1,000 km area) and ratios decreased rapidly with increasing distance from the release point (Mück et al., 2000). This was because these radioactive materials had a

high rate of deposition resulting in their rapid deposition after release from the damaged reactor.

Since the Chernobyl release continued over 10 days (UNSCEAR, 2000a), deposition plumes with differing characteristics were observed in different directions, depending on the state and temperature of the reactor at different times during the accident. Mück et al. (2000) observed that ratios in ground of radionuclides having similar volatility to radiocaesium, such as ^{132}Te were remarkably consistent with direction. For ^{132}Te: ^{137}Cs in three plumes released from Chernobyl NPP: W (the explosive phase), NNW (the slowly heating-up core phase) and S (above 2,000 ºC at core phase) showed remarkably consistent ratios of ^{132}Te: ^{137}Cs. Ratios to ^{137}Cs of other radionuclides including ^{90}Sr, ^{95}Zr, ^{99}Mo, ^{103}Ru,, ^{140}Ba, ^{144}Ce and ^{239}Np were similar in the western and northern plume but the value in south direction was significantly higher. This is due to the fact that the southern plume was caused by a high temperature release with less volatile radionuclides i.e. ^{90}Sr, ^{95}Zr, ^{99}Mo, ^{103}Ru, and ^{140}Ba, released at significantly higher rates than radiocesium, In contrast, the relatively volatile ^{131}I (aerosol+gaseous) showed only higher ratios to ^{137}Cs in the southern plume compared to the western and north-north-western plumes because higher core temperatures released higher amounts of ^{131}I (Mück, et al., 2000). For large distances, the ^{131}I (aerosol+gaseous):^{137}Cs ratio decreased with distance which (Mück et al. (2000)) was because deposition of ^{131}I was dominated by dry deposition of the gaseous form (70%) and deposition velocity of this form was higher than particulate ^{131}I and ^{137}Cs. Mück and coworkers also concluded that deposition velocities of particulate ^{131}I and ^{137}Cs were similar at 1 mm s^{-1} while gaseous ^{131}I was 6 mm s^{-1}.

In another study, Mück and co-workers (2002) derived equations for reconstructing the radioactivity concentration in air, which can be used to estimate internal dose from inhalation. The relationship between the concentration in air and soil at near-zone (30-km area and no rain) was given as:

$$A_i = C_i v_{gi} \tag{2-1}$$

where A_i (Bq m^{-2}) is the deposited radioactivity concentration of the i^{th} nuclide, C_i (Bq s m^{-3}) is the integrated radioactivity concentration in air of the i^{th} nuclide, and v_{gi} (m s^{-1}) is the deposition velocity of the i^{th} nuclide. For longer distances, but no further than 170 km,

the radioactivity concentration in air and soil of long half-life radionuclides which their half-life are greater than the time of plume passage can be calculated as follows:

$$C_i(r) = \frac{1000 \times A_{Cs-137} \times R_{iso} \times R_{nucl} \times c_{dir}}{3.6 \times v_{gi}} \quad (2\text{-}2)$$

where $C_i\,(r)$ (Bq h m^{-3}) is the integrated radioactivity concentration in air of the i^{th} nuclide at distance r from release point, $A_{Cs\text{-}137}$ (kBq m^{-2}) is the deposited radioactivity concentration of ^{137}Cs at distance r from the release point, R_{iso} is the ratio of the i^{th} nuclide to isotopic guide-nuclide in each group. For example, ^{89,90,91}Sr/^{90}Sr, ^{129m,132}Te/^{132}Te, $^{131(aerosol\ and\ gaseous),133}$I/$^{131(aerosol\ and\ gaseous)}$I, and ^{134,136,137}Cs/^{137}Cs, R_{nucl} is the ratio of the isotopic guide-nuclide in each group to ^{137}Cs e.g. ^{90}Sr/^{137}Cs, ^{132}Te /^{137}Cs , $^{131(aerosol\ and\ gaseous)}$I: ^{137}Cs, c_{dir} is a correction factor for direction, resulting from the different amounts of each radionuclide in the three main plumes released from the Chernobyl accident such as 3.0 for ^{89,90,91}Sr 1.7 for $^{131(aerosol\ and\ gaseous),133}$I, and 1 for ^{134,136,137}Cs, and v_{gi} (mm s^{-1}) is the deposition velocity of i^{th} nuclides. After deriving radioactivity concentration in air by Equation 2-1 and 2-2 at the sites where ambient measurement was not performed, the inhalation dose can be estimated (Mück, et al., 2000).

For further distances, other studies focused on the dispersion and deposition of radionuclides released from Chernobyl accident. Clark and Smith (1988) used measured data in air, soil and particularly on grass combined with sufficient meteorology data to evaluate wet and dry deposition in UK. Relatively volatile ^{137}Cs released from Chernobyl accident was mostly in the particulate form, so that the deposition process was dominated by washout of rainfall. ^{131}I, however, was transported both in particulate and gaseous forms and both wet and dry deposition processes were significant. In this study (Clark and Smith, 1988), 50-75% of ^{131}I was found to be in gaseous form the study of, Cambray et al. (1987) also found that 75% of radioiodine was gaseous. In Italy, 68-76% was in gaseous phase (Spezzano and Giacomelli, 1991).

In the initial period of the Chernobyl release, there was no significant rain in the former Soviet Union territory. This meant that the volatile radionuclides such as ^{131}I and ^{134,137}Cs were still found in the atmosphere (Clark & Smith, 1988; Mück, et al., 2002) at large distances from the site. The cloud of radioactive gases moved to other parts of Europe and led to significant deposits to soil by rainfall. In UK in areas of little or no rain,

the ratio ^{131}I: ^{137}Cs on grass (which is likely to be similar to surface soil) was high, at approximately 18, resulting from the high dry deposition velocity of aerosol ^{131}I. For light rainfall conditions, the ^{131}I: ^{137}Cs ratio decreased remarkably to about 4 and declined to lower than 2 in high precipitation areas. This can be explained by the fact that the average of the dry deposition velocity of ^{131}I (both aerosol and gaseous) in the UK was higher than ^{137}Cs by a factor of 60, and that the estimated release of ^{131}I was significantly higher than ^{137}Cs (IAEA, 1986; UNSCEAR, 2000a). This result agrees with another study about the deposition in northern England (Livens, Fowler, & Horrill, 1992) which ^{131}I had high rate of deposition in dry deposition. Smith and Clark (1989) present a method for estimating the deposited radioactivity, D (Bq m^{-2}) in relation to the concentration radioactivity in air:

$$D = v_{part} C_{part} + v_{gas} C_{gas} \quad (2\text{-}3)$$

where C_{part} and C_{gas} are the time-integrated concentration (Bq m^{-3} s) in particulate and gaseous form respectively, v_{part} and v_{gas} are the empirically estimated dry deposition velocity (m s^{-1}) for particulate and gaseous form respectively. In the UK both observed parameters were 4.6×10^{-4} m s^{-1} for v_{part} and 3.6×10^{-3} m s^{-1} for v_{gas} (F. B. Smith & Clark, 1989).

In case of wet deposition in UK (Clark & Smith, 1988), measurements were available for evaluating the interception of the Chernobyl release by rainfall. The deposited radioactivity in the washout process, D (Bq m^{-2}), can be calculated by assuming that it is proportional to the radioactivity concentration in air:

$$D = w_r C R \quad (2\text{-}4)$$

where w_r is the dimensionless washout factor which varies by intensity of rainfall in range $5.8\text{-}7.7\times10^5$ for UK (Clark & Smith, 1988) similar to 6.5×10^5 in Clark and Smith (1988)'s study, C (Bq m^{-3}) is the average concentration radioactivity in air, and R (m) is the total amount of rainfall.

2.3 Deposition of radionuclides following the Fukushima accident

In a recent study on ambient transfer and deposition of radionuclides following the Fukushima accident, Kinoshita and co-workers (2011) measured the deposition ratio from the near-field zone to further distances (from 30 to 300 km approximately) by gamma-ray spectrometry of contaminated radionuclides in surface soil. This allowed mapping of the distribution of contamination. According to metrological data (Section 1.4.1), it is clear that the major transport occurred in 15 March 2011 in N to NW, particularly in NW direction of Fukushima I NPSs (Chino, et al., 2011; Kinoshita, et al., 2011; Morino, et al., 2011). This was followed by more minor releases in the SW to S directions which occurred on 21 March. During the 15-16th March radioactive release, there was rainfall from 17.00 on 15 March to 4.00 on 16 March 2011 in the northern area of Fukushima prefecture up to about 50 km to the N and NW direction from Fukushima I NPSs. For the later release, rainfall occurred between 8.00 on 21 March and 6.00 on 23 March in southern 200-300 km area as show the detail in Figure 1-1.

Kinoshita et al. (2011) reported depositions for ^{131}I, ^{129m}Te, and ^{134,136,137}Cs and ratios for ^{129m}Te:^{137}Cs, ^{131}I:^{137}Cs, and ^{129m}Te:^{131}I (corrected to 29 March 2011) around Fukushima I NPSs. In Figure 2-1, it is shown that the deposited activities of fission products including ^{129m}Te, ^{131}I, $^{134, 136, 137}$Cs were very high in the Iitate and Naka-Dori regions. Iitate is a hilly area located approximately 30 km from Fukushima I NPSs in the NW direction, while Naka-Dori is a basin-shape valley located in the middle of the Fukushima prefecture or NW to SW of Fukushima I NPSs.

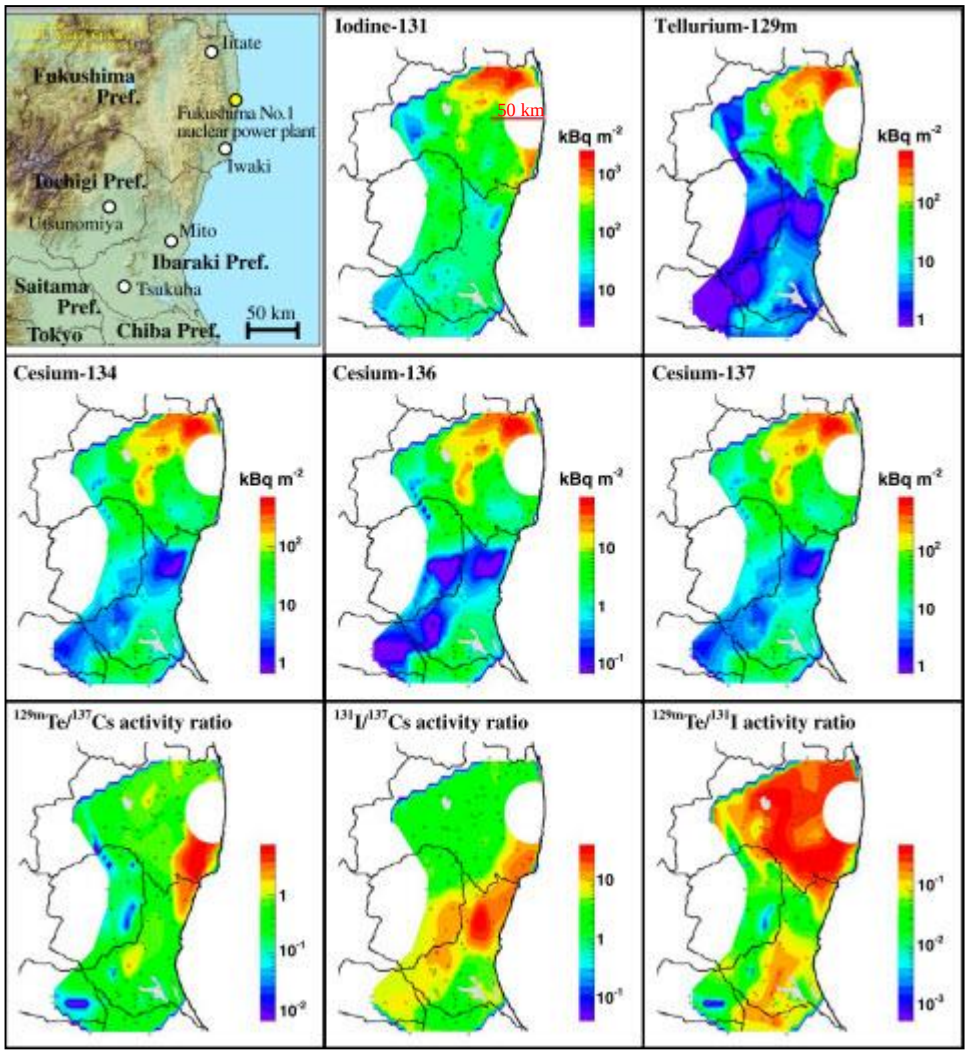

Figure 2-1 Illustration of the topographic map of the depositions for ^{131}I, ^{129m}Te, and ^{134,136,137}Cs and ratios for ^{129m}Te:^{137}Cs, ^{131}I:^{137}Cs, and ^{129m}Te:^{131}I (corrected to March 29, 2011) in the area of Fukushima and further areas in other prefectures including Tokyo; produced by Kinoshita et al. (2011).

The deposited concentrations of all isotopes of radiocesium (^{134,136,137}Cs) were high between 10^2 and 10^3 kBq m^{-2} for ^{134,137}Cs and around 10 and 100 kBq m^{-2} for ^{136}Cs within the 80-km area in the N and NW and the area between 80 and 100 km in the NW. Lower activities of about 10^2 for ^{134,137}Cs and around 10 kBq m^{-2} for ^{136}Cs were seen in the area between 80 and 100 to the NW and SW which was influenced by the changing of wind direction in the first plume. For ^{131}I, the deposition in soil was very high within approximately a 50-km area in the S and an area within 80-100 km in N and NW direction, being approximately 10^3-10^4 kBq m^{-2}. Deposition density in the southern direction was influenced by the second 21 March release, averaging around 10^3 kBq m^{-2}, while other regions (W to SW) were lower, being of the order of ten to a thousand times lower than in the N and NW directions.

The ratio of ^{134} Cs to ^{137}Cs was around 0.8-0.9 in all directions and distances around Fukushima I NPSs, whereas the ratio ^{131}I: ^{137}Cs was much higher to the SW and S being in the range 8-15 but much lower in other regions including the N and NW (ratio around 1-8).

2.4 Model for external gamma dose from deposited radionuclides

UNSCEAR (2000a, 2013) and WHO (2012) show that the majority of radiation dose to the public was dominated by deposited radioactivity and the ingestion pathway while dose from the contaminated cloud is minor. Radionuclides deposited in soils produce an external gamma dose rate in air which depends on the gamma decay energy, the distribution in the soil and soil characteristics (Peter Jacob et al., 1994; Kocher & Sjoreen, 1985). Jacob and co-workers (Peter Jacob, et al., 1994) model the kerma rate in the air as function of ^{137}Cs depth profile and site characteristics, then kerma rate can be converted to an exposure dose rate to humans. Kocher and Sjoreen (1985) model the external exposure produced by emitted photons from soil. In a similar way, the GRANIS model (Khalid & Mann, 2007) calculates the external photon dose by using conversion factors for converting deposited concentration to effective dose rate at various times from a variety of radioisotope materials.

Following the Chernobyl accident, Jacob and co-workers (Peter Jacob, et al., 1994) modelled the kerma rate in the air as function of ^{137}Cs depth profile and site characteristics: soil type, annual precipitation, distance from Chernobyl, and mode of deposition (dry or wet). There are three parameters which can reduce the kerma rate over the grassland. The first parameter is the surface roughness of the interface between air and ground, the second is migration of the radioactive material into the soil, and the last is radiation shielding surrounding the area. This research (Peter Jacob, et al., 1994) focused on the first two parameters, and evaluated attenuation factors due to the combination of the surface roughness and the migration of ^{137}Cs in south Bavaria (clay and silt), in Ukraine (sand), and some sites in Russia (silt and sand) from deposition following Chernobyl accident. In-situ gamma-ray spectrometry was used to measure activity per unit area compare with depth profiles. For dry deposition, surface roughness was less significant than in wet conditions because more radionuclides are deposited on to vegetation in dry conditions while under wet deposition, radionuclides are more quickly washed out and migrated into the soil (P Jacob, Meckbach, & Müller, 1987; Peter Jacob, et al., 1994). Attenuation factors due to the combination of the surface roughness and the migration of ^{137}Cs resulting from in stu gamma-ray spectrometry method agreed with depth profiles method in first year after deposition. After that, in second year, an attenuation factor from in stu gamma-ray spectrometry method was slightly less than

depth profiles method, and less than more in the third year. This is because of the underestimation from an exponential decrease activity in the soil in in stu gamma-ray spectrometry calculation. However, the difference from two methods was not significant which mean the surface roughness did not effect to an attenuation factor in initial period of migration into soil. The kerma rate in air as a function of time after deposition of nuclide i, $\dot{K}$(J kg^{-1}) can be calculated (Peter Jacob, et al., 1994) by

$$\dot{K}(t) = \sum_i A_i \times k_i \times e^{(-\lambda t)} \times r_i\,(t) \qquad (2\text{-}5)$$

When A_i (Bq per unit area) is deposited activity of nuclide i, k_i is a factor for converting activity per unit area to the kerma rate in air of nuclide i which can be applied for estimating human doses depending on type of organs, t (years) is time after deposition, r_i is a modified function of the kerma rate due to an activity distribution depending on type of nuclide, physical and chemical form of radionuclide before deposition, deposited condition (dry or wet), time after deposition, characteristic of site such as properties of soil, the annual precipitation(option). In the Jacob et al. model, the parameter r_i (t) is determined empirically by using measured data from Bavaria, Ukraine and Russia. The value of r_i (t) was defined as a function of the empirical parameters ρ_1, ρ_2, ρ_3 and ρ_4 which can see in detail in Table 2-1.

$$r_i(t) = \rho_1 e^{-\rho_2 t} + \rho_3 e^{-\rho_4 t} \qquad (2\text{-}6)$$

Jacob and co-workers (1994) determined empirical parameter ρ_1, ρ_2, ρ_3 and ρ_4 from Bavarian sites where characteristic of sites were available and condition of deposition is wet resulting in high deposition for caesium. The first set of empirical parameters were derived from Bavarian data ρ_4 was set equal to zero to give an upper estimate of long term dose because measured data were available only for the first 5.5 years after the Chernobyl accident. Later studies (Peter Jacob, et al., 1994) also used longer term data from the New York area which studied dose after the deposition from atomic weapon test ove a 24 year period. This gave a long term continuing decline in dose (positive ρ_4 value). However, this resulted in an underestimated result for long-term predictions due to the fixation process of radiocaesium in soil. Therefore, the third set of parameters (Table 2-1) which has no ρ_4 best predicted the measurements of kerma rate in air

Table 2-1 Empirical parameters ρ_1, ρ_2, ρ_3 and ρ_4 for estimating r_i (t) in Jacob et al .(1994).

Parameters				Area	Reference
ρ_1	ρ_2	ρ_3	ρ_4		
0.34±0.03	0.55±0.14	0.34±0.03	0.0	Bavaria	Jacob et al. (1994)
0.31±0.04	0.61±0.18	0.37±0.04	0.015±0.008	Bavaria and New York	Jacob et al. (1994) and Miller et al. (1990)
0.38±0.03	0.38±0.07	0.28±0.03	0.0	Bavaria and New York	Jacob et al. (1994) and Miller et al. (1990)

2.5 Model for external gamma dose from deposited radionuclides following Fukushima

Similar to the research by Jacob and co-workers, WHO (2012) developed a model for estimating the external dose from contaminated radionuclides in soil to populations affected by Fukushima in Japan. The effective dose rate $\dot{E}_i^{dep}$ Sv/h in *t* time (year) at one metre above the ground was be estimated by converting kerma in free air as follows:

$$\dot{E}_i^{dep}(t) = \dot{K_{air}}(t) \times k_i \times RF_i \qquad (2\text{-}7)$$

Where k_i is a conversion factor from kerma in free air to the effective dose, independent of location and time after the accident: 0.75 Sv/Gy for adults, 0.80 Sv/Gy for children (10 years) and 0.90 Sv/Gy for infants (1 year). RF_i is a reduction factor for population group *i* (assumed to be 0.6 for all population groups in Japan), and $\dot{K_{air}}(t)$ is the kerma rate in free air (μGy/h) which can be determined by

$$\dot{K}_{air}(t) = r(t) \times A_{Cs137} \times \sum_m \left(\frac{A_m}{A_{Cs137}}\right) \times \dot{d}_m^{dep} \times e^{-\lambda_m t} \qquad (2\text{-}8)$$

where A_{Cs137} is the surface activity density of ^{137}Cs on the ground (Bq/m^2), A_m is the surface activity density of radionuclide *m* on the ground (Bq/m^2) which the estimation of $\frac{A_m}{A_{Cs137}}$ of each *m* nuclide corrected back to 15 March 2011. The parameter values used in the WHO model are shown in Table 2-2: $\dot{d}_m^{dep}$ is the dose rate coefficient from surface activity density to kerma rate for height of one metre above ground due to initial distribution of radionuclide *m* in the ground based on the empirical study of Jacob et al. (1990) discussed above, λ_m is the decay constant of radionuclide *m* (year-1), and $r(t)$ is a time dependent attenuation function that accounts for radionuclide penetration in the soil (year) can be estimated (Vladislav Golikov, Balonov, Erkin, & Jacob, 1999; V Golikov, Balonov, & Jacob, 2002; P Jacob & Likhtarev, 1996) by

$$r(t) = \rho_1 e^{-\frac{ln2}{T_1}t} + \rho_2 e^{-\frac{ln2}{T_2}t} \qquad (2\text{-}9)$$

From WHO (2012), ρ_1= 0.34, ρ_2 = 0.66, T_1 = 1.5 year and T_2 = 50 year. Equation 2-9 is similar to Equation 2-6 as both are empirical parameters for site characteristics such as soil type, annual precipitation and distance from release point, the reduction of dose rate

due to the surface roughness of interface between air and ground, and the migration of the radioactive material into the soil.

Table 2-2 the estimation of relative isotopic ratio of radionuclide *m* to ^{137}Cs ($\frac{A_m}{A_{Cs137}}$) in soil on 15 March 2011 were used in WHO'model summarised from (Imanaka, et al., 2012; IRSN, 2011b)

Radionuclide *m*	**Deposited ratio to ^{137}Cs**
^{131}I	7.8
^{132}I	7.6
^{132}Te	7.6
^{134}Cs	0.92
^{136}Cs	0.16

A simpler method to determine the external gamma dose from ground surface is estimation using a conversion factor to calculate gamma dose from deposited concentration (Kocher and Sjoreen (1985)). These workers estimated external gamma dose rate at a height of one metre above ground from radioactive concentration and dose-rate conversion factors which were dependent on, the energy of gamma emitters and depth profiles of discrete energies in soil. To extrapolate dose rate, conversion factors were determined in discrete energies from 0.01 to 10 MeV and depths in soil of radioactive material from the surface to 300-cm depth. Dose rate is defined as the gamma energy emitted per unit of source concentration in soil and it is assumed that the sources of gamma dose rate are divided into uniform infinite surfaces parallel to the ground surface at any depths of soil, or uniform slab sources between ground surface and different depths in soil. Table 2-3 shows examples of conversion factors to estimate gamma dose from long-lived ^{137}Cs. Another study using conversion factors to extrapolate the integrated effective dose rate at 1 metre above ground after an instantaneous of deposition is the GRANIS model (Khalid & Mann, 2007). GRANIS is a computer model for estimation of gamma dose and gamma dose rate from radionuclides in a contaminated layer of finite thickness and infinite plane source. The principle of the model is the calculation of the total photon flux (at 1 metre above ground or above the contaminated layer; the energy of the photon depends on the isotope) from the whole contaminated layer by integrating from each small thickness of layer as a disc (infinite lateral extent). The flux from each disc is reduced by attenuation and scattering in the soil layer and air above, and the

reduction of flux depends on the depth from ground surface including thickness of shielding, and type of material of shield. For contamination in soil, for example, soil is shielding itself which mostly consist of O, Si and C (Khalid & Mann, 2007). Conversion factors for soil of some key radionuclides to gamma dose are shown in Table 2-4.

Table 2-3 Examples of conversion factor (Gy/a per Bq/cm^2) to extrapolate external gamma dose from soil for ^{137}Cs by Kocher and Sjoreen's method (1985).

Depth (cm)	Emitted photon energy (MeV)			
	Uniform infinite surface parallel to the ground surface at any depths		Uniform slab sources between ground surface and deferent depths	
	0.06	0.08	0.06	0.08
0.0	3.62E-05	4.18E-05	4.73E-06	6.65E-06
0.5	9.12E-06	1.36E-05	8.44E-06	1.25E-05
1.0	6.11E-06	1.00E-05	1.30E-05	2.05E-05
2.0	3.38E-06	6.45E-06	1.56E-05	2.59E-05

Table 2-4 Example of conversion factor (Sv/h per Bq/m^2) to extrapolate the integrated effective dose rate at 1 metre above ground after an instantaneous of deposit 1 Bq m^{-2} of ^{131}I, ^{132}I and ^{137}Cs on undisturbed soil by the GRANIS model (Khalid & Mann, 2007).

Time	Conversion factor			
	^{131}I	^{132}I	^{132}Te	^{137}Cs
0	8.49E-13	5.27E-12	4.96E-13	1.39E-12
6 h	8.75E-13	8.63E-13	4.73E-12	1.39E-12
12 h	8.56E-13	1.42E-13	5.18E-12	1.39E-12
1 day	8.20E-13	3.84E-15	4.78E-12	1.39E-12
2 days	7.52E-13	1.13E-17	3.87E-12	1.39E-12
7 days	4.88E-13	1.36E-23	1.33E-12	1.39E-12
30 days	6.66E-14	0	9.97E-15	1.38E-12
1 year	1.49E-22	0	0	1.21E-12
2 years	1.03E-25	0	0	1.06E-12
5 years	0	0	0	7.48E-13
10 years	0	0	0	4.76E-13
50 years	0	0	0	4.37 E-14

,

2.6 AQUASCOPE model for transfer of contaminated radionuclides in aquatic ecosystems

The long-term transfers of radiocaesium in terrestrial and aquatic ecosystems are dependent on slow changes in chemical availability in soil (J. T. Smith, Fesenko, et al., 1998b). In this study, a consistent rate of decline of radiocaesium concentration was seen in three ecosystem components: vegetation, water and milk during five years after the Chernobyl accident. The study, focused on ^{137}Cs, derived the rate of decline by using transfer modelling of ^{137}Cs in ecosystems as shown in Figure 2-3, and these derived rates of vegetation, water and milk showed a remarkably consistent decline over the five years study period for a large set of measurement data. The times for decline of ^{137}Cs to half its initial value were in the range 1-4 years during the first five years after the accident, while for the longer period, the trend of decline reverted to a slower rate at 6-30 years (J. T. Smith et al., 2000).

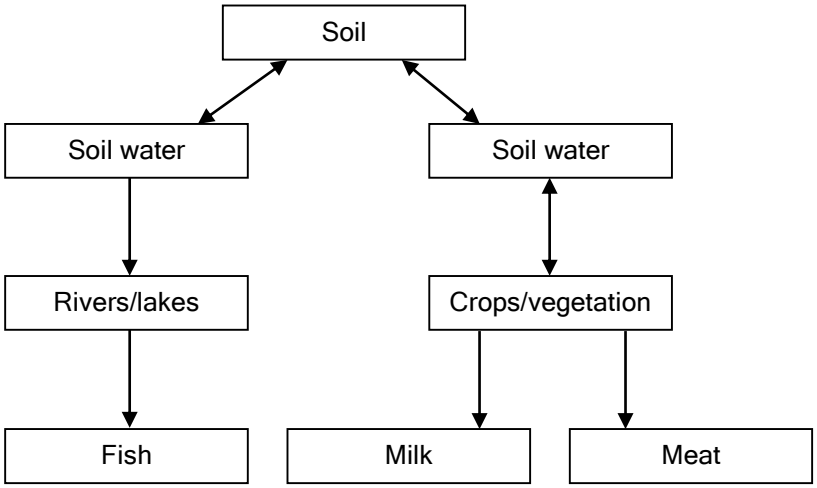

Figure 2-2 Schematic diagram of transfers of ^{137}Cs in ecosystems.

2.6.1 Runoff or river modelling

A key characteristic of runoff or river water is the much more rapid flow rate of water through this ecological system compared with lakes and reservoirs. The activity concentration in runoff water or rivers (Helton, Muller, & Bayer, 1985) can be determined (Helton et al. 1985) as the fractional removal of fallout radioactivity from a catchment, relative to the flow rate of water removal from the catchment. Therefore, the

contamination in runoff water or rivers is most significant in the initial period when deposition is high, and the level of contamination varies with the deposited concentration in a catchment. Radionuclides in aquatic systems are found in the form of both dissolved and particulate phases. The simplified model "AQUASCOPE" (J. T. Smith et al., 2005), however, focused on only the dissolved phase for estimating radionuclides in runoff and rivers because a large proportion of particulate phase activity transfers directly into sediments, and the uptake of radionuclides into fish and other aquatic foodstuffs is mostly from the dissolved phase.

For estimation and prediction of the contamination in runoff water or rivers, Monte (1995) and Smith et al. (2000) showed that the change with time of dissolved radioactivity concentration in runoff and river, C_R (Bq/m^3), can be calculated by:

$$C_R = D_C(\alpha e^{-(k_1+\lambda)t} + \beta e^{-(k_2+\lambda)t} + \gamma e^{-(k_3+\lambda)t}) \qquad 2\text{-}10$$

Where D_C is the radionuclide deposition to the catchment (Bq/m^2) and λ (y^{-1}) is the decay constant of the radionuclide. The constants α, β, γ and k_1, k_2, k_3 *are* empirically determined constants which depend on the specific radionuclide. α and k_1 are the constants for a fast "flush" of activity as a result of rapid washoff processes, β and k_2 are for a slow decline as a result of soil fixation and redistribution processes, and γ and k_3 are for the very long term "equilibrium" situation.

(a) Description of the AQUASCOPE model for radiocaesium in rivers and runoff water

For the initial rapid decline, k_1, the mean rate four rivers in Europe is 18.0 **y**$^{-1}$ (Monte, 1995; Schoer, 1988; Ursula, Von Gunten, & Krähenbühl, 1987; Voitsekhovitch, Borzilov, & Konoplev, 1991). The parameters k_2, k_3 are estimated empirically from studies of the time dependence of radiocaesium activity concentrations in many European rivers after both weapons testing and Chernobyl (J. T. Smith, et al., 2000; J. T. Smith, Fesenko, et al., 1998a; J. T. Smith, Kudelsky, Ryabov, & Hadderingh, 2000), and the estimated values of these are 0.41 and 0.02 y^{-1} for k_2 and k_3 respectively.

During the first year after high fall out from nuclear weapon testing, when the initial runoff had significantly high contamination, Helton et al. (1985) measured the cumulative loss of activity from the catchment, λ_a (Bq/y) for radiocaesium by using:

$$\lambda_a = R \int_0^1 \alpha\, e^{-(k_1+\lambda)t} + \beta e^{-(k_2+\lambda)t} + \gamma e^{-(k_3+\lambda)t} dt \qquad 2\text{-}11$$

Where R (m/y) is the net annual rainfall to the catchment which is equal to the annual flow per unit surface area of water removed from the catchment. This study also found the correlation between α and k_1 is given by:

$$\alpha \approx \frac{k_1 \lambda_a}{R} \qquad 2\text{-}12$$

From Helton et al.(1985), gives λ_a= 0.001-0.02 and R ~ 1 m y^{-1} with k_1 as above, the range of α is 0.013-0.26 m^{-1}. However, Smith et al. (2005) assume that R < 1 m y^{-1} resulting the conservative value of α for model of 0.3 m^{-1}.

To estimate β and γ, the values of both are given by linear relations with the percentage coverage of the catchment by these boggy and organic soils (Hilton, Livens, Spezzano, & Leonard, 1993; J. T. Smith, Howard, et al., 1998). The following linear relations have been used in the model:

$$\beta = \beta_1 \cdot f_{min} + \beta_2 \cdot f_{org} \qquad 2\text{-}13$$

$$\gamma = \gamma_1 \cdot f_{min} + \gamma_2 \cdot f_{org} \qquad 2\text{-}14$$

Where $\beta_{1,2}$ and $\gamma_{1,2}$ are empirically determined constants which are 0.003, 0.05, 0.0002 and 0.007 respectively, f_{org} is the fraction (by area) of the catchment which is covered by boggy and organic soils, and f_{min}: the fraction not covered by boggy and organic soils.

(b) ^{131}I for river modelling

Smith (2005) gives the value of α = 1.0 m^{-1}, , and Monte (1995) gives a value of k_1 = 8.5 y^{-1}. There is no fixation in soil of ^{131}I and physical decay is very short so that both β = 0 and γ = 0.

2.6.2 Open Lake Modelling

A lake can be defined as an open lake when water residence time is less than 1 year or the average depth of lake is greater than 7 metres. The model distinction between open and closed lakes is necessary to identify because the long-term contamination by ^{137}Cs in closed lakes have clearly been shown to be higher than in open lakes which have more rapid flow rate of removal of water (Bulgakov et al., 2002).

For short-term, in the initial period, the contamination of a lake is dominated by a "spike" input or direct deposition to the surface of the lake (J. T. Smith, et al., 2005) which is given by simple dilution:

$$C_L(0) = \frac{D_L}{d} \qquad 2\text{-}15$$

When $C_L(0)$ (Bq/m^3) is the initial mean lake water concentration, D_L (Bq/m^2) is the deposition per square metre of lake surface , and d (m) is the mean depth of the lake. In this period, radionuclides from spike input only sink into sediment. In the long-term period, however, the activity concentration in open lakes is dominated by runoff from the catchment. Radionuclides continue to sink into the bed sediment but there is also transfer from sediment to lake by physical resuspension and chemical remobilisation (J. T. Smith, et al., 2005). In addition, in long-term period, Smith et al. (J. T. Smith, P. Leonard, Hilton, & Appleby, 1997) found that the radioactivity concentration in lake was approximately equal to the concentration in the inlets or streams. Smith and co-workers (J. T. Smith, et al., 2005) calculate the radionuclide activity concentrations in open lakes, $C_L(t)$ (Bq/m^3), by using:

$$C_L(t) = \frac{D_L}{d} e^{-(K+\lambda)t} + \frac{D_C e^{-\lambda t}}{T_W}\left[\frac{\alpha(e^{-k_1 t} - e^{-Kt})}{(K - k_1)} + \frac{\beta(e^{-k_2 t} - e^{-t/T_W})}{(1/T_w - k_2)} + \frac{\gamma(e^{-k_3 t} - e^{-t/T_W})}{(1/T_W - k_3)}\right] \qquad 2\text{-}16$$

Where D_C (Bq/m^2) is the radionuclide deposition to the catchment, D_L (Bq/m^2) the deposition per square metre of lake surface, d (m) is the mean depth of the lake, λ (y^{-1}) is the decay constant of the radionuclide, parameter values of constants k_1, k_2 and k_3 are determined as in the runoff model, and K (y^{-1}) is the rate of removal of radionuclides to the lake bed sediments and outflow.

(a) Parameters for open lake modelling

A key input parameter for modelling radiocaesium and ^{131}I is the rate of removal of radionuclides to the lake bed sediments and outflow (K). For radiocaesium, the removal rate consist of the removal to sediment and the removal to the lake outflow (J. T. Smith, et al., 2005). Therefore, to predict radiocaesium in lakes (both open and closed lakes), the value of parameter K can be determined as below

$$K = \frac{1}{T_W} + \frac{1}{T_L} \quad \text{2-17}$$

T_W *is* the water residence time of the lake (y), and T_L is the rate of removal of radionuclides to bed sediments (y^{-1}), these are given by:

$$T_W \approx \frac{V_L}{RA_C} \quad \text{2-18}$$

$$\frac{1}{T_L} = \frac{f_p v_p}{d} \quad \text{2-19}$$

where R (m/y) is the net rainfall, V_L (m^3) is the lake volume, A_c (m^2) is the catchment area, v_p (m/y) the particle settling velocity, and f_p is the particulate sorbed fraction which can be calculated from the radiocaesium distribution coefficient (K_d, m^3/kg) and the suspended solids concentration (s, mg/l) of the lake water:

$$f_p = \frac{sK_d}{1+sK_d} \quad \text{2-20}$$

Smith and co-workers (1999) observed the rate of removal of radiocaesium to the lake bed sediments and outflow (K) from sixteen Chernobyl contaminated lakes. It can be assumed that the rate of removal depends on the water residence time and the mean depth of the lake as follow

$$K = \frac{1}{T_W} + \psi_1 \quad \text{2-21}$$

$$K = \frac{1}{T_W} + \frac{\psi_2}{d} + \theta \quad \text{2-22}$$

Where Ψ_1, Ψ_2 and θ are empirical parameters (Smith et al. (1999) gives Ψ_1 = 2.0 y^{-1} for estimating K value when only T_w is known, and Ψ_2 = 8.0 m y^{-1} and θ =1.0 y^{-1} if measurements of both Tw and d are available.

(b) ^{131}I for open lake modelling

The removal rate ^{131}I for open lake is based on the transfer to the lake outflow only, there is no significant transfer to the bottom sediment, so decline in concentration is assumed to be by dilution and physical decay only. Therefore, *K* for ^{131}I can be estimated by (J. T. Smith, et al., 2005):

$$K = \frac{1}{T_W} \qquad 2\text{-}23$$

Where T_W can be calculated by using Equation 2-18.

2.6.3 Closed Lake Modelling

Under the AQUASCOPE model, the definition of a closed lake is that the water residence time is more than 1 year and the average depth of lake is less than 7 metres.

(a) Radiocaesium for closed lake modelling

The trend of ^{137}Cs, in the long-term, in closed lakes is much higher than in runoff or river water and in open lakes (Bulgakov, et al., 2002). Another characteristic of closed lake (J. T. Smith, et al., 2005) is that the long-term ^{137}Cs concentration in water is dominated by resuspension and remobilisation from the sediment and the transfer from catchment can be neglected since there is little water inflow or outflow. Resuspension is a physical process in which ^{137}Cs is removed back from sediment to water by wave action while remobilisation (Evans, Alberts, & Clark Iii, 1983) is the chemical transfer by anoxic conditions in the sediment (a total absence of oxygen).

AQUASCOPE estimates radioactive concentration in water, C_L (Bq/m^3) by using

$$C_L = \frac{D_L}{d} e^{-(K+\lambda)t} + D_L\left[\eta_1 e^{-(\lambda+k_2)t} + \eta_2 e^{-(\lambda+k_3)t}\right] \qquad 2\text{-}24$$

Where D_L (Bq/m^2) the deposition per square metre of lake surface, *d* (m) is the mean depth of the lake, λ (y^{-1}) is the decay constant of the radionuclide, *K* is the rate of removal of radionuclides to the lake bed sediments and outflow determined as for the radiocaesium removal rate in open lake modelling. The constants k_2 and k_3 have been observed to be similar to the rates of decline seen in rivers so these are assumed to have the same value, and η_1 and η_2 are the estimated empirically from measurements normalised to unit

deposition to the lake surface (m^{-1}).Smith et al. (2005) gives values of η_1 = 0.04 m^{-1} and η_2 = 0.0085 m^{-1} from observations on nine closed lakes in European countries.

(b) ^{131}I for closed lake modelling

Since physical decay of ^{131}I is significant short lead to the transfer of ^{131}I in lake to bottom sediment and lake outflow can be negligible. Therefore, the estimation of ^{131}I concentration in water can be made by

$$C_L = \frac{D_L}{d} e^{-\lambda t} \qquad 2\text{-}25$$

2.6.4 Fish Modelling

The uptake (Hickey, Keith, & Coon, 1966; Rasmussen, Rowan, Lean, & Carey, 1990; Thomann, 1989) of radionuclides to fish occurs by ingestion and inhalation. The former is a primary pathway which most radionuclieds in food chain can transfer to fish, while the latter, the direct transfer via gills, is less significant. There are four main factors for the uptake into fish: the species of fish, the length of the food chain, water temperature, and the chemical properties of the water (J. T. Smith, et al., 2005).

Basically, the level of radioactive contamination of fish can be defined by the Concentration Factor (*CF*, m^3/kg) which is the factor relative to activity concentration in fish and water as shown below:

$$CF = \frac{Activity\ concentration\ per\ kg\ of\ fish\ (wet\ weight)}{Activity\ concentration\ per\ cubic\ metre\ of\ water} \qquad 2\text{-}26$$

In the short-term phase after the release from a nuclear accident which can be defined as the non-equilibrium phase, the radioactivity concentration in fish (J. T. Smith, et al., 2005) can be determined by using a simple “two-box” model as shown in Figure 2-4.

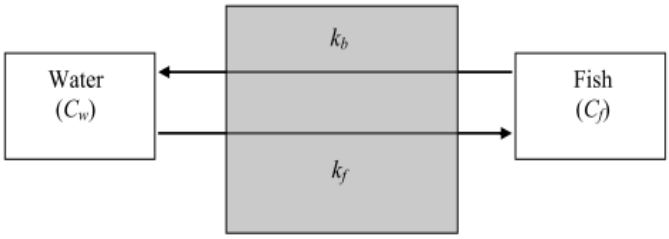

Figure 2-3 A simple "two-box" model describes the uptake and excretion of radioactive material of fish.

Figure 2-4 shows the relation of the transfer of radionuclide between fish and water, where C_f is activity concentration of a radionuclide in fish (Bq/kg), C_w is the activity concentration of a radionuclide in water (Bq/m^3), k_f is the rate constant describing transfers of ^{137}Cs to fish (m^3/kg y) and k_b is the backward rate constant describing excretion of radioactivity from the fish (y^{-1}), and all parameters can be determined for the non-equilibrium phase in the following equation:

$$\frac{dC_f}{dt} = k_f C_w - (k_b + \lambda) C_f \qquad 2\text{-}27$$

When the equilibrium phase is reached, the CF is defined as the ratio of uptake and excretion rate constants:

$$CF = \frac{C_f}{C_w} = \frac{k_f}{k_b + \lambda} \qquad 2\text{-}28$$

(a) Radiocaesium for fish modelling

Smith et al. (2000) and Blaylock (1982) show that *CF* of ^{137}Cs had an inverse relation with potassium concentration in lake water, in which *CF* (J.T. Smith, A.V. Kudelsky, et al., 2000) can be determined as below

$$CF = \frac{Y}{[K^+]} = \frac{k_f}{k_b} \qquad 2\text{-}29$$

To calculate k_f, Equation 2-29 can be rewritten as below

$$k_f = \frac{Y k_b}{[K^+]} \qquad 2\text{-}30$$

Where $[K^+]$ is the potassium concentration of the lake water in units μmol/L≡mmol/m^3 and Y is an empirically determined constant (μmol m^3/kg). From observations from 10 lakes in Russia, Belarus and Ukraine during 6-11 years after Chernobyl accident, Smith et al. (2000) gives Y = 462 and 61.3 μmol m^3/kg, and k_b = 0.511 and 8.4 (y^{-1}) for predatory and non-predatory fish respectively.

Smith and co-worker's study (2000) also concludes that the *CF* of predatory fish is higher twice than non-predatory and there was no observable difference in *CF* for different species of non-predatory. To contrast, predatory fish has the "size effect" for radiocaesium accumulation which is that the contamination increase when the fish size increase (Elliott et al., 1992; Hadderingh, van Aerssen, Ryabov, Koulikov, & Belova, 1997; A. O. Koulikov & Ryabov, 1992). Elliott et al. (1992) found that the radiocaesium accumulation has a logarithmic relation with wet weight of fish which Smith et al. (2002) quantified using a power law to evaluate the radioactivity concentration for fish:

$$C_f \propto w^n \tag{2-31}$$

Where w is wet weight of predatory fish (g), and n is an empirically determined coefficient: n = 0.34 for predatory fish and n = 0 for non-predatory fish.

Therefore, the radioactivity concentration of radiocaesium in both predatory and non-predatory fish in rivers, open lake and closed can be calculated by using Equations 2-32, 2-33 and 2-34 respectively as below

To calculate radioactivity concentration of radiocaesium in fish in runoff or river:

$$\begin{aligned} C_f &= D_c \times e^{-\lambda t} \times w^n \\ &\times \left[\frac{k_f \times \alpha}{k_b - k_1} \times (e^{-k_1 t} - e^{-k_b t}) + \frac{k_f \beta}{k_b - k_2} \times (e^{-k_2 t} - e^{-k_b t}) \right. \\ &\left. + \frac{k_f \gamma}{k_b - k_3} \times (e^{-k_3 t} - e^{-k_b t})\right] \end{aligned} \tag{2-32}$$

Fish in open lake:

$$C_f = e^{-\lambda t} \times w^n \times \left[\left(k_f \times D_L \times \frac{e^{-Kt} - e^{k_b t}}{(k_b - K)d} \right) + D_C \times \alpha \times \frac{k_f}{T_W \times (K - k_1)} \times \left(\frac{e^{-k_1 t} - e^{-k_b t}}{k_b - k_1} - \frac{e^{-Kt} - e^{-k_b t}}{k_b - K} \right) + \times \beta \times \frac{k_f}{T_W \times \left(\frac{1}{T_W} - k_2 \right)} \times \left(\frac{e^{-k_2 t} - e^{-k_b t}}{k_b - k_2} - \frac{e^{-\frac{t}{T_W}} - e^{-k_b t}}{k_b - \frac{1}{T_W}} \right) + D_C \times \gamma \times \frac{k_f}{T_W \times \left(\frac{1}{T_W} - k_3 \right)} \times \left(\frac{e^{-k_3 t} - e^{-k_b t}}{k_b - k_3} - \frac{e^{-\frac{t}{T_W}} - e^{-k_b t}}{k_b - \frac{1}{T_W}} \right) \right] \quad 2\text{-}33$$

And fish in closed lake:

$$C_f = D_L e^{-\lambda t} \times w^n \times \left[\left(\frac{k_f}{d(k_b - K)} \times (e^{-Kt} - e^{-k_b t}) \right) + \left(\frac{k_f \times \eta_1}{k_b - k_2} \times (e^{-k_2 t} - e^{-k_b t}) \right) + \frac{k_f \times \eta_2}{k_b - k_3} \times (e^{-k_3 t} - e^{-k_b t}) \right] \quad 2\text{-}34$$

Note that the value of parameters *n*, k_f and k_b in Equations 2.32-2.34 have to be chosen correctly for predatory or non-predatory fish.

(b) ^{131}I for fish modelling

For ^{131}I in AQUASCOPE, there is no difference between predatory and non-predatory fish, and it is assumed that the "size effect" does not influence the uptake into fish from different weights i.e. $n = 0$ in Equation 2-31.

The uptake is principally via the food chain with assumed that fish feed at their maximum daily rate. Therefore, the uptake rate can be estimated by

$$k_f = \frac{C_{food} \times D_{max} \times \phi \times 365 \times 10^{-3}}{C_w \times w \times 10^{-3}} = \frac{CF_{food} \times D_{max} \times \phi \times 365}{w} \quad 2\text{-}35$$

Where D_{max} is the maximum daily intake (wet weight) of food (g/d), C_{food} is the activity concentration of the food, CF_{food} is the concentration factor of the food (e.g. plankton for

herbivores or herbivorous fish for piscivores), ϕ is the assimilation efficiency (the fraction of amount ingested which is absorbed by the fish). Smith et al. (2005) gives $\phi = 1.0$, $C_{food} = C_w$, and $CF_{food} = CF_{fish} = 0.04$ m^3/kg

D_{max} is the maximum daily intake (wet weight) of food (g/d) and can be determined by using Elliott's model (1975):

$$D_{max} = (4 \times 10^{-3}) A_D \times w^{b_1} \times e^{b_3 T} \qquad 2\text{-}36$$

Where T is water temperatures, and the parameters A_d, b_1, b_2 are the empirically determined constants. From the fish measurements in the Kiev Reservoir following the Chernobyl accident (I. I. Kryshev & Ryazantsev, 2000), Smith et al. (2005) concludes that k_f = 0.593 m^3/kg and k_b = 14.8 y^{-1} which were used for prediction ^{131}I in fish in AQUASCOPE.

The concentration of ^{131}I in both predatory and non-predatory fish in river can be calculated in AQUASCOPE by

$$C_f = D_C \times e^{-\lambda t} \times \frac{k_f \alpha}{k_b - k_1} \times (e^{-k_1 t} - e^{-k_b t}) \qquad 2\text{-}37$$

For open lakes, the ^{131}I concentration can be determined as below

$$\begin{aligned} C_f = {} & e^{-\lambda t} \\ & \times \left[\left(\frac{k_f \times D_L}{d \times (k_b - K)} \right) \times (e^{-Kt} - e^{-k_b t}) \right. \\ & \left. + \left(\frac{D_C \times \alpha \times k_f}{T_W \times (K - k_1)} \right) \times \left(\frac{e^{-k_1 t} - e^{-k_b t}}{k_b - k_1} - \frac{(e^{-Kt} - e^{-k_b t})}{k_b - K} \right) \right] \end{aligned} \qquad 2\text{-}38$$

Finally, in closed lake, ^{131}I contaminate in fish can be calculated by

$$C_f = \frac{D_L \times k_f}{(d \times k_b) \times e^{-\lambda t} \times (1 - e^{-k_b t})} \qquad 2\text{-}39$$

Note that ^{131}I estimations requires D_C for river modeling, D_C and D_L with (T_W and K in Equation 2-38 which can be calculated by using Equation 2-18 and 2-23 respectively) for open lake, and only D_L for closed lake. Other parameters are empirically determined constants as shown in Table 2-5.

Table 2-5 Empirically determined parameters for AQUASCOPE for prediction of radiocaesium in freshwater and fish.

Parameter	Value	Resource and note
k_1	18 y^{-1}	Ursula et al. (1987), Schoer (1988), Voitsekhovitch et al. (1991) and Monte (1995)
k_2	0.41 y^{-1}	Smith et al. (2000; 1998a; 2000)
k_3	0.02 y^{-1}	Smith et al. (2000; 1998a; 2000)
α	0.3 m^{-1}	Helton et al.(1985) and Smith et al. (2005)
β_1	0.003 m^{-1}	Hilton et al. (1993) Smith et al. (1998)
β_2	0.05 m^{-1}	Hilton et al. (1993) Smith et al. (1998)
γ_1	0.0002 m^{-1}	Hilton et al. (1993) Smith et al. (1998)
γ_2	0.007 m^{-1}	Hilton et al. (1993) Smith et al. (1998)
η_1	0.04 m^{-1}	Smith et al. (2005)
η_2	0.0085 m^{-1}	Smith et al. (2005)
$Y_{predatory\ fish}$	492 µmol m^3/kg	Smith et al. (2000)
$Y_{non\text{-}predatory\ fish}$	61.3 µmol m^3/kg	Smith et al. (2000)
$k_{b_{predatory\ fish}}$	0.511 y^{-1}	Smith et al. (2000)
$k_{b_{non-predatory\ fish}}$	8.4 y^{-1}	Smith et al. (2000)

Table 2-6 Emperically determined parameters for AQUASCOPE for prediction ^{131}I in freshwater and fish.

Parameter	Value	Resource and note
k_1	8.5 y^{-1}	Monte (1995)
k_2	0 y^{-1}	no fixation
k_3	0 y^{-1}	short half-life
α	1.0 m^{-1}	Smith (2005)
β	0 m^{-1}	no fixation
γ	0 m^{-1}	short half-life
k_f	0.593 m^3/kg	Smith (2005)
k_b	14.8 y^{-1}	Smith (2005)

2.6.5 Other models for aquatic ecosystems

Following the Chernobyl accident, there were a number of studies focusing on contamination of radiocaesium in aquatic ecosystems.

A dynamic model for estimated contamination of radiocaesium in both freshwater and fish was developed by Koulikov and Meili (2003). The change with time of radiocaesium concentration in water and fish were modelled using these assumptions: "*a) potassium acts as a biogeochemical equivalent of caesium; b) the concentration of potassium in fish and other biota is rather constant; and c) the main source of potassium in freshwater fish is the dietary uptake*".

^{137}Cs concentration in water (A_W) decreased as a two-term of exponential function including "fast" and "slow" decrease of radiocaesium which can be determined at *t* time as below

$$A_W = K_W^F e^{-\lambda_F t} + K_W^S e^{-\lambda_S t} \qquad 2\text{-}40$$

Where $K_W^F$and K_W^S are the transfer coefficients of fast and slow decline of radiocaesium in freshwater, and λ_F and λ_S are the rate constants of fast and slow decline process respectively.

In Koulikov and Meili's model, estimating ^{137}Cs concentration in fish in member *j* of trophic level (A_j) can be calculated as below

$$A_j = e^{-\lambda_j^{Cs} t} \times \left\{ T_{j-1}^{j} \int A_{j-1} e^{\lambda_j^{Cs} t} dt + \left[A_{j_{(t=0)}} - \left(T_{j-1}^{j} \int A_{j-1} e^{\lambda_j^{Cs} t} dt \right)_{(t=0)} \right] \right\} \qquad 2\text{-}41$$

Where $\lambda_j^{Cs}$the empirical is rate constant of radiocaesium in fish at level *j* of food change, and A_{j-1} is radioactivity concentration of radiocaesium in fish at previous level (*j-1*). $T_{j-1}^{j}$is a complex transfer coefficient between level *j* and *j-1* which can be calculated by using the empirical is rate constant of radiocaesium $\left(\lambda_j^{Cs}\right)$ and potassium $\left(\lambda_j^{K}\right)$ in fish at level *j*, the assimilation efficiencies of radiocaesium $\left(\alpha_j^{Cs}\right)$ and potassium $\left(\alpha_j^{K}\right)$, and potassium concentration (C_j and C_{j-1}) in fish at *j* and *j-1* level of food change in equation below

$$T_{j-1}^{j} = \lambda_j^K \times \frac{\alpha_j^{Cs}}{\alpha_j^K} \times \frac{C_j}{C_{j-1}} \qquad 2\text{-}42$$

Similarly to AQUASCOPE, Koulikov and Meili also found that the uptake of radiocaesium in fish was different between predatory and non-predatory fish, and the level of ^{137}Cs contamination depended on potassium concentration in freshwater. [Note that no values of these parameters were given in this study].

Sundbom and co-workers (2003) studied the contamination of ^{137}Cs in fish at three lakes in Sweden namely Ekholmssjön, Flatsjön and Siggeforasjön, the model focused on long-term concentration by using contamination in fish during initial period of deposition to these lakes. The change with time of concentration of ^{137}Cs (Bq kg^{-1} fresh weight, Cs_{fish}) in fish can be determined as below

$$Cs_{fish} = A(Cs_{max} - Cs_{base})\left(e^{\frac{Bt}{t_{max}}} - e^{\frac{Ct}{t_{max}}}\right) + Cs_{base}e^{-\lambda t} \qquad 2\text{-}43$$

Where Cs_{max} (Bq kg^{-1}) is the maximum activity concentration after the time of first deposition into the lake until concentration reach to maximum peak (day, t_{max}) and Cs_{base} (Bq kg^{-1}) is the near steady-state level of ^{137}Cs (slow decline during long-term period). Figure 2-4 shows these key parameters for modelling the change with time of the concentration of ^{137}Cs in pike from Flatsjön Lake in Sweden where Cs_{max} = 10.5×10^3 Bq kg^{-1}, t_{max} = 690 days and Cs_{base} = 2.8×10^3 Bq kg^{-1}.

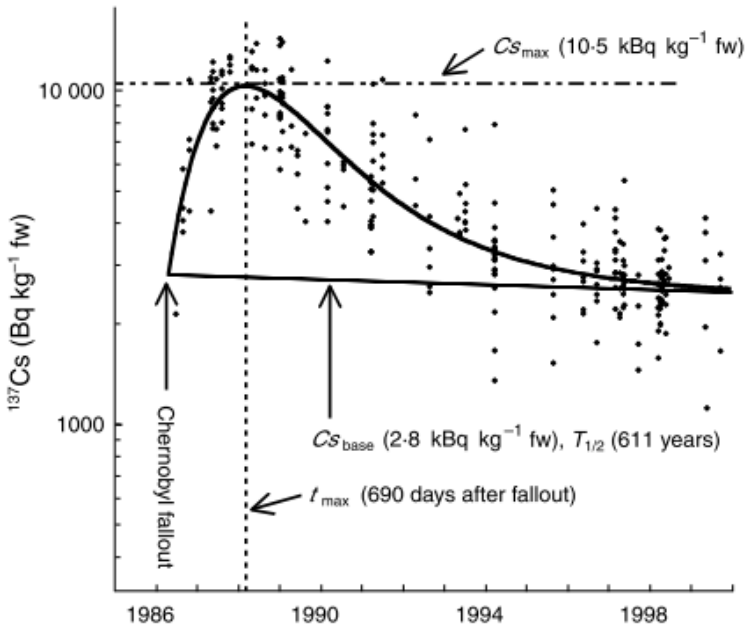

Figure 2-4 Illustration of key parameters for modelling the change with time of the concentration of ^{137}Cs in pike from Flatsjön Lake in Sweden.

The parameter λ is the empirical long-term decline rate of ^{137}Cs in fish which was 0.015 year^{-1} (ecological half-life = $\frac{0.693}{0.015}$ = 46 years which was similar to physical decay of ^{137}Cs) from a study (Sundbom, Meili, Andersson, Östlund, & Broberg, 2003) of these three lakes during 1986-2000, and *A*, *B* and *C* in Equation 2-40 can be calculated by using

$$A = \frac{R^{\frac{R}{R-1}}}{R-1} \quad \text{2-44}$$

$$B = \frac{lnR}{R-1} \quad \text{2-45}$$

$$C = \frac{R\ lnR}{R-1} \quad \text{2-46}$$

R is the ratio of incline and decline rate of ^{137}Cs in fish before and after a peak of deposition in lake.

Sundbom et al. found that t_{max} increased when size of fish increased and trophic level was higher, Cs_{max} also increased with size but it was highest at the bottom of trophic level, and Cs_{base} did not change with size but increased by factor of 1.8 for an upper level of trophic level.

Another model, Kryshev and Ryabov (2000) estimated radiocaesium in fish at many contaminated freshwater systems contaminated by Chernobyl's fallout. The accumulation of radiocaesium in fish was influenced by age class which describes a specific growth rate, diet and activity of metabolic processes.The total radiocaesium activity in the fish (A. Kryshev & Ryabov, 2000) from a particular age class (Bq, *Y*) at *t* time can be given

$$\frac{dY}{dt} = INTAKE_{rad} - \lambda Y - \varepsilon Y \quad \text{2-47}$$

Where $INTAKE_{rad}$the intake of radiocaesium by the fish is, λ is the radioactive decay constant of ^{137}Cs and ε is the rate of biological elimination of ^{137}Cs from the muscles of the fish. Since $INTAKE_{rad} = X\frac{Q_1^A}{Q_0^A}[\frac{dM}{dt} + \varepsilon_A W]$ ($\frac{Q_1^A}{Q_0^A}$ from Kryshev & Ryabov's

observation = 1.0 for carp and 1.2 for pike-perch) and expressing activity concentration in unit Bq per kg of fish ($y = \frac{Y}{M}$), the activity concentration of ^{137}Cs in each discrete generation of fish can be calculated as below

$$\frac{dy}{dt} = \frac{X}{M}\frac{Q_1^A}{Q_0^A}\left[\frac{dM}{dt} + \varepsilon_A W\right] - \left(\lambda + \varepsilon_A \frac{W}{M} + \frac{1}{M}\frac{dM}{dt}\right) y \qquad 2\text{-}48$$

Where X is the concentration of radionuclide in the food of the fish (Bq/kg), M is the fish weight averaged over a particular age class (kg), Q_1^A and Q_0^A are the concentration of the stable bioelement analogue in the fish and the food of the fish respectively, ε_A is a coefficient of proportionality between the elimination rate of the bioelement, and W is the general rate of metabolism (gram per hour) which can be determined (Ivlev, 1962; Winberg, 1956) as below

$$W = 0.0048 \times \alpha_1 M^{\alpha_2} K_{mov} \beta_0 e^{\beta T} \qquad 2\text{-}49$$

Where α_1 and α_2 are empirical parameter which are 0.467 and 0.8 for carp and 0.116 and 0.83 for pike-perch (A. Kryshev & Ryabov, 2000) respectively, K_{mov} is a correction factor allowing for the fact that the fish spend energy on both internal processes and movement (from Ivlev (1962), K_{mov} = 2), β is a parameter for the temperature dependence of the fish metabolism, β_0 is a normalizing factor selected in such a way that at 20°C and term $\beta_0 e^{\beta T}$ = 1, and T is temperature in °C.

Chapter 3 Isotopic Ratio

3.1 Introduction

The various radionuclides (mainly fission products) released from Fukushima have widely different half-lives and potentially different removal rates from air to soil (see Section 1.3). Therefore, the concentration of each nuclide varies significantly with site and time since release as after Chernobyl (Mück, et al., 2002; 2000), decay-corrected isotope ratios will be used to interpret measurement data in soil and air, and to model external dose rates.

In this research, the variation in isotopic ratios will be used to study the geographical changes in radionuclides released from Fukushima to areas worldwide and particularly in the most contaminated near-zone. The isotopic ratio is a simple method, with no necessity to measure the total amount of all nuclides in an environmental compartment and can be used to evaluate contamination back to the initial period after the accident.

3.2 Methodology

During the weeks following the accident, a large number of measurements of various radioisotopes were made in soil and air at sites in Japan and around the world. The main monitoring programme conducted in Japan only provided continuous measurement of ^{131}I and ^{134,137}Cs in air and a range of sites in the near zone (20-80 km) (MEXT, 2011a, 2011b, 2011c). ^{132}Te/^{132}I and ^{136}Cs are key radioelements for formation of external gamma dose in the early phase (See Section 4.2.2), but relatively few measurements of these nuclides were available in soil. Therefore, determination of accurate ratios of ^{132}Te:^{137}Cs and ^{136}Cs:^{137}Cs, and investigation of variation with distance and direction are essential for evaluating contamination characteristics and early-phase external gamma dose.

Other radionuclides, including ^{95}Nb, ^{99}Mo/^{99m}Tc, ^{110m}Ag, ^{129m}Te/^{129}Te, ^{133}I, ^{140}Ba/^{140}La also had few measurements available (JAEA, 2012; Kanai, 2012; Stoehlker, et al., 2011). These radioisotopes, however, were not found to be significant for formation of the external gamma dose. The available measurements of the key dose forming radionuclides were reviewed and their decay corrected ratios RN:^{137}Cs determined. . Since ^{137}Cs is longest fission product, it persists in contaminated soils for long periods of time and hence can be measured in soil for many years following an accident. By determining ratios of

shorter-lived isotopes in relation to ^{137}Cs, early-phase contamination and external dose can be reconstructed at any site if the ^{137}Cs can be measured. This can in principle be used many years after fallout, though the potential for reduction of measured ^{137}Cs with time via soil erosion and migration needs to be taken into account.

3.2.1 Corrected time

All isotope ratios were corrected back to 14:46 on 11 March 2011 (JST) when all reactors shut down automatically as a result of the earthquake and when the production of fission products had stopped. Although radionuclides were also released from spent fuels in the cooling pond of Reactor 4 (Stohl et al., 2011) and the Japanese authorities have not revealed any information of reactor cores and spent fuels, the stopping time of reactors is the best point for correction if the leaks from reactor cores are to be determined.

3.2.2 Key radionuclides for isotopic ratios

As discussed above, a large number of different radionuclides were released in the accident. To develop a model for the external gamma dose rate it is important to determine which of these made a significant contribution to external dose. Because of their significant gamma emissions and high concentrations in soil, Section 4.2.2 will verify that ^{131}I, ^{132}Te/^{132}I, ^{134}Cs, and ^{137}Cs made a significant contribution and ^{136}Cs could also have potentially contributed to dose in the early phase. In addition, it will be shown that external gamma dose in the initial phase was dominated by contaminated radionuclides in soil, while the gamma radiation emitted from radionuclides in the cloud was much less significant (Section 4.2.4).

3.2.3 Isotope ratios as a function of direction and distance

Following the Chernobyl accident, corrected isotopic ratios of nuclides to ^{137}Cs were a function of direction and distance. A study by Muck et al (2000) showed that the ratios ^{134,136}Cs:^{137}Cs and ^{132}Te:^{137}Cs were consistent with direction and distance, while ^{131}I:^{137}Cs was different in different directions around the near-zone and decreased as distance from NPP increased (Mück, et al., 2000).

Available measured data of key radionuclides in both air and soil from many literature sources and monitoring reports following the Fukushima accident were compiled and analysed in terms of decay-corrected isotopic ratios as a function of direction and distance

from Fukushima. The hypothesis of this research, is that decay corrected ratios of volatile radioisotopes should be similar to those observed after the Chernobyl accident.

In particular, in the near-zone where external gamma dose was significantly high for residents and there were differences in contamination between different directions and distances (MEXT, 2011a, 2014), corrected ratios are useful for reconstruction of gamma dose in the near zone.

Note that distance from the NPSs to sampling points were estimated by using vector distances for area within Japan (<1,200 km) while following the pattern of the worldwide plume dispersion (Section 1.4.3) for larger distances.

3.2.4 Data and statistical methods

At each sampling site, the average value calculated from corrected ratios of all samples (each radionuclide) was represented by the mean value for each site. This decay corrected mean was then used to determined correlations with direction and distance. The reason for using the mean at each site is that, for example, if one site had only one measurement while another had lot of measured data, use of raw data would bias the analysis towards sites with more measurements

If it could be shown that, as after the Chernobyl accident (Muck et al 2002), the corrected ratios of ^{132}Te, ^{134,136}Cs to ^{137}Cs were consistent with direction and distance, then general corrected ratios representing the value of each nuclide independent of direction and distance could be determined by taking the overall mean of all sampling sites. The S.E. (Standard Error) representing the real mean of the population (Altman & Bland, 2005; Nagele, 2003) will be used for uncertainty of the general corrected ratios, while S.D. (Standard Deviation) indicates the level of between-site variability. This variability of site-to-site might vary significantly due to a number of factors including different episodes of depositions, characteristics of the ground such as type, density and radionuclide-absorption of soil, whereas the general corrected ratio represents the real mean from the Fukushima release without the influence of these other parameters.

The measurement data were divided into four groups based on distance from Fukushima I NPSs i.e. near zone around NPSs (<80 km), outside near-zone but still in Japan (80-2,000 km), sites in Pacific Ocean and US territory (2,000-12,000 km) and monitoring

sites in EU (>12,000 km). The corrected ratios of key radionuclides in each group were determined for normality by using Shapiro-Wilk test because the number of sites in each group were lower than 30 samples which is the minimum criteria for best test by the Kolmogorov-Smirnov method (D'agostino, Belanger, & D'Agostino Jr, 1990). The hypothesis of normality in Shapiro-Wilk (Razali & Wah, 2011; Shapiro & Wilk, 1965) or Kolmogorov-Smirnov method (Sheskin, 2003) is rejected if the p-value is below 0.05 (95% of confidence). To determine significant differences, a t-test is a method for comparing two normally distribute groups (Sheskin, 2003) in which the p-value has to be less than 0.05 (Hinton, McMurray, & Brownlow, 2014), and a Mann-Whitney test is used for nonparametric-nonparametric or nonparametric-parametric group comparisons (Hole, 2013) in which the correction ratios from two groups are significantly different if U_A from this method is lower than the critical values (Billiet, 2013). Critical values in the Mann-Whitney test can be found in Critical Value for the Mann-Whitney U-Test (Billiet, 2013) in which the value depends on the number of both samples, the minimums are 5 for large sample group and 3 for smaller.

3.2.5 Field measurements

This research collaborated with the Ukrainian Institute of Hydrometeorology who supplied measurements of radioactivity concentration in air in Ukraine as shown in Table 3-1. Their sampling methods will briefly be described here. The air sampling pump and filter were located at Rivnenska NPP (49°32'51.81"N, 30°50'40.01"E), and activity was measured using a gamma spectrometer. Routine monitoring was performed daily. The contaminated cloud including key nuclides except ^{136}Cs (no measurement) reached this site on 24 March 2011. The very short-lived nuclide ^{132}Te was observed in air at this site for 9 days since first detection; ^{131}I and ^{134}Cs were observed longer until 24 April, after which there was only long-lived ^{137}Cs. This site is approximately 2,264 km from Fukushima I NPSs, and the corrected ratios during one month were 65.4, 24.3 and 1.03 for ^{131}I, ^{132}Te and ^{134}Cs respectively.

Table 3-1 Particulate air sampling measurements and corrected ratios to ^{137}Cs at Rivnenska Nuclear Power Plant in Ukraine conducted by the Ukrainian Institute of Hydrometeorology (the date for corrected ratio is 11/03/2012 14:46)

Mid time of Exposure (UTC time)	Radionuclide activity concentration (Bq/m^3)			
	^{131}I	^{132}Te	^{134}Cs	^{137}Cs
24/03/2011 00:00	3.76E-04	2.21E-05	2.21E-05	2.77E-05
26/03/2011 00:00	6.59E-04	-	2.44E-05	3.25E-05
27/03/2011 00:00	2.27E-04	-	3.67E-05	4.40E-05
28/03/2011 12:00	6.22E-04	3.24E-05	1.08E-05	2.16E-05
30/03/2011 00:00	6.32E-03	1.07E-04	5.37E-04	4.16E-04
31/03/2011 00:00	3.63E-03	6.13E-05	4.56E-04	3.20E-04
01/04/2011 00:00	1.93E-03	-	2.68E-04	2.03E-04
02/04/2011 00:00	1.60E-03	9.75E-05	3.97E-04	3.41E-04
03/04/2011 12:00	4.08E-03	1.02E-04	1.23E-03	1.11E-03
05/04/2011 00:00	2.54E-03	-	5.80E-04	5.12E-04
06/04/2011 00:00	1.52E-03	-	5.30E-04	4.17E-04
07/04/2011 00:47	5.87E-04	-	1.13E-04	1.13E-04
08/04/2011 02:35	2.41E-04	-	3.16E-05	3.80E-05
10/04/2011 00:40	1.34E-04	-	2.23E-05	2.23E-05
11/04/2011 22:37	1.97E-04	-	5.09E-05	6.36E-05
13/04/2011 23:02	1.06E-04	-	2.53E-05	2.07E-05
16/04/2011 23:27	9.80E-05	-	2.00E-05	2.45E-05
20/04/2011 12:15	7.01E-05	-	1.88E-05	2.56E-05
24/04/2011 12:50	4.05E-05	-	1.52E-05	1.35E-05
Mean corrected ratio	6.54E+01	2.43E+01	1.03E+00	1.98E-04
(± 2 S.E.)	1.48E+01	1.57E+01	1.16E-01	1.27E-04

3.2.6 Calculated ratios in the fuel inventory

Ratios in the Fukushima reactor cores and spent fuel pools at the time of the accident can be used to compare with corrected ratio in air and soil to help evaluate the transfer of radioactive isotopes. Since there is a lack of data on the inventory of reactor cores and spent fuel pools, the ratio in reactor cores and spent fuel pools can be estimated by using calculations. Nishihara (2012) used the last information before the accident of inventories of cores of Unit 1-3 (all nuclear fuel assemblies in Unit 4 had been removed to spent fuel pool for preparation of new fuel replacement (Povinec, et al., 2013)) and spent fuel pools of Unit 1-4 , burn-up information, and release amount in environment to calculate the amounts of radioactive nuclides present in Fukushima I NPSs. The ratios of key radionuclides to ^{137}Cs from Nishihara's calculation are shown in Table 3-2.

Table 3-2 The calculation of the radionuclide inventory in the reactor cores and spent fuel pools (Kenji Nishihara et al., 2012).

Inventory	Ratio to ^{137}Cs			
	^{131}I	^{132}Te	^{134}Cs	^{136}Cs
Unit 1				
Core	6.65	9.65	0.94	0.27
Spent fuel pool	1.02E-13	-	0.53	1.03E-09
Unit 2				
Core	9.15	13.15	1.08	0.31
Spent fuel pool	2.78E-07	4.39E-17	0.65	7.59E-06
Unit 3				
Core	9.63	13.96	1.04	0.34
Spent fuel pool	2.21E-10	-	0.74	1.13E-07
Unit 4				
Core	-	-	-	-
Spent fuel pool	5.21E-04	1.44E-09	0.68	7.30E-04
Mean ratio in core	8.48	12.25	1.02	0.31
Mean ratio in spent fuel pool	1.30E-04	7.18E-10	0.65	1.84E-04

From Nishihara's calculation, the total amount in all Units of short-lived nuclides ^{131}I, ^{132}Te and ^{136}Cs in spent fuel pools (total amount of each nuclide: 4.61×10^{14}, 1.27×10^{9}, 6.49×10^{14} Bq) were remarkably lower than the total amount in reactors cores (6.02×10^{18}, 8.68×10^{18}, 7.19×10^{17} Bq) due to the decrease by physical decay. The estimated total amount of all reactor cores and all spent fuel pools were 7.04×10^{17} and 1.89×10^{18} Bq respectively for ^{137}Cs and 7.19×10^{17} and 1.27×10^{18} Bq for ^{134}Cs so that it can be concluded that the major amount of ^{131}I, ^{132}Te and ^{136}Cs were from the reactor cores as the amount of these nuclides in spent fuel pools was significantly lower than in reactor cores by magnitudes of four, nine and two respectively. For ^{134}Cs, the decayed amount in spent fuel pools still was around half of ^{137}Cs and total amount was more than in all reactor cores, the ratio ^{134}Cs:^{137}Cs should be from total amount from reactor cores and spent fuel pools of both nuclides which given ratio = 0.77. Therefore, ratio of ^{134}Cs: ^{137}Cs from environmental samples will identify whether the major release of ^{134}Cs was from reactor cores, spent fuel pools or both. In addition, ^{134}Cs is from neutron activation of ^{133}Cs while ^{137}Cs is produced by fission, the behaviour of both nuclides in environment is the same

as the stable element, the activity ratio of ^{134}Cs: ^{137}Cs in reactor from both productions is proportional to integrated neutron flux or therefore to the burnup (Doyle, 2011) and ^{134}Cs: ^{137}Cs ratio is dependent on the value of burnup (Choppin, Liljenzin, & Rydberg, 2002; T. Endo, Sato, & Yamamoto, 2011; Povinec, et al., 2013; Sengupta, 2014).

3.3 Results

3.3.1 Corrected ratios of particulates in air

After the Fukushima accident, continuous monitoring of air was established in the near-field zone (within 80 km) by the Japanese Ministry of Education, Culture, Sports, Science and Technology (MEXT). This monitoring mainly measured particulate radioactivity in air, and concentrated on high concentration radionuclides ^{131}I and ^{134,137}Cs, while ^{132}Te and ^{136}Cs were not measured (MEXT, 2011a). Moreover, most sites started measurements after 20 March, 9 days after the earthquake or 5 days after the time of highest deposition (Kinoshita, et al., 2011) so that ^{131}I:^{137}Cs are not considered because short half-life 8.02 days of ^{131}I resulting the significant decreasing amount by physical decay.

The decrease of radionuclide activity concentration in air was not monotonic: activity concentrations varied depending on weather conditions, wind speed and direction, and precipitation are extremely impact factors in determining activity concentrations, as well as variation in releases from the NPP. Following the Chernobyl accident, around 70% of ^{131}I release was ins gaseous form (Cambray, et al., 1987; Clark & Smith, 1988; Mück, et al., 2002; Spezzano & Giacomelli, 1991) which is similar to the results of JAEA measurements for the Fukushima accident (JAEA, 2012). The deposited velocity of gaseous ^{131}I is higher than ^{137}Cs in dry conditions and lower in wet conditions, while ^{134,136}Cs has same deposited velocity with ^{137}Cs as both are the same elements (F. B. Smith & Clark, 1989). Monitoring of ^{131}I started at 9 days after earthquake which does not properly represent ^{131}I from the initial release because this was not only ^{131}I released from the NPSs in the first plumes (NW plume) but also included ^{131}I released continuously from NPSs with different rates of release after the first plumes. The consequence is that the late starting of this monitoring might influence the calculation of corrected ratio of ^{131}I:^{137}Cs ratio in the near-zone so this is not appropriate for comparison with the ratio at larger distances. So it is important to avoid interference of the different releases of ^{131}I: the details of this are discussed in Section 3.3.6. It is important to note

that ^{131}I data at all larger distances included ^{131}I from both plumes, thus these can be used ^{131}I to determine the corrected ratio. Therefore, only the corrected ratios of ^{134}Cs:^{137}Cs from this monitoring (near-zone) to compare with larger distances.

As shown in Figure 3.1, ratio of ^{134}Cs:^{137}Cs (particulate) in air was constant with distance and also with direction, having mean 1.03 (± S.E. 0.05) based on 68 samples and 17 sites. The ^{131}I: ^{137}Cs ratio varied significantly with distance and direction (Figure 3-2) with mean 31.80 (± S.E. 6.43) from 90 samples and 22 sites. The ratio in the South tended to be higher than in other directions, in agreement with the map of deposited ratios by Kinoshita and co-workers (2011) in Figure 2-1. The details of mean ratios of ^{134}Cs and ^{131}I to ^{137}Cs of all air sample sites within the near-zone are shown in Table B-1, Appendix B.

Outside the near-zone in Japan, there were fewer monitoring sites for airborne radioactivity. Five sites to the southwest and south of Fukushima I NPS (discussed in section 1.4.2 above: JAEA at Ibaraki prefecture (JAEA, 2012), Waku Institute at Saitama prefecture (RIKEN, 2011), CTBT at Gunma prefecture (Stoehlker, et al., 2011), JCAC at Chiba prefecture (Amano, et al., 2012)) were at distances of approximately 100-200 km. Another relevant measurement site for ^{134}Cs and ^{131}I to ^{137}Cs (particulates) in air was Kyushu University, Fukuoka prefecture (Momoshima, et al., 2012) located about 1,100 km to the southwest. All of these sites were in the passage of both significant plumes (Kinoshita, et al., 2011). The ratios obtained at these sites are shown in Table 3-3 (data on ratios each site are shown in Table B-2 in Appendix B). The ratio ^{131}I:^{137}Cs (mean = 70.88, S.E. = 31.78, sample = 234 and sites = 5) was higher than that in the near-zone area by factor of two while ^{134}Cs:^{137}Cs (mean = 0.99, S.E. = 0.10, sample = 217 and sites = 5) and ^{132}Te:^{137}Cs (mean = 17.49, S.E. = 1.07, sample = 226 and sites = 5) were still constant with increasing distance (Figure 3-3).

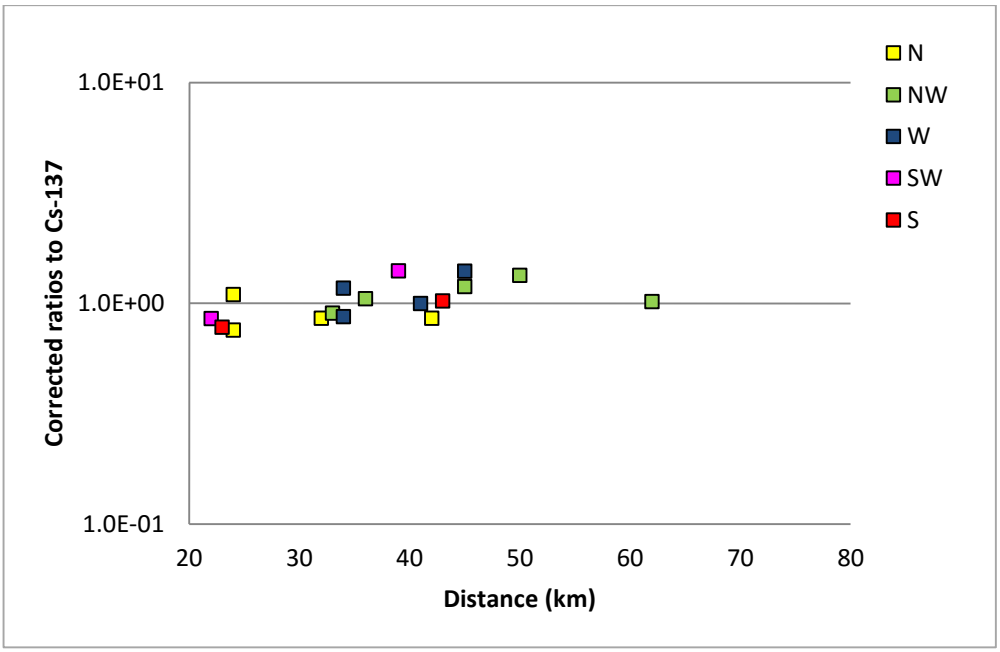

Figure 3-1 Corrected ^{134}Cs:^{137}Cs (both are particulate form) in air in different directions in the "near-zone" of Fukushima I NPSs (>80 km). From data given in MEXT (2011a).

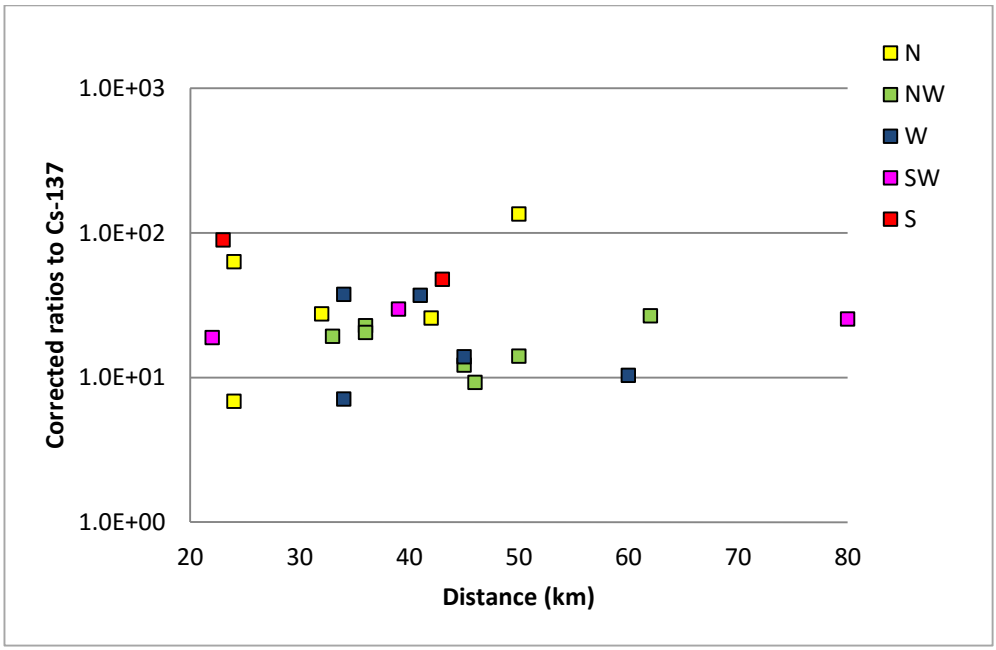

Figure 3-2 Corrected ^{131}I:^{137}Cs (both in particulate form) in air in different directions in the "near-zone" of Fukushima I NPSs (>80 km). From data given in MEXT (2011a).

In the Pacific Ocean and the United States territories, numerous sites (Appendix C-2) were measured for atmospheric radionuclides (Leon et al. (2011), UCB (2011), MacMullin et al. (2012), EPA (2011) and Biegalski et al. (2011)). Table 3-3 and Figure 3-4 illustrate the values and relevant of ratios at longer distances (2,000 to 12,000 km). Comparing these ratios with ratios in Japan, it clear that the corrected ratio of ^{134,136}Cs and ^{132}Te to ^{137}Cs were consistent with distance (mean = 0.99, 0.19 and 17.49 for ^{134,136}Cs and ^{132}Te: ^{137}Cs respectively). ^{131}I:^{137}Cs was similar to the ratio in Japan outside the near-zone, but the mean was much more uncertain than for other nuclides, S.E. = 13.46, 0.03, 0.02 and 2.10 for corrected ratio of ^{131}I, ^{134,136}Cs and ^{132}Te to ^{137}Cs respectively.

In Europe, there were a large number of sites monitoring ambient radioactivity: Pinero et al. (2012), Perrot et al. (2012), Loaiza et al. (2012), Pham et al. (2012), Bossew et al. (2012), Carvalho et al. (2012), HPA (2011), Gudelis et al. (2012) and Chaisan et al. (2013) [196 samples and 22 sites in 10 countries as shown in detail in Table B-2 in Appendix B]. From Figure 3-5 and Table 3-3 it is seen that ^{134}Cs:^{137}Cs and ^{136}Cs:^{137}Cs were relatively constant with distance in Europe. For ^{134}Cs:^{137}Cs, average ratio was 0.91 (with S.E. 0.03) while 0.19 (SE 0.02) was the ratio for ^{136}Cs:^{137}Cs. In the case of ^{132}Te:^{137}Cs, the ratio was 22.01 with a relatively high S.E. of 3.02. Similar to other areas, there was high variability in the ratio of ^{131}I to ^{137}Cs (mean = 77.12 and S.E. = 8.30).

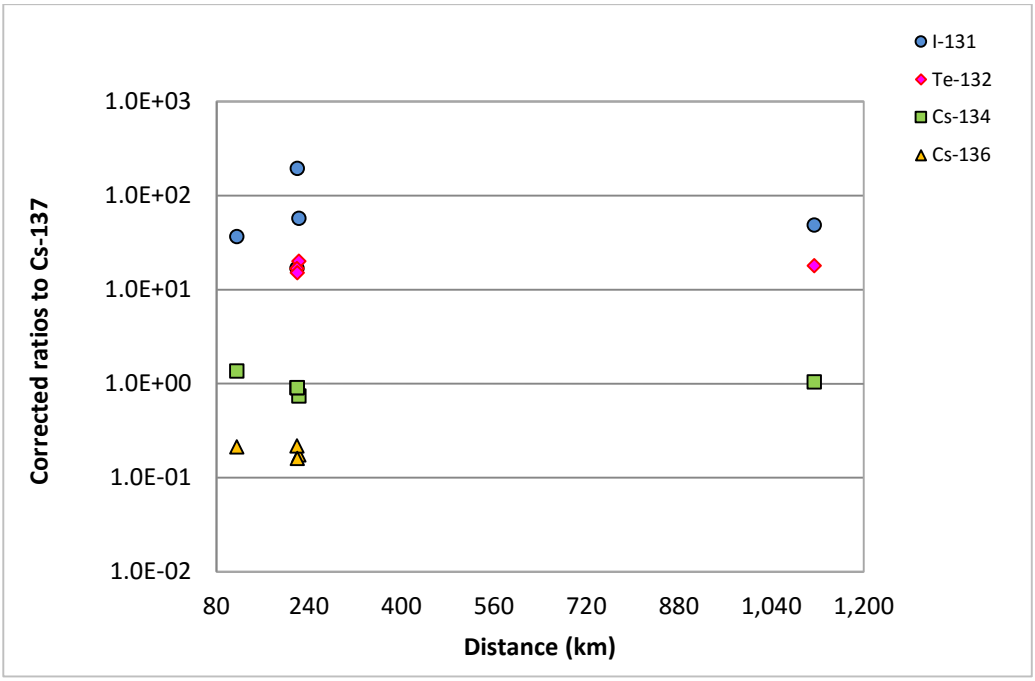

Figure 3-3 Illustration of the ambient particulate ratios (corrected for decay) of ^{134,136}Cs, ^{131}I and ^{132}Te to ^{137}Cs in "outside near-zone" of Fukushima I NPSs (>80 km to 1,200 km).

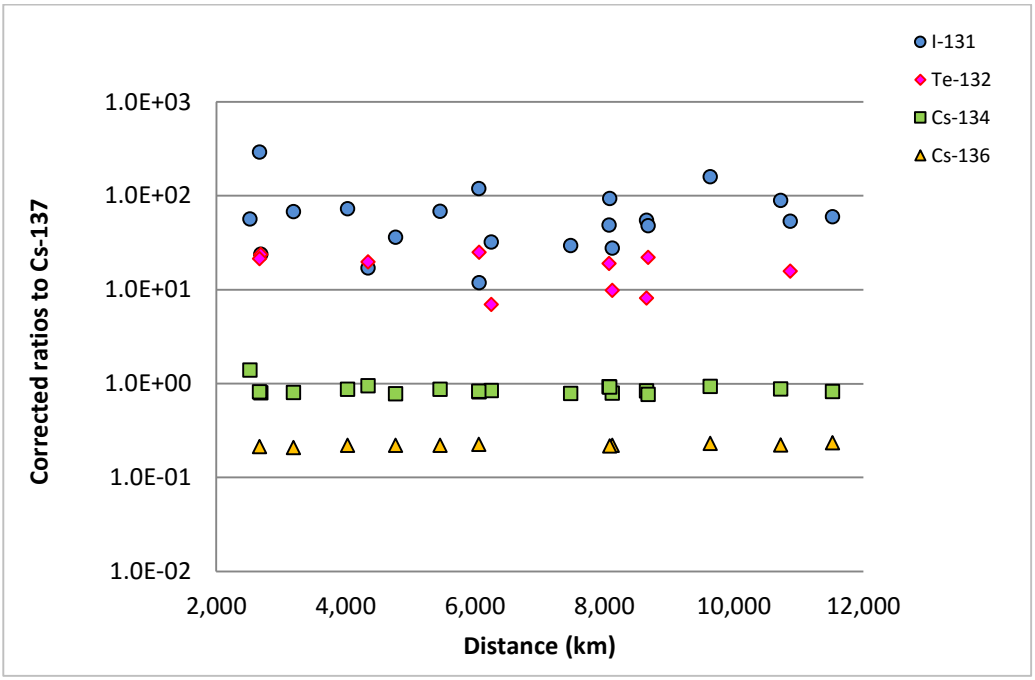

Figure 3-4 Illustration of the ambient particulate corrected ratio of ^{134,136}Cs, ^{131}I and ^{132}Te to ^{137}Cs in Pacific Ocean and United state (1,200 to 12,000 km).

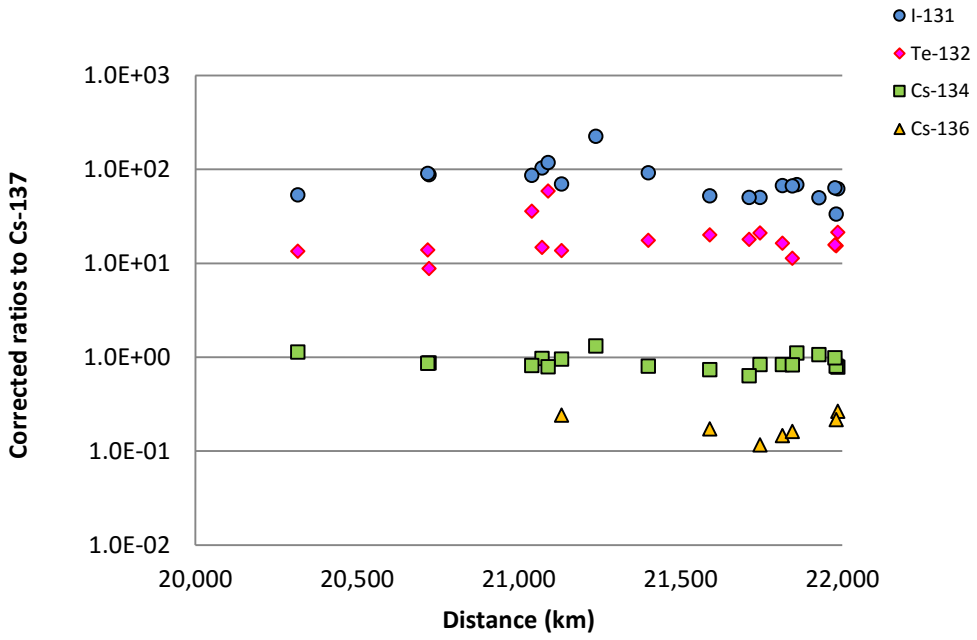

Figure 3-5 Illustration of the ambient particulate corrected ratio of ^{134,136}Cs, ^{131}I and ^{132}Te to ^{137}Cs in Europe (>20,000 km).

Table 3-3 Average corrected mean ratios to ^{137}Cs from release of Fukushima (± S.E., based on variation of means between sites).

Radioisotope	Soil samples in near-zone (<80 km)	Air samples in near-zone (<80 km) Particulate	Air samples in Japan (80-2,000 km) Particulate	Air samples in Pacific Ocean and US (2,000-12,000 km) Particulate	Air samples in EU (>20,000 km) Particulate
^{131}I	22.1±1.8 Sites = 144 Samples = 1,794	31.80±6.43 * Sites = 22 Samples = 90	70.88±31.76 Sites = 5 Samples = 234	69.5±13.46 Sites = 20 Samples = 457	77.12±8.30 Sites = 22 Samples = 196
^{132}Te	18.3±0.9 Sites = 20 Samples = 20	No data	17.49±1.07 Sites = 4 Samples = 226	17.13±2.10 Sites = 21 Samples = 455	22.01±3.02 Sites = 22 Samples = 196
^{134}Cs	0.90±0.01 Sites = 146 Samples = 1,817	1.03±0.05 Sites = 17 Samples = 68	0.99±0.10 Sites = 5 Samples = 217	0.87±0.03 Sites = 20 Samples = 420	0.91±0.03 Sites = 22 Samples = 193
^{136}Cs	0.23±0.01 Sites = 88 Samples = 283	No data	0.19±0.01 Sites = 4 Samples = 105	0.22±0.002 Sites = 11 Samples = 184	0.19±0.02 Sites = 9 Samples = 27

* Note that these measurements began 4-5 days after the passage of the initial plumes so, because the ^{131}I:^{137}Cs ratio varied with release time, cannot be directly compared with other data and are not included in Figure 3-6.

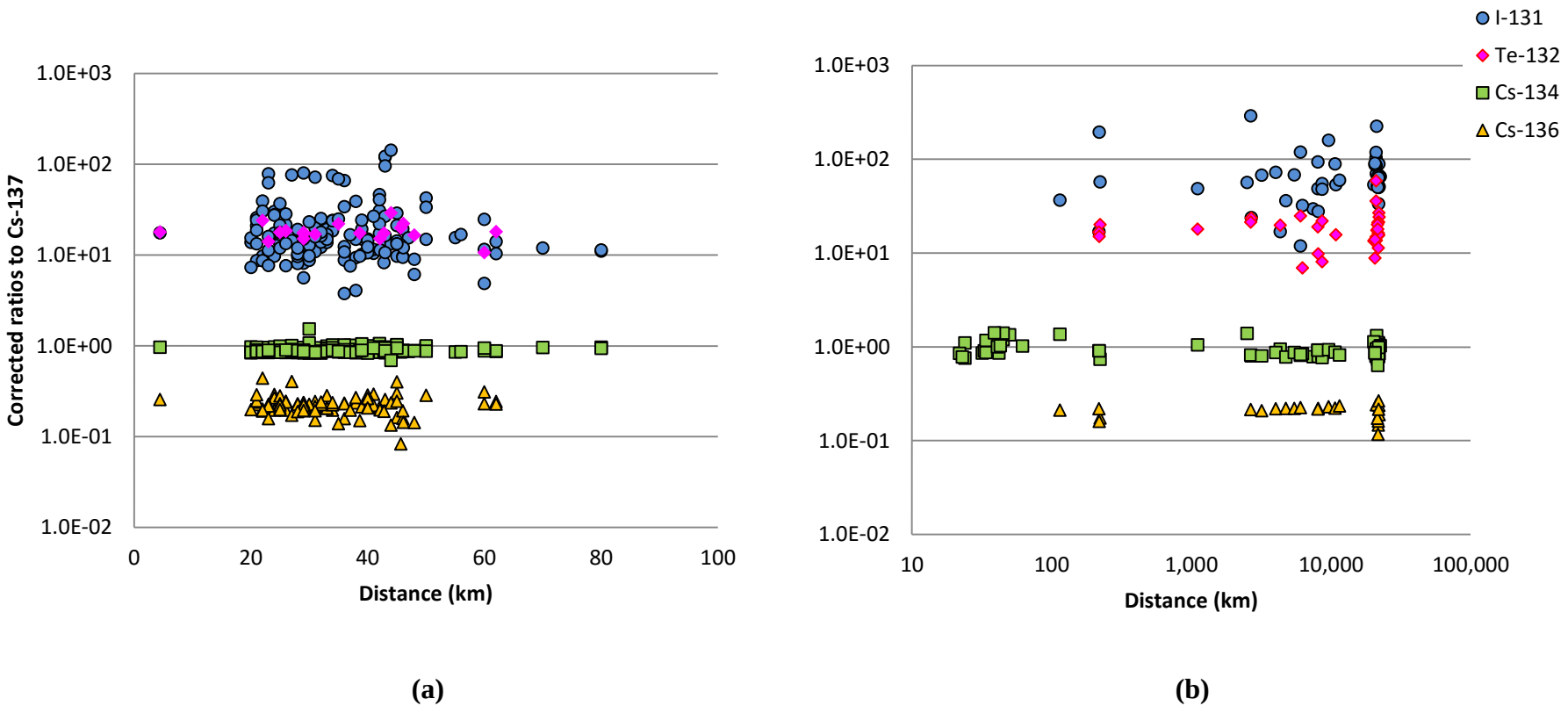

Figure 3-6 Average corrected ratios to ^{137}Cs of ^{131}I, $^{134, 136}$Cs and ^{132}Te in (a) soils and (b) air particulates. Many of the ^{131}I measurements in air taken in the vicinity of Fukushima I NPSs were excluded from (b) as sampling did not begin until some days after the radionuclide release.

The statistical analysis of corrected isotope ratios in air at different distances from Fukushima is shown in Table 3-4. All ratios of key radionuclides were tested for normality by the Shapiro-Wilk test for low sample numbers (N<30), then the change of ratio with increasing distance was investigated by a t-test for ratios between both normal distributions, and using the Mann-Whitney test between both non-normal distribution or between normal and non-normal distribution. The results show that the ratio ^{134}Cs:^{137}Cs was relatively constant with distance, but the ratio in the near zone is likely slightly higher than at further distances. Means of particulate ^{134}Cs:^{137}Cs were normally distributed for the near-zone, in Japan outside near-zone and EU while mean of Pacific Ocean and US was nonparametric. Statistical methods and results to test different ^{134}Cs:^{137}Cs ratio between two groups are presented in Table 3-3 which shows that there is only a significantly different ratio between near-zone area and EU (by t-test between both parametric distributions) while there was no difference between other groups. Therefore, ambient ^{134}Cs:^{137}Cs ratios show low variability and are relatively constant with distance with only a slight difference between near-zone and EU.

For the ratio ^{136}Cs:^{137}Cs (in Table 3-4), there were no measurements in the near zone. Ratios were parametric for the Japan area outside the near-zone and EU and only nonparametric for Pacific Ocean and US Ratios of ^{136}Cs:^{137}Cs were consistent at all distance from the NPSs. The mean ^{132}Te:^{137}Cs ratio in Japan outside the near zone, Pacific Ocean and US were normally distributed and relatively consistent with distance, but the mean in Europe was non-normally distributed and slightly higher. However, using the Mann-Whitney test for low sample numbers and non-normal distribution of the ratios between Pacific Ocean and US and Europe, it is found that there was no significant difference (U_A: 87 > the critical values: 52 at 5% for level of significance for N = 10 and 19)

In contrast, ^{131}I:^{137}Cs ratios in air are significantly more variable, and all means of this ratio at all distances from Fukushima are non-normally distributed. The average ratios are much higher than other nuclides. The ratio in the near-zone was significantly lower than at longer distances, though these data must be interpreted with caution since significant air monitoring in the Fukushima area only began 4-5 days after passage of the initial contamination plumes. Thus much of the local (< 80 km) ^{131}I/^{137}Cs air monitoring data are not shown in Figure 3-6 (b). The ratios in Japan outside the near-zone, Pacific Ocean

and US, and Europe were not significantly different from each other. As shown in Table 3-3, the mean ^{131}I:^{137}Cs ratio in Europe was higher than in the Pacific Ocean, but, like the ^{132}Te:^{137}Cs ratio, not significantly different between the two areas (Mann-Whitney U-test U_A: 168 > the critical values: 150 at 5% for level).

Table 3-4 Method and result for testing the significance of differences of ^{131}I, ^{132}Te and ^{134,136}Cs/^{137}Cs in air between groups at different distances from the NPSs.

Site	Nomality*	p-value$^{\Omega}$ for normality test	Test method^{a} / p-value$^{\theta}$ or U_A^{Δ} comparing with the critical values / result of difference^{+}			
			Near-zone	Outside near-zone	Pacific Ocean and US	EU
$\underline{^{131}I/^{137}Cs}$						
Near-zone	normal	0.000	-	MW / 83>23 / no	MW / 365>150 / no	MW / 435>158 / no
In Japan outside near-zone	n-normal	0.033	-	-	MW / 48>22 / no	MW / 30>23 / no
Pacific Ocean and US	n-normal	0.000	-	-	-	MW / 168>150 / no
EU	n-normal	0.000	-	-	-	-
$\underline{^{132}Te/^{137}Cs}$			-			
Near-zone	-	-	-	-	-	-
In Japan outside near-zone	normal	0.982	-	-	T / 0.920 / no	MW / 38>13 / no
Pacific Ocean and US	normal	0.167	-	-	-	MW / 87>52 / no
EU	n-normal	0.000	-	-	-	-

Table 3-4 (continued) Method and results for testing the significance of differences of ^{131}I, ^{132}Te and $^{134,136}Cs/^{137}Cs$ in air between groups from different distances from the NPSs.

Site	Normality *	p-value$^{\Omega}$ for normality test	Test method[a] / p-value$^{\theta}$ or U_A^{Δ} comparing with the critical values / result of difference^{+}			
			Near-zone	Outside near-zone	Pacific Ocean and US	EU
$^{134}Cs/^{137}Cs$						
Near-zone	normal	0.148	-	T / 0.699 / no	MW / 258>10 / no	T / 0.006 / yes
In Japan outside near-zone	normal	0.556	-	-	MW / 68>20 / no	T / 0.128 / no
Pacific Ocean and US	n-normal	0.000	-	-	-	MW / 178>141 / no
EU	normal	0.180	-	-	-	-
$^{136}Cs/^{137}Cs$						
Near-zone	-		-	-	-	-
In Japan outside near-zone	normal	0.348	-	-	MW / 6.5>6 / no	T / 8.41 / no
Pacific Ocean and US	n-normal	0.008	-	-	-	MW / 38.5>23 / no
EU	normal	0.819	-	-	-	-

Note that: *For normality: "normal" is parametric distribution and "n-normal" is nonparametric distribution.

$^{\Omega}$For Shapiro-Wilk test, ratio is normal distribution if p-value > 0.05 (Razali & Wah, 2011; Shapiro & Wilk, 1965).

[a]Method: T is t-test and MW is Mann-Whitney test.

$^{\theta}$For t- test, p-value is lower than 0.05 means there is significantly difference between two group (Hinton, et al., 2014).

$^{\Delta}$For Mann-Whitney test, U_A is lower than the critical values (at 5% for level of significance) means there is significantly difference between two group (Billiet, 2013; Hole, 2013).

$^{+}$Result from t-test or Mann-Whitney test: "yes" is for significantly different and "no" is for no difference between two groups.

3.3.2 Particulate and gaseous ^{131}I in air

Measurement of both gaseous and particulate phases of ^{131}I in Japan in the early stages of the accident (15/16 March) was only available at one site: JAEA (2012) at Tokai-mura, Ibaraki prefecture (115 km in South direction). Measurements from other sites worldwide began later, but due to longer travel times, captured the peak air concentrations from the early stages of the accident. Figure 3-7 shows the available mean ^{131}I:^{137}Cs ratios of both gaseous and particulate phase ^{131}I as a function of distance.

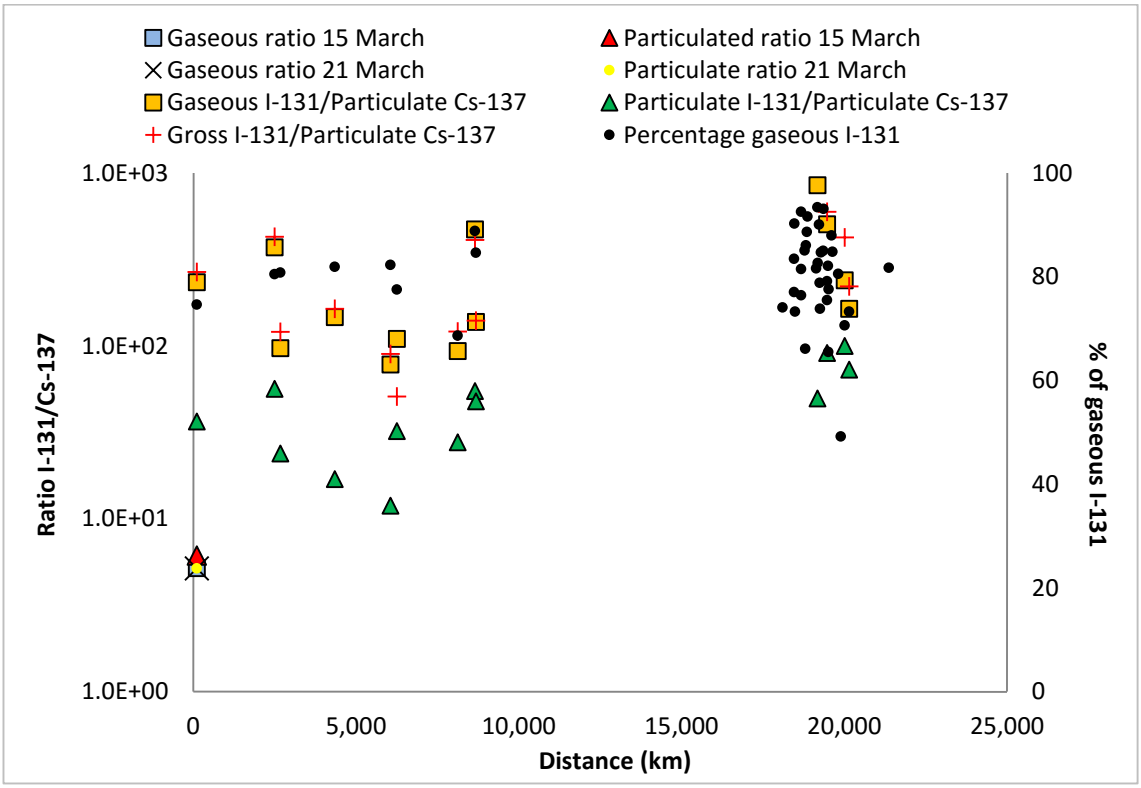

Figure 3-7 Ratios of particulate and gaseous ^{131}I to particulate ^{137}Cs with distance from Fukushima I NPSs. At two sites 120 and 160 km to the south of the accident site, lower ^{131}I:^{137}Cs ratios were observed in both phases on 15 March and 21 March 2011.

Data from the JAEA site measured on 15 March and 21 March (significant peak release periods) suggests lower ^{131}I:^{137}Cs ratios in both particulate and gaseous phases at this time, as shown in Figure 3-7. The ratio of particulate ^{131}I:particulate ^{137}Cs were 6.10 and 5.98 for 15 and 21 March, and 5.18 and 5.16 for gaseous ^{131}I:particulate ^{137}Cs. These values were similar to the reconstruction of ratios of these isotopes in the reactor cores of Units 1-3 which were 6.65, 9.15 and 9.63 (mean = 8.48) respectively (K. Nishihara, et al., 2012) as shown in Table 3-2.

The relatively low ^{131}I:^{137}Cs isotope ratios observed in the areas of high fallout and in the 15 and 21 March air monitoring data in Japan are not observed in the measurements in other countries. The ^{131}I:^{137}Cs ratios in both phases at longer distances were much higher, even in the peak corresponding to the early (12-15 March) releases from Fukushima. Mean values were 73.1 (N = 48 range 12-290) for ^{131}I:^{137}Cs particulate, 269 (N = 13 range 78-853) for the ratio of gaseous ^{131}I to particulate ^{137}Cs, and 253 .12 for gross ^{131}I to particulate ^{137}Cs (N = 12 range 50.91-597.15) (particulate ^{131}I to particulate ^{137}Cs ratios are shown in Table B-2 and B-3, and gaseous ^{131}I to particulate ^{137}Cs and gross ^{131}I to particulate ^{137}Cs are shown in Table B-3).

There is no evidence of a significant change in ^{131}I:^{137}Cs ratio with distance in either particulate, gaseous or total phases. This appears to be in contrast to observations following the Chernobyl accident (Mück, et al., 2002) which showed generally *decreasing* of ratio of gross ^{131}I to particulate ^{137}Cs with distance due to greater dry deposition of gaseous. After Fukushima, the mean of gross ^{131}I to particulate ^{137}Cs in the Pacific Ocean was 190.77 (N = 20 range 50.92-428.16) and distribution was nonparametric (p=0.16) and mean in the EU was 414.45 (N = 3 range 220.93-597.15) and it was normally distributed (p=0.905)> There was no significant different at distances between 12,000-20,000 km using Mann-Whitney test (UA = 12 > critical value = 2). So the data appear to show contrasting behaviour of radioiodine transport between the Fukushima and Chernobyl accidents. It is possible that this is due to different fallout behaviour, though it should also be noted that the observation of decreasing I:Cs ratio after Chernobyl was based on relatively few data and, in the Chernobyl near-zone, radiocaesium deposition rates may have exceeded ^{131}I due to fallout of larger airborne particulates including fuel particles (J. T. Smith & Beresford, 2005a).

Mean fractions of gaseous phase ^{131}I were relatively constant with distance (Table B-3 and Figure 3-7), with mean gaseous fraction 80.4% (S.E. = 1.3 % and range 49.2-93.4%). The consistency of gaseous fractions of ^{131}I over long distances implies relatively little transfer from gaseous to particulate form. As discussed by Masson et al. (2011), "^{131}I [from Fukushima] remains mainly in its gaseous form during transport. Thus, the transfer from gaseous to particulate form, if it exists, was not sufficient within the two-week interval to counterbalance the decrease of particulate ^{131}I due to its deposition, mainly by rain".

3.3.3 Corrected ratios in soil

In a similar way to atmospheric monitoring, MEXT established continuous monitoring of soil and external gamma dose at six sites in the near zone on 18 March. This was then unsystematically extended to a further 50 sites around the near-field zone of Fukushima I NPSs. MEXT also carried out a further survey in which one sample was collected from 71 sites in this area (MEXT, 2011b, 2011c).

Two further studies collected single soil samples for detailed analysis including activity-depth profiles (surface deposition) from each site. Endo and co-workers (2012) measured 15 soil samples on 15 March when deposited concentration reached a peak. In another study, Imanaka et al. (2012) collected 5 samples in the most contaminated area to the northwest between 38 and 46 km on 31 March 2011, 16 days after highest deposition point. All details of the soil measurements are s shown in Table B-4 in Appendix B.

The measurements of radionuclides in soil were analysed by investigating relationships between decay corrected isotope ratios and distance and direction from Fukushima. As shown in Table 3-4, Figure 3-8 and 3-11, ratios of the same element ^{134}Cs: ^{137}Cs was constant with distance. The distribution of this ratio within the near-zone (Figure 3.11) and the constant trend with direction (Figure 3.13) demonstrate that, as with atmospheric data, the ^{134}Cs: ^{137}Cs ratio deposited in soil did not vary significantly with distance or direction. From Table 3-3, average of ratio was 0.90 with 0.01 for S.E. from 146 sites and 1,866 samples. Since N>30, normality can be tested by Shapiro-Wilk or Kolmogorov-Smirnov method and both tests show an insignificant probability of normality (p=0.00 for both). For ^{136}Cs: ^{137}Cs, there was a lack of measured data in the north, southwest and south as shown by the few data in these directions in Figure 3-12. However, the ratio tended to be consistent with distance as shown in all directions from the NPSs in Figure 3-13. As with the atmospheric data and in the previous study of Chernobyl (Mück, et al., 2002), it can be concluded that ^{136}Cs: ^{137}Cs was consistent with distance and direction. The mean of ^{136}Cs: ^{137}Cs (Table 3-4) was 0.23 and 0.01 for S.E. from 88 sites and 297 samples around the near-zone of NPSs. From Shapiro-Wilk and Kolmogorov-Smirnov test, mean of these measured data is also not normally distributed: p=0.00 for both tests.

Measured data of ^{132}Te in soil was available for 18 sites in the high contamination area to the northwest and to the west, southwest and west of Fukushima (Figure 3-10). In contrast

to the measurements of radiocaesium and radioiodine, there was only one sample measured for ^{132}Te at each site. From Figure 3-8 and 3-13, however, it is shown that the mean corrected ratio ^{132}Te:^{137}Cs was also remarkably constant in all directions and distances. The average ratio of ^{132}Te:^{137}Cs was 18.3 and S.E. of 1.7, calculated from 20 samples of 20 sites, the normality test can be determined by only Shapiro-Wilk test (N<30) which shows nonparametric distribution for these data (p=0.006).

As with the atmospheric data, the ^{131}I: ^{137}Cs ratio in soils was much more variable with distance and direction than the primarily particle-bound radionuclides. With regard to direction, it clear that the ratio in the south was much higher than in other directions (Figure 3-8): the mean ratio in the south being 74.72±20.85 a factor of four higher than in other directions ((Table 3-5). There was no significant correlation of ^{131}I: ^{137}Cs ratio with distance in the 20-80 km range (Figure 3-8). It is noted that the ratios ^{131}I:^{137}Cs in soil in the near zone are expected to be more reliable than the air measurements since the latter started sometime after the passage of the main plume, whilst the soil accumulates the deposited radionuclides.

Table 3-5 The corrected ratio of ^{131}I to ^{137}Cs in the near-zone of Fukushima I NPSs.

Direction	Mean	± S.E.	Max.	Min.	No. of samples	No. of sites
N	22.97	7.02	46.17	9.72	240	12
NW	17.00	3.11	119.03	3.76	818	89
W	19.05	3.55	39.12	4.85	413	22
SW	15.25	3.74	30.25	11.01	177	10
S	74.72	20.85	142.39	9.80	196	12

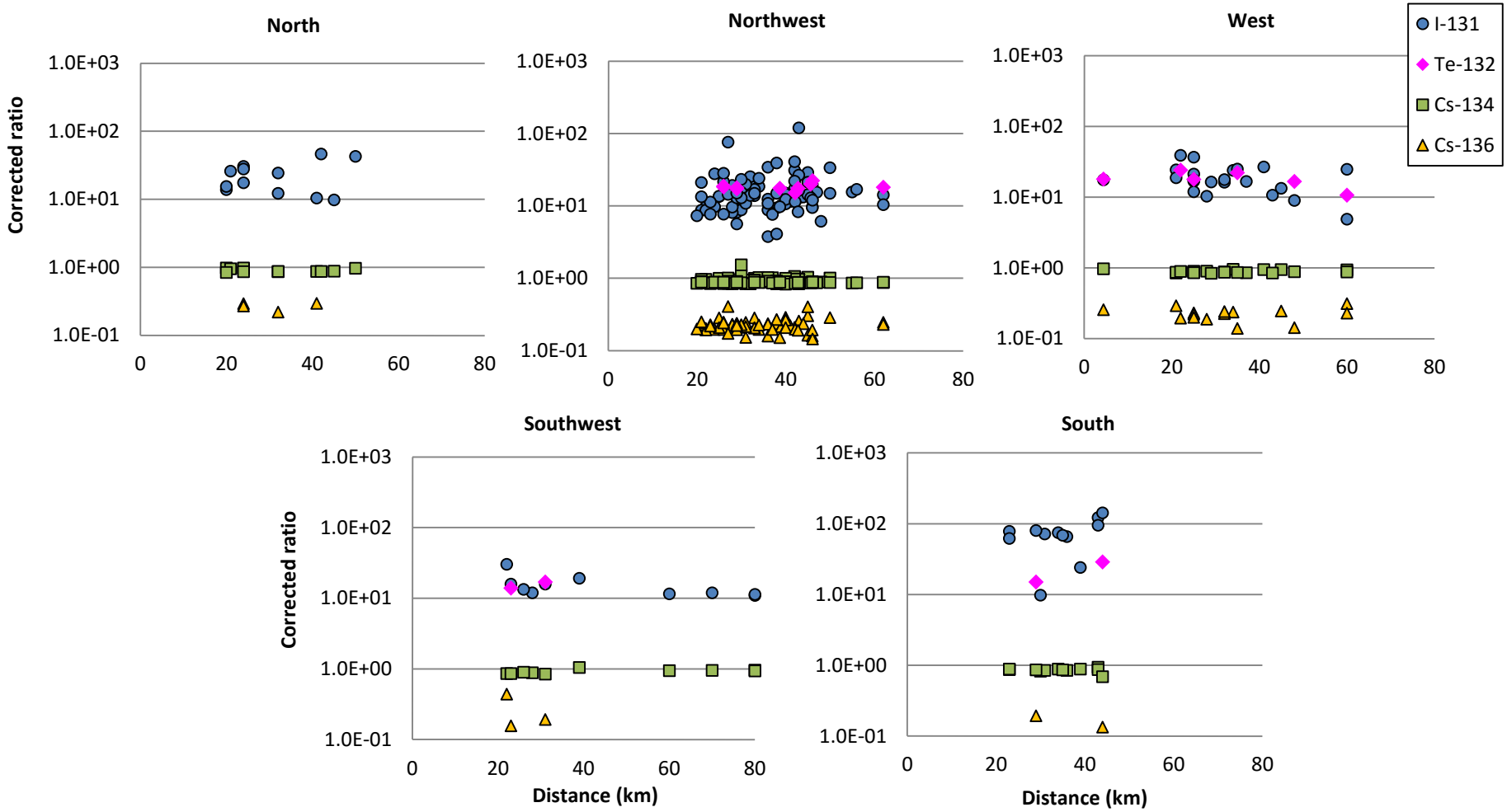

Figure 3-8 The corrected ratios of ^{131}I, ^{132}Te, $^{134,136}Cs$ to ^{137}Cs in soil at near-field zone in each direction of Fukushima I NPSs

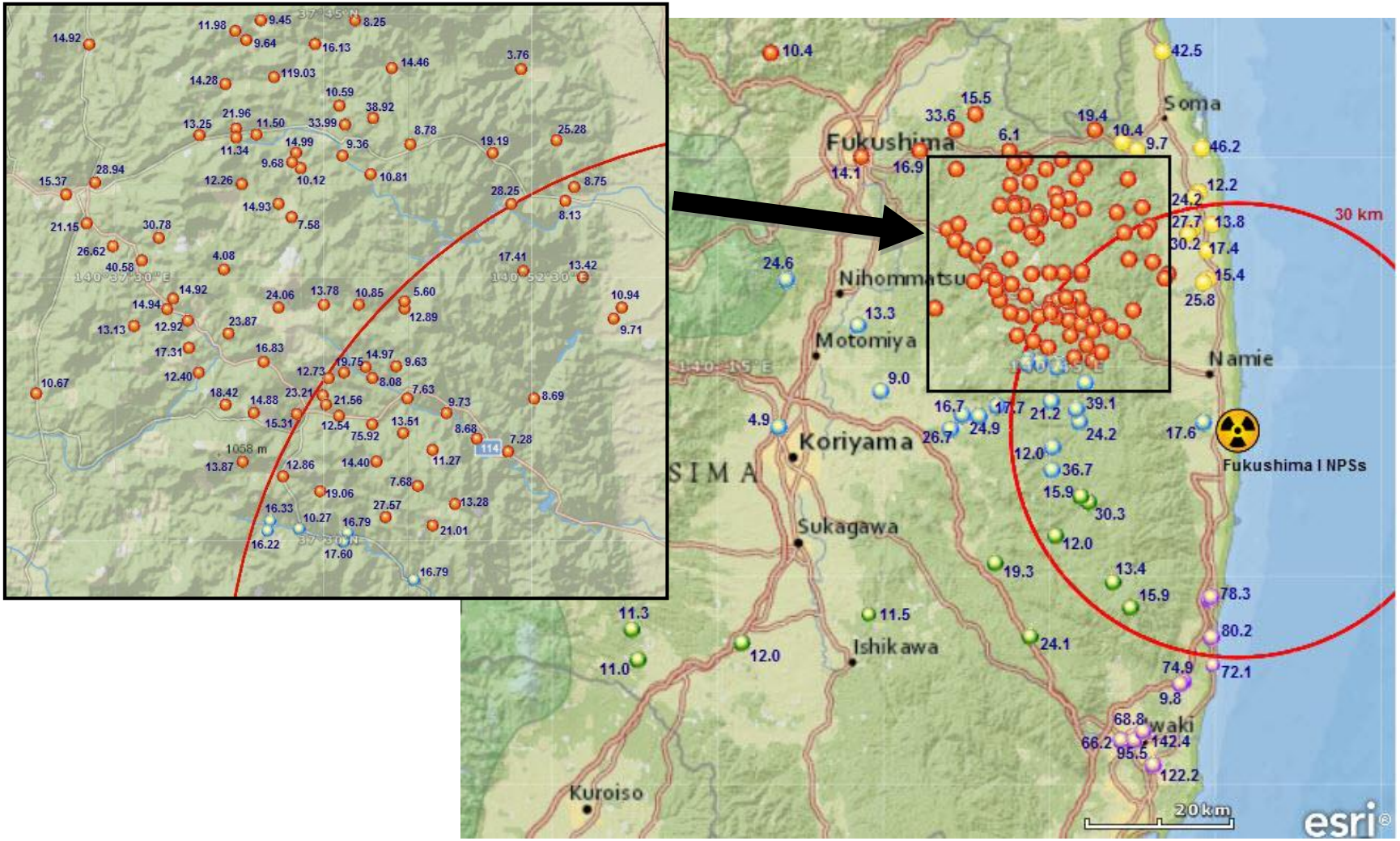

Figure 3-9 Illustration of the distribution map of corrected ratios of ^{131}I to ^{137}Cs in soil at near-field zone of Fukushima I NPSs

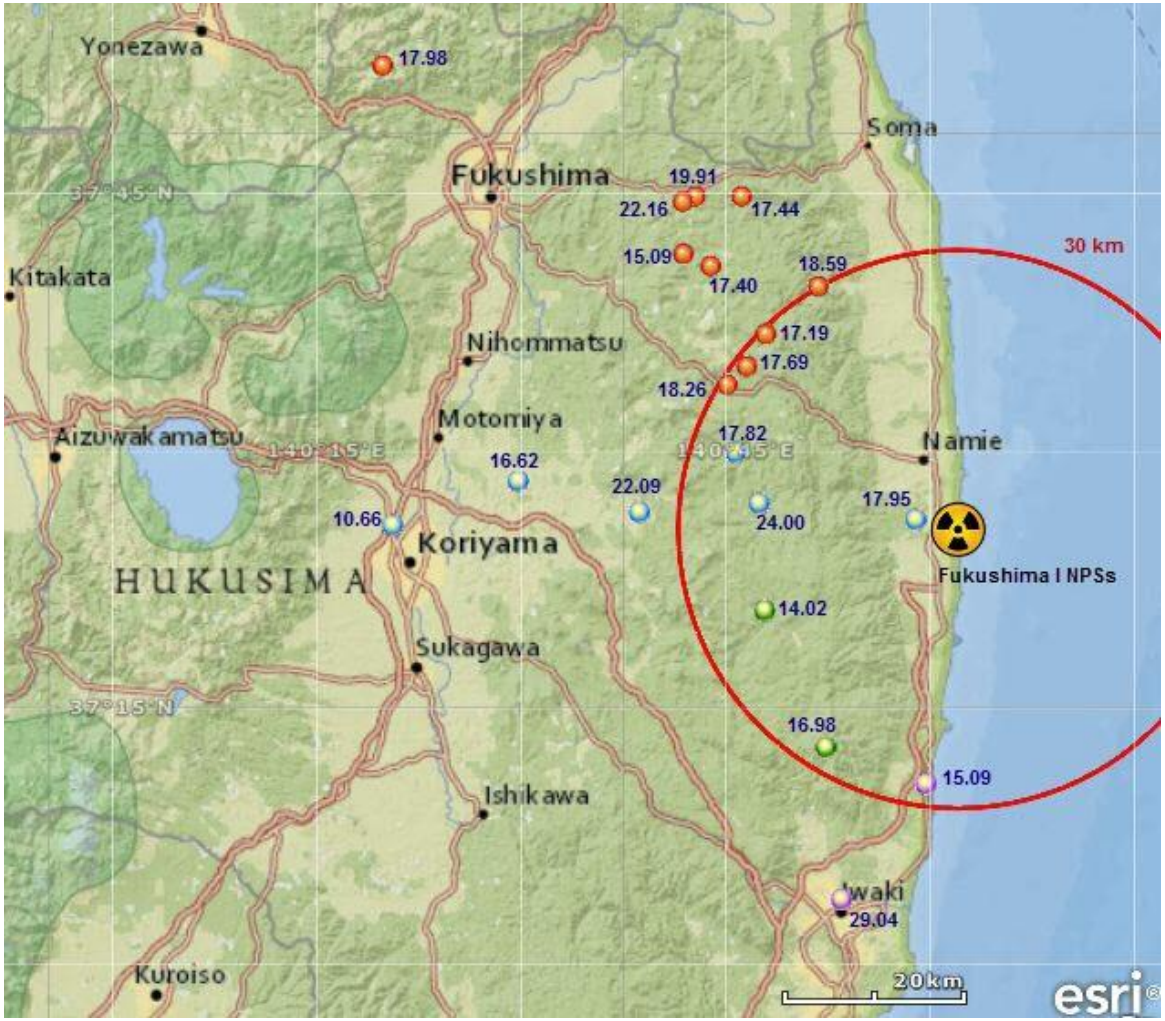

Figure 3-10 Illustration of the distribution map of corrected ratios of ^{132}Te to ^{137}Cs in soil at near-field zone of Fukushima I NPSs

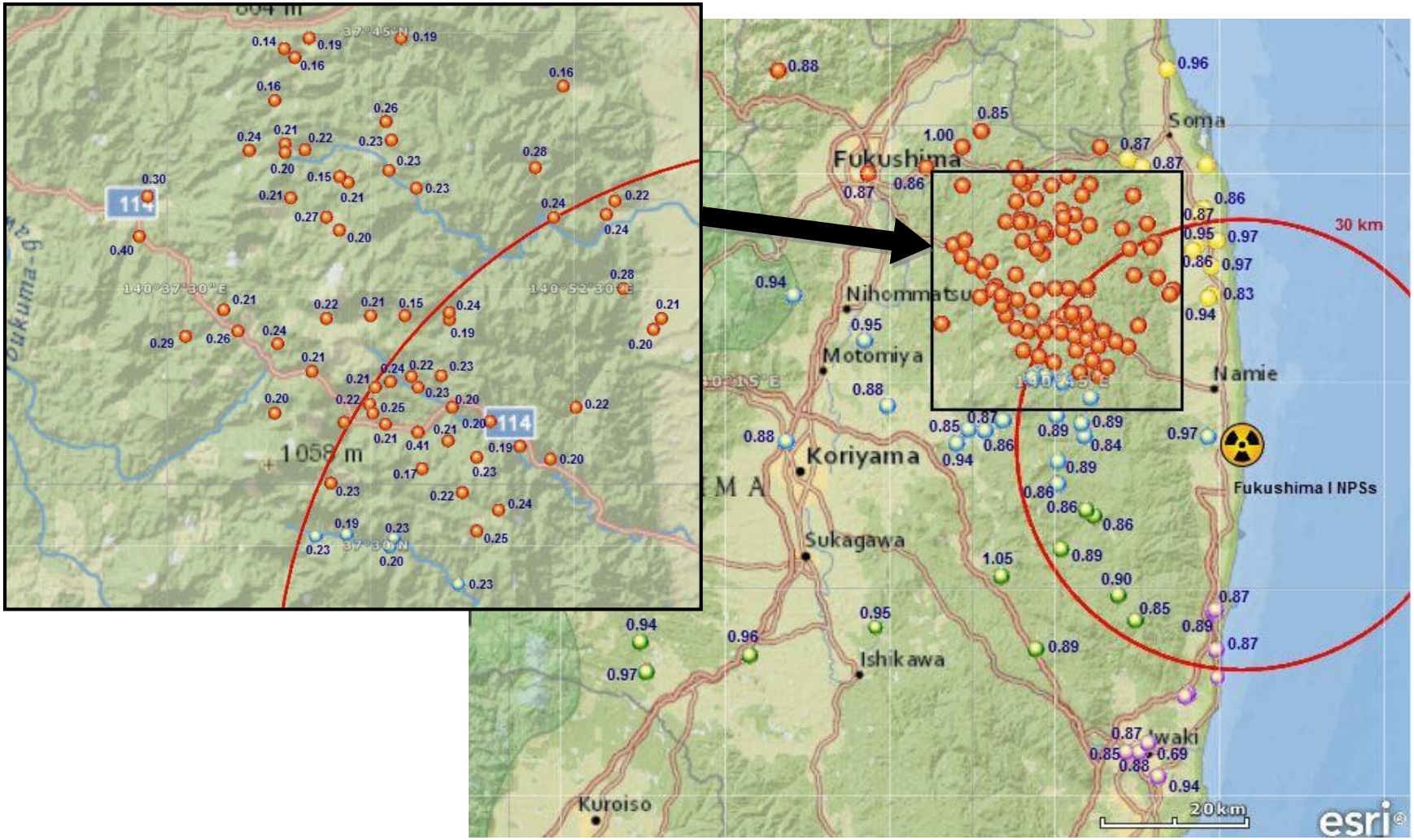

Figure 3-11 Illustration of the distribution map of corrected ratios of ^{134}Cs to ^{137}Cs in soil at near-field zone of Fukushima I NPSs

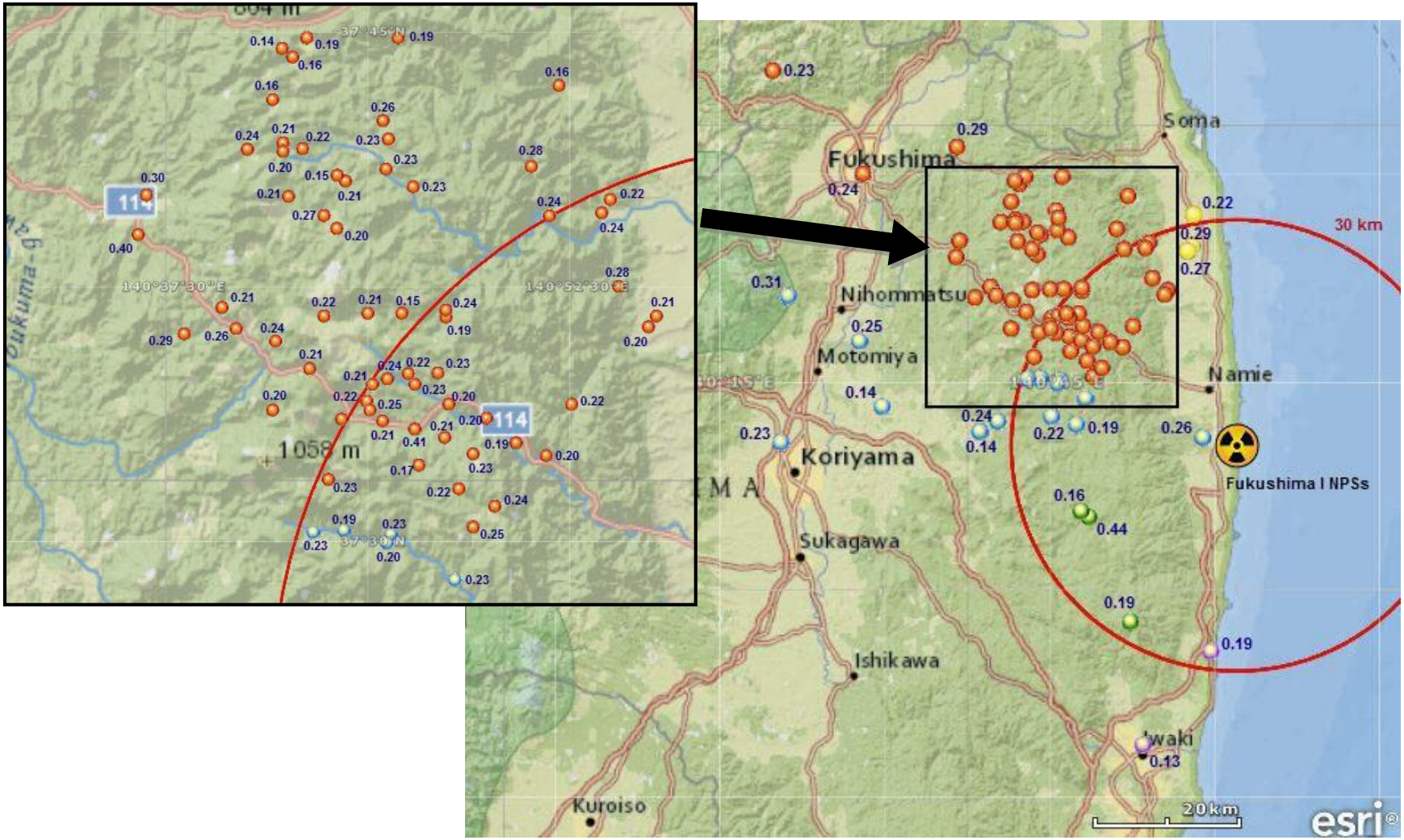

Figure 3-12 Illustration of the distribution map of corrected ratios of ^{136}Cs to ^{137}Cs in soil at near-field zone of Fukushima I NPSs.

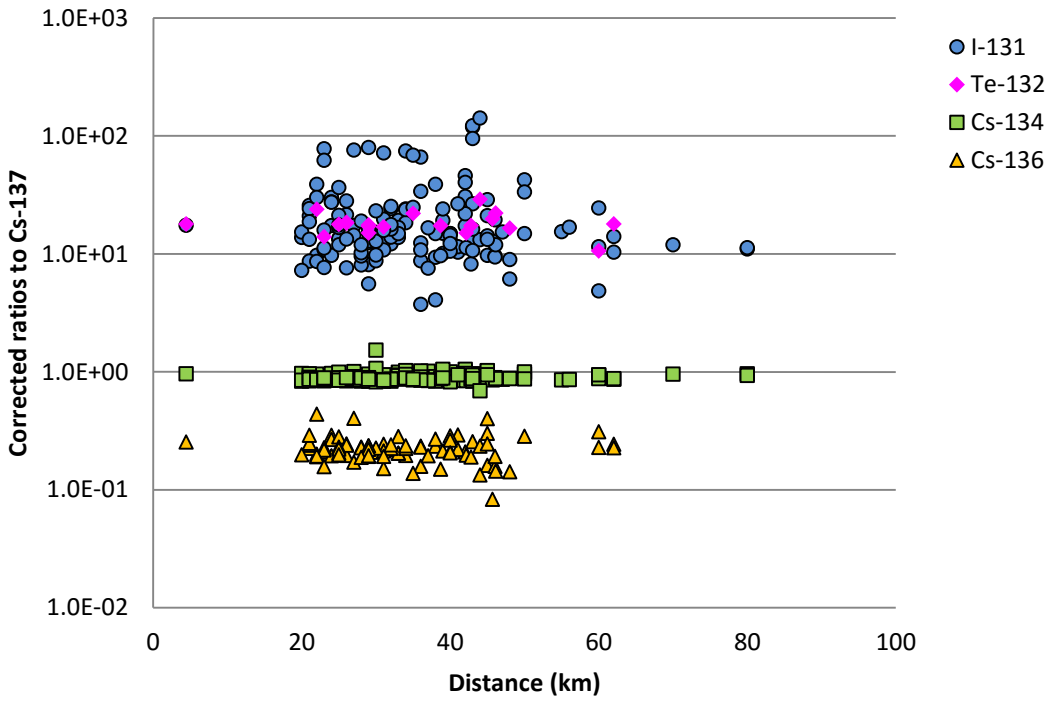

Figure 3-13 Illustration of the Corrected ^{131}I, ^{132}Te, ^{134,136}Cs:^{137}Cs in soil at near-zone of Fukushima I NPSs

Figure 3-19 illustrates the relationships between the corrected ratios of all nuclides in all directions with distance. There were apparently constant ratios of ^{132}Te, and ^{134,136}Cs:^{137}Cs. Only ^{131}I:^{137}C varied with distance. 3.3.5 Deposited ^{131}I/^{137}Cs in the highly contaminated area

As shown in Table 3-3, ^{131}I/^{137}Cs isotope ratios in soil deposits in the area within 80 km of Fukushima I NPSs (mean=22.1) were low compared to those ratios in air particulates worldwide (range ~70-80), and Table 3-5 shows variation in direction. Since high fall out occurred in the Northwest area in the near-zone of Fukushima I NPSs, the measurements in soil in this key region were carried out specially. Figure 3-14 shows a highly significant inverse correlation between the ^{131}I:^{137}Cs ratio and the ^{137}Cs activity concentration (Spearman's correlation coefficient -0.54; N=89; $p<0.001$).

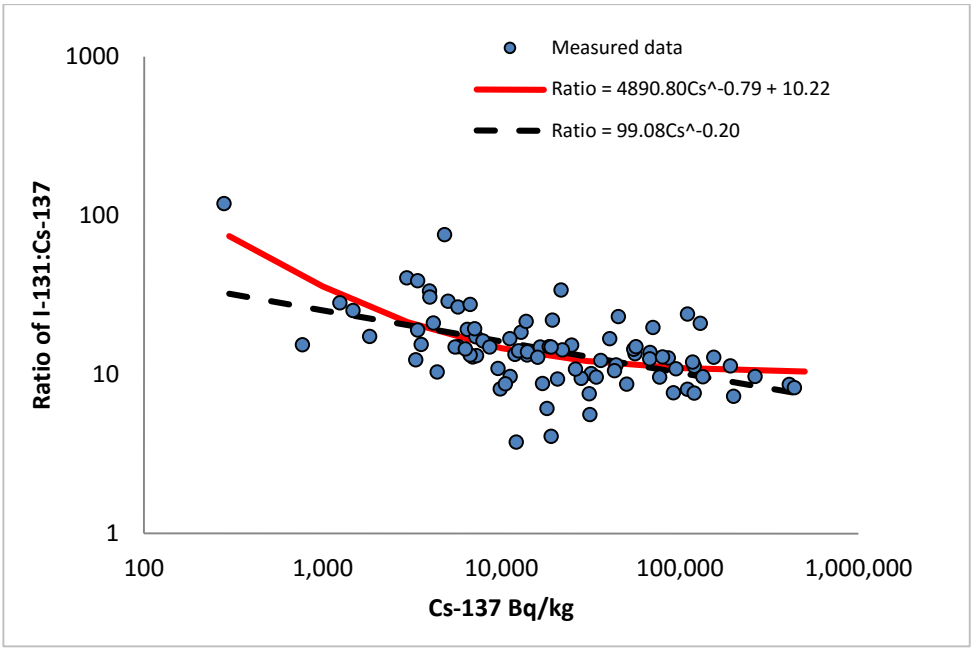

Figure 3-14 Scatter plot of ratio of ^{131}I to ^{137}Cs against activity of ^{137}Cs in soil around Fukushima I NPS. In areas of very high radiocaesium fallout, the ratio ^{131}I:^{137}Cs is much lower than in areas of lower radiocaesium fallout.

The best fit equation (using the Akaike Information Criterion (Bergman, Ider, Bowden, & Cobelli, 1979)) to these data was of the form

$$^{131}I{:}^{137}Cs = a\,(C_{137Cs})^{b} + c \qquad 3\text{-}1$$

Where $^{131}I{:}^{137}Cs$ is the ratio of ^{131}I to ^{137}Cs, C_{137Cs} is the mean activity concentration of ^{137}Cs (Bq/kg) in soil, and *a*, *b* and *c* are fitting constants from the Akaike Information Criterion. As shown in Figure 3-14 in comparison with a standard power law fit (i.e. excluding the intercept *c*). Parameter values for the fitted equations are shown in Figure 3-14. [Model fits were carried out on log-transformed data of the concentration of each isotope in soil (C_{131I} vs C_{137Cs}) then back-transformed and expressed as a ratio ^{131}I:^{137}Cs for presentation of results.] Note that Equation 3-1 is only applicable in the high fallout areas (> *ca*. 300 Bq kg^{-1} ^{137}Cs) to the north, northwest and west of Fukushima I NPS. For lower C_{Cs137} fallout areas, a generic value of 76 could be used (the value of the ratio at 300 Bq kg^{-1} of ^{137}Cs). The value of 300 Bq kg^{-1} is the lower bound of available I^{131}:^{137}Cs measurements in soil. The choice of this lower bound value (^{131}I:^{137}Cs ratio = 76 at 300 Bq kg^{-1} ^{137}Cs) is supported by the far field particulate air monitoring data in Japan, Europe and North America (ratio=70-80, Table 3-4).

3.3.4 Variation in $^{131}I/^{137}Cs$ ratio

From Figure 3-7, it can be seen that the corrected ratio of particulate ^{131}I:^{137}Cs at JAEA resulting from the northwest plume of 15 March was similar to that of the southern plume of 21 March (which had ratios of 6.10 and 5.98 respectively). However, from continuous monitoring in air at JAEA (JAEA, 2012) as shown in Figure 3-15, around a day after the highest peak in the southern plume, the ambient concentration of ^{137}Cs (green line) decreased from 1.56 to 0.42 Bq/m^3 between two measurement at 3:05 on 21 March and 15:05 on 22 March. At the same time, the concentration of ^{131}I (blue line) increased from 3.26 to 28.7 Bq/m^3 resulting in the corrected ratio (red dotted line) increasing dramatically from 4.99 to 169.37. These high ratios were seen for the next 2 days: the mean of ^{131}I:^{137}Cs during these 2 days was 147.80, then the ratio decreased continuously until 28 March, when it increased again for two days with mean of 124.05. This may be explained by the fact that a day after the highest peak of the southern plume, the temperature of the release increased dramatically for 2 days resulting in the release of a large amount of ^{131}I from the reactor core of Unit 2 (see Section 1.2). This phenomenon also occurred for the NW plume but the change in corrected ratio was not so great as in the southern plume: the ratio from 15 March until 20 March to 46.8, then declined to around 4-8 just before 21 March southern plume.

Therefore, this changing reactor temperature when ^{131}I was released from the Fukushima I NPSs apparently influenced the corrected ratio of ^{131}I:^{137}Cs significantly. This meant that a much higher amount of ^{131}I compared with ^{137}Cs in the southern plume was the likely cause of high deposition in the southern area of the near-zone. It should be noted that the 15th March NW plume, after passing the NW area of the near zone, changed direction to the south and reached the JAEA monitoring site. This phenomenon agrees with measurements of soil samples: Figure 3-16 shows corrected ratio of ^{131}I:^{137}Cs and measured concentration of ^{131}I and ^{137}Cs in soil at Umemoto, Taira Aza, Iwaki city located at 43 km to the south of Fukushima I NPS, in which the corrected ratio at around one day after second plume increased dramatically from 59.75 to 109.19 (on 22 March) then the trend of ratio after southern plume was higher than earlier by approximately one order of magnitude.

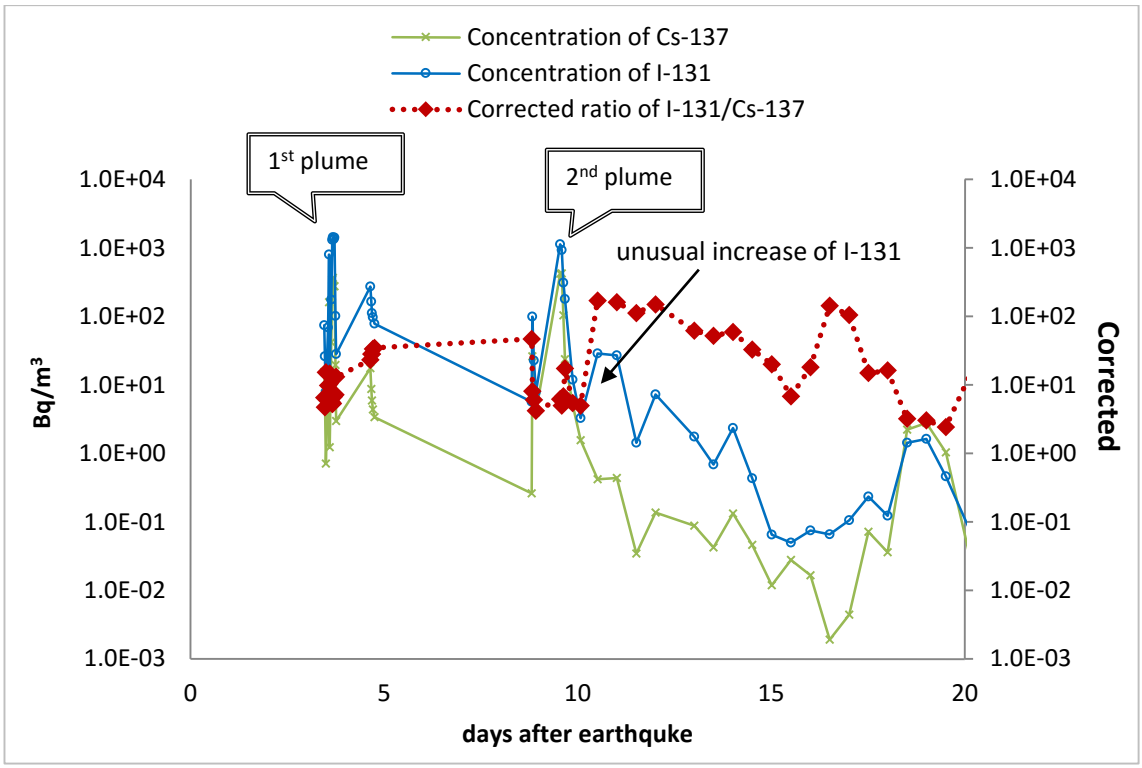

Figure 3-15 Comparison of the amount of radioactivity (Bq/m^3) in air between ^{131}I and ^{137}Cs with corrected ratio ^{131}I:^{137}Cs at JAEA, Tokai-mura, Ibaraki, Japan where the nearest site monitored ambient concentration continuously.

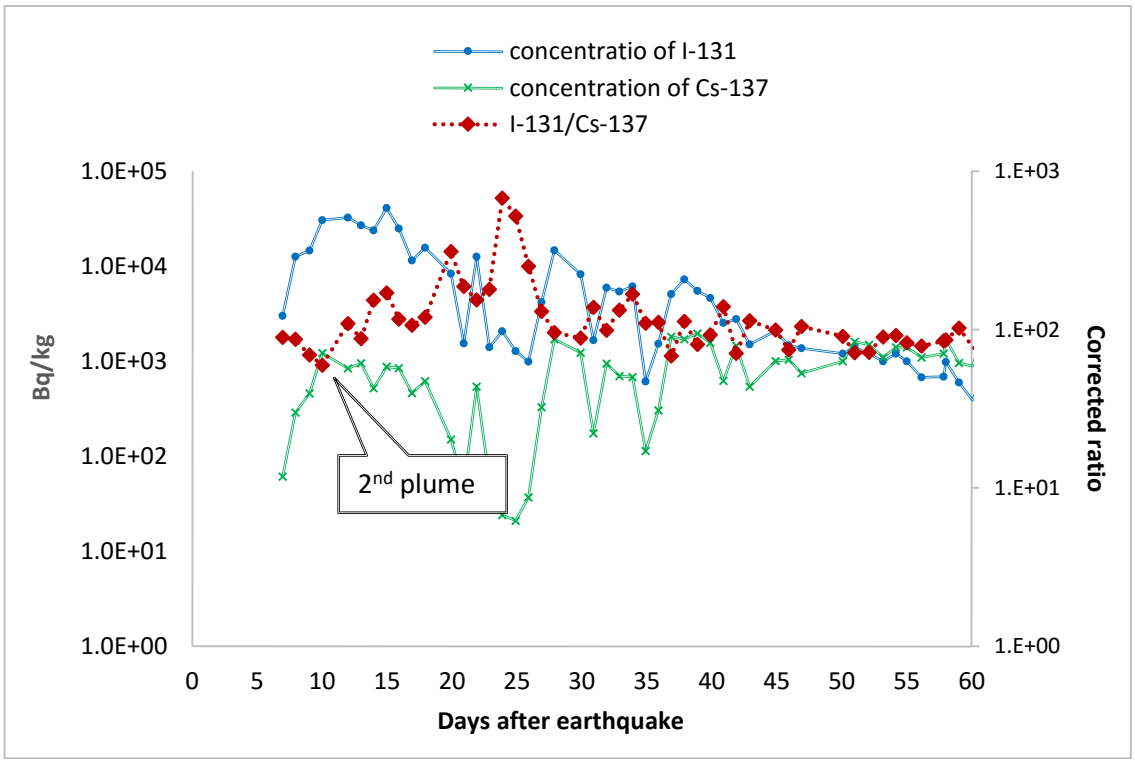

Figure 3-16 Comparing the amount (Bq/m^3) in soil between ^{131}I and ^{137}Cs with corrected ratio ^{131}I:^{137}Cs at Umemoto, Taira Aza, Iwaki city (code 2-6) located at 43 km in the South area of Fukushima I NPS.

In terms of concentration in soil, Figure 3-16 shows that the deposited contamination at this site was dominated by radionuclides from the second plume as the concentrations of both nuclides after the second plume passed this site were higher than the influence from the first plume.

The evidence for different releases of ^{131}I can be determined by comparing the change with time of the corrected isotope ratios. Figure 3-17 shows changes with time of key radionuclides from six sites which are located at different distances from the NPSs (both nuclides in these site were particulate phase). For the nearest site at JAEA and the monitoring station at Takasaki, Gunma, Japan (219 km in southwest direction (Stoehlker, et al., 2011)), the ^{131}I:^{137}Cs ratio in air increased rapidly around one day after the release of second plume, and the highest ratios at both of these sites were higher than earlier by two orders of magnitude. After that, the ratio at JAEA varied between 2.26 and 351.95 (mean=49.77 N=43) compared to the range 4.20-46.83 (mean=13.10 N=28) for the initial period before the second plume: ranges were 3.13-28.08 (mean=11.97 N=9) and 2.95-62.52 (mean=17.99 N=41) for before and after the passage of the second plume. [Note that the change of ^{131}I:^{137}Cs with time at JAEA was more clear than at other sites since the frequency of collecting samples was 10 minutes in the initial phase while accumulated radionuclides in one day were collected for long-term phase and routine sampling at the other station] The trend of higher ratio after the second plume still occurred in the Pacific Ocean and the US, station in Oahu, Hawaii, US (6,055 km (Biegalski, et al., 2011)): the mean was 22.62 with range 9.67-44.75 (N=12) before the second plume then the ratio increased to mean=161.82 with range 31.41-405.77 (N=27). This trend likely disappeared when passage of both plumes reached to European countries. However, it clear that the ratio of ^{131}I to ^{137}Cs had varied with time while other key radionuclides were constant with time at all different distances from the NPSs in particular other radiocaesium isotopes. The ratio ^{132}Te:^{137}Cs only had slight variation because the type and size of ^{132}Te is similar to ^{137}Cs (Jonas, 1984; Slade, 1968).

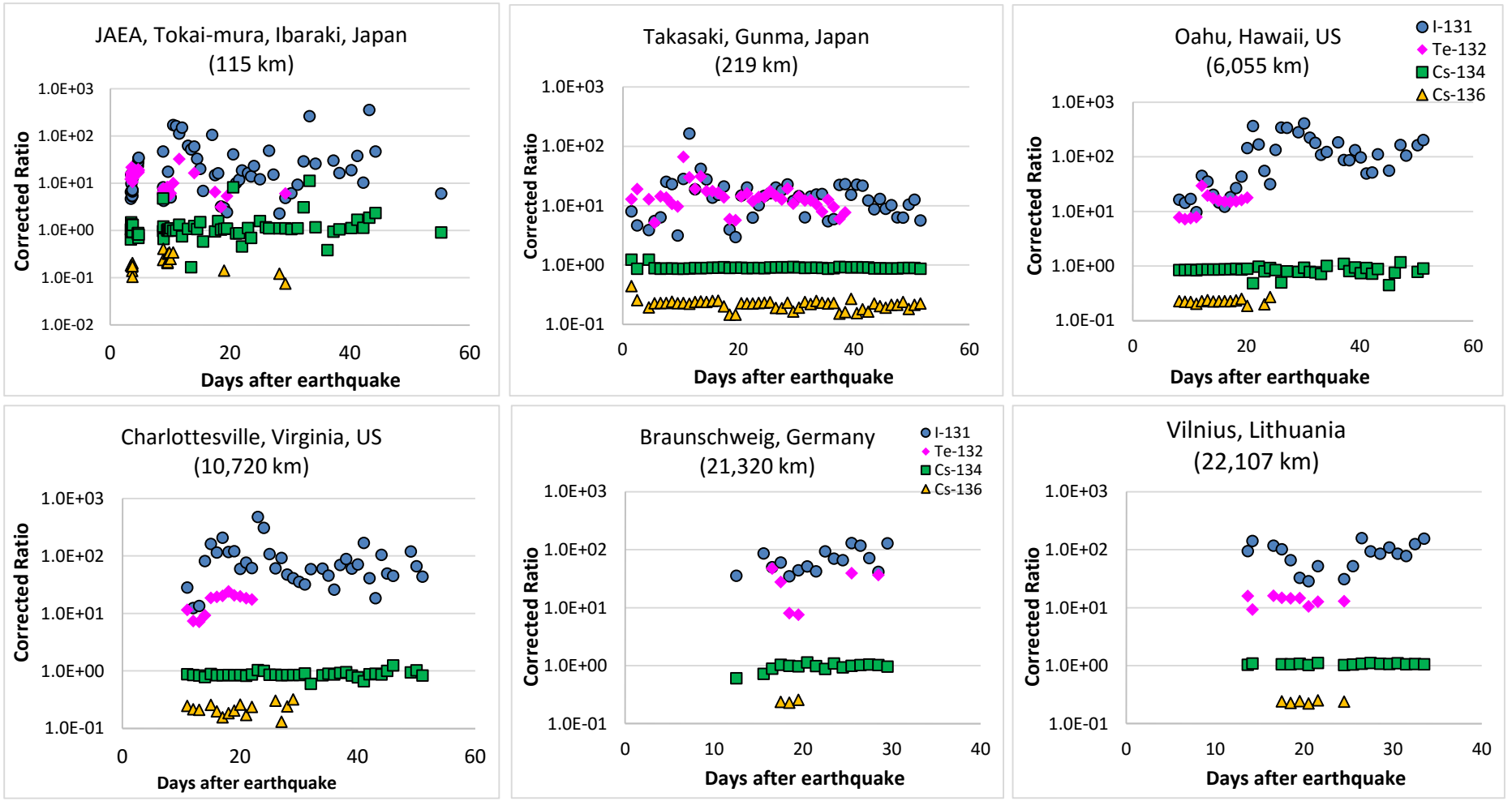

Figure 3-17 Change with time in corrected ratios to ^{137}Cs of ^{131}I, $^{134, 136}$Cs and ^{132}Te at different distances from Fukushima I NPSs.

Even though sites in Japan and the Pacific Ocean observed major changes with time of $^{131}I/^{137}Cs$ in air, the corrected ratio observed in soil did not change with time significantly in the area from North to West where the contamination were influenced by the first plume, as shown in Figure 3-18. There were slight differences in mean values of the ratio between before and after the second plume. For example, at Takami town (north), the mean before the second plume was 19.8 with range 15.7-22.7 while the mean after the second plume was 31.0 with range 10.3-86.5 and mean of whole period which was used to determine correlation between $^{131}I/^{137}Cs$ and ^{137}Cs concentration in soil (Equation 3-1) was 30.3 range 10.3-86.5. As can be seen from Figure 3-18, the mean before the second plume was similar to the minimum ratio of mean after second plume in all three sites. Since all data were used for estimating the $^{131}I/^{137}Cs$ ratio in the dose assessment model (Chapter 4), this increase in ratio over time may result in a slight over-estimate of dose in the early stages, giving a conservative estimate of dose.

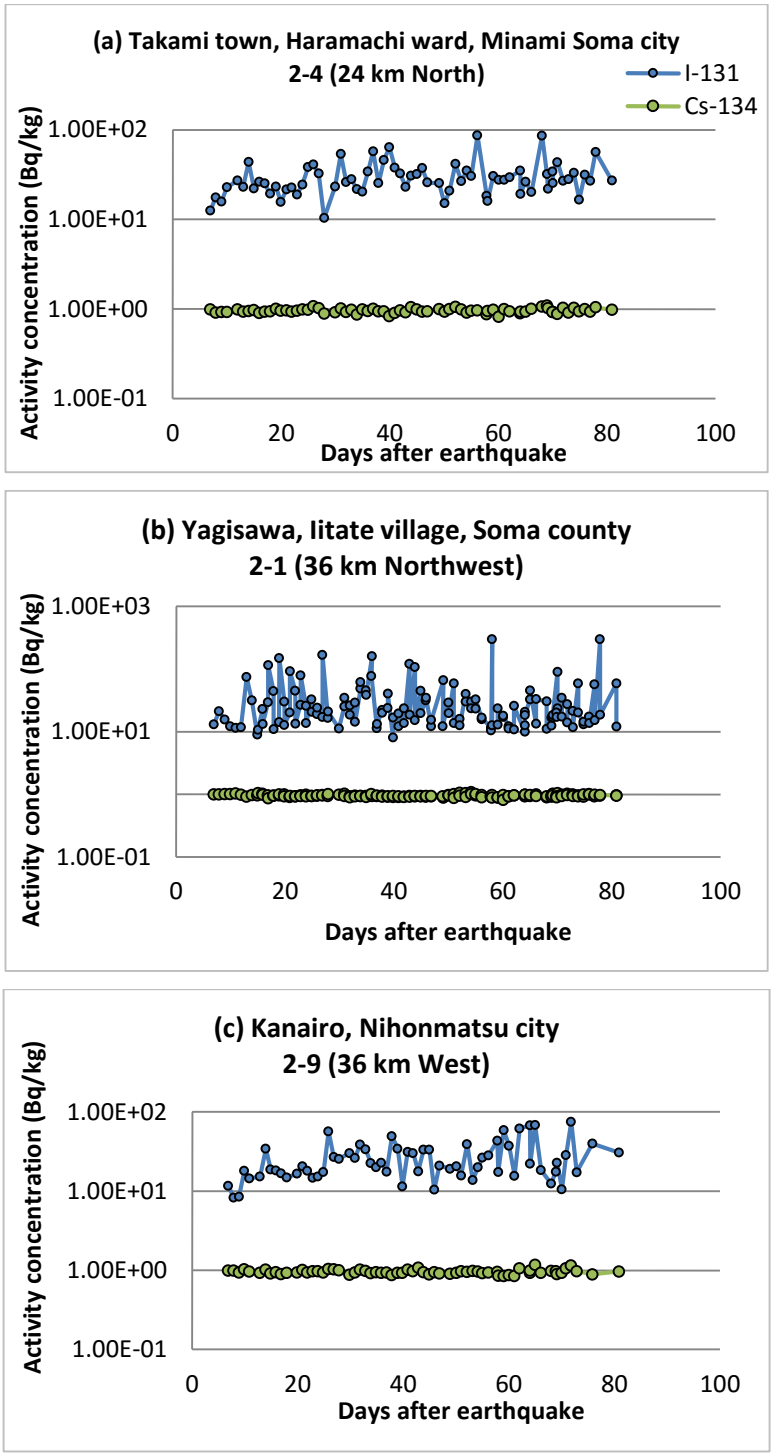

Figure 3-18 Change with time corrected ratios to ^{137}Cs of ^{131}I, $^{134, 136}$Cs and ^{132}Te at different distances from Fukushima I NPSs.

3.4 Summary and conclusions

^{134}Cs/^{137}Cs

Ratios of the radiocaesium isotopes (^{134}Cs:^{137}Cs; ^{136}Cs:^{137}Cs) show low variability and are relatively constant with distance, as observed after the Chernobyl accident (Mück, et al., 2002) and are consistent with the map of ratios in soil around Fukushima I NPSs as evaluated by Kinoshita and co-workers (2011). However, ^{134}Cs:^{137}Cs in air within near-zone (<80 km) of Fukushima I NPS was slightly higher than in the longer distance area in the EU. The reason may be that the ^{134}Cs:^{137}Cs ratio may vary according to the source of contamination depending on fuel age in a given reactor (Kirchner, Bossew, & De Cort, 2012). A shift of this isotope ratio had been noted in Europe and attributed to the small fraction of ^{137}Cs released during the Chernobyl accident or nuclear weapons test fallout still present in the atmosphere (Kirchner, et al., 2012). ^{134}Cs:^{137}Cs in air was constant with distance at ranges from 20 – 20,000 km, mean ratios were 1.03 in the near-zone and between 0.87 and 0.91 for longer distances, similar to the ratio in soil of 0.90 in the near-zone and the mean ratio of 1.02 from calculation of the total inventories of Unit 1-3's reactor core (Kenji Nishihara, et al., 2012). This observation can confirm that the major release of ^{134}Cs was from the reactor cores because the environmental ratio was similar to calculated ratio in the Unit 1-3'reactor cores (note that the calculated ratio of the Unit 1-3 reactor core = 1.02 while ratio of the Unit 1-4 spent fuel pool = 0.65; total amount of ^{134}Cs in all spent fuel > in all reactor cores). The ^{134}Cs:^{137}Cs ratios from Fukushima were higher than Chernobyl which were 0.55-0.59 for ambient ratio, 0.54-0.57 for the deposited ratio, and 0.53-0.65 for the calculated ratio in reactor core.

^{136}Cs/^{137}Cs

Similarly to ^{134}Cs:^{137}Cs, ^{136}Cs:^{137}Cs of Fukushima was constant with distance at about 0.2 in both air and soil which was similar to the calculated ratio from reactor cores of Unit 1-3: 0.3 and Chernobyl ratios which were 0.15-0.27, 0.22-0.27, and 0.27-0.42 for ambient ratio, deposited ratio, and the calculated ratio of the reactor inventory respectively. As expected, the corrected ratios to ^{137}Cs ^{134,136}Cs in air and soil samples were similar to calculated ratios in inventory cores as observed in Chernobyl (Mück, et al., 2000).

^{132}Te/^{137}Cs

Another constant ratio was ^{132}Te:^{137}Cs, the deposited ratio in the near-zone was 18.3, and ambient ratio around the world was 17.13-22.01, and mean of calculated ratio in the three cores was 12.25 that can be compared with the mean ratio of 16-17 in both air and soil for Chernobyl (even in the near-zone of Chernobyl where there were remarkably different temperatures of three plumes.

This analysis of worldwide isotope ratios has provided strong evidence that the radiocaesium and tellurium isotopes were transported and deposited in the same way and that ratios of these isotopes in air and soil were similar to those in the reactors at the time of the accident as^{132}Te and ^{137}Cs were both high volatile nuclides and sizes were similar which is appropriate to attach to each other when released from the reactor core by evaporation, then the reducing of temperature condense to particulate form, and the aerosol are blown by wind or deposited to the ground (Jonas, 1984; Slade, 1968).

^{131}I/^{137}Cs

In contrast, the corrected ratio of particulate ^{131}I:^{137}Cs was not constant with direction and distance. Since the start of measurements of ^{131}I was 9 days after the earthquake it is not sensible to evaluate ^{131}I:^{137}Cs in air at near-zone of Fukushima I NPSs, so ^{131}I:^{137}Cs air ratios from this area might not accurate for comparing with larger distance. However, there was no significant difference in relation to distance in the range 80 – 20,000 km. Moreover, there was no particulate ^{131}I:^{137}Cs in air from Chernobyl for comparison, however, Mück (2000) concluded that deposited velocity of particulate ^{131}I was similar to particulate ^{137}Cs resulting in particulate ^{131}I:^{137}Cs being constant with distance.

For the fraction of gaseous phase ^{131}I in air, the mean from all distances was 80.4% (S.E. = 1.3 %) and range 49.2-93.4% which is similar to the range = ~60-80% from observations after the Chernobyl accident (Cambray, et al., 1987; Clark & Smith, 1988; Mück, et al., 2000; Spezzano & Giacomelli, 1991). However, this fraction depended on the episode of deposition of the plume passage after each accident since deposition of gaseous iodine is remarkably higher than particulate by a factor of six in dry conditions combining with significantly higher amounts in gaseous form (Mück, et al., 2000; F. B. Smith & Clark, 1989). The ratio of gross ^{131}I to particulate ^{137}Cs between after Fukushima varied with distance but there was no significant difference observed at large distances between Pacific Ocean and US, and EU (12,000-20,000 km) while Chernobyl showed a

decrease at distance from the NPP to 1,200 km due to dry deposition, then the ratio increased until 1,400 km (Mück, et al., 2000) when wet deposition likely took place.

In the near-zone, the ratio of ^{131}I to ^{137}Cs in soil in the southern area was significantly higher than in other directions (north to southwest in which ratios were generally similar but also with high variability), and this phenomenon also occurred in the near-zone of Chernobyl which had three release plumes and the highest temperature southern plume showing much higher ^{131}I:^{137}Cs ratios in soil (Mück, et al., 2000). This might be explained by the observation made above that the highest temperature occurred in the southern plume (second plume) resulting in the deposited ^{131}I:^{137}Cs being significantly higher than in the earlier NW plume.

For the key area of high gamma dose in NW direction in the near-zone, the corrected ratio of ^{131}I:^{137}Cs in soil has an inverse correlation with the ^{137}Cs activity concentration in soil as shown in Equation 3-1. This correlation is useful for predicting contaminated iodine in soil where no measurements were performed.

Chapter 4 Early-phase external dose reconstruction at near-zone

4.1 Introduction

On 17 March 2011, 6 days after the Fukushima accident or 2 days after the period of maximum radionuclide deposition (Kinoshita, et al., 2011), MEXT established (MEXT, 2011c) daily measurement of gamma dose rate at nine sites in the near-zone (20-80 km area) around the Fukushima I NPSs. The sampling was subsequently expanded at the end of May to cover 80 km in all directions from the NPSs, including 40 sites for daily monitoring 40 sites for less regular measurement, and more than 54 sites for single measurements. The first report of unusually high gamma dose rate was detected at Tomioka-town, Motooka Shin-yonomori approximately 7 km to the southwest of NPSs (in the 20 km exclusion zone) on 12 March at 08:25, the value of dose rate being 0.18 μSv/h compared to background before the accident of around 0.03-0.06 μSv/h (NISA, 2011c). Following the high deposition period on 15th March (see Section 2.3), the external dose rates declined rapidly due to decay of short-lived radionuclides (Hosoda et al., 2011), therefore the evaluation of radiation effects on humans requires dose reconstruction in the weeks after radionuclide deposition.

Radionuclides deposited in soils produce an external gamma dose rate in air which depends on the gamma decay energy, the distribution in the soil and soil characteristics (Peter Jacob, et al., 1994; Kocher & Sjoreen, 1985). Jacob and co-workers (1994) modelled the kerma rate in the air as function of the ^{137}Cs depth profile and the following site characteristics: soil type, annual precipitation, distance from Chernobyl, and mode of deposition (dry or wet). The kerma rate in air can be converted to an exposure dose rate to humans and biota. In a similar way, Kocher and Sjoreen (1985) modelled the external exposure produced by emitted photons from the soil (see detail of both model in 2.4). The external gamma dose can be estimated from radioactive concentration and dose-rate conversion factors which were dependent on the energy of gamma emitters and depth profiles of discrete energies in soil. However, early-phase radionuclide depth profiles are not in general available for the Fukushima fallout, so this study will investigate the extent to which available dose rate data and isotope ratios can be used for external dose rate reconstruction.

4.2 Methodology

Available data for model calibration and testing

In the main monitoring in soil samples around the Fukushima I NPSs conducting by MEXT, the measurements available were the analysis of radioactivity concentration only without the deposited radioactivity density. The deposited radioactivity density (Bq m^{-2}) is the main parameter for modelling the external gamma dose, as used in the models of Kocher and Sjoreen (1985), Jacob and co-workers (1994), and GRANIS (Khalid & Mann, 2007). Since the depth profiles of each radioisotope or the density of soil samples, as used to evaluate the deposited radioactivity density, were not carried out by MEXT following the Fukushima accident, a simple model using radioactivity concentration parameters will be tested for estimating the dose to humans.

This simple model uses the measured ratios of nuclides which potentially influence the gamma dose, together with an empirical parameter to determine the early-phase gamma dose rate to human from contamination in soil at near-zone area (< 80 km). This empirical parameter can be determined by comparing the measured data between the deposited activity concentration and gamma dose rate in early-phase: such data was available at 6 sites (MEXT, 2011a) around the Fukushima I NPSs: hereinafter these sites are referred to as the "calibration sites". Furthermore, the "early-phase" is here defined as within the first 30 days following the accident before external dose was dominated by relatively long-lived ^{134,137}Cs. All of the 6 calibration sites were in the most contaminated area (Kinoshita, et al., 2011; MEXT, 2011d).

To evaluate the model by "blind testing", there were early-phase external gamma dose measurements at 15 sites (MEXT, 2011a) in the near-zone, with a few measurements of gamma dose available at each site. There were single measurements at 2 sites and the others ranged from 2 measurements at 3 sites to 48 measurements at one site. Fourteen sites were in the north to west area (the highly contaminated area) while only one site was in the lower contamination area to the south of the power plants. Therefore, we can test the model in both contaminated area, though the data is much better for the northwest. Detail of the position and start date of monitoring for the calibration sites and blind testing sites are shown in Figure 4-1. In addition, MEXT (2011a) also collected single soil

samples from 48 sites in the near zone where this model can be applied to estimate the early-phase external gamma dose.

Figure 4-1 The map generated by ESRI's ArcGIS explorer (ESRI, http://www.esri.com/Software/arcgis/explorer) illustrates the positions of 6 sites for model calibration (red circles) and 15 sites for model blind testing (blue squares); the table shows details of these sites.

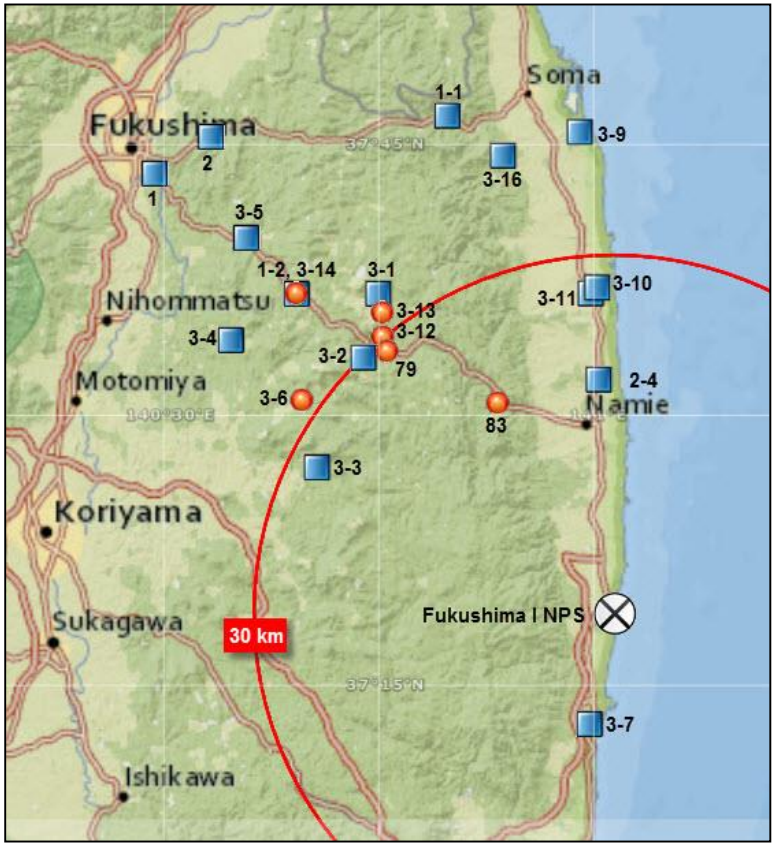

Code[Δ]	Direction	Distance (km)	Start time of measurement	
			Gamma dose rate	Soil
79	NW	29	20/03/2011 13:55	14/04/2011 11:24
83	NW	24	24/03/2011 09:46	30/03/2011 15:40
3-6	NW	32	23/03/2011 14:00	23/03/2011 14:00
3-12	NW	30	17/03/2011 13:10	25/03/2011 14:13
3-13	NW	31	25/03/2011 14:30	25/03/2011 14:30
3-14	NW	40	20/03/2011 11:20	25/03/2011 15:35
3-1*	NW	29	23/03/2011 11:10	23/03/2011 11:10
3-9 *	N	42	25/03/2011 11:24	25/03/2011 11:24
3-11*	N	32	25/03/2011 12:33	25/03/2011 12:33
3-4*	NW	43	23/03/2011 11:08	23/03/2011 11:08
3-5*	NW	47	23/03/2011 10:30	23/03/2011 10:30
3-16*	N	45	28/03/2011 16:18	28/03/2011 16:18
1	NW	62	14/04/2011 18:08	14/04/2011 18:08
2	NW	56	31/03/2011 10:20	31/03/2011 10:20
1-1	NW	46	31/03/2011 11:19	31/03/2011 11:19
1-2	NW	40	03/04/2011 09:52	03/04/2011 09:52
2-4	N	24	03/04/2011 11:57	03/04/2011 11:57
3-10*	N	32	25/03/2011 12:18	25/03/2011 12:18
3-2*	NW	30	23/03/2011 13:17	23/03/2011 13:17
3-3*	NW	32	23/03/2011 12:50	23/03/2011 12:50
3-7*	S	23	23/03/2011 13:00	23/03/2011 13:00

Note that: [Δ]the names of the deposition monitoring sites were show in Table C-2, Appendix C.

[*]Site 3-1, 3-9, 3-11, 3-10, 3-2, 3-3, and 3-7 had only 2-3 samples in first few days after earthquake and 3-4, 3-5 and 3-16 had only single sample resulting the measured data from these sites were not inefficient for calibration.

4.2.1 Model equation

In the initial period, before significant penetration of radionuclides into the soil (Kato, Onda, & Teramage, 2012), the external gamma dose rate is determined primarily by the level of radioisotope deposition and their decay energies. We therefore estimate the external gamma dose rate, D (μSv h^{-1}), at 1 m above the soil surface by:

$$D = AC_{137Cs} \sum E_i R_i e^{-\lambda_i t} \qquad 4\text{-}1$$

Where C_{137Cs} is the mean activity concentration of ^{137}Cs (Bq/kg) in soil, E_i is total gamma decay energy of each nuclide (MeV) (see Table 3.3), R_i is the ratio of deposition of each nuclide to Cs-137, λ_i is the decay constant of each nuclide (d^{-1}), and t is time after the earthquake. A [μSv hr^{-1} MeV^{-1} per 1 Bq/kg of ^{137}Cs] is an empirically-determined constant to convert gamma decay energy to gamma dose. The value of A can be evaluated by using D and R_i from the measurement data at 6 calibration sites at time t , and E_i and $e^{-\lambda_i t}$ can be calculated using Table 4.1. The measured D and R_i values were available from 5-10 days after high deposition on 15 March when short half-lived nuclides such as ^{131}I and ^{132}Te/^{132}I (8.02 and 3.20 days respectively) still influenced the external gamma dose and their radioactivity concentrations in soil were be able to be observed.

4.2.2 Key radionuclides

As discussed in section 3.4.3, the key radionuclides dominating the external gamma dose rate consisted of ^{131}I, ^{132}Te/^{132}I, ^{134}Cs, ^{136}Cs and ^{137}Cs because of the high emitted gamma energy for ^{132}I from ^{132}Te/^{132}I, ^{134}Cs and ^{136}Cs, and the high deposition in soil for ^{131}I, ^{132}I from ^{132}Te/^{132}I, ^{132}Te, ^{134}Cs and ^{137}Cs (^{134}Cs and ^{132}I from ^{132}Te/^{132}I have both high gamma emission and concentration in soil).

The influence of key radionuclides on the early-phase external gamma dose can be determined in term of the value of $E_i R_i e^{-\lambda_i t}$ in Equation 4-1; this is evaluated for the different radionuclidesin Table 4-1.

Table 4-1 Comparison of the parameters of each radionuclide and the calculation of their effect on external gamma dose in terms of $E_i R_i e^{-\lambda_i t}$ in Equation 4-1

Nuclides	Half-life	Factor for model		
		E_i (MeV)	R_i	$E_i R_i e^{-\lambda_i t}$ (t=3.9 d♣)
^{131}I	8.02 d	0.3828	>10.22	>2.79
^{132}Te	3.20 d	0.2344	18.30	1.84
^{132}I (from ^{132}Te/^{132}I)	3.20 d*	2.2645	18.30	17.8
^{132}I (fission product)	2.295 h	2.2645	N/A	N/A
^{134}Cs	2.07 y	1.5551	0.90	1.39
^{136}Cs	13.16 d	2.1283	0.22	3.81×10^{-1}
^{137}Cs	30.17 y	0.5963Δ	1.00	5.96×10^{-1}
^{129m}Te	33.60 d	0.0376	0.03♦	1.04×10^{-3}
^{129}Te (from ^{129m}Te/^{129}Te)	33.60 d*	0.0625	0.03♦	1.73×10^{-3}
^{129}Te (fission product)	69.6 m	0.0625	N/A	N/A
^{140}Ba	12.75 d	0.1826	0.07Ω	1.03×10^{-2}
^{140}La (from ^{140}Ba/^{140}La)	12.75 d*	2.3084	0.07Ω	1.31×10^{-1}
^{140}La (fission product+ from ^{140}Ba/^{140}La)	1.68 d	2.3084	0.40ɵ	1.85×10^{-1}

Note that: Emitted energy (MeV) of the released photon when parent nuclide decay to its daughter

Δ 94.4% of Cs-137 decays to Ba-137m and emitted gamma energy of Ba-137m is 0.5963 MeV/nuclear transformation.

* Using half-life from their parent when they reach equilibrium.

♣ Time of high deposition was on 15 March 2011.

♦ Corrected ratio to 11 March 2011 14:46 from the average of a single sample at 4 sites in the northwest direction of NPSs (Imanaka, et al., 2012), collected samples on 31 March 2011 as shown in Table C-3, Appendix C.

Ω Corrected ratio to 11 March 2011 14:46 from the average of a single sample at 13 sites in northwest to south direction on (S. Endo, et al., 2012), collected samples on 15 March 2011 as shown in Table C-4, Appendix C.

ɵ Corrected ratio to 11 March 2011 14:46 from the average of a single sample at 9 sites in northwest to south direction (S. Endo, et al., 2012), collected samples on 15 March 2011 as shown in Table C-4, Appendix C.

N/A means not available because the activities of very short half-lived radionuclides had already disappeared on 15 March 2011.

From Table 4-1, at the highest point of deposition (3.9 days after earthquake (Kinoshita, et al., 2011)), the value of $E_i R_i e^{-\lambda_i t}$ was highest for ^{132}I from ^{132}Te/^{132}I with a value of 17.8 MeV resulting from the highest gamma emission energy: E_i = 2.2645 MeV and a high decay-corrected ratio to long-lived ^{137}Cs: R_i= 18.30.

The isotopes ^{132}Te/^{132}I are in secular equilibrium, and therefore have a common radionuclide decay rate if the half-life of the parent nuclide is significantly greater than that of the daughter (Brezonik, 1993; Bushberg & Boone, 2011; Kendall & McDonnell, 1999; L'Annunziata, 2012). At the beginning of decay, there is only an amount of parent' radioactivity (A_{0_p}) while the daughter activity (A_{0_d}) = 0. At time t > 0, the radioactivity of the parent decays by its longer half-life ($t_{1/2_p}$) as follows

$$A_{t_p} = A_{0_p} e^{-\lambda_p t} \qquad 4\text{-}2$$

Where A_{t_p} is radioactivity (Bq) of the parent nuclide at time *t*, and λ_p is the decay constant of parent: $\lambda_p = \frac{1}{t_{1/2_p}}$. The activity of the daughter grows as the rate of parent decay which is relatively slower than the rate of daughter decay from its very short half-life ($t_{1/2_d}$) and activity of daughter at time *t* (from L'Annunziata (2012)) can be calculated by

$$A_{t_d} = \frac{\lambda_p A_{0_p}}{\lambda_d}[1 - e^{-(\lambda_d t)}] \qquad 4\text{-}3$$

where λ_d is the decay constant of the daughter. After about five to six half-lives of the daughter isotope (Bushberg & Boone, 2011), the activity of both nuclides are the same. ^{132}Te/^{132}I reaches secular equilibrium in 12 h as shown in Figure E-1 (a) in Appendix E so that the corrected ratio of ^{132}I:^{137}Cs is equal to ^{132}Te:^{137}Cs).

^{131}I is also shown to be important in the early stages, the value being >2.79 due to its high corrected ratio to ^{137}Cs: R_i= >10.22 (this ratio was discussed in Section 3.3.4). Initially, there was a much lower effect of ^{134,137}Cs on external dose rate with a values of 1.39 and 5.96×10^{-1} respectively, but over time these isotopes came to dominatedue to high amounts deposited. For example, mean ^{137}Cs was 2.7×10^{6} Bq/m^2 in the northwest area (S. Endo, et al., 2012; Imanaka, et al., 2012; MEXT, 2011b, 2011c). In the case of ^{136}Cs, even though it is a high energy gamma emitter (E_i = 2.1283 MeV) it apparently had only a slight effect on external dose rate with a low value of $E_i R_i e^{-\lambda_i t}$ of only 3.81×10^{-1} resulting

from the low corrected ratio to ^{137}Cs of 0.22. ^{136}Cs only slightly influenced the external gamma dose compared with other key nuclides as the value of the term $E_i R_i e^{-\lambda_i t}$ for ^{136}Cs is fifty times lower than the highest value for ^{132}I from ^{132}Te/^{132}I. However, ^{136}Cs also is considered in the model as the minimum effect radionuclide.

The radionuclides, ^{132}I (directly released from the reactor: ingrowth from ^{132}Te was included), ^{129}Te and ^{140}La, were not included in the model. The levels of these radionuclides released directly from reactor cores can be ignored when evaluating the external gamma dose. Since ^{132}I and ^{129}Te have very short half-life (2.30 h for ^{132}I and 69.60 m for ^{129}Te), both nuclides had already disappeared before the high deposition period on 15 March. In the case of ^{140}La, there was only one measurement collected on 15 March, 4 days after reactors shutdown. The corrected ratio (R_i= 0.07 (S. Endo, et al., 2012)) from this measurement consists of ^{140}La releasing directly from reactor cores and ^{140}La decay from ^{140}Ba. From Equation 4-1 and 4.2, ^{140}Ba/^{140}La slowly reaches secular equilibrium in 5.5 days as shown in Figure E-1 (b). However, the value of $E_i R_i e^{-\lambda_i t}$ of both forms of ^{140}La still was a factor of 2 lower than ^{136}Cs, and ^{140}La (1.68 d) decays more rapidly than ^{136}Cs and ^{134}Cs (13.16 d and 2.07 y respectively). Therefore ^{140}La does not significantly contribute to gamma dose rate. ^{129}Te from decay of metastable ^{129m}Te also rapidly reaches secular equilibrium in only 7.5 h (as shown in Figure E-1 (c) and also has a low value of $E_i R_i e^{-\lambda_i t}$. ^{129m}Te and ^{140}Ba have low ratios to ^{137}Cs (R_i = 0.03 and 0.07 respectively) and low gamma emission energies (E_i = 0.0376 and 0.1826 respectively). In addition, Tagami (Tagami, et al., 2011) observed very low activity concentrations of other radioelements in soil including ^{95}Nb, ^{110m}Ag and ^{140}Ba, and ^{95}Zr, ^{103,106}Ru, and ^{140}Ba which, though found in the Chernobyl accident as a result of fuel particle release, were not found in significant quantities following Fukushima. For the noble gases, most nuclides emit low gamma energies (0.0474 MeV for ^{133}Xe, and 0.0206 for ^{131m}Xe. 0.0410 for ^{133m}Xe, only short half-lived ^{135}Xe (9.14 h) has a relatively low energy (0.2483 MeV) and do not significantly deposit to the ground surface. Therefore, these noble gases do not affect the gamma dose. Therefore, all of these nuclides did not contribute significantly to external gamma dose rate and can be ignored for evaluating gamma dose in this model. According to the main monitoring around Fukushima I NPSs (MEXT, 2011a, 2011b), this nuclide was not measured. However, there were a few measurements of deposited activity in t near-zone area conducted by Endo (2012) and Imanaka (2012) which showed corrected ratios of ^{132}Te to ^{137}Cs which were remarkably consistent in all directions and

distances, with mean 18.3 and S.E. 1.7 (further details were given in Section 3.3.4). From Table 4-1, the highest value of $E_i R_i e^{-\lambda_i t}$ is 17.8 for ^{132}I from the ^{132}Te/^{132}I decay, therefore the early-phase external gamma dose rate was dominated by this radionuclide.

The significant advantage of this simple model, therefore, is that we can estimate the early-phase external gamma dose by using the mean ratio of a few key radionuclides when measured data was not available, particularly when dose was most influenced by the key nuclide: ^{132}I (from ^{132}Te/^{132}I decay).. Figure 4-2 shows how much each nuclide contributes to the external gamma dose by the calculation of this model (a representation of the value of $E_i R_i e^{-\lambda_i t}$ as a function of time after the earthquake). The greatest contribution to dose was from ^{132}I (from ^{132}Te/^{132}I) until around 25 days after the earthquake while the secondary influence was from ^{131}I until 40 days. In the early phase, the gamma dose also was influenced by ^{132}Te for about 15 days. The contributions from these nuclides were longer than their half-life because their influence came from the combination of amount deposited and gamma energy released. This can explain why ^{132}I dominates gamma dose longer than ^{132}Te even though they have the same half-life and deposited activity: ^{132}I from ^{132}Te/^{132}I has a much higher energy of gamma emission.

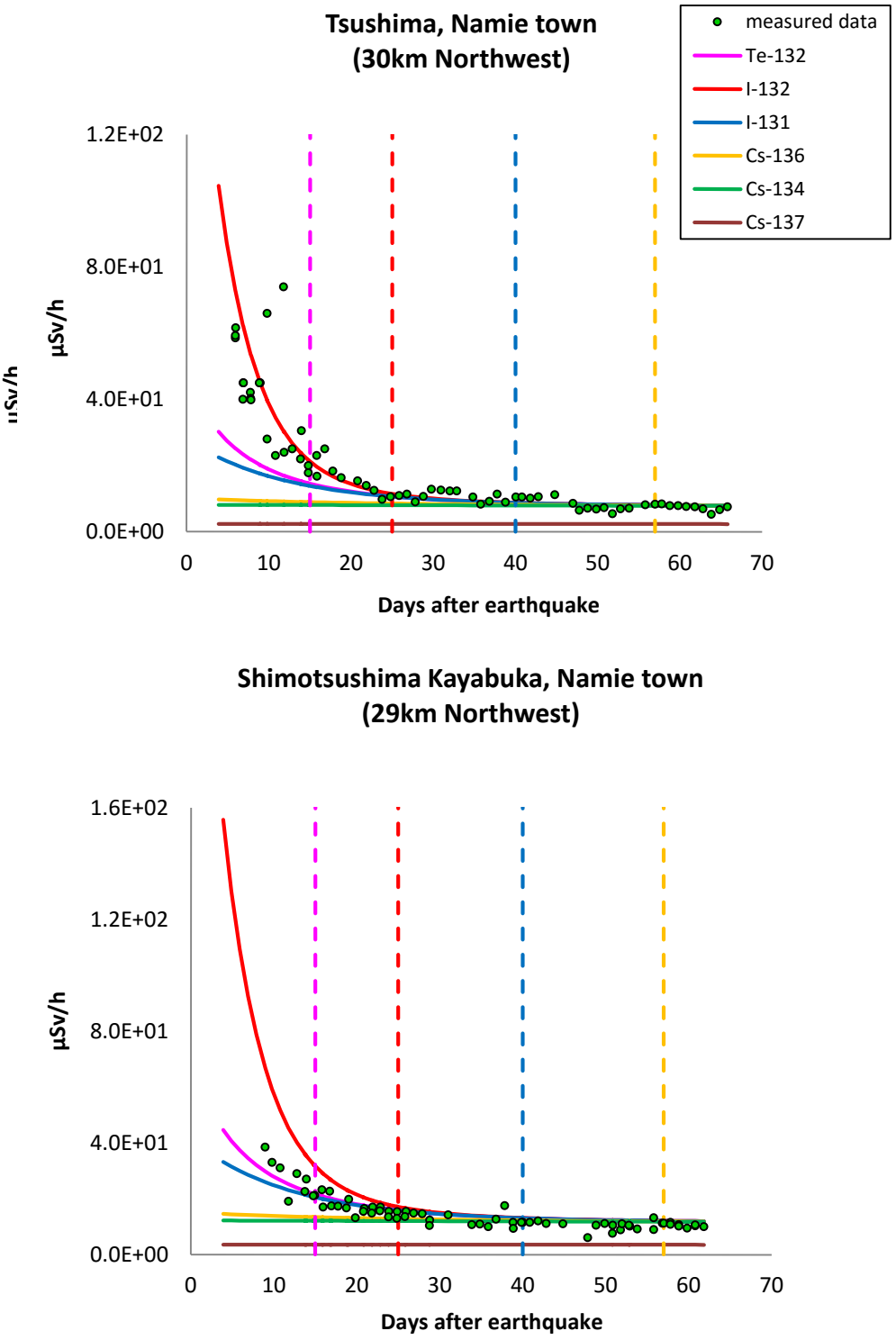

Figure 4-2 the contribution of external gamma dose from each key nuclide, and the region of the period influencing dose (dash line: pink for ^{132}Te, red for ^{132}I, blue for ^{131}I and yellow for ^{136}Cs), the calculation started at the time of highest deposition on 15 March 2014.

After the early phase, the external gamma dose was dominated by radiocaesium, particularly ^{134}Cs, followed by ^{137}Cs and ^{136}Cs respectively. From the calculations, ^{136}Cs had a little effect until approximately 58-60 days after earthquake. After that, the gamma dose was dominated by long-lived nuclides: ^{134}Cs and ^{137}Cs.

Table 4-2 Summary of the mean ratio values used in the predictive model, ^{131}I:^{137}Cs from 3.3.5, and ^{132}Te, ^{134,6}Cs:^{137}Cs from 3.3.4.

Nuclide	Decay constant (d^{-1})	Emitted gamma energy (MeV/nt)	Ratio to ^{137}Cs
^{131}I	8.64E-02	0.3828	$4.89 \times 10^3 \times C_{137Cs}^{-0.76} + 10.22$
^{132}Te	2.16E-01	0.2344	18.30
^{132}I	2.16E-01	2.2645	18.30
^{134}Cs	9.20E-04	1.5551	0.90
^{136}Cs	5.27E-02	2.1283	0.22
^{137}Cs	6.29E-05	0.5963	1.00

Table 4-2 shows a summary of the corrected ratio of each radionuclide to ^{137}Cs (R_i), as well as the emitted gamma energy (E_i), and the decay constant (λ_i) of all key radionuclides which were used to determine the change in gamma dose rate with time. For ^{131}I:^{137}Cs, the corrected ratio is estimated by using Equation 3-1 in areas where there was high fallout (C_{137Cs} is greater than 300 Bq kg^{-1}) while in areas of lower fallout (C_{137Cs} < 300) a value of ^{131}I:^{137}Cs = 76 is used. For ^{132}I from ^{132}Te/^{132}I, this isotope is in secular equilibrium with ^{132}Te hence ^{132}I follows the ^{132}Te decay curve and uses the same R_i and λ_i.

Since the model is intended to be generic (not site-specific), it uses generic isotope ratios determined from mean data (see Section 3.2.1). Table 4-3 shows the differences of ratios between the observations at each of the six calibration sites and the generic ratios used in the model. No data of ^{132}Te/^{137}Cs (which was equal to the radionuclide which most influenced early-phase dose: ^{132}I/^{137}Cs) was available in these six calibration sites, however, it clear that (from Figure 3-8, Chapter 3) the deposited corrected ratio of ^{132}Te/^{137}Cs was consistent in direction and distance allowing it to be assumed that the mean of this ratio can be used in the model. Similarly to ^{132}Te/^{137}Cs, ^{134,136}Cs/^{137}Cs were also remarkably consistent with direction and distance and we can see that the means were generally very similar to the measured data at all six calibration sites (except the site in Tsushima, Namie town for ^{134}Cs/^{137}Cs). For ^{131}I:^{137}Cs, the extrapolated value generally agrees with observations except at two sites in which the model underestimates this twice: this can be a cause for incorrect estimation of the external gamma dose rate in these two

sites (Tsushima, Namie town and Akougi, Namie town). Therefore, in terms of the corrected ratios, the estimation of ^{131}I:^{137}Cs will be the major cause for uncertainty of this model.

Table 4-3 The comparision of the corrected ratios between measurements at the six calibration sites and model generic isotope ratios.

Code[Δ]	Direction	Distance (km)	Measured data				Extrapolated data			
			^{131}I	^{132}Te	^{134}Cs	^{136}Cs	$^{131}I^{*}$	$^{132}Te^{\Phi}$	$^{134}Cs^{\Phi}$	$^{136}Cs^{\Phi}$
79	NW	29	12.54	-	0.90	0.21	11.23	18.30	0.90	0.22
83	NW	24	9.73	-	0.90	0.20	10.58	18.30	0.90	0.22
3-6	NW	32	16.22	-	0.87	0.23	14.57	18.30	0.90	0.22
3-12	NW	30	23.21	-	0.93	0.22	11.60	18.30	0.90	0.22
3-13	NW	31	19.75	-	0.95	0.25	11.20	18.30	0.90	0.22
3-14	NW	40	14.91	-	0.87	0.21	13.19	18.30	0.90	0.22

Note that: [Δ]The names of the deposition monitoring sites were show in Table E-1, Appendix E.

[*]Note that the corrected ratio was estimated by using Equation 3-1.

[Φ]Note that these corrected ratios were from the mean measured data.

4.2.3 *A* parameter

An empirically-determined constant, the *"A"* parameter, was used to convert the term of $C_{137Cs} \sum E_i R_i e^{-\lambda_i t}$ to external gamma dose (the units of this parameter are μSv hr^{-1} MeV^{-1}) per 1 Bq/kg of ^{137}Cs. The value of the *A* parameter is dependent on gamma ray absorption in soil and air. The *A* parameter accounts for potentially different distributions of radionuclides with depth at different sites and represents to a large extent soil shielding. Note that the external gamma dose in the early phase was from the combination of radioactivity in air and soil. Further details of the potential interference of radionuclides in the dispersion cloud on external gamma dose is discussed in Section 4.2.4.

Under conditions of high rainfall, radiocaesium can penetrate relatively deeply into the soil profile (Bunzl et al., 1997), however in most areas affected by Chernobyl (J. T. Smith & Beresford, 2005b), and at Fukushima (Kato, et al., 2012; Tanaka et al., 2012), the majority of radioactivity remained near the soil surface, limiting gamma-ray absorption within the soil. Over years to decades after fallout, gamma dose rates will decline due to radioactive decay and further slow penetration of radiocaesium into the soil profile (Bunzl, et al., 1997; J. T. Smith & Beresford, 2005b).

Using mean deposited ratios of each radionuclide to ^{137}Cs, Equation (4-1) was fitted to measurements of changes in external gamma dose rate with time at six sites at a distance 24-40 km from Fukushima I NPSs. Model fits were carried out by using SAS software (PROC Nlin; SAS Institute Inc.) to determine the value of the one unknown parameter, *A*. The fitted value of the *A* parameter at each site was then correlated with total ^{137}Cs activity concentration. From Figure 4-4, using only one site-specific input parameter or the activity concentration ^{137}Cs and one fitting parameter of *A* in the model, the fits show good agreement with measured data. This confirms the accuracy of the derived mean isotope ratios. A slight tendency to under-predict dose rates in the period from 20 – 80 days is likely due to differences in absorption in soil at different sites, and (relatively small) local variation in isotope ratios.

The fitted values of the *A* parameter at the six calibration sites were shown in Table 4-4, range was 5.70×10^{-5} – 14.6×10^{-5}, and mean was 9.2×10^{-5}. This relatively narrow range gives confidence that values of this unknown parameter can be extrapolated to reconstruct external dose rates at other sites, on the basis only of the measured ^{137}Cs activity

concentration. It also implies that, in the early phase, soil self-shielding was broadly similar across the different sites.

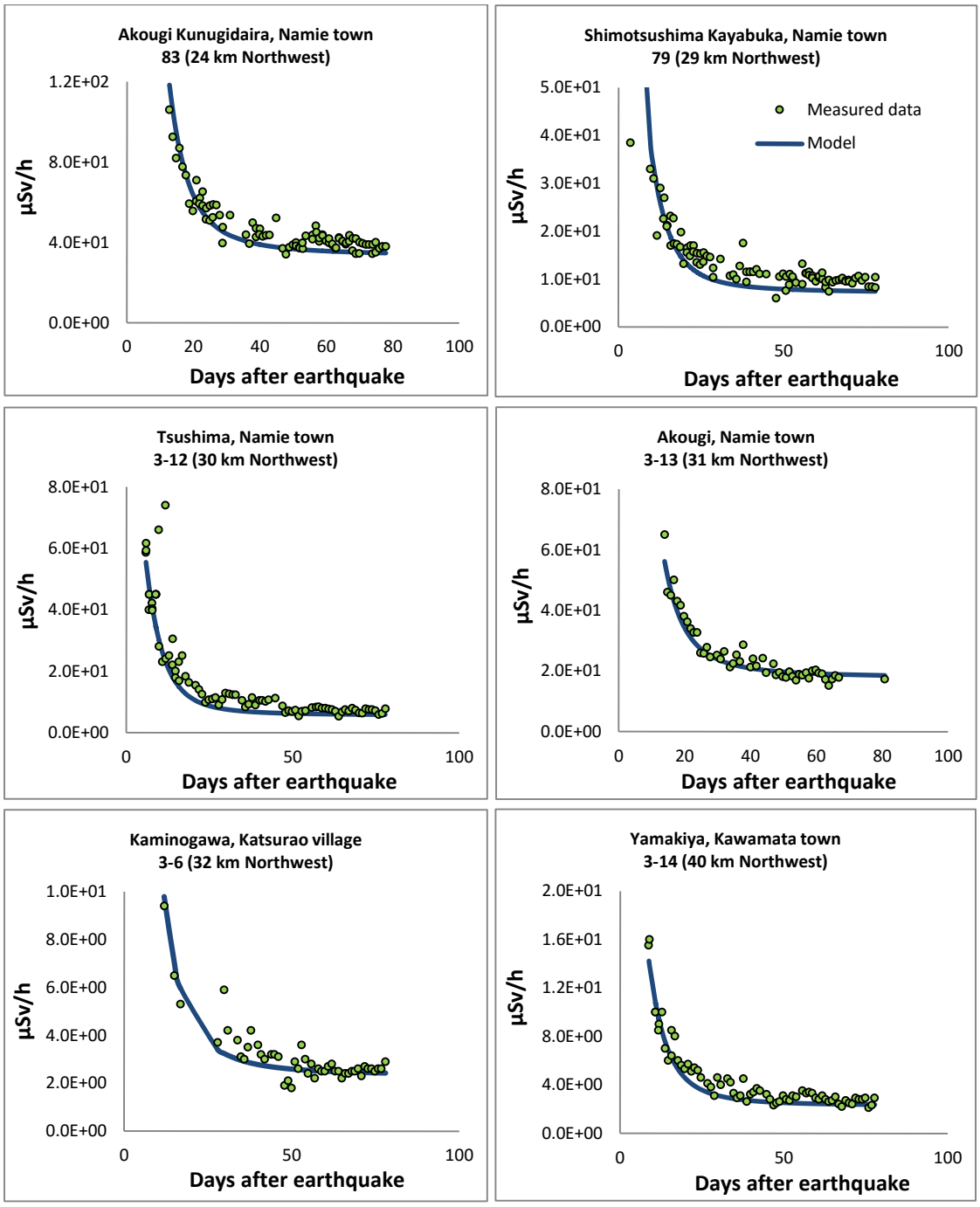

Figure 4-3 Model fits to measured gamma dose rates obtained using generic isotope ratios for radiocaesium isotopes and ^{132}Te, and using a regression Equation (Eq. 3-1) for ^{131}I; the *A* parameter is fitted to the data using SAS (SAS Institute Inc.).

Table 4-4 The *A* parameter is fitted to the data at calibration sites by using SAS (SAS Institute Inc.).

Code[Δ]	Direction	Distance (km)	Concentration of ^{137}Cs (Bq/kg) Mean ± S.E.	*A*		
				Mean	Lower limit[*]	Upper limit[*]
79	NW	29	$6.77\times10^{4} \pm 3.81\times10^{3}$	6.00×10^{-5}	5.70×10^{-5}	6.30×10^{-5}
83	NW	24	$2.63\times10^{5} \pm 2.57\times10^{4}$	7.10×10^{-5}	6.90×10^{-5}	7.30×10^{-5}
3-6	NW	32	$1.00\times10^{4} \pm 8.04\times10^{2}$	1.29×10^{-4}	1.22×10^{-4}	1.37×10^{-4}
3-12	NW	30	$4.53\times10^{4} \pm 7.47\times10^{3}$	7.10×10^{-5}	6.60×10^{-5}	7.60×10^{-5}
3-13	NW	31	$7.05\times10^{4} \pm 5.73\times10^{3}$	1.42×10^{-4}	1.38×10^{-4}	1.46×10^{-4}
3-14	NW	40	$1.65\times10^{4} \pm 1.09\times10^{3}$	7.70×10^{-5}	7.40×10^{-5}	8.10×10^{-5}
			Mean	9.17×10^{-5}	8.77×10^{-5}	9.60×10^{-5}

Note that: [Δ]The names of the deposition monitoring sites were show in Table E-1, Appendix E.

[*] Note that the lower and upper limits are 95% confidence limits in *A* parameter.

4.2.4 The potential influence of radionuclides in air on external dose rate

This section will discuss the minor contribution to dose rate from radionuclides in the dispersion cloud. The dose rate from radionuclides in the cloud can calculated by using a conversion factors converting the radioactivity concentration in air to the external gamma dose rate at 1 metre above the ground (DOE, 1988; Eckerman & Ryman, 1993; Yoo, Jang, Lee, Noh, & Cho, 2013). To calculate the gamma dose from radionuclides in air, the key radionuclides i.e. ^{131}I, ^{132}Te/^{132}I and ^{134,136,137}Cs were taken into account. Another majority of the contamination in air was noble gases such as $^{131m,133m,133 \text{ and } 135}$Xe (Stoehlker, et al., 2011; Stohl, et al., 2011): these radionuclides have to be included for calculating the gamma dose rate. However, the most predominant nuclide of the noble gases is ^{133}Xe (Stoehlker, et al., 2011; Stohl, et al., 2011) whilst ^{131m,135}Xe have a conversion factor less than ^{133}Xe by a factor of 10 (DOE, 1988; Yoo, et al., 2013). The conversion factors of these nuclides were shown in Table 4-5. There was no influence from noble gas in soil because most of them didn't deposited into ground (Stoehlker, et al., 2011; Stohl, et al., 2011; UNSCEAR, 2013).

Table 4-5 The conversion factors for radioactivity concentration in air to the external gamma dose rate above the ground about 1 metre.

Nuclide	The conversion factors μSv/h per Bq/m^3		
	DOE (1988)	Eckerman and Ryman (1993)	Yoo et al. (2013)
^{131}I	5.89E-05	6.55E-05	5.83E-05
^{132}Te	3.36E-05	-	-
^{132}I	3.67E-04	4.03E-04	3.67E-04
^{133}Xe	5.43E-06	5.62E-06	4.43E-06
^{134}Cs	2.47E-04	2.73E-04	2.47E-04
^{136}Cs	3.49E-04	3.82E-04	3.47E-04
^{137}Cs/^{137m}Ba	9.44E-05	1.04E-04	9.36E-05

The measured data in air was lacking during first few days after the accident. There were few sites where measured ambient and deposited data were available. Hosoda and co-workers (2013) measured gamma dose rate and collected both soil and air samples from four sites in near-zone of Fukushima I NPSs during the early phase after accident on 17-19 of March 2011, but only 2 sites were able to detect contamination (FU and IW-2 in Table 4-6). Another available 2 sites were studied by MEXT (2011a) in this period (1 and

2-4 in Table 4-6) . However, none of these sites observed ^{132}Te, ^{136}Cs and gaseous ^{131}I, so these were estimated using the general ratios of these nuclides in Japan (within 80-2,000 km from NPSs) as shown in Table 3-4 (17.49 for ^{132}Te and 0.19 for ^{136}Cs) and gaseous ^{131}I can be estimated by using the mean fraction of gaseous form of 80.4% from Section 3.3.2. In addition, the measured ambient data in MEXT (2011a) provided the density of contamination in terms of radioactivity to mass of dust in air or Bq per kg of dust in air (Bq/kg_{dust}). This allowed data to be converted to Bq per cubic metre of air using the average mass of dust in a cubic metre of air (kg_{dust}/m^3) from the world-wide survey by the World Bank (2014) which gave a particulate matter concentration (PM10) in Japan in 2011 of 19 $\mu g_{dust}/m^3$.

A comparison of external gamma dose from cloud shine and soil are shown in Table 4-6. It is clear that the majority of gamma dose in the few days after the accident (when significant concentrations of radionuclides still occurred in air) was dominated by the contamination in soil since the ratios of dose calculated from soil to dose calculated from air are around 10^3 to 10^5 while the measured dose to dose calculated from air had a ratio which varied from 10^4 to 10^{10}.

Table 4-6 The comparison dose rate from soil model (Equation 4-1) and air model (the conversion factors of DOE (1988) and Yoo et al. (2013)).

Code	Direction	Distance (km)	Sampling date	Dose rate (μSv/h)			Ratio		
				Measurement	Soil	Air	Measurement/Air	Soil/Air	Measurement/Soil
FU♦	NW	62.9	17/03/2011	7.39E+00	4.84E+01	5.77E-05	1.28E+05	8.39E+05	1.53E-01
IW-2♦	SW	44.4	18/03/2011	1.09E+00	8.12E-01	1.16E-04	9.40E+03	7.00E+03	1.34E+00
1Δ	NW	62	20/03/2011	5.00E+00	1.46E+01	5.63E-09	8.88E+08	2.60E+09	3.42E-01
2-4Δ	N	24	21/03/2011	2.80E+00	2.35E+00	1.80E-10	1.56E+10	1.31E+10	1.19E+00

ΔNote that these two sites from MEXT (2011a), the names of the deposition monitoring sites were show in Table C-2, Appendix 2.

♦These two sites from Hosoda et al. (2013), FU is in Fukushima city, Fukushima and IW-2 is in Iwaki, Fukushima.

Table 4-7 The external gamma dose from radionuclides in air at Takasaki, Gunma prefecture located approximately 220 km in the southwest direction of Fukushima I NPSs, calculated by the conversion factors of DOE (1988) and Yoo et al. (2013).

Sampling date	Dose rate from air (μSv/h)			Ratio	
	Total with ^{133}Xe (1)	Total without ^{133}Xe (2)	Only ^{133}Xe (3)	(1)/(2)	(3)/(2)
13/03/2011	1.02E-07	1.01E-07	1.70E-09	1.02	0.02
14/03/2011	5.00E-06	5.00E-06	1.37E-09	1.00	0.01
16/03/2011	2.32E-02	2.22E-02	9.34E-04	1.04	0.04
17/03/2011	2.25E-03	4.96E-05	2.20E-03	45.47	44.47
18/03/2011	1.83E-04	4.78E-05	1.35E-04	3.83	2.83
19/03/2011	1.07E-04	6.50E-05	4.18E-05	1.64	0.64
20/03/2011	8.70E-05	6.01E-05	2.70E-05	1.45	0.45
21/03/2011	6.37E-03	6.32E-03	5.07E-05	1.01	0.01
22/03/2011	2.13E-03	1.88E-03	2.50E-04	1.13	0.13
23/03/2011	1.36E-03	1.32E-03	3.65E-05	1.03	0.03
24/03/2011	5.31E-05	3.72E-05	1.59E-05	1.43	0.43
25/03/2011	4.77E-05	3.19E-05	1.58E-05	1.50	0.50
26/03/2011	1.91E-05	1.59E-05	3.19E-06	1.20	0.20
27/03/2011	1.68E-05	5.00E-06	1.18E-05	3.37	2.37
28/03/2011	1.30E-05	4.99E-06	8.03E-06	2.61	1.61
29/03/2011	1.39E-05	1.01E-05	3.84E-06	1.38	0.38
30/03/2011	1.03E-04	1.01E-04	2.12E-06	1.02	0.02
31/03/2011	4.21E-05	4.07E-05	1.44E-06	1.04	0.04

For ^{133}Xe, where the amount was significant in air in the first few days after the accident (JAEA, 2012; Stoehlker, et al., 2011), the contribution to gamma dose rate was also much less significant than from soil. The monitoring site nearest Fukushima I NPSs where there was sufficient information of ^{133}Xe and key nuclides to evaluate the gamma dose rate was in Gunma prefecture approximately 220 km in the southwest (Stoehlker, et al., 2011). Using the conversion factors from Table 4-5, the results in Table 4-7 show that the contribution to gamma dose from ^{133}X was less than the combination of key radionuclides as ratio of calculated dose from ^{133}X to calculated dose from key radionuclide were lower than 0.7. There was only a notably high influence from ^{133}X on 17 March (ratio = 44.47) and higher influence (ratio ≈ 2-3) on 18th, 27th and 28th of March.

On 17 March, the external gamma dose rate from cloud shine at 1 metre above the contaminated ground, was dominated by ^{133}Xe from air media, however, the highest influence from ^{133}Xe in air (ratio to all nuclides in air = 44.47) was still significantly lower than the influence from all nuclides in soil (ratio of all nuclides in soil to all nuclides in air was in the range $10^3 – 10^5$). Thus, it can be concluded that ^{133}Xe in air had lower effect to the external gamma dose compared with the effect from deposited radionuclides.

4.3 Sensitivity of the model

The variability in model predictions results from the following key factors: the attenuation and shift of the energy spectrum by penetration of fallout into the soil; geometry of the dose rate monitors (i.e. response to given contamination); possibly different fallout episodes with different radionuclide ratios. These factors lead to uncertainty in input parameters used in the model such as the *A* parameter, the measured ^{137}Cs activity concentration in soil, and the corrected ratios in soil. This is because that all of these input parameters were extrapolated from measured data for which some data sets were quite small, for example, the corrected ratio of ^{132}Te to ^{137}Cs. Another important factor which can affect the results of the model, is the lack of measured gamma dose rate data particularly during the highest deposition on 15 March (as seen in Table 4-1 the measured gamma dose from six sites started very late around 5-10 days after 15 March). The measured gamma dose around 15 March will be useful to extrapolate more accurate values of the *A* parameter, and also useful for validation of this model.

This section will discuss the errors in the model, the most important of which can be determined by analysis of measured data. These are: the deposited concentration of ^{137}Cs, the *A* parameter, and the corrected ^{131}I/^{137}Cs ratio. A Monte Carlo simulation will be used to estimate the error of means of other corrected ratios. Monte Carlo simulation was also performed for evaluating the error from all parameters, including generating the values of ^{137}Cs concentration, *A* parameter and corrected ^{131}I/^{137}Cs by using randomly generated data sets for each characteristic.

4.3.1 *A* parameter

As shown in Table 4-4, *A* parameter calibrated from six calibration sites has mean = 9.17×10^{-5}. The sensitivity of the estimation of the *A* parameter can be determined by the SAS software: with a confidence level of 95%, the upper limit from six calibration sites is 1.46×10^{-4} and the lower limit 5.7×10^{-5}. This range of *A* parameter values was used to determine the sensitivity of model at six calibration sites where there were available data for evaluating the model. Figure 4-4 show the sensitivity to the *A* parameter (all other parameters were constant, using general corrected ratios and average ^{137}Cs concentrations), the result shows a good agreement, there was under estimation in Akougi, Namie town and Kaminogawa (code: 3-13 and direction: 31 km Northwest) and Katsurao village (code: 3-6 and direction: 32 km Northwest) where the estimates of ^{131}I/^{137}Cs in these areas are significantly different to measured data (other sites have very close values to measured data). The details of the differences between measured corrected ratio and extrapolated ratio were shown in Table 4-3, the extrapolated ratios of ^{131}I/^{137}Cs at sites 3-6 and 3-13 were 14.57 and 11.20 respectively while measured ratios were 16.22 and 19.75.

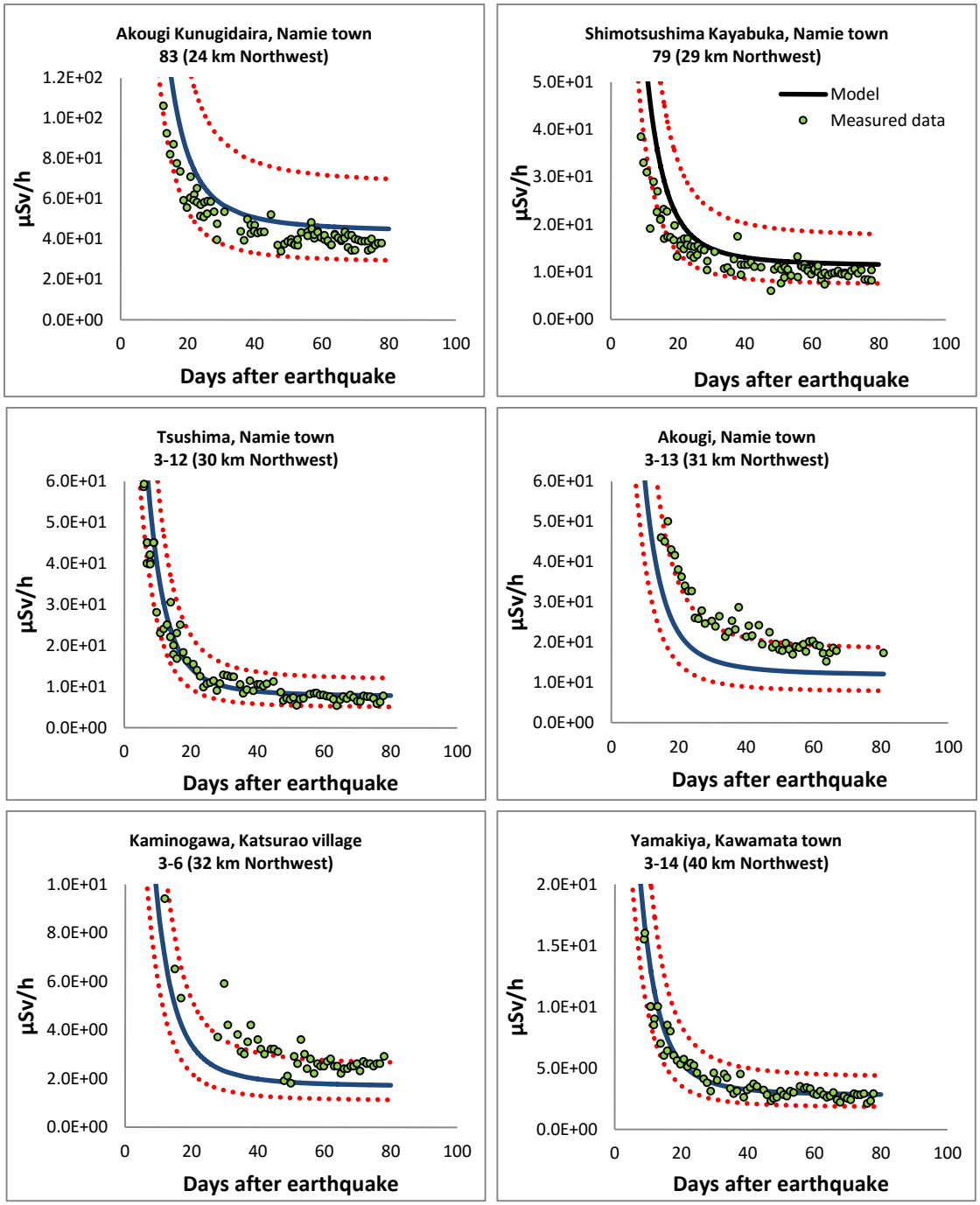

Figure 4-4 Model results with sensitivity in estimation of *A* parameter compared with the measurement data at all six calibration sites.

4.3.2 $^{131}I/^{137}Cs$

The corrected ratio $^{131}I/^{137}Cs$ was determined by Equation 3-1 which was derived from measurements in soil in the northwest areas where there was the highest contamination. The corrected ratios calculated by Equation 3-1 (R_{model}) and the corrected ratios by observation ($R_{measurement}$) are not normally distributed (Kolmogorov-Smirnov test in IBM SPSS Statistics 20: $p < 0.01$ for both). Moreover, $\frac{R_{measurement}}{R_{model}}$ (from all sites) is also not normally distributed ($p < 0.01$). However, the $\log_{10}$ transformation of $\frac{R_{measurement}}{R_{model}}$ is normally distributed (Kolmogorov-Smirnov's test; $p = 0.05$) and from visual inspection of the histograms in Figure 4-5. Figure 4-5 shows that both $R_{measurement}$ and R_{model} show a distribution with a long tail on the right (positively skewed). $\frac{R_{measurement}}{R_{model}}$ appears to be normally distributed in shape but still has long tail on the right.The histogram is clearly symmetrically distributed for $Log(\frac{R_{measurement}}{R_{model}})$.

The mean of $Log(\frac{R_{measurement}}{R_{model}})$ is -3.0024×10^{-5}, standard deviation is 1.9016×10^{-1}, and the upper and lower bounds of $Log(\frac{R_{measurement}}{R_{model}} \pm 2\sigma)$ are 3.8029×10^{-1} and -3.8035×10^{-1} respectively. Then, anti-log of these values give the upper and lower of $\frac{R_{measurement}}{R_{model}}$ which are 24.0 and 4.1653×10^{-1} respectively (the details of these values are shown in Table C-5, Appendix C). Therefore, the upper and lower of the corrected ratio of ^{131}I:^{137}Cs from equation 3-1 at each site $(R_{measurement} \pm 2\sigma_1)_i$ can be calculated as follows

$$(R_{measurement} \pm 2\sigma_1)_i = [10^{\left(Log\left(\frac{R_{measurement}}{R_{model}} \pm 2\sigma_2\right)_{all}\right)}] \times (R_{model})_i \quad (4\text{-}2)$$

where $Log\left(\frac{R_{measurement}}{R_{model}} \pm 2\sigma_2\right)_{all}$ is the mean anti log of $\frac{R_{measurement}}{R_{model}}$ from all sites, $(R_{model})_i$ is the corrected ratio of ^{131}I:^{137}Cs in each site calculated from equation 3-1, σ_1 is the standard deviation of $R_{measurement}$ at each site and σ_2 is the standard deviation of mean of $Log(\frac{R_{measurement}}{R_{model}})$ from all sites.

Figure 4-6 shows the model sensitivity to uncertainty in ^{131}I:^{137}Cs ratio at the six calibration sites when othar input parameters are fix with their default values. The sensivity of ^{131}I:^{137}Cs is more narrow compared with that of the *A* parameter, showing

that it has less influence on overall model sensitivity. As with the sensivity to the *A* parameter, a relatively high error also occured in two sites at Akougi, Namie town and Kaminogawa (code: 3-13 and direction: 31 km Northwest), Katsurao village (code: 3-6 and direction: 32 km Northwest) due to the significantly high error in estimates of ^{131}I:^{137}Cs. In these two sites, the ratio ^{131}I:^{137}Cs estimated from Equation 3-1 are twice as low as the measured data (see the detail in Table 4-3) resulting in the model predicting an underestimated gamma dose rate.

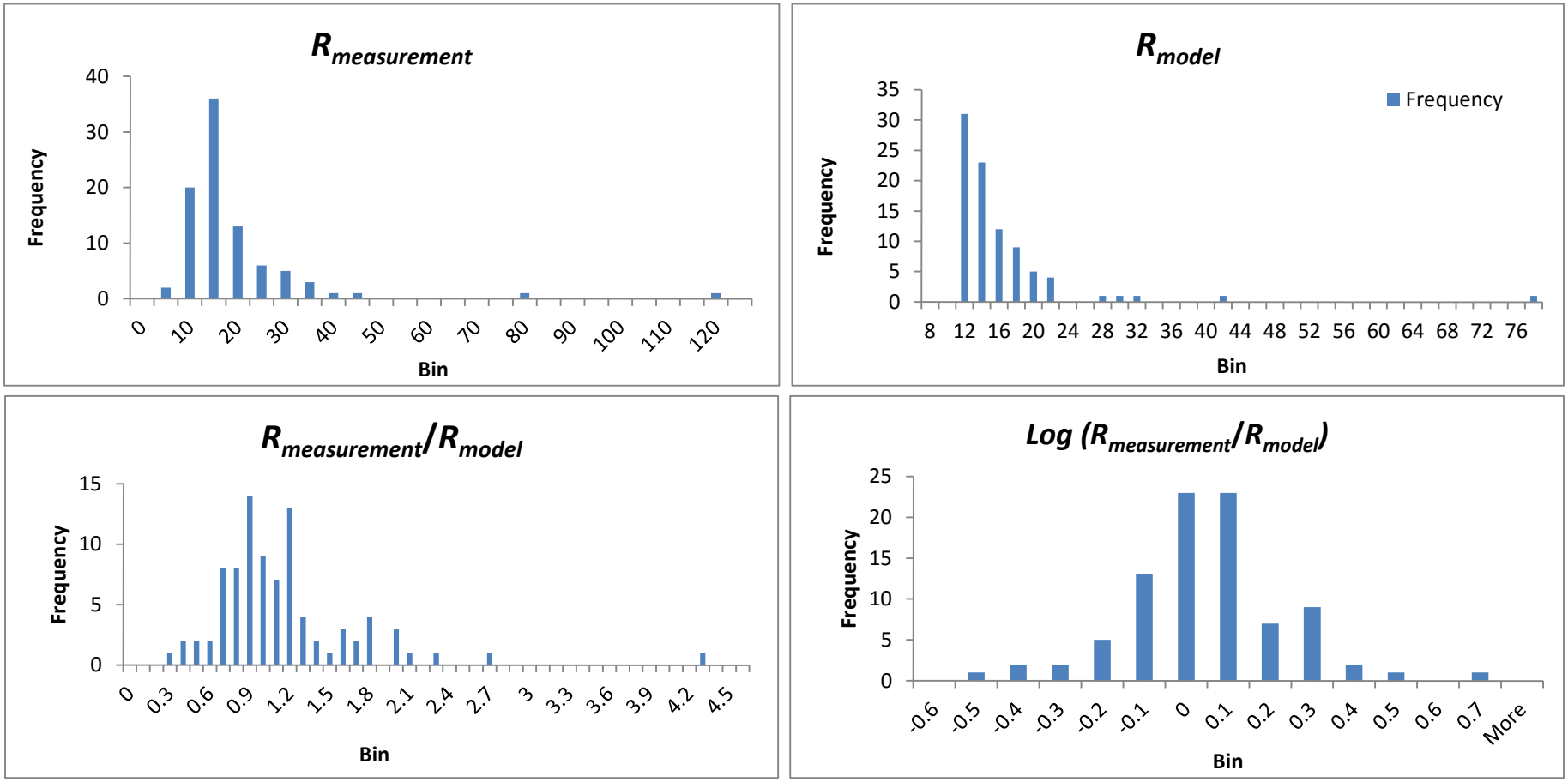

Figure 4-5 Illustration of the histograms of the corrected ratio from measured data and model (by Equation 3-1), the ratio of both, and the log transform of this ratio.

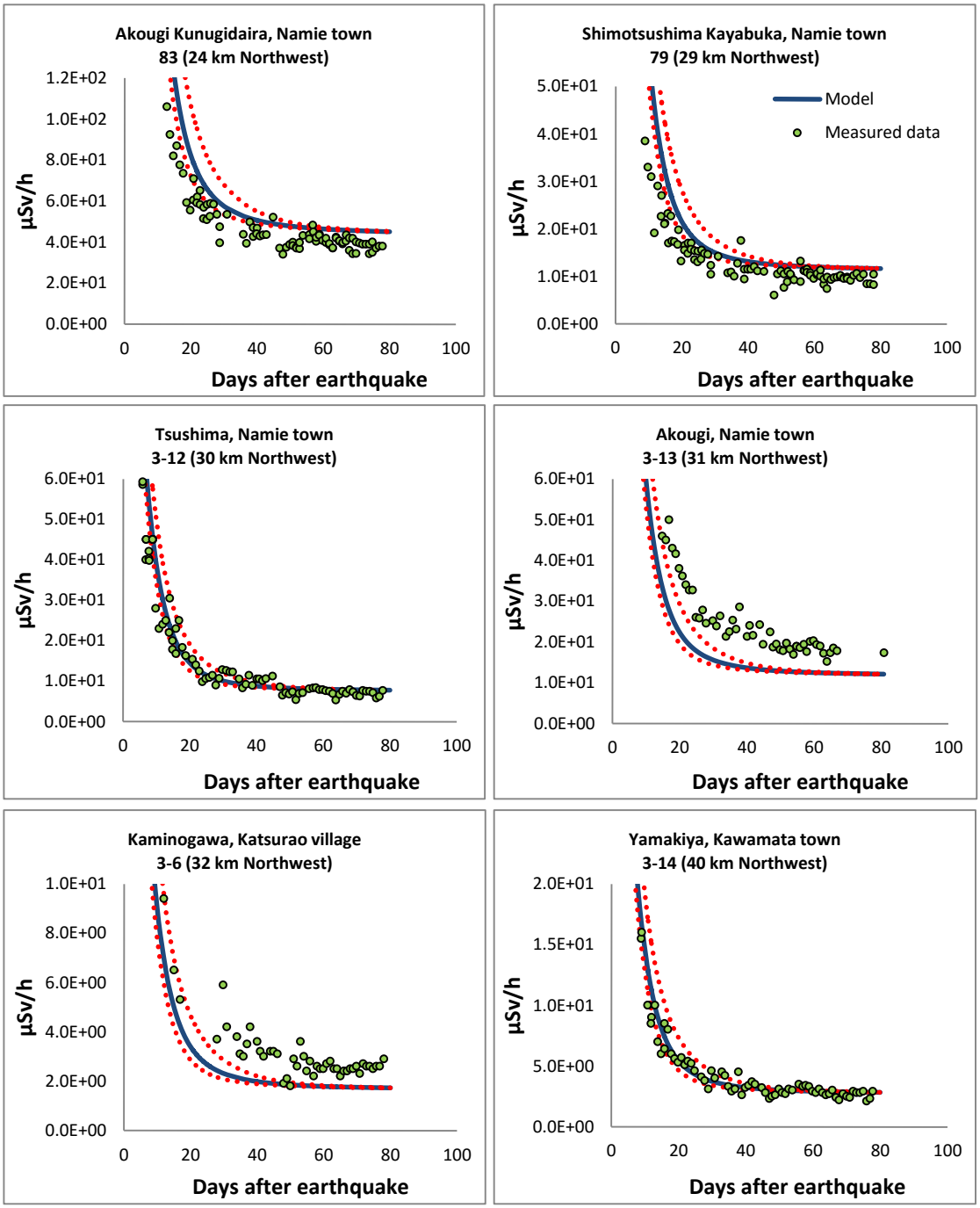

Figure 4-6 Model results with ±2σ uncertainty in estimation of $^{131}I/^{137}Cs$ ratio, compared with the measurement data at all six calibration sites.

4.3.3 ^{137}Cs activity

The parameter with the most influence in this model is the deposited activity of ^{137}Cs. This is because the other parameters are functions of ^{137}Cs activity: the measured ^{137}Cs activities at six calibration sites are used to evaluate the value of the *A* parameter for converting the sum of gamma energies and corrected ratios to gamma dose rate. In addition, the activities of other key radionuclides in soil are evaluated using the average corrected ratios, and particularly the estimation of ^{131}I/^{137}Cs from Equation 3-1 which extrapolates the ratio by using the ^{137}Cs activity. This is a strength of the model because it only needs one easily measurable input parameter, but also a weakness as it makes the model sensitive to uncertainty in the value of ^{137}Cs activity concentration.

The deposited activity of ^{137}Cs at all available sites where there were a sufficient number of samples ($n>50$) as shown in Table 4-5 were not significantly different to a normal distribution (Kolmogorov-Smirnov's test $p > 0.05$) . Therefore, the means of these data are an effective representation of the values at each site and can be used as the input to this model. Because ^{137}Cs activity at available sites are all normal, it is assumed that the ^{137}Cs activity data at smaller sample sites ($n<50$) are also normally distribution.

Since measured radioactivities of ^{137}Cs in soils are normally distributed, the variability of this parameter can be determined by using the S.E. or S.D for modelling. The S.D. indicates that how much variability there is between individuals in a sample are while S.E. is the uncertainty of the sample mean which represents the real mean of the population (Altman & Bland, 2005; Nagele, 2003). The S.D. in deposited radioactivity at a particular site, measures the variability due to differences factors including, for example, different episodes of depositions, characteristics of the ground such as type, density and radionuclide-absorption of soil, and removal factor of radioactivity in ground due to slope and erosion. In particular, the S.D. is the best uncertainty parameter to evaluate radioactivities from different sites where these influenced factors are significantly different. However, S.E. is a better choice to indicate the precision of the mean of measured data or samples to represent the exact mean radioactivity in soil at a given site. This is because all ratios of key nuclides estimated by correlation to ^{137}Cs activity in soil, the error from deposited ^{137}Cs might be the major error of modelling.

Table C-6 in Appendix C shows mean, S.E., S.D. and C.V. (coefficient of variation) of deposited radioactivity of ^{137}Cs at all sites around the near-zone of Fukushima I NPSs. To consider the distribution of ^{137}Cs activity at all sites, the % C.V. can be used. The distribution at all sites are vary significantly, most sites (31) have coefficient of variation between 40 and 60%, only 9 sites have less variation, but 16 sites have much higher variation (70-140%) as shown in Figure 4-7. At high variation sites, the error from the activity concentration of ^{137}Cs is significant when modelling the external gamma dose rate.

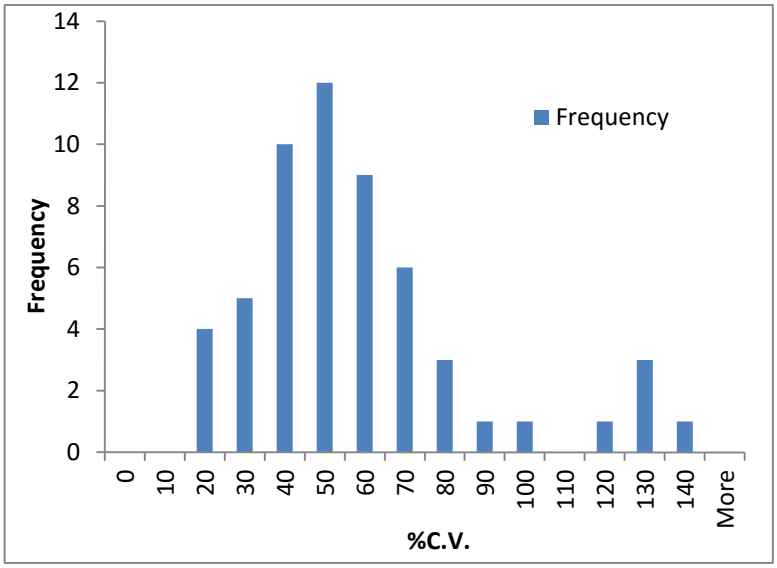

Figure 4-7 Illustrate the histogram of %C.V. of deposited concentration of ^{137}Cs in soil at near zone of Fukushima I NPSs

4.3.4 $^{132}Te/^{137}Cs$ and $^{132}I/^{137}Cs$

To estimate the external gamma dose by this modelmean of measured ratios of other key radionuclides (except $^{131}I^{137}Cs$) is used. As shown in Chapter 3, the deposited corrected ratios of ^{132}Te, ^{132}I, $^{134,136}Cs$ to ^{137}Cs are consistent with direction and distance from the NPP. From Table 4-2, the mean of $^{132}Te/^{137}Cs$ is 18.30, calculated from 20 samples of 20 sites, from Section 3.3.4 this mean is from a non-normal distribution. The histogram of this ratio in Figure 4-8 seems to be a parametric distribution. But because of the lack of measured data, it cannot be concluded that the distribution is normal. Therefore, an empirical probability density function was used to generate this ratio in Monte Carlo simulation.

Table 4-8 shows the available measurements of $^{132}Te/^{137}Cs$ and unit frequency of each ratio value determined from measured data at near zone of NPSs. There are many ratio values dispersed between 10.75 and 29.25. The highest frequency of this ratio is apparently at ratio 18.00 (unit frequency=0.15) that is very close to the mean value (18.30).

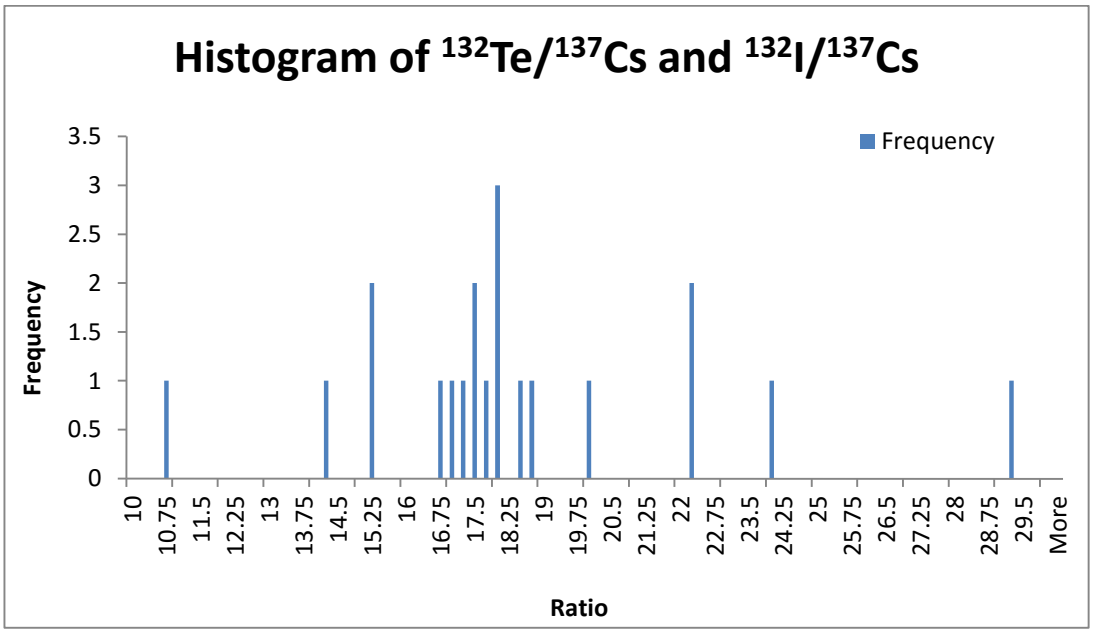

Figure 4-8 Histogram of $^{132}Te/^{137}Cs$ in soil which is equal to $^{132}I/^{137}Cs$ from measured data at near zone of Fukushima I NPSs.

Table 4-8 the ratio value and its unit frequency of $^{132}Te/^{137}Cs$ from measured data (n=20) at near zone of Fukushima I NPSs.

Ratio	Unit Frequency	Ratio	Unit Frequency	Ratio	Unit Frequency
10	0	16.75	0.05	23.5	0
10.25	0	17	0.05	23.75	0
10.5	0	17.25	0.05	24	0.05
10.75	0.05	17.5	0.1	24.25	0
11	0	17.75	0.05	24.5	0
11.25	0	18	0.15	24.75	0
11.5	0	18.25	0	25	0
11.75	0	18.5	0.05	25.25	0
12	0	18.75	0.05	25.5	0
12.25	0	19	0	25.75	0
12.5	0	19.25	0	26	0
12.75	0	19.5	0	26.25	0
13	0	19.75	0	26.5	0
13.25	0	20	0.05	26.75	0
13.5	0	20.25	0	27	0
13.75	0	20.5	0	27.25	0
14	0	20.75	0	27.5	0
14.25	0.05	21	0	27.75	0
14.5	0	21.25	0	28	0
14.75	0	21.5	0	28.25	0
15	0	21.75	0	28.5	0
15.25	0.1	22	0	28.75	0
15.5	0	22.25	0.1	29	0
15.75	0	22.5	0	29.25	0.05
16	0	22.75	0	29.5	0
16.25	0	23	0	29.75	0
16.5	0	23.25	0	30	0

4.3.5 $^{134}Cs/^{137}Cs$

In addition to the large number of measurements of ^{137}Cs concentration in soil at near zone, there were many samples measuring ^{134}Cs: 1,817 samples from 146 sites, with mean 0.90 with 0.01 for S.E. and 0.06 for S.D (see Figure C-1, Appendix C for details). From Section 3.3.4, the mean of these measured data are not normally distributed and it is clear from the histogram in Figure-4.9 that the data show a positive skew with a very long right tail.

From Table 4-9, the highest ratio is 0.88 and highest region is between 0.85 and 0.89. There are many ratios greater than highest region from 0.93 to 1.08 while the lower is only 0.83 – 0.84. The significant frequencies occur at 0-94-0.97 and a little frequencies are at 1.00 – 1.03. This pattern clears that we cannot use only S.E. and S.D. to determine the variation from $^{134}Cs/^{137}Cs$, an empirical probability density function is a best method to evaluate variation of this ratio.

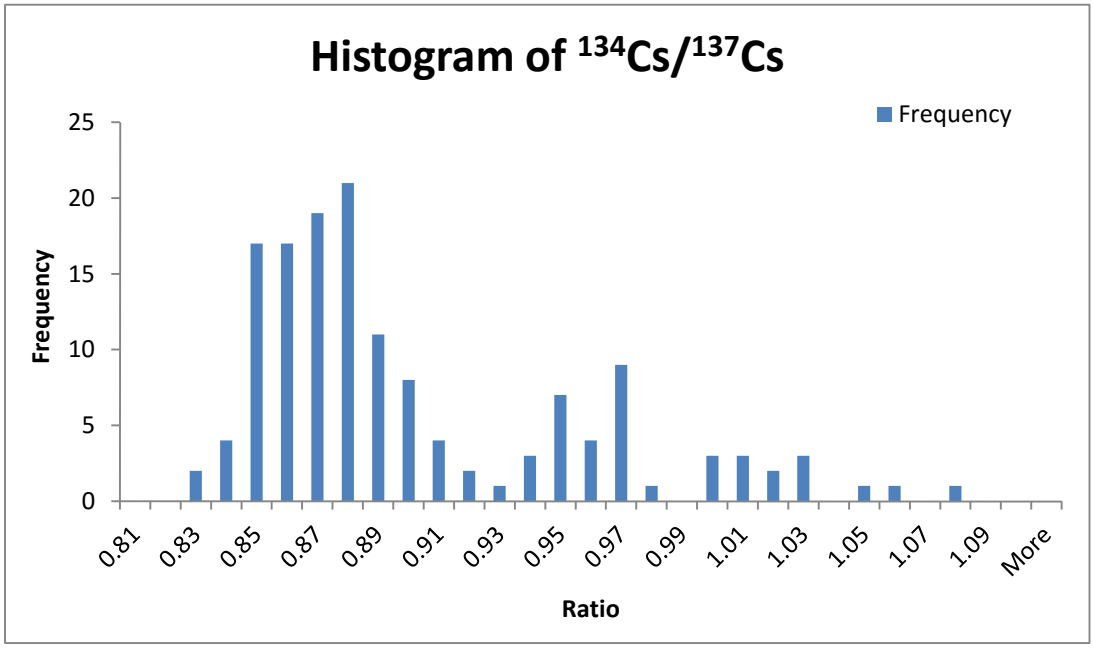

Figure 4-9 Histogram of $^{134}Cs/^{137}Cs$ in soil from measured data at near zone of Fukushima I NPSs.

Table 4-9 the value of the ratio and its unit frequency for $^{134}Cs/^{137}Cs$ from measured data (n=144) at near zone of Fukushima I NPSs.

Ratio	Unit Frequency	Ratio	Unit Frequency	Ratio	Unit Frequency
0.81	0	0.91	0.027778	1.01	0.020833
0.82	0	0.92	0.013889	1.02	0.013889
0.83	0.013889	0.93	0.006944	1.03	0.020833
0.84	0.027778	0.94	0.020833	1.04	0
0.85	0.118056	0.95	0.048611	1.05	0.006944
0.86	0.118056	0.96	0.027778	1.06	0.006944
0.87	0.131944	0.97	0.062500	1.07	0
0.88	0.145833	0.98	0.006944	1.08	0.006944
0.89	0.076389	0.99	0	1.09	0
0.9	0.055556	1	0.020833	1.1	0

4.3.6 $^{136}Cs/^{137}Cs$

For $^{136}Cs/^{137}Cs$, the histogram in Figure 4-10 and Section 3.3.4 show the nonparametric distribution of this ratio. The shape of distribution is a little positive skewed. An empirical probability distribution as shown in Table 4-10 was therefore used to generate random numbers for the Monte Carlo simulation.

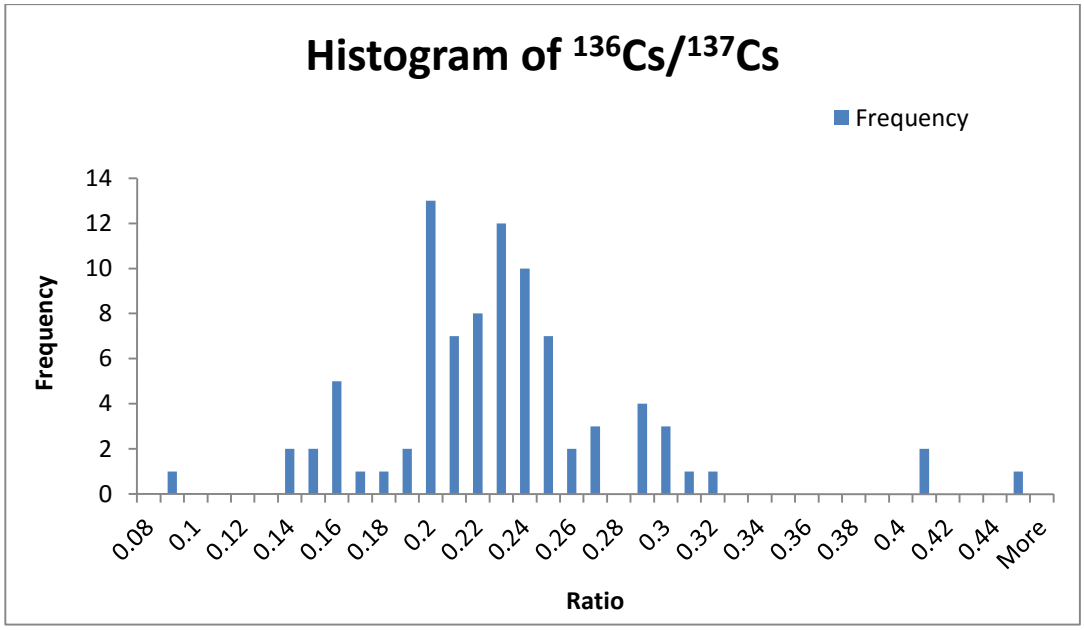

Figure 4-10 Histogram of $^{136}Cs/^{137}Cs$ in soil from measured data at near zone of Fukushima I NPSs.

Table 4-10 the ratio value and its unit frequency of $^{136}Cs/^{137}Cs$ from measured data (n=88) at near zone of Fukushima I NPSs.

Ratio	Unit Frequency	Ratio	Unit Frequency
0.08	0	0.27	0.034091
0.09	0.011364	0.28	0
0.1	0	0.29	0.045455
0.11	0	0.3	0.034091
0.12	0	0.31	0.011364
0.13	0	0.32	0.011364
0.14	0.022727	0.33	0
0.15	0.022727	0.34	0
0.16	0.056818	0.35	0
0.17	0.011364	0.36	0
0.18	0.011364	0.37	0
0.19	0.022727	0.38	0
0.2	0.147727	0.39	0
0.21	0.079545	0.4	0
0.22	0.090909	0.41	0.022727
0.23	0.136364	0.42	0
0.24	0.113636	0.43	0
0.25	0.079545	0.44	0
0.26	0.022727	0.45	0.011364

4.4 The individual and total error from input parameters

Monte Carlo simulation is used to determine the error from input parameters for this model. The method uses random samples, of a parameter to determine the behaviour of parameter in a complex system (Kalos & Whitlock, 2008; Seco & Verhaegen, 2013). Since there were differences between the errors of parameters as discussed above in Section 4.3.1-4.3.6, this simulation is appropriate to determine the error from this model. In each parameter, the tool of random number generator in Microsoft Excel will generate 1,000 samples from the behaviour of variation of each parameter. For individual parameter, Monte Carlo is used to random samples for determined parameter, then these samples and mean values of other parameters are used in the model calculation to evaluate the upper and lower error from the determined parameter. For total errors from all input parameters, 1,000 random values of each parameter are the input to determine the total error of the model.

4.4.1 The individual error from each input parameter

The error from each individual parameter and from the combination of all parameters can be determined by using Monte Carlo simulation. The simulation was performed at six calibration sites where have measured data of the external gamma dose rate was available in the first few days after deposition.

For the evaluation of sensitivity for each individual parameter, the values of the parameter which is being determined were generated for the Monte Carlo simulation using each error distribution while other parameters are using their mean values. For the analysis sensitivity to ^{137}Cs concentration, uncertainty in both the ^{131}I/^{137}Cs ratio and the ^{137}Cs concentration was generated. This is because, the value of ^{131}I/^{137}Cs depends on the ^{137}Cs concentration via Equation 3-1. Figure 4-18 (a) – (f) shows the results of the simulation for individual parameters varied and the combination of all parameters varied at the six calibration sites. The error in the *A* parameter was generated by using the uniform distribution between 1.46×10^{-4} and 5.70×10^{-5} which are the upper and lower limits evaluated by the SAS software; both values are consistent with the range for all sites). In terms of ^{131}I/^{137}Cs, the distribution is assumed to be uniform distribution is used between the upper and lower limits (Equation 4-2) at each site are taken to analyse the error from this parameter. For the error from the deposited concentration of ^{137}Cs, two S.E. (95% confidence) will be applied for evaluating the error from all parameters. Since the concentration of ^{137}Cs is normally distributed, the mean and S.E. is appropriate. Finally, the deposited corrected ratios of ^{132}Te, ^{132}I, ^{134,136}Cs to ^{137}Cs which are non-parametrically distributed, and an empirical probability density function is used to determine the error from these parameters.

It is clear that, in Figure 4-17 (a) – (f), the largest error is from the value of the *A* parameter and the radioactivity concentration of ^{137}Cs in soil. Since this is an empirical parameter converting the term from all other factors to the external gamma dose rate, the error from this parameter already includes errors from the other parameters: the error from the *A* parameter is almost the same as the error in all parameters combined. Figure 4-11 shows the uncertainty in the *A* parameter was high in the early period from 15 March in two of the six calibration sites. After this period, the variation continuously deceased until 30 days after earthquake, after that the variation is constant.

For the uncertainty in deposited concentration of ^{137}Cs, the error at each site depends on the S.E. in the mean value at each site. This error is important as other corrected ratios are a function of this parameter. The uncertainty in ^{137}Cs (Figure 4-13) concentration has the same trend with time as the *A* parameter. Initially, the gamma dose was determined by all key radionuclides so variation in all isotope ratios is important, then as key short-lived radionuclides decayed the gamma dose became dominated by long-lived ^{134,137}Cs, reducing the uncertainty to that of the estimation of the ^{137}Cs concentration since the ^{134}Cs:^{137}Cs ratio is relatively constant. Figures 4-17 (a) – (f) show that the error from uncertainty in the ^{131}I/^{137}Cs ratio is less than that of the *A* parameter and ^{137}Cs concentration but the error from this parameter is significantly greater than ^{134,136}Cs to ^{137}Cs ratios. ^{131}I has a significantly higher release amount, and lower gamma decay energy and half-life than ^{134,136}Cs. This means that the influence of the release amount has more effect on the gamma dose in this case. The model is least sensitive to uncertainty in ^{134,136}Cs:^{137}Cs (Figure 4-15 and 4-16) because the variation in their ratios to ^{137}Cs is relatively small and because ^{136}Cs had a very low deposited concentration in soil (even though ^{136}Cs has higher gamma decay energy).

4.4.2 The total error from all input parameters

For error from the combination of all parameters, 1000 randomly distributed values of all parameters are generated. As shown in Figure 4-17 (a) – (f), when variation in all parameters is considered, the majority of the total error is from the deposited concentration of ^{137}Cs and the *A* parameter. The total error also was influenced by uncertainty in the ratios ^{131}I/^{137}Cs and ^{132}Te/^{137}Cs (with its daughter: ^{132}I/^{137}Cs) during the first few days after 15 March, while the ratio of radiocaesium (^{134,137}Cs) isotopes has little effect during the entire period. These results are in agreement with the assessment of individual errors discussed above. Using 95% confidence in the simulation results of total error allows us to determine the upper and lower of total errors as shown in Figure 4-18. The yellow dotted line is the upper and lower of the errors from all parameters (include the errors from *A* parameter and ^{131}I/^{137}Cs), and red dotted line for *A* parameter and back dash line for ^{131}I/^{137}Cs individually (by calculation in Section 4.3.1 and 4.3.2 respectively). Since the total error includes error from all parameters, this error has good agreement with the range in measured data at six calibration sites including site 3-13 and 3-6 where the error from the *A* parameter and ^{131}I/^{137}Cs were underestimated. This is

because the error from deposited concentration of ^{137}Cs used to estimate $^{131}I/^{137}Cs$ was included in the total error. Therefore, the sensitivity from all parameters evaluated by Monte Carlo simulation can be used to evaluate uncertainty in the model as they show good agreement with early measured data (when gamma dose rate high with a contribution of all key radionuclides).

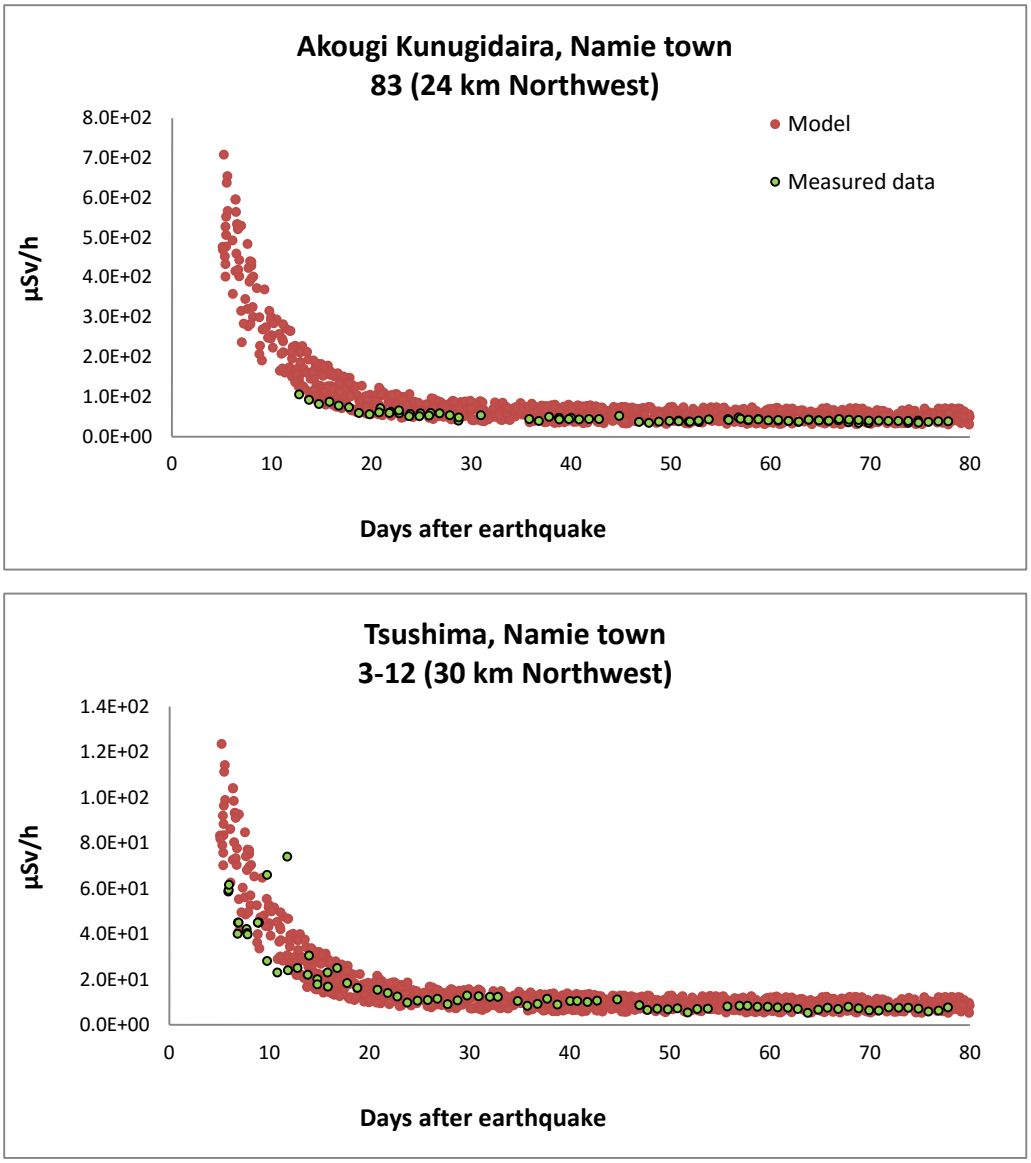

Figure 4-11 Results from Monte Carlo simulation for the error from *A* parameter since 15 March.

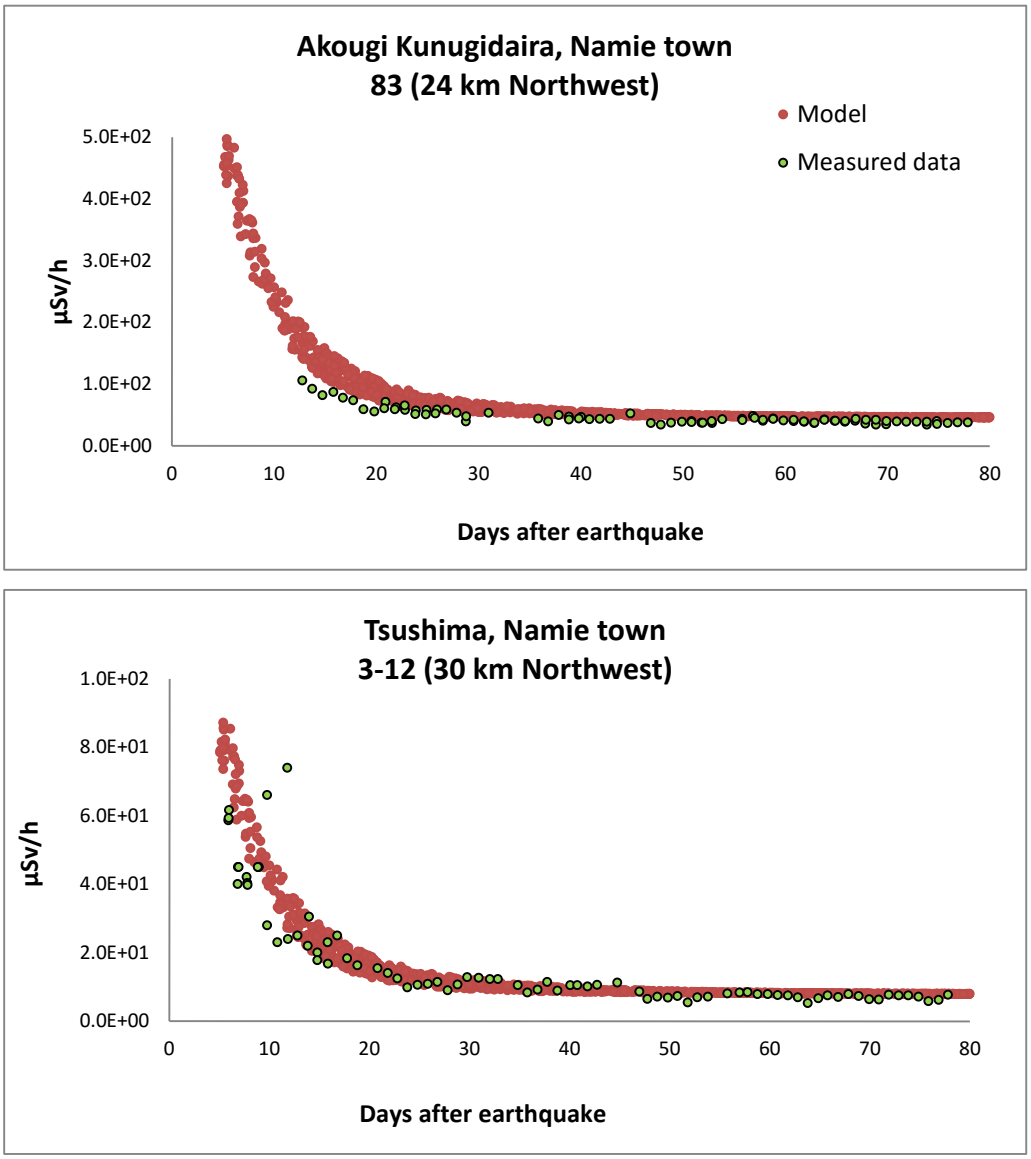

Figure 4-12 Results from Monte Carlo simulation for the error from $^{131}I/^{137}Cs$ in soil since 15 March.

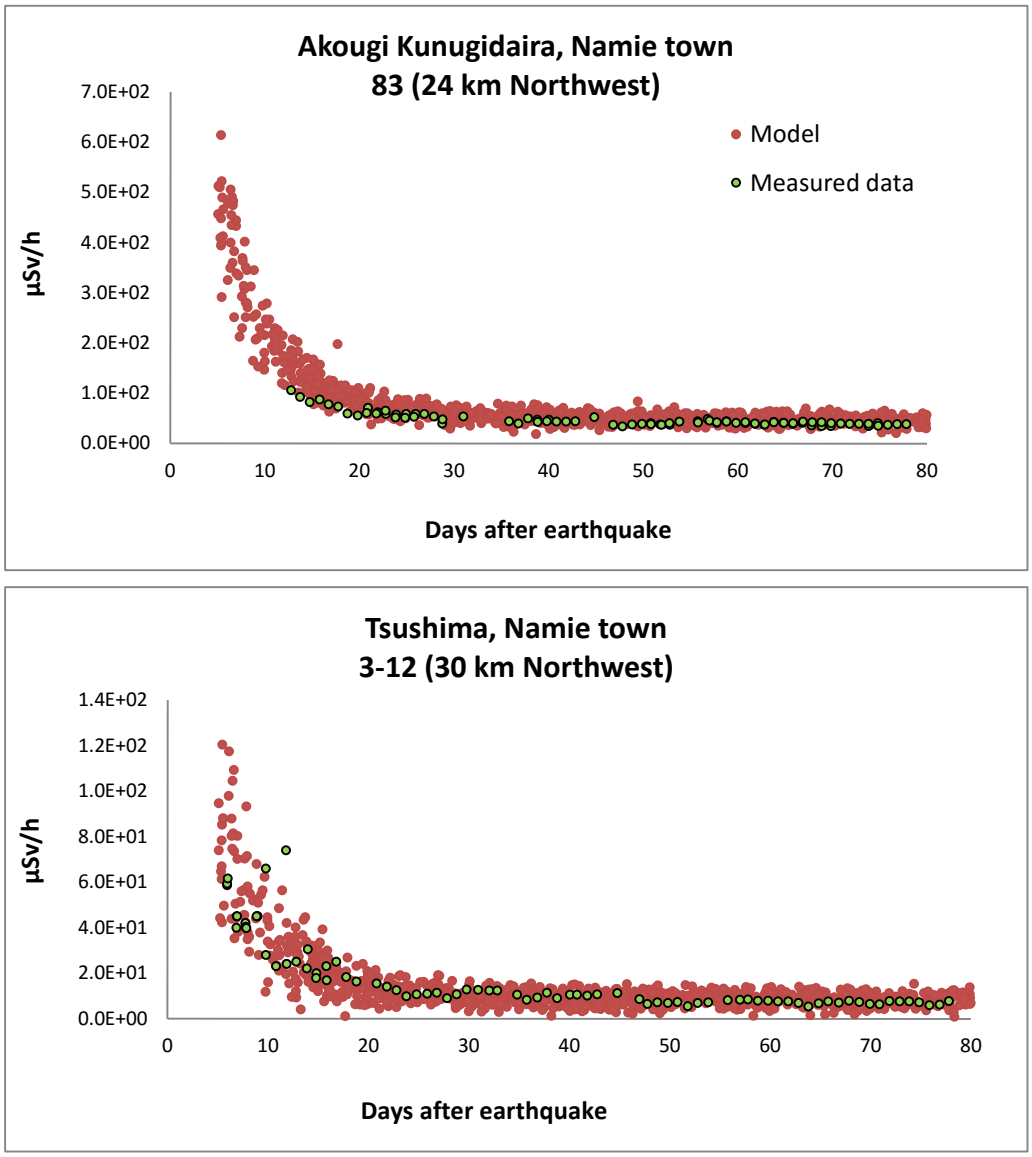

Figure 4-13 Results from Monte Carlo simulation for the error from concentration of ^{137}Cs in soil since 15 March.

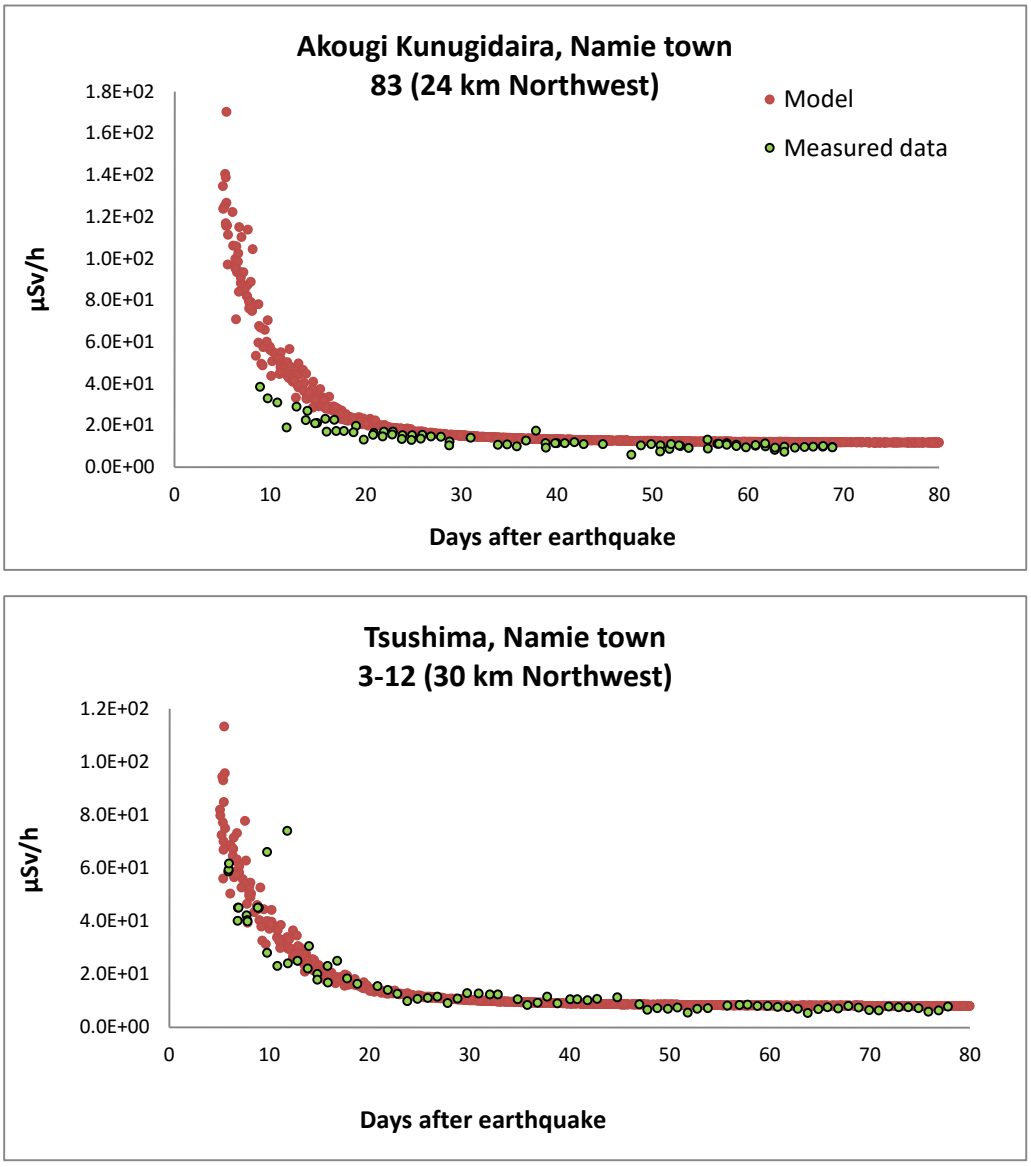

Figure 4-14 Results from Monte Carlo simulation for the error from concentration of $^{132}Te/^{137}Cs$ in soil which is equal to $^{132}I/^{137}Cs$ since 15 March.

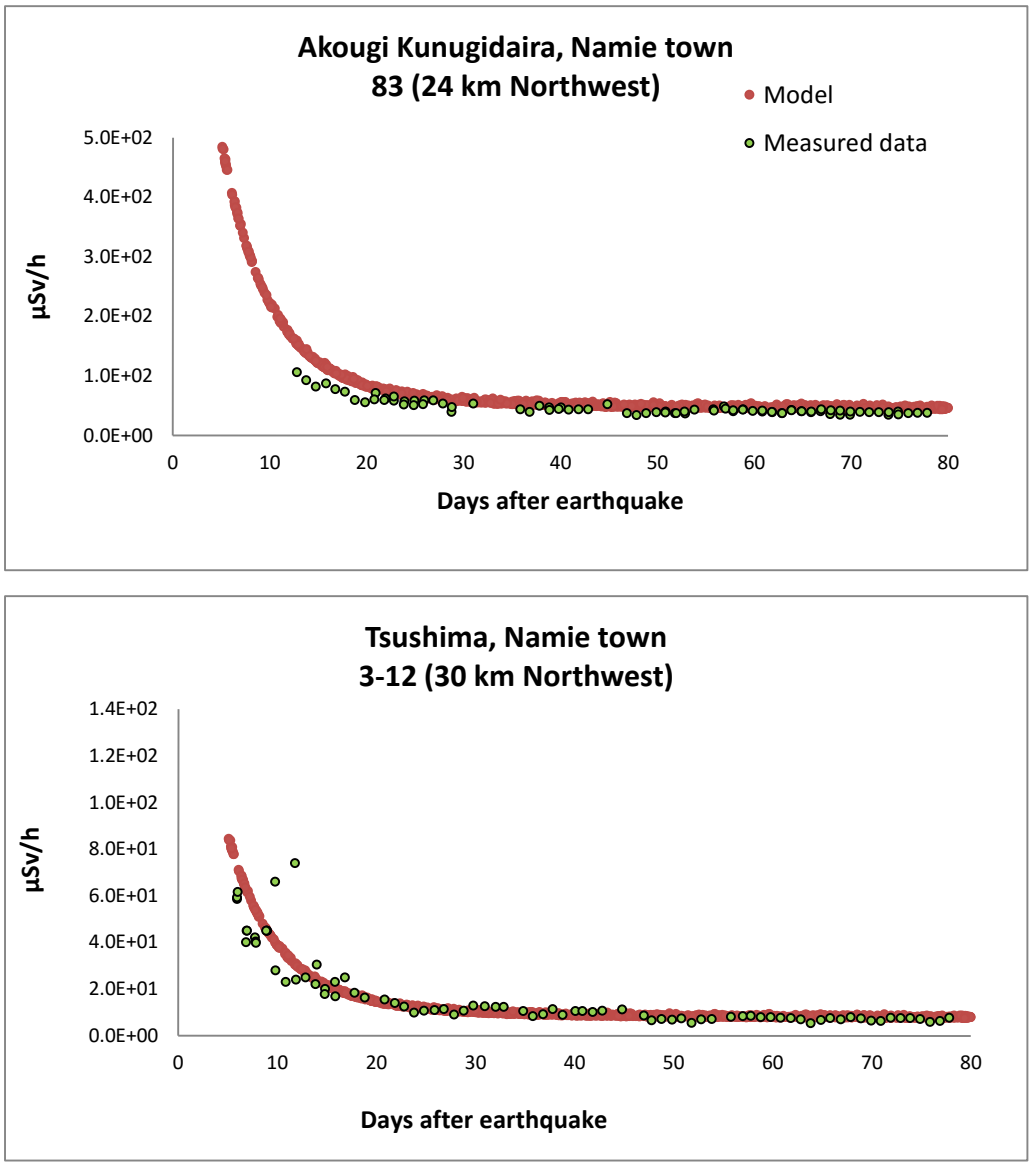

Figure 4-15 Results from Monte Carlo simulation for the error from concentration of $^{134}Cs/^{137}Cs$ in soil since 15 March.

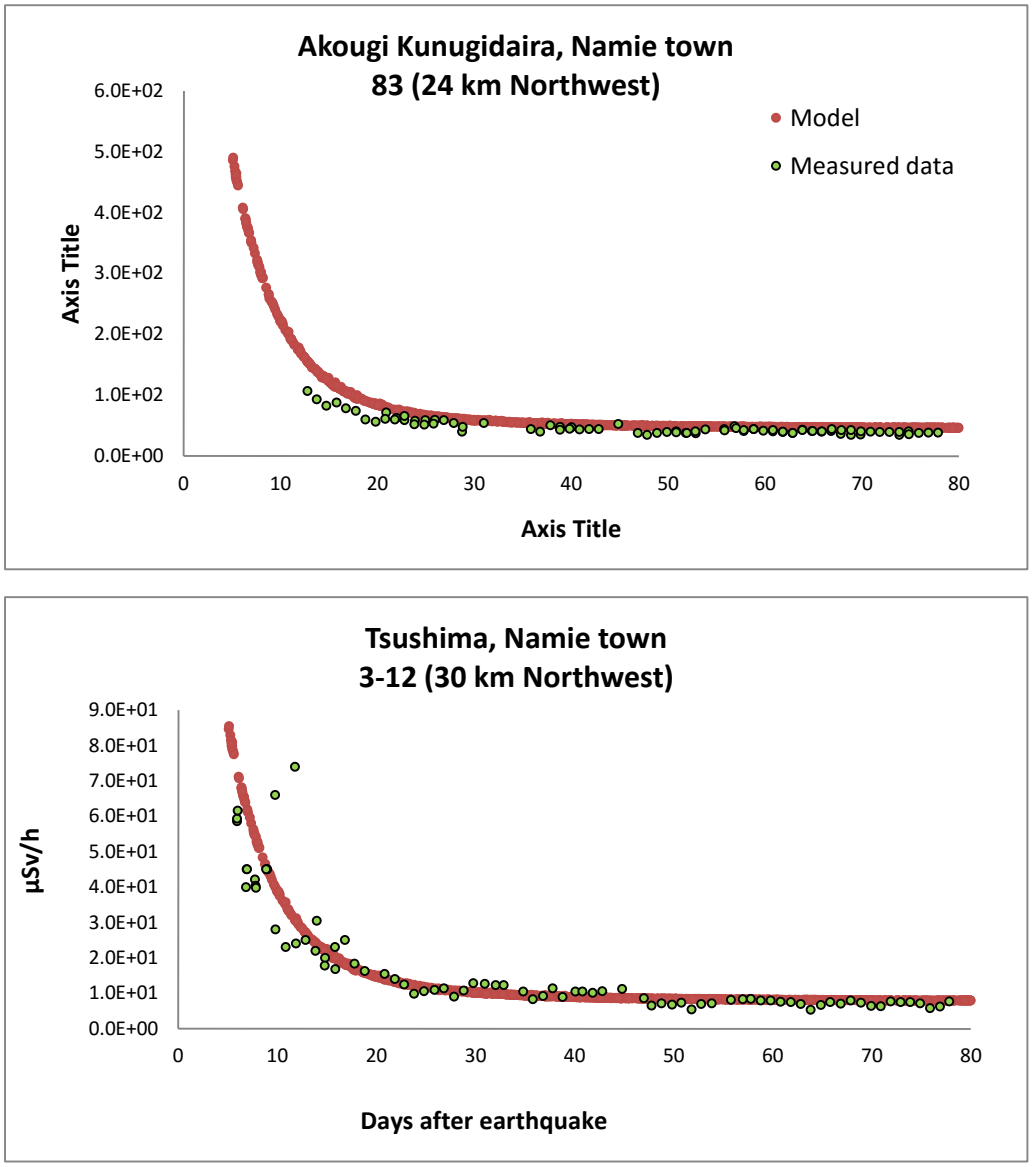

Figure 4-16 Results from Monte Carlo simulation for the error from concentration of $^{136}Cs/^{137}Cs$ in soil since 15 March.

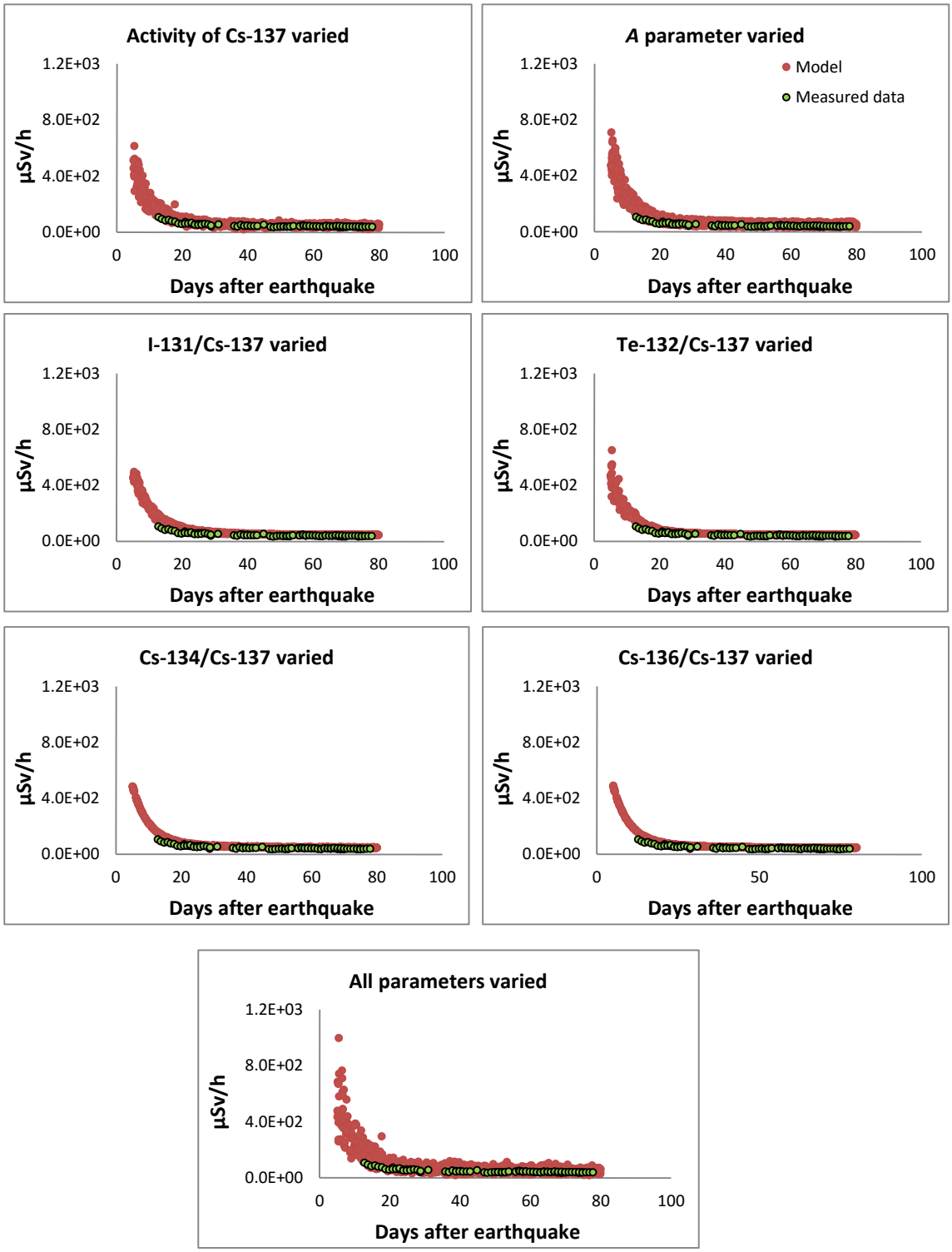

(a) Akougi Kunugidaira, Namie town (code: 83 and Direction: 24 km Northwest)

Figure 4-17 The comparisons between measured data and model results from the randomly generated parameters of activity of ^{137}Cs in soil, *A* parameter, and the deposited corrected ratios of ^{131}I (Equation 3-1), ^{132}Te (with ^{132}I), ^{134,136}Cs to ^{137}Cs and all parameters at calibration sites.

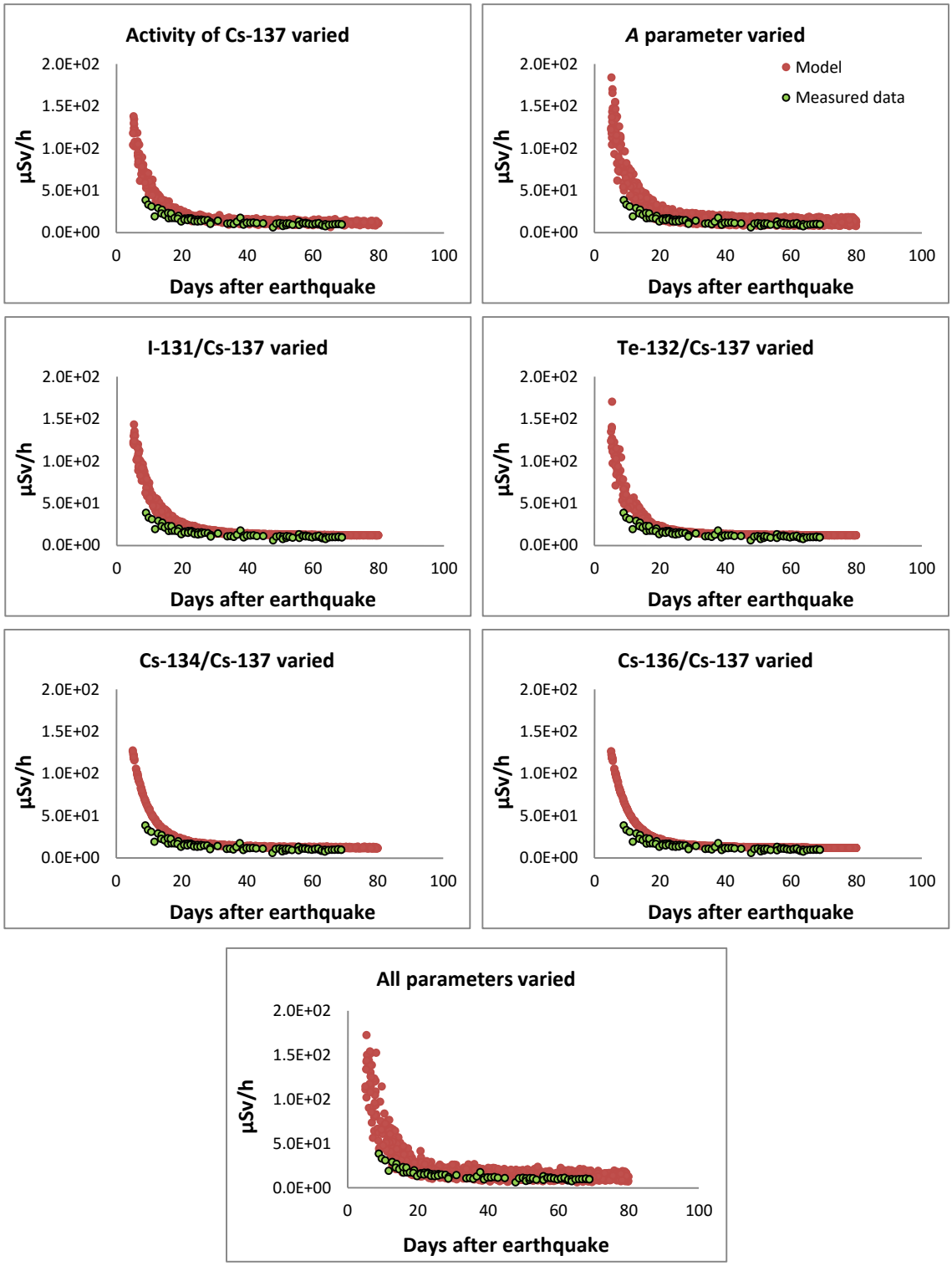

(b) Shimotsushima Kayabuka, Namie town (code: 79 and Direction: 29 km Northwest)

Figure 4-17 (continued) The comparisons between measured data and model results from the randomly generated parameters of activity of ^{137}Cs in soil, *A* parameter, and the deposited corrected ratios of ^{131}I (Equation 3-1), ^{132}Te (with ^{132}I), ^{134,136}Cs to ^{137}Cs and all parameters at calibration sites.

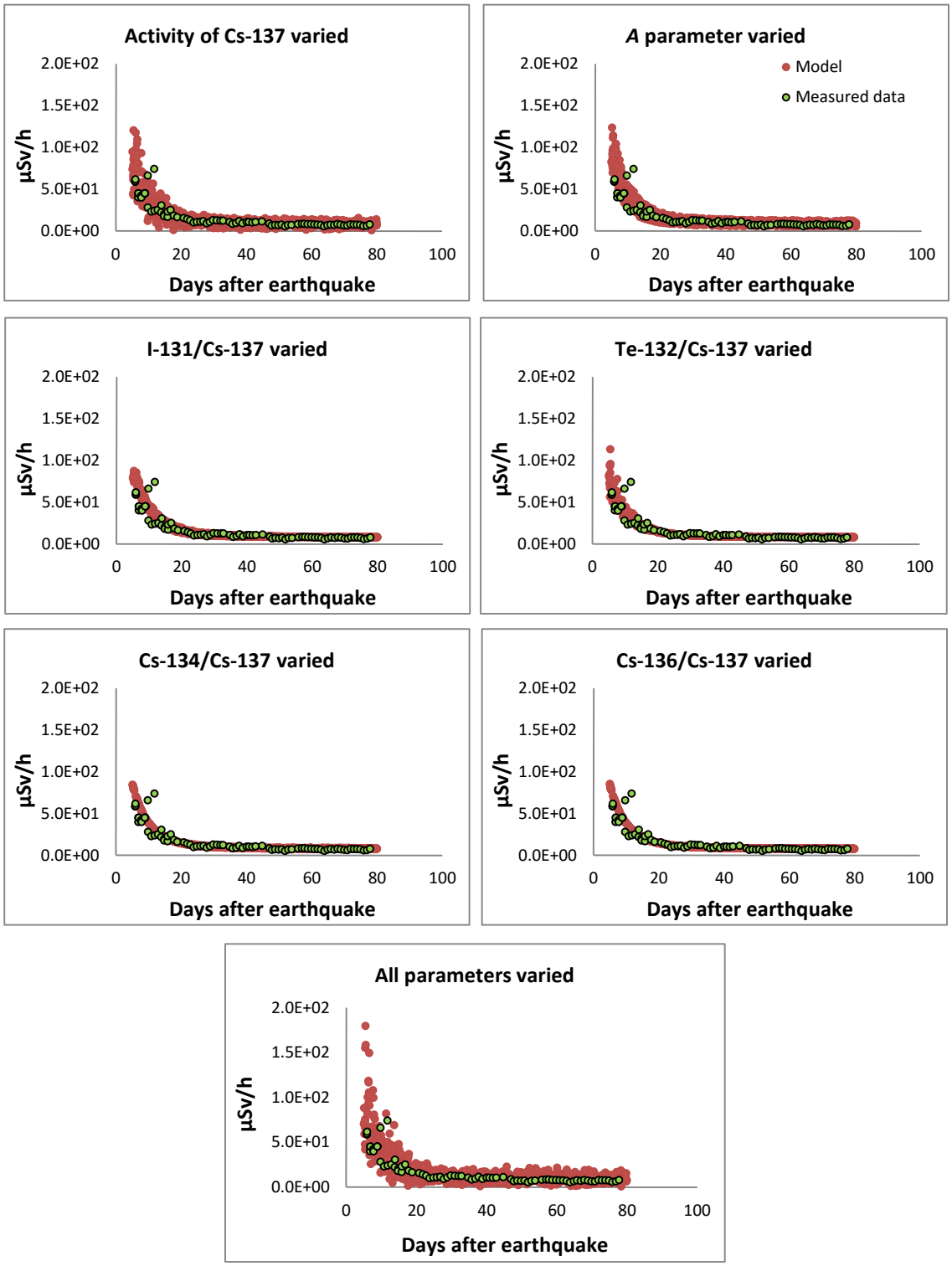

(c) Tsushima, Namie town (code: 3-12 and Direction: 30 km Northwest)

Figure 4-17(continued) The comparisons between measured data and model results from the randomly generated parameters of activity of ^{137}Cs in soil, *A* parameter, and the deposited corrected ratios of ^{131}I (Equation 3-1), ^{132}Te (with ^{132}I), ^{134,136}Cs to ^{137}Cs and all parameters at calibration sites.

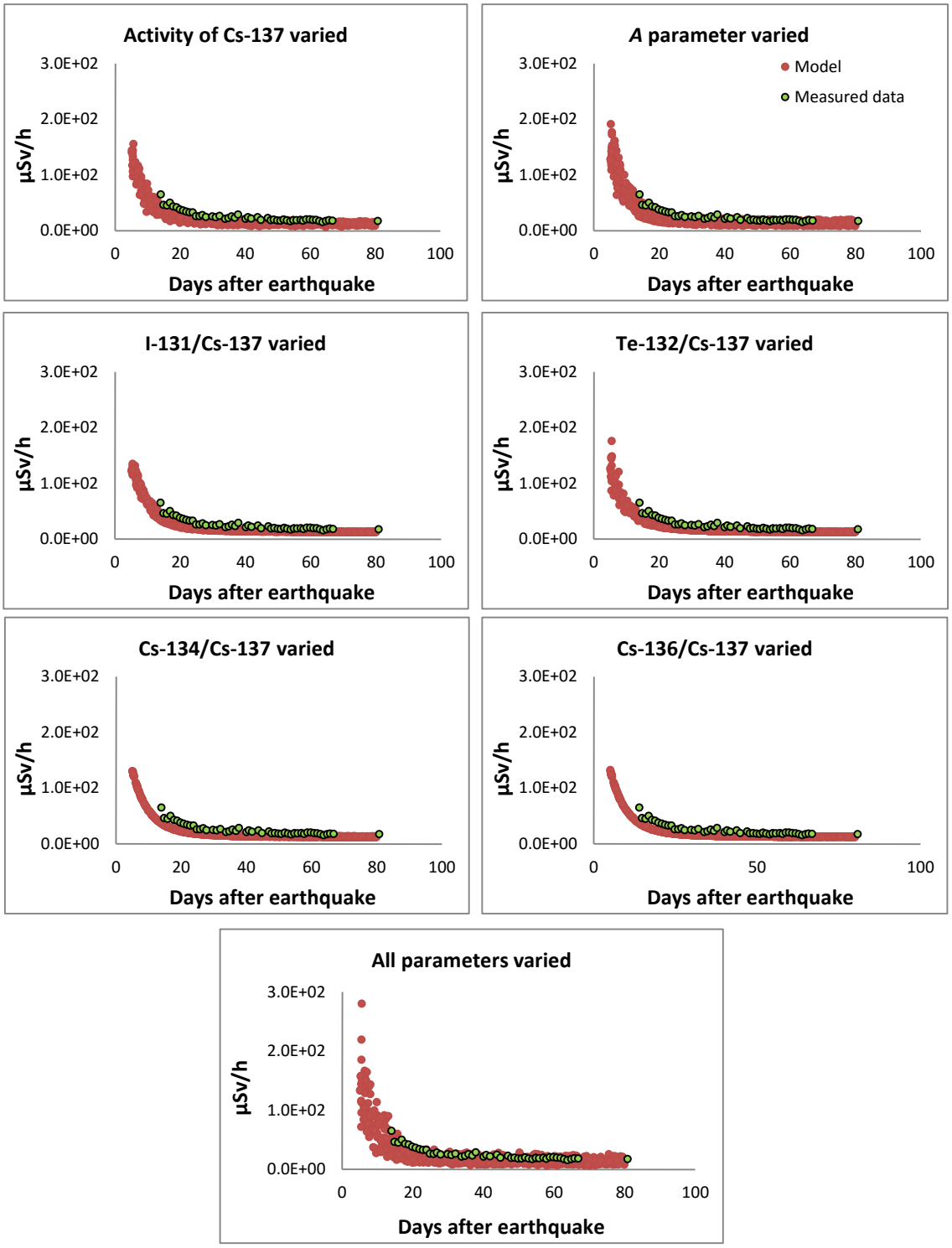

(d) Akougi, Namie town (code: 3-13 and Direction: 31 km Northwest)

Figure 4-17 (continued) The comparisons between measured data and model results from the randomly generated parameters of activity of ^{137}Cs in soil, *A* parameter, and the deposited corrected ratios of ^{131}I (Equation 3-1), ^{132}Te (with ^{132}I), ^{134,136}Cs to ^{137}Cs and all parameters at calibration sites.

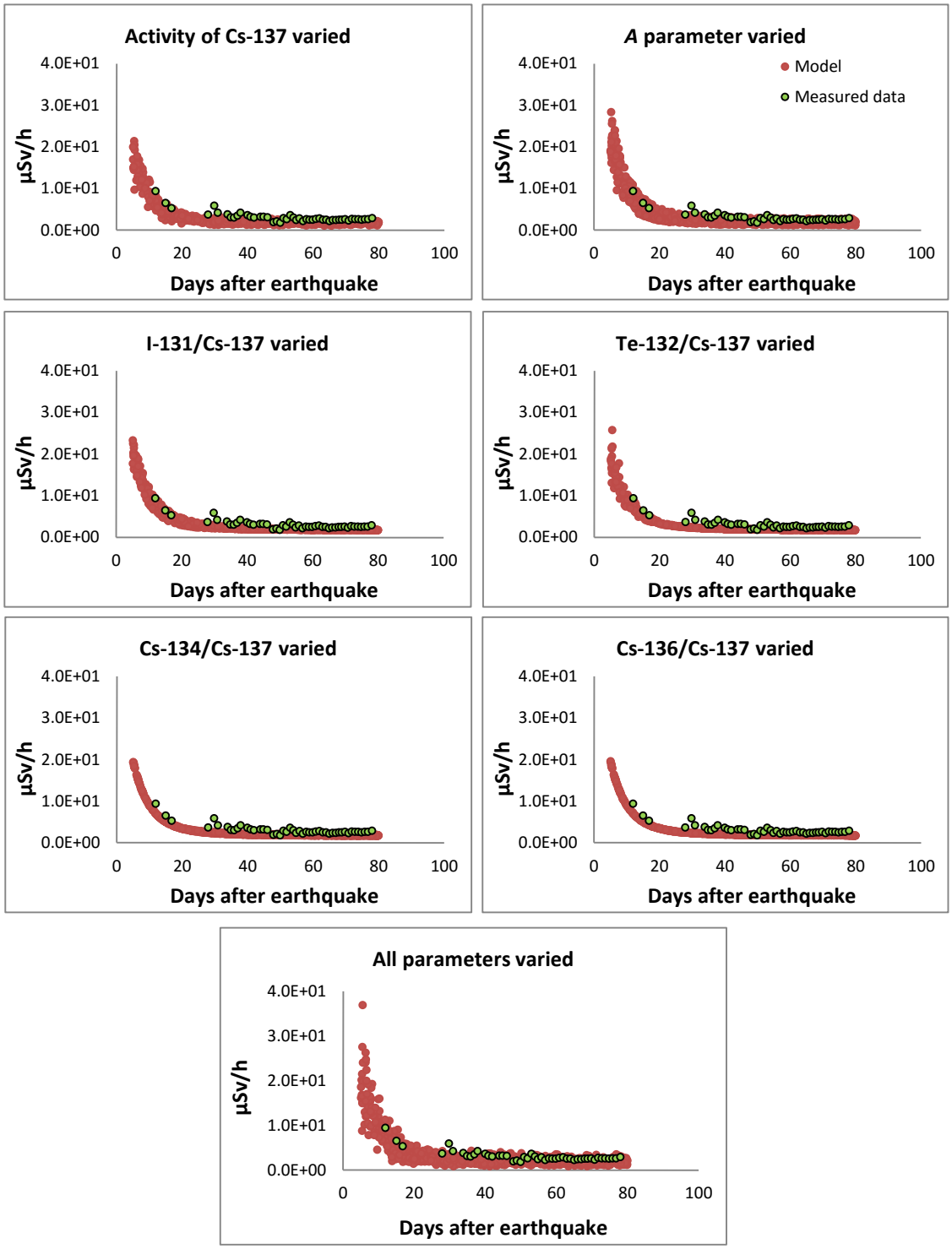

(e) Kaminogawa, Katsurao village (code: 3-6 and Direction: 32 km Northwest)

Figure 4-17 (continued) The comparisons between measured data and model results from the randomly generated parameters of activity of ^{137}Cs in soil, *A* parameter, and the deposited corrected ratios of ^{131}I (Equation 3-1), ^{132}Te (with ^{132}I), ^{134,136}Cs to ^{137}Cs and all parameters at calibration sites.

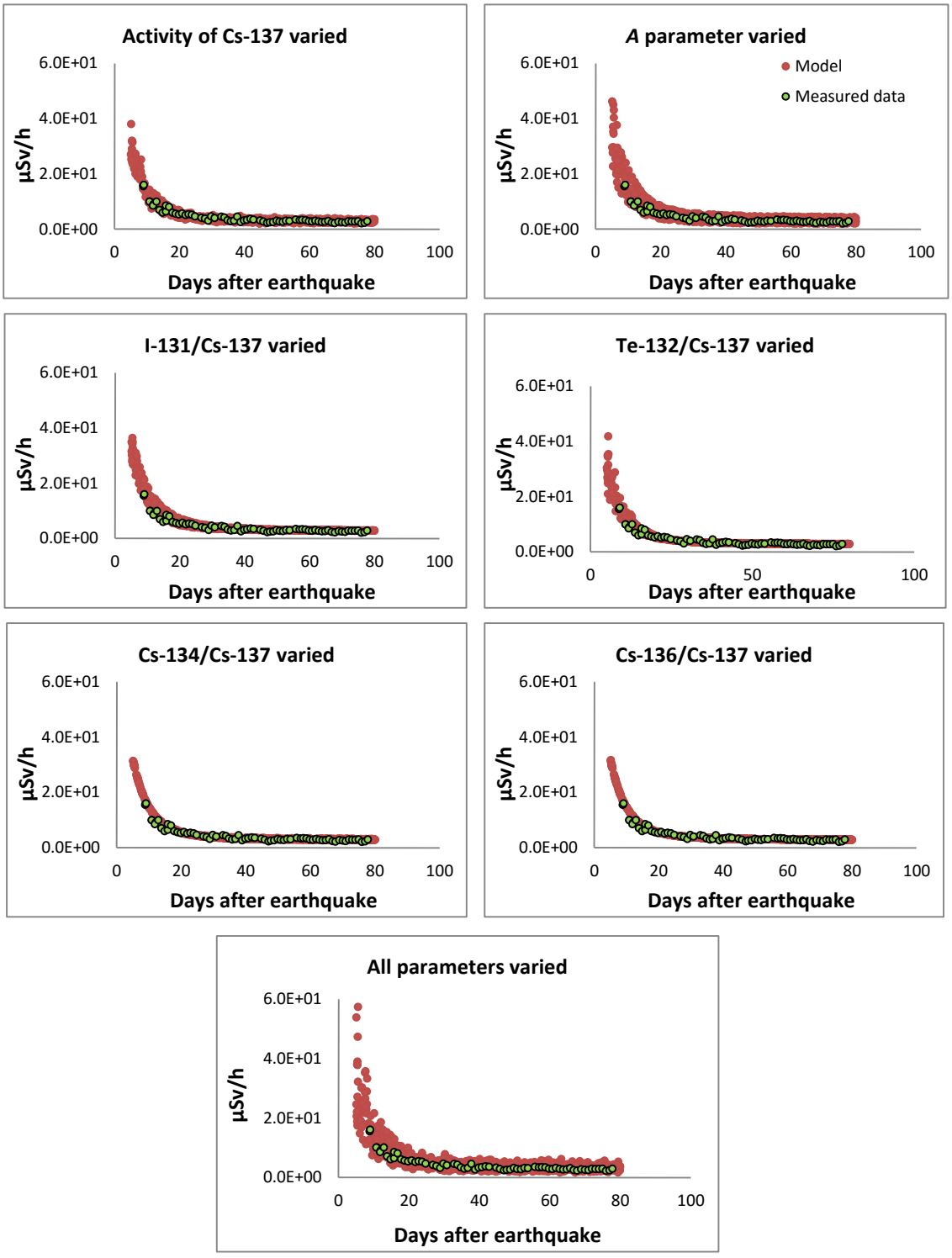

(f) Yamakiya, Kawamata town (code: 3-14 and Direction: 40 km Northwest)

Figure 4-17 (continued) The comparisons between measured data and model results from the randomly generated parameters of activity of ^{137}Cs in soil, *A* parameter, and the deposited corrected ratios of ^{131}I (Equation 3-1), ^{132}Te (with ^{132}I), ^{134,136}Cs to ^{137}Cs and all parameters at calibration sites.

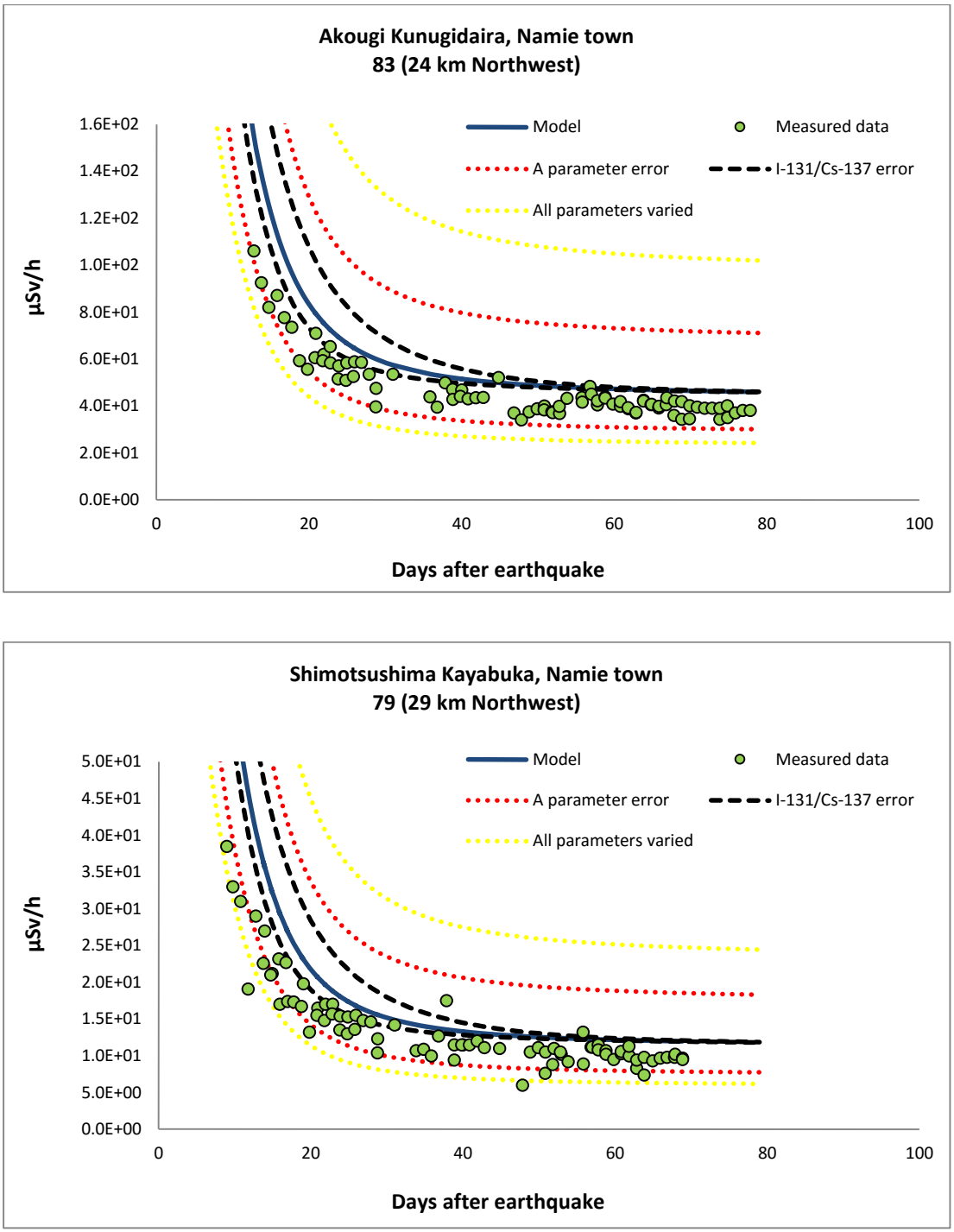

Figure 4-18 Comparison of errors from *A* parameter, $^{131}I/^{137}Cs$, and all parameters at six calibration sites.

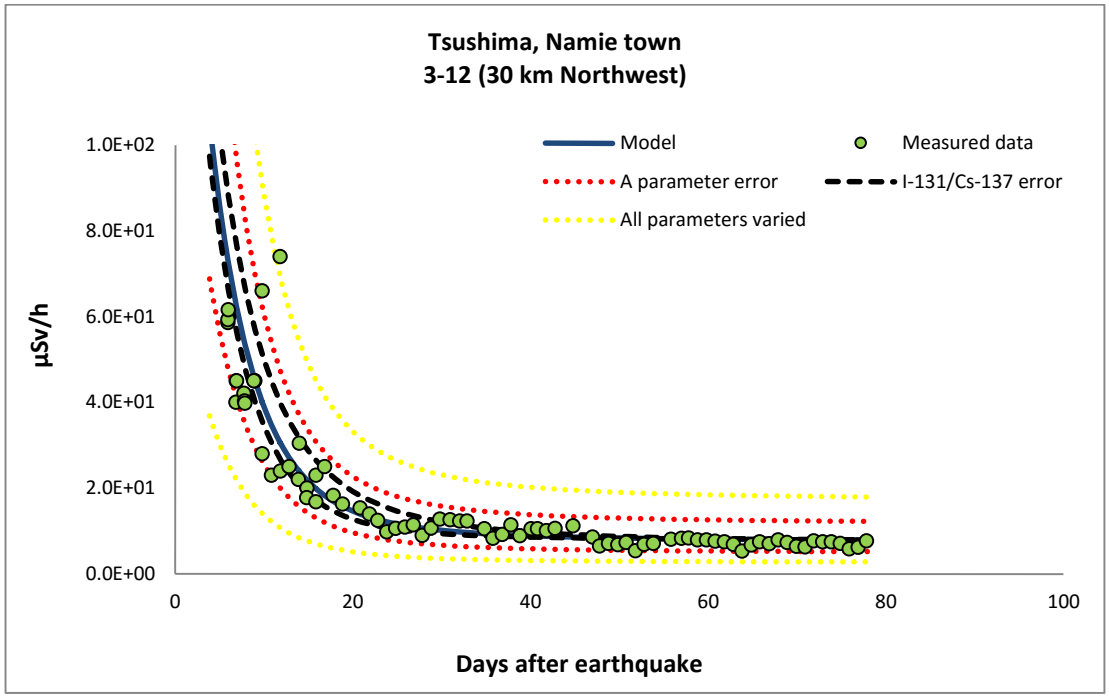

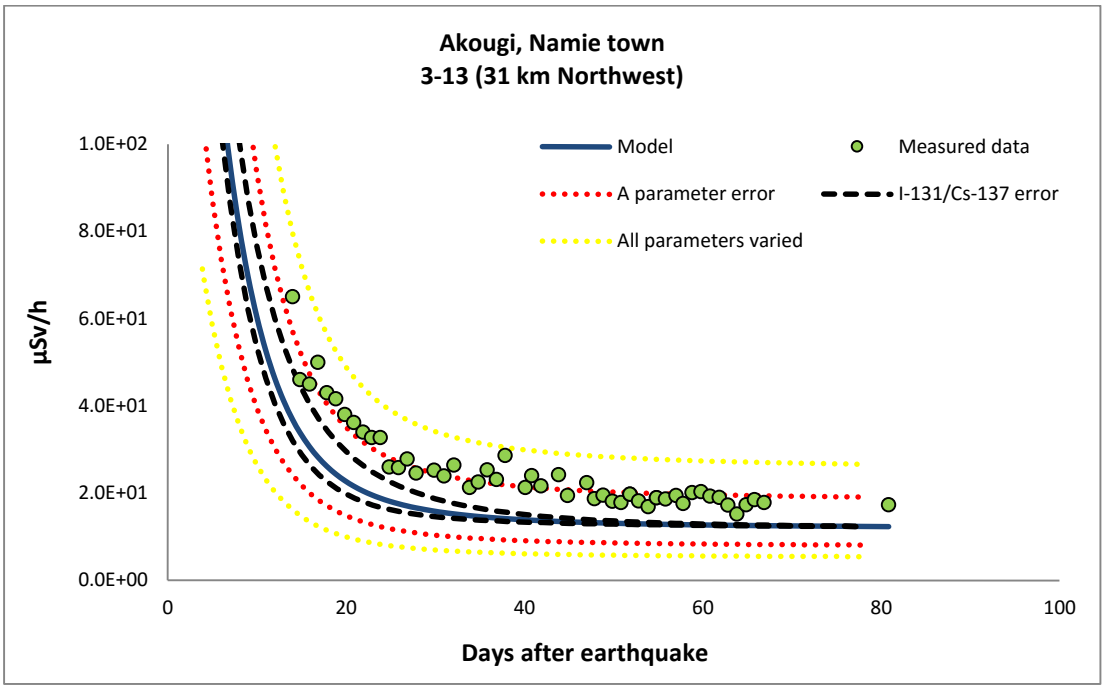

Figure 4-18 (continued) Comparison of errors from *A* parameter, $^{131}I/^{137}Cs$, and all parameters at six calibration sites.

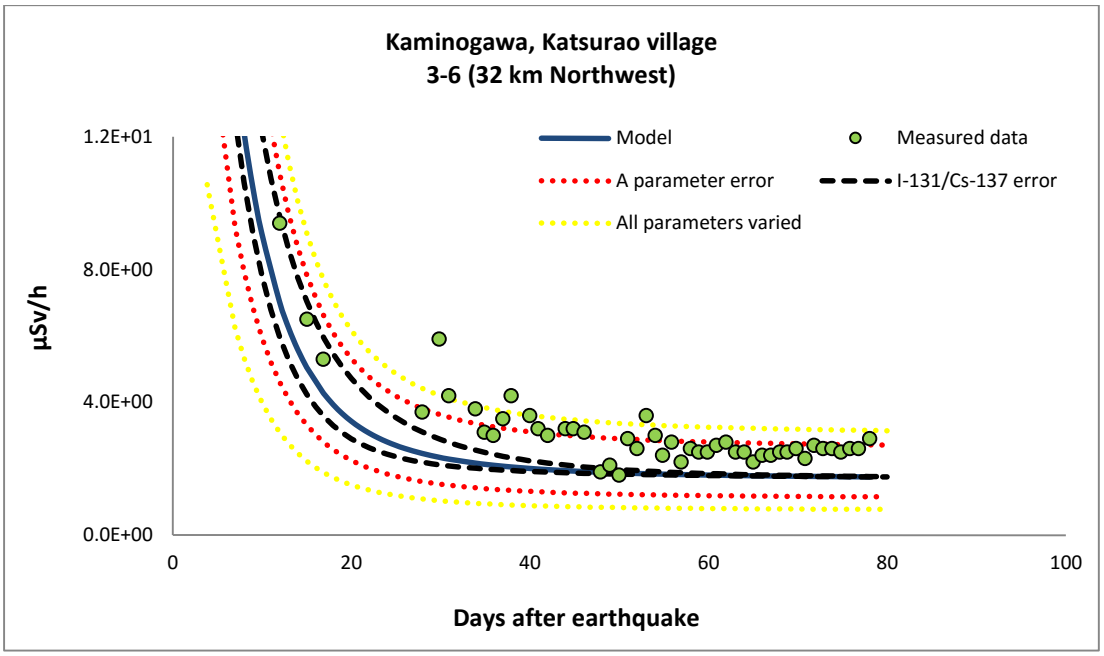

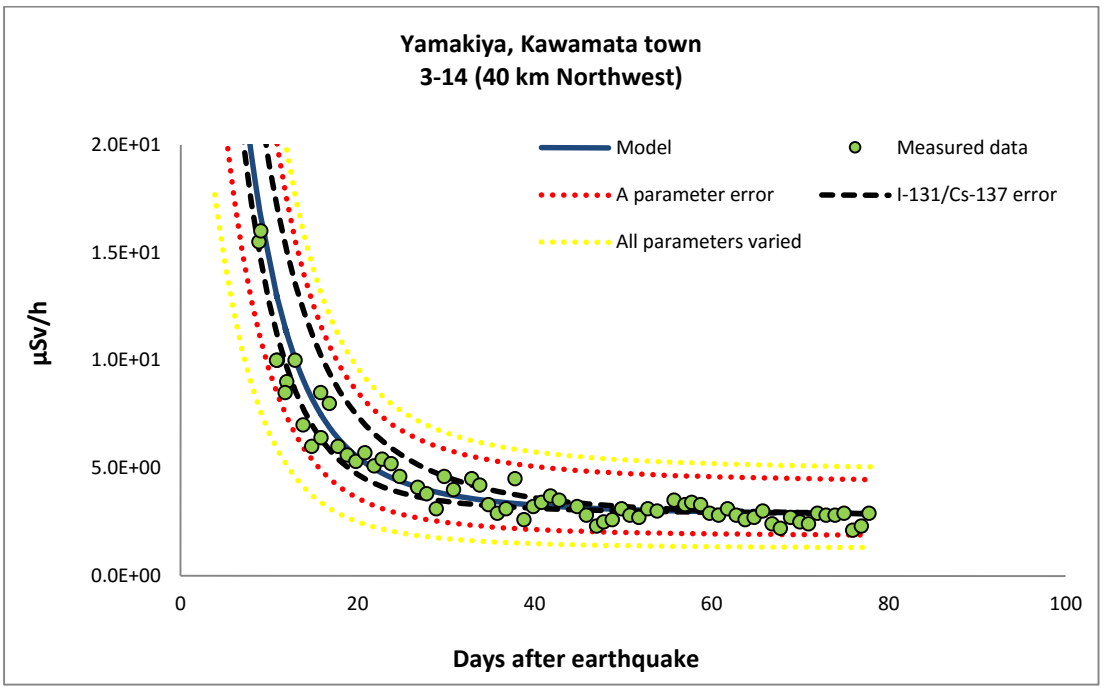

Figure 4-18 (continued) Illustrates comparison of errors from *A* parameter, $^{131}I/^{137}Cs$, and all parameters at six calibration sites.

4.5 Results of the model

4.5.1 Comparison of the results to earliest available measured data

Equation 4-1 was used to determine the change of external gamma dose rate with time at each of the six calibration sites. The measured radiocaesium activity concentration in soil at each site was used as an input parameter, and activity concentrations of other radioisotopes were estimated using the generic RN:^{137}Cs ratios given in Table 4-2. For ^{131}I, the correlation between ^{131}I:^{137}Cs ratio and measured ^{137}Cs activity concentration can be determined by using Equation 3-1. Model fits to measured external gamma dose rate are shown in Figure 4-19 for the six sites for which long time-series of dose rate were available. However, as an advantage of this model, estimations can be extrapolated back to the high dose period on 15 March (it is expected that this is a good estimation point for the highest dose rate since it follows the time of maximum fallout. The extrapolation back to 15th March is shown in Figure 4-20 when the highest deposition occurred (Kinoshita, et al., 2011) but no measured data were available (note that the highest gamma dose was dominated by contaminated radionuclides in soil compared to cloud shine from the air, as discussed in Section 4.2.4).

These results reveal that the highest gamma dose rate to people who lived in these contaminated areas were very significant compared with the first measured data. The highest gamma dose for the calibration site at Akougi Kunugidaira, Namie town (code 83) located 24 km in northwest of NPSs, on 15 March is around 500 μSv/h while the first measured data on 24 March was 106 μSv/h. Another site, Kaminogawa, Katsurao village (code: 3-6, direction: 32 km Northwest), the measurements started on 23 March with 9.4 μSv/h and the model estimated gamma dose on 15 March was 24.02 μSv/h. Estimation of gamma dose on 15 March is very useful for evaluating the radiation impact on humans for this accident, particularly since no measurements were performed at this time.

Using only one site-specific input parameter (^{137}Cs activity concentration) and one fitting parameter (*A*), the model shows excellent agreement with the earliest available measured values at six calibration sites, reflecting accuracy of the derived isotope ratios. Therefore, this simplified model can be used to reconstruct the external gamma dose at any site where only a deposited activity concentration of ^{137}Cs is available. Note that the first available measurement of both gamma dose rate and deposited activities at the same site of six

calibration sites were performed around 17 – 25 March, only one site at Tsushima, Namie town (code 3-6) started on 17 March, the details are shown in Figure 4-1.

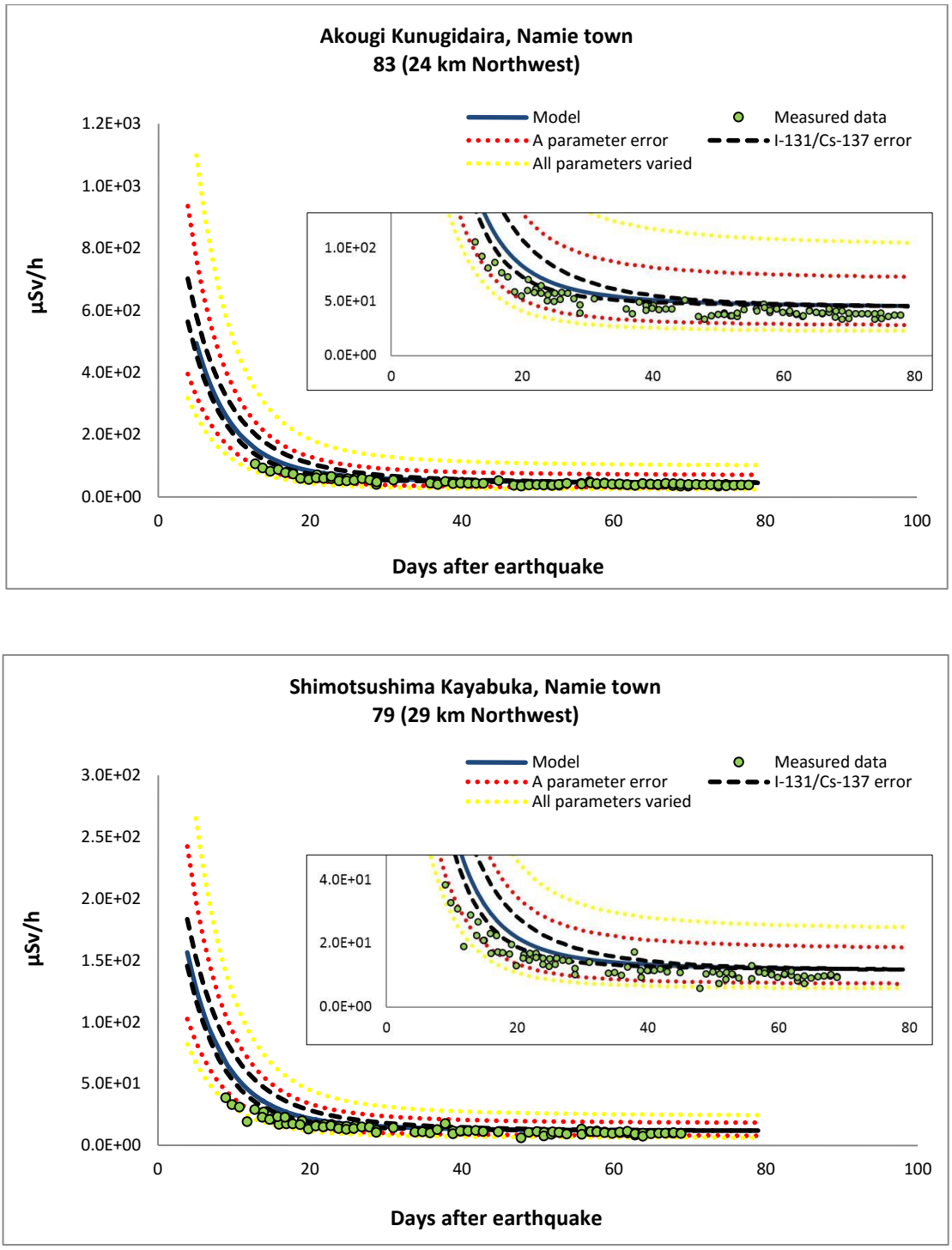

Figure 4-19 the results of the model at six calibration sites: the results were evaluated back to highest dose period on 15 March 2011.

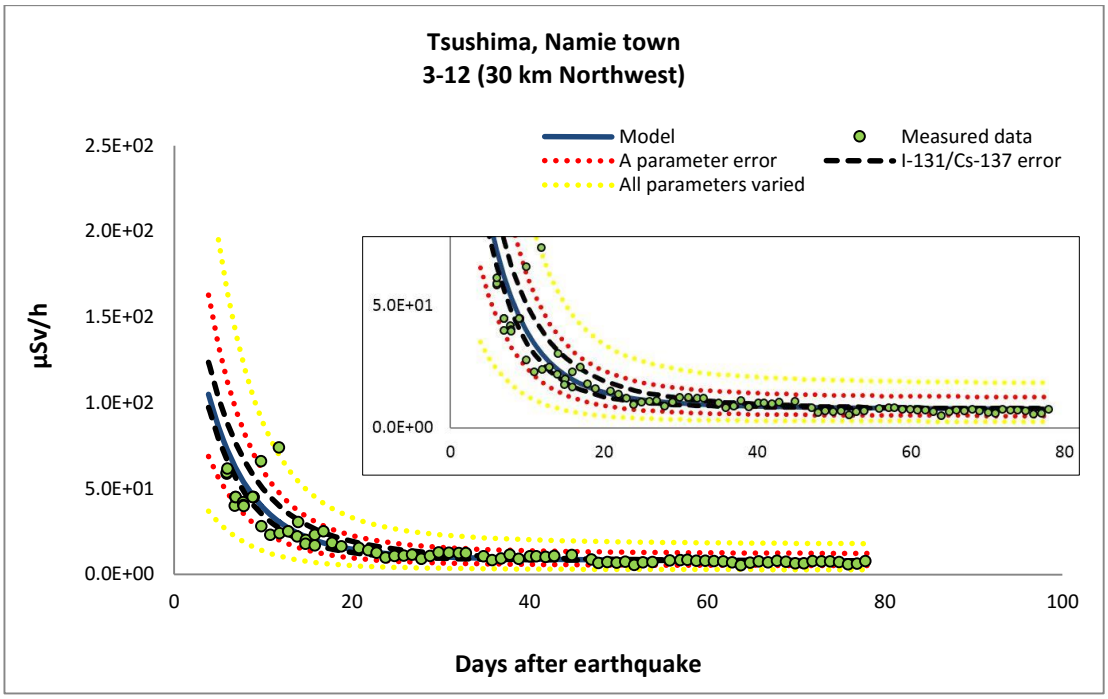

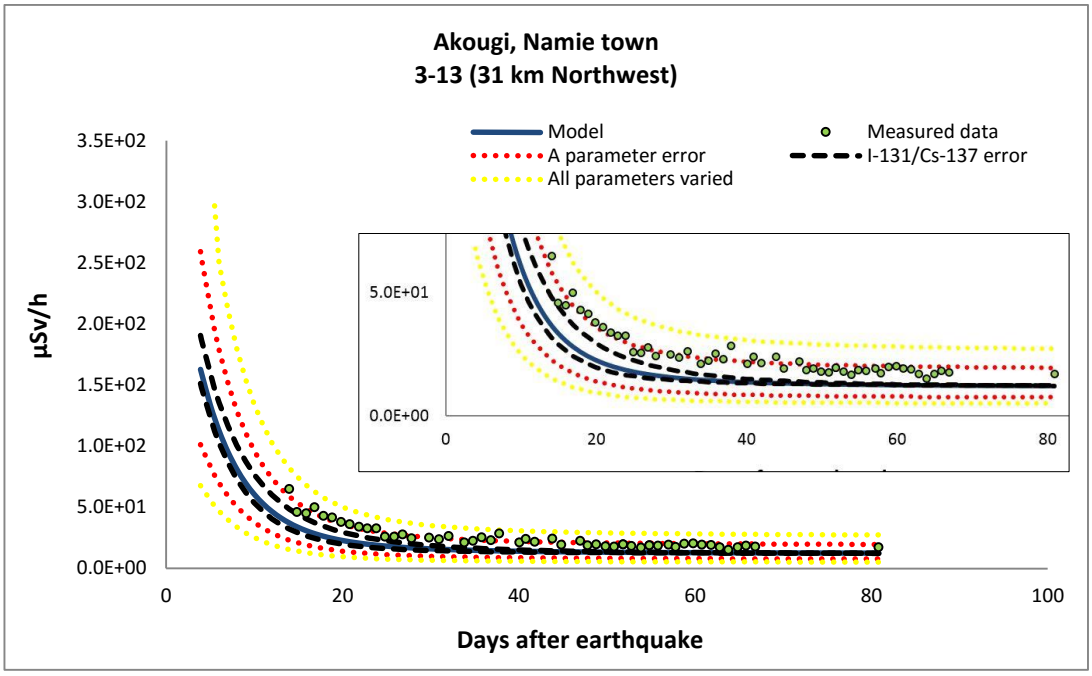

Figure 4-19 (continued) The results from the model at six calibration sites, the results were evaluated back to highest dose period on 15 March 2011.

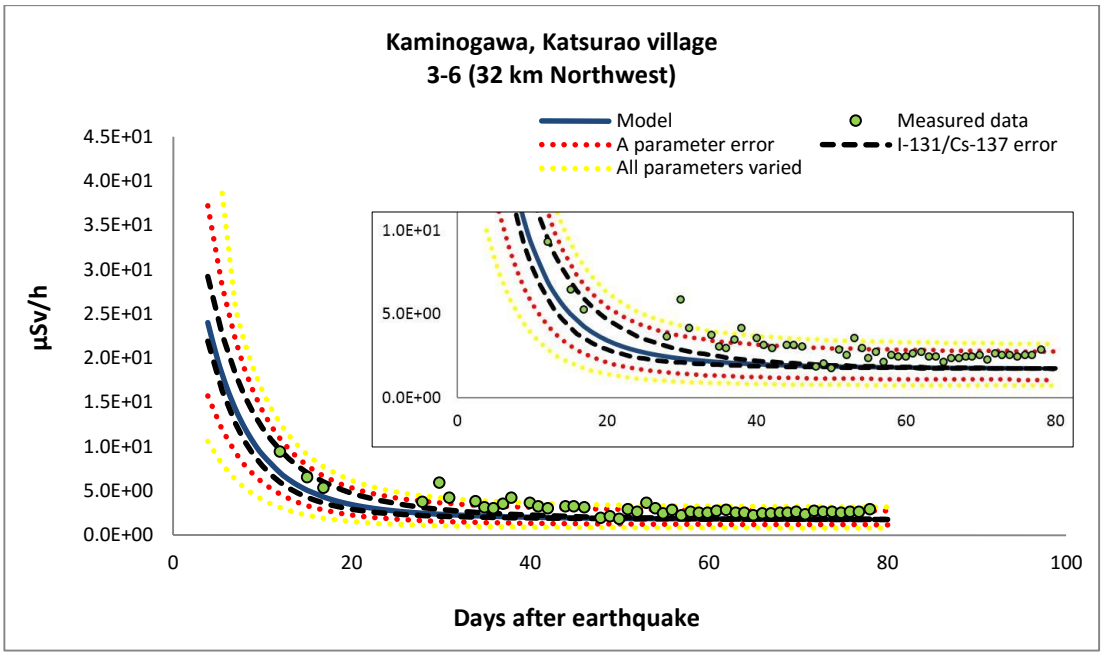

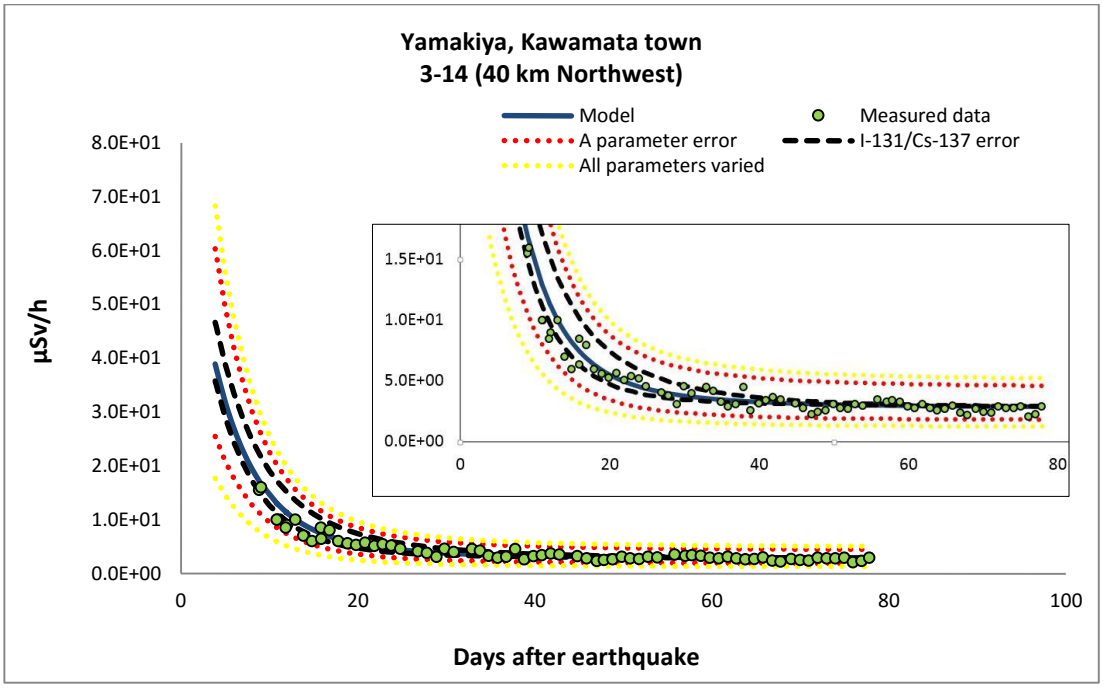

Figure 4-19 (continued) The results from the model at six calibration sites, the results were evaluated back to highest dose period on 15 March 2011.

4.5.2 Blind test of the model

The external dose model was "blind" tested by comparing predictions of the change in external gamma dose rate with time against measurements. Figure 4-20 illustrates model "blind" predicted dose rates against those measured at fifteen test sites. The graphs illustrate the good fit in regions to the North and West, but, as expected, relatively poorer fit at the one site to the South. In the North to West direction, some measured data in the early phase are available for comparing with the results from the model. Most of results are excellent agreement with measured data, the uncertaintyestimated from variation of all parameters used in the model covers the variation in all measured data. There are some sites where the results of the model are slighly underestimated at sites 3-11, and 3-5. Althrough the estimated $^{131}I/^{137}Cs$ from Equation 3-1 are similar to observation data in site 3-11 (measured ratio = 24.2, calculated ratio = 25.6), gamma dose from the model was lower than measurements by a factor of about two. This might be that the *A* parameter was not appropiate for this site (probably soil type is different to others) as other ratios (both calculation and measurements) were similar to other sites. For site 3-5, calculated $^{131}I/^{137}Cs$ was 41.0 and measurement was 15.13, giving a three times underestimation of gamma dose at this site maybe from lack of variation of ^{137}Cs activity from single measurement (^{137}Cs activity maybe too low resulting estimation of main nuclide in very early phase $^{132}Te/^{132}I$ too low as well). A significantly poorer result (dose model lower than mesurement by a factor eight) occurs in the South direction at Shimokitaba, Hirono town (code: 3-7 and direction 23 km South). The reason of the poorer fit in the South might be that the observed corrected deposited ratio of ^{131}I to ^{137}Cs was 78.27, but the corrected ratio calculated by Equation 3-1 is 24.14, nearly three times lower. As discussed in Section 3.6, the corrected ratio of ^{131}I:^{137}Cs in the South area of Fukushima I NPSs was significantly higher than other directions.

Since there is a lack of measurements in the highly contaminated area in the Northwest direction and particularly gamma dose rate on 15-17th March, it is useful to use the model to determine the gamma dose rate at sites where measurement of ^{137}Cs activity concentration in soil was available. The value of ^{137}Cs concentration used in this model can be from a sample collected during at any period since the ^{137}Cs migration in soil is not significant over the first few years (J. T. Smith, Fesenko, et al., 1998b). Under conditions of high rainfall, ^{137}Cs can penetrate relatively deeply into the soil profile

(Bunzl, et al., 1997), however in most areas affected by Chernobyl (J. T. Smith & Beresford, 2005b), and at Fukushima (Kato, et al., 2012), the majority of radioactivity remained near the soil surface, limiting self-shielding. Over years-decades after fallout, gamma dose rates will decline due to further slow penetration of radiocaesium into the soil profile (Bunzl, et al., 1997; J. T. Smith & Beresford, 2005b). Note that the ^{137}Cs concentration in soil in this study was from the soil samples had been collected from the first few days after earthquake until the end of May 2011.

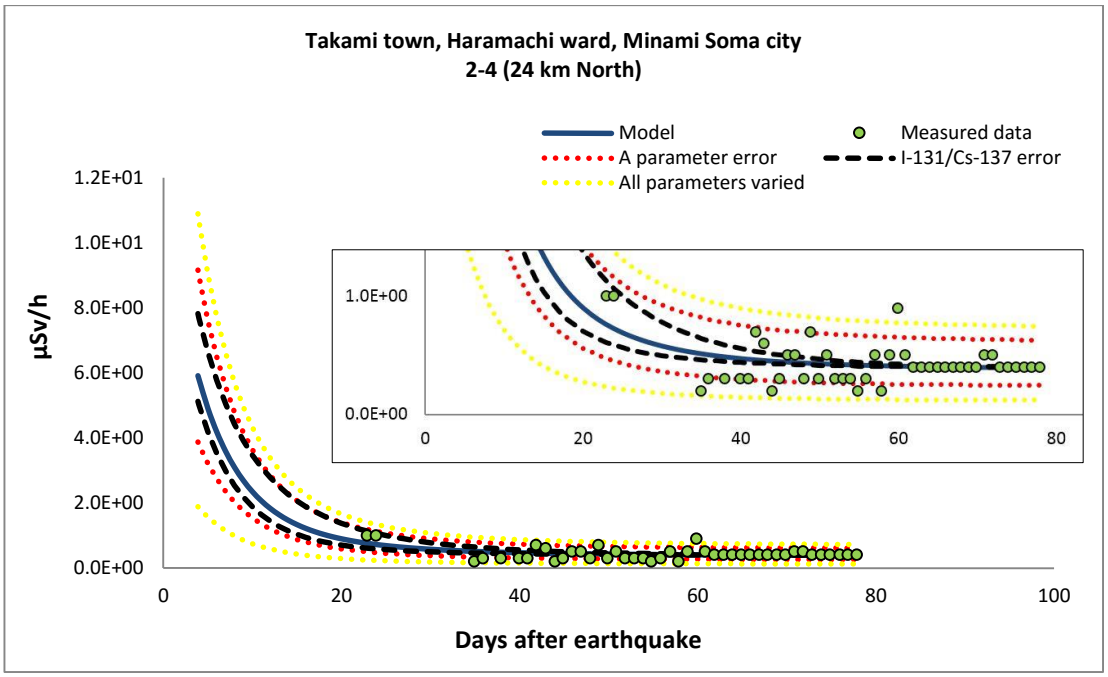

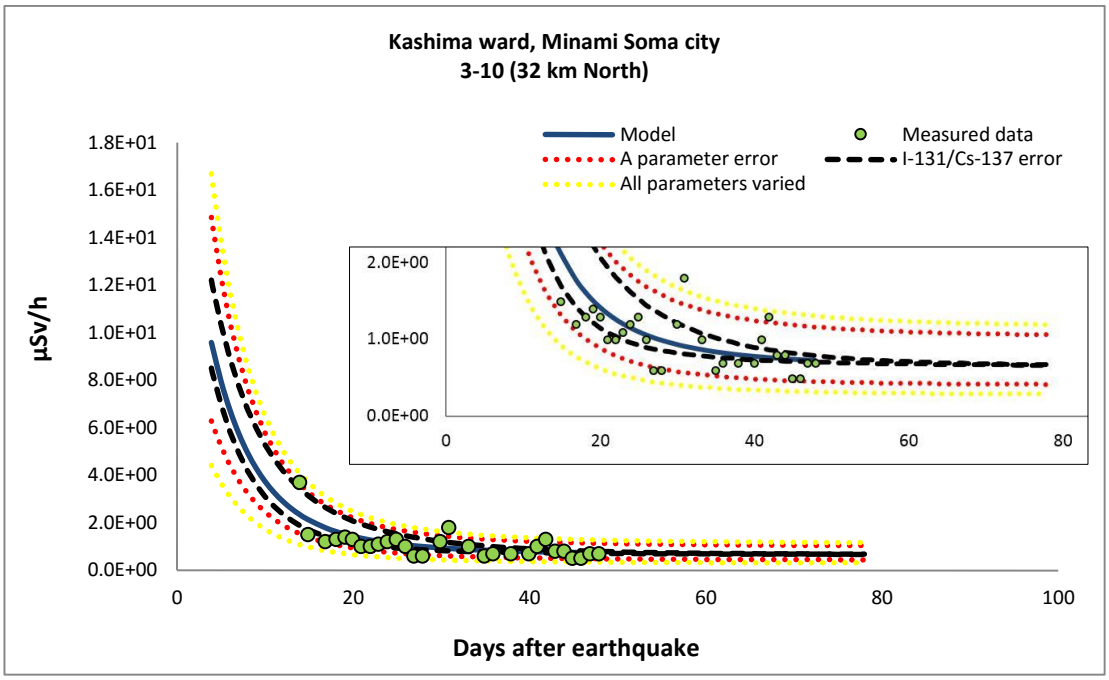

Figure 4-20 Blind prediction of external gamma dose vs days since 15 March using only measured ^{137}Cs concentration at each of fifteen sites as an input variable.

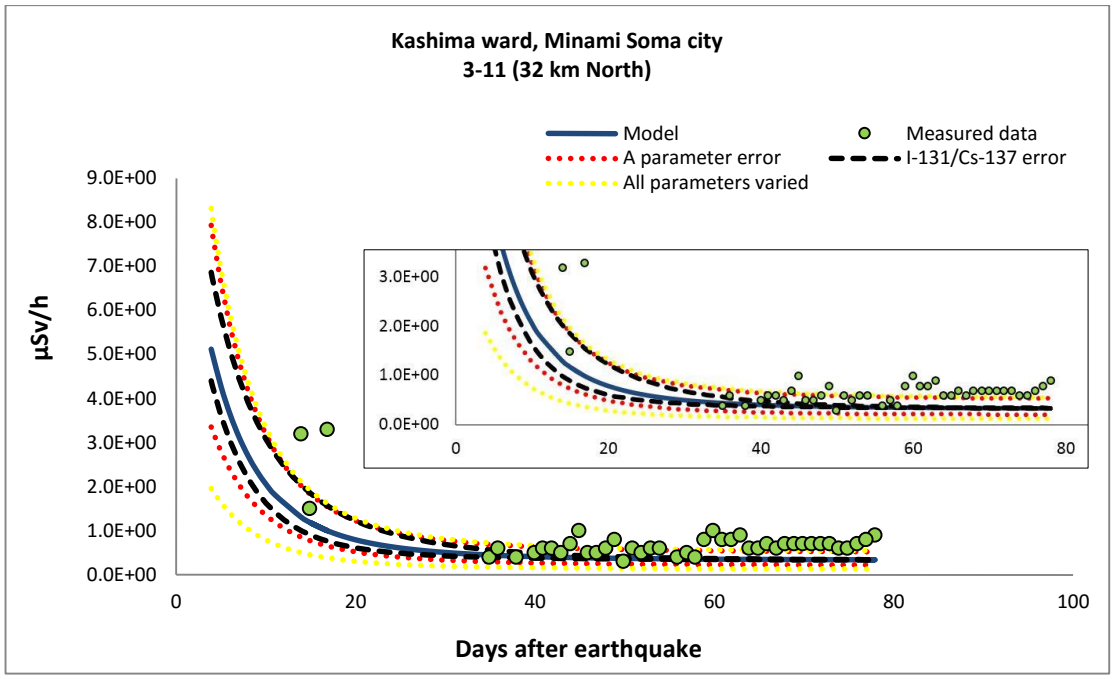

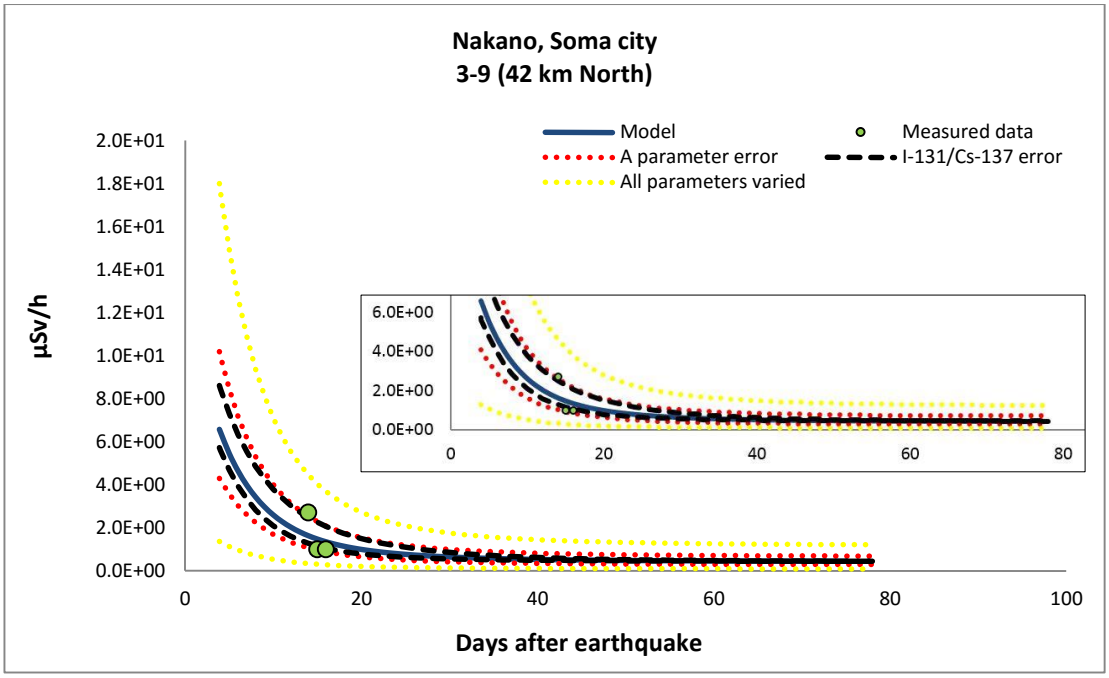

Figure 4-20 (continued) Blind prediction of external gamma dose vs days since 15 March using only measured ^{137}Cs concentration at each of fifteen sites as an input variable.

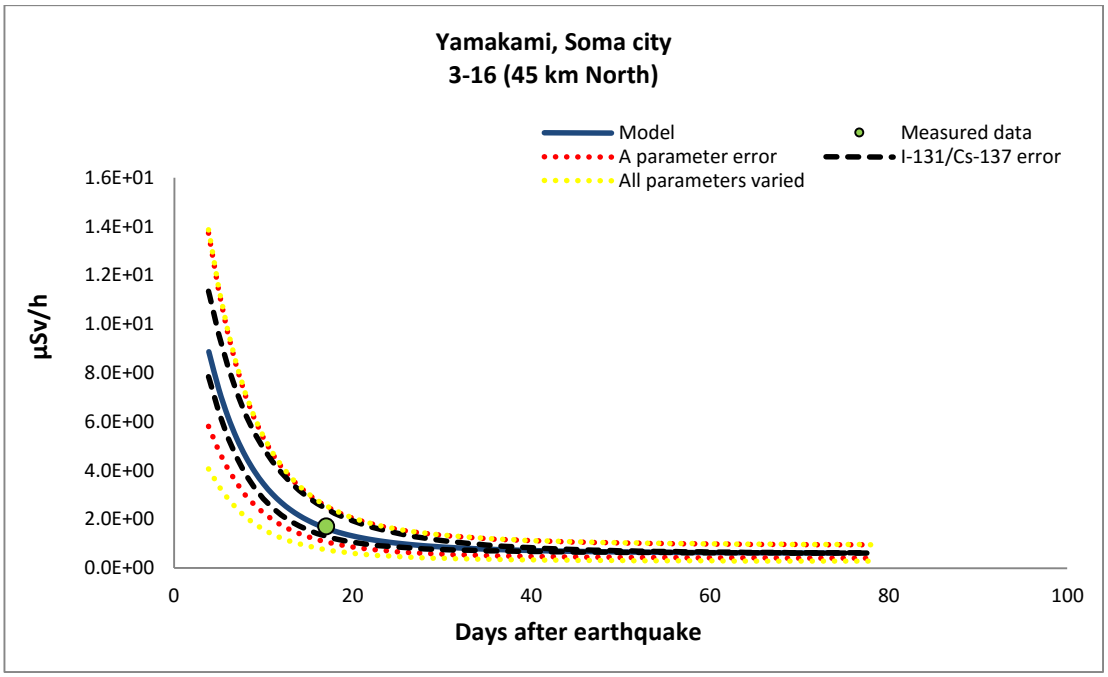

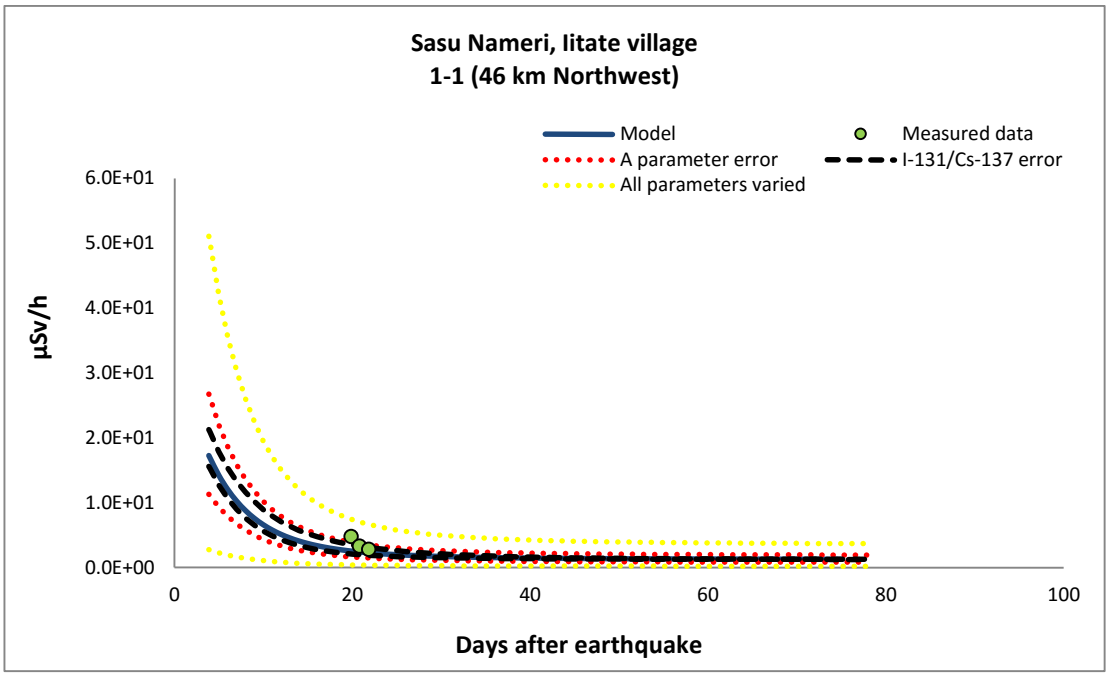

Figure 4-20 (continued) Blind prediction of external gamma dose vs days since 15 March using only measured ^{137}Cs concentration at each of fifteen sites as an input variable.

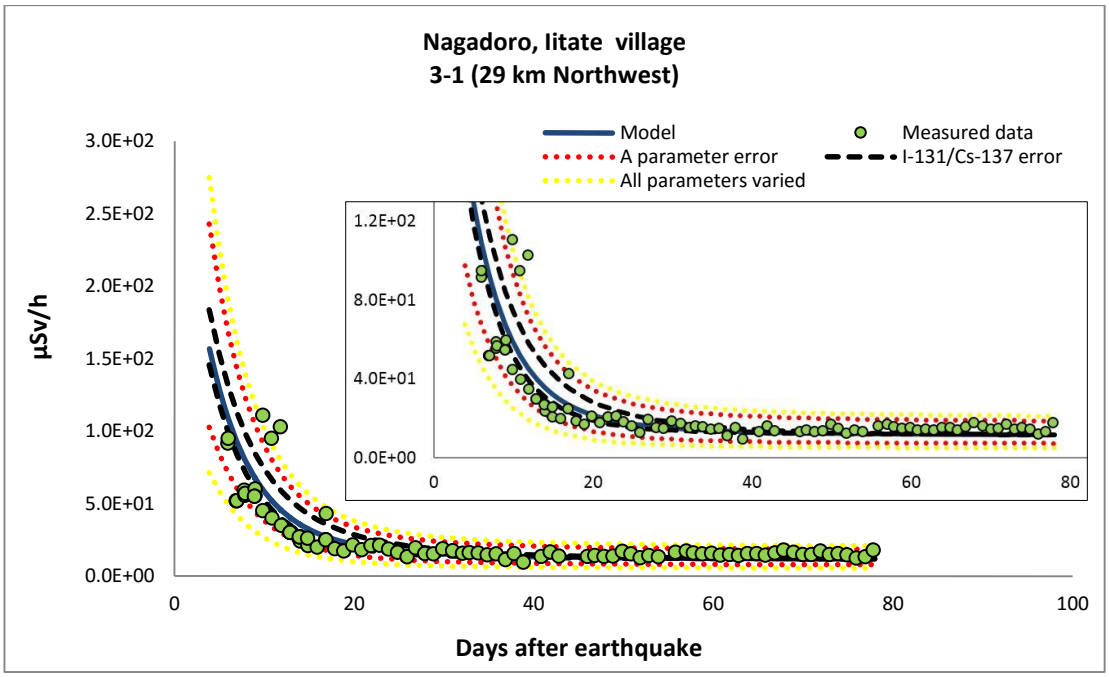

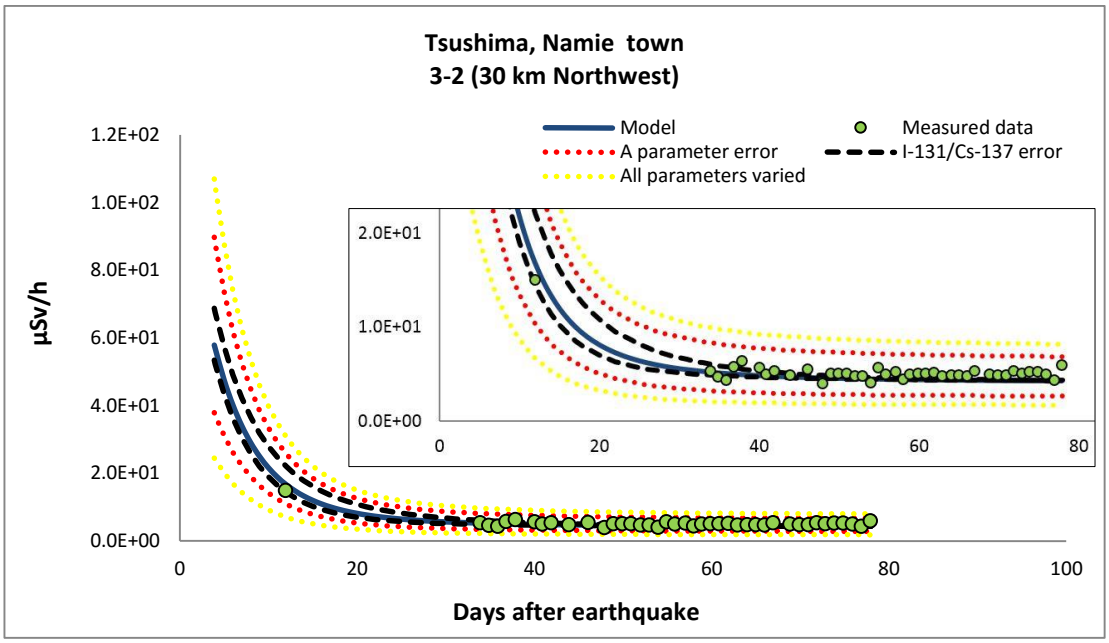

Figure 4-20 (continued) Blind prediction of external gamma dose vs days since 15 March using only measured ^{137}Cs concentration at each of fifteen sites as an input variable.

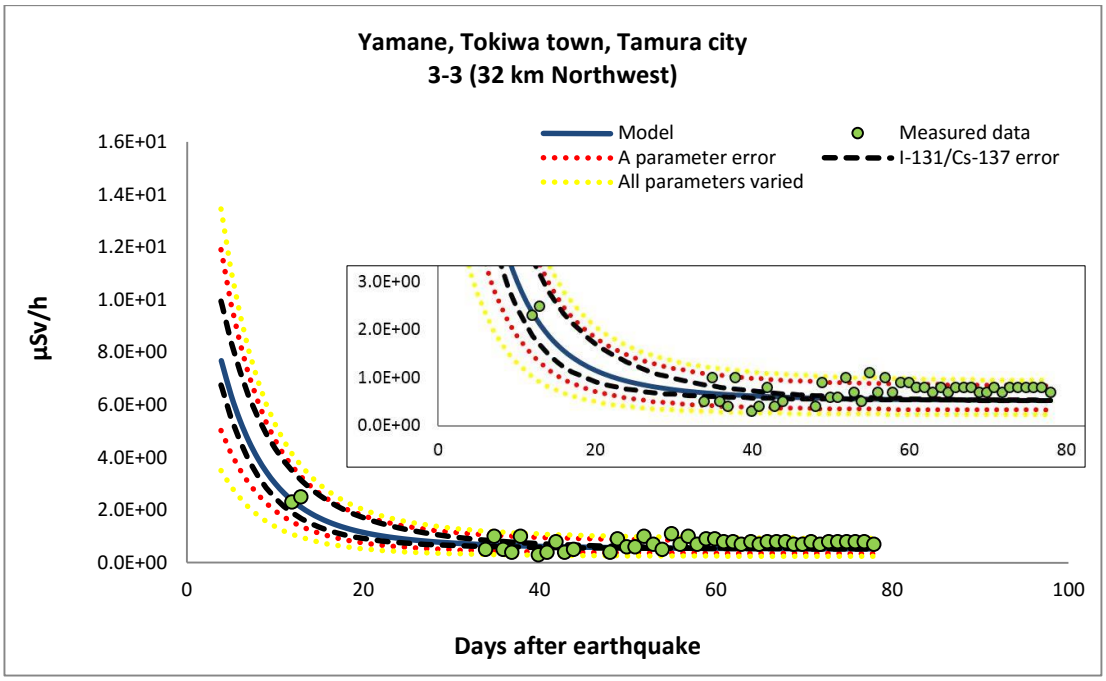

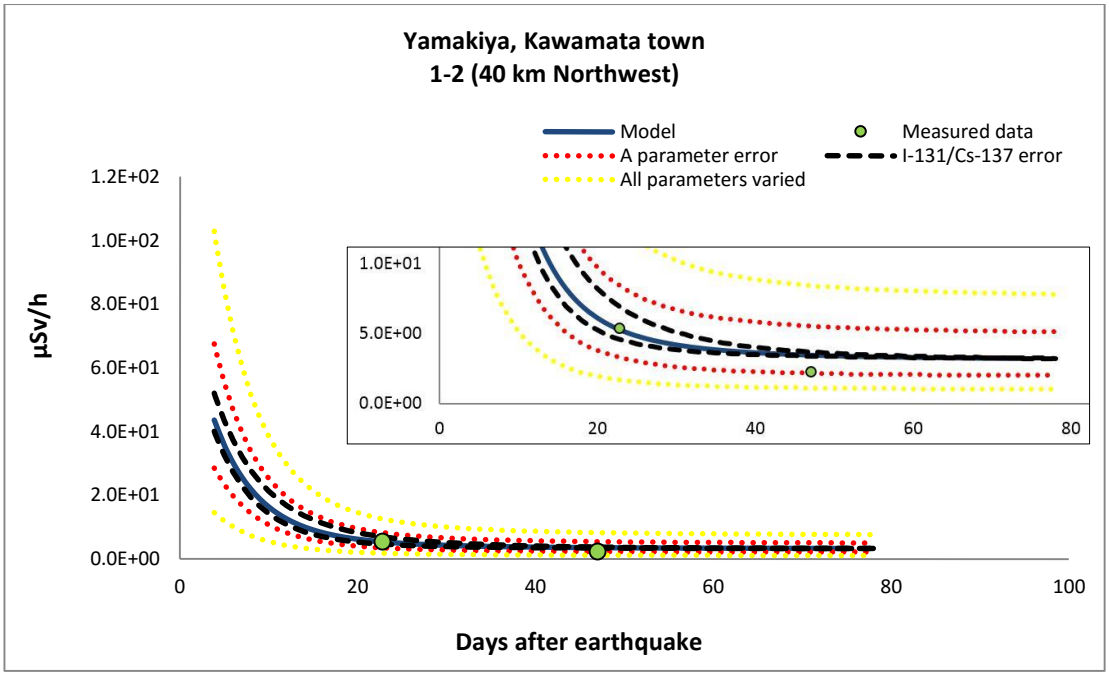

Figure 4-20 (continued) Blind prediction of external gamma dose vs days since 15 March using only measured ^{137}Cs concentration at each of fifteen sites as an input variable.

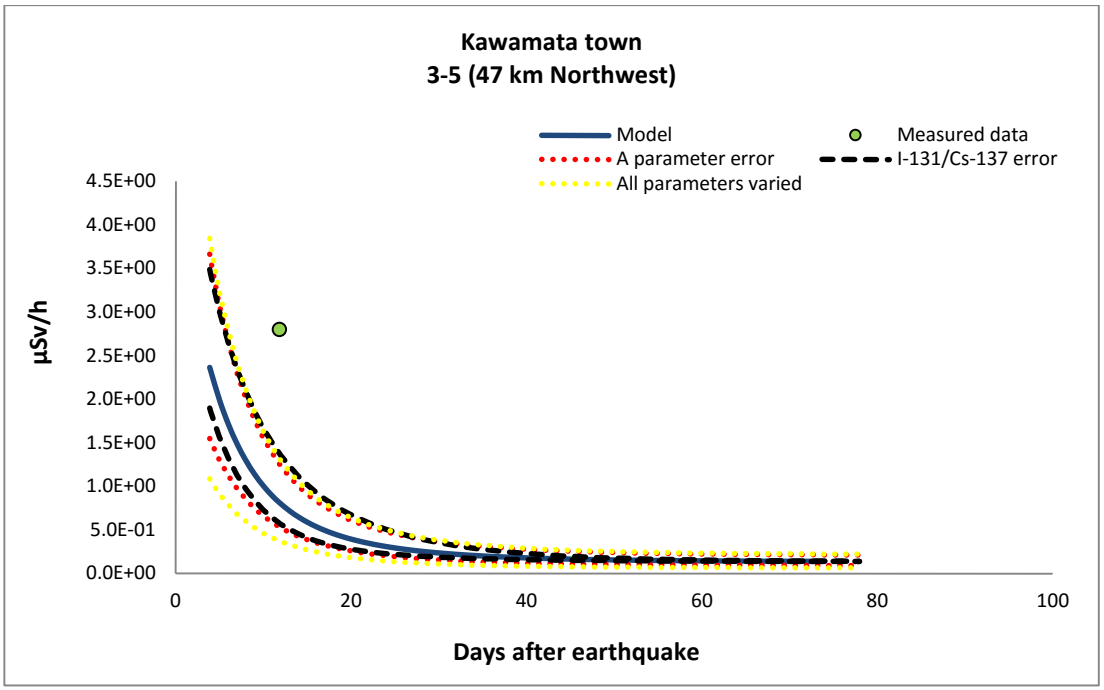

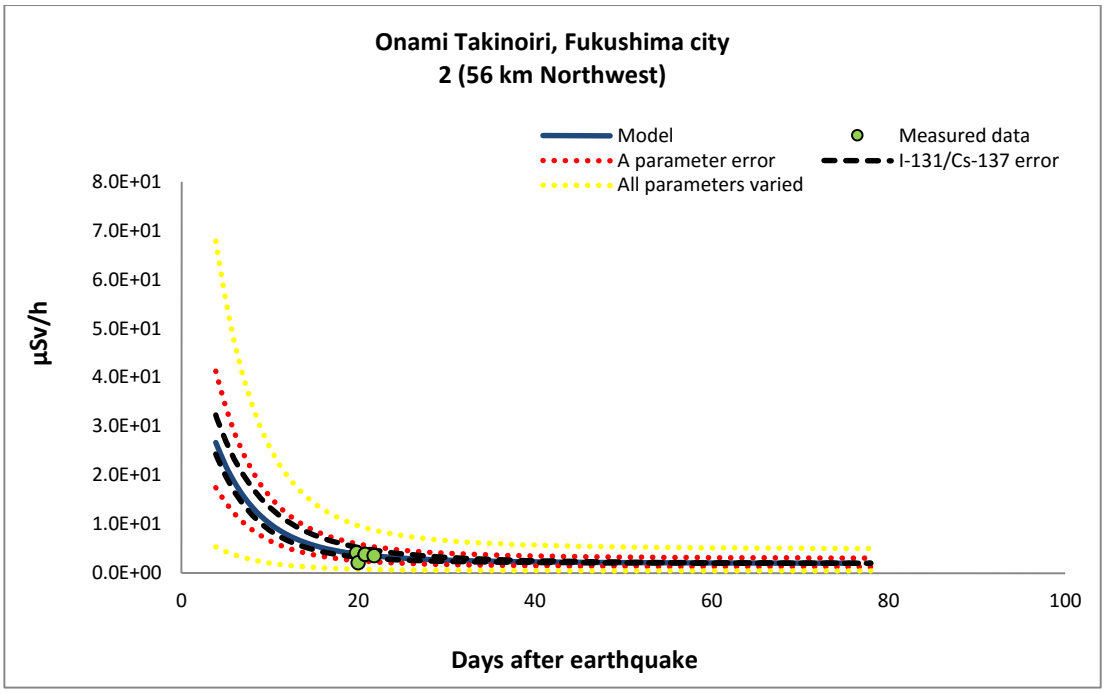

Figure 4-20 (continued) Blind prediction of external gamma dose vs days since 15 March using only measured ^{137}Cs concentration at each of fifteen sites as an input variable.

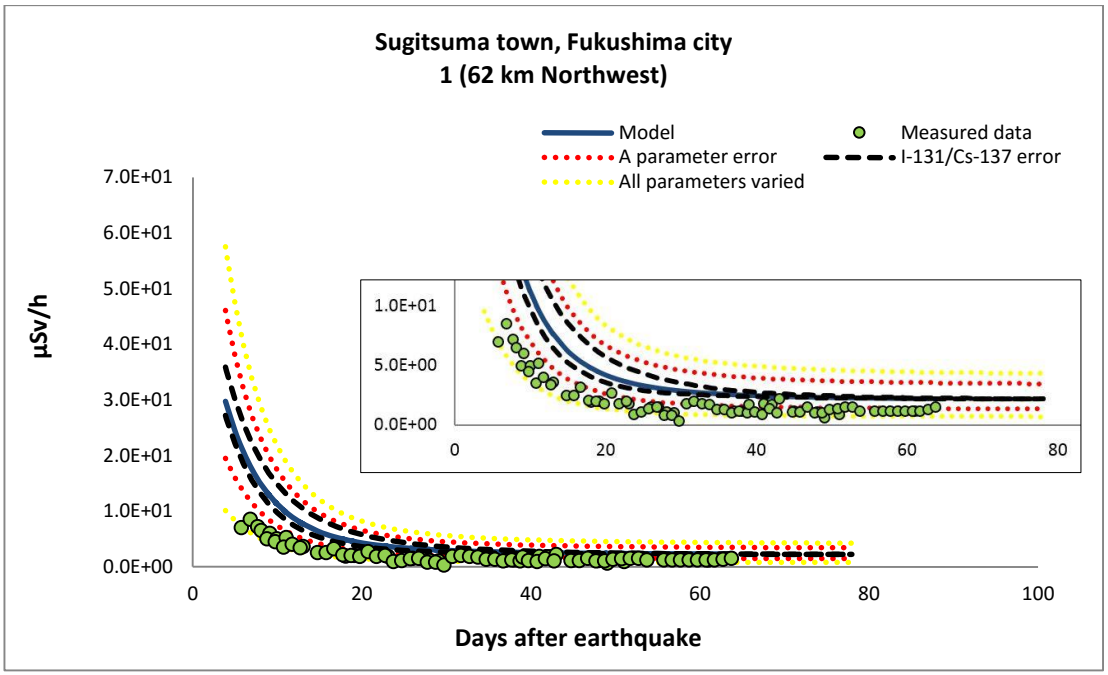

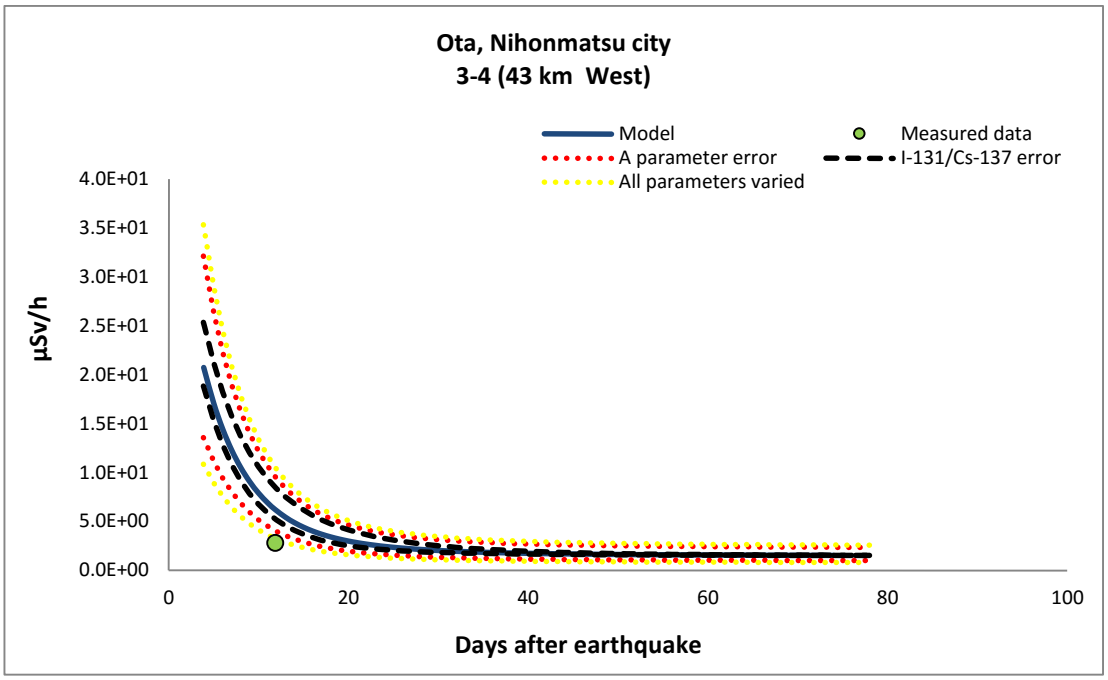

Figure 4-20 (continued) Blind prediction of external gamma dose vs days since 15 March using only measured ^{137}Cs concentration at each of fifteen sites as an input variable.

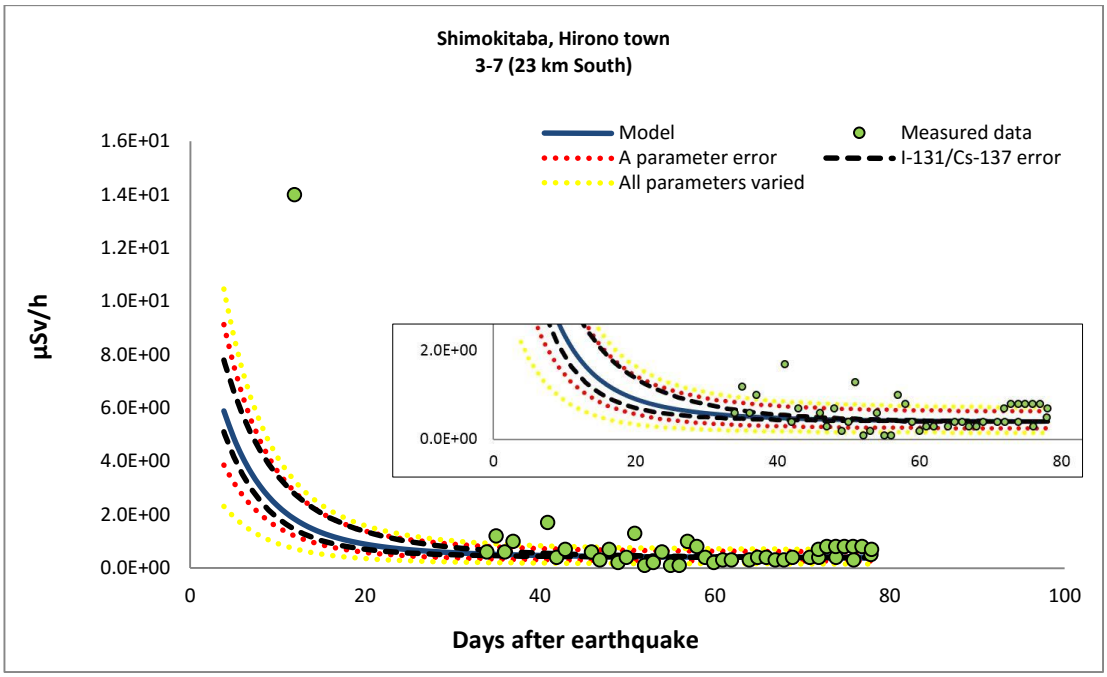

Figure 4-20 (continued) Blind prediction of external gamma dose vs days since 15 March using only measured ^{137}Cs concentration at each of fifteen sites as an input variable.

Figure 4-21 compares model predictions against data from the six calibration sites plus the fifteen test sites, (a) represents the gamma dose rate which was dominated by both short-lived (^{131}I and ^{132}Te/^{132}I) and long-lived (^{134,137}Cs) (> 30 days) radionuclides (b) represents the period when only long-lived radionuclides made a significant contribution to dose. The dotted lines show a factor of two over- and under-estimation of model predictions. In the early phase at the areas from north to west, the results from model have good agreement with measured data. This confirms that the value of empirical *A* parameter, the equation for estimating ^{131}I/^{137}Cs, means of isotopic ratios of key contaminated nuclides are effective to predict the external gamma dose rate in these areas. As expected, model predictions at one site to the south of the NPSs are poorer than those to the north and northwest due to the poor estimation of ^{131}I/^{137}Cs by Equation 3-1 (as discuss before, the consequence of March 21 fallout event to the south resulting the corrected ratio of ^{131}I/^{137}Cs in this direction much higher than the others).

Ninety-five percent of dose rate predictions are within a factor of two of measured values. There is likely to be uncertainty in the measurement of external dose rate, but this is expected to be insignificant in comparison with uncertainties introduced by varying isotope ratios at individual sites (particularly ^{131}I:^{137}Cs ratio) and varying early phase depth distributions. The results of this sensitivity analysis are consistent with the factor of two uncertainty of model predictions in blind testing, implying that these are the greatest source of model uncertainty. In general the model shows excellent agreement with measured dose rates against test data, providing strong evidence for the ability of such models to extrapolate dose rates at sites for which early phase dose rates and isotopic compositon are not available.

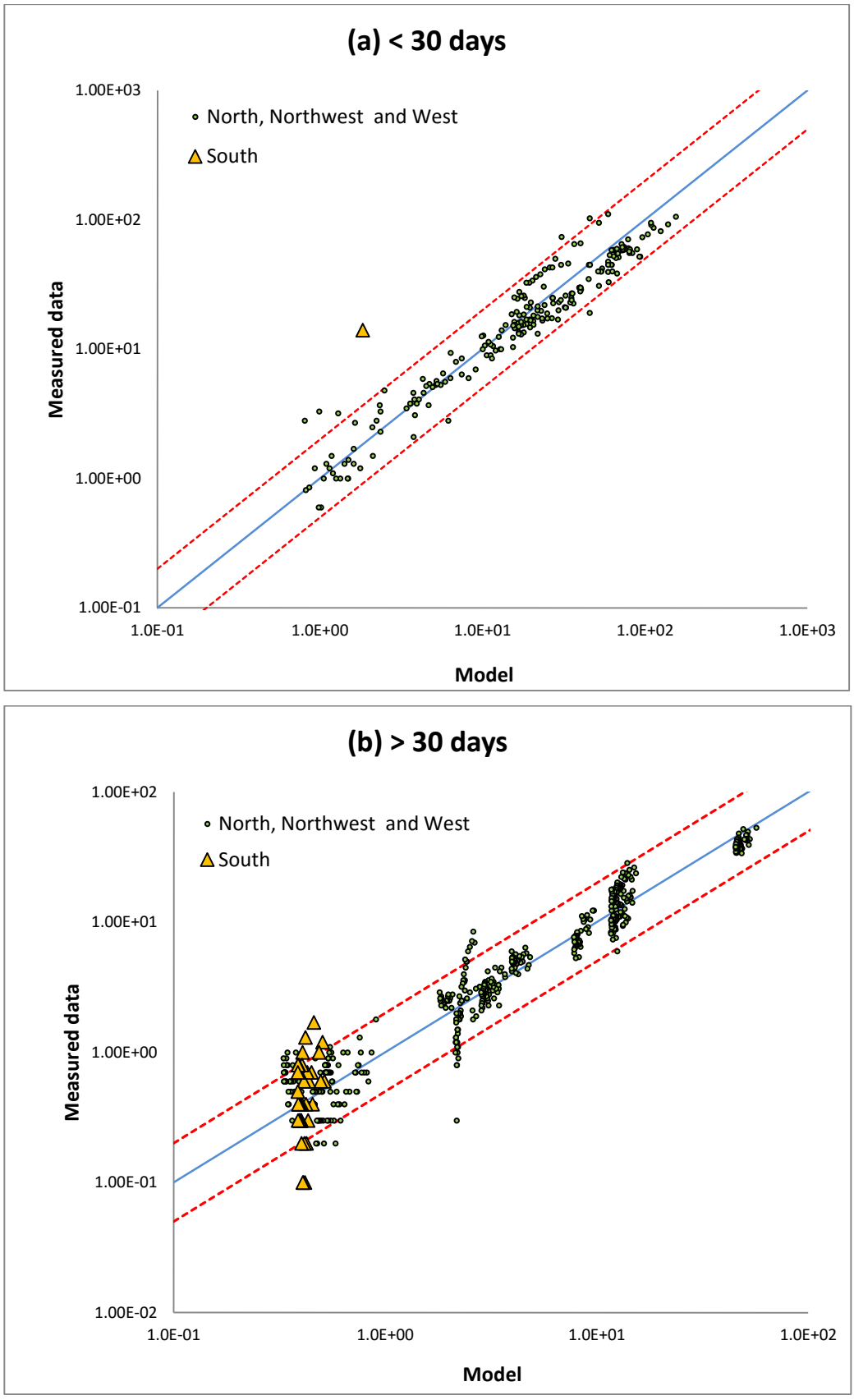

Figure 4-21 Comparison of predicted dose rates (μSv/h) and measured data from (a) first measurement up to 30 days and (b) more than 30 days after the accident.

4.6 Discussion and conclusion

The biggest advantage of this simple model is that it uses only one input measurement, the concentration of ^{137}Cs in soil to predict the external gamma dose rate back to the period of highest contamination on 15 March 2011 (WHO, 2012). This is an effective methodology to reconstruct the external gamma dose in the early phase (within 30 days after earthquake) in areas where there are no measurements of other radioactive materials. The estimation can determine the dose at any time back to the high dose period and also can predict forward to future times after the early phase when external gamma dose became dominated by only long-lived nuclides ^{134,137}Cs. However, this research focuses on the reconstruction of dose to humans in the highly contaminated area in the early phase, so that the validation of model is considered for the early-phase after the accident only.

Following the Fukushima accident there were huge difficulties in monitoring radioactivity and dose rates due to the combination of the nuclear accident and the consequences of the earthquake and tsunami. A lot of analytical equipment was destroyed, and the electricity supply failed. So, the network of dose rate measurements was very patchy: using ^{137}Cs concentration in this model allows estimation of past dose rate to other sites.

In terms of methodology to evaluate the transfer behavior of different isotopic material, this study is similar to Mück and co-workers's research (2002) at Chernobyl which used the corrected isotopic ratio of key gamma-ray-emitter nuclides to ^{137}Cs to estimate the missing values at the sites where measured data was not performed. For the <30-km area, Mück et al. used a correlation between concentration air and soil (concentration in air = concentration in soil × the deposition velocity) as the concentration in soil was measureable longer than in air and lot of soil samples were conducted compared with few rapidly dispersed samples in air. This situation also occurred after the Fukushima accident: there was a lack of ambient measurements while many more soil sample measurements were performed. At longer distances (30-170 km) from Chernobyl, the corrected isotopic ratios relative to distance and direction were used to estimate radioactivity concentration in air for investigate inhalation dose to human (Mück, et al., 2000). Both at Chernobyl and Fukushima, ^{132}Te and ^{134,136}Cs/^{137}Cs ratios were consistent with distance and direction and mean ratios in soil and air were almost the same as both

have same type and size, and ^{131}I depended on plume transport characteristics (the details were discussed in Chapter 3). This analysis of available monitoring data has shown that ^{132}Te is also a very important nuclide in external gamma dose rate particularly in the first few days after the high deposition on 15 March (approximately until 25 days after the earthquake). However, the influence is not directly from ^{132}Te; the dose was dominated by very short-lived ^{132}I which is a daughter of ^{132}Te and has very high gamma energy decay and the high release amount in term of ratio to ^{137}Cs. Since ^{132}Te/^{132}I was not included in the main monitoring conducted by Japanese authority and only a few measurements were performed by few researchers (S. Endo, et al., 2012; Imanaka, et al., 2012), the consistent ratio of ^{132}I to ^{137}Cs (equal to its parent, ^{132}Te/^{137}Cs) with time and direction found in this study is very useful to estimation the release amount of this nuclide where there are no measured data.

To contrast with other models, the parameters of this model are simpler to analyse while other models require more complicated parameters and methods. Another method using a conversion factor to estimate gamma dose rate from deposited density concentration was developed by Kocher and Sjoreen (1985) and the Health Protection Agency GRANIS model (Khalid & Mann, 2007). However, these are still difficult to apply to estimate gamma dose, especially for the Fukushima accident situation.

Both models need deposited density concentration of ^{137}Cs but also density or diameter of soil samples to evaluate deposited density concentration, or depth profile measurement which was not available in main monitoring by MEXT (2011b, 2011c). Also the calculation of total gamma dose from both are complicated as they require the summation from monoenergetic photons emitted from each key radionuclide, and the dose-rate results are not interpreted in continuous time series. Particularly Kocher and Sjoreen's model has to identify deposited density concentration at specific times, though the GRANIS model can interpret the result at a few discrete times after deposition (0, 6, 12 h; 1, 2, 7, 30 day; 1, 2, 5, 10, 50 year). Generally the results of these models agree with the simpler model developed here. From the conversion factor in GRANIS for ^{132}Te which includes the influence on dose rate from its daughter ^{132}I also has high contribution to dose in the period from 0 h until 30 days after an instantaneous deposition as shown in Table 2-4. This fact shows that ^{132}Te/^{132}I from GRANIS also dominated the gamma dose

rate in early phase, as was found in the calculation of inhalation dose following Chernobyl by Mück and his coworkers (2002; 2000).

More complex models, such as the Jacob and co-workers's model (Peter Jacob, et al., 1994) and WHO's model (2012), can interpret dose rate with time but there are numerous parameters. Beside the deposited density concentration, both of these models require more information about (1) site characteristics such as soil type, annual precipitation and distance from release point, (2) the reduction of dose rate from the surface roughness of the interface between air and ground, and (3) the migration of the radioactive material into the soil also have to be accounted for using empirical parameters.

In addition, the WHO model, developed to estimate gamma dose rate following the Fukushima accident also requires other specific and complex parameters and the dose rate coefficient from surface activity density to kerma rate at a height of one metre above ground due to the initial distribution of the radionuclide. However, the similarity between the model from this research and the WHO model is that the calculations both use isotopic ratios to deposited density concentration of ^{137}Cs to estimate the values of other key nuclides. Note, however, that WHO does not consider the remarkably different ratios of ^{131}I/^{137}Cs with direction, unlike this research and the previous Mück et al. (2002) study of Chernobyl: the WHO model uses a single value of 7.8 for this ratio in all directions. This is likely to underestimate, dose rates as deposited ratios were generally much higher than this. Another similarity is that the WHO model uses as its starting point the highest gamma dose rate on 15 March 2011 when the fallout was at its peak.

For the possible influence of dose rate from the cloud of contamination, using conversion factors (DOE, 1988; Eckerman & Ryman, 1993; Yoo, et al., 2013) to convert radioactivity in air to the gamma dose rate at 1 metre above ground it was shown that the dose from cloud shine is not significant compared to external gamma dose at the ground surface. The most important radionuclides in air released from the Fukushima accident were ^{131}I, ^{132}Te/^{132}I, ^{137}Cs and the noble gas ^{133}Xe, but all nuclides except ^{133}Xe produced gamma dose rate significantly lower than produced by deposited activity in soil. In the case of ^{133}X, this noble gas had produced a very high dose in short period in the very early phase (dose from soil was remarkably greater than the highest dose from ^{133}X in air by about 200-2,000 times estimated from available at JAEA (JAEA, 2012)) but it did not deposit on the ground (WHO, 2012) so it can be concluded that there was no significant

interference to gamma dose rate at ground level by this radionuclide. This observation agrees with other studies: UNSCEAR (2013) and WHO (2012) for the Fukushima accident and UNSCEAR (1998b) for Chernobyl conclude that the majority of radiation dose to the public was dominated by deposited radioactivity and the ingestion pathway.

This model can be used to estimate the integrated gamma dose from soil. Since the Japanese Government announced a voluntary evacuation area for the 20 to 30 km zone around Fukushima on 25th March (NISA, 2011a), the residents in this area were exposed significantly from the highest deposition date on 15th March until 25th March. Table 4-11 illustrates the integrated gamma dose based on deposited concentration density in Figure 1-9 and the date of evacuation.

Table 4-11 also shows the 30-days integrated gamma dose corresponding to the map of deposited radiocaesium at the near-zone area of Fukushima I NPSs produced by MEXT (2011d) as shown in Figure 1-9. The fraction of ^{137}Cs = 52.63% (estimated by using ratio ^{134}Cs/^{137}Cs = 0.9, not including ^{136}Cs due to the fact that MEXT (MEXT, 2011b 4-4 monitored only ^{134}Cs and ^{137}Cs), estimated depth of sample = 5 cm and general soil density = 1,500 kg/m^3 were used to convert surface deposition (Bq/m^2) of radiocaesium from map to activity concentration of ^{137}Cs (Bq/kg) which is the input of this model as follows

$$\text{activity (Bq/kg)} = \frac{0.5263 \times \text{surface deposition (Bq/m}^2\text{)}}{\text{depth (m)} \times \text{soil density (kg/m}^3\text{)}}$$

Integrated gamma dose in Table 4-10 is given by the area under the graph of results from Equation 4.1 from 15th of March to 15th of April 2011

For the highest contaminated area in Northwest direction of NPSs (red area in Figure 1-9), the first month integrated gamma dose to population was 3.6×10^3 - 3.6×10^2 μSv compared with a dose limit = 5 mSv/y for people from Japanese law which was enforced on April 2012 (MHLW, 2012). If people lived in this area for a year, the integrated gamma dose would have been 15 mSv.

Table 4-11 The integrated gamma dose (μSv) from soil at near-zone of Fukushima I NPSs corresponding to the map of deposited radiocaesium produced by MEXT (2011d) as shown in Figure 1-9 and the date of evacuation.

date of evacuation	Surface deposition of ^{137}Cs (Bq/m^2) in Figure 1-9				
	3×10^7 - 3×10^6	3×10^6 - 1×10^6	1×10^6 - 6×10^5	6×10^5 - 3×10^5	< 3×10^5
	Activity concentration of ^{137}Cs (Bq/kg)				
	2×10^5 - 2×10^4	2×10^4 - 7×10^3	7×10^3 - 4×10^3	4×10^3 - 2×10^3	< 2×10^3
	Integrated gamma dose (μSv) since 15 March until evacuation				
16 March	0.43 - 0.044 ×10^3	44 - 15	15 - 9	9 - 5	< 5
17 March	0.80 - 0.082 ×10^3	82 - 28	28 - 17	17 - 9	< 9
18 March	1.10 - 0.113 ×10^3	113 - 39	39 - 24	24 - 13	< 13
19 March	1.36 - 0.140 ×10^3	140 - 49	49 - 30	30 - 16	< 16
20 March	1.59 - 0.163 ×10^3	163 - 57	57 - 35	35 - 19	< 19
21 March	1.78 - 0.183 ×10^3	183 - 64	64 - 39	39 - 21	< 21
22 March	1.94 - 0.200 ×10^3	200 - 70	70 - 43	43 - 23	< 23
23 March	2.09 - 0.215 ×10^3	215 - 75	75 - 47	47 - 25	< 25
24 March	2.22 - 0.229 ×10^3	229 - 80	80 - 50	50 -27	< 27
25 March	2.33 - 0.240 ×10^3	240 - 84	84 - 52	52 - 28	< 28
26 March	2.44 - 0.251 ×10^3	251 - 88	88 - 55	55 - 30	< 30
27 March	2.53 - 0.261 ×10^3	261 - 91	91 - 57	57 - 31	< 31
28 March	2.61 - 0.270 ×10^3	270 - 94	94 - 59	59 - 32	< 32
29 March	2.69 - 0.278 ×10^3	278 - 97	97 - 61	61 - 33	< 33
30 March	2.77 - 0.286 ×10^3	286 - 100	100 - 62	62 - 34	< 34
31 March	2.83 - 0.293 ×10^3	293 - 102	102 - 64	64 - 34.6	< 34.6
01 April	2.90 - 0.299 ×10^3	299 - 105	105 - 65	65 - 35.5	< 35.5
02 April	2.96 - 0.306 ×10^3	306 - 107	107 - 67	67 - 36.2	< 36.2
03 April	3.02 - 0.312 ×10^3	312 - 109	109 - 68	68 - 37.0	< 37.0
04 April	3.07 - 0.318 ×10^3	318 - 111	111 - 69	69 - 37.7	< 37.7
05 April	3.13 - 0.323 ×10^3	323 - 113	113 - 71	71 - 38.3	< 38.3
06 April	3.18 - 0.328 ×10^3	328 - 115	115 - 72	72 - 38.9	< 38.9
07 April	3.23 - 0.334 ×10^3	334 - 117	117 - 73	73 - 39.6	< 39.6
08 April	3.28 - 0.339 ×10^3	339 - 119	119 - 74	74 - 40.1	< 40.1
09 April	3.33 - 0.344 ×10^3	344 - 120	120 - 75	75 - 40.7	< 40.7
10 April	3.37 - 0.348 ×10^3	348 - 122	122 - 76	76 - 41.2	< 41.2
11 April	3.42 - 0.353 ×10^3	353 - 124	124 - 77	77 - 41.8	< 41.8
12 April	3.46 - 0.358 ×10^3	358 - 125	125 - 78	78 - 42.3	< 42.3
13 April	3.51 - 0.362 ×10^3	362 - 127	127 - 79	79 - 42.8	< 42.8
14 April	3.55 - 0.367 ×10^3	367 - 128	128 - 80	80 - 43.3	< 43.3

To summarise, the results show that the model predictions are generally in good agreement with measured data for sites located from north to west of Fukushima I NPSs. As expected, the results are poor for southern area as this area had a remarkably high ratio ^{131}I/^{137}Cs which resulted from the second plume on 21 March. The sensitivity analysis showed that the, empirical *A* parameter and ^{137}Cs concentration are the greatest source of model uncertainty. Since the *A* parameter is the conversion factor to convert all parameters to gamma dose, the error from the empirically determined *A* parameter likely

includes errors from all parameters. The error in this parameter is similar from both direct calculation using upper and lower ranges of the calibration sites and when using the Monte Carlo simulation. For ^{137}Cs concentration in soil, the statistical error from each site is taken into account in this model. As other corrected ratios of key nuclides are a function of ^{137}Cs, the resulting error in this parameter is highly significant. Sensitivity form all parameters by Monte Carlo simulation had an excellent agreement with measured data of northern-to-western area showing that it can be used as a measure of the sensitivity of this model. As shown in blind test results, the model can reconstruct the external gamma dose at height 1 m above the ground back to maximum dose period after 15 March 2011 from the sites where there is a lack of measured data using only later measurements of ^{137}Cs concentration in soil.

Chapter 5 Transfers of radionuclides in freshwater ecosystems

5.1 Introduction

Many rivers and lakes in Japan have been affected by fallout from the Fukushima accident. This part of the study will focus on the application of the simplified model "AQUASCOPE" to predict the concentration of the key radionuclides ^{134}Cs, ^{137}Cs and ^{131}I in surface waters and freshwater fish near the Fukushima I NPSs where contamination densities were high. The AQUASCOPE model (J. T. Smith, et al., 2005; J.T. Smith et al., 2002; J. T. Smith et al., 2001) had been developed based on the long-term empirical data in European surface water systems affected by the atmospheric nuclear weapons testing and the Chernobyl accident fallout events. The model had been verified against measured data from these fallout events plus data from the Kyshtym accident. This dynamic model can predict the contamination of freshwater ecosystems from the time of the accident until the long-term period of more than ten years. As discussed in the Methods chapter (Chapter 2), the minimum required input parameters for this model are relatively basic parameters such as catchment area, depth, surface deposition, fraction of organic and boggy soil and net annual rainfall on the catchment. For calculation of the uptake of radiocaesium to fish, the potassium concentration of the lake or river water and wet weight of fish (both predatory and non-predatory) is required. It clear that these parameters are relatively easily available for prediction of long term contamination of freshwater systems. This research intends to use this for prediction of contamination of freshwater systems in Japan and test the results with available field measurements following the Fukushima accident. It is possible that there will be significant differences between model parameters from European ecosystems and those in Japan so that the results of AQUASCOPE need to be validated for long term predictions in water and fish affected by Fukushima.

The significant advantage of AQUASCOPE is that it is a simple model which requires basic parameters while other models require complex parameters (Section 2.6.5) such as a complex transfer coefficient between trophic level in Koulikov and Meili's model (2003), contamination in fish during initial period of deposition (the maximum activity concentration and time from first deposition to maximum point) in Sundbom et al.'s model (2003), and a coefficient of proportionality between the elimination rate of the

bioelement, the general rate of metabolism and the concentration of the stable bioelement analogue in the fish and the food of the fish which were used in the model developed by Kryshev and Ryabov (2000). AQUASCOPE also divided characteristic of freshwater system which describes the level of contamination (lowest in river and highest in closed lake) while others model did not determine these resulting in more accurate result from the AQUASCOPE model. Another remarkable benefit of AQUASCOPE is that it can estimate contamination of ^{131}I in water bodies and fish as the amount of ^{131}I was highest in initial period (Section 1.3 and 3.3).

5.2 Methodology

The simplified model, AQUASCOPE, was developed by observing field measurement data of the surface water systems in European countries following the fall out from atmospheric nuclear weapons explosions and large scale nuclear accident of Chernobyl resulting in large areas of land being contaminated by the long-lived radionuclides ^{137}Cs and ^{90}Sr. The model (J. T. Smith, et al., 2005; J.T. Smith, et al., 2002; J. T. Smith, et al., 2001) shows that the activity concentration in water and fish in surface water ecosystems primarily depends on the level of surface deposition (Bq m^{-2}) and some key characteristics of catchments, lakes and rivers. The model is based on key processes of water and sediment transfer in these systems, but model parameters are empirically estimated from a wide range of measurement data. These parameters might be different than those seen in Japan so that the verification of the model is necessary.

5.2.1 Rivers and lake measurements used in this research

After the Fukushima accident, there has been monitoring of contaminated rivers and lakes in Japan, conducted by research institutions and the Japanese authorities. Radiocaesium is found in dissolved and particulate adsorbed forms in aquatic systems: this research will focus on the dissolved form because the uptake to fish is mainly from this form (Jinks, 1975; Morgan, Tytler, & Bell, 1994; Wang & Wong, 2003; Zhao, Wang, Yu, & Lam, 2001)). Only one lake in Iitate, Fukushima Prefecture had been monitored daily by MEXT (MEXT, 2011b): sampling occurred from seven days after the accident until the end of July 2011. For rivers, three research studies have monitored rivers in near zone of Fukushima I NPSs: at the Wariki and Hiso Rivers (Ueda and co-workers (2013)), at the Matsu, Sugita, Gohyaku and Yashiro Rivers (Yasutaka et al. (2014)), and at Natsui and

Same rivers (Nagao et al, 2013). Figure 5-1 shows the locations of all five rivers where data were available. The Wariki and Hiso Rivers are located in the high contamination area (1-3×10^6 Bq m^{-2} region) to the northwest of the power plants at a distance of approximately 45 km. These two rivers are branches of the Niida River. The Abukuma River is the main stream of the Matsu, Sugita, Gohyaku and Yashiro Rivers, the first three of these being located in the 3-6×10^5 Bq m^{-2} region and the Yashiro River is in the less contaminated <3×10^5 Bq m^{-2} region.

This study collaborated with Chiba Institute of Technology in Japan to carry out measurements and determine catchment characteristics of Iitate Lake. Lake water samples were collected to obtain data over a longer period than the measurements conducted by MEXT on this lake. Iitate Lake is located in a highly contaminated area within the catchment of the Wariki River. In addition, monitoring data was obtained from Chiba Institute of Technology on concentration of fish in Teganuma Lake, this lakes being in about 160 km from the NPSs in the southwest direction.

Surface deposition (Bq m^{-2}) measurements in the catchments of all rivers and lakes were performed by MEXT (2014). MEXT collected many soil samples in a large area of about 200 km radius from Fukushima I NPSs. The first measurement data from the catchments of all rivers and Iitate Lake were collected on 14 June 2011, while the samples of soils in catchments of Kasumigaura and Teganuma Lake were performed very late on 1 March 2012. For modelling, surface deposition measurements were decay corrected to the high deposition on 15 March 2011.

In studies in Europe, the runoff of radiocaesium from catchments depended on the degree of coverage with organic, boggy soils (J. T. Smith, Howard, et al., 1998; J. T. Smith et al., 2004), but evidence of such boggy soils was observed in the study areas in Japan by Chiba Institute of Technology (Yutaka Kameda, pers. comm.) so this fraction is assumed to be zero for all rivers and lakes in this research. The potassium concentration of the water is important for modelling radioactivity of radiocaesium in fish because the rate of uptake of radiocaesium into fish is inversely proportional to the potassium concentration in water (Blaylock, 1982; J.T. Smith, A.V. Kudelsky, et al., 2000). There was a lack of available potassium concentration data in some of the rivers and lakes studied. However, UNEP (2008) concludes that the average of potassium concentration of surface waters in Asian countries is 2 mg L^{-1}, so this value was used as a best estimate.

The catchment areas of all rivers and lakes were measured by the Department of Mineral Resources (DMR), Thailand. DMR (Namphone Khampilang, Geologist) used ArcGIS® software version 10 of ESRI to analysis catchment areas and produce the maps of eight rivers and three lakes. The position sites of surface deposition are estimated on all maps (both rivers and lakes) because no GIS data is provided by MEXT (2014).

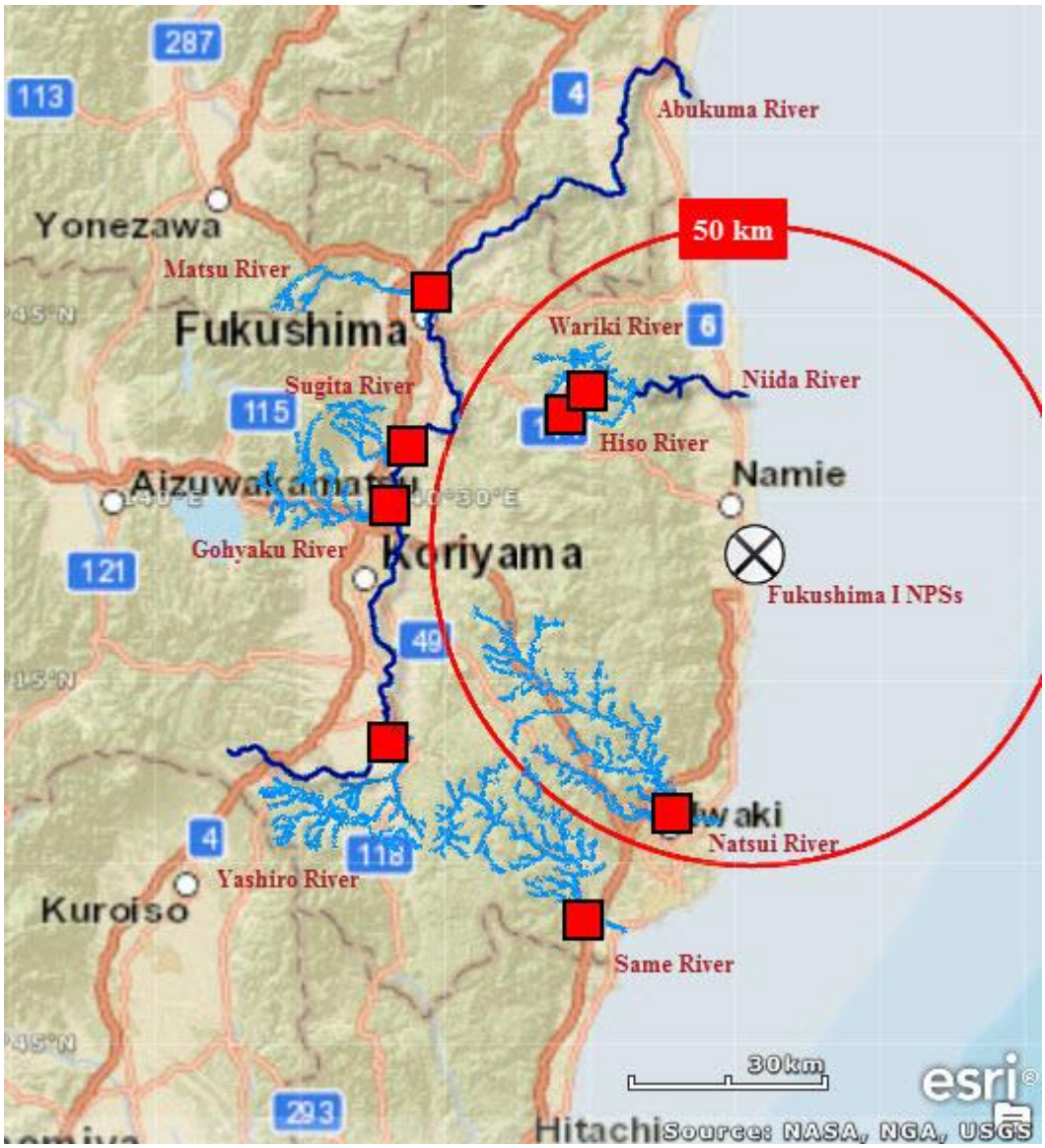

Figure 5-1 Illustration of the five rivers used in this research (the red squares represent the sampling points). The map was generated by ESRI's ArcGIS explorer (ESRI, http://www.esri.com/Software/arcgis/explorer) by the author.

Figure 5-2 the Location of Iitate, Kasumigaura and Teganuma Lakes. The map was generated by ESRI's ArcGIS explorer (ESRI, http://www.esri.com/Software/arcgis/explorer) and produced by the author.

(a) Wariki River

The Wariki (Figure 5.1) is a short river consisting of many branches, one of which begins at Iitate Lake, also studied here. Ueda at al. (2013) collected samples for fifteen different times between July and November in 2011 (Table 5-1) at one site of the river. The exact location of the sampling point is not available but it is located roughly at the beginning of one branch of the river and this point was near the Wariki River as shown in Figure 5-3 (a). The potassium concentration in river water at the sample point was also collected by taking four samples during July – November 2011: the mean value was 1.3 mg L^{-1}.

The catchment area of this branch of the river is relatively small, and surface deposition measurements are available for two points in this part of the catchment (MEXT, 2014). Since this river is locatedin the highly contaminated area, the means of surface depositions (corrected back to the highest deposition date on 15 March 2011) are remarkably high at 7.72×10^5, 8.00×10^5 and 8.57×10^6 Bq m^{-2} for ^{134,137}Cs and ^{131}I respectively.

(b) Hiso River

The Hiso River (Figure 5.1) has a short main stream with few branches. The sampling point is on the beginning of the main stream (Ueda, et al., 2013). At this sampling point, four samples of river water were collected for measuring potassium concentration, 2.9 mg L^{-1} was for mean and 1.3-4.2 mg L^{-1} was the range (Ueda et al. 2013).

The catchment of the sampling point used by Ueda and co-workers is small area: there were available three sites of soil sampling from MEXT (2014), these site have one single sample for each and the details are shown in Figure 5-3 (b). The mean deposited concentration density of ^{134,137}Cs and ^{131}I corrected to 15 March 2011 were 8.95×10^5, 9.15×10^5 and 7.79×10^6 Bq m^{-2} respectively which had the highest surface deposition compared with other rivers.

Table 5-1 Dissolved concentration and percentage of dissolved form of ^{137}Cs of water in Wariki and Hiso Lakes (Ueda, et al., 2013).

Time of Sampling	Years after deposition	*s* (mg L^{-1})	^{134}Cs			^{137}Cs		
			Particulate$^{\Delta}$ (Bq kg^{-1})	Dissolved (Bq m^{-3})	K_d (L kg^{-1})	Particulate$^{\Delta}$ (Bq kg^{-1})	Dissolved (Bq m^{-3})	K_d (L kg^{-1})
Wariki River								
20/07/2011 16:40	0.35	2.87E+01	2.16E+05	6.00E+02	3.60E+05	2.41E+05	7.00E+02	3.44E+05
21/07/2011 08:52	0.35	2.07E+01	2.23E+05	5.00E+02	4.46E+05	2.34E+05	6.00E+02	3.90E+05
21/07/2011 15:23	0.35	7.70E+00	2.34E+05	4.00E+02	5.85E+05	2.65E+05	4.00E+02	6.63E+05
22/07/2011 07:00	0.35	3.80E+00	2.51E+05	4.00E+02	6.28E+05	3.10E+05	4.00E+02	7.75E+05
10/08/2011 14:00	0.41	1.16E+01	1.95E+05	4.00E+02	4.88E+05	2.18E+05	4.00E+02	5.45E+05
20/09/2011 14:10	0.52	7.11E+01	1.34E+05	5.00E+02	2.68E+05	1.63E+05	6.00E+02	2.72E+05
20/09/2011 16:30	0.52	6.15E+01	1.25E+05	5.00E+02	2.50E+05	1.51E+05	6.00E+02	2.52E+05
21/09/2011 09:45	0.52	1.31E+02	1.18E+05	5.00E+02	2.36E+05	1.38E+05	5.00E+02	2.76E+05
21/09/2011 15:30	0.52	6.40E+01	1.17E+05	3.00E+02	3.90E+05	1.34E+05	4.00E+02	3.35E+05
22/09/2011 10:20	0.52	2.50E+01	5.50E+04	2.00E+02	2.75E+05	6.60E+04	2.00E+02	3.30E+05
21/11/2011 13:15	0.69	1.00E+00*	8.80E+04*	1.20E+02*	7.33E+05*	1.06E+05*	1.50E+02*	7.07E+05*
22/11/2011 10:50	0.69	1.00E+00*	1.08E+05*	1.00E+02*	1.08E+06*	1.20E+05*	1.30E+02*	9.23E+05*
	Average	4.26E+01	1.67E+05	4.30E+02	3.93E+05	1.92E+05	4.80E+02	4.18E+05

Table 5-1 (continued) Dissolved concentration and percentage of dissolved form of ^{137}Cs of water in Wariki and Hiso Lakes (Ueda, et al., 2013).

Time of Sampling	Years after deposition	*s* (mg L^{-1})	^{134}Cs			^{137}Cs		
			Particulate$^{\Delta}$ (Bq kg^{-1})	Dissolved (Bq m^{-3})	K_d (L kg^{-1})	Particulate$^{\Delta}$ (Bq kg^{-1})	Dissolved (Bq m^{-3})	K_d (L kg^{-1})
Hiso River								
20/07/2011 14:42	0.35	4.73E+01	1.81E+05	1.10E+03	1.65E+05	2.05E+05	1.30E+03	1.58E+05
20/07/2011 17:33	0.35	5.92E+01	1.71E+05	1.30E+03	1.32E+05	2.09E+05	1.50E+03	1.39E+05
21/07/2011 08:00	0.35	2.39E+01	1.65E+05	1.30E+03	1.27E+05	1.87E+05	1.40E+03	1.34E+05
21/07/2011 15:53	0.35	1.18E+01	1.57E+05	8.30E+02	1.89E+05	1.92E+05	9.10E+02	2.11E+05
22/07/2011 06:30	0.35	7.50E+00	1.86E+05	7.10E+02	2.62E+05	2.26E+05	8.10E+02	2.79E+05
10/08/2011 15:00	0.41	1.74E+01	5.40E+04	5.90E+02	9.15E+04	1.89E+05	7.10E+02	2.66E+05
20/09/2011 13:00	0.52	5.34E+01	1.11E+05	9.30E+02	1.19E+05	1.28E+05	1.10E+03	1.16E+05
20/09/2011 16:00	0.52	3.54E+01	1.15E+05	1.00E+03	1.15E+05	1.39E+05	1.10E+03	1.26E+05
21/09/2011 09:00	0.52	5.76E+01	9.40E+04	7.10E+02	1.32E+05	1.12E+05	8.00E+02	1.40E+05
21/09/2011 11:00	0.52	4.01E+01	1.05E+05	8.10E+02	1.30E+05	1.23E+05	1.00E+03	1.23E+05
21/09/2011 15:00	0.52	3.72E+01	9.80E+04	7.90E+02	1.24E+05	1.18E+05	1.00E+03	1.18E+05
22/09/2011 10:00	0.52	1.51E+01	5.80E+04	5.80E+02	1.00E+05	7.00E+04	6.80E+02	1.03E+05
22/09/2011 11:00	0.52	1.67E+01	5.40E+04	5.40E+02	1.00E+05	6.10E+04	6.60E+02	9.24E+04
21/11/2011 15:30	0.69	1.30E+00*	8.00E+04*	1.70E+02*	4.71E+05*	9.90E+04*	2.00E+02*	4.95E+05*
22/11/2011 10:00	0.69	1.50E+00*	1.67E+05*	1.60E+02*	1.04E+06*	1.91E+05*	2.00E+02*	9.55E+05*
	Average	3.25E+01	1.19E+05	8.61E+02	1.37E+05	1.51E+05	9.98E+02	1.54E+05

Note that: *There was Typhoon over this period resulting to the percentage of dissolved form of ^{137}Cs increased rapidly than usual and these values are not used to calculate the mean.

$^{\Delta}$For dry weight.

(c) Yashiro River

The Abukuma is a long river which runs through the Fukushima Prefecture with many tributaries, the catchment of 234-km river is 5,390 km^2 covered mainly by forest and has very steep gradients in many of its sub-catchments as most of these are located in volcanic mountains (Kabir, Dutta, & Hironaka, 2011; Kinouchi, Seino, & Takase, 2012). Many of the tributaries of the Abukuma River, including the Yashiro River, had high fall out on their catchments. The Yashiro River is located at the beginning of the Abukuma River. Yasutaka and co-workers (2014) collected one water sample about 62 km to the southwest of the NPSs, the concentration of dissolved $^{134,137}Cs$ being 9 and 16 Bq m^{-2} on 14 September 2012. The surface deposition on the Yashiro River catchment is lower than other rivers studied in this research. MEXT (2014) collected soil samples in this large catchment on 14 June 2014 as shown the detail in Figure 5-4 (a) – (c), and the corrected means are 2.76×10^4, 2.80×10^4 and 2.21×10^5 Bq m^{-2} for $^{134,137}Cs$ and ^{131}I respectively.

For potassium concentrations, there is no available data in any of the tributaries of the Abukuma River. However, Sakaguchi and co-workers (2014) measured potassium concentrations in the main stream of the Abukuma River at three sites all of which are downstream of the Yarisho River. The values measured were 2.5, 2.7 and 2.5 mg L^{-1} and the mean is 2.56 mg L^{-1} (another site in the estuary of the river was not used for estimating the mean due to its salinity). It is assumed that the potassium concentration of the tributaries is similar to the main river, so this wil be used for the Yashiro model and other tributaries of the Abukuma.

(d) Gohyaku River

The Gohyaku River is a tributary of the Abukuma River located further downstream in the middle section of the main river. The sampling point is in the western area, at a distance from the power plant of around 56 km. Measurements of radioactivity concentrations in water from a sample at this point collecting on 14 September 2012 were 11 and 22 Bq m^{-3} for dissolved ^{134}Cs and ^{137}Cs (Yasutaka, et al., 2014). The catchment is smaller than Yashiro River (Figure 5-5 (a) – (c)), and the means of surface deposition (from data in MEXT 2014) corrected back to 15 March 2011 were found to be 9.05×10^4, 9.14×10^4 and 7.66×10^5 Bq m^{-2} for $^{134,137}Cs$ and ^{131}I respectively.

(e) Sugita River

Next to Gohyaku River in the downstream direction is the Sugita River. Yasutaka and co-workers (2014) measured dissolved ^{134}Cs and ^{137}Cs at this point (~56 km to the west direction of the NPSs) in one water sample on 14 September 2011, finding 11 and 25 Bq m^{-3} respectively Figures 5-6 (a) – (c) illustrate the corrected surface deposition of key radionuclides (from data in (MEXT, 2014), and 9.71×10^{4} Bq m^{-2} was the mean for deposited ^{134}Cs, 1.02×10^{5} for ^{137}Cs and 6.32×10^{6} for ^{131}I.

(f) Matsu River

The last branch of Abukuma River used in this research is the Matsu River. The dissolved concentrations of ^{134}Cs and ^{137}Cs (Yasutaka, et al., 2014) were, 9.45×10^{4} and 7.66×10^{5} Bq m^{-3} respectively at a sampling point located approximately 62 km to the southwest of the NPS. Corrected surface deposition in this catchment was 2.36×10^{5}, 2.36×10^{5} and 3.25×10^{6} Bq m^{-2} for $^{134,137}Cs$ and ^{131}I respectively, from monitoring on 14 June 2011 (see Figure 5-7 (a) – (c)).

Table 5-2 Summary of radioactivity concentrations of radiocaesium in river water (dissolved phase) in four branches of the Abukuma River monitored by Yasutaka et al. (2014).

River	Time of Sampling	Years after deposition	Particulate phase (Bq m^{-3})		Dissolved phase (Bq m^{-3})	
			^{134}Cs	^{134}Cs	^{134}Cs	^{137}Cs
Yashiro	14/09/2012	1.5	5.00E+00	1.30E+01	9.00E+00	1.60E+01
Gohyaku	14/09/2012	1.5	9.20E+01	1.49E+02	1.10E+01	2.20E+01
Sugita	14/09/2012	1.5	4.20E+01	7.10E+01	1.10E+01	2.50E+01
Matsu	14/09/2012	1.5	8.00E+00	1.30E+01	4.30E+01	8.30E+01

Table 5-2 shows the concentration of radiocaesium in river water in four branches of the Abukuma River. The Matsu River had the highest concentration, probably due to the highest atmospheric fall out to its catchment; both Gohyaku and Sugita rivers had lower concentrations than the Matsu by a factor of four, and the lowest concentration occurred in the Yashiro. This confirms that the concentration of radiocaesium in river water in these mineral catchments depended mainly on surface deposition to the catchment area similar to studies of nuclear weapons test fallout and the Chernobyl accident (Helton, et al., 1985; J. T. Smith, et al., 2005; J. T. Smith, et al., 2004).

(g) Natsui and Same Rivers

Outside the near zone of the Fukushima I NPSs, there are available measurements of radiocaesium in both dissolved and particulate phases from the Natsui and Same Rivers in the southwest area. Observations of radioactivity concentration of river water were made from July 2011 to December 2011 (five samples from one site on each river) by Nagao et al. (2013). The dissolved phase fraction of radiocaesium can be estimated from the total using the mean percentage of dissolved phase activity. Since there was a Typhoon on 22 September 2011, the percentage of dissolved phase changed rapidly making this estimation uncertain, so the measured data after the Typhon were not used in this research. The mean percentage of dissolved phase $^{134, 137}$Cs before the Typhoon was 60% for the Natsui and 74% for Same (from Nagao et al. (2013) Estimates of dissolved-phase activity in these rivers from before the Typhoon are shown in Table 5-3.

The sites for collecting river water samples from the Natsui and Same Rivers are downstream of most tributaries (about 42 km from Fukushima I NPSs). The details of surface deposition in Natsui' and Same catchments (monitored by MEXT (2014) on 14 June 2011) are shown in Figures 5-8 and 5.9.The corrected surface depositions on 15 March 2011 were 2.09×10^4, 2.77×10^4 and 1.26×10^6 Bq m^{-2} for ^{134,137}Cs and ^{131}I (respectively) in the Natsui (Figure 5-8 (a)-(c)) and 2.21×10^4, 2.23×10^4 and 1.60×10^6 Bq m^{-2} in the Same (Figure 5-9 (a)-(c)).

Since there are no available potassium concentration measurements for the Natsui and Same Rivers, the mean value of 2 mg L^{-1} for Asian countries (UNEP, 2008) is used for estimation in model. This mean is similar to other rivers which are shown in the summation of input parameters of all rivers used in this research (Table 5-4).

Since the catchments of the Natsui and Same rivers are farther than previous rivers from the NPSs (about 40 and 60 km for Natsui and Same respectively), the surface deposition are significantly lower than the other rivers, being about one order of magnitude lower than the highly contaminated Wariki and Hiso Rivers.

Table 5-3 Summary of radioactivity concentrations of radiocaesium in river water in the Natsui and Same Rivers Nagao et al. (2013)).

Time of Sampling	Years after deposition	Particulate phase (Bq m^{-3})		Dissolved phase (Bq m^{-3})	
		^{134}Cs	^{134}Cs	^{134}Cs	^{137}Cs
Natsui					
12/07/2011	0.33	1.96E+01	2.08E+01	2.94E+01	3.12E+01
27/07/2011	0.37	3.56E+01	3.92E+01	5.34E+01	5.88E+01
13/09/2011	0.50	1.01E+01	1.04E+01	1.51E+01	1.56E+01
Same					
12/07/2011	0.33	1.94E+01	2.11E+01	5.51E+01	5.99E+01
27/07/2011	0.37	1.24E+01	1.35E+01	3.52E+01	3.85E+01
13/09/2011	0.50	4.13E+00	4.91E+00	1.18E+01	1.40E+01

Table 5-4 shows the summary of minimum input parameters for all eight rivers which were analysed in this research. Since potassium concentrations in the water of the Natsui and Same River were not available, the general value of rivers in Asian countries (UNEP, 2008) was assumed. Measurement of potassium concentrations were available for Wariki and Hiso River while all branches of Abukuma River (Yashiro, Gohyaku, Sugita and Matsu River) use measured data (mean of 2.56 mg L^{-1}) from three-sites downstream of these four tributaries. For the fraction of the catchment covered by organic and boggy soils (f_{org}), Chiba Institute of Technology observed many catchments of rivers and lakes in Japan and confirmed that there is no content of boggy soil (Yutaka Kameda, pers. commun.).There were no available measurements of radiocaesium in fish data in these rivers so comparison with the model results was not possible. For prediction of activity concentrations in fish, a wet weight of fish of 1 kg was assumed.

Table 5-4 Summary of input parameters for all eight rivers.

River	mean surface deposition on catchment* (D_C, Bq m^{-2})			Potassium concentration (mg L^{-1})	fraction of the catchment covering by organic, boggy soils (f_{org})	Wet weight of fish (kg)
	^{131}I	^{134}Cs	^{137}Cs			
Wariki	8.57E+06	7.72E+05	8.00E+05	1.30	0.0$^{\Delta}$	1.0$^{\Omega}$
Hiso	7.79E+06	8.95E+05	9.15E+05	2.90	0.0$^{\Delta}$	1.0$^{\Omega}$
Yashiro	2.21E+05	2.76E+04	2.80E+04	2.56$^{\theta}$	0.0$^{\Delta}$	1.0$^{\Omega}$
Gohyaku	7.66E+05	9.05E+04	9.14E+04	2.56$^{\theta}$	0.0$^{\Delta}$	1.0$^{\Omega}$
Sugita	6.32E+06	9.71E+04	1.02E+05	2.56$^{\theta}$	0.0$^{\Delta}$	1.0$^{\Omega}$
Matsu	3.25E+06	2.36E+05	2.36E+05	2.56$^{\theta}$	0.0$^{\Delta}$	1.0$^{\Omega}$
Natsui	1.26E+06	2.09E+04	2.77E+04	2.00$^{\infty}$	0.0$^{\Delta}$	1.0$^{\Omega}$
Same	1.60E+06	2.21E+04	2.23E+04	2.00$^{\infty}$	0.0$^{\Delta}$	1.0$^{\Omega}$

Note that: *the measured data was monitored by MEXT (2014)

$^{\theta}$Mean value at downstream of Abukuma River monitored by Sakaguchi and co-workers (2014)

$^{\infty}$The general value of rivers in Asain countries (UNEP, 2008).

$^{\Delta}$Chiba Institute of Technology confirms that there is no content of boggy soil in these catchments.

$^{\Omega}$The default value of model.

(a) Wariki River

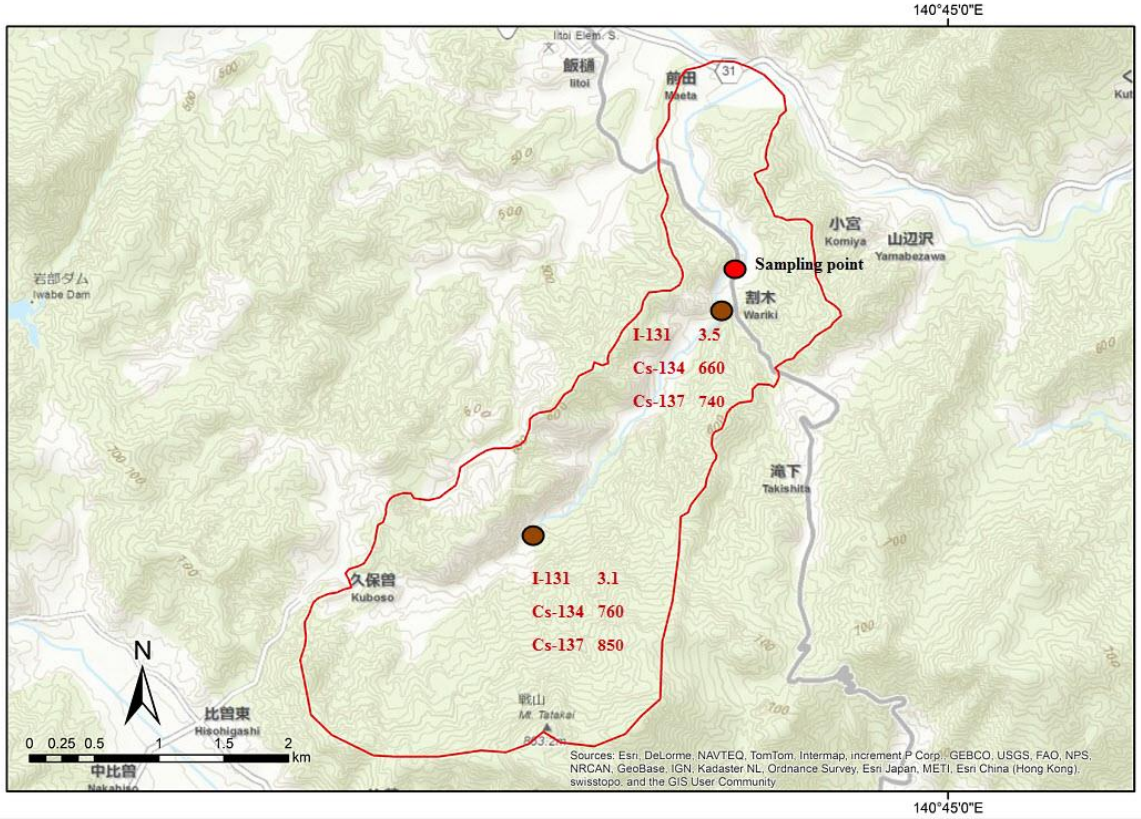

Figure 5-3 Estimated points of water sampling and surface deposition (kBq m^{-2}) of $^{134,137}Cs$ and ^{131}I at (a) Wariki River and (b) Hiso river (kBq m^{-2}), these two maps are generated by using ArcGIS® software, ESRI, and produced by DMR and the author. "NM" in (b) means no measurement at a site.

(b) Hiso River

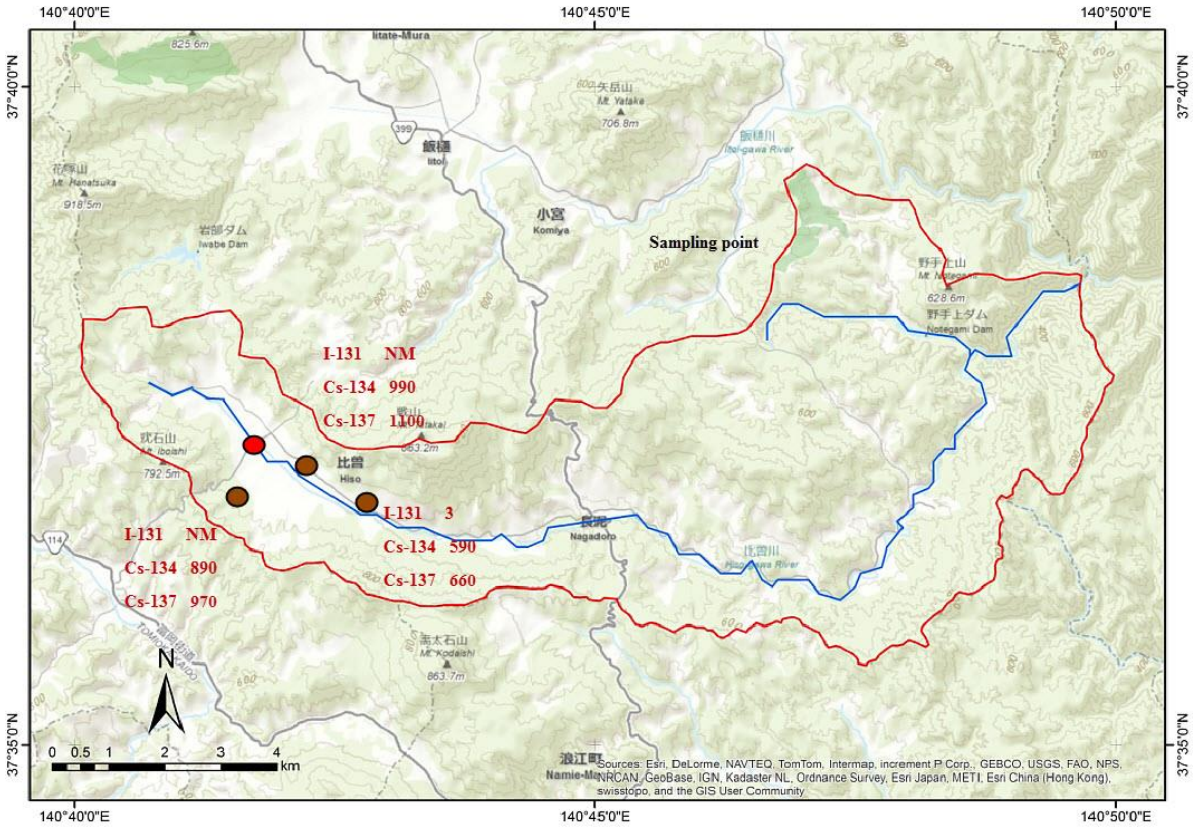

Figure 5-3 (continued) Estimated points of water sampling and surface deposition (kBq m^{-2}) of $^{134,137}Cs$ and ^{131}I at (a) Wariki River and (b) Hiso river (kBq m^{-2}), these two maps are generated by using ArcGIS® software, ESRI, and produced by DMR and the author. "NM" in (b) means no measurement at a site.

(a)

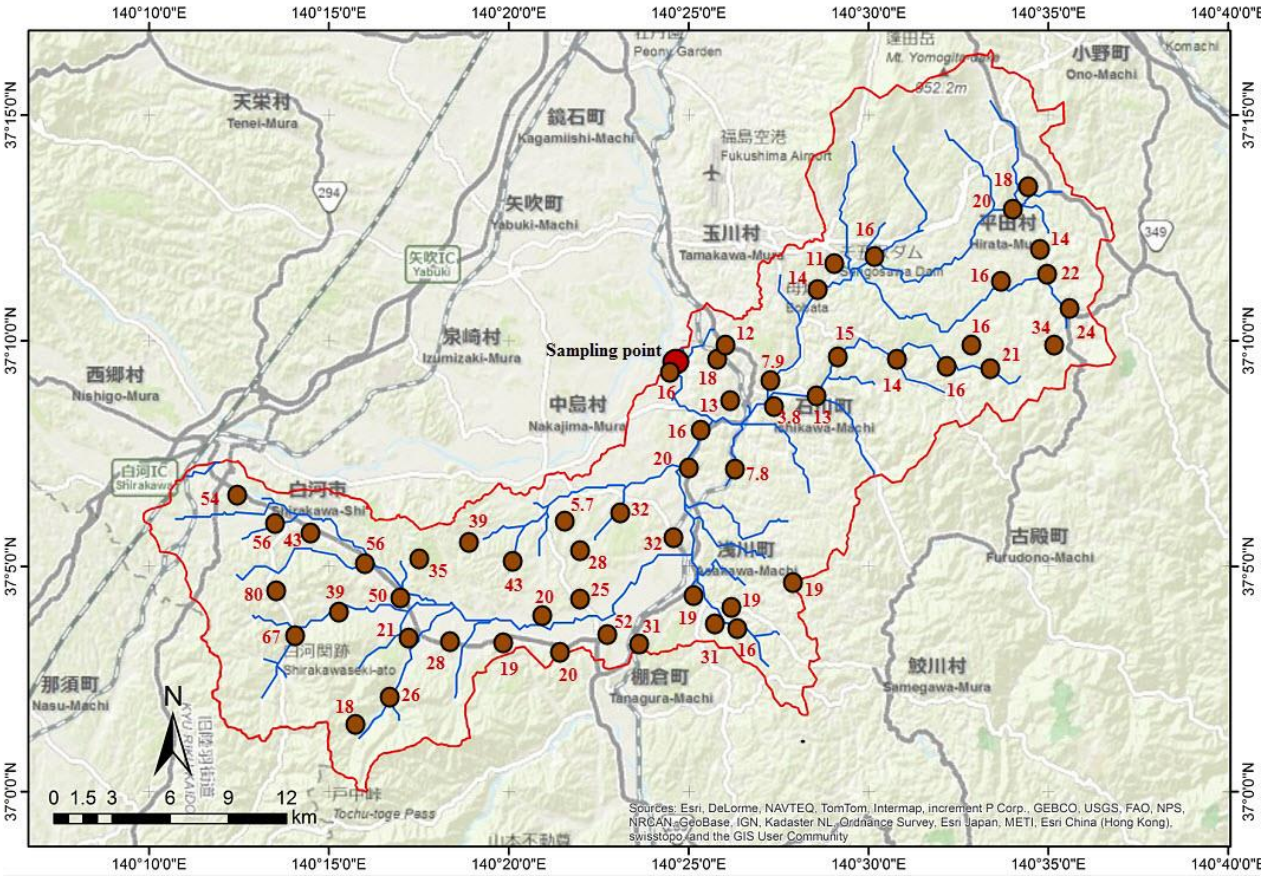

Figure 5-4 The surface deposition (kBq m^{-2}) of ^{134}Cs in (a), ^{137}Cs in (b) and ^{131}I in (C) within the catchment area of the Yashiro River, these measurement were made on14 June 2011. The maps were created by using ArcGIS® software, ESRI, and produced by DMR and the author.

(b)

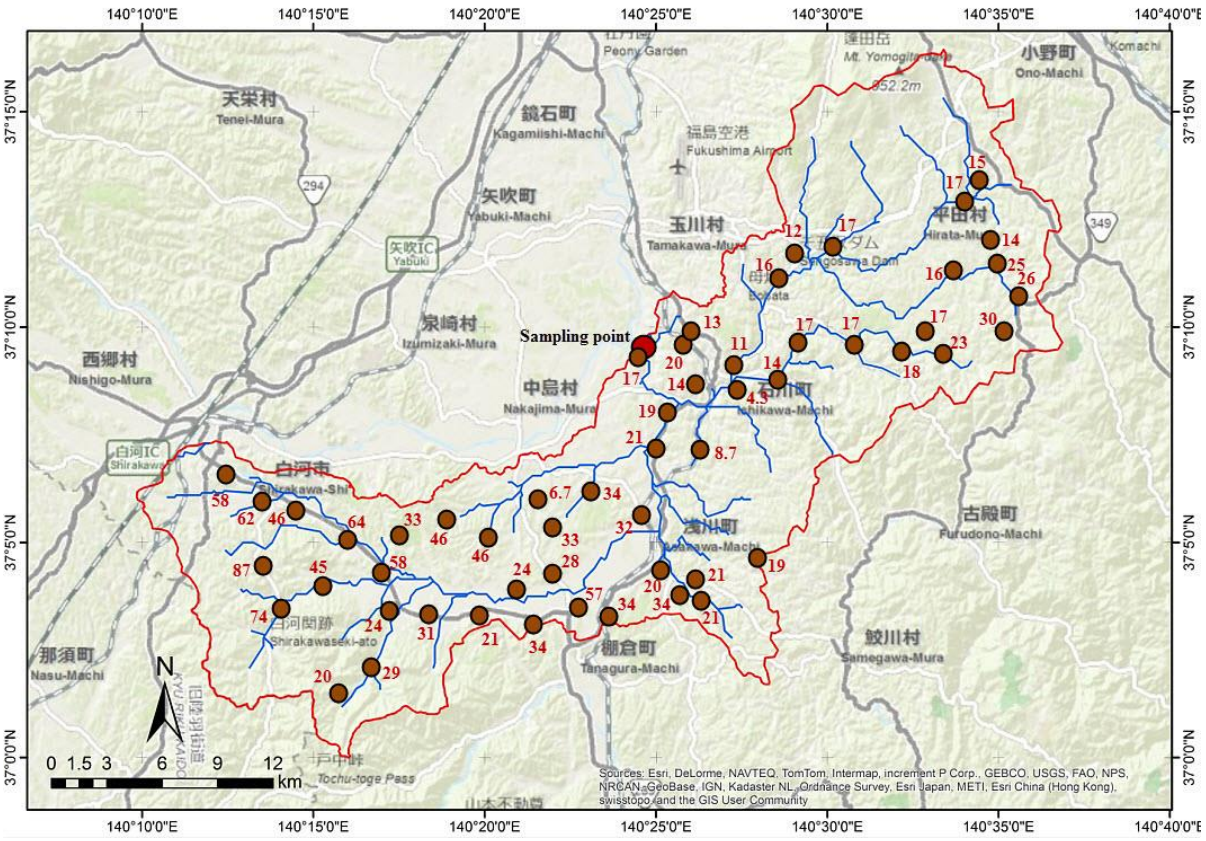

Figure 5-4 (continued) The surface deposition (kBq m^{-2}) of ^{134}Cs in (a), ^{137}Cs in (b) and ^{131}I in (C) within the catchment area of the Yashiro River. These measurements were made on14 June 2011. The maps were created by using ArcGIS® software, ESRI, and produced by DMR and the author.

(c)

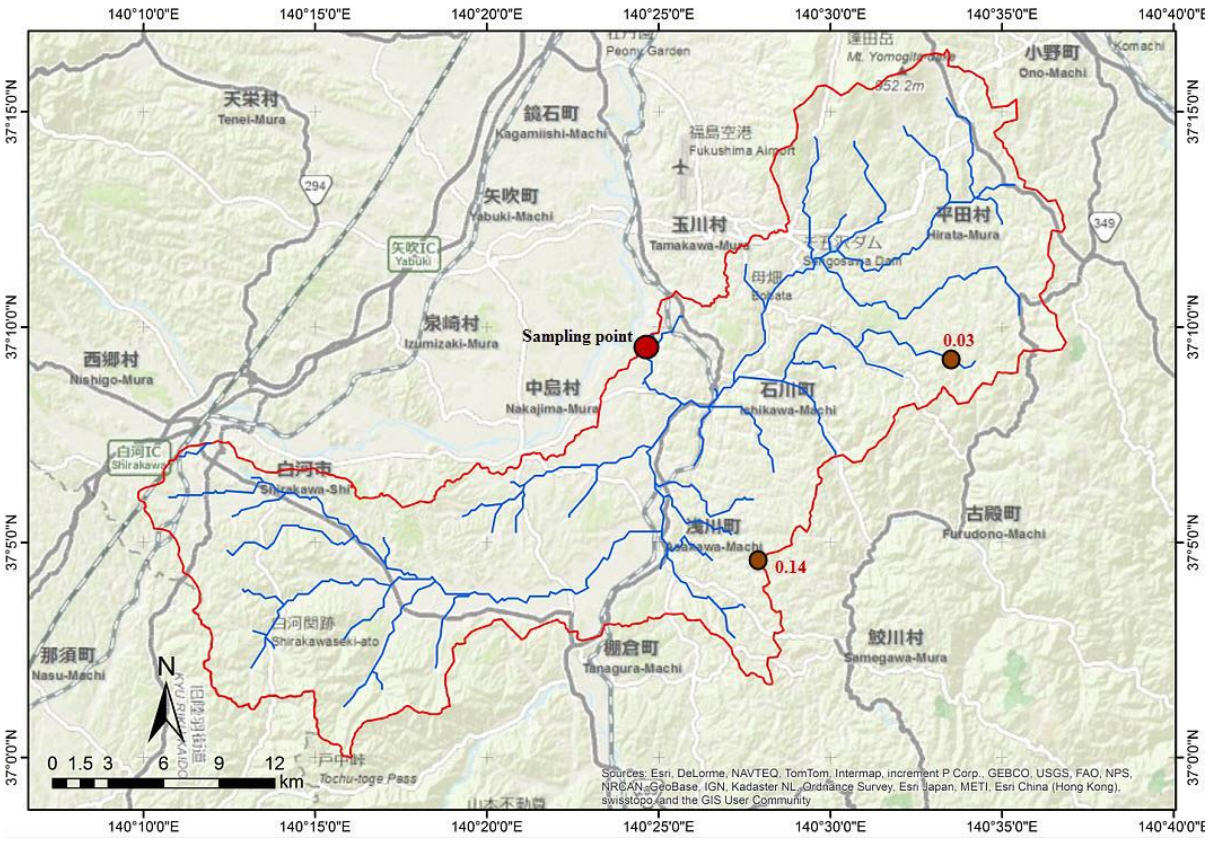

Figure 5-4 (continued) The surface deposition (kBq m^{-2}) of ^{134}Cs in (a), ^{137}Cs in (b) and ^{131}I in (C) within the catchment area of the Yashiro River. These measurements were made on14 June 2011. The maps were created by using ArcGIS® software, ESRI, and produced by DMR and the author..

(a)

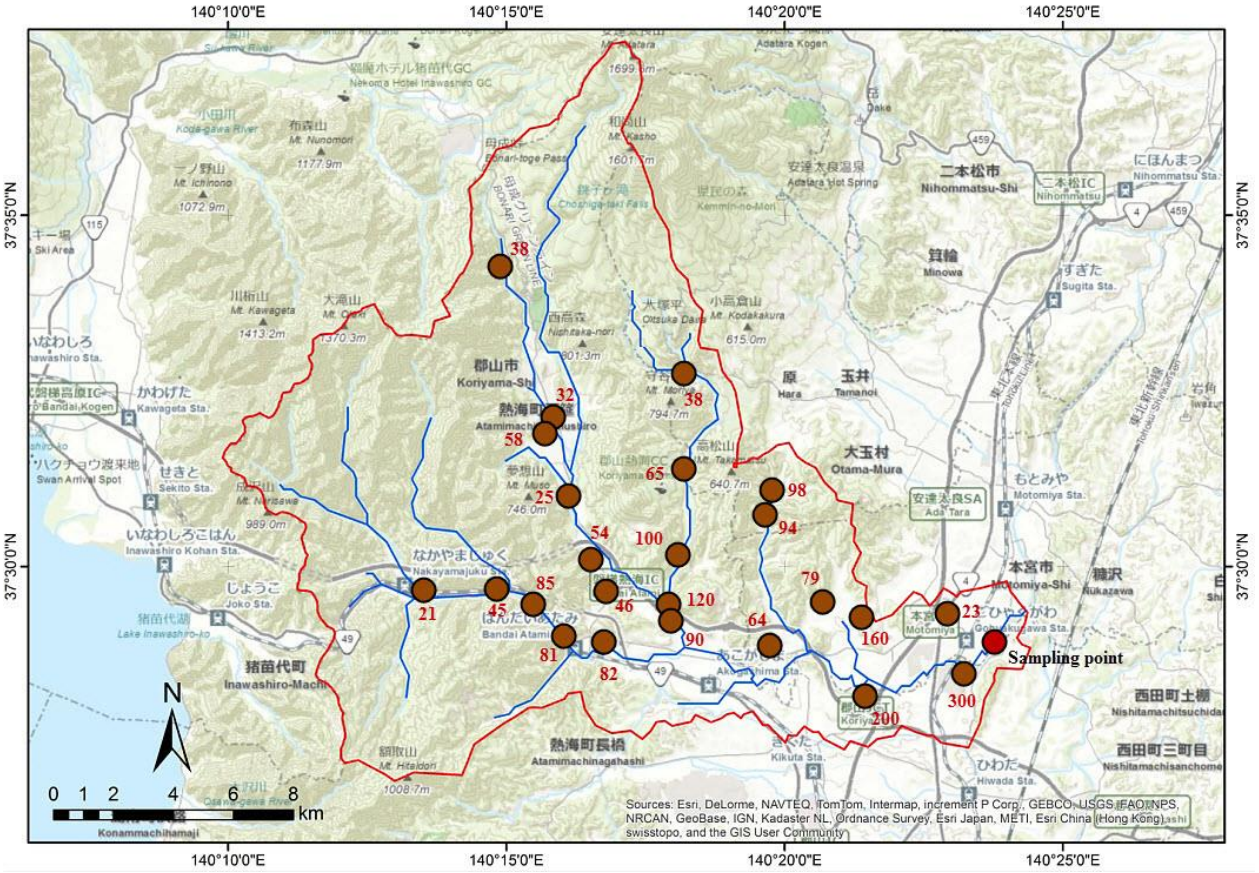

Figure 5-5 The surface deposition (kBq m^{-2}) of ^{134}Cs in (a), ^{137}Cs in (b) and ^{131}I in (C) within the catchment area of the Gohyaku River. These measurements were made on14 June 2011. The maps were created by using ArcGIS® software, ESRI, and produced by DMR and the author..

(b)

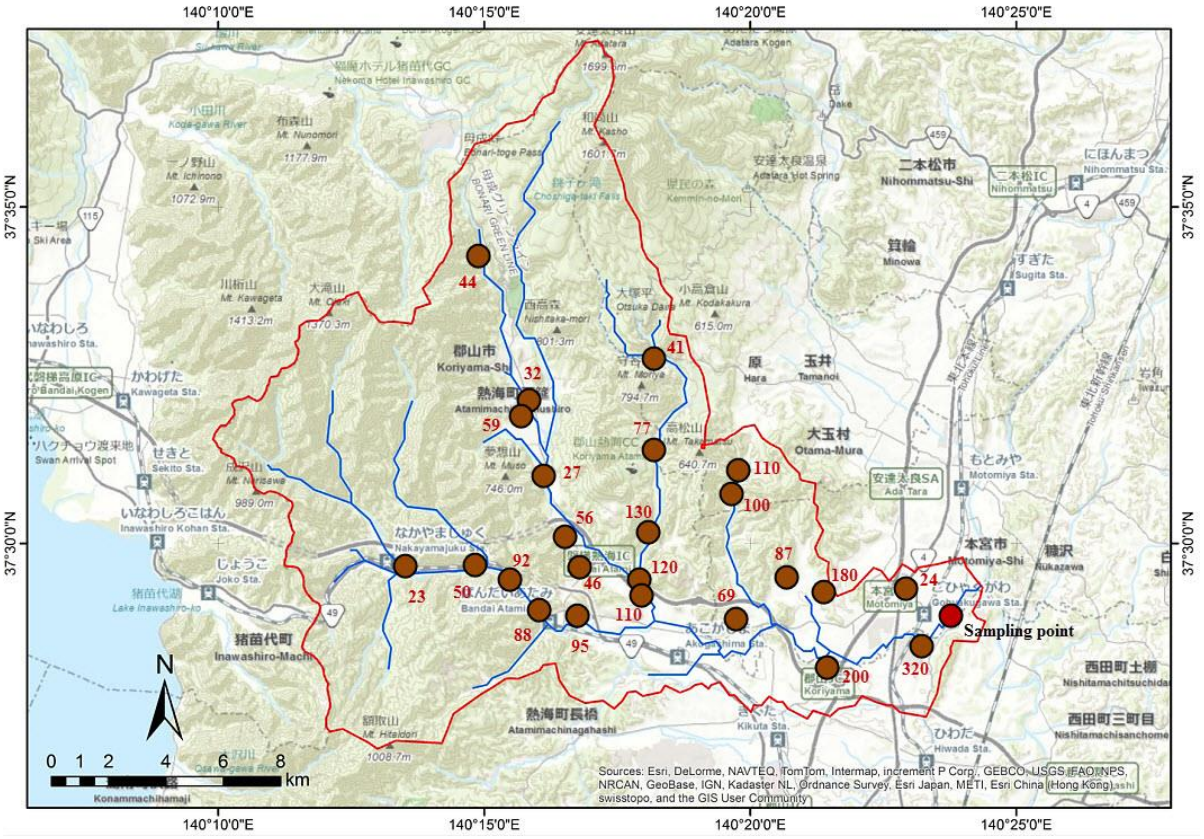

Figure 5-5 (continued) The surface deposition (kBq m^{-2}) of ^{134}Cs in (a), ^{137}Cs in (b) and ^{131}I in (C) within the catchment area of the Gohyaku River. These measurements were made on14 June 2011. The maps were created using ArcGIS® software, ESRI, and produced by DMR and the author.

(c)

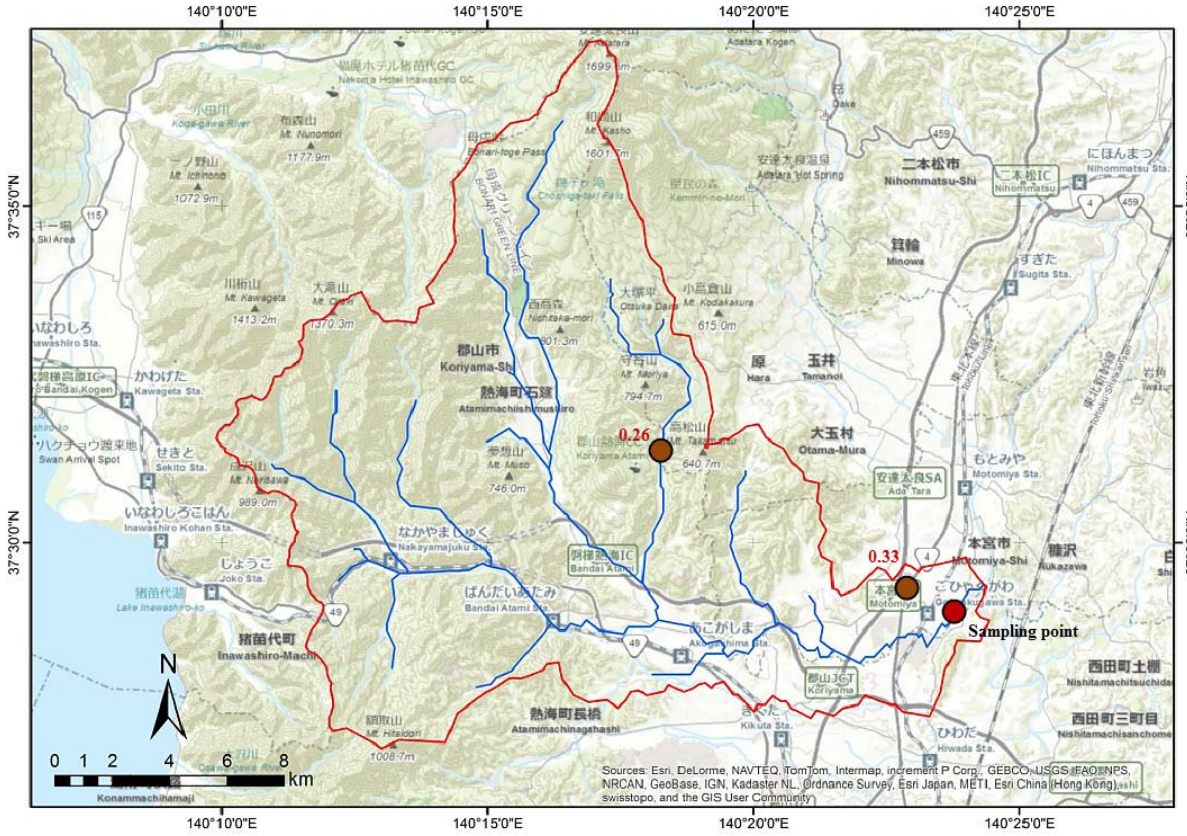

Figure 5-5 (continued) The surface deposition (kBq m^{-2}) of ^{134}Cs in (a), ^{137}Cs in (b) and ^{131}I in (C) within the catchment area of the Gohyaku River. These measurements were made on14 June 2011. The maps were created using ArcGIS® software, ESRI, and produced by DMR and the author.

(a)

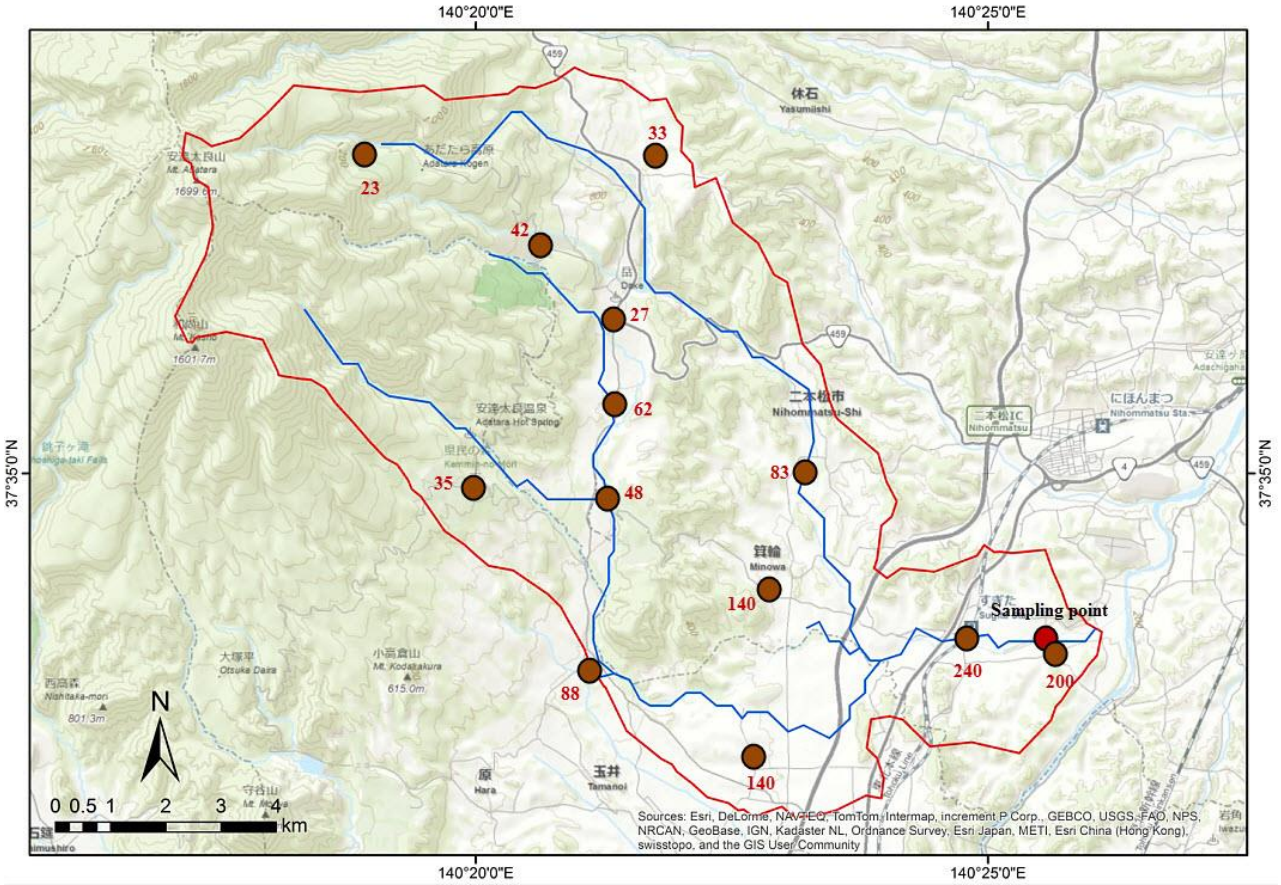

Figure 5-6 The surface deposition (kBq m^{-2}) of ^{134}Cs in (a), ^{137}Cs in (b) and ^{131}I in (C) within the catchment area of the Sugita River. These measurements were made on14 June 2011. The maps were created using ArcGIS® software, ESRI, and produced by DMR and the author.

(b)

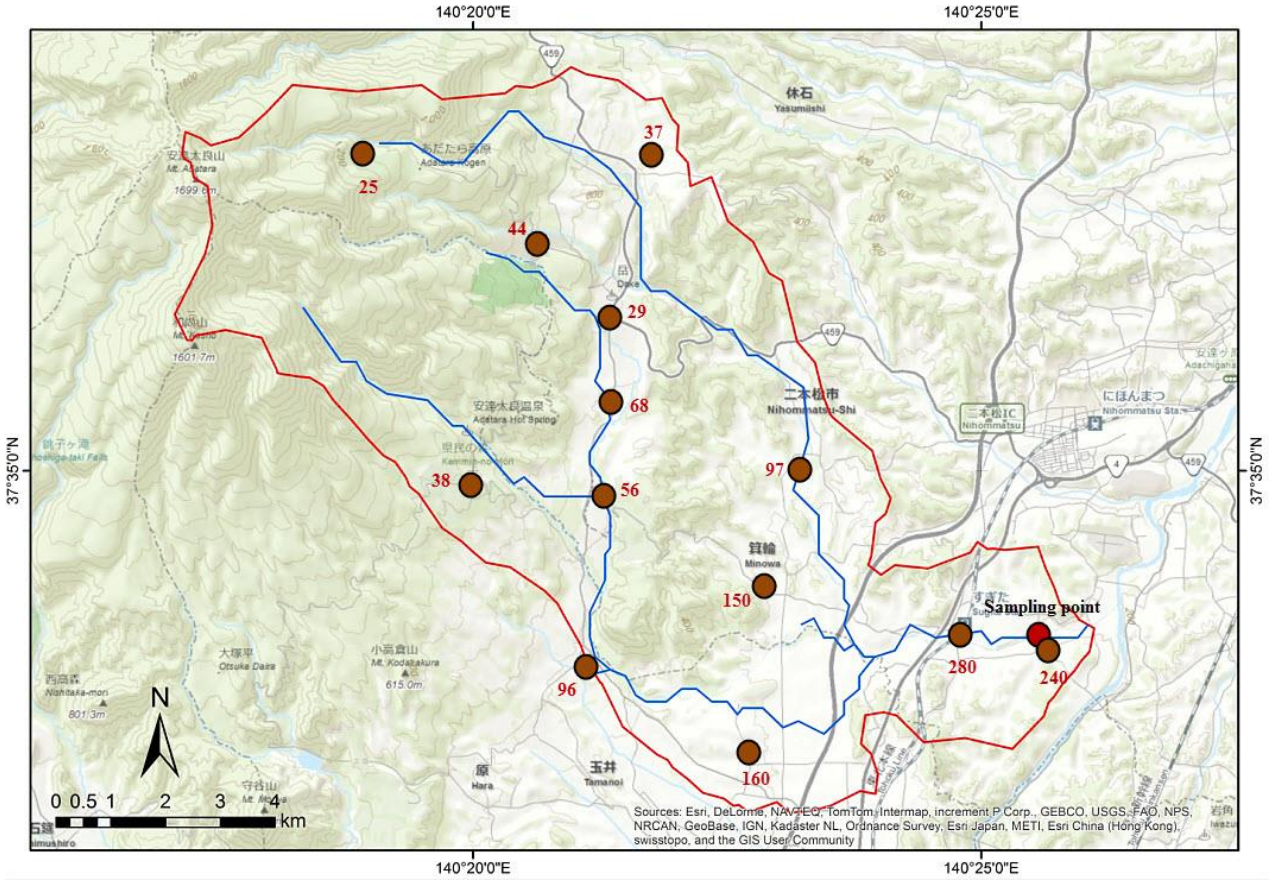

Figure 5-6 (continued) The surface deposition (kBq m^{-2}) of ^{134}Cs in (a), ^{137}Cs in (b) and ^{131}I in (C) within the catchment area of the Sugita River. These measurements were made on14 June 2011. The maps were created using ArcGIS® software, ESRI, and produced by DMR and the author.

(c)

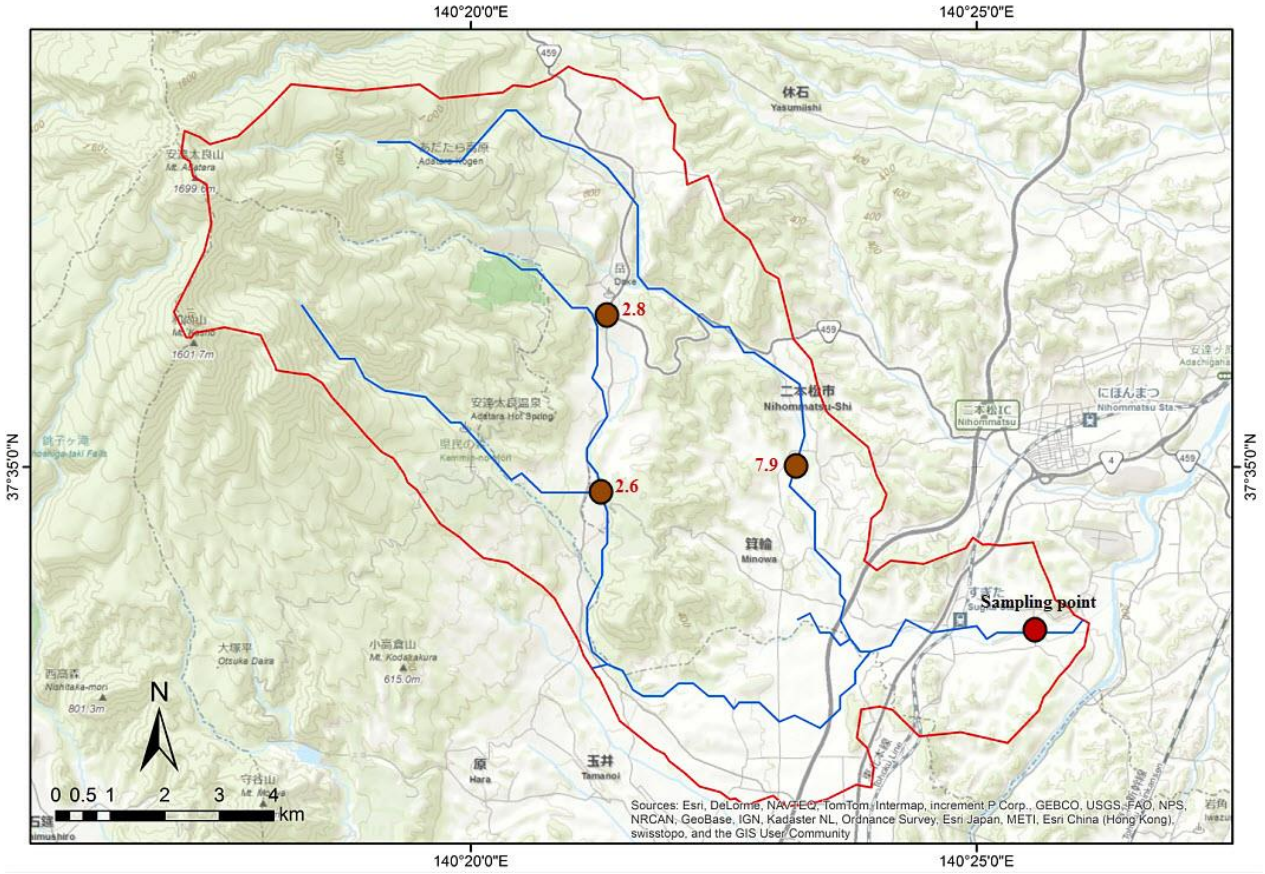

Figure 5-6 (continued) The surface deposition (kBq m^{-2}) of ^{134}Cs in (a), ^{137}Cs in (b) and ^{131}I in (C) within catchment area of Sugita River, these measurement were monitored on14 June 2011. The maps were created by using ArcGIS® software, ESRI, and produced by DMR and the author.

(a)

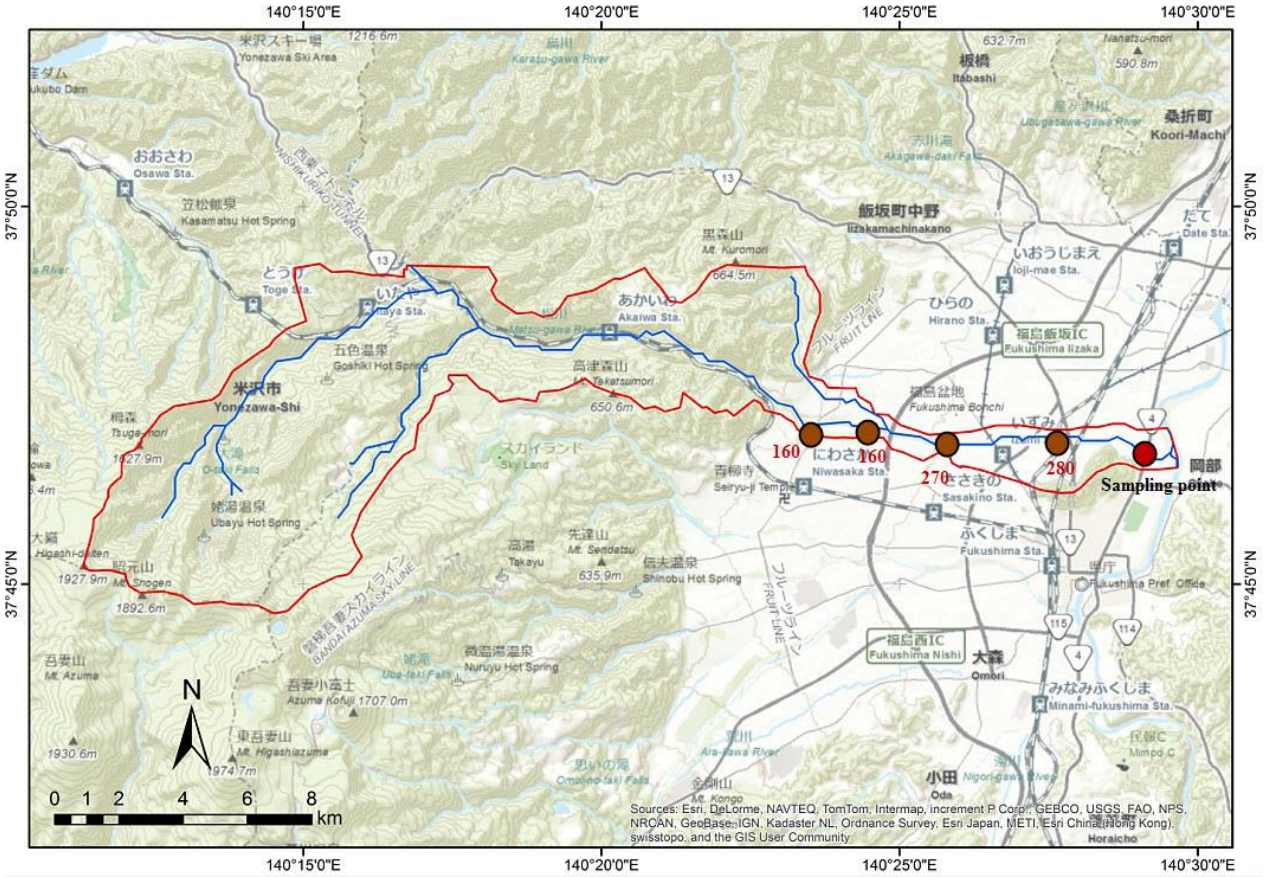

Figure 5-7 The surface deposition (kBq m^{-2}) of ^{134}Cs in (a), ^{137}Cs in (b) and ^{131}I in (C) within catchment area of Matsu River, these measurement were monitored on14 June 2011. The maps were created by using ArcGIS® software, ESRI, and produced by DMR and the author.

(b)

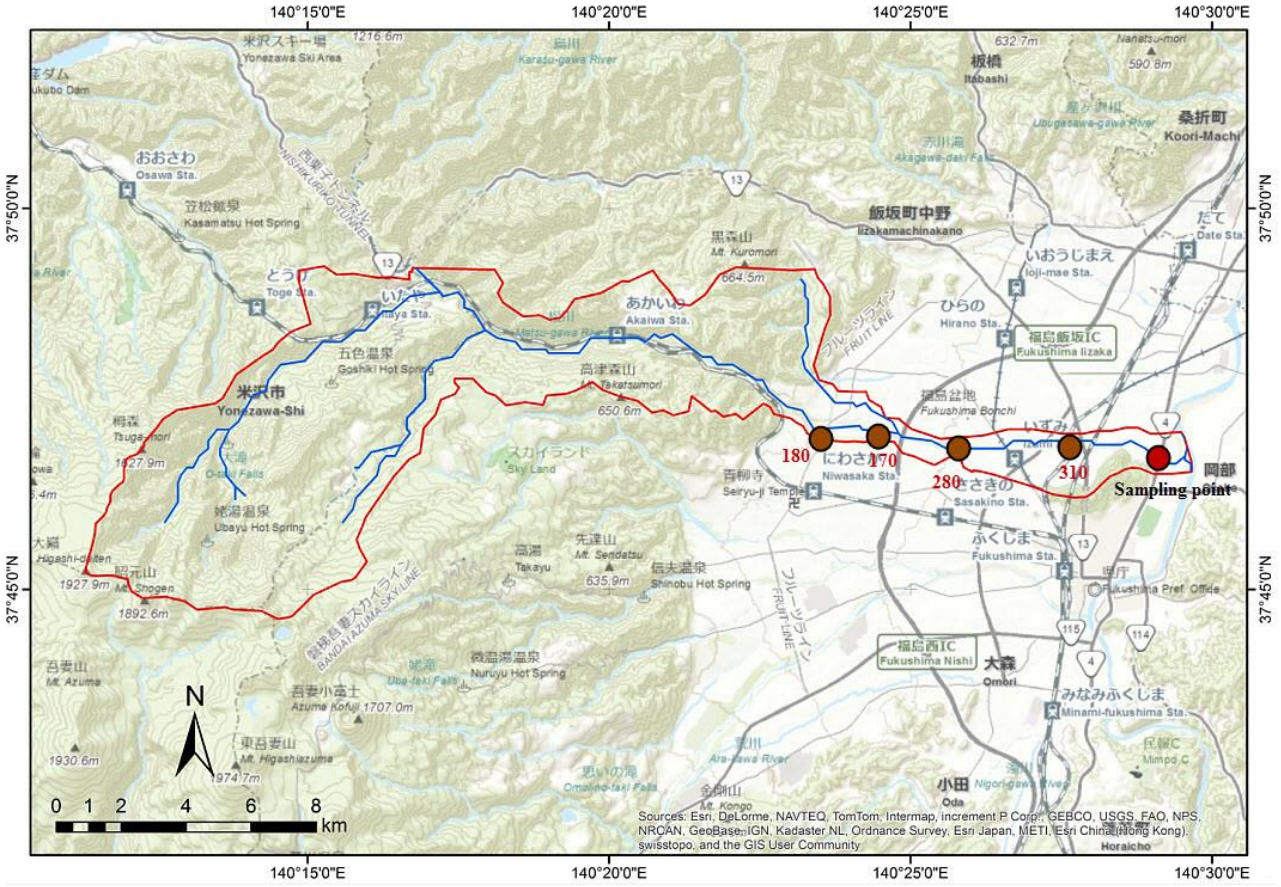

Figure 5-7 (continued) The surface deposition (kBq m^{-2}) of ^{134}Cs in (a), ^{137}Cs in (b) and ^{131}I in (C) within catchment area of Matsu River, these measurement were monitored on14 June 2011. The maps were created by using ArcGIS® software, ESRI, and produced by DMR and the author.

(c)

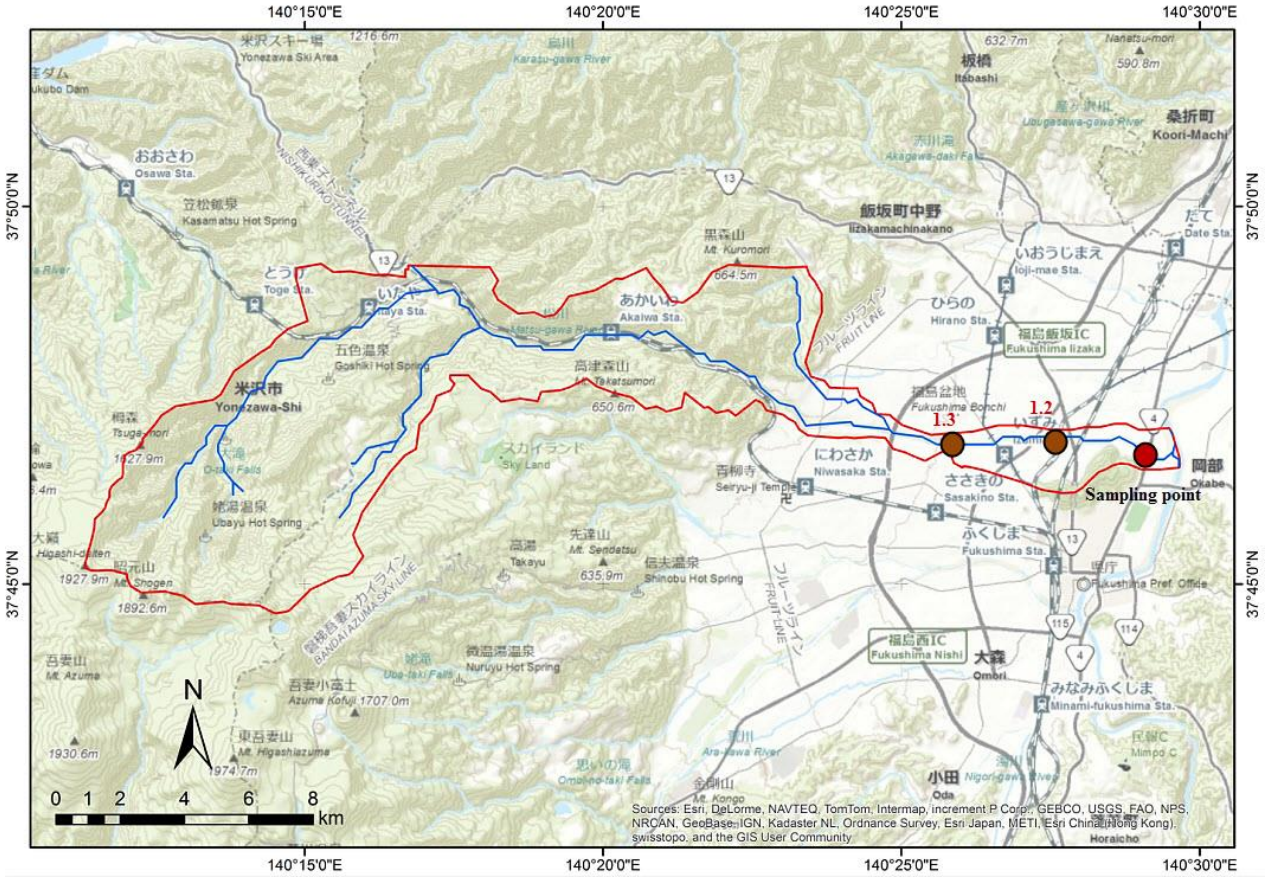

Figure 5-7 (continued) The surface deposition (kBq m^{-2}) of ^{134}Cs in (a), ^{137}Cs in (b) and ^{131}I in (C) within catchment area of Matsu River, these measurement were monitored on14 June 2011. The maps were created by using ArcGIS® software, ESRI, and produced by DMR and the author.

(a)

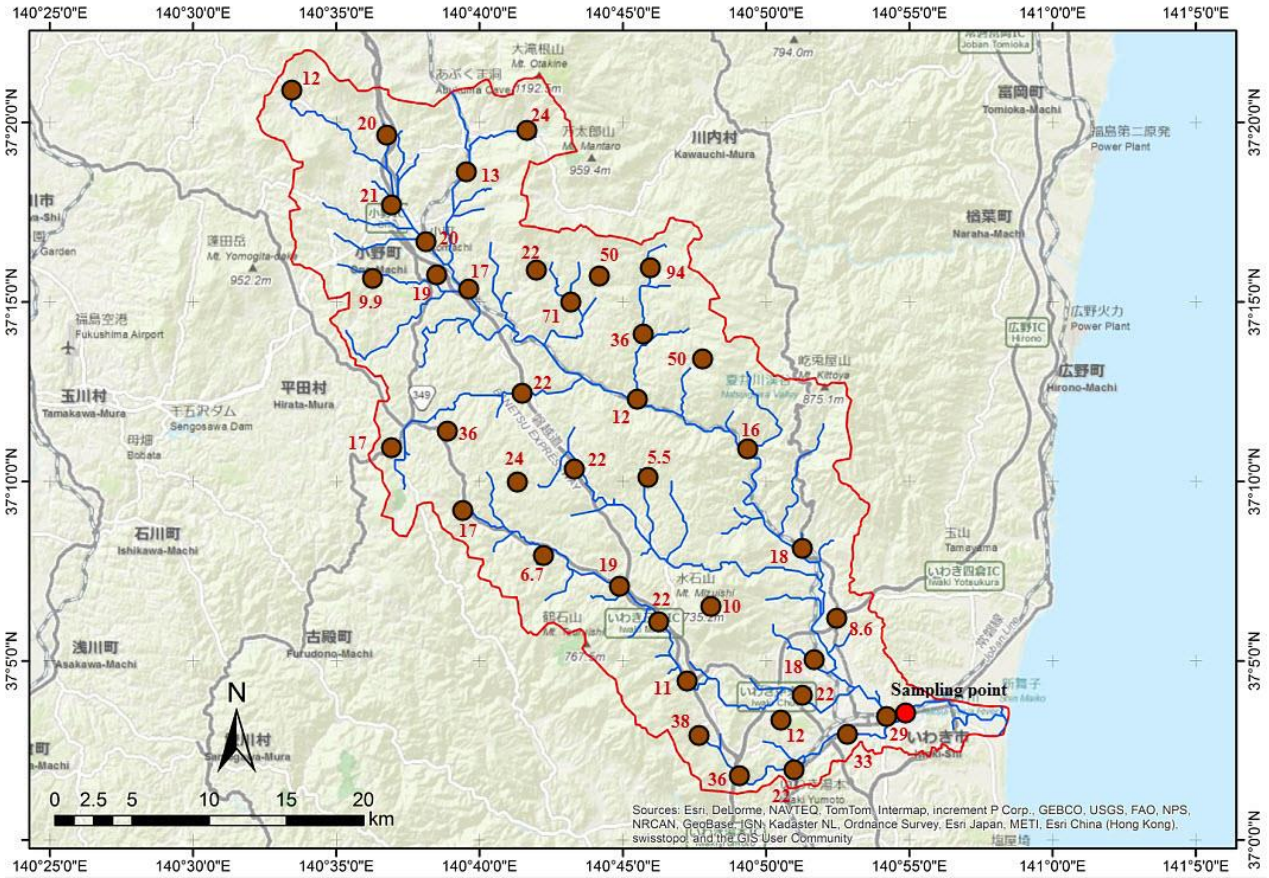

Figure 5-8 The surface deposition (kBq m^{-2}) of ^{134}Cs in (a), ^{137}Cs in (b) and ^{131}I in (C) within catchment area of Natsui River, these measurement were monitored on14 June 2011. The maps were created by using ArcGIS® software, ESRI, and produced by DMR and the author.

(b)

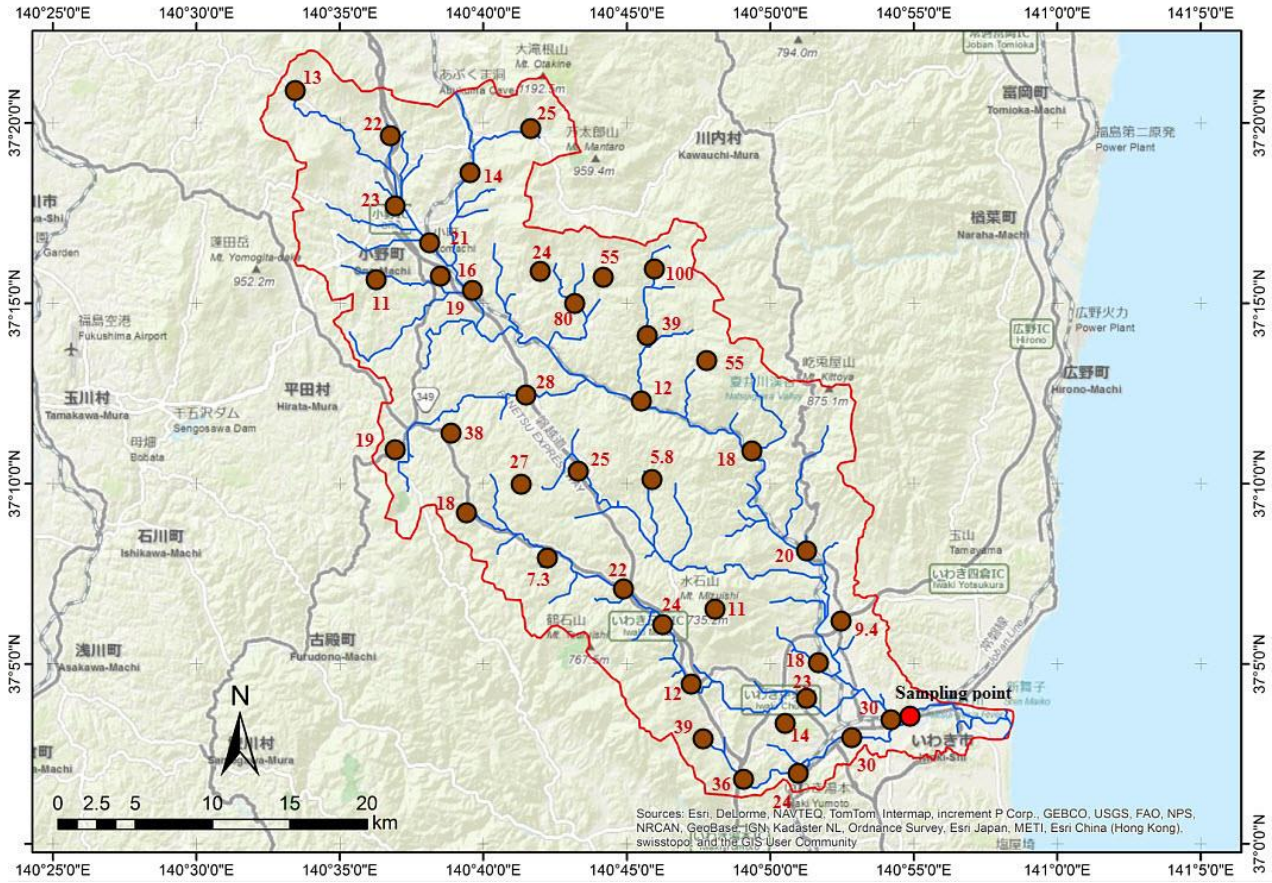

Figure 5-8 (continued) The surface deposition (kBq m^{-2}) of ^{134}Cs in (a), ^{137}Cs in (b) and ^{131}I in (C) within catchment area of Natsui River, these measurement were monitored on14 June 2011. The maps were created by using ArcGIS® software, ESRI produced by DMR and the author.

(c)

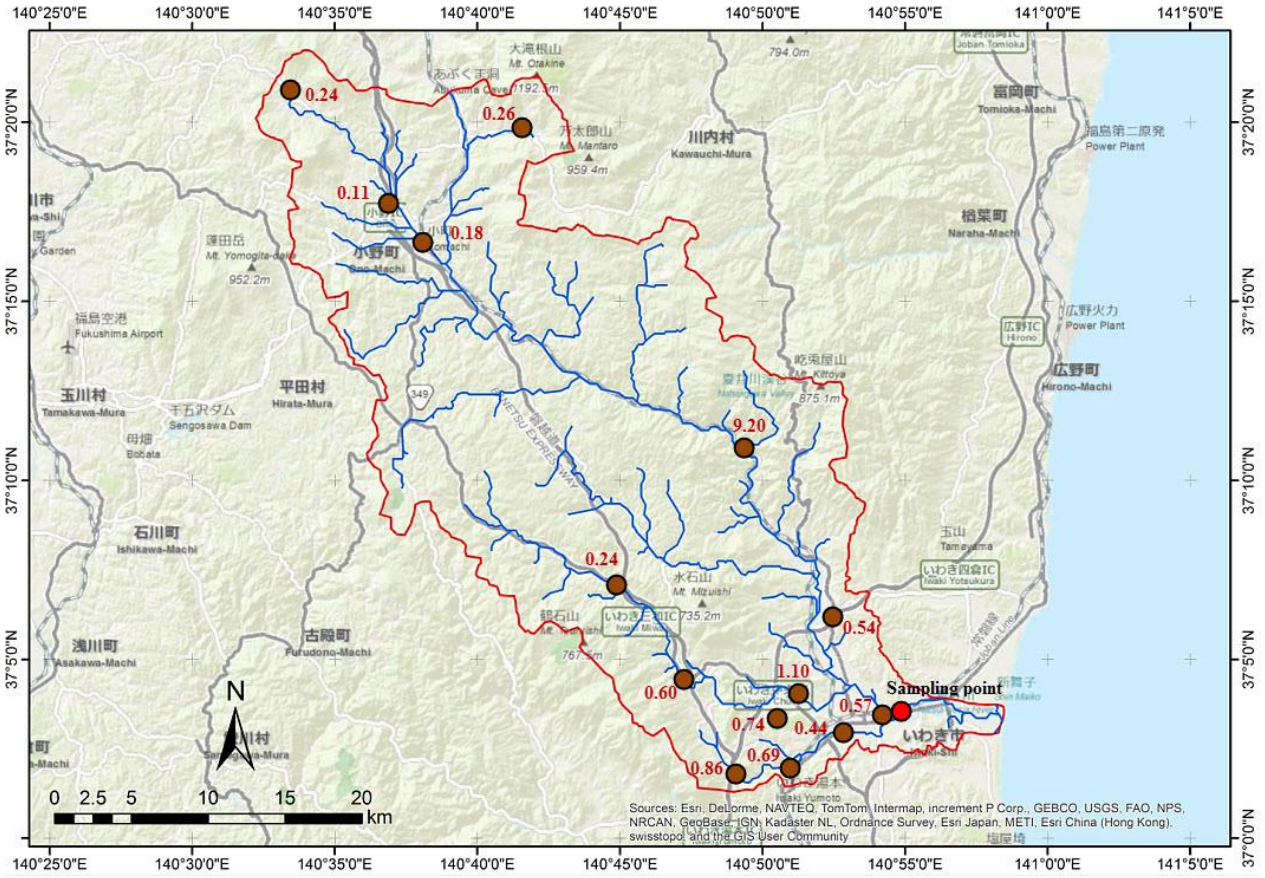

Figure 5-8 (continued) The surface deposition (kBq m^{-2}) of ^{134}Cs in (a), ^{137}Cs in (b) and ^{131}I in (C) within catchment area of Natsui River, these measurement were monitored on14 June 2011. The maps were created by using ArcGIS® software, ESRI, and produced by DMR and the author.

(a)

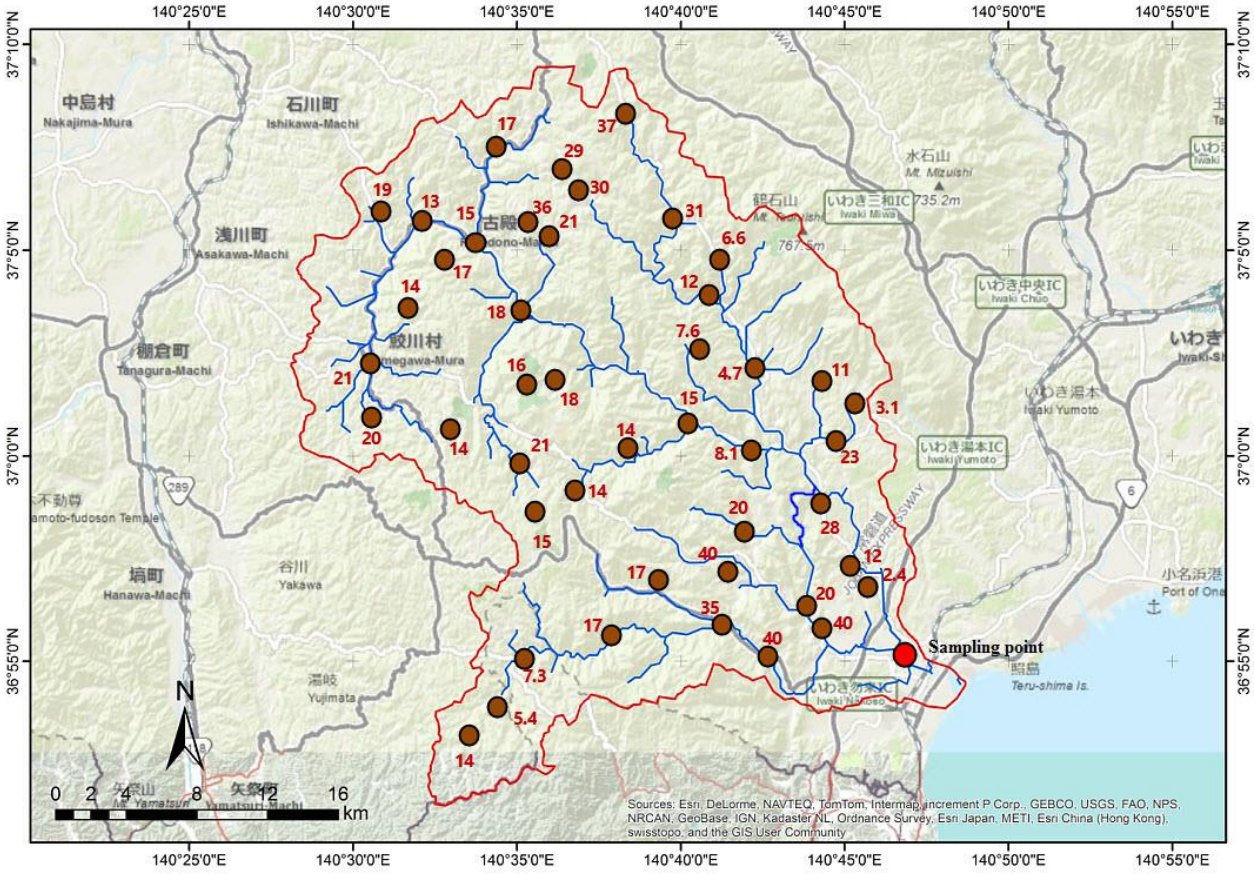

Figure 5-9 The surface deposition (kBq m^{-2}) of ^{134}Cs in (a), ^{137}Cs in (b) and ^{131}I in (C) within catchment area of Same River, these measurement were monitored on14 June 2011. The maps were created by using ArcGIS® software, ESRI, and produced by DMR and the author.

(b)

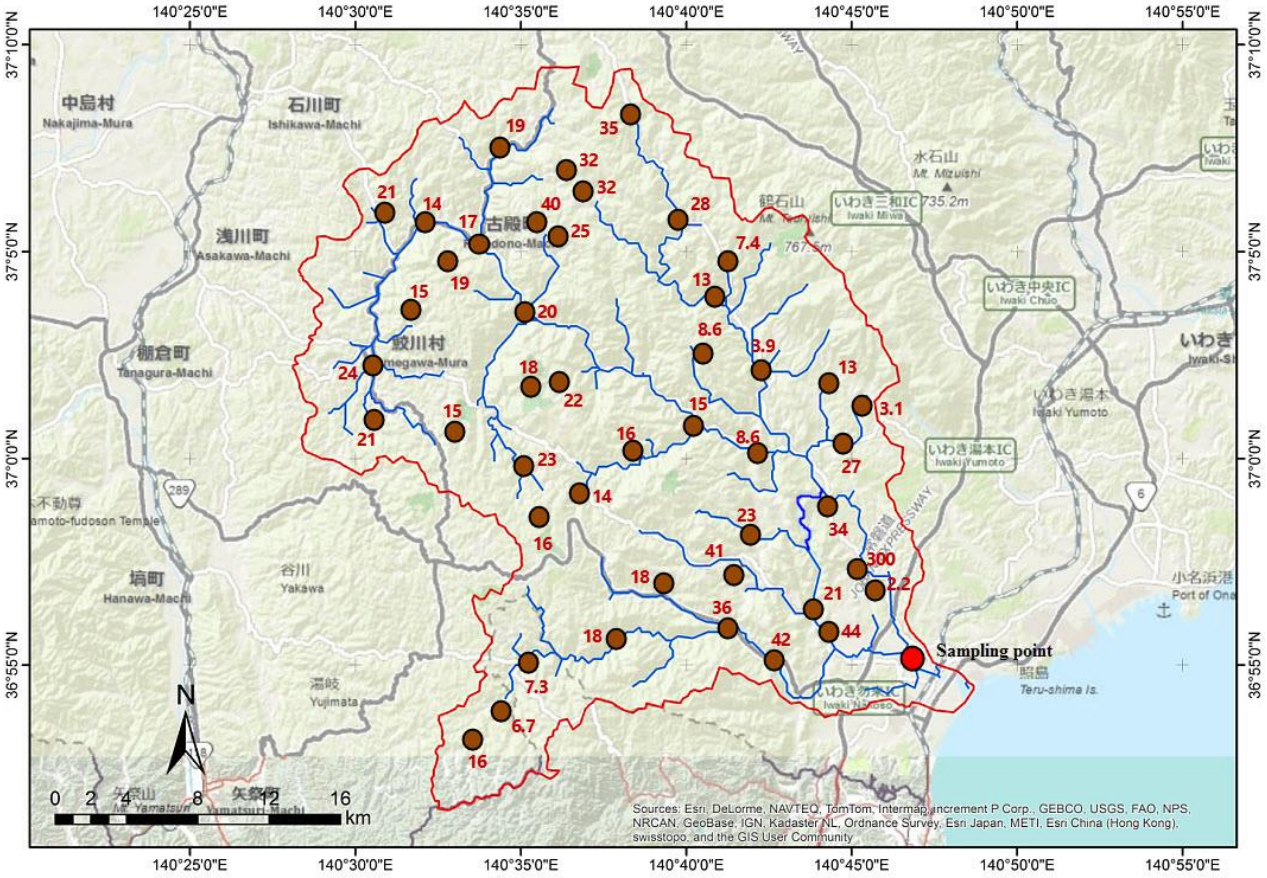

Figure 5-9 (continued) The surface deposition (kBq m^{-2}) of ^{134}Cs in (a), ^{137}Cs in (b) and ^{131}I in (C) within catchment area of Same River, these measurement were monitored on14 June 2011. The maps were created by using ArcGIS® software, ESRI, and produced by DMR and the author.

(c)

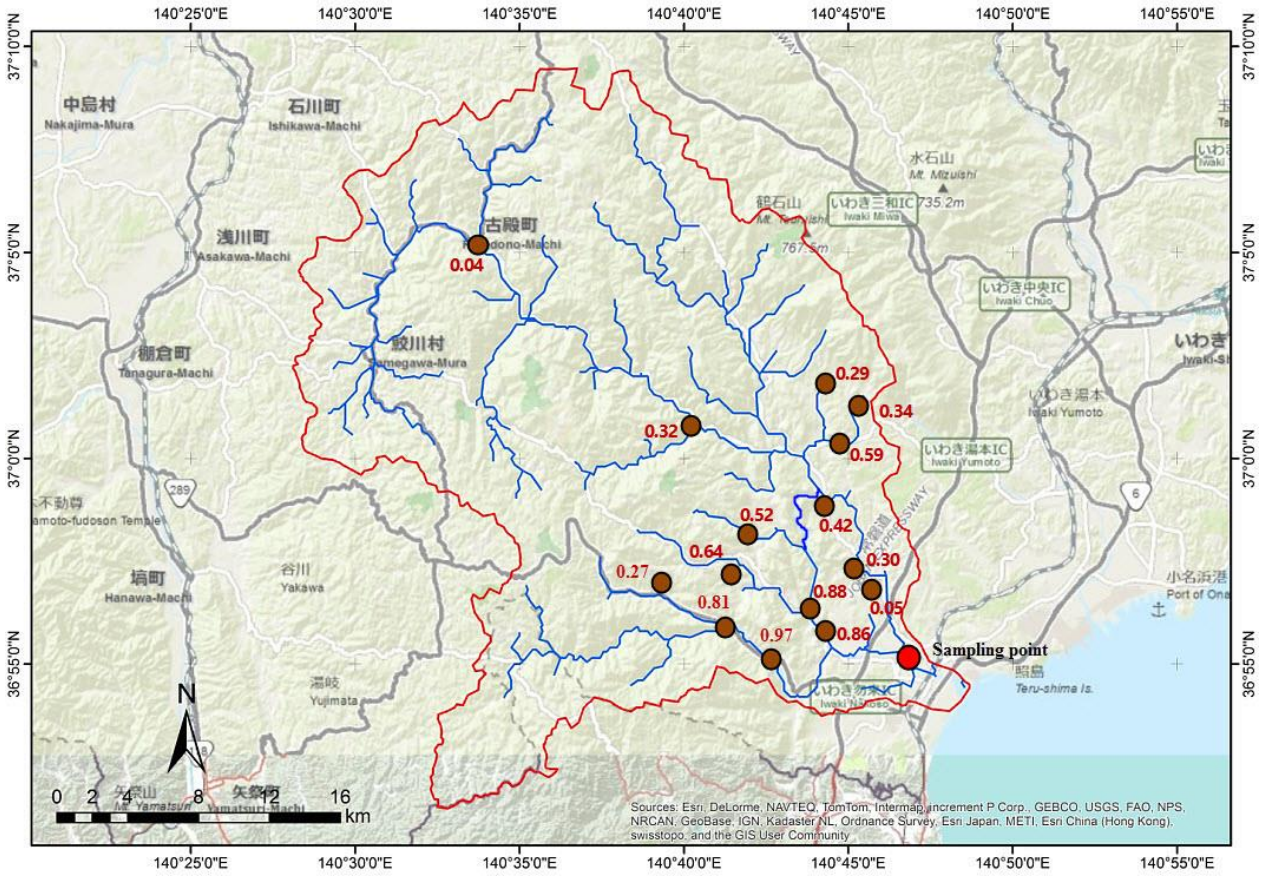

Figure 5-9 (continued) The surface deposition (kBq m^{-2}) of ^{134}Cs in (a), ^{137}Cs in (b) and ^{131}I in (C) within catchment area of Same River, these measurement were monitored on14 June 2011. The maps were created by using ArcGIS® software, ESRI, and produced by DMR and the author.

(h) Iitate Lake

This lake was highly affected by the distribution of atmospheric fallout following the Fukushima accident and is situated in an evacuated zone. The location of the Lake is close to the Fukushima I NPSs, being around 50 km from the NPSs in the highly contaminated area in the northwest region. This lake was a place for leisure activities such as boating, fishing and camping, and there was no fishing for commercial purposes. The Japanese authorities carried out daily monitoring of the radioactivity concentration of ^{131}I and ^{134,137}Cs in water (total phase consisting of dissolved and particulate phase) from 18 March to 1 August 2011. The details of the monitoring are shown Table 5-5. Since the radioactivity of all nuclides in MEXT's monitoring was the total phase, the dissolved phase fraction of radiocaesium was estimated by using the information from Wariki and Hiso River observed by Ueda at al. (2013). Both rivers are tributaries of Niida River, and the sampling points at Wariki and Hiso River were only 6-7 km from Iitate Lake. Iitate Lake is the beginning of a tributary of the Wariki River. Therefore, the amount of dissolved phase can be estimated by using the K_d and s (Section 2.6.2 (a)) from Wariki River. Since the total phase of radiocaesium consists of particulate and dissolved phases, this is given by:

$$T_{Cs} = P_{Cs} + D_{Cs} \qquad 5\text{-}1$$

Where T_{Cs} is Total concentration, P_{Cs} in particulate concentration and D_{Cs} is dissolved concentration of radiocaesium in water, all in units Bq L^{-1}.

K_d is the radiocaesium distribution coefficient:

$$K_d = \frac{P_{Cs}\ in\ dry\ weight}{D_{Cs}} \qquad 5\text{-}2$$

P_{Cs} in dry weight can be calculated suspended solids concentration (s, mg L^{-1}) as follow

$$P_{Cs}\ in\ dry\ weight = \frac{P_{Cs}}{s \times 10^6} \qquad 5\text{-}3$$

The constant of 10^6 is for converting mg L^{-1} to kg L^{-1}, and from Equation 5-1 to 5-3, the amount of dissolved concentration of radiocaesium can be calculated by using:

$$D_{Cs} = \frac{T_{Cs}}{1 + (K_d \times s \times 10^6)} \qquad 5\text{-}4$$

This research has cooperated with Chiba Institute of Technology, Japan to survey the physical environment of Iitate Lake and has monitored the radioactivity concentration in water for long term period (Table 5-6). The first survey conducted by the author and his colleagues at Chiba Institute of Technology in July 2012 which was dry season (summer). The lake average depth (*d*) was measured to be 2.56 metre from 6 points across the bridge which crosses the middle of the river from northeast to southwest as shown in Figure 5-10 (a) and 5-11. Since there is the dam at the outlet of lake, the water level in the lake does not change significantly between the dry season and wet season.

The potassium concentration in water [K^+] is assumed to be equal to the value from Wariki River (1.3 mg L^{-1} = 33.28 μmol L^{-1}) resulting in a value of k_f for radiocaesium from Equation 2-30 of 4.47 m^3 kg^{-1} y^{-1} for predatory fish and 15.47 for non-predatory fish.

From the ArcGIS® software, the lake area of Iitate Lake is 2.3×10^{-2} km^2 while the catchment area is 7.5×10^{-1} km^2 as can be seen in detail in Figures 6-1 and 6-2. From the figures, we can see that the lake has two main inlets at the north and west, while there is one man-made outlet from a dam at the east of lake (the height of dam is about 1 metre from the water surface).

The annual rainfall in Iitate Village (*R*) is approximately 0.10 m, as reported by the Japan Meteorological Agency (JMA, 2012). Therefore, the water residence time (T_W) is calculated by equation 2.18 to be approximately 0.75 years. Since the water residence time is less than a year, we can defines this lake as an open lake (J. T. Smith, et al., 2005) in which the short-term dissolved concentration in the lake can be determined by "spike" input while the longer term component is dominated by deposition on the catchment.

The rate of removal of radiocaesium to the lake bed sediments and outflow (*K*) of Itate Lake is 5.45 y^{-1} estimated by using Equation 2-22, when water residence time and mean depth are known. The value of *K* for predicting ^{131}I can be calculated by using Equation 2-23 which gives *K* = 1.33 y^{-1}.

The available surface deposition in this area was only one site monitored on 14 June 2011 by MEXT (2014) as shown in Figure 5-10 (b). However, from Figure 5-11 to 5-14 it can

be seen that the area of the lake and its catchment is not large, so it is assumed that the surface deposition on catchment similar to lake area. Therefore, the one site monitoring surface deposition can represent the fallout on both catchment and lake. The corrected surface deposition (Bq m^{-2}) to 15 March 2011 at this site were 8.15×10^5, 8.05×10^5 and 5.72×10^6 Bq m^{-2} for ^{134,137}Cs and ^{131}I respectively.

For the fraction of the catchment covered by organic and boggy soils (f_{org}), it is clear from visual inspection that there was no evidence of organic and boggy soils in this catchment. Figures 5-15-5.17 show that the soils of the catchment are dry and mineral soils.

Table 5-5 Radioactivity concentration in freshwater of Iitate Lake, monitored by MEXT (2011b). The result is in total phase and dissolved phase was estimated by using K_d and s of Wariki River in Equation 5-4.

Date of sampling	Years after deposition	Total phase (Bq m^{-3})			Estimation of dissolved phase (Bq m^{-3})	
		^{131}I	^{134}Cs	^{137}Cs	^{134}Cs	^{137}Cs
18/03/2011	0.01	2.09E+06	4.64E+05	5.11E+05	2.62E+04	2.72E+04
19/03/2011	0.01	2.45E+06	8.62E+05	9.40E+05	4.86E+04	5.00E+04
20/03/2011	0.01	2.01E+06	4.49E+05	4.37E+05	2.53E+04	2.32E+04
21/03/2011	0.02	1.72E+06	2.40E+05	2.46E+05	1.35E+04	1.31E+04
22/03/2011	0.02	1.33E+06	1.73E+05	1.72E+05	9.76E+03	9.14E+03
23/03/2011	0.02	1.26E+06	1.45E+05	1.45E+05	8.18E+03	7.71E+03
24/03/2011	0.02	1.33E+06	2.52E+05	2.68E+05	1.42E+04	1.42E+04
25/03/2011	0.03	1.28E+06	4.81E+05	5.07E+05	2.71E+04	2.70E+04
26/03/2011	0.03	8.35E+05	1.64E+05	1.62E+05	9.25E+03	8.61E+03
27/03/2011	0.03	8.28E+05	1.39E+05	1.45E+05	7.84E+03	7.71E+03
28/03/2011	0.04	8.84E+05	1.62E+05	1.83E+05	9.14E+03	9.73E+03
29/03/2011	0.04	7.01E+05	1.54E+05	1.58E+05	8.69E+03	8.40E+03
30/03/2011	0.04	6.29E+05	1.09E+05	1.13E+05	6.15E+03	6.01E+03
31/03/2011	0.04	6.10E+05	1.50E+05	1.92E+05	8.46E+03	1.02E+04
01/04/2011	0.05	6.12E+05	1.66E+05	1.92E+05	9.37E+03	1.02E+04
02/04/2011	0.05	4.65E+05	1.33E+05	1.39E+05	7.51E+03	7.39E+03
03/04/2011	0.05	3.93E+05	1.10E+05	1.06E+05	6.21E+03	5.63E+03
04/04/2011	0.05	4.39E+05	8.90E+04	7.50E+04	5.02E+03	3.99E+03
05/04/2011	0.06	3.57E+05	9.30E+04	8.60E+04	5.25E+03	4.57E+03
06/04/2011	0.06	3.06E+05	9.20E+04	9.10E+04	5.19E+03	4.84E+03
07/04/2011	0.06	3.03E+05	2.25E+05	2.68E+05	1.27E+04	1.42E+04
08/04/2011	0.07	2.90E+05	1.23E+05	1.23E+05	6.94E+03	6.54E+03
09/04/2011	0.07	3.34E+05	1.10E+05	1.18E+05	6.21E+03	6.27E+03
10/04/2011	0.07	2.42E+05	1.05E+05	9.47E+04	5.93E+03	5.03E+03
11/04/2011	0.07	2.02E+05	7.50E+04	7.19E+04	4.23E+03	3.82E+03
12/04/2011	0.08	2.18E+05	9.20E+04	9.52E+04	5.19E+03	5.06E+03
13/04/2011	0.08	1.89E+05	7.50E+04	8.45E+04	4.23E+03	4.49E+03
14/04/2011	0.08	1.79E+05	1.10E+05	1.14E+05	6.21E+03	6.06E+03
15/04/2011	0.08	1.51E+05	6.40E+04	6.50E+04	3.61E+03	3.46E+03
16/04/2011	0.09	1.22E+05	5.80E+04	3.80E+04	3.27E+03	2.02E+03
17/04/2011	0.09	1.09E+05	5.30E+04	5.20E+04	2.99E+03	2.76E+03
18/04/2011	0.09	1.12E+05	4.00E+04	5.30E+04	2.26E+03	2.82E+03
19/04/2011	0.10	1.17E+05	9.10E+04	8.87E+04	5.14E+03	4.72E+03
20/04/2011	0.10	1.09E+05	5.30E+04	4.38E+04	2.99E+03	2.33E+03
21/04/2011	0.10	8.50E+04	3.98E+04	2.90E+04	2.25E+03	1.54E+03
22/04/2011	0.10	6.86E+04	4.11E+04	3.99E+04	2.32E+03	2.12E+03
23/04/2011	0.11	6.58E+04	4.21E+04	5.65E+04	2.38E+03	3.00E+03

Table 5-5 (continued) Radioactivity concentration in freshwater of Iitate Lake monitoring by MEXT (2011b). The result is in total phase and dissolved phase was estimated by using K_d and s of Wariki River in Equation 5-4.

Date of sampling	Years after deposition	Total phase (Bq m^{-3})			Estimation of dissolved phase (Bq m^{-3})	
		^{131}I	^{134}Cs	^{137}Cs	^{134}Cs	^{137}Cs
24/04/2011	0.11	6.38E+04	2.79E+04	3.80E+04	1.57E+03	2.02E+03
25/04/2011	0.11	4.30E+04	4.03E+04	3.21E+04	2.27E+03	1.71E+03
26/04/2011	0.11	3.66E+04	6.42E+04	5.72E+04	3.62E+03	3.04E+03
27/04/2011	0.12	4.28E+04	3.29E+04	3.83E+04	1.86E+03	2.04E+03
28/04/2011	0.12	2.60E+04	2.64E+04	2.67E+04	1.49E+03	1.42E+03
29/04/2011	0.12	2.63E+04	2.94E+04	3.97E+04	1.66E+03	2.11E+03
30/04/2011	0.13	3.61E+04	1.18E+05	1.17E+05	6.66E+03	6.22E+03
01/05/2011	0.13	3.37E+04	2.12E+05	2.04E+05	1.20E+04	1.08E+04
02/05/2011	0.13	2.67E+04	2.50E+04	2.20E+04	1.41E+03	1.17E+03
03/05/2011	0.13	1.89E+04	4.41E+04	5.70E+04	2.48E+03	3.03E+03
04/05/2011	0.14	1.90E+04	1.90E+04	2.90E+04	1.07E+03	1.54E+03
05/05/2011	0.14	1.78E+04	2.60E+04	2.50E+04	1.47E+03	1.33E+03
06/05/2011	0.14	1.77E+04	1.90E+04	2.30E+04	1.07E+03	1.22E+03
07/05/2011	0.15	1.49E+04	6.33E+04	5.64E+04	3.57E+03	3.00E+03
08/05/2011	0.15	-	8.65E+04	1.02E+05	4.88E+03	5.42E+03
11/05/2011	0.16	-	-	-	-	-
12/05/2011	0.16	-	-	-	-	-
13/05/2011	0.16	-	3.42E+04	4.28E+04	1.93E+03	2.28E+03
14/05/2011	0.16	6.20E+03	2.10E+04	2.10E+04	1.19E+03	1.12E+03
16/05/2011	0.17	7.37E+03	2.20E+04	2.60E+04	1.24E+03	1.38E+03
17/05/2011	0.17	5.81E+03	8.81E+03	1.10E+04	4.97E+02	5.85E+02
18/05/2011	0.18	-	-	-	-	-
19/05/2011	0.18	-	1.43E+04	1.93E+04	8.07E+02	1.03E+03
21/05/2011	0.18	-	3.24E+04	3.89E+04	1.83E+03	2.07E+03
22/05/2011	0.19	-	-	1.47E+04	-	7.81E+02
23/05/2011	0.19	-	-	-	-	-
24/05/2011	0.19	-	-	-	-	-
25/05/2011	0.19	-	-	-	-	-
26/05/2011	0.20	-	-	1.47E+04	-	7.81E+02
27/05/2011	0.20	-	-	-	-	-
28/05/2011	0.20	-	-	1.86E+04	-	9.89E+02
29/05/2011	0.21	-	1.97E+04	1.85E+04	1.11E+03	9.83E+02
30/05/2011	0.21	-	2.04E+04	-	1.15E+03	-
31/05/2011	0.21	-	5.75E+04	6.96E+04	3.24E+03	3.70E+03
01/06/2011	0.21	-		-	-	-
02/06/2011	0.22	-	2.75E+04	4.27E+04	1.55E+03	2.27E+03

Table 5-5 (continued) Radioactivity concentration in freshwater of Iitate Lake monitoring by MEXT (2011b). The result is in total phase and dissolved phase was estimated by using K_d and s of Wariki River in Equation 5-4.

Date of sampling	Years after deposition	Total phase (Bq m^{-3})			Estimation of dissolved phase (Bq m^{-3})	
		^{131}I	^{134}Cs	^{137}Cs	^{134}Cs	^{137}Cs
03/06/2011	0.22	-	-	-	-	-
04/06/2011	0.22	-	-	1.66E+04	-	8.82E+02
05/06/2011	0.22	-	4.73E+04	5.04E+04	2.67E+03	2.68E+03
06/06/2011	0.23	-	2.19E+04	1.87E+04	1.24E+03	9.94E+02
07/06/2011	0.23	-	7.39E+04	8.71E+04	4.17E+03	4.63E+03
08/06/2011	0.23	-	-	-	-	-
09/06/2011	0.24	-	-	-	-	-
10/06/2011	0.24	-	-	-	-	-
11/06/2011	0.24	-	-	-	-	-
12/06/2011	0.24	-	-	-	-	-
13/06/2011	0.25	-	-	-	-	-
14/06/2011	0.25	-	-	-	-	-
15/06/2011	0.25	-	-	-	-	-
16/06/2011	0.25	-	-	-	-	-
17/06/2011	0.26	-	-	-	-	-
18/06/2011	0.26	-	-	1.09E+04	-	5.79E+02
19/06/2011	0.26	-	-	-	-	-
20/06/2011	0.27	-	-	-	-	-
21/06/2011	0.27	-	-	-	-	-
22/06/2011	0.27	-	6.82E+04	9.74E+04	3.85E+03	5.18E+03
23/06/2011	0.27	-	1.81E+04	1.90E+04	1.02E+03	1.01E+03
24/06/2011	0.28	-	2.04E+04	2.98E+04	1.15E+03	1.58E+03
29/06/2011	0.29	-	-	-	-	-
04/07/2011	0.30	-	-	1.22E+04	-	6.49E+02
08/07/2011	0.31	-	1.80E+04	1.57E+04	1.02E+03	8.35E+02
11/07/2011	0.32	-	-	-	-	-
15/07/2011	0.33	-	1.63E+04	-	9.20E+02	
18/07/2011	0.34	-	-	-	-	-
22/07/2011	0.35	-	-	1.31E+04	-	6.96E+02
25/07/2011	0.36	-	-	-	-	-
29/07/2011	0.37	-	-	-	-	-
01/08/2011	0.38	-	-	-	-	-

(a)

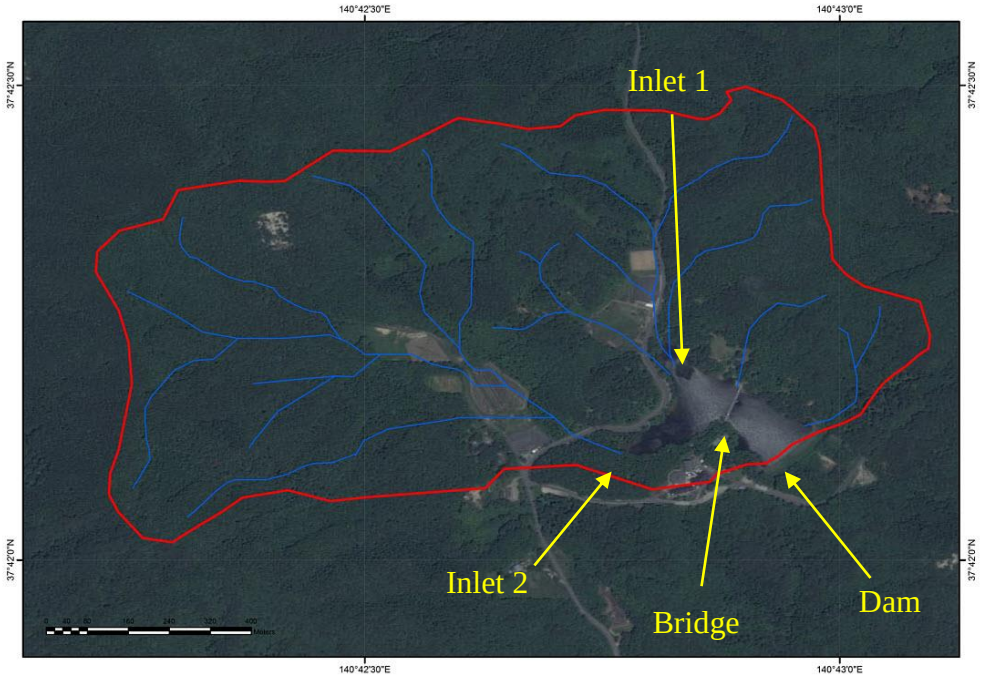

(b)

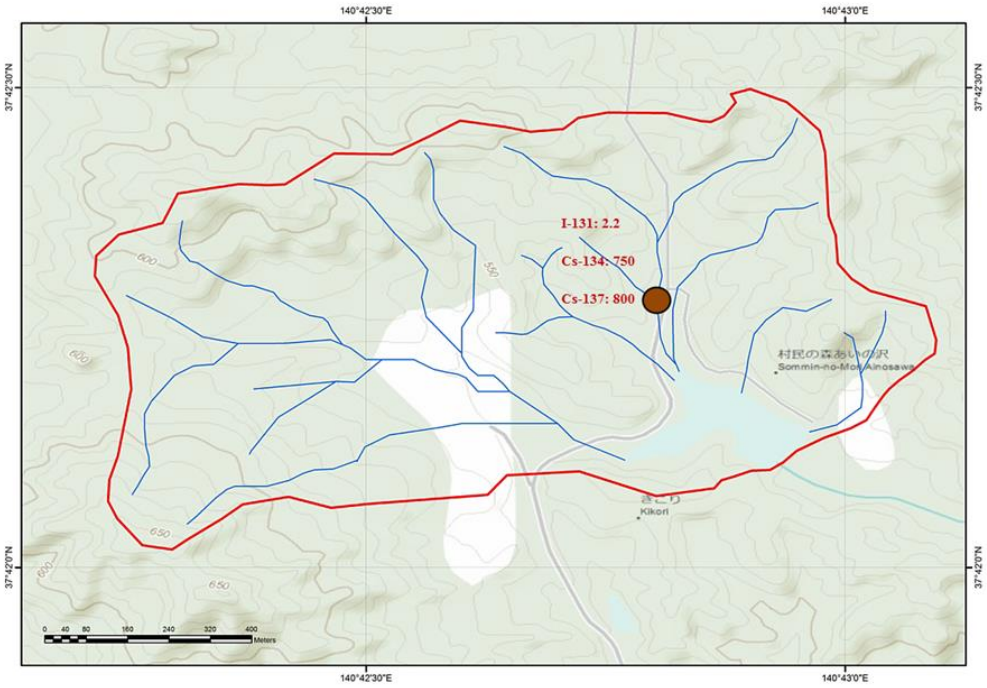

Figure 5-10 Illustration of (a) the satellite map and (b) Topographical map with surface deposition (units of all nuclides are in kBq m^{-2}) sampling of Iitate Lake. The maps were created by using ArcGIS® software, ESRI, and produced by DMR and the author.

Figure 5-11 The photograph of the bridge at the centre of Iitate Lake

Figure 5-12 The photograph of Inlet 1 of Iitate Lake taken from the centre of the bridge.

Figure 5-13 The photograph of Inlet 2 of Iitate Lake taken from the centre of the bridge.

Figure 5-14 The photograph of dam in outlet of Iitate Lake taken from the centre of the bridge.

Figure 5-15 The Photograph shows the soil at the Inlet 2 of Iitate Lake. The soil type is mineral which is similar to the soil around the lake.

Figure 5-16 The Photograph illustrates the characteristics of soils in the catchment of Iitate Lake near the bridge at the south side.

Figure 5-17 The Photograph illustrates the characteristics of soil in the catchment of Iitate Lake near the bridge at the north side.

Table 5-6 Measurements of dissolved ^{137}Cs (Bq m^{-3}) in lake water at Iitate Lake for long term period of measurement following fall out (Chiba Institute of Technology, unpubl. res.).

Date of sampling	**Years after deposition**	**dissolved phase of ^{137}Cs (Bq m^{-3})**
31/07/2012	1.38	5.02E+02
31/07/2012	1.38	3.56E+02
15/12/2012	1.76	1.61E+02

(i) Teganuma Lake

Around 195 km to the southwest of Fukushima I NPS, in Chiba Prefecture, Teganuma Lake is an important water source for the irrigation water supply for this area and it is also used for leisure and fisheries (Inamori, 2010). The mean depth of Teganuma lake is just 0.86 m (Inamori, 2010). From ArcGIS® software, the lake area was found to be 5.3 km^2 and the catchment area is 1.10×10^2 km^2. The Japan Meteorological Agency (JMA, 2012) reports the annual rainfall of 0.14 m for Kashiwa in Chiba Prefecture.

On the basis of these data, the water residence time (Equation 2-18) is 0.29 y which is characteristic of an open lake. The rate of removal of radiocaesium to the lake bed sediments and outflow from Equation 2-22 (for the case where T_W and d are known) is 13.69 y^{-1}, and K for ^{131}I (Equation 2-23) is 3.39 y^{-1}. At the time of writing, there were no potassium concentration data available for Teganuma Lake. However, assuming the mean in Asian countries $[K^+]$ = 2.0 mg L^{-1} = 51.2 µmol L^{-1} resulting in uptake parameters k_f for radiocaesium (Equation 2-30) of 2.90 m^3 kg^{-1} y^{-1} for predatory fish and 10.06 for non-predatory fish.

Chiba Institute of Technology collected fish samples for three species and measured the radioactivity in these fish as shown in Table 5-7. However, there is currently no available measurement of radioactivity concentration in lake water.

For surface deposition from MEXT (2014) in the catchment and lake area, the radicaesium were measured for one site near the centre of the lake (the blue circle in Figure 5-18) and the other four sites were distributed in the catchment area (brown circles). So, the corrected surface depositions (Bq m^{-2}) were used for the model giving 5.11×10^4 and 4.98×10^4 for ^{134}Cs in the lake and catchment area respectively (Figure 5-18 (a)), 4.81×10^4 and 4.78×10^4 for ^{137}Cs (Figure 5-18 (b)). Since all surface deposition measurements at this lake were performed on 1 March 2012, there was no ^{131}I. However, Amano and co-workers (2012) collected fallout in Chiba Prefecture on 11 May 2011 which gave a corrected ratio of ^{131}I to ^{137}Cs of 8.79 resulting in an estimated corrected surface deposition of ^{131}I of 4.22×10^5 for the lake area and 4.21×10^5 for the catchment. It is assumed that the fraction of the catchment covered by organic and boggy soils (f_{org}) is zero (Kameda, Y. Chiba Inst. of Technology).

Table 5-7 Measurements of ^{137}Cs (Bq kg^{-1}) in fish at Teganuma Lake for the long term following fall out (Kameda, Y, unpubl. res.)

Date of sampling	Years after deposition	Activity concentration of ^{137}Cs (Bq kg^{-1})
Stone Moroko - *Pseudorasbora parva*		
09/11/2011	0.65	1.15E+02
17/01/2012	0.84	1.28E+02
06/03/2012	0.98	1.10E+02
03/03/2012	0.97	1.71E+02
14/03/2012	1.00	9.40E+01
09/04/2012	1.07	1.10E+02
25/06/2012	1.28	4.50E+01
20/07/2012	1.35	9.40E+00
31/08/2012	1.46	1.47E+01
01/10/2012	1.55	2.15E+01
Gold Fish - *Carassius Auratus Langsdorfii*		
23/06/2012	1.28	2.40E+02
28/06/2012	1.29	6.30E+01
22/08/2012	1.44	3.60E+01

(a) ^{134}Cs

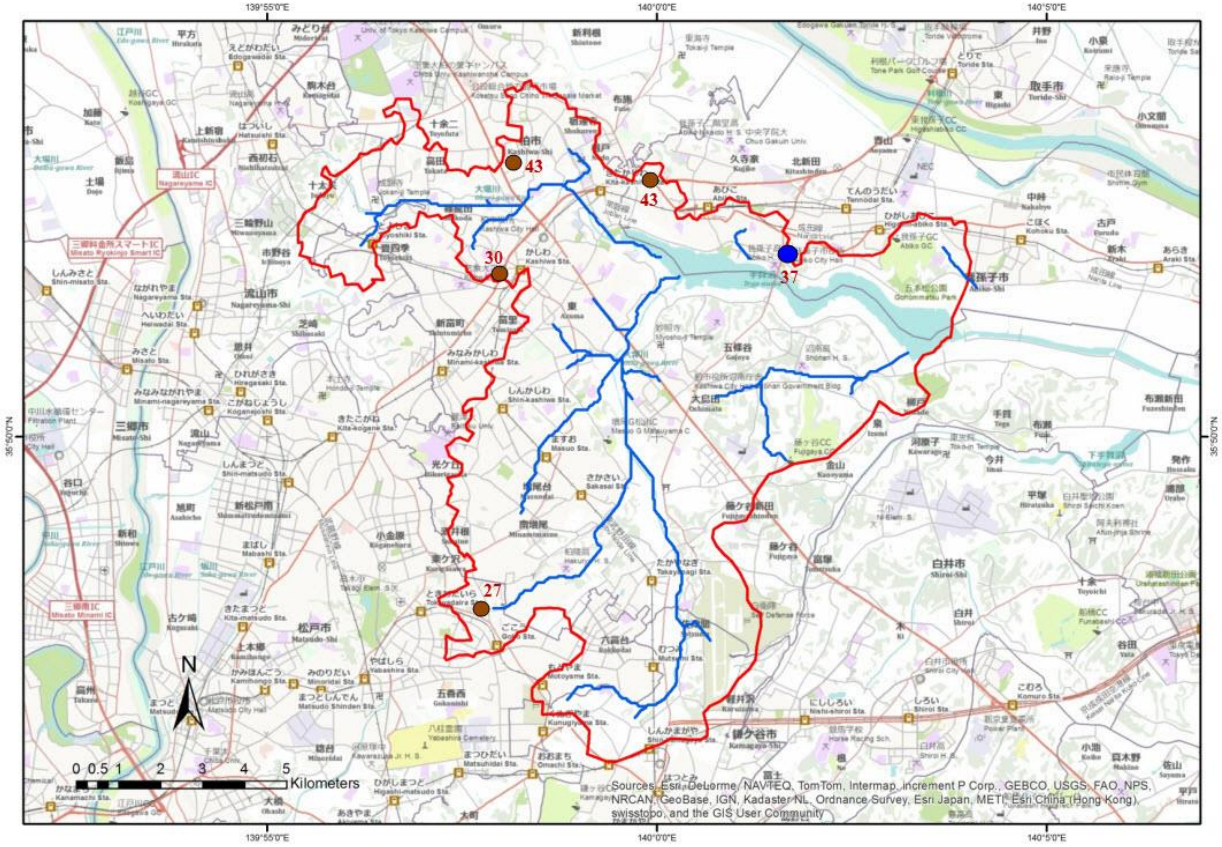

Figure 5-18 Illustration of the surface deposition (kBq m^{-2}) on 1 March 2012 of (a) ^{134}Cs and (b) ^{137}Cs in the catchment area of Tegamura Lake. The blue circle is assumed to represent the value of fallout on the lake area and the brown circles are the surface deposition into catchment. The map was created by using ArcGIS® software, ESRI, and produced by DMR and the author.

(b) ^{137}Cs

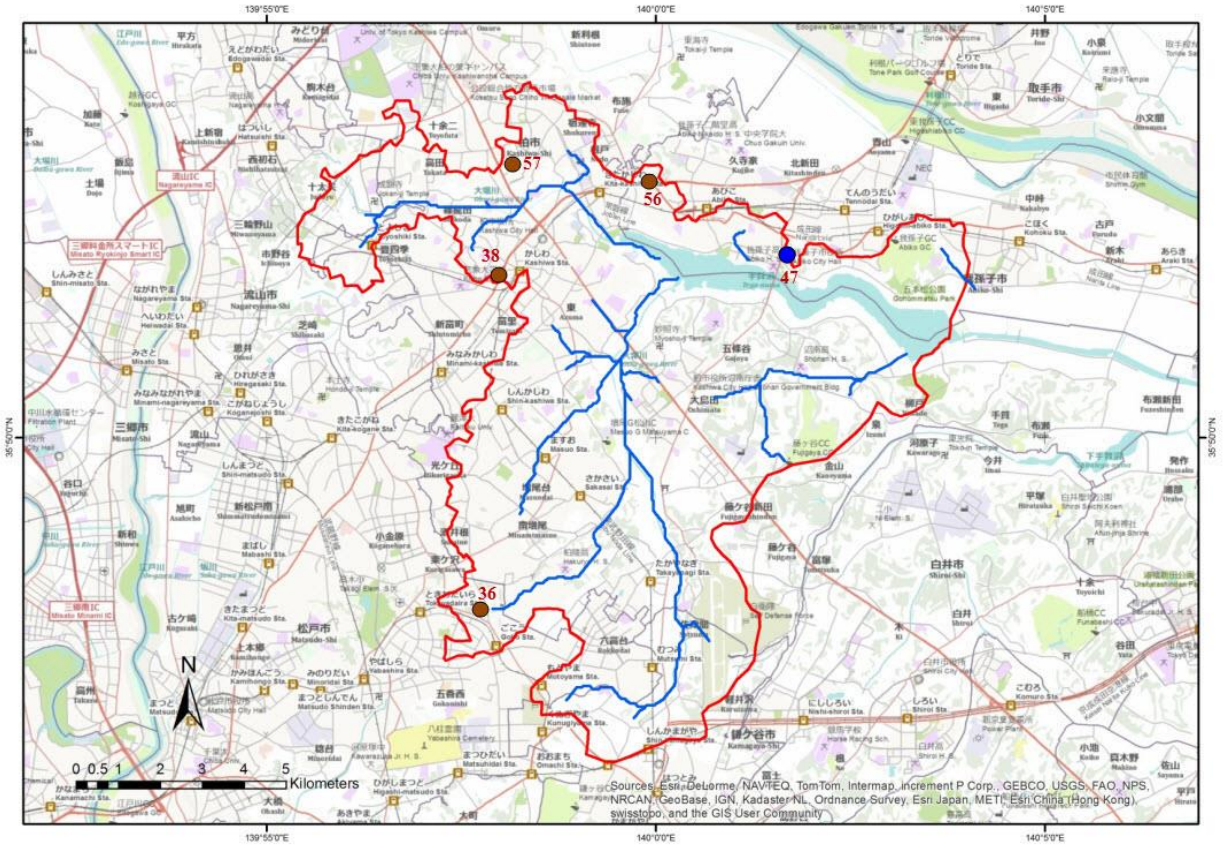

Figure 5-18 (continued) Illustration of the surface deposition (kBq m^{-2}) on 1 March 2012 of (a) ^{134}Cs and (b) ^{137}Cs in the catchment area of Tegamura Lake. The blue circle is assumed to represent the value of fallout onto lake area and the brown circles are the surface deposition into catchment. The map was created by using ArcGIS® software, ESRI, and produced by DMR and the author.

(j) Kasumigaura Lake

To the northeast of Teganuma Lake, there is a larger lake, Kasumigaura Lake (at approximately 163 km from Fukushima I NPS). Kasumigaura Lake (Inamori, 2010) is the second largest lake in Japan and is a valuable water supply for irrigation, domestic, and industrial purposes. There are also leisure activities and inland water fisheries at this lake. The analysis by ArcGIS® software shows that the lake area is 2.57×10^2 km^2 and very large catchment area is 1.71×10^2 km^2.

The mean depth of Kasumigaura Lake is 4.0 m (Inamori, 2010) and annual net rainfall in Ishioka, Ibaraki Prefecture is about 0.04 m (reported by Japan Meteorological Agency (JMA, 2012)). The water residence time (Equation 2-18) is 16.64 y so this lake can be classified as a closed lake. Therefore, K for ^{134,137}Cs (Equation 2-22) is 13.69 y^{-1} and 3.91 y^{-1} for ^{131}I (Equation 2-23).

Similarly to other catchments, there is no organic and boggy soils content in the catchment of this lake which gives $f_{org} = 0$. For potassium concentration in water, NIES (2014) had collected sample monthly from April 1980 to March 2011 which gives a mean $[K^+] = 4.1$ mg L^{-1} = 104.84 μmol L^{-1}. As a result, k_f values for radiocaesium (Equation 2-30) are 1.42 m^3 kg^{-1} y^{-1} for predatory fish and 4.91 for non-predatory fish.

The available surface depositions into the lake following the Fukushima accident are shown in Figure 5-19. Similarly to Teganuma Lake, measurements of radiocaesium were conducted on 12 March 2012 without ^{131}I measurement. The decay corrected mean surface deposition (to 15 March 2011) around the lake (blue circles) were 2.19×10^4 and 2.01×10^4 Bq m^{-2} for ^{134,137}Cs and 1.77×10^5 Bq m^{-2} for ^{131}I (using corrected ^{131}I/^{137}Cs = 8.79 from Amano et al. (2012) to estimate corrected surface depositions of ^{131}I into the lake).

(a) ^{134}Cs

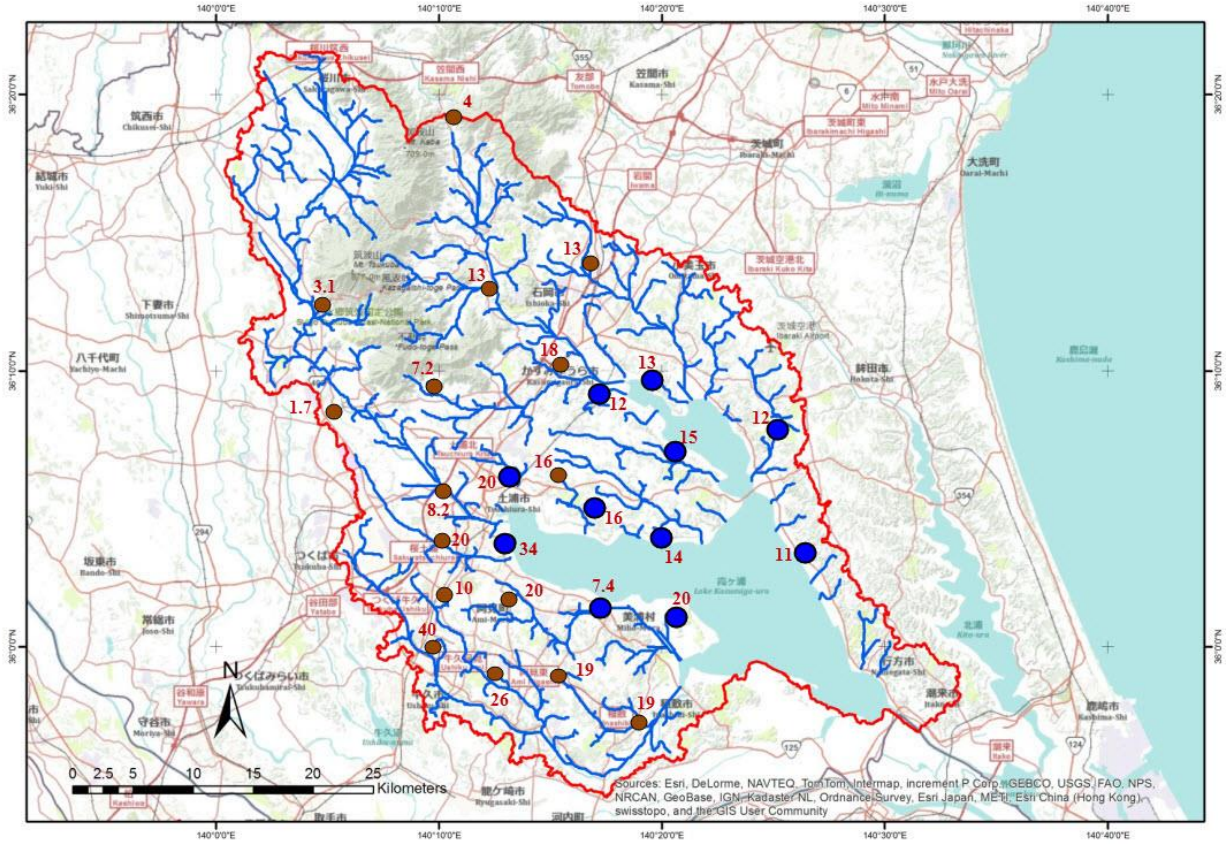

Figure 5-19 Illustration of the surface deposition (kBq m^{-2}) on 1 March 2012 of (a) ^{134}Cs and (b) ^{137}Cs in the catchment area of Kasumigaura Lake. The blue circles are assumed to represent the fallout onto the lake area and the brown circles are the surface deposition into the catchment. The map was created by using ArcGIS® software, ESRI, and produced by DMR and the author.

(b) ^{137}Cs

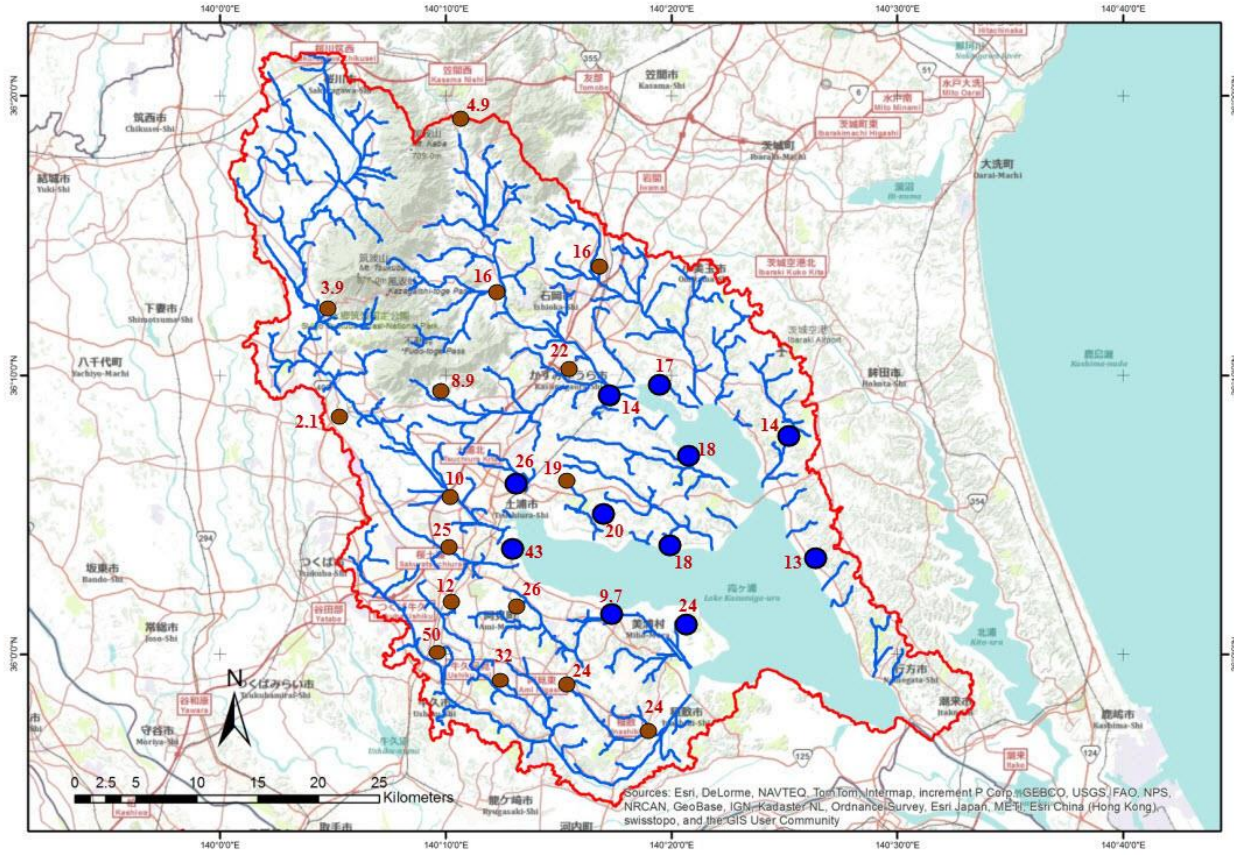

Figure 5-19 (continued) Illustration the surface deposition (kBq m^{-2}) on 1 March 2012 of (a) ^{134}Cs and (b) ^{137}Cs in the catchment area of Kasumigaura Lake. The blue circles are assumed to represent the value into lake area and the brown circles are the surface deposition into catchment. The map was created by using ArcGIS® software, ESRI, and produced by DMR and the author.

Table 5-8 Summary of input parameters for all lakes.

Lake	Depth (m)	Water residence time[η] (y)	Mean surface deposition* (Bq m^{-2})						Potassium concentration (mg L^{-1})	fraction of the catchment covering by organic, boggy soils (f_{org})	Wet weight of fish (kg)
			Lake area			Catchment area					
			^{131}I	^{134}Cs	^{137}Cs	^{131}I	^{134}Cs	^{137}Cs			
Iitate	2.56	0.75	5.72E+06	8.15E+05	8.05E+05	5.72E+06	8.15E+05	8.05E+05	1.3[ω]	0.0[Δ]	1.0[Ω]
Teganuma	0.86	0.29	4.22E+05[θ]	5.11E+04	4.81E+04	4.21E+05	4.98E+04	4.78E+04	2.00[∞]	0.0[Δ]	1.0[Ω]
Kasumigaura	4.00	16.64	1.77E+05[θ]	2.19E+04	2.01E+04	1.70E+05	2.11E+04	1.93E+04	2.90[τ]	0.0[Δ]	1.0[Ω]

Note that: [*]The measured data of radiocaesium was monitored by MEXT (2014).

[η]Water residence time for all types of lakes can be estimated by using Equation 2-18.

[θ]The corrected surface deposition of ^{131}I of these two sites were estimated by using corrected ratio (on 15 March 2011) of near-area at Chiba Prefecture measured by Amano and co-workers (2012).

[ω]The value from measurement at Wariki River (Ueda, et al., 2013) which Iitate Lake is a branch of Wariki River.

[∞]The general value in Asain countries (UNEP, 2008).

[τ]The average of measurement data during 25 April 1980 - 9 March 2011 measured by NIES (2014).

[Δ]Chiba Institute of Technology confirms that there is no content of boggy soil.

[Ω]The default value of the model.

5.2.3 Verification and adjustment of the model for Fukushima accident

The empirical parameters in AQUASCOPE (which were summarised in Tables 2-5 and 2-6) were from observation of rivers and lakes in European countries following nuclear weapons testing and the Chernobyl accident. To use these parameters for prediction of contamination in water and fish in rivers and lakes following the Fukushima accident, it is necessary to verify the model results against available field measurement data. An adjustment of model parameter values and investigation of any differences might be considered if there is a significant difference in radionuclide transport in Japanese freshwater systems compared to European.

Note that there was a mistake in which the wrong value of Y=291 for predatory fish was used in the Microsoft Excel file (CSmaster1.xls) provided in Smith et al. (2005) for using model to calculate contamination: the correct value of Y is 462 and is used in this research.

(a) Verification of the model

Figure 5-20 illustrates the results of blind testing of AQUASCOPE using all empirically determined parameters observed from the European catchments to predict concentration of radiocaesium in four rivers and one open lake. Model validation was carried out where continuous measurement data is available to compare the change of concentration with time. It clear from Figure 5-20 that the results of the model are over estimates for all rivers and lakes. The results of AQUASCOPE for ^{137}Cs at Waraki, and Hiso River (both are in the NW area of high contamination) were significantly greater than measured data by about a factor of five for both rivers (the dashed lines in all graphs are upper and lower error of a factor of five). In the Natsui and Same River in the southerly direction of the NPSs, both results of ^{134}Cs and ^{137}Cs vary over the time of measurement. Although the variations were still within a factor of five of model, in both cases the activity concentrations are over-estimated. In the case of Iitate Lake, defined as an open lake, the trends of radiocaesium model predictions were again greater than measurements by approximately a factor of five in the first month after deposition, then the differences increased to around six or seven times of the measured values. For the measured data in the longer-term period (1.38 and 1.75 years after deposition) the difference between model and measured data was again about five times.

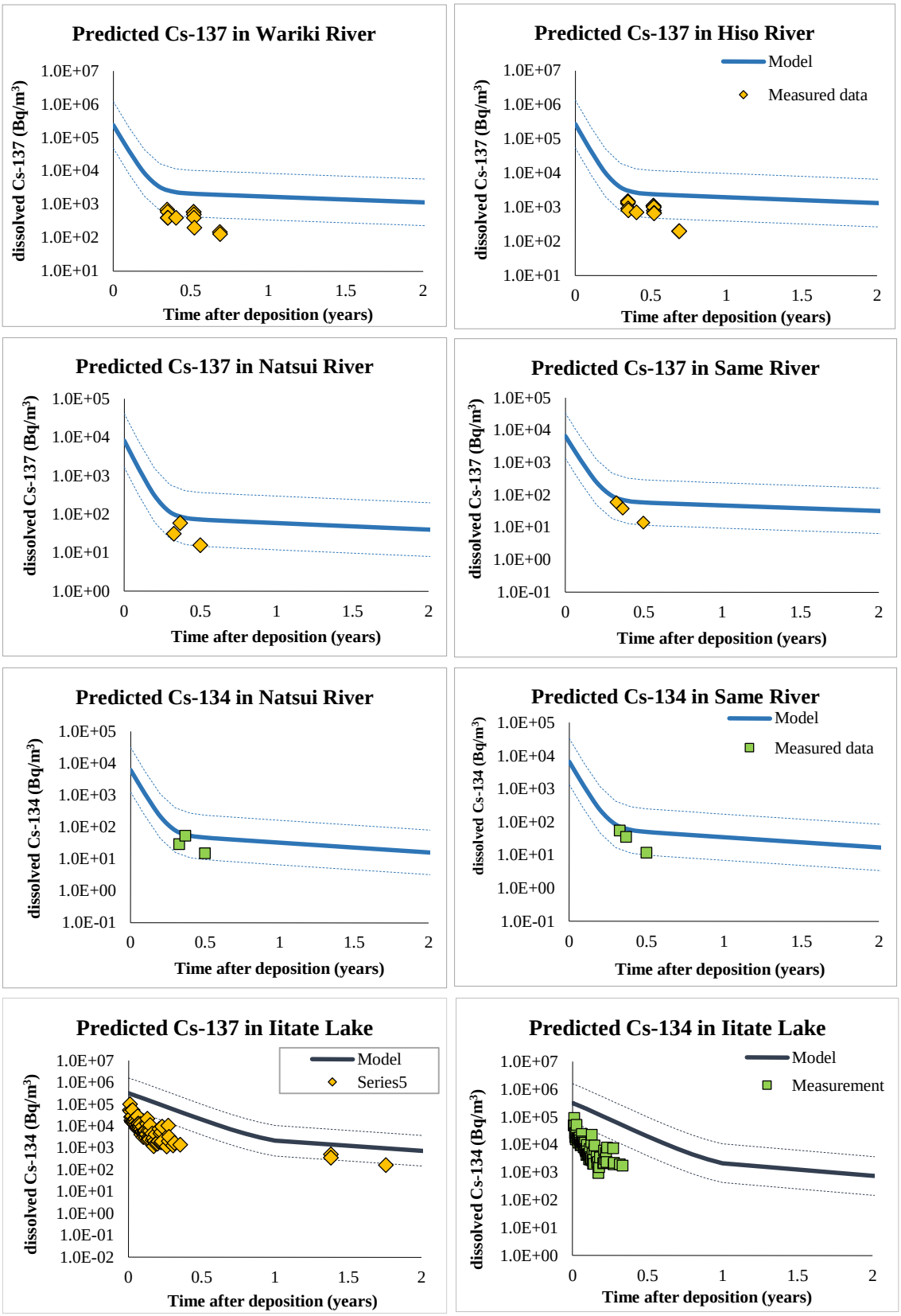

Figure 5-20 The blind prediction from AQUASCOPE by using all empirically determined parameters from rivers and lakes in Europe after Chernobyl.

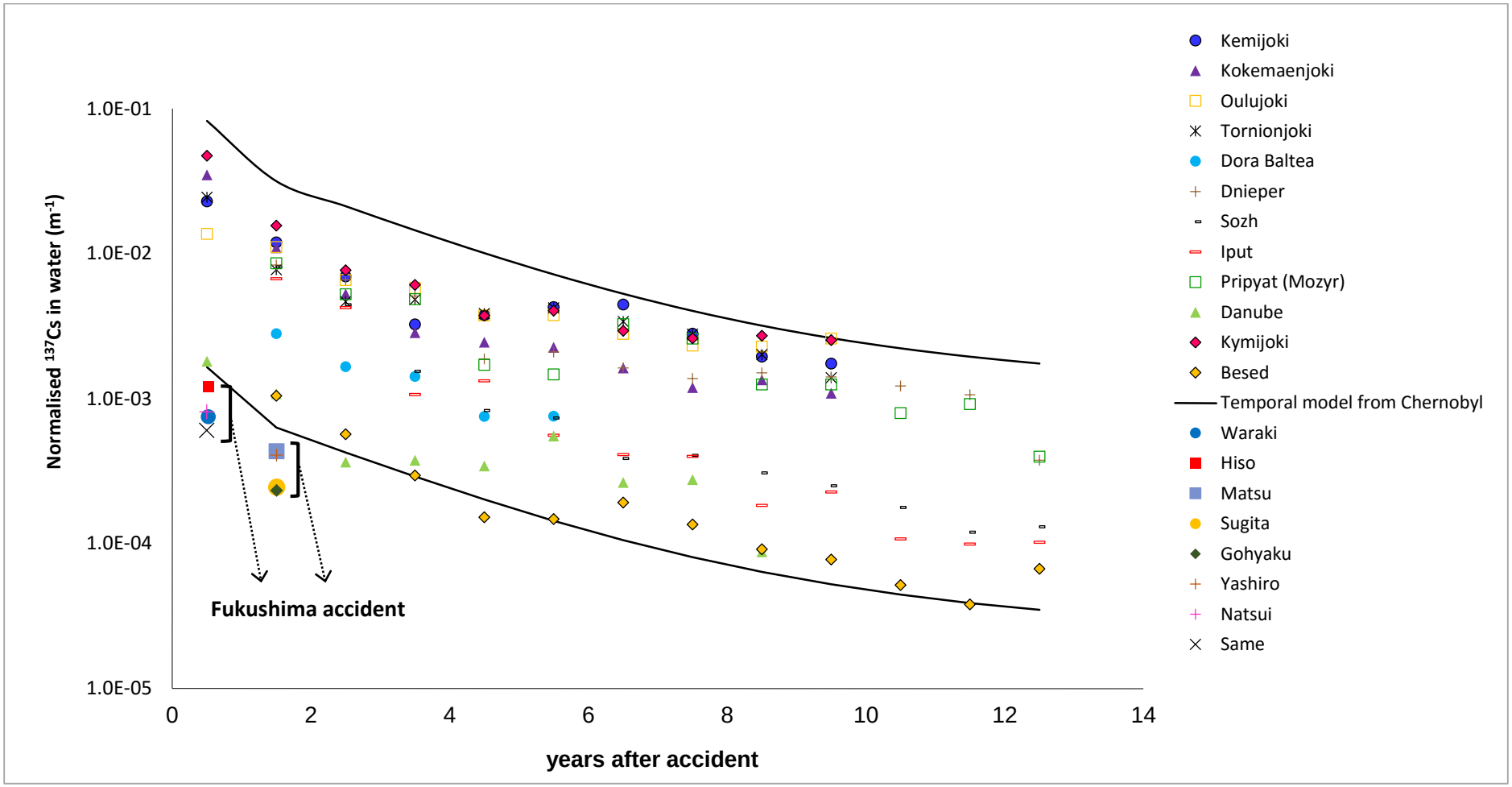

Figure 5-21 Illustrates the comparison the normalized concentration in river per unit of surface deposition between eight rivers in Japan following Fukushima accident and twelve rivers in Europe following the Chernobyl accident.

Overall, the results of the model using empirically determined parameters from previous studies at European rivers and lakes were greater than measured data approximately by a factor of five, but the changes with time of radioactivity concentrations from model decreased similarly with measurements. Figure 5-21, shows the variation of the normalized radioactivity concentration in rivers per unit of surface deposition (the runoff coefficient) of the long-lived nuclide ^{137}Cs from eight rivers in Japan in comparison with twelve rivers in European countries. As discussed above, the measurements following the Fukushima accident are consistently less than the range in values seen after Chernobyl (generated by Smith et al. (2004)). This shows that the mobility of ^{137}Cs transferred from catchments to rivers in Japan was less than European countries, but that during the first years after Fukushima, the time trend was similar. A possible explanation for this is that the absorption of ^{137}Cs in soil of catchments in Japan is stronger than in catchments in European countries.

For radiocesium in soils having high clay mineral content, ^{137}Cs is highly absorbed by "Frayed Edge Sites" (FES) on the illitic clay fraction (Cremers, Elsen, Preter, & Maes, 1988; Kato, et al., 2012; Valcke & Cremers, 1994) while the soils containing a highly organic peat bog soils have low absorption (Hansen & Aarkrog, 1990; Hilton, et al., 1993; J. T. Smith, Howard, et al., 1998). Therefore, the concentration of radiocaesium in runoff water has an inverse relation with the amount of content of clay in catchment soil. Following Chernobyl, runoff of radiocaesium in dissolved phase was highest in catchments covered by a high fraction of organic and boggy soils (Hilton, et al., 1993; Kudelsky, Smith, Ovsiannikova, & Hilton, 1996; J. T. Smith, et al., 2004). Fujiwara and co-workers (2012) collected fifty soil sample within 60 km around Fukushima I NPSs (N to S) and found that the absorption of ^{137}Cs in soil samples were very high due to the high clay content in soil. A similar result was observed by Tanaka and co-workers (Tanaka, et al., 2012) who collected two samples in NW about 65 km from NPSs and one sample in 55-km area in west direction.

Analysis of the soil type map (Hashimoto, Ugawa, Nanko, & Shichi, 2012) for this part of Japan (Figure 5-22) shows that there is no peaty soil around the near zone of Fukushima I NPSs resulting no high concentration in river water from this area. This Map also shows that most types of soils around Fukushima I NPSs are Brown forest soils (Cambisols: in the classification of the Food and Agriculture Organization and Andosols:

soils found in volcanic areas) and Black soils (Andosols). So it can be assumed that the soils in this area are of similar type to those in which Fujiwara and co-workers (2012) and Tanaka and co-workers (2012) observed the high absorption of radiocaesium.

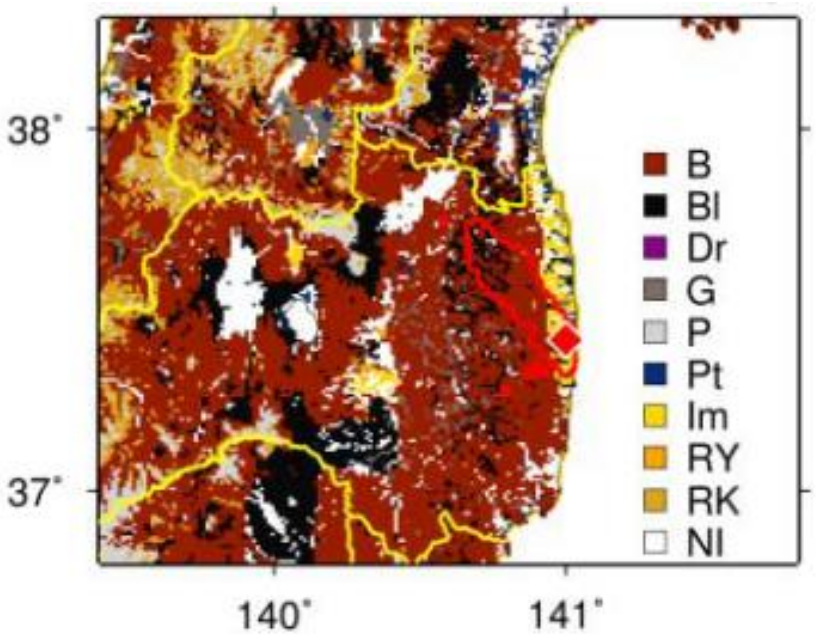

Figure 5-22 Map of soil type around Fukushima I NPSs, the red diamond is the site of the NPSs and the red line is the highly contaminated area, B is Brown forest soils, Bl is Black soils, Dr is Dark red soils, G is Gley soils, P is Podzolic soils, Pt is Peaty soils, Im is Immature soils, RY is Red and Yellow soils, RK is Rock and debris, and NI is not classified.

For K_d of radiocasium, Table 5-10 shows the comparison of K_d between European rivers and lakes and in rivers in the near-zone of Fukushima I NPSs. Apparently, rivers in the near-zone of Fukushima I NPSs had higher K_d values than European rivers and lakes by an order of magnitude at least. Since K_d is the proportion of particulate to dissolved phase, significantly high attachment of radiocasium to soil particles results in a high K_d. This seems to confirm recent findings (Alexie Konoplev, Fukushima University, pers. comm.) that the absorption of radiocaesium in Japanese soil is stronger than soil in European catchments. In addition, all rivers studied in this research are in the same area at the near-zone of NPSs which has the same type of soil (soil in volcanic area (Hashimoto, et al., 2012)) so that K_d values were similar to each other (range (1.5-5.5)×10^5 L kg^{-1} for ^{137}Cs, except Abukuma River: range (1.2-27.0)×10^5 L kg^{-1}.

Table 5-9 Comparison of K_d between in European rivers and lakes and in rivers in near-zone of Fukushima I NPSs.

Nuclide	K_d (L kg^{-1})	River	Reference
Chernobyl			
^{134,137}Cs	50 – (8×10^4)	[a]	IAEA (1994)
	2×10^4	[b]	Coughtrey and Thorne (1983)
	$(3.7\text{-}9.4) \times 10^4$	[b]	Konoplev et al.(1992)
	$(4.6\text{-}270) \times 10^4$	[c]	Konoplev et al. (2002)
	$(0.8\text{-}42) \times 10^4$	[e]	Smith and Beresford (2005a)
Cs	370 – (19×10^4)	[a]	IAEA (2009)
Fukushima			
^{134}Cs	3.9×10^5	Wariki	review from Ueda et al. (2013) in Table 5-1
	1.4×10^5	Hiso	review from Ueda et al. (2013) in Table 5-1
	$(1.3\text{-}25.0) \times 10^5$	Abukuma	Ishikawa et al. (2014)
^{137}Cs	4.2×10^5	Wariki	review from Ueda et al. (2013) in Table 5-1
	1.5×10^5	Hiso	review from Ueda et al. (2013) in Table 5-1
	$(4.3\text{-}5.5) \times 10^5$	Natsui	Nagao et al. (2013)
	$(4.1\text{-}5.0) \times 10^5$	Same	Nagao et al. (2013)
	$(1.2\text{-}27.0) \times 10^5$	Abukuma	Ishikawa et al. (2014)

Note that: [a]Data base from various rivers and lakes in EU.

[b]Not available

[c]Measurement data Lake Constance in Germany, Lake Lugano in Switzerland and Lake Vorsee in Germany.

[d]Measurement data from 18 rivers and lakes in EU.

(b) Calibration of the model for Fukushima conditions

Since the results of ^{137}Cs concentrations in Japanese rivers calculated by AQUASCOPE are overestimated but the changes with time appear to be similar, the model can be adjusted for stronger absorption of radiocaesium to soils to improve model predictions. An empirical parameter, *B* (dimensionless), will be used to represent the fraction to reduce the overestimated radioactivity concentration of radiocaesium. This parameter is evaluated by fitting the measured data from five rivers (the red circles in Figure 5-23) against the results from AQUASCOPE. Then, using a "Blind test" approach, the predictions of radioactivity concentration from the improved model (that includes the correction using the *B* parameter) can be compared with measured data from the other three rivers (blue squares in Figure 5-23).

Figure 5-23 The map illustrates the position of five rivers in red circles (sampling point of each river) to evaluate the correction parameter *B* and three rivers in blue squares for model blind test.

Therefore, Equation 2-10, which is used to determine the radioactivity concentration of radiocaesium in river water as a function of time can be rewritten as:

$$C_R = B \times D_C(\alpha e^{-(k_1+\lambda)t} + \beta e^{-(k_2+\lambda)t} + \gamma e^{-(k_3+\lambda)t}) \qquad 5\text{-}5$$

Where B is the parameter to adjust the overestimated prediction of AQUASCOPE due to the combination of the high absorption of high clay content and no peaty content in Japanese soils. The B parameter was fitted to the data at five rivers by using Microsoft Excel (2013), giving $B = 0.189$. Figure 5-24 illustrates the comparison of the results from modelled and measured data before and after applying B parameter for adjustment the overestimated results of model. The adjusted calculation shows good agreement between prediction and measured data for all five rivers. Before adjustment, all predictions from the model were overestimated approximately by factors of five (some prediction from Wariki and a measurement from Sugita were greater than factors of five). After applying the B parameter, there was excellent agreement between model and measurement from Matsu, Sugita and Yashiro River including estimated middle values of all measurements from Wariki and Natsui River, and all predictions are within the error range in the model.

Since radioactivity concentration in open lakes are influenced by radioactivity on its surface and catchment (runoff water), B parameter was also applied as a correction in Equation 2-24 to adjust the overestimation by high absorption. Similar to the calculation for river, the B parameter can be applied for adjustment directly to the open lake calculation (Equation 2-16), and the radioactivity concentration change with time of radiocaesium in open lakes in Japan can be estimated by

$$C_L(t) = B \times \left\{ \frac{D_L}{d} e^{-(K+\lambda)t} + \frac{D_c e^{-\lambda t}}{T_W} \left[\frac{\alpha(e^{-k_1 t} - e^{-Kt})}{(K - k_1)} + \frac{\beta(e^{-k_2 t} - e^{-t/T_W})}{(1/T_w - k_2)} + \frac{\gamma(e^{-k_3 t} - e^{-t/T_W})}{(1/T_W - k_3)} \right] \right\} \qquad 5\text{-}6$$

For closed lakes, the contamination by radiocaesium depends on the direct fallout onto surface of lake only so there is no influence of the fixation process on catchment soils so that the B parameter is not involved in the calculation. In addition, there is a lack of measured data of closed lakes in Japan following the accident therefore calibration of the AQUASCOPE model was not performed in this research.

For estimating radiocaesium in fish in rivers and open lakes, the *B* parameter is also applied, therefore, the adjusted equation for radiocaesium concentration in fish for rivers is:

$$C_f = B \times \left\{ D_c \times e^{-\lambda t} \times w^n \times \left[\frac{k_f \times \alpha}{k_b - k_1} \times (e^{-k_1 t} - e^{-k_b t}) + \frac{k_f \beta}{k_b - k_2} \times (e^{-k_2 t} - e^{-k_b t}) + \frac{k_f \gamma}{k_b - k_3} \times (e^{-k_3 t} - e^{-k_b t}) \right] \right\} \quad 5\text{-}7$$

In open lakes, the radiocaesium concentration is fish can be estimated by using

$$C_f = B \times \left\{ w^n \left[\left(k_f \times D_L \frac{e^{-Kt} - e^{k_b t}}{(k_b - K)d} \right) + D_C \alpha \times \frac{k_f e^{-\lambda t}}{T_W \times (K - k_1)} \times \left(\frac{e^{-k_1 t} - e^{-k_b t}}{k_b - k_1} - \frac{e^{-Kt} - e^{-k_b t}}{k_b - K} \right) + D_c \beta \times \frac{k_f e^{-\lambda t}}{T_W \times \left(\frac{1}{T_W} - k_2 \right)} \times \left(\frac{e^{-k_2 t} - e^{-k_b t}}{k_b - k_2} - \frac{e^{-\frac{t}{T_W}} - e^{-k_b t}}{k_b - \frac{1}{T_W}} \right) + D_C \gamma \times \frac{k_f e^{-\lambda t}}{T_W \times \left(\frac{1}{T_W} - k_3 \right)} \times \left(\frac{e^{-k_3 t} - e^{-k_b t}}{k_b - k_3} - \frac{e^{-\frac{t}{T_W}} - e^{-k_b t}}{k_b - \frac{1}{T_W}} \right) \right] \right\} \quad 5\text{-}8$$

The blind test of radioactivity concentration of radiocaesium in open lake water can be performed at Iitate Lake to evaluate the results of adjusted modelling, while the prediction of radiocaesium in non-predatory fish for open lakes can be evaluated in Teganuma Lake.

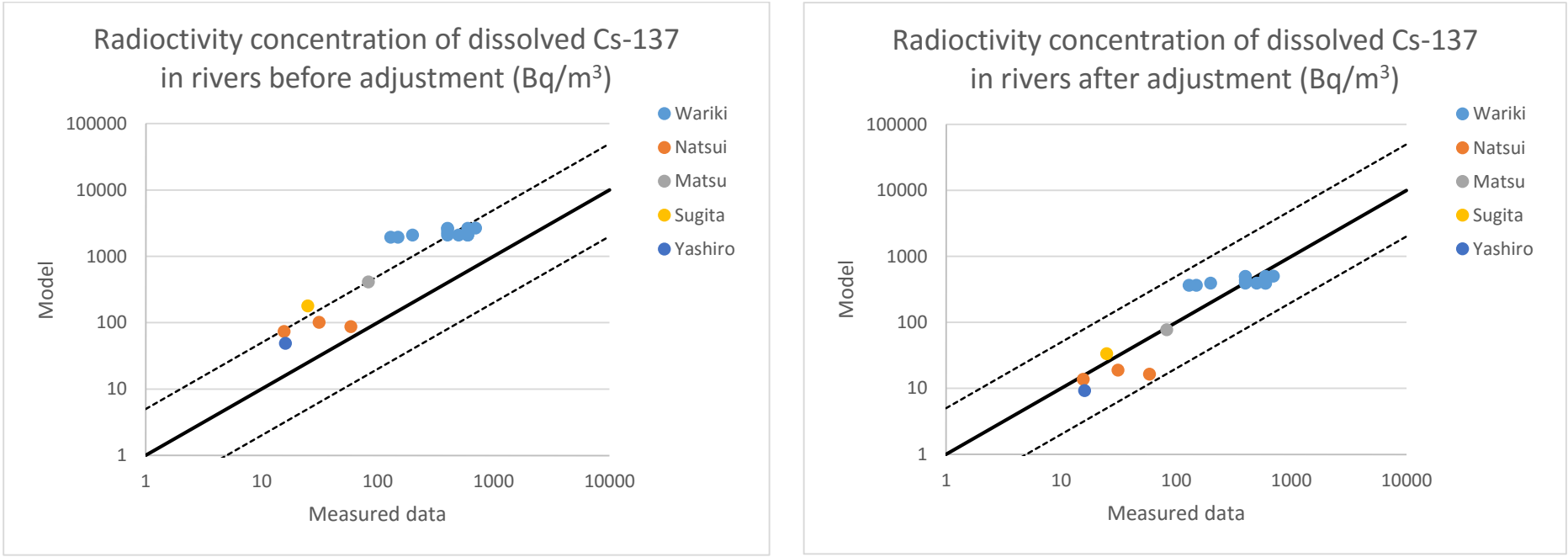

Figure 5-24 Comparison of the results from AQUASCOPE and measured data before and after applying *B* parameter for adjustment of the model. Dotted lines show a factor of five over- and under-estimation.

5.3 Results of the model

5.3.1 Results for river modelling

Figure 5-25 illustrates the results of blind test, after applying the correction parameter for modelling radiocaesium in three rivers (Hiso, Gohyaku and Same as shown in Figure 5-23) whose measured data were not used to determine the *B* parameter. The results of the adjusted model are good agreements with measured data, and the error range of a factor of five(Smith et al. (2005)) covers the variation in all measured data. This confirms that the value of empirical *B* parameter for adjustment of AQUASCOPE is effective to predict radioactivity concentration of radiocaesium in Japanese aquatic systems.

Predictions in all eight rivers are shown in Figure 5-26 (a) and (b): showing excellent agreement with measured data for the period up to 1.5 years after fallout.

For ^{131}I concentration in rivers, there are no measurements for comparison with models, however, the model estimates of the contamination in all eight rivers as shown in Figure 5-26 (c). Similarly to ^{131}I in river water, there were no available measurements for comparing with predictions of ^{134,137}Cs in predatory fish in Figure D-1 (a) and (b) and in non-predatory D-2 (a) and (b) respectively, and ^{131}I in fish (no difference between predatory and non-predatory) in Figure D-3.

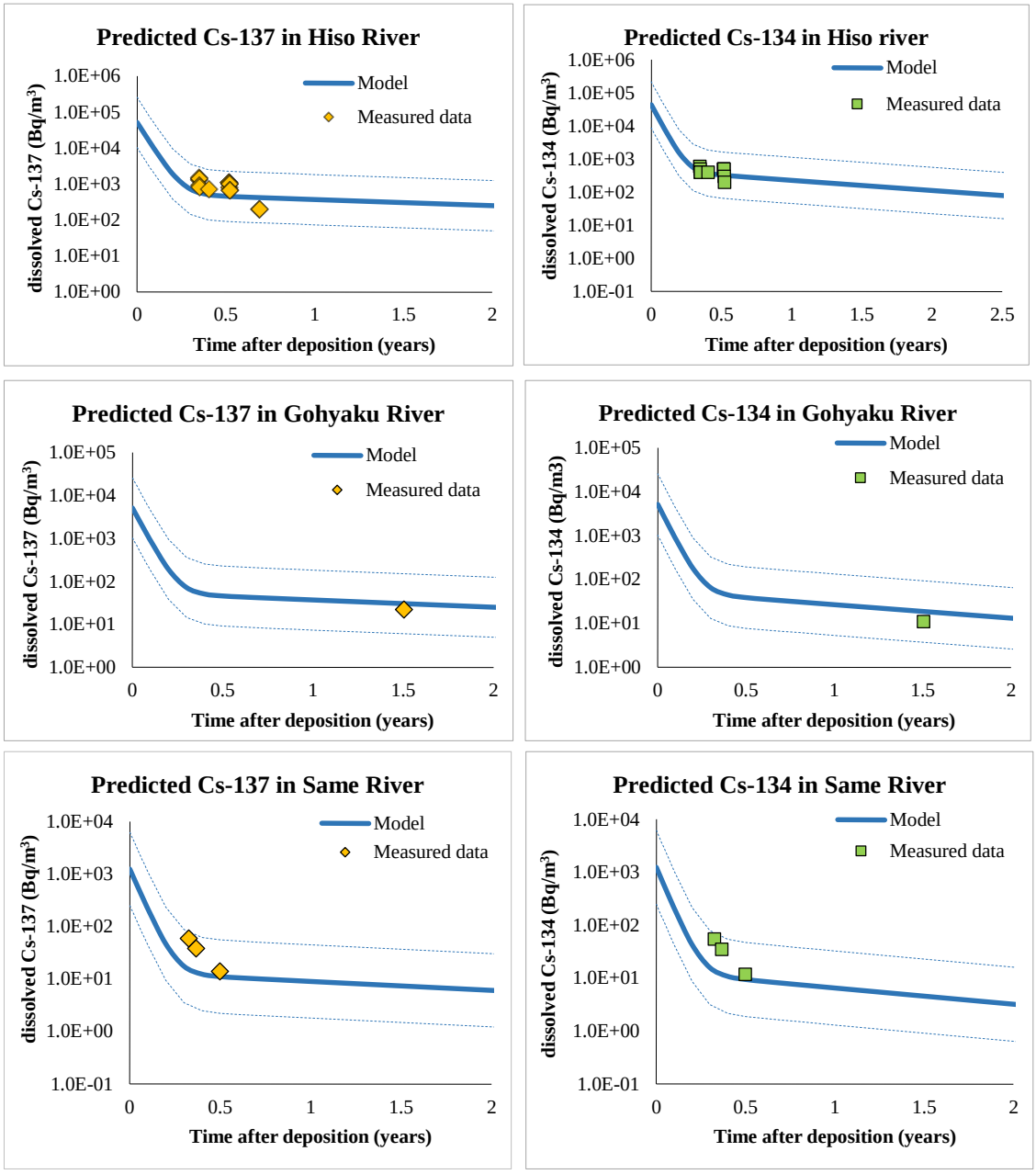

Figure 5-25 ”Blind test” of radiocaesium in three rivers around near-zone of Fukushima I NPSs.

(a) ^{134}Cs in river water

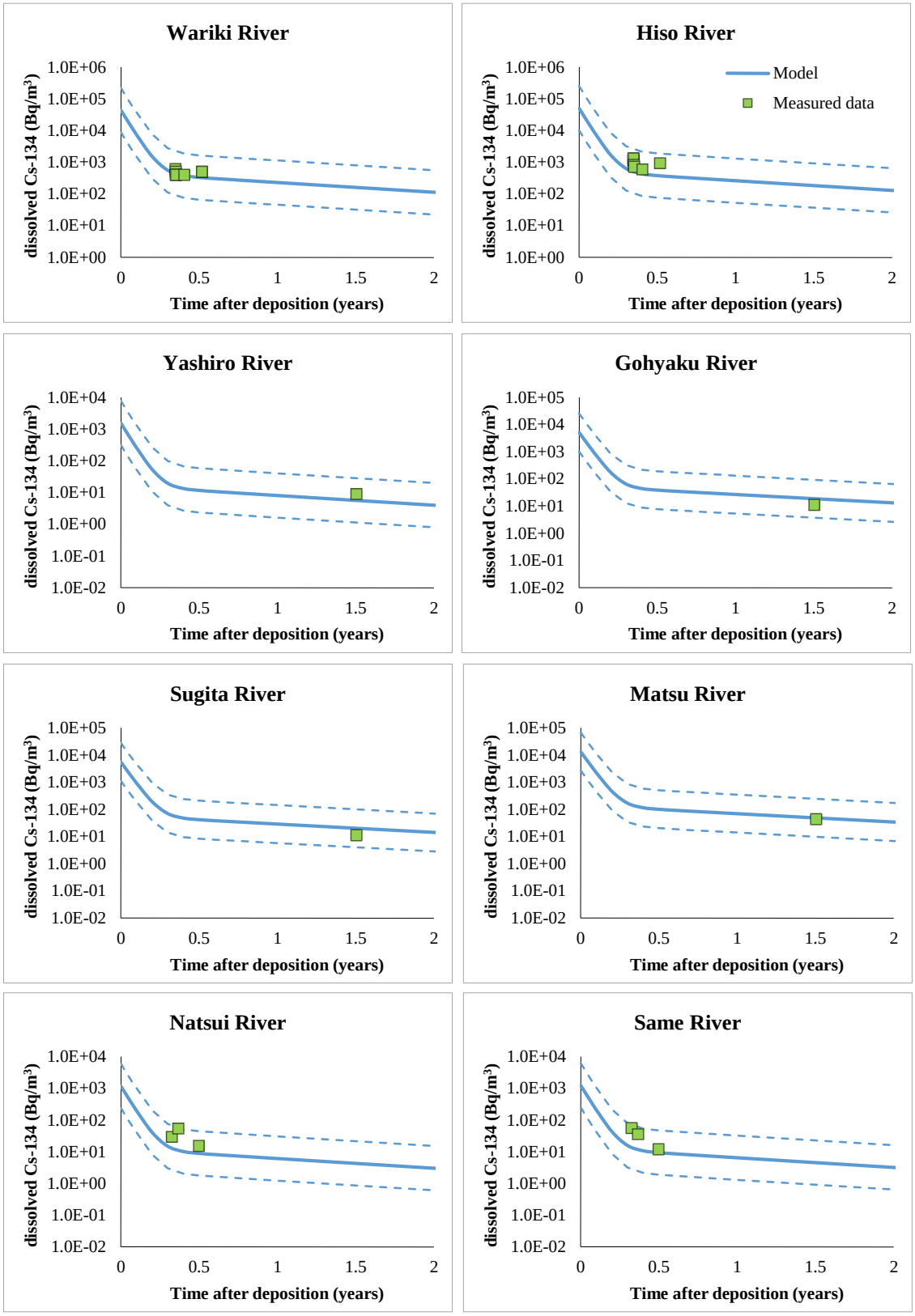

Figure 5-26 Predictions of concentration (Bq m^{-3}) in water at all eight rivers around Fukushima I NPSs, (a) ^{137}Cs, (b) ^{134}Cs and (c) ^{131}I.

(b) ^{137}Cs in river water

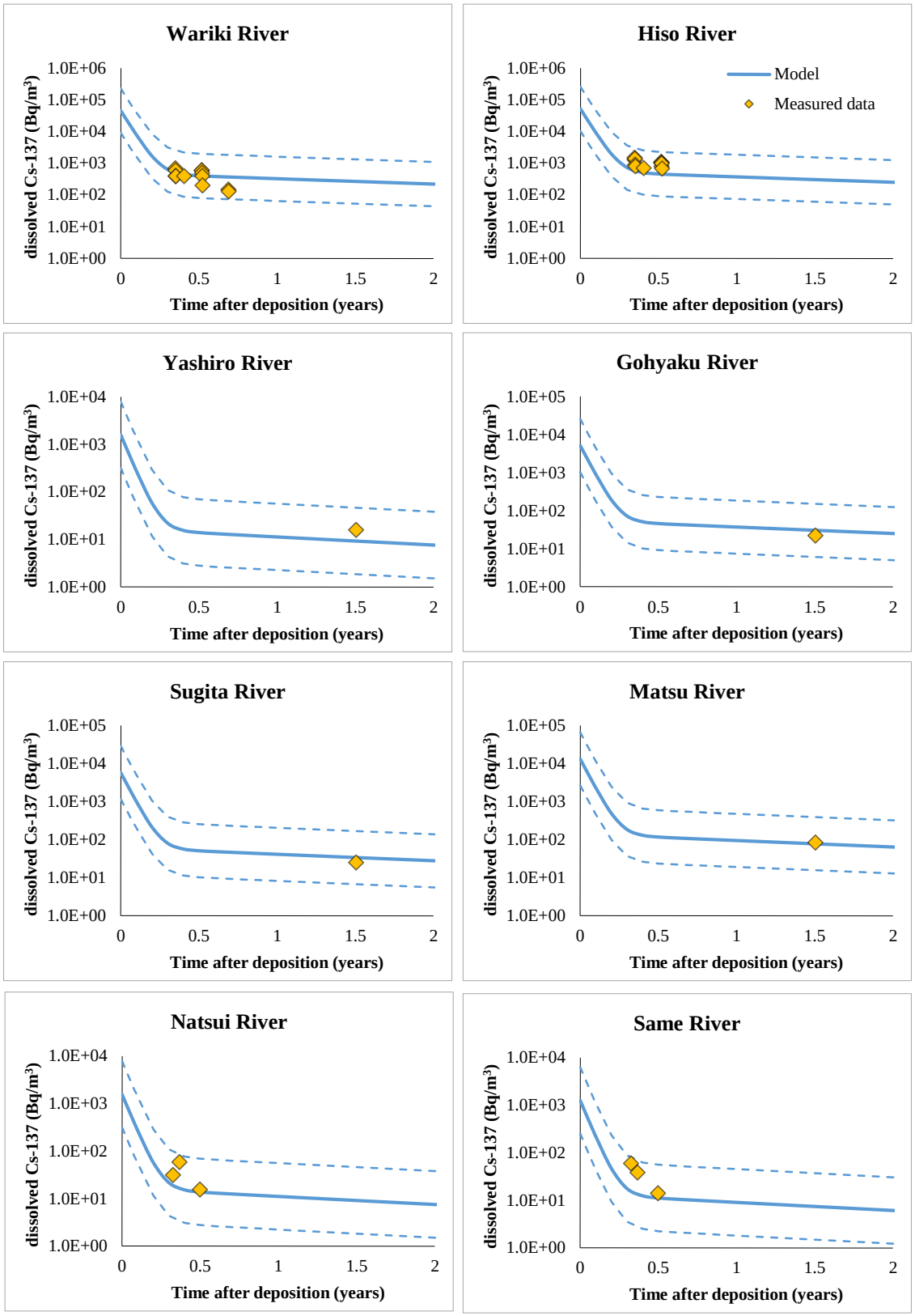

Figure 5-26 (continued) Predictions of concentration (Bq m^{-3}) in water at all eight rivers around Fukushima I NPSs, (a) ^{137}Cs, (b) ^{134}Cs and (c) ^{131}I.

(c) ^{131}I in river water

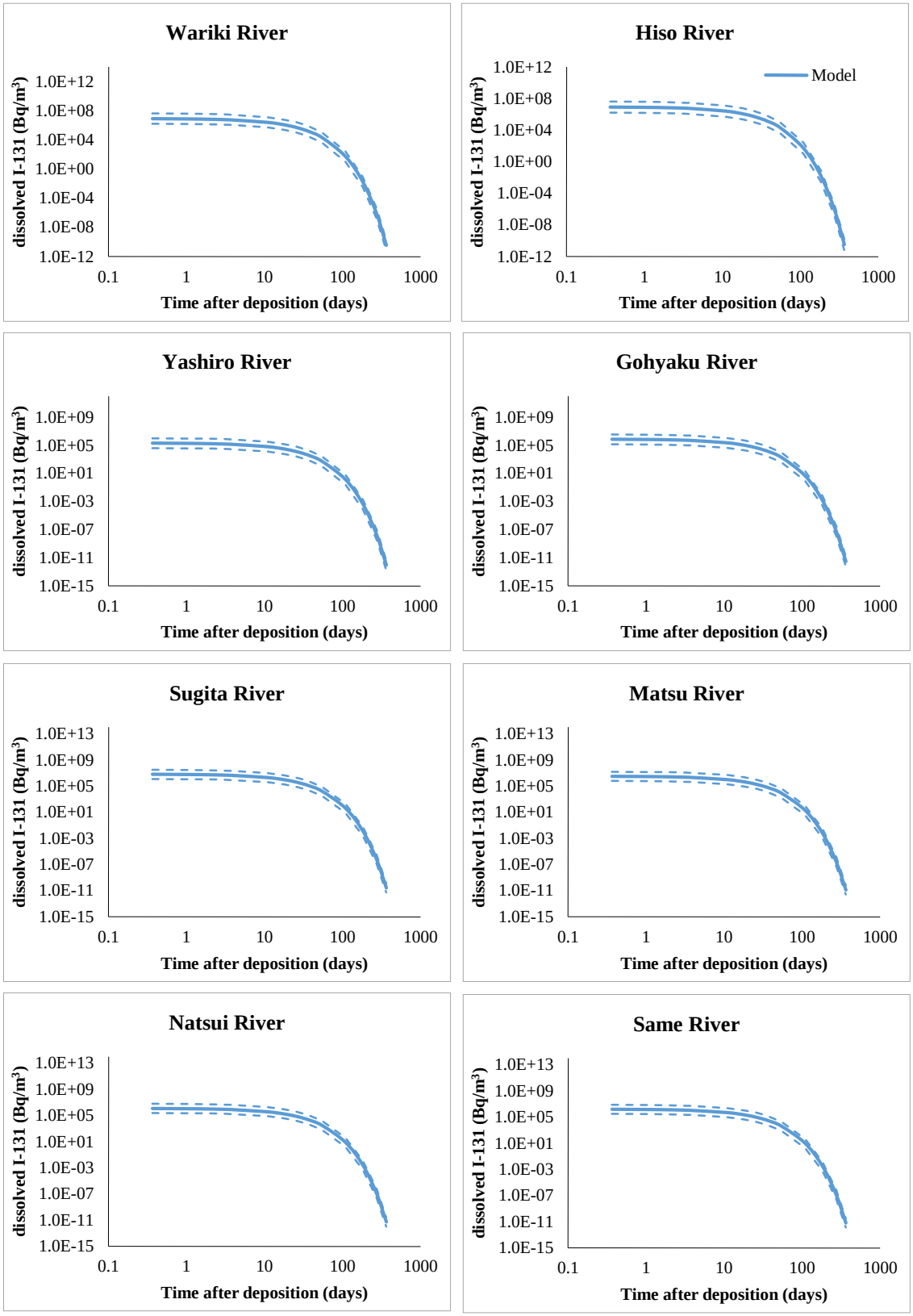

Figure 5-26 (continued) Predictions of concentration (Bq m^{-3}) in water at all eight rivers around Fukushima I NPSs, (a) ^{137}Cs, (b) ^{134}Cs and (c) ^{131}I.

5.3.2 Results of lake modelling

For open lakes, in which radiocaesium is influenced by surface deposition on to both catchment and lake surface, the adjustment parameter *B* is taken into account for prediction of radiocaesium, while prediction of ^{131}I uses all of the same parameters as in the original AQUASCOPE model. After the Fukushima accident, there has been a lack of measured data of contamination in water and fish for model testing in open and closed lakes. Measurements of ^{131}I and ^{134,137}Cs in water are available at Iitate Lake and ^{137}Cs in non-predatory fish data are available for Teganuma Lake.

For ^{131}I and ^{134,137}Cs in open lakes, the blind test was carried out at Iitate Lake using initial measurements by MEXT (2011b) and long-term of ^{137}Cs measured by this research. Dissolved radiocaesium can be subtracted from total phase by using K_d from the Wariki River as discussed above in 5.2.1.(j) However, there were no literature measurements for estimating dissolved ^{131}I following the accident but the distribution coefficient (K_d, L kg^{-1}) (which is the radioacitivity per kg of solid matter divided by the activity per dcubic metre of water) can be used to estimate dissolved ^{131}I in lake water. From previous studies in Table 5-10 (IAEA (1994, 2009) summarized from available literature) shows that the K_d of I is lower than Cs by an order of magnitude or more. This means that the percentage of dissolved form of I is likely to be significantly higher than Cs.

Table 5-10 Comparison of K_d values between ^{131}I and ^{134,137}Cs

Nuclide or element	K_d (L kg^{-1})	Source
^{131}I	0-80	IAEA (1994)
I	58-3.4×10^5	IAEA (2009)
^{134,137}Cs	50-8×10^4	IAEA (1994)
Cs	3.7×10^2-1.9×10^5	IAEA (2009)

Since the ranges of K_d of both nuclides are very large, it is not sensible to use mean values to estimate the proportion of dissolved ^{131}I. In the worst case scenario, for the highest uptake of ^{131}I to aquatic organismsit is assumed that all of the ^{131}I in the lake is in the dissolved form (as seen in Table 5-10, the lower bound of K_d of ^{131}I from IAEA (1994) was 0, or all of ^{131}I in the dissolved phase). Therefore, the blind test of ^{131}I concentration in water at Iitate Lake assumes that the total phase is equal to the dissolved phase.

The blind test of radioactivity concentration of ^{131}I and $^{134,137}Cs$ by using the adjusted AQUASCOPE model at Iitate Lake shows that the model has good agreement with measured data for all nuclides. The model has an excellent prediction for ^{131}I (Figure 5-27 (a)), however, the estimation of dissolved ^{131}I is still in question. For radiocaesium, (Figure 5-27 (b) and (c)) similar to the blind test in rivers, there were slight differences in prediction when the decline of radioactivity concentration in water was dominated by the initial rapid fixation process (up to around 0.1-0.3 years after deposition). The adjusted AQUASCOPE model gives excellent predictions for ^{137}Cs in the longer-term period at 1.4 and 1.8 years after deposition, as shown in detail in Figure 5-27 (c). This also confirms that the *B* parameter can be applied for predictions at any rivers and open lakes outside the near-zone of Fukushima I NPSs. Prediction of uptake into fish for Iitata Lake is shown in Figure D-4 in Appendix D.

The adjusted AQUASCOPE model was also tested against measurements of radioactivity concentration of ^{137}Cs in non-predatory fish at Teganuma Lake where the measurd data of Stone Moroko (*Pseudorasbora parva*) and Gold Fish (*Carassius Auratus Langsdorfii*) were available during 0.65 -1.55 years after deposition. Figure 5-28 illustrates the results from both species: most measured data varied within the error of the model. During 0.65-1.44 years after deposition, the trend of radiocaesium concentrations was underestimated for both species; after that, the prediction of Stone Moroko was overestimated (no measured data for Gold Fish). All prediction of radioactivity concentration in lake water and fish are shown in Figure D-5 in Appendix D.

There were no measurement data available for testing the model on closed lakes. Lake Kasumigaura, however, had the required parameter data for prediction by AQUASCOPE: and the results of the model are provided in Figure D-6, Appendix D.

(a) ^{131}I in water at Iitate Lake

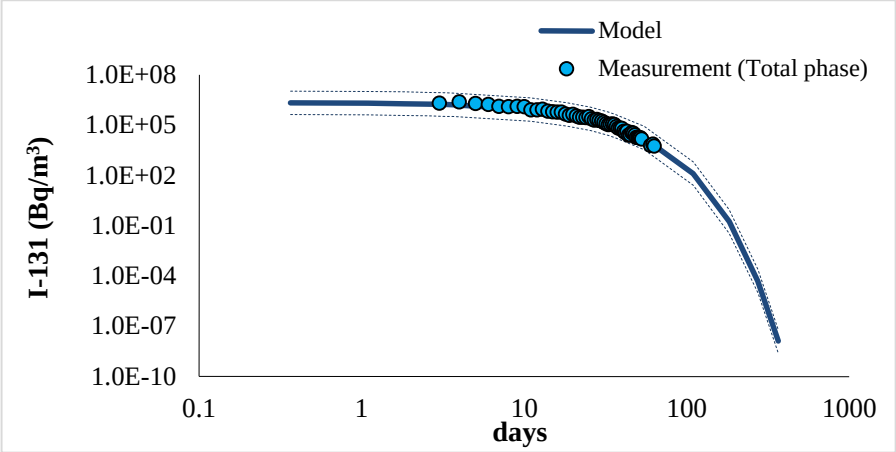

(b) ^{134}Cs in water at Iitate Lake

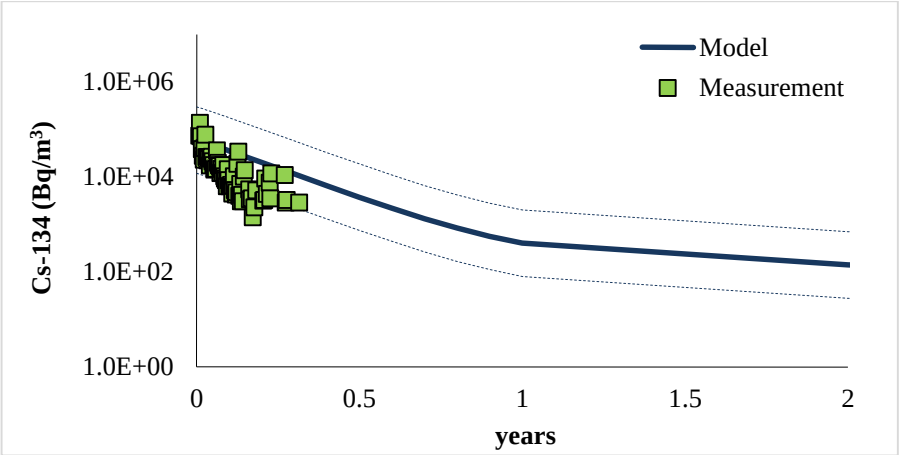

(c) ^{137}Cs in water at Iitate Lake

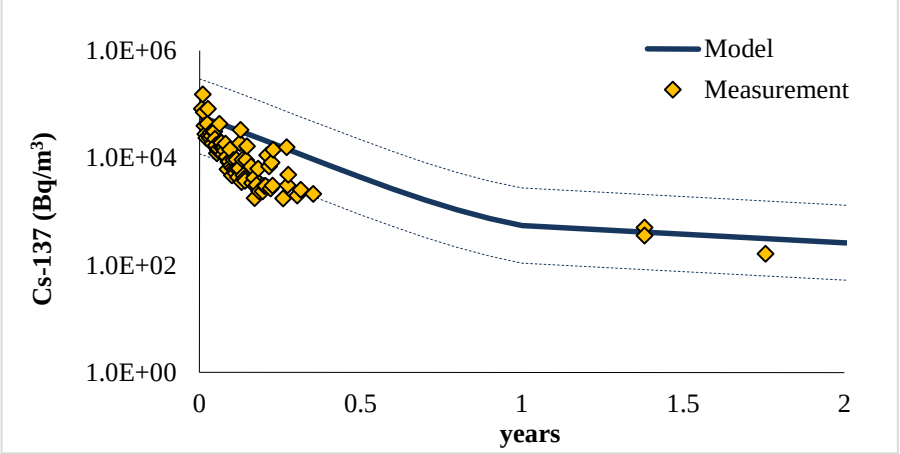

Figure 5-27 Results of the model of radioactivity concentration in lake water at Iitate Lake compared with available measured data from MEXT (2011b) and this research.

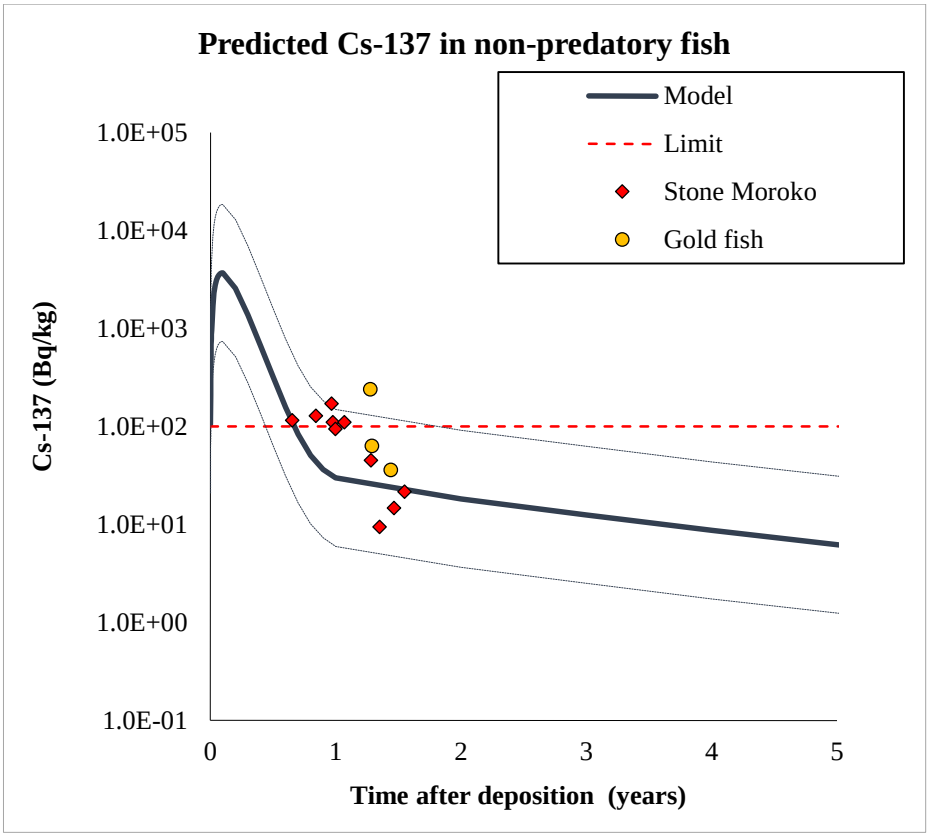

Figure 5-28 Results of radioactivity concentration of ^{137}Cs in fish at Teganuma Lake compared with available measured data from this research. The 100 Bq kg^{-1} limit for consumption of fish in Japan is also shown.

5.4 Conclusion

In contrast with the contamination of rivers following the Chernobyl accident, the normalized concentration in river per unit of surface deposition for radiocaesium in Japanese rivers show significantly lower transfer from the catchment. This is because the soil in Japanese catchments have strong absorption of radiocaesium: the combination of high clay contents and no peat or boggy contents in catchment soils supports this hypothesis since the clay soil has high 'fixation' of radiocaesium while peat or boggy soil has the opposite property. Therefore, to apply AQUASCOPE to predict the changes with time of radiocaesium in rivers and open lakes required the calibration of the model to achieve an accurate. A correction factor, the *B* parameter, of approximately a factor of five, was applied to reduce the over estimation resulting from the combination of the high absorption of high clay content and no peaty content in Japanese soils.

The adjusted model showed excellent predictions of radiocaesium in rivers and open lakes during the period up to 1.5 years after fallout. There are slight differences of prediction in the initial phase when the removal of radiocaesium was dominated by a rapid fixation process in the catchment but the error of a factor of five still covered most of the measured data. For short-lived ^{131}I, the original AQUASCOPE model could be used for prediction. The blind test showed generally good prediction of ^{131}I in the initial phase (by assuming that the dissolved form equalled the total phase). With limited data for fish modelling, only predictions of ^{137}Cs concentration in two non-predatory fish at one open lake could be performed. However, the results showed that the model was mostly in agreement with measured data. It can be assumed that the prediction of radiocaesium in water and fish for closed lakes by the original AQUASCOPE model is acceptable since the contamination in closed lakes is not influenced by the contamination in the catchment.

It can be concluded that the adjusted AQUASCOPE model is sufficient to predict contamination of radiocaesium in water and fish (both predatory and non-predatory) for rivers and open lakes. The original AQUASCOPE model gave good estimates contamination of radiocaesium in water and both fish types and for ^{131}I in closed lake water. There were no available data for testing the model for ^{131}I in rivers and closed lakes.

For closed lake modelling, there was no influence from deposited soil (radiocaesium) in catchment to lakes in Europe (Section 2.6.3) because there was little water inflow and outflow resulting in negligible radiocaesium transferred to and out of closed lakes. However, the strong absorption of radiocaesium for Japanese soil might influence the mobility of radiocaesium from catchment to closed lake, the amount of radiocaesium in runoff may be significant even though the amount of runoff is little. Since there is no measurement data from closed lakes in Japan, this research cannot evaluate this hypothesis.

On April 2012, new limits for radionuclide contamination in foods were enforced by the Ministry of Health, Labour and Welfare of Japan (MHLW, 2012). The new limit values for radioactive caesium are 10 Bg kg^{-1} (10^4 Bq m^{-3}) for drinking water and 100 Bq kg^{-1} for general foodstuffs including fish. Since Teganuma and Kasumigaura Lake are resources for water supply and theses lakes (Inamori, 2010) plus Iitate Lake are used for fisheries. The adjusted AQUASCOPE model can make long-term predictions of radiocaesium contamination in these systems which can estimate the approximate time when water use and fish consumption will be below the limit in these rivers and lakes. The model upper error band of a factor of five can be used to estimate the maximum time before each aquatic system will be below the contamination limit. Figure 5-29 shows total radiocaesium (combination of ^{134}Cs and ^{137}Cs) in (a) Teganuma and (b) Kasumigaura Lake. Teganuma Lake had higher contamination resulting from higher surface deposition than Kasumigaura Lake by about a factor of two. In Teganuma Lake (an open lake) water lake could be consumed approximately three months after deposition, while it took a longer period, around 10 months, in Kasumigaura Lake. Although deposition in catchment and lake surface of Teganuma Lake was higher than lake surface of Kasumigaura Lake, the removal rate of radiocasium of this closed lake was significantly less than in the open Teganuma lake: Kasumigaura Lake has a very long water residence time : T_w = 16.64 years.

For total radiocaesium in fish, in Hiso River which has is the highest contamination, it could take more than 50 and 15 years (Figure 5-30 (a) and (b)) for safe consumption of predatory and non-predatory fish respectively. In Iitate Lake where the contamination is similar to the Hiso River (surface deposition on catchment were 8.05×10^5 and 9.15×10^5 Bq m^{-2} for ^{134}Cs and 1^{37}Cs respectively), the period before safe consumption of fish is

longer than the Hiso River due to the fact that the removal rate of radiocaesium of river is faster than open lake, being up to 60 and 20 years for predatory and non-predatory fish respectively (Figure 5-30 (c) and (d)). Since deposition in Teganuma Lake is less than Iitate Lake by about one magnitude, fish in this lake will be available for consumption sooner than Iitate Lake, around 13 and 3 years for predatory and non-predatory respectively (Figure 5-30 (e) and (f)). In the closed lake, Kasumigaura Lake, where deposition was also lower than Iitate Lake by about one order of magnitude time before safe consumption of fish is potentially very long: up to 90 years for predatory fish and 40 years for non-predatory fish as shown detail in Figure 5-30 (g) and (h).

These predictions of the AQUASCOPE model for rivers and lakes in Japan are potentially very useful to help the Japanese authorities to estimate the time for safe consumption of water and fish in contaminated rivers and lakes in the contaminated areas.

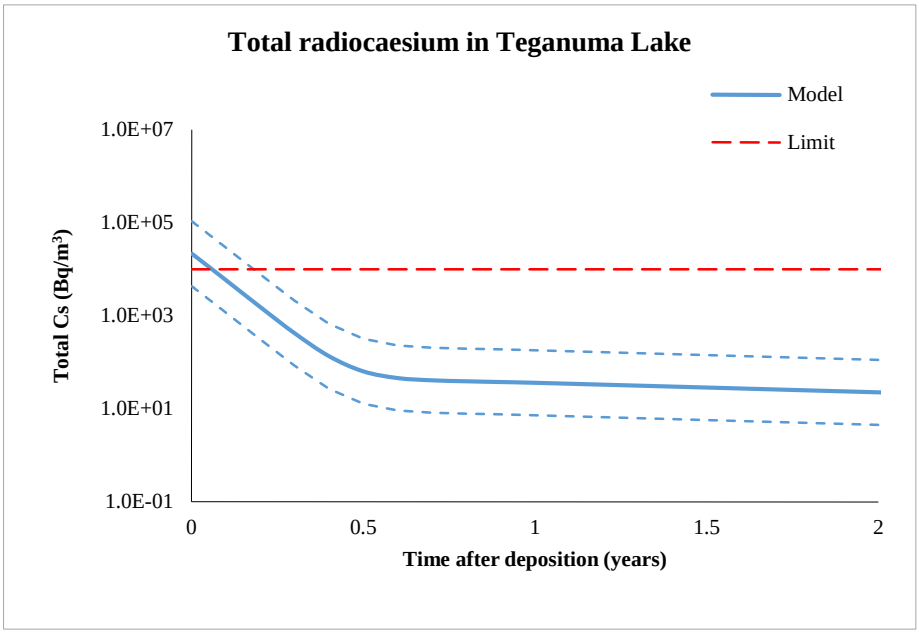

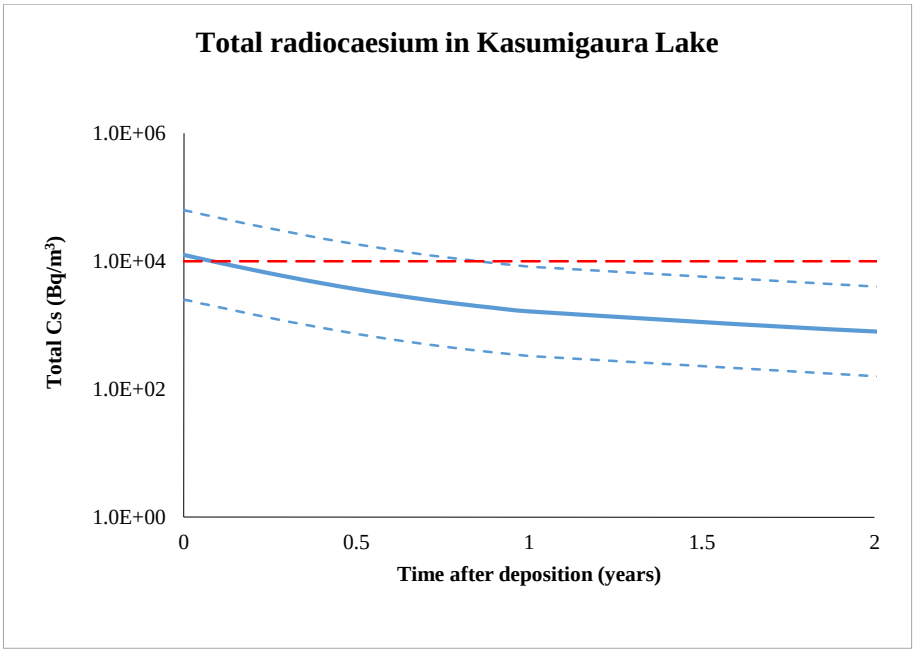

Figure 5-29 Results from model of radioactivity concentration of total radioactive caesium in at Teganuma and Kasigaura Lake where are water supply resources.

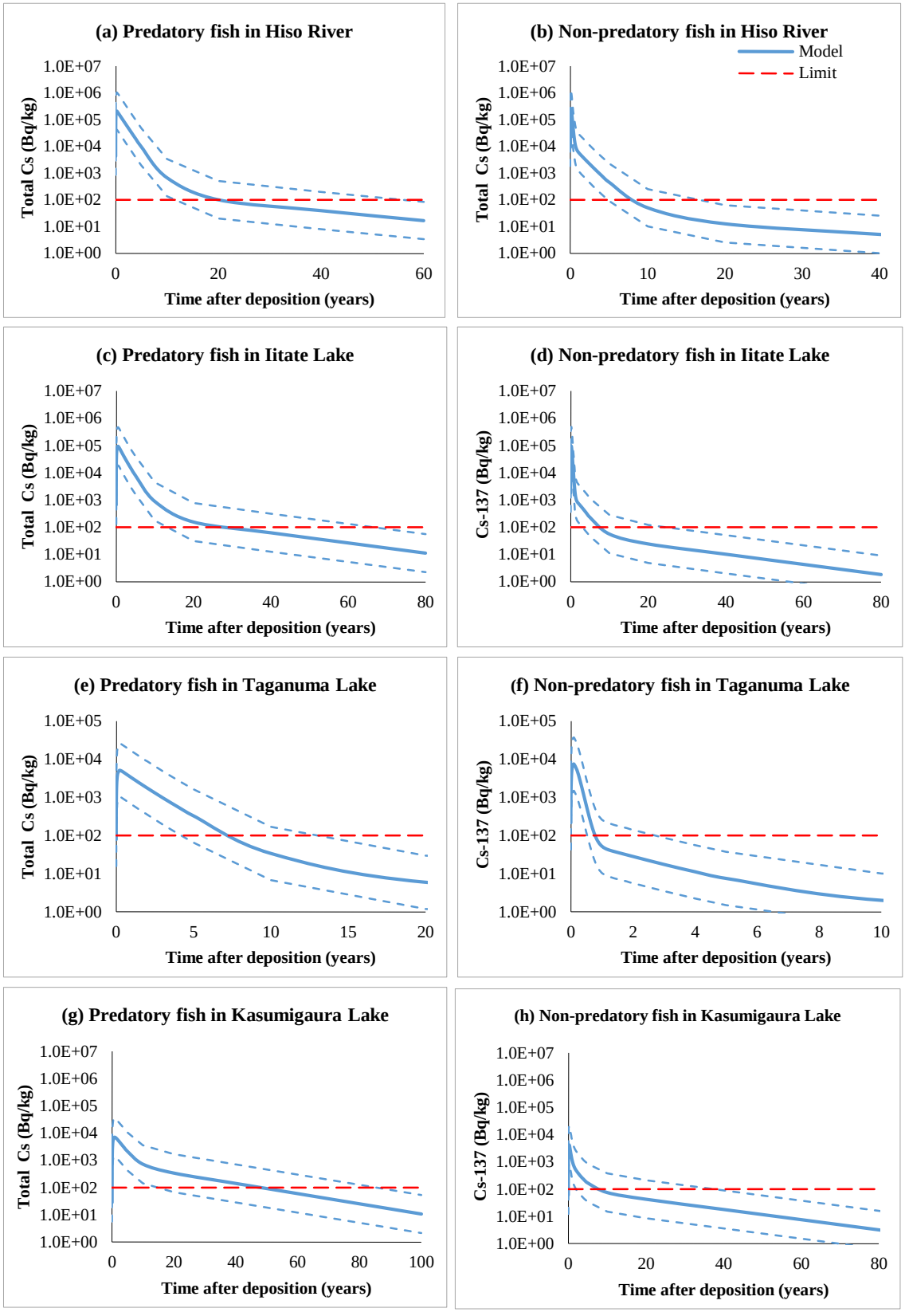

Figure 5-30 Results from model of radioactivity concentration of total radioactive caesium in fish at Hiso River, and Iitate, Teganuma and Kasigaura for determining the safe period of fish consumption.

Chapter 6 General Conclusions

The explosions at the four reactors of the Fukushima Dai-ichi (I) Nuclear Power Stations (Fukushima I NPSs) in Japan released a large radioactive cloud into the atmosphere. Consequently, there were two highly contaminated plumes released from Fukushima I NPSs, the North-Western on 15 March 2011 and Southern plume on 21 March 2011. These releases led to large-scale radioactive contamination in air which was transported around the World. The emphasis of this study was the area in the near-zone of the NPSs where soil and aquatic ecosystems were affected by high deposition and particularly high external gamma dose rates in areas influenced by the North-Western plume. Due to the lack of measurements in three major ecosystem compartments i.e. air, soil and river water, understanding and highest impact early-phase period after high fall out and the interpretation of long-term impacts were limited and unclear. Three model based analyses carried out in this research helps understanding of the transfer of contaminated nuclides, and the reconstruct of the environmental contamination and irradiation of humans in the early-phase. The developed models for aquatic systems also allow prediction of long-term contamination in the future.

Isotopic Ratio

The method of studying decay-corrected ratios of radioisotopes to the long-lived nuclide ^{137}Cs is an effective and simple method to estimate concentrations of other key radionuclides in areas where measurements of these nuclides, in particular very short-lived nuclides ^{131}I and ^{132}Te, are not available.

This analysis of isotope ratios found that the ratios of ^{134,136}Cs and ^{132}Te to ^{137}Cs are relatively constant with distance and direction in both contaminated air and soil. The lowest variability is for the ratios of radiocaesium isotopes as these three nuclides are isotope of same element and behave in the same way in the environment, even though the mechanism of production in the reactor is different (^{136,137}Cs is fission product and ^{134}Cs is activation product). ^{132}Te/^{137}Cs has slightly higher variability than the radiocaesium ratio resulting from a lack of measured data due to its very short half-life, combined with the slightly different behaviour from different elements of similar size and type. Corrected ratios of these three nuclides were similar between air around the World and in soil within the near-zone. The general ratio for ^{136}Cs:^{137}Cs is 0.2, ~0.9-1.0 is for ^{134}Cs:^{137}Cs, and

mean of ratio of both highly volatile elements ^{132}Te and ^{137}Cs is approximately 17-22. The ratio of ^{132}Te:^{137}Cs is very useful for investigation back to initial times when this nuclide dominated external gamma dose since the measurement of this nuclide was very rare: there were no measurements in the main monitoring in the near-zone around the NPPs.

In contrast with these three consistent ratios, the ^{131}I:^{137}Cs ratio is not constant with direction and distance, and it is not constant with time at particular monitoring sites while other key nuclides were relatively constant. The best hypothesis is that the release amount of ^{131}I depends on the temperature in the reactor core (high temperature releases high amounts (Mück, et al., 2002)). To prove this hypothesis, the time-line information of temperature at reactor cores of Unit 1-3 are required. The Worldwide ratio of ^{131}I:^{137}Cs in air had remarkably high variation which might be not accurate for estimating contamination by iodine, with mean = 73.1 and range 12-290 for ^{131}I:^{137}Cs particulate, mean = 269 and range 78-853 for the ratio of gaseous ^{131}I to particulate ^{137}Cs, mean = 253 .12 and range 50.91-597.15 for gross ^{131}I to particulate ^{137}Cs, and the mean gaseous fraction of ^{131}I was 80.4% and range 49.2-93.4%.

For the deposited ratio in the near-zone area, the ratio of the highly contaminated area in NW had inverse correlation with activity concentration of ^{137}Cs. This correlation is very useful to estimate the contamination of ^{131}I at this key region, and after testing in the gamma dose rate model invented by this research it is shown that it can estimate reliable values of the ratios in the N and W since the results of the model also agree with measured data in these areas. There are no measurements of both gamma dose and deposition at the same time in the SW area for model testing, but the deposited ratio was similar to the ratio from the N to W directions.

From Figure 2-1, it was found that the behaviour of deposition of ^{131}I was similar to ^{129m}Te, only these two nuclides were deposited in significant amounts in south direction and the highest corrected ratios of both also occurred in this direction. Therefore, further study about the corrected ratio of ^{131}I to ^{129m}Te around Fukushima I NPSs (both ambient and deposited ratio) might be useful for evaluating the transfers of these nuclides following the Fukushima accident.

Early-phase external dose reconstruction at near-zone

The prediction of external gamma dose rate at 1 metre above contaminated soil in the area from north to west of Fukushima I NPSs can be simply determined by using an empirical constant *A* to convert gamma energy (MeV) emitted from all key radionuclides in soil to external gamma dose rate in air (μSv h^{-1}). The model only requires ^{137}Cs activity as an input parameter while all other parameters are constants. These include total gamma decay energy of each nuclide, mean corrected ratio of ^{32}Te and $^{134,136}Cs$ to ^{137}Cs as observed in soil at near-zone plus estimated ratio of ^{131}I to ^{137}Cs calculated by the inverse correlation to ^{137}Cs activity. The empirically-determined constant *A* was evaluated from six calibration sites at the highest contaminated area to the Northwest, however, model predictions are generally in good agreement with measured data for sites located other directions i.e. North and West. Poor predictions in the southern area are due to a remarkably high ratio $^{131}I/^{137}Cs$ influenced by the southern plume on 21 March. The main uncertainty of the model is shown by Monte Carlo simulation to be the *A* parameter and ^{137}Cs concentration.

For the southern area, the external gamma dose could be estimated by further investigation of the *A* parameter and of the high ^{131}I to low ^{137}Cs ratio for the specific area affected by the southern plume. Long-lived ^{137}Cs is still in the surface of soil due to its strong absorption: Kato and co-workers (2012) observed that greater than 86% of ^{137}Cs is still present in the first 2 cm of soil surface in an area far from Fukushima I NPSs about 40 km in northwest direction. This is similar to the finding that more than 70% of ^{137}Cs was absorbed within the upper 2 cm of soil profile at area from N to NW between 10 and 40 km from NPSs in Fujiwara et al. (Fujiwara et al., 2012). It can be assumed that strong absorption also occur in southern area as Hashimoto and co-workers (Hashimoto, et al., 2012) showed that the soil type around Fukushima I NPSs within 100 km is the same type. Collecting soil samples at sites where there had been measurements of the external gamma dose rate in the initial phase could determine an empirical constant *A* for the southern plume. There were 12 samples of soil available from the southern area to determine a correlation between ^{131}I:^{137}Cs ratio and ^{137}Cs activity. Further investigating of deposited activity of ^{137}Cs can be also applied at any sites in area from North to Southwest where initial gamma dose was available (no soil measurement) to strengthen the *A* parameter for more accurate predictions.

From this study it is shown that a post-accident gamma dose rate monitoring programme should collect soil samples and further information onsoils i.e. type, density and depth, and depth profile of contamination at the site of monitoring which can be used to evaluate correlations of gamma dose rate and contamination in soil. This information will be useful for reconstruction of gamma dose rate by this model and also by other models at areas where measured data in initial period after high fallout are not performed.

Applying AQUASCOPE to predict contamination in freshwater ecosystems

The simplified AQUASCOPE model can predict the contamination of aquatic systems in the long-term period after an accident to evaluate the contamination in future and for reconstruction to study doses during the highest impact initial period. The required input parameters of the model are very simple and available even a short time after the accident. The minimum parameters, for example, the surface deposition (Bq/m^2) could be found in the large data base of measurements made by MEXT (2014) which covers 200-km area around Fukushima I NPSs (most available values were of ^{137}Cs but the corrected ratios from Chapter 3 could be used to estimate ^{134}Cs and ^{131}I). In addition, the surface deposition at any catchment could be evaluated by measuring concentration of ^{137}Cs in soil and density of soil because most of ^{137}Cs is still in the first few centimetres of the soil surface (Fujiwara, et al., 2012; Kato, et al., 2012; Tanaka, et al., 2012). For prediction of radiocaesium in fish, the mean value of potassium concentration in rivers and lakes is another parameter which can be measured at any time. Other parameters, including net rainfall on to the catchment, depth, catchment area and/or surface area of lake are relatively simple parameters to measure. Therefore, AQUASCOPE has been shown to be a simple and effective model to determine the contamination of $^{134,137}Cs$ and ^{131}I at any freshwater ecosystem in Japan after the high fallout from the Fukushima accident.

Further investigation should be carried out to investigate the influence of strong absorption of radiocaesium in Japanese catchment soils, particularly for rivers and open lakes where radioactivity concentration in water is strongly influenced by contamination in catchment. Since there was a lack of initial measurements, it is a limit of this research that there were no observations of these empirical constants for Japanese catchments, i.e. α and k_1 for a fast "flush" of activity as a result of rapid wash off processes and β and k_2 for a slow decline as a result of soil fixation. The author is currently in contact with the Japanese National Institute of Radiological Sciences, Chiba, to find measurements from

before the Fukushima accident (nuclear weapons test period) to help evaluate transfers of radiocaesium from catchment to lake in the very long term. This investigation may provide a more accurate estimate of radiocaesium concentration in water and fish in the long term after Fukushima. In addition, it would be wise to test the adjusted AQUASCOPE for predicting contamination in predatory species of fish in rivers and other open lakes to validate the model results because only data for non-predatory fish was available for these systems. Since potassium concentration in water is very important for estimating uptake of radiocaesium, using measurement of this parameter at rivers and lakes will interpreted accurate prediction.

It clear that the contamination in open lake also depends on direct deposition on the water surface (as well as deposition on catchment), and only on deposition to the surface of the lake for contamination in closed lakes. The remarkably important lakes for people, such as Kasumigaura Lake (the second biggest lake in Japan which is used for water supply and fisheries) and Teganuma Lake (irrigation water supply) should have real time monitoring systems of surface deposition (Bq/m^2) in their catchments and water surfaces because these information are key parameters for evaluating contamination in water and fish.

These three simplified and effective models from this research are powerful tools to reconstruct and predict the effects of contamination from Fukushima on humans and ecosystems which is the key for countermeasures to mitigate the radiological consequences of the Fukushima Accident.

References

Altman, D. G., & Bland, J. M. (2005). Standard deviations and standard errors. *Bmj, 331*(7521), 903.

Amano, H., Akiyama, M., Chunlei, B., Kawamura, T., Kishimoto, T., Kuroda, T., et al. (2012). Radiation measurements in the Chiba Metropolitan Area and radiological aspects of fallout from the Fukushima Dai-ichi Nuclear Power Plants accident. *Journal of Environmental Radioactivity, 111*, 42-52.

Bank, t. W. (2014). *World Development Indicators: Traffic and congestion*.

Bergman, R. N., Ider, Y. Z., Bowden, C. R., & Cobelli, C. (1979). Quantitative estimation of insulin sensitivity. *American Journal of Physiology - Endocrinology And Metabolism, 236*(6), E667-677.

Biegalski, S. R., Bowyer, T. W., Eslinger, P. W., Friese, J. A., Greenwood, L. R., Haas, D. A., et al. (2011). Analysis of data from sensitive US monitoring stations for the Fukushima Daiichi nuclear reactor accident. *Journal of Environmental Radioactivity*.

Billiet, P. (2013). Critical Values for the Mann-Whitney U-Test. Retrieved from http://www.saburchill.com/IBbiology/downloads/002.pdf

Blaylock, B. G. (1982). Radionuclide data bases available for bioaccumulation factors for freshwater biota. *Journal Name: Nucl. Saf.; (United States); Journal Volume: 23:4*, Medium: X; Size: Pages: 427-438.

Bossew, P., Kirchner, G., De Cort, M., de Vries, G., Nishev, A., & de Felice, L. (2012). Radioactivity from Fukushima Dai-ichi in air over Europe; part 1: spatio-temporal analysis. *Journal of Environmental Radioactivity, 114*(0), 22-40.

Brezonik, P. L. (1993). *Chemical kinetics and process dynamics in aquatic systems*: CRC Press.

Bulgakov, A. A., Konoplev, A. V., Smith, J. T., Hilton, J., Comans, R. N. J., Laptev, G. V., et al. (2002). Modelling the long-term dynamics of radiocaesium in closed lakes. *61*(1), 41-53.

Bunzl, K., Jacob, P., Schimmack, W., Alexakhin, R. M., Arkhipov, N. P., Ivanov, Y., et al. (1997). Cs-137 mobility in soils and its long-term effect on the external radiation exposure. *Radiation and Environmental Biophysics, 36*(1), 31-37.

Bushberg, J. T., & Boone, J. M. (2011). *The essential physics of medical imaging*: Lippincott Williams & Wilkins.

Cambray, R. S., Cawse, P., Garland, J., Gibson, J. A. B., Johnson, P., Lewis, G., et al. (1987). Observations on radioactivity from the Chernobyl accident. *Nuclear Energy, 26*(2), 77-101.

Carvalho, F. P., Reis, M. C., Oliveira, J. M., Malta, M., & Silva, L. (2012). Radioactivity from Fukushima nuclear accident detected in Lisbon, Portugal. *Journal of Environmental Radioactivity, 114*(0), 152-156.

Chaisan, K., Smith, J. T., Bossew, P., Kirchner, G., & Laptev, G. V. (2013). Worldwide isotope ratios of the Fukushima release and early-phase external dose reconstruction. *Scientific reports, 3*.

Chino, M., Nakayama, H., Nagai, H., Terada, H., Katata, G., & Yamazawa, H. (2011). Preliminary Estimation of Release Amounts of 131I and 137Cs Accidentally Discharged from the Fukushima Daiichi Nuclear Power Plant into the Atmosphere. *Journal of Nuclear Science and Technology, 48*(7), 1129-1134.

Choppin, G. R., Liljenzin, J.-O., & Rydberg, J. (2002). *Radiochemistry and nuclear chemistry*: Butterworth-Heinemann.

Clark, M., & Smith, F. (1988). Wet and dry deposition of Chernobyl releases.

Coughtrey, P. J., & Thorne, M. C. (1983). *Radionuclide distribution and transport in terrestrial and aquatic ecosystems. A critical review of data. Volume 1*: AA Balkema.

Cremers, A., Elsen, A., Preter, P. D., & Maes, A. (1988). Quantitative analysis of radiocaesium retention in soils. [10.1038/335247a0]. *Nature, 335*(6187), 247-249.

D'agostino, R., Belanger, A., & D'Agostino Jr, R. (1990). A suggestion for using powerful and informative tests of normality. *The American Statistician, 44*(4), 316-321.

DOE. (1988). *External dose-rate conversion factors for calculation of dose to the public* (No. DOE/EH-0070; Other: ON: DE88014691; TRN: 88-030899 United States10.2172/6953527Other: ON: DE88014691; TRN: 88-030899Fri Feb 08 08:56:08 EST 2008NTIS, PC A11/MF A01; 1.TIC; ERA-13-049698; EDB-88-157779English): the US Department of Energy.

Doyle, J. (2011). *Nuclear Safeguards, Security and Nonproliferation: Achieving Security with Technology and Policy*: Elsevier.

Eckerman, K., & Ryman, J. (1993). Dose Coefficients for external exposure to radionuclides distributed in air, water and soil, Federal Guidance report 12. *USEPA, Washington*.

Elliott, J. M. (1975). Number of meals in a day, maximum weight of food consumed in a day and maximum rate of feeding for brown trout, Salmo trutta L. *Freshwater Biology, 5*(3), 287-303.

Elliott, J. M., Hilton, J., Rigg, E., Tullett, P. A., Swift, D. J., & Leonard, D. R. P. (1992). Sources of Variation in Post-Chernobyl Radiocaesium in Fish from Two Cumbrian Lakes (North-West England). *Journal of Applied Ecology, 29*(1), 108-119.

Endo, S., Kimura, S., Takatsuji, T., Nanasawa, K., Imanaka, T., & Shizuma, K. (2012). Measurement of soil contamination by radionuclides due to the Fukushima Dai-ichi Nuclear Power Plant accident and associated estimated cumulative external dose estimation. *Journal of Environmental Radioactivity, 111*(0), 18-27.

Endo, T., Sato, S., & Yamamoto, A. (2011). *Estimation of average burnup of damaged fuels loaded in Fukushima Dai-ichi reactors* Paper presented at the Proceedings of the 2011 Symposium on Nuclear Data.

EPA. (2011). Japanese Nuclear Emergency: Radiation Monitoring. Retrieved from http://epa.gov/japan2011/rert/radnet-sampling-data.html#air

Evans, D. W., Alberts, J. J., & Clark Iii, R. A. (1983). Reversible ion-exchange fixation of cesium-137 leading to mobilization from reservoir sediments. *Geochimica et Cosmochimica Acta, 47*(6), 1041-1049.

Fujiwara, T., Saito, T., Muroya, Y., Sawahata, H., Yamashita, Y., Nagasaki, S., et al. (2012). Isotopic ratio and vertical distribution of radionuclides in soil affected by the accident of Fukushima Dai-ichi nuclear power plants. *Journal of Environmental Radioactivity, 113*, 37-44.

Golikov, V., Balonov, M., Erkin, V., & Jacob, P. (1999). Model validation for external doses due to environmental contaminations by the Chernobyl accident. *Health Physics, 77*(6), 654-661.

Golikov, V., Balonov, M., & Jacob, P. (2002). External exposure of the population living in areas of Russia contaminated due to the Chernobyl accident. *Radiation and Environmental Biophysics, 41*(3), 185-193.

Gudelis, A., Druteikienė, R., Lujanienė, G., Maceika, E., Plukis, A., & Remeikis, V. (2012). Radionuclides in the ground-level atmosphere in Vilnius, Lithuania, in

March 2011, detected by gamma-ray spectrometry. *Journal of Environmental Radioactivity, 109*(0), 13-18.
Hadderingh, R. H., van Aerssen, G. H. F. M., Ryabov, I. N., Koulikov, A. O., & Belova, N. (1997). Contamination offish with 137Cs in Kiev reservoir and old river bed of Pripyat near Chernobyl *Studies in Environmental Science* (Vol. Volume 68, pp. 339-351): Elsevier.
Hansen, H. J. M., & Aarkrog, A. (1990). A different surface geology in Denmark, the Faroe islands and Greenland influences the radiological contamination of drinking water. *Water research, 24*(9), 1137-1141.
Hashimoto, S., Ugawa, S., Nanko, K., & Shichi, K. (2012). The total amounts of radioactively contaminated materials in forests in Fukushima, Japan. *Scientific reports, 2*.
Helton, J. C., Muller, A. B., & Bayer, A. (1985). Contamination of surface-water bodies after reactor accidents by the erosion of atmospherically deposited radionuclides. *Health physics, 48*(6), 757-771.
Hickey, J. J., Keith, J., & Coon, F. B. (1966). An exploration of pesticides in a Lake Michigan ecosystem. *Journal of Applied Ecology*, 141-154.
Hilton, J., Livens, F. R., Spezzano, P., & Leonard, D. R. P. (1993). Retention of radioactive caesium by different soils in the catchment of a small lake. *Science of The Total Environment, 129*(3), 253-266.
Hinton, P. R., McMurray, I., & Brownlow, C. (2014). *SPSS explained*: Routledge.
Hole, G. (2013). The Mann-Whitney test. Retrieved from http://www.sussex.ac.uk/Users/grahamh/RM1web/MannWhitneyHandout%202011.pdf
Hosoda, M., Tokonami, S., Sorimachi, A., Monzen, S., Osanai, M., Yamada, M., et al. (2011). The time variation of dose rate artificially increased by the Fukushima nuclear crisis. [10.1038/srep00087]. *Sci. Rep., 1*.
HPA. (2011). Update on the Fukushima Incident: 14 July 2011. Retrieved 14/04/12, 2012, from http://www.hpa.org.uk/web/HPAweb&HPAwebStandard/HPAweb_C/1309968917992
IAEA. (1986). *SAFETY SERIES* (No. 75-INSAG-4). Vienna.
IAEA. (1991). *The International Chernobyl Project* (No. ISBN 92-0-129191-4). Vienna.
IAEA. (1994). *Handbook of Parameter Values for the Prediction of Radionuclide Ttransfer in Temperate Environments*. Vienna: IAEA.
IAEA. (2009). *Quantification of Radionuclide Ttransfer in Terrestrial and Freshwater Environments for radiological Assessments*. Vienna: IAEA.
ICRP. (2008). *Nuclear Decay Data for Dosimetric Calculations. ICRP Publication 107*: International Commission on Radiological Protection.
Imanaka, T., Endo, S., Sugai, M., Ozawa, S., Shizuma, K., & Yamamoto, M. (2012). Early Radiation Survey of Iitate Village, Which Was Heavily Contaminated by the Fukushima Daiichi Accident, Conducted on 28 and 29 March 2011. *Health Physics, 102*(6), 680-686 610.1097/HP.1090b1013e31824cfe31818.
Inamori, Y. (2010). Manual of Measures against Lake Eutrophication. Retrieved from www.env.go.jp/earth/coop/coop/document/15-pdf/ma_lake_eutrophic_e.pdf
IRSN. (2011a). IRSN publishes assessment of radioactivity released by the Fukushima Daiichi Nuclear Power Plant (Fukushima I) through 22 March 2011. Retrieved

from http://www.irsn.fr/EN/news/Documents/IRSN_fukushima-radioactivity-released-assessment-EN.pdf
IRSN. (2011b). Synthèse des informations disponibles sur la contamination radioactive de
l'environnement terrestre japonais provoquée par l'accident de Fukushima Daiichi.
.
Ishikawa, Y., Kawaguchi, T., Ho-daka, T., & Haruyuki, H. (2014). Numerical simulation of radioactive cesium in Abukuma water system. *Journal of Japan Society on Water Environment, 37*(2), 29-43.
ISIS. (2011). *Fukushima Crisis: Unmonitored Releases Preliminary Assessment of Accident Sequences and Potential Atmospheric Radiation Releases*: The Institute for Science and International Security.
Ivlev, V. (1962). The method for calculation of food amount consumed by growing fish. *Biologiya vnutrennih vodoyomov Pribaltiki (Biology of surface water bodies of Baltic Region). USSR Academy of Sciences, Moscow*, 132-138.
Jacob, P., & Likhtarev, I. (1996). *Pathway analysis and dose distributions*: ECSC-EC-EAEC Brussels.
Jacob, P., Meckbach, R., & Müller, H. (1987). Reduction of external exposure from deposited Chernobyl activity by run-off, weathering, street cleaning and migration in the soil. *Radiation protection dosimetry, 21*(1-3), 51-57.
Jacob, P., Meckbach, R., Paretzke, H., Likhtarev, I., Los, I., Kovgan, L., et al. (1994). Attenuation effects on the kerma rates in air after cesium depositions on grasslands. *Radiation and Environmental Biophysics, 33*(3), 251-267.
Jacob, P., Rosenbaum, H., Petoussi-Henss, N., & Zankl, M. (1990). *Calculation of organ doses from environmental gamma rays using human phantoms and Monte Carlo methods, Part II: radionuclides distributed in the air or deposited on the ground*. Neuherberg, Germany: National Research Center for Environment and Health.
JAEA. (2012). Emergency Monitoring of Environmental Radiation and Atmospheric Radionuclides at Nuclear Science Research Institute, JAEA Following the Accident of Fukushima Daiichi Nuclear Power Plant. Retrieved from http://jolissrch-inter.tokai-sc.jaea.go.jp/pdfdata/JAEA-Data-Code-2012-010.pdf
Jinks, S. M. (1975). Investigation of the factors influencing radiocesium concentrations of fish inhabiting natural aquatic ecosystems.
JMA. (2012). Tables of Monthly Climate Statistics. Retrieved 17/7/2013, from http://www.data.jma.go.jp/obd/stats/data/en/smp/
Jonas, R. (1984). Deposition and attachment of air pollutants to vegetation and other atmosperic boundaries. *Jülich: Research Centre Jülich*.
JST. (2011). Great East Japan Earthquake and the seismic damage to the NPSs. Retrieved from http://www.meti.go.jp/
english/earthquake/nuclear/pdf/110515_1400_factsheet. pdf
Kabir, M. A., Dutta, D., & Hironaka, S. (2011). Process-based distributed modeling approach for analysis of sediment dynamics in a river basin. *Hydrology and Earth System Sciences, 15*(4), 1307-1321.
Kalos, M. H., & Whitlock, P. A. (2008). *Monte carlo methods*: John Wiley & Sons.
Kanai, Y. (2012). Monitoring of aerosols in Tsukuba after Fukushima Nuclear Power Plant incident in 2011. *Journal of Environmental Radioactivity, 111*(0), 33-37.
Kantei. (2011). Retrieved from http://www.kantei.go.jp/jp/topics/2011/pdf/06-kankyo.pdf

Katata, G., Ota, M., Terada, H., Chino, M., & Nagai, H. (2012). Atmospheric discharge and dispersion of radionuclides during the Fukushima Dai-ichi Nuclear Power Plant accident. Part I: Source term estimation and local-scale atmospheric dispersion in early phase of the accident. *Journal of Environmental Radioactivity, 109*, 103-113.

Katata, G., Terada, H., Nagai, H., & Chino, M. (2012). Numerical reconstruction of high dose rate zones due to the Fukushima Dai-ichi Nuclear Power Plant accident. *Journal of Environmental Radioactivity, 111*, 2-12.

Kato, H., Onda, Y., & Teramage, M. (2012). Depth distribution of 137Cs, 134Cs, and 131I in soil profile after Fukushima Dai-ichi Nuclear Power Plant Accident. *Journal of Environmental Radioactivity, 111*(0), 59-64.

Kawamura, H., Kobayashi, T., Furuno, A., In, T., Ishikawa, Y., Nakayama, T., et al. (2011). Preliminary numerical experiments on oceanic dispersion of 131I and 137Cs discharged into the ocean because of the Fukushima Daiichi nuclear power plant disaster. *Journal of Nuclear Science and Technology, 48*(11), 1349-1356.

KEK. (2011, 04/05/2011). Measurement result of airborne nuclide and air radiation level in Tsukuba area. from http://legacy.kek.jp/quake/radmonitor/GeMonitor-e.html

Kendall, C., & McDonnell, J. J. (1999). *Isotope tracers in catchment hydrology*: Elsevier.

Khalid, M., & Mann, S. (2007). *GRANIS: a model for the assessment of external photon irradiation from contaminated media of infinite lateral extent*: Health Protection Agency, Radiation Protection Division.

Kim, C.-K., Byun, J.-I., Chae, J.-S., Choi, H.-Y., Choi, S.-W., Kim, D.-J., et al. (2012). Radiological impact in Korea following the Fukushima nuclear accident. *Journal of Environmental Radioactivity, 111*(0), 70-82.

Kinoshita, N., Sueki, K., Sasa, K., Kitagawa, J.-i., Ikarashi, S., Nishimura, T., et al. (2011). Assessment of individual radionuclide distributions from the Fukushima nuclear accident covering central-east Japan. *Proceedings of the National Academy of Sciences*.

Kinouchi, T., Seino, A., & Takase, T. (2012). In-stream phosphate removal by suspended sediments transported from volcanic catchments. *Journal of Hydrology, 448*, 129-138.

Kirchner, G., Bossew, P., & De Cort, M. (2012). Radioactivity from Fukushima Dai-ichi in air over Europe; part 2: what can it tell us about the accident? *Journal of Environmental Radioactivity, 114*, 35-40.

Kocher, D. C., & Sjoreen, A. L. (1985). Dose-rate Conversion Factors for External Exposure to Photon Emitters in Soil. *Health Physics, 48*(2), 193-205.

Konoplev, A., Kaminski, S., Klemt, E., Konopleva, I., Miller, R., & Zibold, G. (2002). Comparative study of< sup> 137</sup> Cs partitioning between solid and liquid phases in Lakes Constance, Lugano and Vorsee. *Journal of Environmental Radioactivity, 58*(1), 1-11.

Konoplev, A. V., Kopylova, L. P., Bobovnikova, T. I., Bulgakov, A. A., & Siverina, A. A. (1992). Distribution of ^{90}Sr and ^{137}Cs within the system of bottom sediment-water of the reservoirs in the areas adjacent to the Chernobyl NPP. *Soviet Meteorology and Hydrology, 1*, 35-32.

Koulikov, A. O., & Meili, M. (2003). Modelling the dynamics of fish contamination by Chernobyl radiocaesium: an analytical solution based on potassium mass balance. *Journal of Environmental Radioactivity, 66*(3), 309-326.

Koulikov, A. O., & Ryabov, I. N. (1992). Specific cesium activity in freshwater fish and the size effect. *Science of The Total Environment, 112*(1), 125-142.
Kryshev, A., & Ryabov, I. (2000). A dynamic model of 137Cs accumulation by fish of different age classes. *Journal of Environmental Radioactivity, 50*(3), 221-233.
Kryshev, I. I., & Ryazantsev, E. P. (2000). Ecological security of Russian nuclear-energy complex ("IZDAT"Moscow). 384.
Kudelsky, A. V., Smith, J. T., Ovsiannikova, S. V., & Hilton, J. (1996). Mobility of Chernobyl-derived ^{137}Cs in a peatbog system within the catchment of the Pripyat River, Belarus. *Science of The Total Environment, 188*(2), 101-113.
L'Annunziata, M. F. (2012). *Handbook of radioactivity analysis*: Academic Press.
Leon, J. D., Jaffe, D. A., Kaspar, J., Knecht, A., Miller, M. L., Robertson, R. G. H., et al. (2011). Arrival time and magnitude of airborne fission products from the Fukushima, Japan, reactor incident as measured in Seattle, WA, USA. *Journal of Environmental Radioactivity, 102*(11), 1032-1038.
Livens, F., Fowler, D., & Horrill, A. (1992). Wet and dry deposition of< sup> 131</sup> I,< sup> 134</sup> Cs and< sup> 137</sup> Cs at an upland site in Northern England. *Journal of Environmental Radioactivity, 16*(3), 243-254.
Loaiza, P., Brudanin, V., Piquemal, F., Reyss, J. L., Stekl, I., Warot, G., et al. (2012). Air radioactivity levels following the Fukushima reactor accident measured at the Laboratoire Souterrain de Modane, France. *Journal of Environmental Radioactivity, 114*(0), 66-70.
Lujaniene, G., Bycenkiene, S., Sciglo, T., Povinec, P. P., Gera, M., Bartok, J., et al. (2011, 26-28 July 2011). *Radionuclides from the Fukushima accident in Europe - Modelling the air mass transport.* Paper presented at the Fuzzy Systems and Knowledge Discovery (FSKD), 2011 Eighth International Conference on.
MacMullin, S., Giovanetti, G. K., Green, M. P., Henning, R., Holmes, R., Vorren, K., et al. (2012). Measurement of airborne fission products in Chapel Hill, NC, USA from the Fukushima Dai-ichi reactor accident. *Journal of Environmental Radioactivity, 112*(0), 165-170.
Masson, O., Baeza, A., Bieringer, J., Brudecki, K., Bucci, S., Cappai, M., et al. (2011). Tracking of Airborne Radionuclides from the Damaged Fukushima Dai-Ichi Nuclear Reactors by European Networks. *Environmental Science & Technology, 45*(18), 7670-7677.
MEXT. (2011a). Readings of dust sampling (All Results for May 2011). Retrieved 10/07/11, 2011, from http://www.mext.go.jp/component/english/__icsFiles/afieldfile/2011/06/15/1306621_053110.pdf
MEXT. (2011b). Readings of environmental monitoring sample (All Results for May 2011). Retrieved 10/07/11, 2011, from http://www.mext.go.jp/component/english/__icsFiles/afieldfile/2011/06/15/1306623_053110.pdf
MEXT. (2011c). Readings of soil monitoring (All Results for May 2011). Retrieved 10/07/11, 2011, from http://www.mext.go.jp/component/english/__icsFiles/afieldfile/2011/06/15/1306622_053110.pdf
MEXT. (2011d). Results of Airborne Monitoring by the Ministry of Education, Culture, Sports, Science and Technology and the U.S. Department of Energy. Retrieved from http://www.mext.go.jp/component/english/__icsFiles/afieldfile/2011/05/10/1304797_0506.pdf

MEXT. (2014, 19/05/2014). Extension Site of Distribution Map of Radiation Dose, etc. Retrieved 30/05/2014, 2014, from http://ramap.jmc.or.jp/map/eng/map.html
MHLW. (2012). *New Standard limits for Radionuclides Radionuclides in Foods in Foods*. Retrieved from http://www.mhlw.go.jp/english/topics/2011eq/dl/new_standard.pdf.
Miller, K. M., Kuiper, J. L., & Helfer, I. K. (1990). < sup> 137</sup> Cs fallout depth distributions in forest versus field sites: Implications for external gamma dose rates. *Journal of Environmental Radioactivity, 12*(1), 23-47.
Momoshima, N., Sugihara, S., Ichikawa, R., & Yokoyama, H. (2012). Atmospheric radionuclides transported to Fukuoka, Japan remote from the Fukushima Dai-ichi nuclear power complex following the nuclear accident. *Journal of Environmental Radioactivity, 111*(0), 28-32.
Monte, L. (1995). Evaluation of radionuclide transfer functions from drainage basins of fresh water systems. *Journal of Environmental Radioactivity, 26*(1), 71-82.
Morgan, I., Tytler, P., & Bell, M. (1994). The use of a perfused, whole-body preparation to measure the branchial and intestinal influx of 137-caesium in the rainbow trout (Oncorhynchus mykiss). *Journal of fish biology, 45*(2), 247-256.
Morino, Y., Ohara, T., & Nishizawa, M. (2011). Atmospheric behavior, deposition, and budget of radioactive materials from the Fukushima Daiichi nuclear power plant in March 2011. *Geophysical research letters, 38*(7).
Mück, K., Pröhl, G., Likhtarev, I., Kovgan, L., Meckbach, R., & Golikov, V. (2002). A Consistent Radionuclide Vector After the Chernobyl Accident. *Health Physics, 82*(2), 141-156.
Mück, K., Pröhl, G., Meckbach, R., Likhtarev, I., Kovgan, L., & Golikov, S. (2000). *A new aproach to assess the doses to the population in the 30 km-zone after the Chernobyl accident.* Paper presented at the 10th Conf. IRPA, Hiroshima.
Nagao, S., Kanamori, M., Ochiai, S., Tomihara, S., Fukushi, K., & Yamamoto, M. (2013). Export of 134 Cs and 137 Cs in the Fukushima river systems at heavy rains by Typhoon Roke in September 2011. *Biogeosciences Discussions, 10*(2), 2767-2790.
Nagele, P. (2003). Misuse of standard error of the mean (SEM) when reporting variability of a sample. A critical evaluation of four anaesthesia journals. *British journal of anaesthesia, 90*(4), 514-516.
NIES. (2014). Lake Kasumigaura Database. Retrieved from http://db.cger.nies.go.jp/gem/moni-e/inter/GEMS/database/kasumi/index.html
NISA. (2011a). The 2011 off the Pacific coast of Tohoku Pacific Earthquake and the seismic damage to the NPPs. Retrieved from http://www.nuceng.ca/refer/japan/en20110406-1-1.pdf
NISA. (2011b). Evaluation of the amount of radioactive materials discharged to the air. Retrieved from http://www.kantei.go.jp/foreign/kan/topics/201106/pdf/attach_06.pdf
NISA. (2011c). Regarding the Results of Emergency Monitoring (March 11-15 Samples) in the Vicinity of Fukushima Dai-ichi and Dai-ni Nuclear Power Stations Retrieved from http://www.nsr.go.jp/archive/nisa/english/press/2011/06/en20110615-4.pdf
Nishihara, K., Iwamoto, H., & Suyama, K. (2012). Estimation of fuel compositions in Fukushima-Daiichi Nuclear Power Plant. Retrieved from http://jolissrch-inter.tokai-sc.jaea.go.jp/search/servlet/search?5036485&language=1

Nishihara, K., YAMAGISHI, I., YASUDA, K., ISHIMORI, K., TANAKA, K., KUNO, T., et al. (2012). Radionuclide release to stagnant water in Fukushima-1 nuclear power plant. *Tranacations of the Atomic Energy Society of Japan, 11*(1), 13-19.
Perrot, F., Hubert, P., Marquet, C., Pravikoff, M. S., Bourquin, P., Chiron, H., et al. (2012). Evidence of 131I and 134,137Cs activities in Bordeaux, France due to the Fukushima nuclear accident. *Journal of Environmental Radioactivity, 114*(0), 54-60.
Pham, M. K., Eriksson, M., Levy, I., Nies, H., Osvath, I., & Betti, M. (2012). Detection of Fukushima Daiichi nuclear power plant accident radioactive traces in Monaco. *Journal of Environmental Radioactivity, 114*(0), 131-137.
Piñero García, F., & Ferro García, M. A. (2012). Traces of fission products in southeast Spain after the Fukushima nuclear accident. *Journal of Environmental Radioactivity, 114*(0), 146-151.
Povinec, P. P., Hirose, K., & Aoyama, M. (2013). *Fukushima Accident: Radioactivity Impact on the Environment*: Elsevier.
Qiao, F., Wang, G., Zhao, W., Zhao, J., Dai, D., Song, Y., et al. (2011). Predicting the spread of nuclear radiation from the damaged Fukushima Nuclear Power Plant. *Chinese Science Bulletin, 56*(18), 1890-1896.
Rasmussen, J., Rowan, D., Lean, D., & Carey, J. (1990). Food chain structure in Ontario lakes determines PCB levels in lake trout (Salvelinus namaycush) and other pelagic fish. *Canadian Journal of Fisheries and Aquatic Sciences, 47*(10), 2030-2038.
Razali, N., & Wah, Y. (2011). Power comparisons of shapiro-wilk, kolmogorov-smirnov, lilliefors and anderson-darling tests. *Journal of Statistical Modeling and Analytics, 2*(1), 21-33.
RIKEN. (2011). Report on the γ-ray measurement after the accident of Fukushima I Nuclear Power Station. Retrieved 09/10/2011, 2011, from http://www.radiochem.org/kinkyu/49.pdf
Sakaguchi, A., Tanaka, K., Iwatani, H., Chiga, H., Fan, Q., Onda, Y., et al. (2014). Size distribution studies of ^{137}Cs in river water in the Abukuma Riverine system following the Fukushima Dai-ichi Nuclear Power Plant accident. *Journal of environmental radioactivity*.
Schoer, J. (1988). Investigation of transport-processes along the Elbe river using Chernobyl radionuclides as tracers. *Environmental Technology, 9*(4), 317-324.
Seco, J., & Verhaegen, F. (2013). *Monte Carlo techniques in radiation therapy*: CRC Press.
Sengupta, D. (2014). Recent Trends in Modelling of Environmental Contaminants.
Shapiro, S. S., & Wilk, M. B. (1965). An analysis of variance test for normality (complete samples). *Biometrika*, 591-611.
Sheskin, D. (2003). *Handbook of parametric and nonparametric statistical procedures*: crc Press.
Slade, D. H. (1968). *METEOROLOGY AND ATOMIC ENERGY, 1968*: Environmental Science Services Administration, Silver Spring, Md. Air Resources Labs.
Smith, F. B., & Clark, M. J. (1989). *The Transport and Deposition of Airborne Debris from the Chernobyl Nuclear Power Plant Accident with Special Emphasis on the Consequences to the United Kingdom*.
Smith, J. T., Belova, N. V., Bulgakov, A. A., Comans, R. N. J., Konoplev, A. V., Kudelsky, A. V., et al. (2005). THE "AQUASCOPE" SIMPLIFIED MODEL FOR PREDICTING 89,90Sr, 131I, and 134,137Cs IN SURFACE WATERS

AFTER A LARGE-SCALE RADIOACTIVE FALLOUT. *Health Physics, 89*(6).
Smith, J. T., & Beresford, N. A. (2005a). *Chernobyl – Catastrophe and Consequences*: Springer-Praxis.
Smith, J. T., & Beresford, N. A. (2005b). *Chernobyl – Catastrophe and Consequences*. Berlin: Springer-Praxis.
Smith, J. T., Clarke, R. T., & Saxén, R. (2000). Time-dependent behaviour of radiocaesium: A new method to compare the mobility of weapons test and Chernobyl derived fallout. *Journal of Environmental Radioactivity, 49*(1), 65-83.
Smith, J. T., Comans, R. N. J., Beresford, N. A., Wright, S. M., Howard, B. J., & Camplin, W. C. (2000). Pollution: Chernobyl's legacy in food and water. *Nature, 405*, 1.
Smith, J. T., Comans, R. N. J., & Elder, D. G. (1999). Radiocaesium removal from European lakes and reservoirs: key processes determined from 16 Chernobyl-contaminated lakes. *33*(18), 3762-3774.
Smith, J. T., Fesenko, S. V., Howard, B. J., Horrill, A. D., Sanzharova, N. I., Alexakhin, R. M., et al. (1998a). Temporal Change in Fallout 137Cs in Terrestrial and Aquatic Systems: A Whole Ecosystem Approach. *Environmental Science & Technology, 33*(1), 49-54.
Smith, J. T., Fesenko, S. V., Howard, B. J., Horrill, D. A., Sanzharova, N. I., Alexakhin, R. M., et al. (1998b). Temporal Change in Fallout 137Cs in Terrestrial and Aquatic Systems: A Whole Ecosystem Approach. *Environmental Science & Technology, 33*(1), 49-54.
Smith, J. T., Howard, D. C., Wright, S. M., Naylor, C., Brookes, A. M., Hilton, J., et al. (1998). Use of a satellite-derived land cover map to estimate transport of radiocaesium to surface waters. *209*(1), 1-15.
Smith, J. T., Konoplev, A. V., Bulgakov, A. A., Comans, R. N. J., Cross, M. A., Kaminski, S., et al. (2002). *AQUASCOPE Technical Deliverable. Simplified models for predicting 89Sr, 90Sr, 134Cs, 137Cs, 131I in water and fish of rivers, lakes and reservoirs*.
Smith, J. T., Konoplev, A. V., Bulgakov, A. A., Comans, R. N. J., Cross, M. A., Khristuk, B., et al. (2001). Dorset: Centre for Ecology and Hydrology; AQUASCOPE Final Report. *European Commission project IC15-CT98-0205, 114*.
Smith, J. T., Kudelsky, A. V., Ryabov, I. N., Daire, S. E., Boyer, L., Blust, R. J., et al. (2002). Uptake and elimination of radiocaesium in fish and the “size effect”. *Journal of Environmental Radioactivity, 62*(2), 145-164.
Smith, J. T., Kudelsky, A. V., Ryabov, I. N., & Hadderingh, R. H. (2000). Radiocaesium concentration factors of Chernobyl-contaminated fish: a study of the influence of potassium, and “blind” testing of a previously developed model. *Journal of Environmental Radioactivity, 48*(3), 359-369.
Smith, J. T., P. Leonard, D. R., Hilton, J., & Appleby, P. G. (1997). Towards a Generalized Model for the Primary and Secondary Contamination of Lakes by Chernobyl-Derived Radiocesium. *Health Physics, 72*(6).
Smith, J. T., Wright, S. M., Cross, M. A., Monte, L., Kudelsky, A. V., Saxén, R., et al. (2004). Global analysis of the riverine transport of 90Sr and 137Cs. *Environmental Science & Technology, 38*(3), 850-857.
Spezzano, P., & Giacomelli, R. (1991). Transport of< sup> 131</sup> I and< sup> 137</sup> Cs from air to cows' milk produced in North-Western Italian farms

following the Chernobyl accident. *Journal of Environmental Radioactivity, 13*(3), 235-250.
Stoehlker, U., Nikkinen, M., & Gheddou, A. (2011). Detection of radionuclides emitted during the Fukushima nuclear accident with the CTBT radionuclide network. *Monitoring Research Review: Ground-Based Nuclear Explosion Monitoring Technologies*, 715-724.
Stohl, A., Seibert, P., Wotawa, G., Arnold, D., Burkhart, J. F., Eckhardt, S., et al. (2011). Xenon-133 and caesium-137 releases into the atmosphere from the Fukushima Dai-ichi nuclear power plant: determination of the source term, atmospheric dispersion, and deposition. *Atmospheric Chemistry and Physics Discussions, 11*(10), 75.
Sundbom, M., Meili, M., Andersson, E., Östlund, M., & Broberg, A. (2003). Long-term dynamics of Chernobyl 137Cs in freshwater fish: quantifying the effect of body size and trophic level. *Journal of Applied Ecology, 40*(2), 228-240.
Tagami, K., Uchida, S., Uchihori, Y., Ishii, N., Kitamura, H., & Shirakawa, Y. (2011). Specific activity and activity ratios of radionuclides in soil collected about 20km from the Fukushima Daiichi Nuclear Power Plant: Radionuclide release to the south and southwest. *Science of the Total Environment, 409*(22), 4885-4888.
Takemura, T., Nakamura, H., Takigawa, M., Kondo, H., Satomura, T., Miyasaka, T., et al. (2011). A numerical simulation of global transport of atmospheric particles emitted from the Fukushima Daiichi Nuclear Power Plant. *Sola, 7*(0), 101-104.
Tanaka, K., Takahashi, Y., Sakaguchi, A., Umeo, M., Hayakawa, S., Tanida, H., et al. (2012). Vertical profiles of iodine-131 and cesium-137 in soils in Fukushima prefecture related to the Fukushima Daiichi Nuclear Power Station accident. *Geochemical Journal, 46*(1), 73-76.
Thomann, R. V. (1989). Bioaccumulation model of organic chemical distribution in aquatic food chains. *Environmental Science & Technology, 23*(6), 699-707.
Tsumune, D., Tsubono, T., Aoyama, M., & Hirose, K. (2012). Distribution of oceanic< sup> 137</sup> Cs from the Fukushima Dai-ichi Nuclear Power Plant simulated numerically by a regional ocean model. *Journal of Environmental Radioactivity, 111*, 100-108.
UCB. (2011). Air Sampling Results. Retrieved 04/09/11, 2011, from http://www.nuc.berkeley.edu/UCBAirSampling/AirSamplingResults
Ueda, S., Hasegawa, H., Kakiuchi, H., Akata, N., Ohtsuka, Y., & Hisamatsu, S. (2013). Fluvial discharges of radiocaesium from watersheds contaminated by the Fukushima Dai-ichi Nuclear Power Plant accident, Japan. *Journal of environmental radioactivity, 118*, 96-104.
UNEP. (2008). *Water Quality for Ecosystem and Human Health* (2nd Edition ed.): the United Nations Environment Programme Global Environment Monitoring System (GEMS)/Water Programme.
UNSCEAR. (2000a). ANNEX J: Exposures and effects of the Chernobyl accident. *Sources and Effects of Ionizing Radiation: The United Nations Scientific Committee on the Effects of Atomic Radiation UNSCEAR*, 451-566.
UNSCEAR. (2000b). *Source and effects of ionizing radiation.* New York: United Nations.
UNSCEAR. (2013). *Scientific Annex A: SOURCES, EFFECTS AND RISKS OF IONIZING RADIATION*.
Ursula, W., Von Gunten, H. R., & Krähenbühl, U. (1987). The impact of the Chernobyl accident on a river/groundwater aquifer. *Radiochimca Acta, 41*(4), 191-198.

Valcke, E., & Cremers, A. (1994). Sorption-desorption dynamics of radiocaesium in organic matter soils. *Science of The Total Environment, 157*(0), 275-283.

Voitsekhovitch, O. V., Borzilov, V. A., & Konoplev, A. V. (1991). *Hydrological aspects of Radionuclide Migration in Water Bodies Following the Chernobyl Accident*. Paper presented at the Proceeding of Seminar on Comparative Assessment of the Environmental Impact of Radionuclides Released during Three Major Nuclear Accident: Kyshtym, Windscale, Chernobyl.

Wang, W.-X., & Wong, R. S. (2003). Bioaccumulation kinetics and exposure pathways of inorganic mercury and methylmercury in a marine fish, the sweetlips Plectorhinchus gibbosus. *Marine Ecology Progress Series, 261*, 257-268.

WHO. (2012). Preliminary dose estimation from the nuclear accident after the 2011 Great East Japan Earthquake and Tsunami.

Winberg, G. (1956). Rate of metabolism and food requirements of fishes. *Fish. Res. Bd Can., Trans. Ser., 194*, 1-202.

Yablokov, A. V., Nesterenko, V. B., Nesterenko, A. V., & Sherman-Nevinger, J. D. (2010). *Chernobyl: Consequences of the Catastrophe for People and the Environment* (Vol. 39): Wiley. com.

Yamamoto, M., Takada, T., Nagao, S., Koike, T., Shimada, K., Hoshi, M., et al. (2012). An early survey of the radioactive contamination of soil due to the Fukushima Dai-ichi Nuclear Power Plant accident, with emphasis on plutonium analysis. *Geochemical Journal, 46*(4), 341.

Yasutaka, T., Kawabe, Y., Kurosawa, A., & Komai, T. (2014). Monitoring dissolved radioactive cesium in Abukuma River in Fukushima Prefecture.

Yoo, S. J., Jang, H.-K., Lee, J.-K., Noh, S., & Cho, G. (2013). External dose-rate conversion factors of radionuclides for air submersion, ground surface contamination and water immersion based on the new ICRP dosimetric setting. *Radiation protection dosimetry*, nct045.

Zhao, X., Wang, W.-X., Yu, K., & Lam, P. K. (2001). Biomagnification of radiocesium in a marine piscivorous fish. *Marine Ecology Progress Series, 222*, 227-237.

Appendices

Appendix A Measurement data from air and soil samples

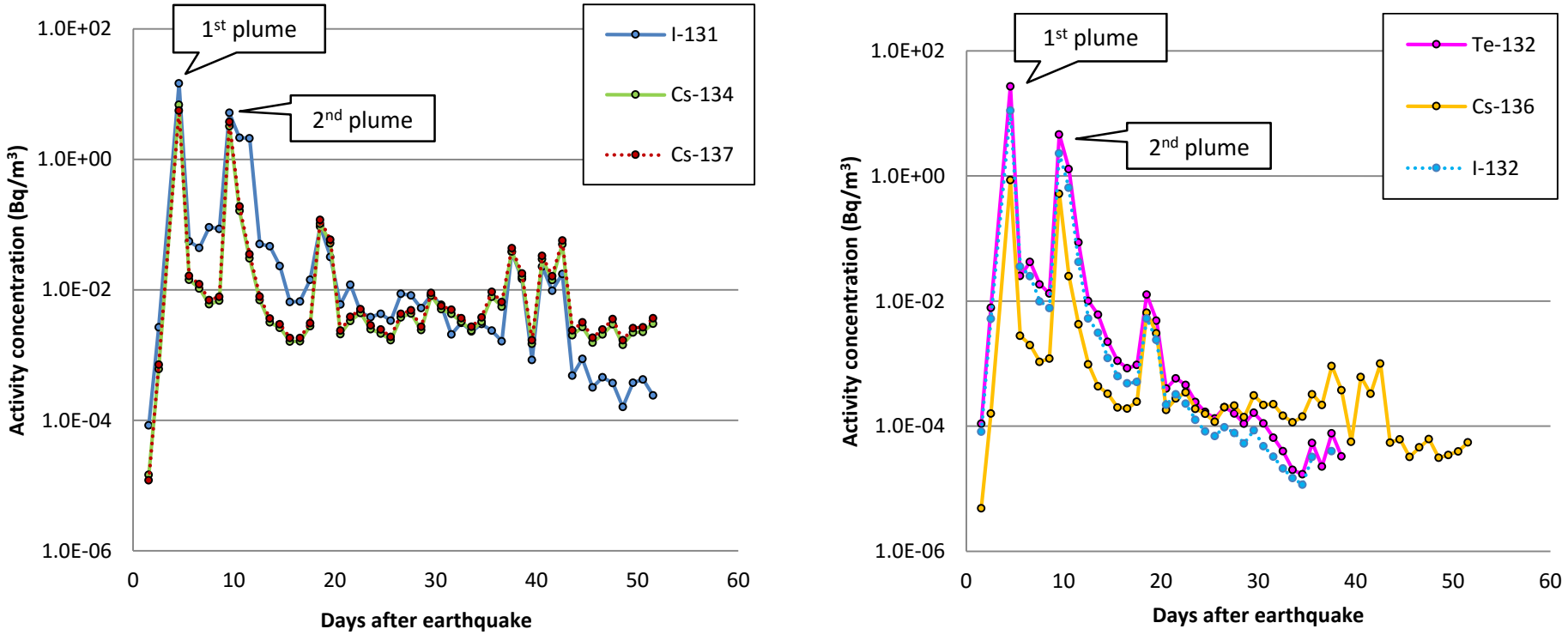

Figure A-1 The monitoring of contaminated concentration in air of key radionuclides in particulate form at Takasaki, Gunma prefecture located approximately 220 km in southwest direction of Fukushima I NPSs (Stoehlker, et al., 2011).

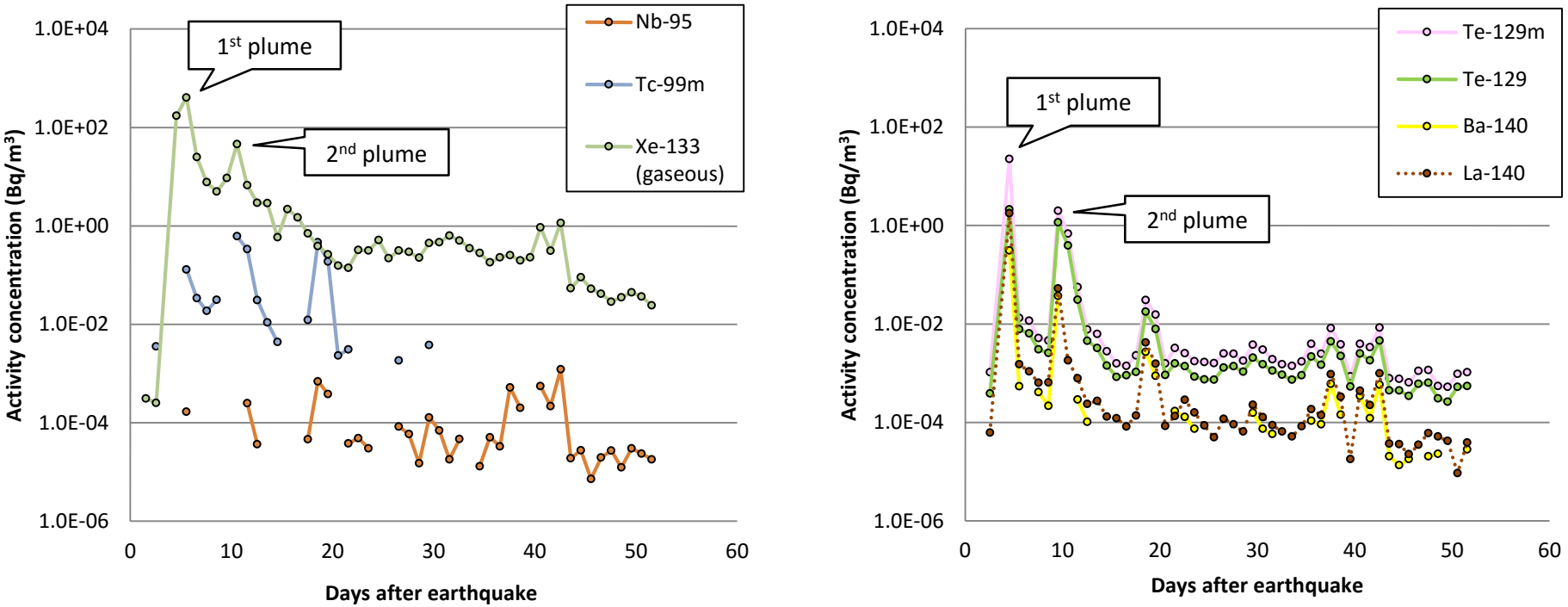

Figure A-2 The monitoring of contaminated concentration in air of other radionuclides at Takasaki, Gunma prefecture located approximately 220 km in southwest direction of Fukushima I NPSs, the form of radionuclies were particulate, except the noble gas ^{133}Xe was a gaseous form and the data including background around 1×10^{-3} Bq/m^3 (Stoehlker, et al., 2011).

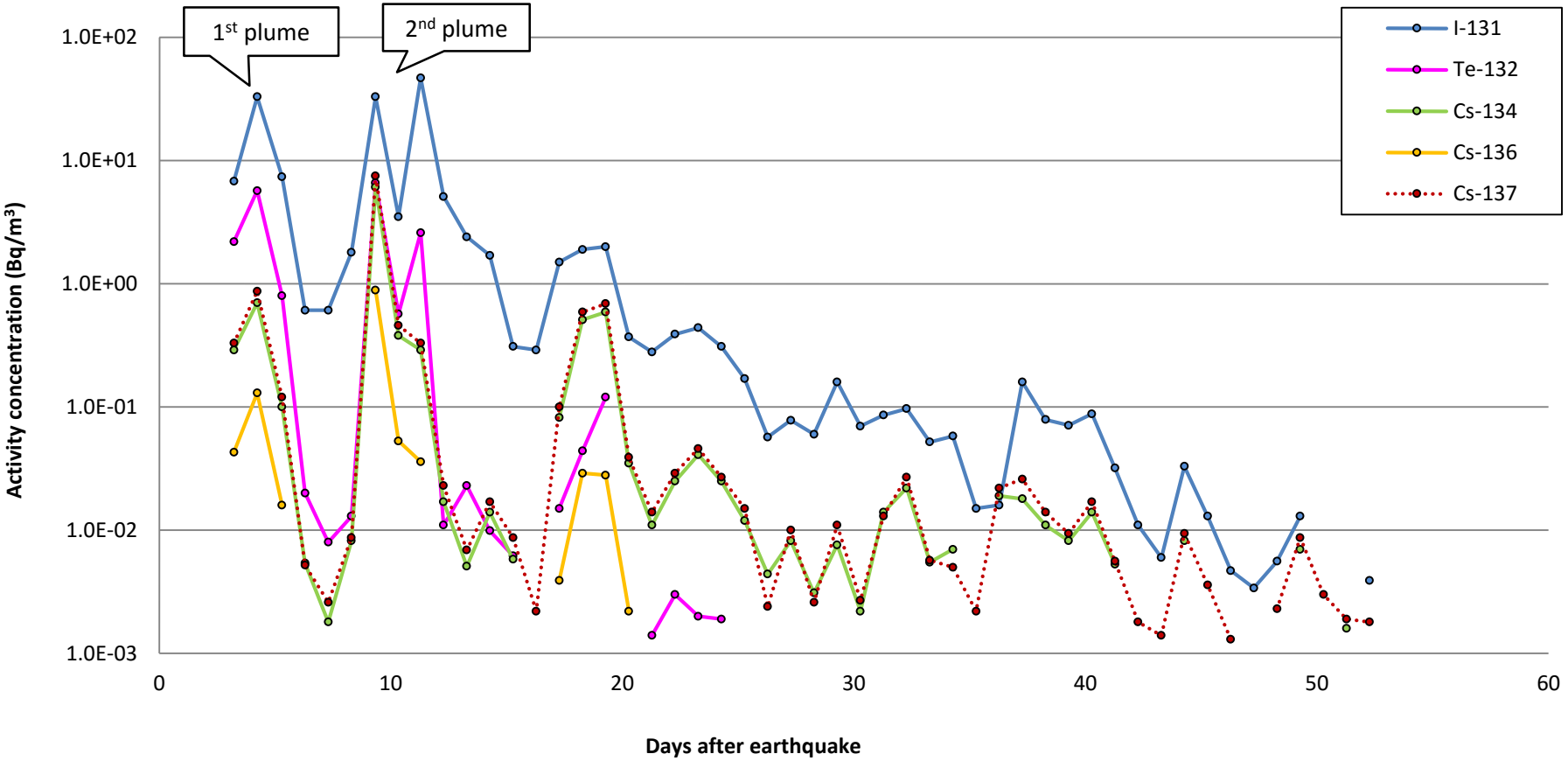

Figure A-3 The particulate concentration in air at Japan Chemical Analysis Center (JCAC), Chiba prefecture located about 220 km in southwest direction of Fukushima I NPSs (Amano, et al., 2012).

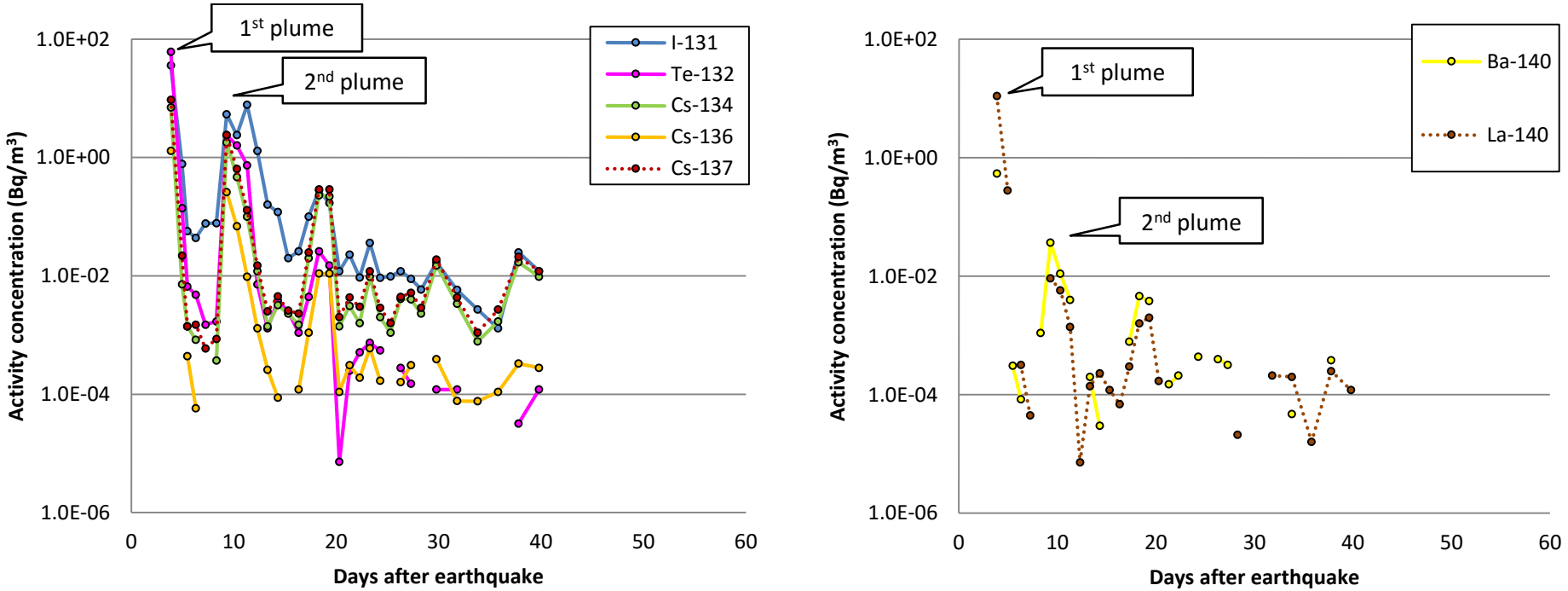

Figure A-4 The particulate concentration in air at Waku Institute, Saitama prefecture located about 220 km in southwest direction of Fukushima I NPSs (RIKEN, 2011).

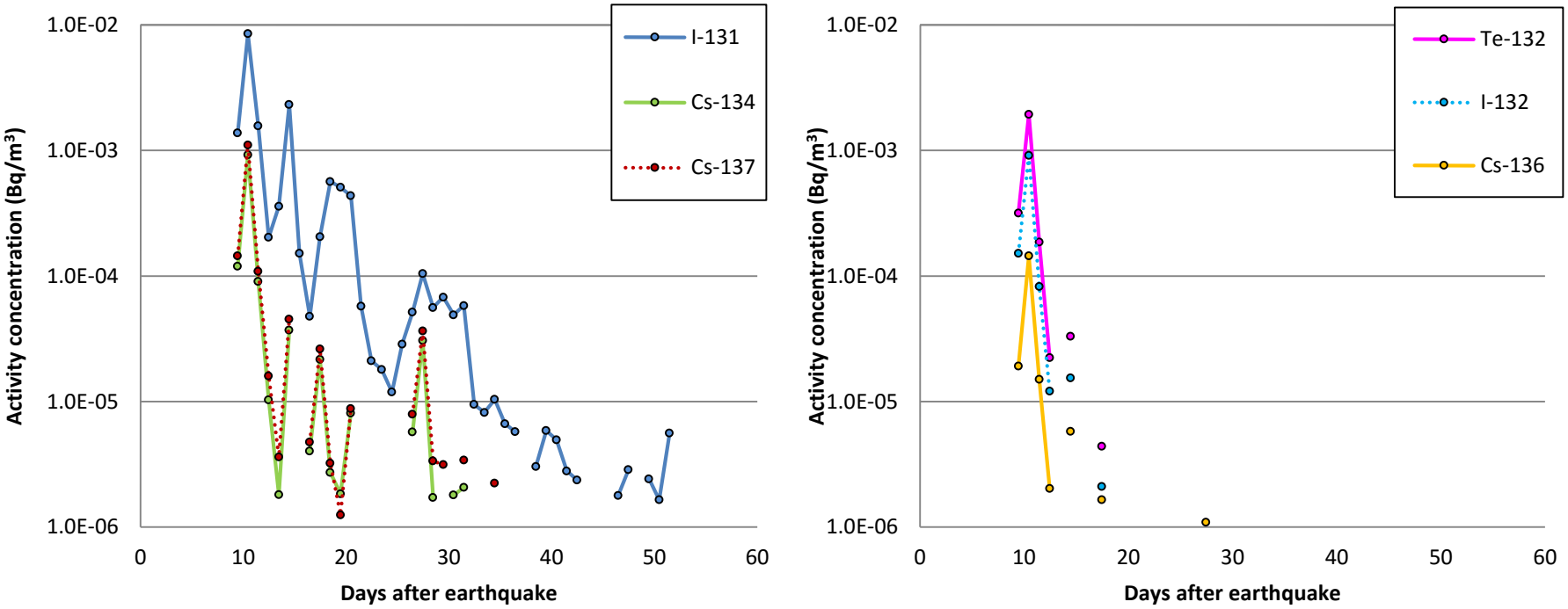

Figure A-5 The particulate concentration in air at Guam, the United States of America located about 2,700 km from Fukushima I NPSs (Biegalski, et al., 2011).

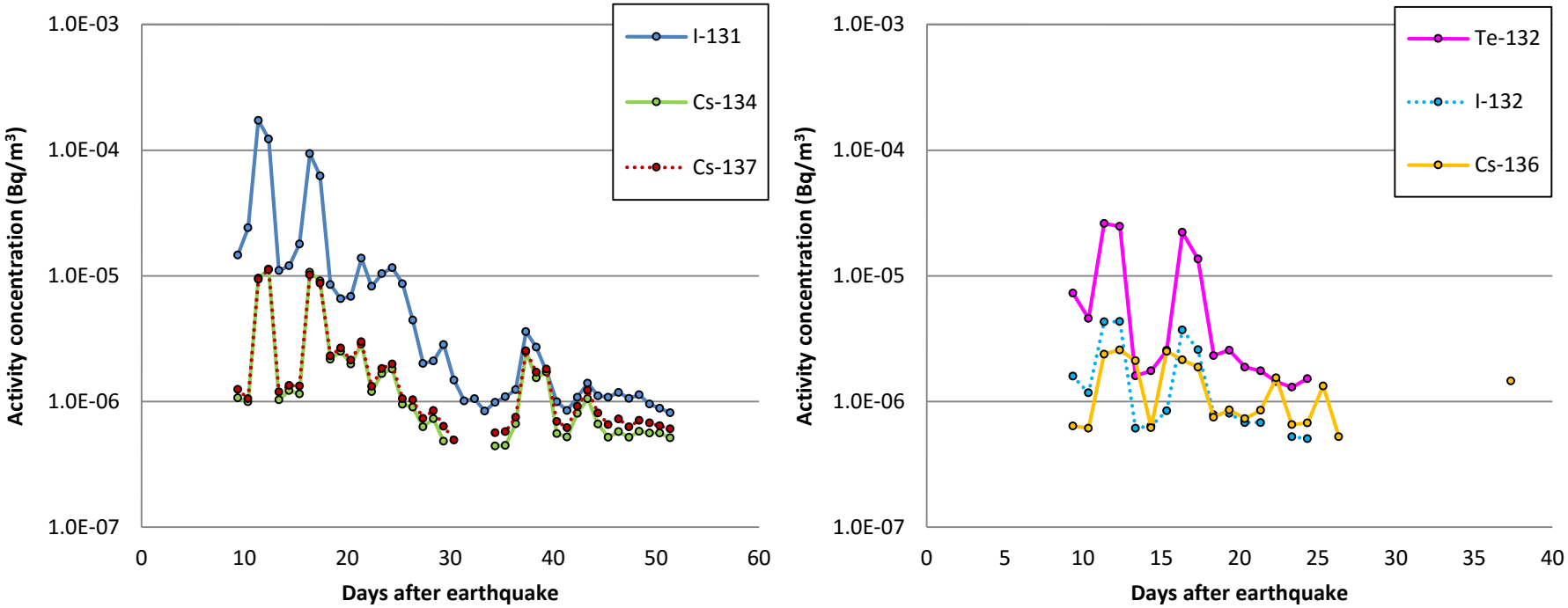

Figure A-6 The particulate concentration in air at Midway Islands, the United States of America located about 4,000 km from Fukushima I NPSs (Biegalski, et al., 2011).

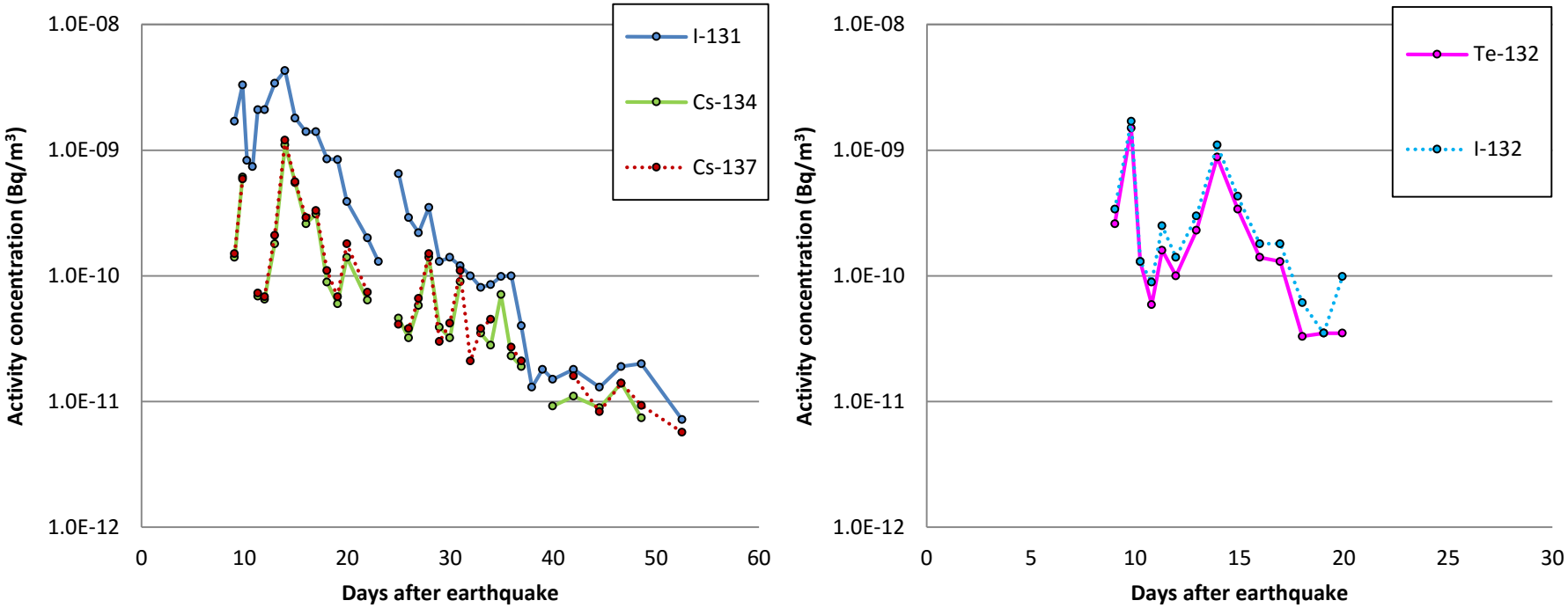

Figure A-7 The particulate concentration in air at University of California, the United States of America located about 8,000 km from Fukushima I NPSs (UCB, 2011).

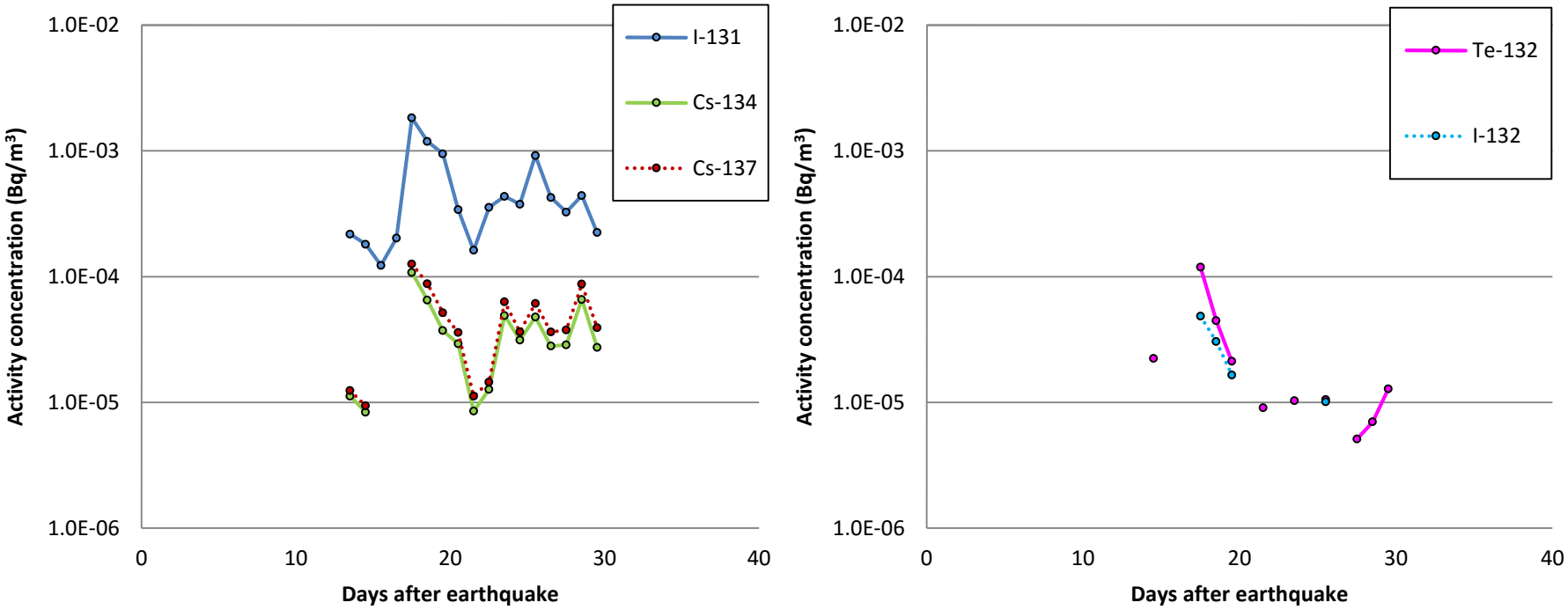

Figure A-8 The particulate concentration in air at Offenbach, Germany located about 21,000 km from Fukushima I NPSs (Bossew, et al., 2012).

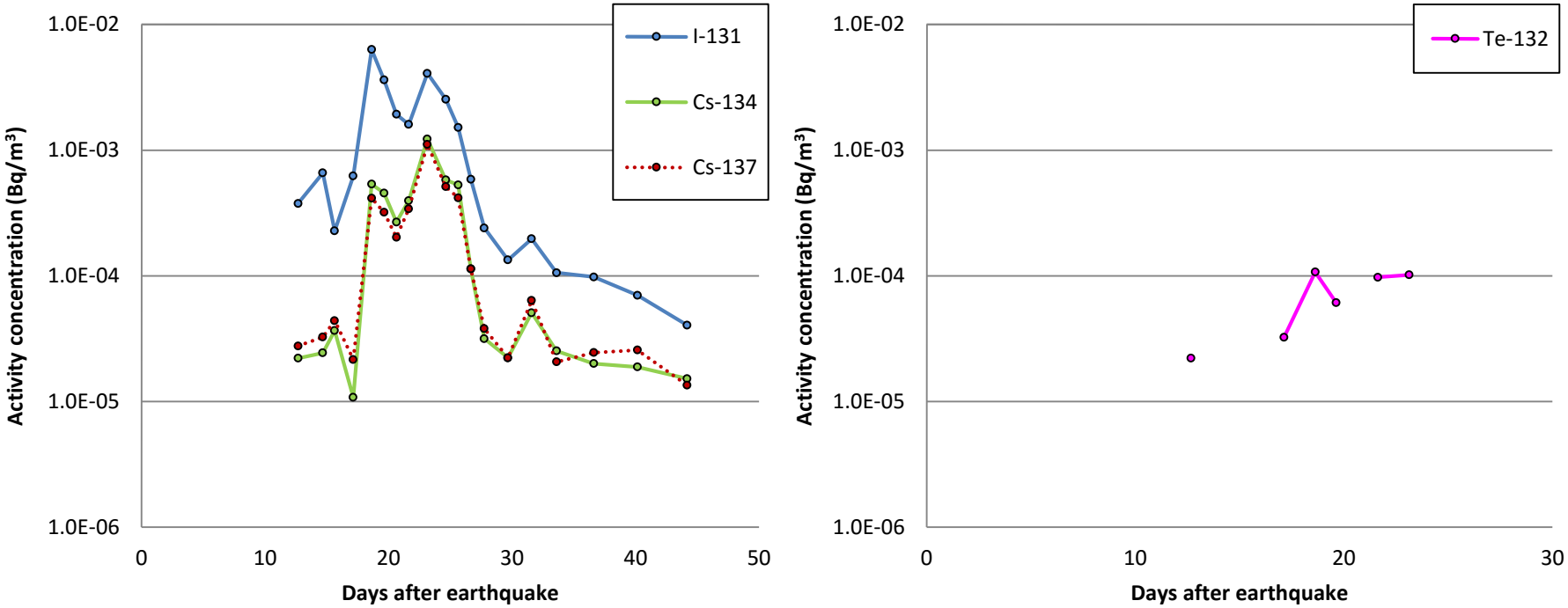

Figure A-9 The particulate concentration in air at Ukrainian Institute of Hydrometeorology, Ukraine located about 22,600 km from Fukushima I NPSs (measured data from this research).

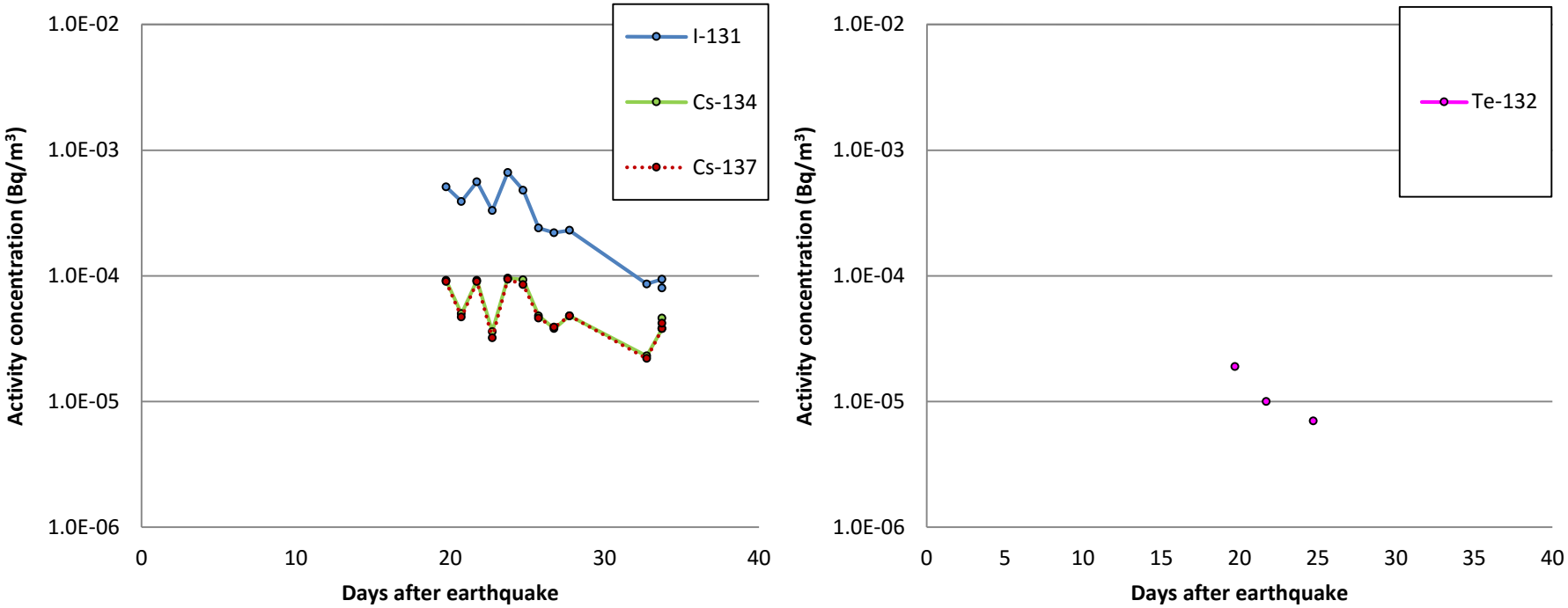

Figure A-10 The particulate concentration in air at The Health Protection Agency, Oxon, United Kingdom located about 22,000 km from Fukushima I NPSs (HPA, 2011).

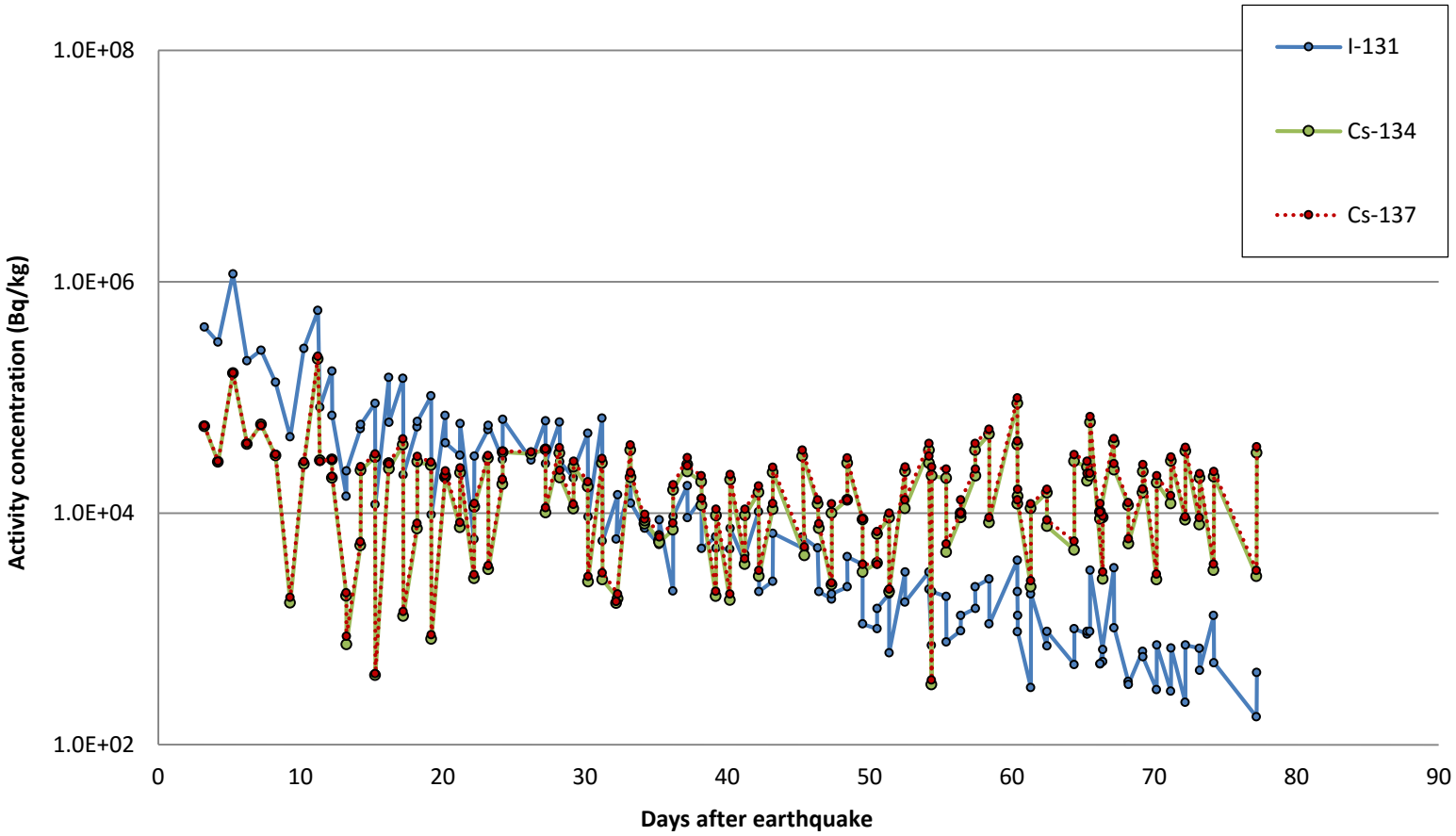

Figure A-11 the deposited concentration at Takami town, Haramachi ward, Minami Soma city located 24 km in north direction of Fukushima I NPSs (MEXT, 2011b).

Table A-1 Average deposited density of ^{134}Cs and ^{137}Cs at near-zone of Fukushima I NPSs (S. Endo, et al., 2012; Imanaka, et al., 2012; MEXT, 2011b, 2011c).

Code	Direction	Distance (km)	Site	Deposited density (Bq/m^2)			
				^{134}Cs		^{137}Cs	
				Mean	S.E.	Mean	S.E.
103	N	20	Mamegarauchi, Taka, Haramachi ward, Minami Soma city	1.6E+05	4.7E+04	1.9E+05	5.6E+04
ms-8	N	20	Kanezawa, Haramachi ward, Minami Soma city	1.1E+05	-	1.2E+05	-
ms-10	N	21	Taka, Haramachi ward, Minami Soma city	2.0E+05	-	2.2E+05	-
2-4	N	24	Takami town, Haramachi ward, Minami Soma city	1.5E+05	1.5E+04	1.7E+05	1.6E+04
2-4	N	24	Takami town, Haramachi ward, Minami Soma city	1.6E+05	1.2E+04	2.0E+05	1.4E+04
ms-9	N	24	Takami town, Haramachi ward, Minami Soma city	3.1E+05	-	3.4E+05	-
3-10	N	32	Kashima ward, Minami Soma city	2.4E+05	1.4E+04	2.9E+05	1.8E+04
3-11	N	32	Kashima ward, Minami Soma city	1.2E+05	1.1E+04	1.4E+05	1.2E+04
39	N	41	Kaminamiki, Yamakami, Soma city	2.5E+05	1.2E+04	3.0E+05	1.5E+04
3-9	N	42	Nakano, Soma city	1.7E+05	4.3E+04	1.9E+05	4.5E+04
3-16	N	45	Yamakami, Soma city	2.3E+05	-	2.6E+05	-
2-10	N	50	Shinchi town, Soma county	1.5E+04	-	1.6E+04	-

Table A-1 (continued) Average deposited density of ^{134}Cs and ^{137}Cs at near-zone of Fukushima I NPSs (S. Endo, et al., 2012; Imanaka, et al., 2012; MEXT, 2011b, 2011c).

Code	Direction	Distance (km)	Site	Deposited density (Bq/m^2)			
				^{134}Cs		^{137}Cs	
				Mean	S.E.	Mean	S.E.
n11	NW	20	Hirusone, Namie town, Futaba county	1.2E+07	-	1.5E+07	-
ms-6	NW	21	Baba, Haramashi ward, Minami Soma city	3.4E+06	-	3.8E+06	-
K8	NW	21	Noyuki, Katsurao, Katsurao village , Futaba county	8.3E+06	-	9.8E+06	-
K9	NW	21	Ozasa, Ochiai, Katsurao village, Futaba county	4.2E+05	-	5.0E+05	-
ms-7	NW	22	Baba, Haramashi ward, Minami Soma city	7.6E+05	-	8.4E+05	-
n5	NW	22	Kurabeishi, Hirusone, Namie town, Futaba county	2.5E+07	-	3.1E+07	-
107	NW	23	Shimonakanouchi, Baba, Haramachi ward, Minami Soma city	5.8E+05	3.7E+04	7.2E+05	4.6E+04
K7	NW	23	Kashiwabara, Katsurao, Katsurao village, Futaba county	5.6E+06	-	6.9E+06	-
n7	NW	23	Shimohiyada, Minamitsushima, Namie town, Futaba county	7.4E+06	-	9.0E+06	-
83	NW	24	Akougi Kunugidaira, Namie town	1.7E+07	1.5E+06	2.0E+07	1.9E+06
K10	NW	24	Ozasa, Ochiai, Katsurao village, Futaba county	2.9E+05	-	3.5E+05	-
ms-5	NW	25	Takanokura, Haramachi ward, Minami Soma city	8.3E+05	-	8.9E+05	-
n6	NW	25	Shimohiyada, Minamitsushima, Namie town, Futaba county	3.4E+06	-	4.2E+06	-
ed2	NW	26	Namie Tsushima	4.6E+05	-	5.1E+05	-

Table A-1 (continued) Average deposited density of ^{134}Cs and ^{137}Cs at near-zone of Fukushima I NPSs (S. Endo, et al., 2012; Imanaka, et al., 2012; MEXT, 2011b, 2011c).

Code	Direction	Distance (km)	Site	Deposited density (Bq/m^2)			
				^{134}Cs		^{137}Cs	
				Mean	S.E.	Mean	S.E.
ed11	NW	26	Minami Soma	3.6E+04	-	4.1E+04	-
n4	NW	26	Shiobite, Akougi, Namie town, Futaba county	7.1E+06	-	9.0E+06	-
ms-4	NW	27	Takanokura, Haramachi ward, Minami Soma city	1.3E+05	-	1.4E+05	-
K6	NW	27	Hiroyaji, Katsurao, Katsurao village, Futaba county	3.3E+06	-	4.1E+06	-
n8	NW	27	Kotsuka, Shimotsushima, Namie town, Futaba county	3.1E+05	-	3.6E+05	-
K3	NW	28	Higashidaira, Katsurao, Katsurao village, Futaba county	2.0E+05	-	2.6E+05	-
n2	NW	28	Teshichiro, Akougi, Namie town, Futaba county	6.5E+06	-	8.3E+06	-
n3	NW	28	Shiraoi, Akougi, Namie town, Futaba county	4.7E+06	-	5.8E+06	-
79	NW	29	Kayabuka, Shimotsushima, Namie town, Futaba county	4.1E+06	2.3E+05	5.1E+06	2.9E+05
ms-11	NW	29	Ohara, Haramachi ward, Minami Soma city	6.7E+05	-	7.4E+05	-
ed3	NW	29	Iitate Warabidaira	1.7E+06	-	1.8E+06	-
ed4	NW	29	Namie Akogi	1.9E+06	-	2.2E+06	-
i25	NW	29	Warabidaira, Iitate village, Soma county	4.8E+06	-	6.0E+06	-
108	NW	30	Daihata, Ohara, Haramachi ward, Minami Soma city	6.5E+05	3.0E+04	7.9E+05	3.8E+04

Table A-1 (continued) Average deposited density of ^{134}Cs and ^{137}Cs at near-zone of Fukushima I NPSs (S. Endo, et al., 2012; Imanaka, et al., 2012; MEXT, 2011b, 2011c).

Code	Direction	Distance (km)	Site	Deposited density (Bq/m^2)			
				^{134}Cs		^{137}Cs	
				Mean	S.E.	Mean	S.E.
3-12	NW	30	Tsushima, Namie town	3.1E+06	5.2E+05	3.4E+06	5.6E+05
3-2	NW	30	Tsushima, Namie town	1.6E+06	1.4E+05	1.9E+06	1.8E+05
K2	NW	30	Nakadaira, Katsurao, Katsurao village, Futaba county	9.8E+05	-	1.2E+06	-
3-13	NW	31	Akougi, Namie town	4.8E+06	3.8E+05	5.3E+06	4.3E+05
i26	NW	31	Nagadoro, Iitate village, Soma county	5.6E+06	-	7.1E+06	-
n1	NW	31	Teshichiro, Akougi, Namie town, Futaba county	5.1E+06	-	6.5E+06	-
ms-12	NW	32	Jisabara Maeta, Kashima ward, Minami Soma city	9.5E+04	-	1.1E+05	-
K1	NW	32	Kazakoshi, Katsurao, Katsurao village, Futaba county	8.3E+05	-	1.1E+06	-
3-1	NW	33	Nagadoro, Iitate village, Soma county	4.5E+06	2.9E+05	5.1E+06	3.4E+05
kw-6	NW	33	Hirokuboyama, Yamakiya, Kawamta town, Date county	2.7E+06	-	3.0E+06	-
ms-1	NW	33	Ohara, Haramachi ward, Minami Soma city	4.5E+05	-	4.8E+05	-
n10	NW	33	Tatenosawa, Hatsuke, Namie town, Futaba county	4.1E+05	-	5.0E+05	-
kw-5	NW	34	Isshoutatsuyama, Yamakiya, Kawamta town, Date county	9.3E+05	-	9.7E+05	-
i28	NW	34	Hiso, Iitate village, Soma county	6.8E+06	-	8.3E+06	-

Table A-1 (continued) Average deposited density of ^{134}Cs and ^{137}Cs at near-zone of Fukushima I NPSs (S. Endo, et al., 2012; Imanaka, et al., 2012; MEXT, 2011b, 2011c).

Code	Direction	Distance (km)	Site	Deposited density (Bq/m^2)			
				^{134}Cs		^{137}Cs	
				Mean	S.E.	Mean	S.E.
2-1	NW	36	Yagisawa, Iitate village, Soma county	1.5E+06	1.6E+05	1.6E+06	1.7E+05
ms-3	NW	36	Kamitochikubo, Kashima ward, Minami Soma city	7.8E+05	-	9.1E+05	-
ni-2	NW	36	Shimomagariyama, Tazawa, Nihonmatsu city	2.4E+05	-	2.5E+05	-
i18	NW	36	Yagisawa, Iitate village, Soma county	1.1E+06	-	1.3E+06	-
i20	NW	36	Hashiba, Sekisawa, Iitate village, Soma county	1.7E+06	-	2.0E+06	-
kw-4	NW	37	Boyoshi, Yamakiya, Kawamta town, Date county	5.3E+05	-	5.6E+05	-
i32	NW	37	Iitoi , Iitate village, Soma county	1.9E+06	-	2.3E+06	-
i17	NW	38	Kusano, Iitate village, Soma county	2.2E+05	-	2.6E+05	-
i19	NW	38	Sekisawa, Iitate village, Soma county	1.2E+06	1.3E+05	1.5E+06	1.7E+05
i29	NW	38	Kamihiso, Hiso, Iitate village, Soma county	1.1E+06	-	1.4E+06	-
i31	NW	38	Iitoi , Iitate village, Soma county	1.1E+06	-	1.4E+06	-
im4	NW	39	Village office, Iitate village, Soma county	5.8E+05	-	6.7E+05	-
i1	NW	39	Itamizawa, Iitate village, Soma county	1.9E+06	-	2.4E+06	-
i2	NW	39	Itamizawa, Iitate village, Soma county	3.5E+05	2.0E+05	4.3E+05	2.5E+05

Table A-1 (continued) Average deposited density of ^{134}Cs and ^{137}Cs at near-zone of Fukushima I NPSs (S. Endo, et al., 2012; Imanaka, et al., 2012; MEXT, 2011b, 2011c).

Code	Direction	Distance (km)	Site	Deposited density (Bq/m^2)			
				^{134}Cs		^{137}Cs	
				Mean	S.E.	Mean	S.E.
1-2	NW	40	Yamakiya, Kawamata town	1.2E+06	1.5E+05	1.4E+06	1.9E+05
3-14	NW	40	Yamakiya, Kawamata town	1.0E+06	6.9E+04	1.2E+06	8.2E+04
kw-3	NW	40	Shimonagahashi, Yamakiya, Kawamta town, Date county	5.1E+05	-	5.5E+05	-
i14	NW	40	Kusano, Iitate village, Soma county	2.6E+06	-	3.2E+06	-
i15	NW	40	Ookura, Iitate village, Soma county	3.9E+05	-	4.7E+05	-
i16	NW	40	Ookura, Iitate village, Soma county	7.5E+04	-	9.0E+04	-
i30	NW	40	Ohi, Iitoi, Iitate village, Soma county	2.1E+06	-	2.7E+06	-
i6	NW	41	Fukaya, Iitate village, Soma county	2.6E+06	-	3.3E+06	-
kw-1	NW	42	Ushirozawa, Kotsunagi, Kawamata town, Date county	2.8E+05	-	3.0E+05	-
kw-10	NW	42	Kotsunagi, Kawamata town, Date county	4.9E+05	-	5.4E+05	-
kw-2	NW	42	Kotsunagi Kamihagane, Kawamata town, Date county	2.2E+05	-	2.2E+05	-
i7	NW	42	Usuishi, Iitate village, Soma county	1.2E+06	3.4E+05	1.4E+06	4.1E+05
im1	NW	42	Usuishi, Iitate village, Soma county	8.0E+05	-	9.6E+05	-
im5	NW	43	Magata, Iitate village, Soma county	1.9E+06	-	2.2E+06	-

Table A-1 (continued) Average deposited density of ^{134}Cs and ^{137}Cs at near-zone of Fukushima I NPSs (S. Endo, et al., 2012; Imanaka, et al., 2012; MEXT, 2011b, 2011c).

Code	Direction	Distance (km)	Site	Deposited density (Bq/m^2)			
				^{134}Cs		^{137}Cs	
				Mean	S.E.	Mean	S.E.
kw-8	NW	43	Kotsunagi, Kawamata town, Date county	3.9E+05	-	4.3E+05	-
kw-9	NW	43	Kotsunagi, Kawamata town, Date county	4.7E+05	-	5.2E+05	-
i12	NW	43	Sasu, Iitate village, Soma county	4.7E+05	-	5.9E+05	-
i13	NW	43	Maeta, Iitate village, Soma county	1.7E+04	-	2.1E+04	-
i8	NW	44	Nimaibashi, Iitate village, Soma county	8.5E+05	1.4E+05	1.0E+06	1.8E+05
2-2	NW	45	Kawamata town, Date county	3.6E+05	2.6E+04	3.8E+05	2.7E+04
kw-7	NW	45	Kotsunagi, Kawamata town, Date county	3.0E+05	-	3.1E+05	-
i9	NW	45	Maeta, Iitate village, Soma county	1.4E+06	-	1.7E+06	-
im2	NW	46	Sasu, Iitate village, Soma county	6.5E+05	-	7.7E+05	-
1-1	NW	46	Sasu Nameri, Iitate village	4.7E+05	1.4E+05	5.3E+05	1.6E+05
i10	NW	46	Sasu, Iitate village, Soma county	2.1E+06	-	2.6E+06	-
i11	NW	46	Sasu, Iitate village, Soma county	1.7E+06	-	2.1E+06	-
im3	NW	46	Yamstsumi shrine, Iitate village, Soma county	5.1E+05	-	5.9E+05	-
3-5	NW	47	Kawamata town	5.0E+04	-	5.8E+04	-

Table A-1 (continued) Average deposited density of ^{134}Cs and ^{137}Cs at near-zone of Fukushima I NPSs (S. Endo, et al., 2012; Imanaka, et al., 2012; MEXT, 2011b, 2011c).

Code	Direction	Distance (km)	Site	Deposited density (Bq/m^2)			
				^{134}Cs		^{137}Cs	
				Mean	S.E.	Mean	S.E.
37	NW	48	Hojizawa, Ishida, Ryozen town, Date city	1.2E+06	3.8E+04	1.4E+06	1.5E+05
102	NW	50	Tsukidate town, Date city	3.5E+05	4.1E+04	4.1E+05	5.1E+04
2-8	NW	50	Tsukidate town, Date city	2.7E+05	1.9E+04	3.0E+05	2.2E+04
101	NW	55	Oishi, Ryozen town, Date city	2.2E+05	3.8E+04	2.7E+05	4.4E+04
2	NW	56	Onami Takinoiri, Fukushima city	7.1E+05	1.8E+05	8.4E+05	2.1E+05
1	NW	62	Sugitsuma town, Fukushima city	7.7E+05	5.3E+04	9.4E+05	6.4E+04
ed10	NW	62	Niihama Park, Fukushima city	3.4E+05	-	3.9E+05	-
ed1	W	4.4	Futaba Yamada	9.8E+06	-	1.0E+07	-
105	W	21	Furumichi, Miyakoji town, Tamura city	1.4E+05	1.4E+04	1.7E+05	1.7E+04
K11	W	21	Ohanachi, Ochiai, Katsurao village, Futaba county	4.3E+05	-	5.3E+05	-
ed6	W	22	Miyakoji Junior High School	7.2E+04	-	8.2E+04	-
104	W	25	Ochiai, Oaza, Katsurao Village, Futaba County	6.4E+05	3.9E+04	7.8E+05	4.8E+04
110	W	25	Furumichi, Miyakoji town, Tamura city	3.4E+05	-	4.1E+05	-
113	W	25	Iwaisawa, Miyakoji town, Tamura city	1.1E+06	3.2E+05	1.3E+06	3.9E+05

Table A-1 (continued) Average deposited density of ^{134}Cs and ^{137}Cs at near-zone of Fukushima I NPSs (S. Endo, et al., 2012; Imanaka, et al., 2012; MEXT, 2011b, 2011c).

Code	Direction	Distance (km)	Site	Deposited density (Bq/m^2)			
				^{134}Cs		^{137}Cs	
				Mean	S.E.	Mean	S.E.
181	W	25	Kamikawauchi, Kawauchi village, Futaba county	7.3E+04	-	9.0E+04	-
ed8	W	25	Katsurao Junior High School	2.2E+05	-	2.6E+05	-
K4	W	28	Nakanouchi, Nogawa, Katsurao village, Futaba county	1.2E+06	-	1.4E+06	-
K5	W	29	Yuden, Nogawa, Katsurao village, Futaba county	3.9E+05	-	5.0E+05	-
3-3	W	32	Yamane, Tokiwa town, Tamura city	1.9E+05	1.2E+04	2.2E+05	1.5E+04
3-6	W	32	Kaminogawa, Katsurao village	6.3E+05	5.1E+04	7.5E+05	6.0E+04
2-7	W	34	Yamakiya, Kawamata town, Date county	9.9E+05	7.8E+04	1.1E+06	8.5E+04
ed5	W	35	Tokiwa Junior High School	2.6E+04	-	3.0E+04	-
13	W	37	Yakata, Nishimuki, Tokiwa town, Tamura city	7.5E+04	-	9.0E+04	-
2-3	W	41	Funehiki, Funehiki town, Tamura city	5.3E+04	4.9E+03	5.9E+04	5.2E+03
3-4	W	43	Ota, Nihonmatsu city	5.4E+05	-	6.5E+05	-
2-9	W	45	Kanairo, Nihonmatsu city	8.1E+05	6.1E+04	8.9E+05	6.6E+04
ed9	W	48	Miharu Town	7.3E+03	-	8.3E+04	-
4-3	W	60	Otama village, Adachi county	1.8E+05	2.4E+04	2.0E+05	2.6E+04

Table A-1 (continued) Average deposited density of ^{134}Cs and ^{137}Cs at near-zone of Fukushima I NPSs (S. Endo, et al., 2012; Imanaka, et al., 2012; MEXT, 2011b, 2011c).

Code	Direction	Distance (km)	Site	Deposited density (Bq/m^2)			
				^{134}Cs		^{137}Cs	
				Mean	S.E.	Mean	S.E.
ed12	W	60	Ohshima-Higashi Park, Kouriyama	1.1E+04	-	1.2E+04	-
76	SW	22	Hayawata, Kamikawauchi, Kawauchi village, Futaba county	9.3E+04	4.6E+03	1.1E+05	5.5E+03
ed7	SW	23	Kawauchi Elementary School	4.7E+04	-	5.5E+04	-
114	SW	26	Kamiogawa, Ogawa town, Iwaki city	3.9E+05	-	4.7E+05	-
111	SW	28	Kamikawauchi, Kawauchi village, Futaba county	8.3E+04	-	9.8E+04	-
ed15	SW	31	Kittoya Mountain, Miharu Town	4.4E+04	-	5.2E+04	-
2-5	SW	39	Ononiimachi, Ono town, Tamura county	5.7E+04	6.1E+03	6.0E+04	6.2E+03
4-2	SW	60	Hachiman town, Sukagawa city	8.9E+04	8.4E+03	9.6E+04	8.5E+03
4-4	SW	70	Izumizaki village, Shirakawa county	1.4E+05	2.0E+04	1.5E+05	2.2E+04
4-1	SW	80	Shirakawa city	1.9E+05	2.6E+04	2.1E+05	2.8E+04
4-5	SW	80	Saigou village, Nishishirakawa county	2.2E+05	2.6E+04	2.5E+05	2.9E+04
106	S	30	Hokita, Shiraiwa, Kawamae town, Iwaki city	7.0E+04	4.4E+03	8.8E+04	6.8E+03
3-15	S	23	Shimokitaba, Hirono town, Futaba county	8.0E+04	2.7E+04	9.3E+04	3.2E+04
3-7	S	23	Shimokitaba, Hirono town	1.4E+05	1.0E+04	1.7E+05	1.2E+04

Table A-1 (continued) Average deposited density of ^{134}Cs and ^{137}Cs at near-zone of Fukushima I NPSs (S. Endo, et al., 2012; Imanaka, et al., 2012; MEXT, 2011b, 2011c).

Code	Direction	Distance (km)	Site	Deposited density (Bq/m^2)			
				^{134}Cs		^{137}Cs	
				Mean	S.E.	Mean	S.E.
ed14	S	29	Suetsugi Station	2.1E+04	-	2.5E+04	-
72	S	31	Hisanohama, Hisanohama town, Iwaki city	1.2E+05	1.2E+04	1.5E+05	1.6E+04
38	S	34	Hokita, Shiraiwa, Yotsukura town, Iwaki city	1.7E+05	4.0E+04	2.0E+05	4.4E+04
73	S	35	Takahagi, Ogawa town, Iwaki city	7.0E+04	8.4E+03	8.3E+04	9.2E+03
74	S	36	Takahagi, Ogawa town, Iwaki city	3.0E+04	5.5E+03	3.5E+04	6.2E+03
84	S	39	Saiso, Miwa town, Iwaki city	4.6E+04	3.3E+03	5.4E+04	3.8E+03
2-6	S	43	Umemoto, Taira Aza, Iwaki city	6.4E+04	5.2E+03	7.2E+04	5.9E+03
75	S	43	Uchigoumimaya town, Iwaki city	7.2E+04	1.1E+04	8.3E+04	1.2E+04
ed13	S	44	Chuo Interchange, Iwaki	1.6E+03	-	2.3E+03	-

Appendix B Corrected ratios in Air

Table B-1 Average of corrected ratios of particulate ^{134}Cs and particulate ^{131}I to particulate ^{137}Cs in air at near-zone of Fukushima I NPSs (MEXT, 2011a).

Code	Direction	Distance (km)	Sites	Corrected ratio in air			
				^{134}Cs:^{137}Cs		^{131}I:^{137}Cs	
				Mean	±S.E.	Mean	±S.E.
2-4	N	24	Takami town, Haramachi ward, Minami Soma city	0.76	0.02	6.83	1.09
2-4	N	24	Takami town, Haramachi ward, Minami Soma city	1.10	0.07	63.00	15.19
2-10	N	50	Shinchi town, Soma county	-	-	134.85	-
1-7	N	32	Kashima ward, Minami Soma city	0.86	0.03	27.47	19.93
1-8	N	42	Nakano, Soma city	0.86	-	25.74	-
3-1	NW	33	Nagadoro, Iitate village, Soma county	0.90	0.15	19.25	11.53
2-1	NW	36	Yagisawa, Iitate village, Soma county	-	-	22.78	2.15
2-1	NW	36	Yagisawa, Iitate village, Soma county	1.05	0.10	20.50	10.45
2-2	NW	45	Kawamata town, Date county	1.19	0.16	12.19	6.61
1-1	NW	46	Sasu Nameri, Iitate village, Soma county	-	-	9.26	-
2-8	NW	50	Tsukidate town, Date city	1.34	-	14.07	-
1	NW	62	Sugitsuma town, Fukushima city	1.02	0.11	26.68	11.62
2-7	W	34	Yamakiya, Kawamata town, Date county	0.87	-	7.10	0.46

Table B-1 (continued) Average corrected ratios of particulate ^{134}Cs and particulate ^{131}I to particulate ^{137}Cs in air at near-zone of Fukushima I NPSs (MEXT, 2011a).

Code	Direction	Distance (km)	Sites	Corrected ratio in air			
				^{134}Cs:^{137}Cs		^{131}I:^{137}Cs	
				Mean	±S.E.	Mean	±S.E.
2-7	W	34	Yamakiya, Kawamata town, Date county	1.17	0.16	37.63	28.14
2-9	W	45	Kanairo, Nihonmatsu city	1.40	-	13.87	3.47
2-3	W	41	Funehiki, Funehiki town, Tamura city	1.00	0.15	36.96	24.22
4-3	W	60	Ootama village, Adachi county	-	-	10.32	-
76	SW	22	Kamikawauchi, Kawauchi village, Futaba county	0.85	0.06	18.91	3.21
2-5	SW	39	Ononiimachi, Ono town, Tamura county	1.41	-	29.76	-
4-5	SW	80	Nishigou village, Nishishirakawa county	-	-	25.30	-
2-6	S	43	Umemoto, Taira Aza, Iwaki city	1.03	0.09	47.74	17.59
1-5	S	23	Shimokitaba, Hirono town, Futaba county	0.78	0.08	89.42	22.78

*Note that all ratios are corrected back to 11/03/2011 14:46.

Table B-2 Average of corrected ratios of particulate ^{131}I, ^{132}Te, and $^{134,136}Cs$ to particulate ^{137}Cs in air around the World.

Site	Average corrected ratio* in air of								References
	^{131}I: ^{137}Cs		^{132}Te: ^{137}Cs		^{134}Cs: ^{137}Cs		^{136}Cs: ^{137}Cs		
	Mean	S.E.	Mean	S.E.	Mean	S.E.	Mean	S.E.	
Air samples in Japan (80-2,000 km)									
JAEA, Tokai-mura, Ibaraki, Japan	36.55	6.97	20.13	6.49	1.36	0.18	0.21	0.02	JAEA (2012)
Waku Institute, Saitama, Japan	57.34	12.40	16.70	2.81	0.74	0.03	0.17	0.02	RIKEN (2011)
Takasaki, Gunma, Japan	16.90	3.18	15.09	1.69	0.90	0.01	0.22	0.01	Stoehlker et al. (2011)
JCAC, Chiba, Japan	195.00	28.02	18.02	4.59	0.91	0.03	0.16	0.01	Amano et al. (2012)
Kyushu University, Fukuoka, Japan	48.61	11.10	-	-	1.05	0.06	-	-	Momoshima et al. (2012)
Air samples in Pacific Ocean and US (2,000-12,000 km)									
University of Washington, Washington, US	29.47	5.95	19.05	4.13	0.78	0.05	-	-	Leon et al. (2011)
University of California, California, US	48.77	6.25	15.71	1.38	0.92	0.03	-	-	UCB (2011)
University of North Carolina, North Carolina, US	53.43	7.16	-	-	-		-	-	MacMullin et al. (2012)
Saipan, CNMI, US	56.4	-	23.59	-	1.39	-	-		EPA (2011)
Guam, US	23.87	8.59	19.77	4.20	0.80	0.07	-		EPA (2011)
Dutch Harbor, Alaska, US	15.95	5.13	22.88	3.52	0.88	0.11	-	-	EPA (2011)
Oahu, Hawaii, US	11.90	2.65	6.96	0.56	0.81	0.01	-		EPA (2011)
Juneau, Alaska, US	32.12	5.54	9.74	1.20	0.84	0.04	-	-	EPA (2011)
Boise, Idaho, US	27.74	6.87	8.10	2.06	0.79	0.05	0.22	-	EPA (2011)
Anaheim, California, US	54.86	22.91	21.98	4.73	0.83	0.05	-	-	EPA (2011)
San Bernardino, California, US	19.69	2.62	15.65	1.74	0.71	0.10	-	-	EPA (2011)
Upi Guam, US	290.81	128.82	16.47	1.98	0.81	0.06	0.21	0.02	Biegalski et al. (2011)
Wake Island, US	67.65	17.65	17.55	1.89	0.80	0.01	0.21	0.01	Biegalski et al. (2011)
Midway Islands, US	72.71	10.05	15.06	1.34	0.87	0.02	0.22	0.01	Biegalski et al. (2011)

Table B-3 (continued) Average of corrected ratios of particulate ^{131}I, ^{132}Te, and $^{134,136}Cs$ to particulate ^{137}Cs in air around the World.

Site	Average corrected ratio* in air of								References
	^{131}I: ^{137}Cs		^{132}Te: ^{137}Cs		^{134}Cs: ^{137}Cs		^{136}Cs: ^{137}Cs		
	Mean	**S.E.**	**Mean**	**S.E.**	**Mean**	**S.E.**	**Mean**	**S.E.**	
Sand Point, Alaska, US	36.04	3.28	21.02	1.04	0.78	0.01	0.22	0.01	Biegalski et al. (2011)
Salchaket, Alaska, US	68.34	7.80	24.11	1.19	0.87	0.01	0.22	0.01	Biegalski et al. (2011)
Oahu, Hawaii, US	118.99	17.21	14.69	1.72	0.83	0.02	0.22	0.01	Biegalski et al. (2011)
Sacramento, California, US	93.72	12.52	22.94	1.83	0.92	0.02	0.22	0.01	Biegalski et al. (2011)
Ashland, Kansas, US	158.77	16.64	22.55	2.63	0.93	0.04	0.23	0.02	Biegalski et al. (2011)
Charlottesville, Virginia, US	89.47	14.13	16.19	1.67	0.88	0.02	0.22	0.01	Biegalski et al. (2011)
Melbourne, Florida, US	59.59	5.59	17.61	0.97	0.82	0.02	0.23	0.01	Biegalski et al. (2011)
Air samples in EU (>12,000 km)									
Granada, Spain	53.52	-	-	-	1.13	-	-	-	Pinero et al. (2012)
Bordeaux, France	103.86	30.22	-	-	0.97	0.07	-	-	Perrot et al. (2012)
the French Alps, France	224.86	45.64	17.53	5.02	1.31	0.15	-	-	Loaiza et al. (2012)
the IAEA-NAEL building, Monaco	91.87	13.42	-	-	0.80	0.05	-	-	Pham et al. (2012)
Saclay, France	90.65	11.59	50.84	17.69	0.86	0.11	-	-	Bossew et al. (2012)
Orsay, France	87.48	36.28	13.90	2.19	0.87	0.04	-	-	Bossew et al. (2012)
Offenbach, Germany	86.10	8.68	58.81	15.81	0.81	0.02	-	-	Bossew et al. (2012)
Schauinsland, Germany	118.72	22.03	16.34	1.50	0.79	0.02	-	-	Bossew et al. (2012)
Braunschweig, Germany	69.90	8.03	35.87	9.99	0.95	0.03	0.24	0.01	Bossew et al. (2012)
Wroclaw, Poland	52.30	9.37	15.42	5.05	0.74	0.04	0.17	0.01	Bossew et al. (2012)
Katowice, Poland	50.20	8.26	8.81	0.66	0.63	0.03	-	-	Bossew et al. (2012)

Table B-4 (continued) Average of corrected ratios of particulate ^{131}I, ^{132}Te, and $^{134,136}Cs$ to particulate ^{137}Cs in air around the World.

Site	Average corrected ratio* in air of								References
	^{131}I: ^{137}Cs		^{132}Te: ^{137}Cs		^{134}Cs: ^{137}Cs		^{136}Cs: ^{137}Cs		
	Mean	**S.E.**	**Mean**	**S.E.**	**Mean**	**S.E.**	**Mean**	**S.E.**	
Lodz, Poland	50.24	7.53	11.34	3.03	0.83	0.02	0.12	0.01	Bossew et al. (2012)
Krakow, Poland	67.16	8.74	21.45	6.72	0.83	0.05	0.15	0.03	Bossew et al. (2012)
Warszawa, Poland	66.46	12.09	20.03	1.94	0.83	0.03	0.16	0.02	Bossew et al. (2012)
Byalistok, Poland	33.47	6.23	15.70	1.67	0.80	0.08	0.22	-	Bossew et al. (2012)
Sanok, Poland	62.17	5.69	21.04	2.59	0.79	0.06	0.27	0.05	Bossew et al. (2012)
Reykjavik, Iceland	50.86	3.70	13.69	2.75	0.85	0.10	0.19	-	Bossew et al. (2012)
Gdynia, Poland	63.64	9.33	18.01	2.51	0.99	0.05	-	-	Bossew et al. (2012)
Sacavém, Lisbon, Portugal	68.81	9.58	26.80	4.30	1.11	0.07	-	-	Carvalho et al. (2012)
HPA, Oxon, UK	50.06	3.45	14.81	1.47	1.07	0.01	-	-	HPA (2011)
Vilnius, Lithuania	88.92	9.55	13.44	0.78	1.06	0.01	0.24	0.01	Gudelis et al. (2012)
Kiev, Ukraine	65.40	7.40	24.27	7.87	1.03	0.06	-	-	This research

* Note that all ratios are corrected back to 11/03/2011 14:46

Table B-3 Average percentage of gaseous ^{131}I and corrected ratio of particulate and gaseous of ^{131}I to particulate ^{137}Cs, in air sampling around the World.

Site	Average percentage of $^{131}I(g)$	Average corrected ratio* in air of				References
		$^{131}I(p)/^{137}Cs$ (p)		$^{131}I(g)/^{137}Cs$ (p)		
		Mean	S.E.	Mean	S.E.	
KEK, Tsukuba, Ibaraki, Japan	28.59	20.85	13.01	8.17	4.92	KEK (2011)
JAEA, Tokai-mura, Ibaraki, Japan	74.67	36.55	6.97	233.79	59.44	JAEA (2012)
Saipan, CNMI, US	80.50	56.4	-	371.7		EPA (2011)
Guam, US	80.81	23.87	8.59	96.93	21.69	EPA (2011)
Dutch Harbor, Alaska, US	81.93	16.95	6.50	147.14	102.74	EPA (2011)
Oahu, Hawaii, US	82.31	11.90	2.65	77.98	35.41	EPA (2011)
Juneau, Alaska, US	77.57	32.12	5.56	110.13	10.99	EPA (2011)
Boise, Idaho, US	68.63	27.74	6.87	93.62	47.89	EPA (2011)
Anaheim, California, US	88.86	54.86	22.91	473.57	238.82	EPA (2011)
San Bernardino, California, US	84.67	47.87	52.19	138.05	52.87	EPA (2011)
Cherbourg, France	82.11	-	-	-	-	Bossew et al. (2012)
Saclay, France	79.17	91.22	28.82	505.92	434.44	Bossew et al. (2012)
Orsay, France	75.50	-	-	-	-	Bossew et al. (2012)
Guipavas, France	93.10	-	-	-	-	Bossew et al. (2012)
Brest, France	85.02	-	-	-	-	Bossew et al. (2012)
Mol, Belgium	80.55	-	-	-	-	Bossew et al. (2012)
Helsinki, Finland	81.73	-	-	-	-	Bossew et al. (2012)
Fessenheim, France	88.00	-	-	-	-	Bossew et al. (2012)
Le Péage-de-Roussillon, France	73.84	-	-	-	-	Bossew et al. (2012)
Romans-sur-Isère, France	78.86	-	-	-	-	Bossew et al. (2012)
Valence, France	90.10	-	-	-	-	Bossew et al. (2012)
Grenoble, France	84.69	-	-	-	-	Bossew et al. (2012)
Montélimar, France	82.70	-	-	-	-	Bossew et al. (2012)
Santander, Spain	66.15	-	-	-	-	Bossew et al. (2012)

Table B-5 (continued) Average percentage of gaseous ^{131}I and corrected ratio of particulate and gaseous of ^{131}I to particulate ^{137}Cs, in air sampling around the World.

Site	Average percentage of $^{131}I(g)$	Average corrected ratio* in air of				References
		$^{131}I(p)/^{137}Cs$ (p)		$^{131}I(g)/^{137}Cs$ (p)		
		Mean	S.E.	Mean	S.E.	
Bilbao, Spain	85.06	-	-	-	-	Bossew et al. (2012)
Avignon, France	81.64	-	-	-	-	Bossew et al. (2012)
Oviedo, Spain	86.05	-	-	-	-	Bossew et al. (2012)
Cadarache, France	93.40	91.22	28.82	853.10	11.66	Bossew et al. (2012)
Milan, Italy	65.48	-	-	-	-	Bossew et al. (2012)
Puigcerdà, Spain	88.63	-	-	-	-	Bossew et al. (2012)
Piacenza, Italy	77.60	-	-	-	-	Bossew et al. (2012)
Gerona, Spain	91.64	-	-	-	-	Bossew et al. (2012)
Ascó, Spain	76.43	-	-	-	-	Bossew et al. (2012)
Linz, France	70.60	99.87	20.00	240.37	40.00	Bossew et al. (2012)
Vandellòs, Spain	81.48	-	-	-	-	Bossew et al. (2012)
Calafat, Spain	92.54	-	-	-	-	Bossew et al. (2012)
Madrid, Spain	90.29	-	-	-	-	Bossew et al. (2012)
Ljubljana, Slovenia	49.20	-	-	-	-	Bossew et al. (2012)
Vienna, Austria	73.28	72.92	23.67	164.45	70.18	Bossew et al. (2012)
Valencia, Spain	73.28	-	-	-	-	Bossew et al. (2012)
Cáceres, Spain	77.03	-	-	-	-	Bossew et al. (2012)
Badajoz, Spain	83.46	-	-	-	-	Bossew et al. (2012)
Granada, Spain	74.09	-	-	-	-	Bossew et al. (2012)
San Cristóbal de La Laguna, Spain	84.86	-	-	-	-	Bossew et al. (2012)

*Note that all ratios are corrected back to 11/03/2011 14:46

Appendix C Corrected ratio in Soil

Table C-1 Average corrected ratios of ^{131}I, ^{132}Te, and $^{134,136}Cs$ to ^{137}Cs. in the near-zone of Fukushima I NPSs.

Code	Direction	Distance (km)	Average corrected ratio* in soil of											
			^{131}I:^{137}Cs			^{134}Cs:^{137}Cs			^{132}Te:^{137}Cs			^{136}Cs:^{137}Cs		
			Mean	S.E.	S.D.	Mean	S.E.	S.D.	Mean	S.E.	S.D.	Mean	S.E.	S.D.
2-4	N	24	3.0E+01	1.7E+00	1.4E+01	9.5E-01	6.4E-03	5.4E-02	-	-	-	2.9E-01	-	-
2-10	N	50	4.3E+01	-	-	9.6E-01	-	-	-	-	-	-	-	-
ms-8	N	20	1.4E+01	-	-	9.7E-01	-	-	-	-	-	-	-	-
ms-9	N	24	1.7E+01	-	-	9.7E-01	-	-	-	-	-	-	-	-
ms-10	N	21	2.6E+01	-	-	9.4E-01	-	-	-	-	-	-	-	-
2-4	N	24	2.8E+01	2.1E+00	1.4E+01	8.6E-01	5.5E-03	3.6E-02	-	-	-	2.7E-01	3.3E-02	6.5E-02
3-9	N	42	4.6E+01	3.2E+01	6.4E+01	8.7E-01	2.5E-02	5.1E-02	-	-	-	-	-	-
3-10	N	32	1.2E+01	4.6E-01	2.5E+00	8.6E-01	4.3E-03	2.3E-02	-	-	-	-	-	-
3-11	N	32	2.4E+01	1.1E+00	7.3E+00	8.7E-01	2.3E-02	1.6E-01	-	-	-	2.2E-01	-	-
39	N	41	1.0E+01	6.7E-01	4.1E+00	8.6E-01	4.5E-03	2.8E-02	-	-	-	2.9E-01	9.5E-03	1.9E-02
103	N	20	1.5E+01	2.2E+00	5.3E+00	8.3E-01	1.1E-02	2.8E-02	-	-	-	-	-	-
3-16	N	45	9.7E+00	-	-	8.7E-01	-	-	-	-	-	-	-	-
2-1	NW	36	3.4E+01	3.7E+00	4.4E+01	9.5E-01	3.5E-03	4.1E-02	-	-	-	2.3E-01	1.3E-02	7.7E-02
2-2	NW	45	2.9E+01	2.0E+00	1.7E+01	1.0E+00	6.7E-02	5.6E-01	-	-	-	3.0E-01	3.9E-02	1.0E-01
2-8	NW	50	3.4E+01	2.5E+00	2.0E+01	1.0E+00	7.0E-02	5.7E-01	-	-	-	2.9E-01	2.9E-02	5.7E-02
ms-1	NW	33	1.9E+01	-	-	9.9E-01	-	-	-	-	-	2.8E-01	-	-
ms-3	NW	36	3.8E+00	-	-	9.2E-01	-	-	-	-	-	1.6E-01	-	-
ms-4	NW	27	1.7E+01	-	-	1.0E+00	-	-	-	-	-	-	-	-
ms-5	NW	25	1.3E+01	-	-	9.9E-01	-	-	-	-	-	2.8E-01	-	-
ms-6	NW	21	8.7E+00	-	-	9.6E-01	-	-	-	-	-	2.2E-01	-	-
ms-6	NW	21	8.7E+00	-	-	9.6E-01	-	-	-	-	-	2.2E-01	-	-
ms-7	NW	22	9.7E+00	-	-	9.6E-01	-	-	-	-	-	2.0E-01	-	-
ms-11	NW	29	8.1E+00	-	-	9.6E-01	-	-	-	-	-	2.4E-01	-	-
ms-12	NW	32	2.5E+01	-	-	9.1E-01	-	-	-	-	-	-	-	-

Table C-1 (continued) Average corrected ratios of ^{131}I, ^{132}Te, and $^{134,136}Cs$ to ^{137}Cs in the near-zone of Fukushima I NPSs.

Code	Direction	Distance (km)	Average corrected ratio* in soil of											
			^{131}I:^{137}Cs			^{134}Cs:^{137}Cs			^{132}Te:^{137}Cs			^{136}Cs:^{137}Cs		
			Mean	S.E.	S.D.	Mean	S.E.	S.D.	Mean	S.E.	S.D.	Mean	S.E.	S.D.
kw-1	NW	42	3.1E+01	-	-	1.0E+00	-	-	-	-	-	-	-	-
kw-2	NW	42	4.1E+01	-	-	1.1E+00	-	-	-	-	-	-	-	-
kw-3	NW	40	1.3E+01	-	-	1.0E+00	-	-	-	-	-	2.9E-01	-	-
kw-4	NW	37	-	-	-	1.0E+00	-	-	-	-	-	-	-	-
kw-5	NW	34	1.8E+01	-	-	1.0E+00	-	-	-	-	-	2.0E-01	-	-
kw-6	NW	33	1.7E+01	-	-	9.4E-01	-	-	-	-	-	2.1E-01	-	-
kw-7	NW	45	2.1E+01	-	-	1.0E+00	-	-	-	-	-	4.0E-01	-	-
kw-8	NW	43	2.7E+01	-	-	9.7E-01	-	-	-	-	-	-	-	-
kw-9	NW	43	1.3E+01	-	-	9.6E-01	-	-	-	-	-	2.6E-01	-	-
kw-10	NW	42	1.7E+01	-	-	9.7E-01	-	-	-	-	-	-	-	-
ni-2	NW	36	1.2E+01	-	-	1.0E+00	-	-	-	-	-	-	-	-
1	NW	62	1.4E+01	7.0E-01	4.6E+00	8.7E-01	3.8E-03	2.5E-02	-	-	-	2.4E-01	1.1E-02	4.1E-02
2	NW	56	1.7E+01	1.3E+00	3.0E+00	8.6E-01	4.9E-03	1.1E-02	-	-	-	-	-	-
3-1	NW	33	1.4E+01	1.1E+00	7.7E+00	9.3E-01	8.4E-03	6.1E-02	-	-	-	2.1E-01	5.5E-03	2.0E-02
3-2	NW	30	1.5E+01	8.9E-01	5.7E+00	1.1E+00	2.1E-01	1.3E+00	-	-	-	2.1E-01	9.8E-03	3.7E-02
3-12	NW	30	2.3E+01	3.9E+00	2.8E+01	9.3E-01	6.0E-01	4.3E+00	-	-	-	2.2E-01	1.5E-02	5.0E-02
3-13	NW	31	2.0E+01	1.9E+00	1.3E+01	9.5E-01	7.9E-03	5.7E-02	-	-	-	2.4E-01	5.1E-03	1.8E-02
3-14	NW	40	1.5E+01	5.2E-01	3.7E+00	8.7E-01	3.7E-03	2.6E-02	-	-	-	2.1E-01	1.9E-02	5.8E-02
37	NW	48	6.1E+00	4.7E-01	6.6E-01	8.8E-01	7.0E-02	9.8E-02	-	-	-	-	-	-
79	NW	29	1.3E+01	5.3E-01	3.3E+00	8.6E-01	3.2E-03	2.0E-02	-	-	-	2.1E-01	4.9E-03	2.1E-02
83	NW	24	9.7E+00	3.3E-01	1.0E+00	8.8E-01	1.7E-02	5.3E-02	-	-	-	2.0E-01	7.1E-03	1.0E-02
101	NW	55	1.6E+01	2.1E+00	5.6E+00	8.5E-01	7.8E-03	2.1E-02	-	-	-	-	-	-
102	NW	50	1.5E+01	8.0E-01	2.1E+00	8.7E-01	1.5E-02	3.8E-02	-	-	-	-	-	-
107	NW	23	1.1E+01	8.0E-01	5.3E+00	8.4E-01	3.9E-03	2.6E-02	-	-	-	2.1E-01	1.0E-02	3.2E-02
108	NW	30	8.7E+00	5.2E-01	3.5E+00	8.6E-01	4.1E-03	2.8E-02	-	-	-	2.2E-01	1.6E-02	4.9E-02
i1	NW	39	1.0E+01	3.2E-01	7.7E-01	8.6E-01	6.2E-03	1.5E-02	-	-	-	2.1E-01	4.1E-02	5.8E-02

Table C-1 (continued) Average corrected ratios of ^{131}I, ^{132}Te, and $^{134,136}Cs$ to ^{137}Cs in the near-zone of Fukushima I NPSs.

Code	Direction	Distance (km)	Average corrected ratio* in soil of											
			^{131}I:^{137}Cs			^{134}Cs:^{137}Cs			^{132}Te:^{137}Cs			^{136}Cs:^{137}Cs		
			Mean	S.E.	S.D.	Mean	S.E.	S.D.	Mean	S.E.	S.D.	Mean	S.E.	S.D.
i2	NW	39	1.5E+01	2.4E+00	4.9E+00	8.9E-01	1.1E-02	2.5E-02	-	-	-	-	-	-
i7	NW	42	2.2E+01	5.6E+00	1.3E+01	8.7E-01	9.0E-03	2.0E-02	-	-	-	2.1E-01	-	-
i8	NW	44	1.3E+01	1.0E+00	2.2E+00	8.7E-01	4.1E-03	9.1E-03	-	-	-	2.4E-01	7.1E-02	1.0E-01
i19	NW	38	9.4E+00	1.1E+00	2.5E+00	8.4E-01	7.4E-03	1.6E-02	-	-	-	2.3E-01		
1-1	NW	46	1.9E+01	1.8E+00	3.0E+00	8.9E-01	1.0E-02	1.8E-02	-	-	-	-	-	-
1-2	NW	40	1.5E+01	9.6E-01	1.4E+00	8.9E-01	1.8E-02	2.6E-02	-	-	-	-	-	-
3-5	NW	47	1.5E+01	-	-	8.7E-01	-	-	-	-	-	-	-	-
K1	NW	32	1.4E+01	-	-	8.3E-01	-	-	-	-	-	-	-	-
K2	NW	30	1.3E+01	-	-	8.6E-01	-	-	-	-	-	2.3E-01		
K3	NW	28	1.9E+01	-	-	8.4E-01	-	-	-	-	-	-	-	-
K6	NW	27	1.4E+01	-	-	8.5E-01	-	-	-	-	-	1.7E-01	-	-
K7	NW	23	7.7E+00	-	-	8.5E-01	-	-	-	-	-	2.2E-01	-	-
K8	NW	21	1.3E+01	-	-	9.0E-01	-	-	-	-	-	2.4E-01	-	-
K9	NW	21	2.1E+01	-	-	8.9E-01	-	-	-	-	-	2.5E-01	-	-
K10	NW	24	2.8E+01	-	-	8.8E-01	-	-	-	-	-	-	-	-
n1	NW	31	1.3E+01	-	-	8.4E-01	-	-	-	-	-	2.1E-01	-	-
n2	NW	28	8.1E+00	-	-	8.4E-01	-	-	-	-	-	2.3E-01	-	-
n3	NW	28	9.6E+00	-	-	8.7E-01	-	-	-	-	-	2.3E-01	-	-
n4	NW	26	7.6E+00	-	-	8.4E-01	-	-	-	-	-	2.0E-01	-	-
n5	NW	22	8.7E+00	-	-	8.6E-01	-	-	-	-	-	1.9E-01	-	-
n6	NW	25	1.4E+01	-	-	8.6E-01	-	-	-	-	-	2.1E-01	-	-
n7	NW	23	1.1E+01	-	-	8.7E-01	-	-	-	-	-	2.3E-01	-	-
n8	NW	27	7.6E+01	-	-	9.1E-01	-	-	-	-	-	4.1E-01	-	-
n10	NW	33	1.5E+01	-	-	8.7E-01	-	-	-	-	-	-	-	-
n11	NW	20	7.3E+00	-	-	8.5E-01	-	-	-	-	-	2.0E-01	-	-
i6	NW	41	1.2E+01	-	-	8.5E-01	-	-	-	-	-	2.2E-01	-	-

Table C-1 (continued) Average corrected ratios of ^{131}I, ^{132}Te, and $^{134,136}Cs$ to ^{137}Cs in the near-zone of Fukushima I NPSs.

Code	Direction	Distance (km)	Average corrected ratio* in soil of											
			^{131}I:^{137}Cs			^{134}Cs:^{137}Cs			^{132}Te:^{137}Cs			^{136}Cs:^{137}Cs		
			Mean	S.E.	S.D.	Mean	S.E.	S.D.	Mean	S.E.	S.D.	Mean	S.E.	S.D.
i9	NW	45	1.4E+01	-	-	8.7E-01	-	-	-	-	-	1.6E-01	-	-
i10	NW	46	9.6E+00	-	-	8.8E-01	-	-	-	-	-	1.6E-01	-	-
i11	NW	46	9.5E+00	-	-	8.8E-01	-	-	-	-	-	1.9E-01	-	-
i12	NW	43	1.6E+01	-	-	8.4E-01	-	-	-	-	-	-	-	-
i13	NW	43	1.2E+02	-	-	8.8E-01	-	-	-	-	-	-	-	-
i14	NW	40	1.1E+01	-	-	8.4E-01	-	-	-	-	-	2.6E-01	-	-
i15	NW	40	1.4E+01	-	-	8.8E-01	-	-	-	-	-	-	-	-
i16	NW	40	-	-	-	8.9E-01	-	-	-	-	-	-	-	-
i17	NW	38	3.9E+01	-	-	9.1E-01	-	-	-	-	-	-	-	-
i18	NW	36	8.8E+00	-	-	8.8E-01	-	-	-	-	-	-	-	-
i20	NW	36	1.1E+01	-	-	9.0E-01	-	-	-	-	-	2.3E-01	-	-
i25	NW	29	1.3E+01	-	-	8.5E-01	-	-	-	-	-	1.9E-01	-	-
i26	NW	31	1.1E+01	-	-	8.4E-01	-	-	-	-	-	1.5E-01	-	-
i28	NW	34	2.4E+01	-	-	8.7E-01	-	-	-	-	-	2.2E-01	-	-
i29	NW	38	4.1E+00	-	-	8.4E-01	-	-	-	-	-	-	-	-
i30	NW	40	1.2E+01	-	-	8.3E-01	-	-	-	-	-	2.1E-01	-	-
i31	NW	38	1.5E+01	-	-	8.4E-01	-	-	-	-	-	2.7E-01	-	-
i32	NW	37	7.6E+00	-	-	8.6E-01	-	-	-	-	-	2.0E-01	-	-
ed2	NW	26	2.2E+01	-	-	-	-	-	1.8E+01	-	-	2.5E-01	-	-
ed3	NW	29	5.6E+00	-	-	9.0E-01	-	-	1.7E+01	-	-	2.4E-01	-	-
ed4	NW	29	1.5E+01	-	-	8.8E-01	-	-	1.8E+01	-	-	2.2E-01	-	-
ed10	NW	62	1.0E+01	-	-	8.8E-01	-	-	1.8E+01	-	-	2.3E-01	-	-
ed11	NW	26	2.8E+01	-	-	8.8E-01	-	-	1.9E+01	-	-	2.4E-01	-	-
im1	NW	42	1.1E+01	-	-	8.5E-01	-	-	1.5E+01	-	-	2.0E-01	-	-
im2	NW	46	1.3E+01	-	-	8.6E-01	-	-	2.0E+01	-	-	8.3E-02	-	-
im3	NW	46	1.2E+01	-	-	8.8E-01	-	-	2.2E+01	-	-	1.4E-01	-	-

Table C-1 (continued) Average corrected ratios of ^{131}I, ^{132}Te, and $^{134,136}Cs$ to ^{137}Cs in the near-zone of Fukushima I NPSs.

Code	Direction	Distance (km)	Average corrected ratio* in soil of											
			^{131}I:^{137}Cs			^{134}Cs:^{137}Cs			^{132}Te:^{137}Cs			^{136}Cs:^{137}Cs		
			Mean	S.E.	S.D.	Mean	S.E.	S.D.	Mean	S.E.	S.D.	Mean	S.E.	S.D.
im4	NW	39	9.7E+00	-	-	8.8E-01	-	-	1.7E+01	-	-	1.5E-01	-	-
im5	NW	43	8.3E+00	-	-	8.7E-01	-	-	1.7E+01	-	-	1.9E-01	-	-
2-6	S	43	1.2E+02	1.2E+01	9.6E+01	9.4E-01	1.3E-02	1.1E-01	-	-	-	-	6.6E+04	-
3-7	S	23	7.8E+01	5.7E+00	3.4E+01	8.7E-01	6.4E-03	3.8E-02	-	-	-	-	-	-
3-15	S	23	6.2E+01	3.3E+01	5.7E+01	8.9E-01	4.4E-02	7.6E-02	-	-	-	-	-	-
38	S	34	7.5E+01	2.5E+00	1.5E+01	8.9E-01	6.0E-03	3.6E-02	-	-	-	-	-	-
72	S	31	7.2E+01	5.9E+00	1.2E+01	8.5E-01	1.1E-02	2.1E-02	-	-	-	-	-	-
73	S	35	6.9E+01	6.7E+00	1.3E+01	8.7E-01	1.3E-02	2.5E-02	-	-	-	-	-	-
74	S	36	6.6E+01	5.8E+00	1.2E+01	8.5E-01	4.5E-02	9.1E-02	-	-	-	-	-	-
75	S	43	9.5E+01	8.7E+00	1.7E+01	8.8E-01	2.2E-02	4.5E-02	-	-	-	-	-	-
84	S	39	2.4E+01	1.1E+00	5.9E+00	8.9E-01	1.0E-02	5.7E-02	-	-	-	-	-	-
106	S	30	9.8E+00	1.0E+00	2.1E+00	8.3E-01	2.1E-02	4.2E-02	-	-	-	-	-	-
ed13	S	44	1.4E+02	-	-	6.9E-01	-	-	2.9E+01	-	-	1.3E-01	-	-
ed14	S	29	8.0E+01	-	-	8.7E-01	-	-	1.5E+01	-	-	1.9E-01	-	-
2-5	SW	39	1.9E+01	1.5E+00	1.2E+01	1.0E+00	1.2E-01	1.0E+00	-	-	-	-	6.6E+04	-
4-1	SW	80	1.1E+01	4.7E-01	1.9E+00	9.7E-01	1.1E-02	4.5E-02	-	-	-	-	6.6E+04	-
4-2	SW	60	1.2E+01	5.3E-01	2.2E+00	9.5E-01	1.1E-02	4.4E-02	-	-	-	-	6.6E+04	-
4-4	SW	70	1.2E+01	5.1E-01	2.1E+00	9.6E-01	9.8E-03	4.1E-02	-	-	-	-	6.6E+04	-
4-5	SW	80	1.1E+01	7.9E-01	3.2E+00	9.4E-01	1.1E-02	4.6E-02	-	-	-	-	6.6E+04	-
76	SW	22	3.0E+01	9.3E-01	5.9E+00	8.6E-01	6.7E-03	4.3E-02	-	-	-	4.4E-01	-	-
111	SW	28	5.0E+01	-	-	9.0E-01	-	-	-	-	-	-	-	-
114	SW	26	1.3E+01	-	-	9.0E-01	-	-	-	-	-	-	-	-
ed7	SW	23	1.6E+01	-	-	8.6E-01	-	-	1.4E+01	-	-	1.6E-01	-	-
ed15	SW	31	1.6E+01	-	-	8.5E-01	-	-	1.7E+01	-	-	1.9E-01	-	-
2-3	W	41	2.7E+01	1.9E+00	1.5E+01	9.4E-01	1.1E-02	9.4E-02	-	-	-	-	-	-

Table C-1 (continued) Average of corrected ratios of ^{131}I, ^{132}Te, and $^{134,136}Cs$ to ^{137}Cs in near-zone of Fukushima I NPSs.

Code	Direction	Distance (km)	Average corrected ratio* in soil of											
			^{131}I:^{137}Cs			^{134}Cs:^{137}Cs			^{132}Te:^{137}Cs			^{136}Cs:^{137}Cs		
			Mean	S.E.	S.D.	Mean	S.E.	S.D.	Mean	S.E.	S.D.	Mean	S.E.	S.D.
2-7	W	34	2.4E+01	2.0E+00	1.6E+01	9.5E-01	4.7E-03	3.8E-02	-	-	-	2.4E-01	8.0E-03	3.5E-02
2-9	W	45	1.3E+01	7.4E-01	6.0E+00	9.5E-01	4.2E-03	3.4E-02	-	-	-	2.5E-01	1.5E-02	5.7E-02
4-3	W	60	2.5E+01	1.7E+00	1.2E+01	9.4E-01	8.5E-03	6.1E-02	-	-	-	3.1E-01	-	-
3-3	W	32	1.8E+01	1.3E+00	8.7E+00	8.7E-01	4.6E-03	3.0E-02	-	-	-	2.4E-01	-	-
3-6	W	32	1.6E+01	7.9E-01	5.5E+00	8.7E-01	3.7E-03	2.6E-02	-	-	-	2.3E-01	9.7E-03	3.2E-02
104	W	25	1.7E+01	5.7E-01	3.7E+00	8.7E-01	3.8E-03	2.5E-02	-	-	-	2.3E-01	1.5E-02	4.0E-02
105	W	21	2.4E+01	8.4E-01	1.7E+00	8.4E-01	6.6E-03	1.3E-02	-	-	-	-	-	-
113	W	25	2.1E+01	3.3E+00	1.3E+01	8.9E-01	5.3E-03	2.1E-02	-	-	-	2.2E-01	1.4E-02	4.4E-02
13	W	37	1.7E+01	-	-	8.5E-01	-	-	-	-	-	-	-	-
3-4	W	43	1.1E+01	-	-	8.5E-01	-	-	-	-	-	-	-	-
110	W	25	1.2E+01	-	-	8.9E-01	-	-	-	-	-	-	-	-
181	W	25	3.7E+01	-	-	8.6E-01	-	-	-	-	-	-	-	-
K4	W	28	1.0E+01	-	-	8.9E-01	-	-	-	-	-	1.9E-01	-	-
K5	W	29	1.6E+01	-	-	8.4E-01	-	-	-	-	-	-	-	-
K11	W	21	1.9E+01	-	-	8.7E-01	-	-	-	-	-	2.9E-01	-	-
ed1	W	4.4	1.8E+01	-	-	9.7E-01	-	-	1.8E+01	-	-	2.6E-01	-	-
ed5	W	35	2.5E+01	-	-	8.6E-01	-	-	2.2E+01	-	-	1.4E-01	-	-
ed6	W	22	3.9E+01	-	-	8.9E-01	-	-	2.4E+01	-	-	1.9E-01	-	-
ed8	W	25	1.8E+01	-	-	8.5E-01	-	-	1.8E+01	-	-	2.0E-01	-	-
ed9	W	48	9.0E+00	-	-	8.8E-01	-	-	1.7E+01	-	-	1.4E-01	-	-
ed12	W	60	4.9E+00	-	-	8.8E-01	-	-	1.1E+01	-	-	2.3E-01	-	-
Average			22.46	1.87	22.50	0.90	0.01	0.06	18.30	0.87	3.87	0.22	0.01	0.05
No. of samples			1,795			1,817					20	283		
No. of sites			145			146					20	88		

[Δ]Note that the names of the deposition monitoring sites and source of data are shown in Table C-2, Appendix C.

[*]Note that all ratios are corrected back to 11/03/2011 14:46

Table C-2 the name and source of the deposition monitoring sites in near zone of Fukushima I NPSs.

Code	Site
Monitoring by MEXT (2011b)	
2-1	Yagisawa, Iitate village, Soma county
2-2	Kawamata town, Date county
2-3	Funehiki, Funehiki town, Tamura city
2-4	Takami town, Haramachi ward, Minami Soma city
2-5	Ononiimachi, Ono town, Tamura county
2-6	Umemoto, Taira Aza, Iwaki city
2-7	Yamakiya, Kawamata town, Date county
2-8	Tsukidate town, Date city
2-9	Kanairo, Nihonmatsu city
4-1	Shirakawa city
4-2	Hachiman town, Sukagawa city
4-3	Otama village, Adachi county
4-4	Izumizaki village, Shirakawa county
4-5	Saigou village, Nishishirakawa county
2-10	Shinchi town, Soma county
ms-1	Ohara, Haramachi ward, Minami Soma city
ms-3	Kamitochikubo, Kashima ward, Minami Soma city
ms-4	Takanokura, Haramachi ward, Minami Soma city
ms-5	Takanokura, Haramachi ward, Minami Soma city
ms-6	Baba, Haramashi ward, Minami Soma city
ms-7	Baba, Haramashi ward, Minami Soma city
ms-8	Kanezawa, Haramachi ward, Minami Soma city
ms-9	Takami town, Haramachi ward, Minami Soma city
ms-10	Taka, Haramachi ward, Minami Soma city
ms-11	Ohara, Haramachi ward, Minami Soma city
ms-12	Jisabara Maeta, Kashima ward, Minami Soma city
kw-1	Ushirozawa, Kotsunagi, Kawamata town, Date county
kw-2	Kotsunagi Kamihagane, Kawamata town, Date county
kw-3	Shimonagahashi, Yamakiya, Kawamta town, Date county
kw-4	Boyoshi, Yamakiya, Kawamta town, Date county
kw-5	Isshoutatsuyama, Yamakiya, Kawamta town, Date county

Table C-2 (continued) the name and source of the deposition monitoring sites in near zone of Fukushima I NPSs.

Code	Site
kw-6	Hirokuboyama, Yamakiya, Kawamta town, Date county
kw-7	Kotsunagi, Kawamata town, Date county
kw-8	Kotsunagi, Kawamata town, Date county
kw-9	Kotsunagi, Kawamata town, Date county
kw-10	Kotsunagi, Kawamata town, Date county
ni-2	Shimomagariyama, Tazawa, Nihonmatsu city
Monitoring by MEXT (2011c)	
1	Sugitsuma town, Fukushima city
2	Onami Takinoiri, Fukushima city
2-4	Takami town, Haramachi ward, Minami Soma city
3-1	Nagadoro, Iitate village, Soma county
3-2	Tsushima, Namie town
3-3	Yamane, Tokiwa town, Tamura city
3-6	Kaminogawa, Katsurao village
3-7	Shimokitaba, Hirono town
3-9	Nakano, Soma city
3-10	Kashima ward, Minami Soma city
3-11	Kashima ward, Minami Soma city
3-12	Tsushima, Namie town
3-13	Akougi, Namie town
3-14	Yamakiya, Kawamata town
3-15	Shimokitaba, Hirono town, Futaba county
37	Hojizawa, Ishida, Ryozen town, Date city
38	Hokita, Shiraiwa, Yotsukura town, Iwaki city
39	Kaminamiki, Yamakami, Soma city
72	Hisanohama, Hisanohama town, Iwaki city
73	Takahagi, Ogawa town, Iwaki city
74	Takahagi, Ogawa town, Iwaki city
75	Uchigoumimaya town, Iwaki city
76	Hayawata, Kamikawauchi, Kawauchi village, Futaba county
79	Shimotsushima Kayabuka, Namie town, Futaba county

Table C-2 (continued) the name and source of the deposition monitoring sites in near zone of Fukushima I NPSs.

Code	Site
83	Akougi Kunugidaira, Namie town
84	Saiso, Miwa town, Iwaki city
101	Oishi, Ryozen town, Date city
102	Tsukidate town, Date city
103	Mamegarauchi, Taka, Haramachi ward, Minami Soma city
104	Ochiai, Oaza, Katsurao Village, Futaba County
105	Furumichi, Miyakoji town, Tamura city
106	Hokita, Shiraiwa, Kawamae town, Iwaki city
107	Shimonakanouchi, Baba, Haramachi ward, Minami Soma city
108	Daihata, Ohara, Haramachi ward, Minami Soma city
113	Iwaisawa, Miyakoji town, Tamura city
i1	Itamizawa, Iitate village, Soma county
i2	Itamizawa, Iitate village, Soma county
i7	Usuishi, Iitate village, Soma county
i8	Nimaibashi, Iitate village, Soma county
i19	Sekisawa, Iitate village, Soma county
1-1	Sasu Nameri, Iitate village
1-2	Yamakiya, Kawamata town
13	Yakata, Nishimuki, Tokiwa town, Tamura city
3-4	Ota, Nihonmatsu city
3-5	Kawamata town
3-16	Yamakami, Soma city
110	Furumichi, Miyakoji town, Tamura city
111	Kamikawauchi, Kawauchi village, Futaba county
114	Kamiogawa, Ogawa town, Iwaki city
181	Kamikawauchi, Kawauchi village, Futaba county
K1	Kazakoshi, Katsurao, Katsurao village, Futaba county
K2	Nakadaira, Katsurao, Katsurao village, Futaba county
K3	Higashidaira, Katsurao, Katsurao village, Futaba county
K4	Nakanouchi, Nogawa, Katsurao village, Futaba county
K5	Yuden, Nogawa, Katsurao village, Futaba county
K6	Hiroyaji, Katsurao, Katsurao village, Futaba county

Table C-2 (continued) the name and source of the deposition monitoring sites in near zone of Fukushima I NPSs.

Code	Site
K7	Kashiwabara, Katsurao, Katsurao village, Futaba county
K8	Noyuki, Katsurao, Katsurao village , Futaba county
K9	Ozasa, Ochiai, Katsurao village, Futaba county
K10	Ozasa, Ochiai, Katsurao village, Futaba county
K11	Ohanachi, Ochiai, Katsurao village, Futaba county
n1	Teshichiro, Akougi, Namie town, Futaba county
n2	Teshichiro, Akougi, Namie town, Futaba county
n3	Shiraoi, Akougi, Namie town, Futaba county
n4	Shiobite, Akougi, Namie town, Futaba county
n5	Kurabeishi, Hirusone, Namie town, Futaba county
n6	Shimohiyada, Minamitsushima, Namie town, Futaba county
n7	Shimohiyada, Minamitsushima, Namie town, Futaba county
n8	Kotsuka, Shimotsushima, Namie town, Futaba county
n10	Tatenosawa, Hatsuke, Namie town, Futaba county
n11	Hirusone, Namie town, Futaba county
i6	Fukaya, Iitate village, Soma county
i9	Maeta, Iitate village, Soma county
i10	Sasu, Iitate village, Soma county
i11	Sasu, Iitate village, Soma county
i12	Sasu, Iitate village, Soma county
i13	Maeta, Iitate village, Soma county
i14	Kusano, Iitate village, Soma county
i15	Ookura, Iitate village, Soma county
i16	Ookura, Iitate village, Soma county
i17	Kusano, Iitate village, Soma county
i18	Yagisawa, Iitate village, Soma county
i20	Hashiba, Sekisawa, Iitate village, Soma county
i25	Warabidaira, Iitate village, Soma county
i26	Nagadoro, Iitate village, Soma county
i28	Hiso, Iitate village, Soma county
i29	Kamihiso, Hiso, Iitate village, Soma county
i30	Ohi, Iitoi, Iitate village, Soma county

Table C-2 (continued) the name and source of the deposition monitoring sites in near zone of Fukushima I NPSs.

Code	Site
i31	Iitoi , Iitate village, Soma county
i32	Iitoi , Iitate village, Soma county
Monitoring by Endo and co-workers (2012)	
ed1	Futaba Yamada
ed2	Namie Tsushima
ed3	Iitate Warabidaira
ed4	Namie Akogi
ed5	Tokiwa Junior High School
ed6	Miyakoji Junior High School
ed7	Kawauchi Elementary School
ed8	Katsurao Junior High School
ed9	Miharu Town
ed10	Niihama Park, Fukushima city
ed11	Minami Soma
ed12	Ohshima-Higashi Park, Kouriyama
ed13	Chuo Interchange, Iwaki
ed14	Suetsugi Station
ed15	Kittoya Mountain, Miharu Town
Monitoring by Imanaka and co-workers (2012)	
im1	Usuishi, Iitate village, Soma county
im2	Sasu, Iitate village, Soma county
im3	Yamstsumi shrine, Iitate village, Soma county
im4	Village office, Iitate village, Soma county
im5	Magata, Iitate village, Soma county

Table C-3 Average of corrected ratios of ^{129m}Te to ^{137}Cs in near-zone of Fukushima I NPSs.

Code[Δ]	Direction	Distance (km)	Average corrected ratio[*] in soil of		
			^{129m}Te:^{137}Cs	^{140}Ba:^{137}Cs	^{140}La:^{137}Cs
im1	NW	42.12	0.02	-	-
im2	NW	45.68	0.04	-	-
im3	NW	46.1	0.03	-	-
im4	NW	38.67	0.04	-	-
im5	NW	42.78	0.03	-	-
Mean corrected ratio			0.03	-	-
(± 2 S.E.)			0.006	-	-

[Δ]Note that the names of the deposition monitoring sites were show in Table C-2, Appendix C.

Table C-4 Average of corrected ratios of ^{140}Ba and ^{140}La (fission product) to ^{137}Cs in near-zone of Fukushima I NPSs from Endo (2012).

Code[Δ]	Direction	Distance (km)	Average corrected ratio[*] in soil of		
			^{129m}Te:^{137}Cs	^{140}Ba:^{137}Cs	^{140}La:^{137}Cs
ed1	W	4.4	-	-	-
ed2	NW	26	-	0.04	0.10
ed3	NW	29	-	0.07	-
ed4	NW	29	-	0.05	-
ed5	W	35	-	0.04	-
ed6	W	22	-	0.04	
ed7	SW	23	-	0.09	0.26
ed8	W	25	-	0.02	0.47
ed9	W	48	-	0.02	0.18
ed10	NW	62	-	0.03	0.19
ed11	NW	26	-	0.08	-
ed12	W	60	-	0.04	-
ed13	S	44	-	0.37	-
ed14	S	29	-	-	1.76
ed15	SW	31	-	-	0.11
Mean corrected ratio			-	0.07	0.40
(± 2 S.E.)			-	0.06	0.34

[Δ]Note that the names of the deposition monitoring sites were show in Table C-2, Appendix C.

Table C-5 Details of the corrected ratio $^{131}I/^{137}Cs$ in soil from measurement and from model (Equation 3-1) in the northwest area of Fukushima I NPSs.

Code[Δ]	Direction	Distance (km)	Measurement ($R_{measurement}$)	Model (R_{model})	$\frac{R_{measurement}}{R_{model}}$	$Log\ (\frac{R_{measurement}}{R_{model}})$
2-1	NW	36	33.99	12.64	2.69	0.43
2-2	NW	45	28.94	17.58	1.65	0.22
2-8	NW	50	33.60	19.05	1.76	0.25
ms-1	NW	33	19.19	16.32	1.18	0.07
ms-3	NW	36	3.76	13.99	0.27	-0.57
ms-5	NW	25	13.42	14.04	0.96	-0.02
ms-7	NW	22	9.71	14.22	0.68	-0.17
ms-11	NW	29	8.13	14.62	0.56	-0.25
ms-12	NW	32	25.28	28.94	0.87	-0.06
ms-4	NW	27	17.41	26.14	0.67	-0.18
ms-6	NW	21	8.69	11.49	0.76	-0.12
kw-1	NW	42	30.78	19.04	1.62	0.21
kw-2	NW	42	40.58	21.28	1.91	0.28
kw-7	NW	45	21.15	18.73	1.13	0.05
kw-8	NW	43	26.62	16.89	1.58	0.20
kw-9	NW	43	12.92	15.99	0.81	-0.09
kw-10	NW	42	17.31	15.82	1.09	0.04
kw-3	NW	40	13.13	15.78	0.83	-0.08
kw-5	NW	34	18.42	13.81	1.33	0.13
kw-6	NW	33	16.83	11.72	1.44	0.16
ni-2	NW	36	12.40	20.33	0.61	-0.21
107	NW	23	10.94	14.73	0.74	-0.13
108	NW	30	8.75	14.41	0.61	-0.22
83	NW	24	9.73	10.58	0.92	-0.04
3-13	NW	31	19.75	11.20	1.76	0.25
3-1	NW	33	13.78	11.23	1.23	0.09
i19	NW	38	9.36	12.73	0.74	-0.13
i1	NW	39	10.12	12.02	0.84	-0.07
i2	NW	39	14.99	16.87	0.89	-0.05
i7	NW	42	21.96	12.86	1.71	0.23
i8	NW	44	13.25	13.60	0.97	-0.01
1-1	NW	46	19.44	15.88	1.22	0.09
37	NW	48	6.12	13.00	0.47	-0.33

Table C-5 (continued) Details of the corrected ratio $^{131}I/^{137}Cs$ in soil from measurement and from model (Equation 3-1) in the northwest area of Fukushima I NPSs.

Code[Δ]	Direction	Distance (km)	Measurement ($R_{measurement}$)	Model (R_{model})	$\frac{R_{measurement}}{R_{model}}$	$Log\ (\frac{R_{measurement}}{R_{model}})$
102	NW	50	14.92	17.08	0.87	-0.06
101	NW	55	15.50	19.81	0.78	-0.11
2	NW	56	16.85	14.23	1.18	0.07
1	NW	62	14.09	13.90	1.01	0.01
3-12	NW	30	23.21	11.59	2.00	0.30
79	NW	29	12.54	11.23	1.12	0.05
3-2	NW	30	15.31	12.40	1.23	0.09
3-14	NW	40	14.92	13.20	1.13	0.05
1-2	NW	40	14.94	12.95	1.15	0.06
3-5	NW	47	15.37	41.03	0.37	-0.43
n1	NW	31	12.73	11.06	1.15	0.06
n2	NW	28	8.08	10.92	0.74	-0.13
n3	NW	28	9.63	11.14	0.86	-0.06
n4	NW	26	7.63	10.87	0.70	-0.15
n5	NW	22	8.68	10.47	0.83	-0.08
n6	NW	25	13.51	11.39	1.19	0.07
n7	NW	23	11.27	10.87	1.04	0.02
n8	NW	27	75.92	17.85	4.25	0.63
K8	NW	21	13.28	16.14	0.82	-0.08
n11	NW	20	7.28	10.66	0.68	-0.17
i6	NW	41	11.50	11.63	0.99	0.00
i9	NW	45	14.28	12.61	1.13	0.05
i10	NW	46	9.64	11.93	0.81	-0.09
i11	NW	46	9.45	12.21	0.77	-0.11
i12	NW	43	16.31	15.44	1.06	0.02
i13	NW	43	119.03	76.85	1.55	0.19
i14	NW	40	10.59	11.65	0.91	-0.04
i15	NW	40	14.46	16.42	0.88	-0.06
i17	NW	38	38.92	20.15	1.93	0.29
i18	NW	36	8.78	13.13	0.67	-0.17
i20	NW	36	10.81	12.32	0.88	-0.06
i25	NW	29	12.89	11.11	1.16	0.06
i26	NW	31	10.85	11.00	0.99	-0.01
i28	NW	34	24.06	10.92	2.20	0.34

Table C-5 (continued) Details of the corrected ratio $^{131}I/^{137}Cs$ in soil from measurement and from model (Equation 3-1) in the northwest area of Fukushima I NPSs.

Code[Δ]	Direction	Distance (km)	Measurement ($R_{measurement}$)	Model (R_{model})	$\frac{R_{measurement}}{R_{model}}$	$Log\ (\frac{R_{measurement}}{R_{model}})$
i29	NW	38	4.08	12.89	0.32	-0.50
i30	NW	40	12.26	11.86	1.03	0.01
i31	NW	38	14.93	12.89	1.16	0.06
i32	NW	37	7.58	12.06	0.63	-0.20
K1	NW	32	13.87	13.59	1.02	0.01
K2	NW	30	12.86	13.26	0.97	-0.01
K3	NW	28	19.06	20.15	0.95	-0.02
K6	NW	27	14.40	11.41	1.26	0.10
K7	NW	23	7.68	11.02	0.70	-0.16
K9	NW	21	21.01	10.83	1.94	0.29
K10	NW	24	27.57	16.14	1.71	0.23
n10	NW	33	14.88	15.11	0.98	-0.01
ed2	NW	26	21.56	13.63	1.58	0.20
ed3	NW	29	5.60	12.04	0.46	-0.33
ed4	NW	29	14.97	11.38	1.32	0.12
ed10	NW	62	10.37	18.40	0.56	-0.25
ed11	NW	26	28.25	31.51	0.90	-0.05
im1	NW	42.12	11.34	10.68	1.06	0.03
im2	NW	45.68	12.86	10.76	1.20	0.08
im3	NW	46.1	11.98	10.88	1.10	0.04
im4	NW	38.67	9.68	10.82	0.90	-0.05
im5	NW	42.78	8.25	10.46	0.79	-0.10

[Δ]Note that the names of the deposition monitoring sites were show in Table C-2, Appendix C.

Table C-6 Mean radioactivity concentration of ^{137}Cs in soil (with statistical parameters) in the near-zone of Fukushima I NPSs.

Code[Δ]	Direction	Distance (km)	Activity of ^{137}Cs					
			Mean	S.E.	S.D.	%C.V.	No. of samples	p value in test of normality (Kolmogorov-Smirnov)
2-4	N	24	2.2E+03	2.1E+02	1.8E+03	7.9E+01	71	0.130
2-10	N	50	2.1E+02	-	-	-	1	-
ms-8	N	20	1.6E+03	-	-	-	1	-
ms-9	N	24	4.6E+03	-	-	-	1	-
ms-10	N	21	3.0E+03	-	-	-	1	-
2-4	N	24	2.6E+03	1.9E+02	1.2E+03	4.8E+01	44	-
3-9	N	42	2.5E+03	6.0E+02	1.2E+03	4.7E+01	4	-
3-10	N	32	3.8E+03	2.3E+02	1.3E+03	3.3E+01	29	-
3-11	N	32	1.9E+03	1.6E+02	1.0E+03	5.5E+01	44	-
39	N	41	4.1E+03	1.9E+02	1.2E+03	3.0E+01	40	-
103	N	20	2.5E+03	7.4E+02	1.8E+03	7.1E+01	6	-
3-16	N	45	3.5E+03	-	-	-	1	-
2-1	NW	36	2.2E+04	2.3E+03	2.7E+04	1.2E+02	135	0.213
2-2	NW	45	5.0E+03	3.6E+02	3.0E+03	6.0E+01	71	0.123
2-8	NW	50	4.0E+03	2.9E+02	2.4E+03	5.9E+01	66	0.089
ms-1	NW	33	6.4E+03	-	-	-	1	-
ms-3	NW	36	1.2E+04	-	-	-	1	-
ms-4	NW	27	1.8E+03	-	-	-	1	-
ms-5	NW	25	1.2E+04	-	-	-	1	-
ms-6	NW	21	5.0E+04	-	-	-	1	-
ms-7	NW	22	1.1E+04	-	-	-	1	-
ms-11	NW	29	9.9E+03	-	-	-	1	-

Table C-6 (continued) Average of radioactivity concentration of ^{137}Cs in soil with statistic description at near-zone of Fukushima I NPSs.

Code[Δ]	Direction	Distance (km)	Activity of ^{137}Cs					
			Mean	S.E.	S.D.	%C.V.	No. of samples	p value in test of normality (Kolmogorov-Smirnov)
ms-12	NW	32	1.5E+03	-	-	-	1	-
kw-1	NW	42	4.0E+03	-	-	-	1	-
kw-2	NW	42	3.0E+03	-	-	-	1	-
kw-3	NW	40	7.3E+03	-	-	-	1	-
kw-4	NW	37	7.4E+03	-	-	-	1	-
kw-5	NW	34	1.3E+04	-	-	-	1	-
kw-6	NW	33	4.1E+04	-	-	-	1	-
kw-7	NW	45	4.2E+03	-	-	-	1	-
kw-8	NW	43	5.7E+03	-	-	-	1	-
kw-9	NW	43	6.9E+03	-	-	-	1	-
kw-10	NW	42	7.2E+03	-	-	-	1	-
ni-2	NW	36	3.3E+03	-	-	-	1	-
1	NW	62	1.2E+04	8.5E+02	5.6E+03	4.5E+01	43	-
2	NW	56	1.1E+04	2.8E+03	6.2E+03	5.5E+01	5	-
3-1	NW	33	6.8E+04	4.5E+03	3.3E+04	4.8E+01	5	-
3-2	NW	30	2.5E+04	2.4E+03	1.5E+04	6.2E+01	41	-
3-12	NW	30	4.5E+04	7.5E+03	5.4E+04	1.2E+02	52	0.210
3-13	NW	31	7.0E+04	5.7E+03	4.1E+04	5.9E+01	52	0.073
3-14	NW	40	1.6E+04	1.1E+03	7.8E+03	4.7E+01	51	0.113
37	NW	48	1.8E+04	2.0E+03	2.8E+03	1.6E+01	2	-
79	NW	29	6.8E+04	3.8E+03	2.4E+04	3.5E+01	39	-
83	NW	24	2.6E+05	2.6E+04	8.1E+04	3.1E+01	10	-
101	NW	55	3.6E+03	5.9E+02	1.6E+03	4.4E+01	7	-

Table C-6 (continued) Average of radioactivity concentration of ^{137}Cs in soil with statistic description at near-zone of Fukushima I NPSs.

Code[Δ]	Direction	Distance (km)	Activity of ^{137}Cs					
			Mean	S.E.	S.D.	%C.V.	No. of samples	p value in test of normality (Kolmogorov-Smirnov)
102	NW	50	5.5E+03	6.7E+02	1.8E+03	3.2E+01	7	-
107	NW	23	9.6E+03	6.1E+02	4.1E+03	4.3E+01	45	-
108	NW	30	1.1E+04	5.1E+02	3.4E+03	3.2E+01	45	-
i1	NW	39	3.2E+04	3.9E+03	9.5E+03	3.0E+01	6	-
i2	NW	39	5.8E+03	3.4E+03	7.6E+03	1.3E+02	5	-
i7	NW	42	1.9E+04	5.4E+03	1.2E+04	6.3E+01	5	-
i8	NW	44	1.4E+04	2.4E+03	5.4E+03	3.8E+01	5	-
i19	NW	38	2.1E+04	2.2E+03	4.9E+03	2.4E+01	5	-
1-1	NW	46	7.1E+03	2.1E+03	3.6E+03	5.1E+01	3	-
1-2	NW	40	1.9E+04	2.5E+03	3.5E+03	1.9E+01	2	-
3-5	NW	47	7.7E+02	-	-	-	1	-
K1	NW	32	1.4E+04	-	-	-	1	-
K2	NW	30	1.6E+04	-	-	-	1	-
K3	NW	28	3.4E+03	-	-	-	1	-
K6	NW	27	5.5E+04	-	-	-	1	-
K7	NW	23	9.2E+04	-	-	-	1	-
K8	NW	21	1.3E+05	-	-	-	1	-
K9	NW	21	6.7E+03	-	-	-	1	-
K10	NW	24	4.6E+03	-	-	-	1	-
n1	NW	31	8.6E+04	-	-	-	1	-
n2	NW	28	1.1E+05	-	-	-	1	-
n3	NW	28	7.7E+04	-	-	-	1	-
n4	NW	26	1.2E+05	-	-	-	1	-

Table C-6 (continued) Average of radioactivity concentration of ^{137}Cs in soil with statistic description at near-zone of Fukushima I NPSs.

Code[Δ]	Direction	Distance (km)	Activity of ^{137}Cs					
			Mean	S.E.	S.D.	%C.V.	No. of samples	p value in test of normality (Kolmogorov-Smirnov)
n5	NW	22	4.1E+05	-	-	-	1	-
n6	NW	25	5.6E+04	-	-	-	1	-
n7	NW	23	1.2E+05	-	-	-	1	-
n8	NW	27	4.8E+03	-	-	-	1	-
n10	NW	33	6.7E+03	-	-	-	1	-
n11	NW	20	2.0E+05	-	-	-	1	-
i6	NW	41	4.4E+04	-	-	-	1	-
i9	NW	45	2.2E+04	-	-	-	1	-
i10	NW	46	3.4E+04	-	-	-	1	-
i11	NW	46	2.8E+04	-	-	-	1	-
i12	NW	43	7.9E+03	-	-	-	1	-
i13	NW	43	2.8E+02	-	-	-	1	-
i14	NW	40	4.3E+04	-	-	-	1	-
i15	NW	40	6.3E+03	-	-	-	1	-
i16	NW	40	1.2E+03	-	-	-	1	-
i17	NW	38	3.4E+03	-	-	-	1	-
i18	NW	36	1.7E+04	-	-	-	1	-
i20	NW	36	2.6E+04	-	-	-	1	-
i25	NW	29	8.0E+04	-	-	-	1	-
i26	NW	31	9.5E+04	-	-	-	1	-
i28	NW	34	1.1E+05	-	-	-	1	-
i29	NW	38	1.9E+04	-	-	-	1	-
i30	NW	40	3.6E+04	-	-	-	1	-

Table C-6 (continued) Average of radioactivity concentration of ^{137}Cs in soil with statistic description at near-zone of Fukushima I NPSs.

Code[Δ]	Direction	Distance (km)	Activity of ^{137}Cs					
			Mean	S.E.	S.D.	%C.V.	No. of samples	p value in test of normality (Kolmogorov-Smirnov)
i31	NW	38	1.9E+04	-	-	-	1	-
i32	NW	37	3.1E+04	-	-	-	1	-
ed2	NW	26	1.4E+04	-	-	-	1	-
ed3	NW	29	3.1E+04	-	-	-	1	-
ed4	NW	29	5.7E+04	-	-	-	1	-
ed10	NW	62	4.4E+03	-	-	-	1	-
ed11	NW	26	1.3E+03	-	-	-	1	-
im1	NW	42	1.9E+05	-	-	-	1	-
im2	NW	46	1.5E+05	-	-	-	1	-
im3	NW	46	1.2E+05	-	-	-	1	-
im4	NW	39	1.3E+05	-	-	-	1	-
im5	NW	43	4.4E+05	-	-	-	1	-
2-6	S	43	9.6E+02	7.8E+01	6.5E+02	6.8E+01	69	0.075
3-7	S	23	2.2E+03	1.6E+02	9.8E+02	4.4E+01	36	-
3-15	S	23	1.2E+03	4.2E+02	7.3E+02	5.9E+01	3	-
38	S	34	2.7E+03	5.9E+02	3.5E+03	1.3E+02	35	-
72	S	31	2.0E+03	2.1E+02	4.2E+02	2.2E+01	4	-
73	S	35	1.1E+03	1.2E+02	2.4E+02	2.2E+01	4	-
74	S	36	4.7E+02	8.3E+01	1.7E+02	3.5E+01	4	-
75	S	43	1.1E+03	1.6E+02	3.1E+02	2.8E+01	4	-
84	S	39	7.2E+02	5.1E+01	2.9E+02	4.0E+01	32	-
106	S	30	1.2E+03	9.1E+01	1.8E+02	1.6E+01	4	-
ed13	S	44	7.4E+01	-	-	-	1	-

Table C-6 (continued) Average of radioactivity concentration of ^{137}Cs in soil with statistic description at near-zone of Fukushima I NPSs.

Code[Δ]	Direction	Distance (km)	Activity of ^{137}Cs					
			Mean	S.E.	S.D.	%C.V.	No. of samples	p value in test of normality (Kolmogorov-Smirnov)
ed14	S	29	7.3E+02	-	-	-	1	-
2-5	SW	39	8.0E+02	8.3E+01	7.0E+02	8.8E+01	72	0.180
4-1	SW	80	2.8E+03	3.7E+02	1.5E+03	5.5E+01	17	-
4-2	SW	60	1.3E+03	1.1E+02	4.7E+02	3.7E+01	17	-
4-4	SW	70	2.0E+03	3.0E+02	1.2E+03	6.3E+01	17	0.227
4-5	SW	80	3.3E+03	3.8E+02	1.5E+03	4.6E+01	16	0.135
76	SW	22	1.5E+03	7.4E+01	4.7E+02	3.1E+01	41	0.360
111	SW	28	1.3E+03	-	-		1	-
114	SW	26	6.2E+03	-	-		1	-
ed7	SW	23	1.3E+03	-	-		1	-
ed15	SW	31	1.3E+03	-	-		1	-
2-3	W	41	7.8E+02	7.0E+01	5.9E+02	7.5E+01	71	0.123
2-7	W	34	1.4E+04	1.1E+03	9.1E+03	6.3E+01	65	0.131
2-9	W	45	1.2E+04	8.8E+02	7.1E+03	6.0E+01	65	0.113
4-3	W	60	2.6E+03	3.5E+02	2.5E+03	9.7E+01	52	0.208
3-3	W	32	3.0E+03	1.9E+02	1.3E+03	4.2E+01	43	0.104
3-6	W	32	1.0E+04	8.0E+02	5.6E+03	5.6E+01	49	0.082
104	W	25	1.0E+04	6.5E+02	4.2E+03	4.0E+01	42	0.134
105	W	21	2.3E+03	2.2E+02	4.4E+02	2.0E+01	4	0.382
113	W	25	1.7E+04	5.1E+03	2.1E+04	1.2E+02	16	0.272
13	W	37	1.2E+03	-	-	-	1	-
3-4	W	43	8.6E+03	-	-	-	1	-
110	W	25	5.4E+03	-	-	-	1	-

Table C-6 (continued) Average of radioactivity concentration of ^{137}Cs in soil with statistic description at near-zone of Fukushima I NPSs.

Code[Δ]	Direction	Distance (km)	Activity of ^{137}Cs					
			Mean	S.E.	S.D.	%C.V.	No. of samples	p value in test of normality (Kolmogorov-Smirnov)
181	W	25	1.2E+03	-	-	-	1	-
K4	W	28	1.9E+04	-	-	-	1	-
K5	W	29	6.6E+03	-	-	-	1	-
K11	W	21	7.0E+03	-	-	-	1	-
ed1	W	4.4	1.9E+05	-	-	-	1	-
ed5	W	35	3.4E+02	-	-	-	1	-
ed6	W	22	1.0E+03	-	-	-	1	-
ed8	W	25	4.9E+03	-	-	-	1	-
ed9	W	48	1.2E+03	-	-	-	1	-
ed12	W	60	4.6E+03	-	-	-	1	-

[Δ]Note that the names of the deposition monitoring sites were show in Table C-2, Appendix C.

Appendix D Measurements and results for adjusted AQUASCOPE

(a) ^{134}Cs in predatory fish

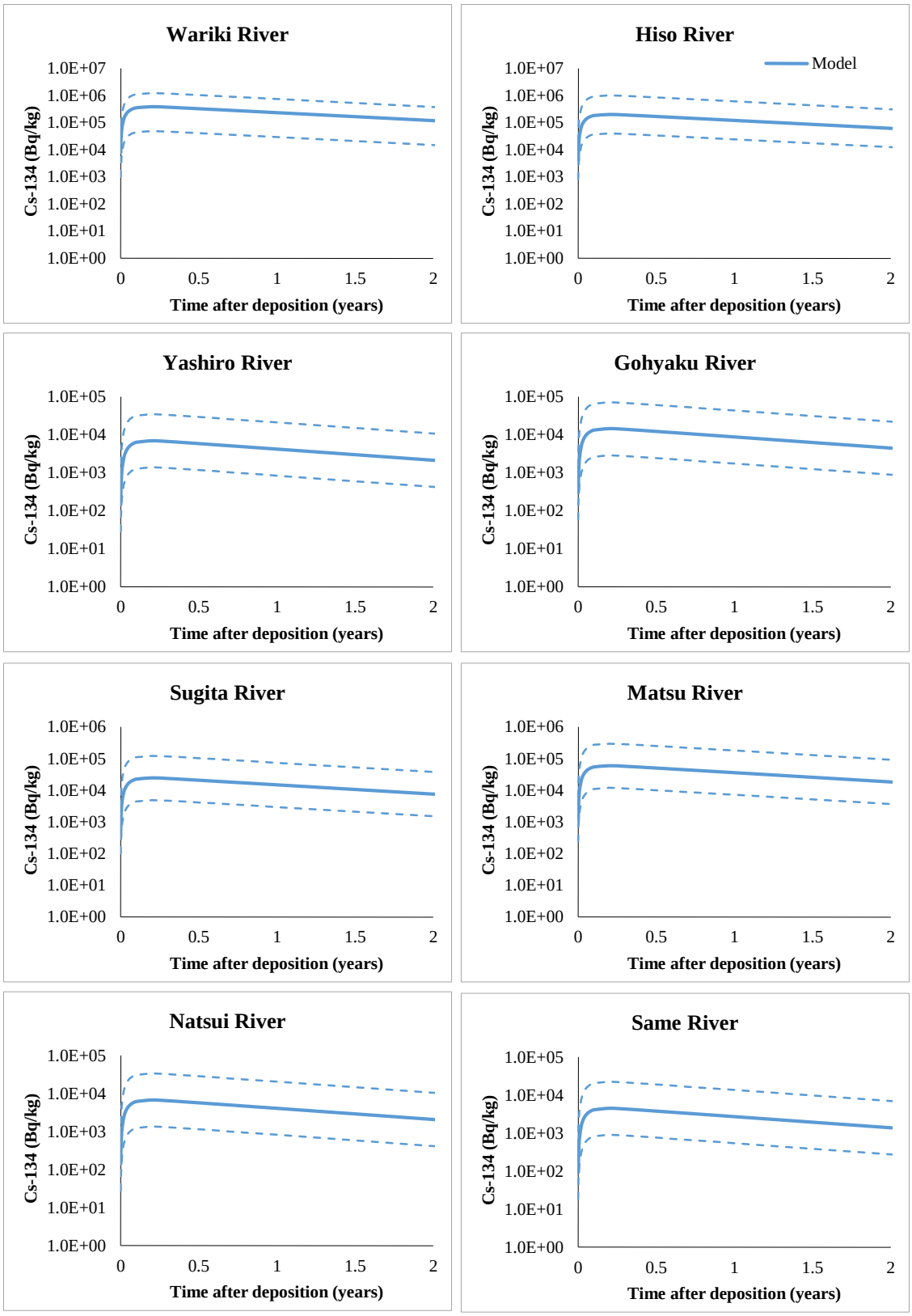

Figure D-1 Predictions of concentration (Bq/kg) in predatory fish at all eight rivers around Fukushima I NPSs, (a) ^{134}Cs in and (b) ^{137}Cs.

(b) ^{137}Cs in predatory fish

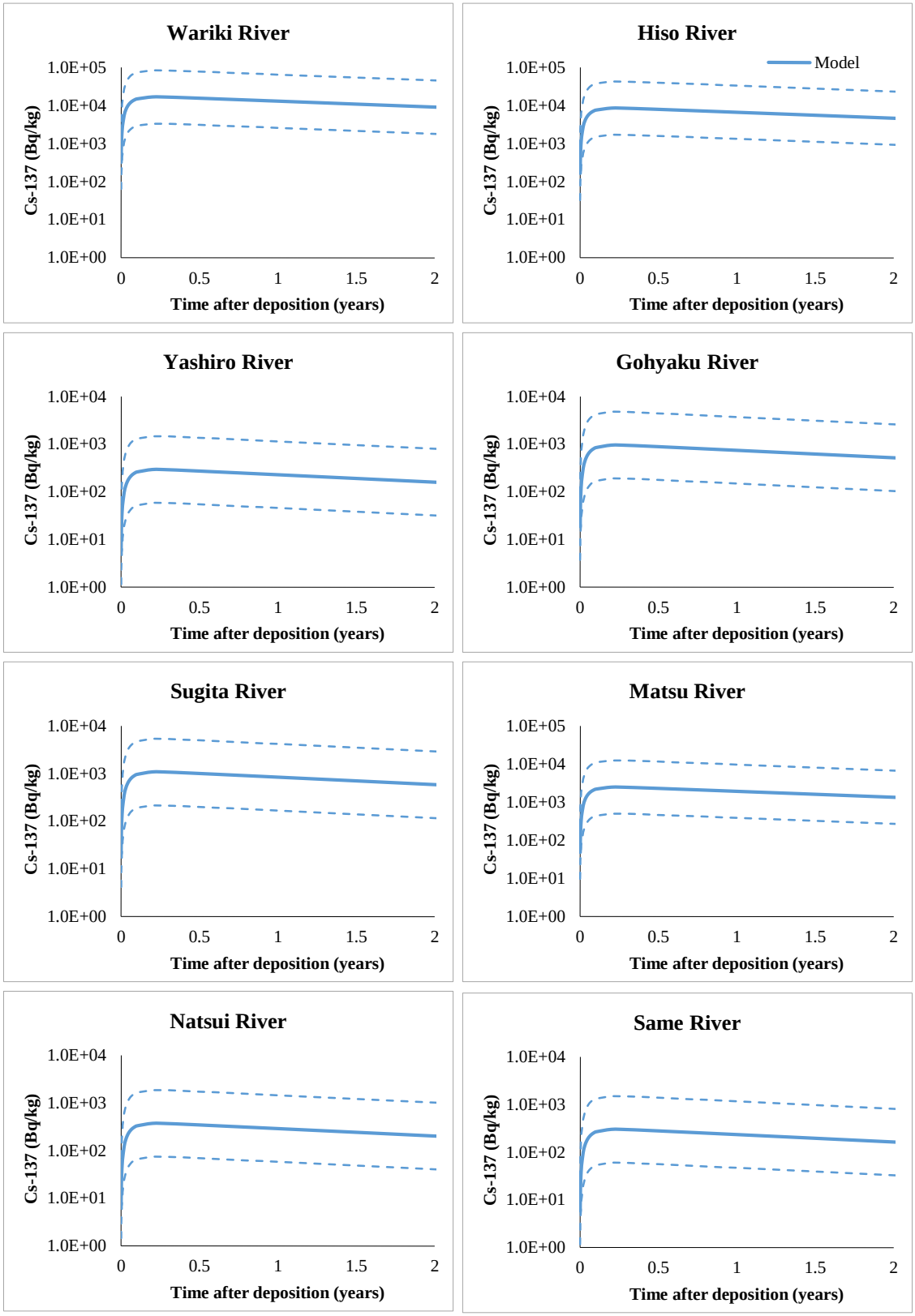

Figure D-1 (continued) Predictions of concentration (Bq kg^{-1}) in predatory fish at all eight rivers around Fukushima I NPSs, (a) ^{134}Cs in and (b) ^{137}Cs.

(a) ^{134}Cs in non-predatory fish

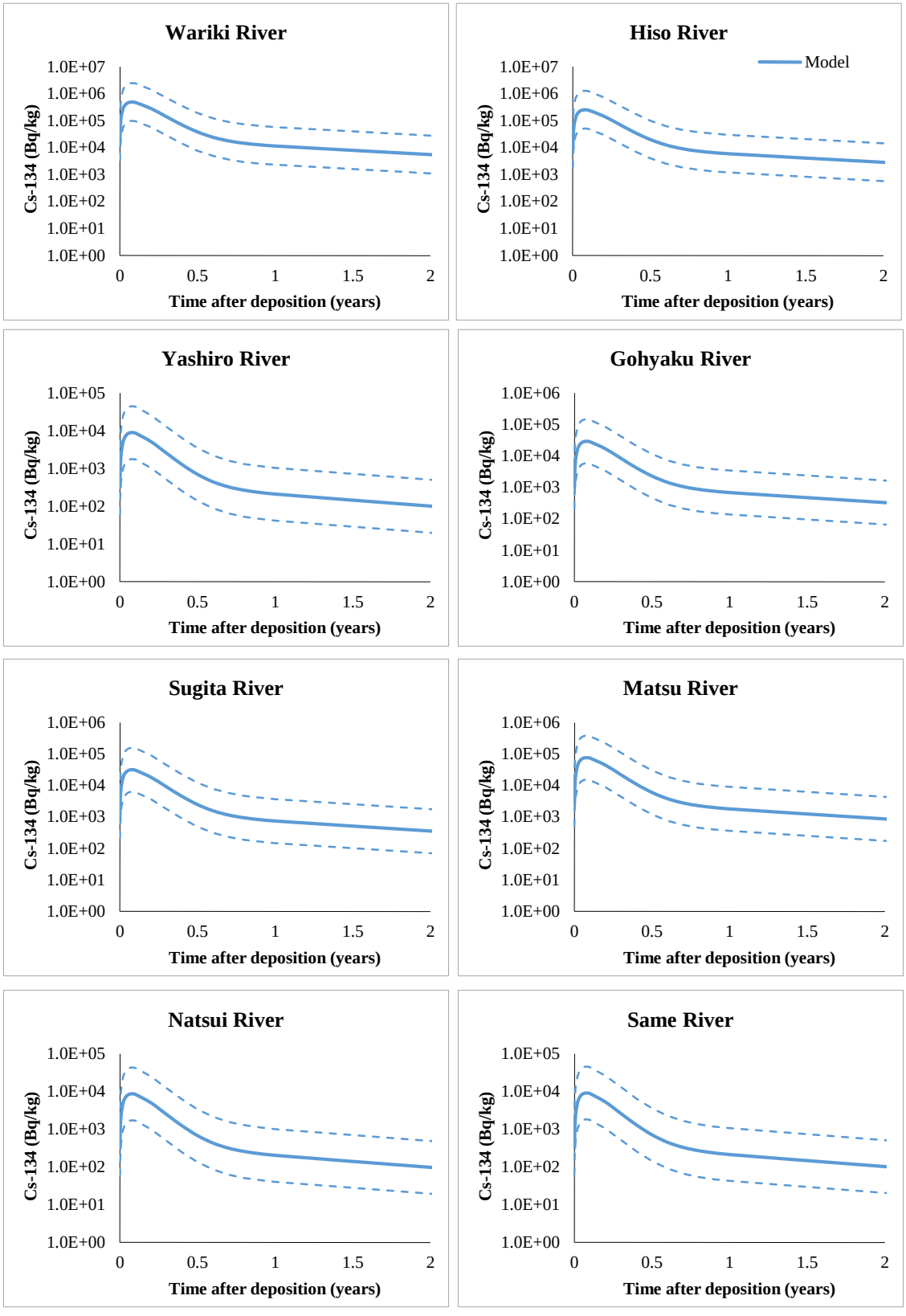

Figure D-2 Predictions of concentration (Bq kg^{-1}) in non-predatory fish at all eight rivers around Fukushima I NPSs, (a) ^{134}Cs in and (b) ^{137}Cs.

(b) ^{137}Cs in non-predatory fish

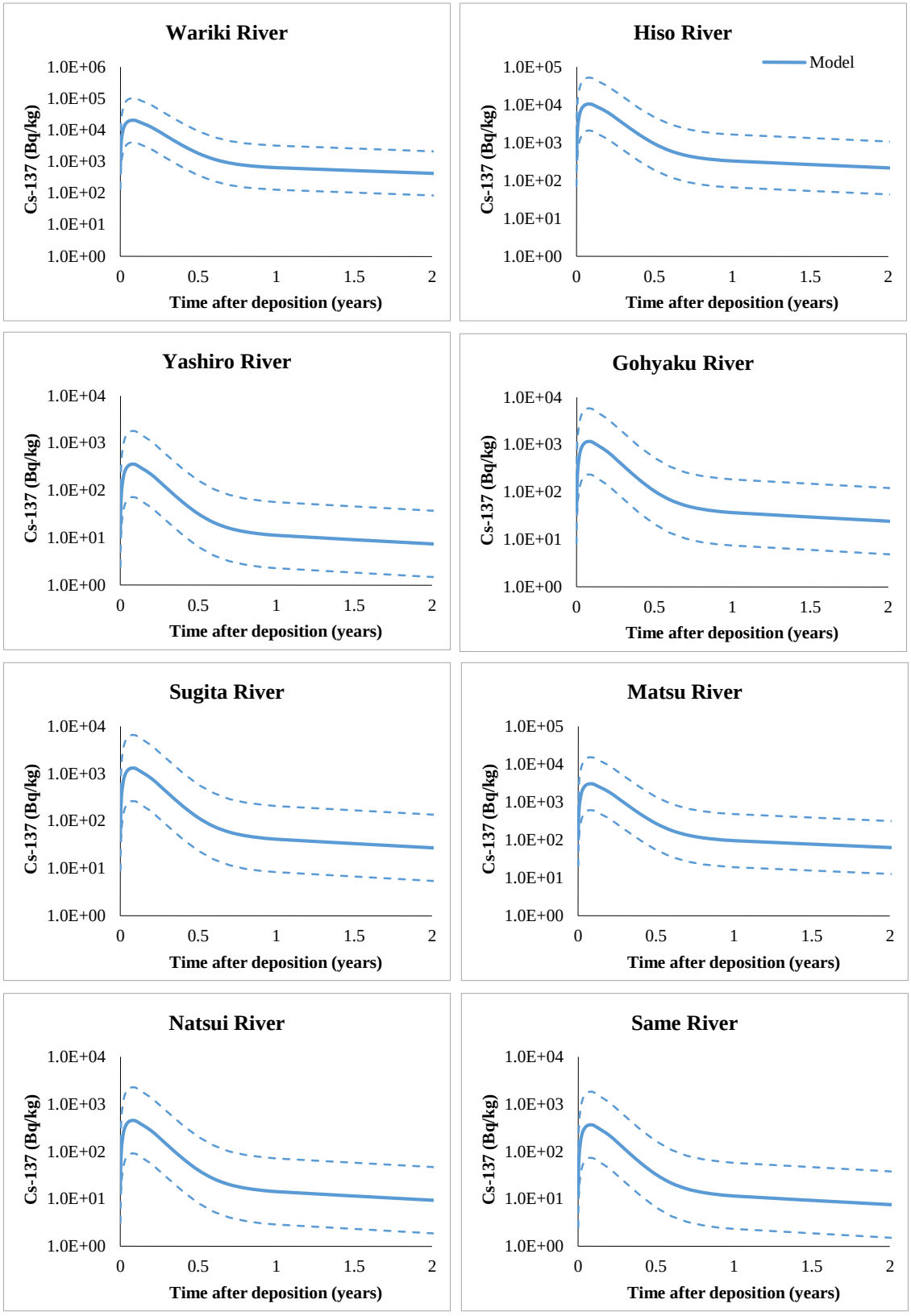

Figure D-2 (continued) Predictions of concentration (Bq kg^{-1}) in non-predatory fish at all eight rivers around Fukushima I NPSs, (a) ^{134}Cs in and (b) ^{137}Cs.

^{131}I in both predatory and non-predatory fish

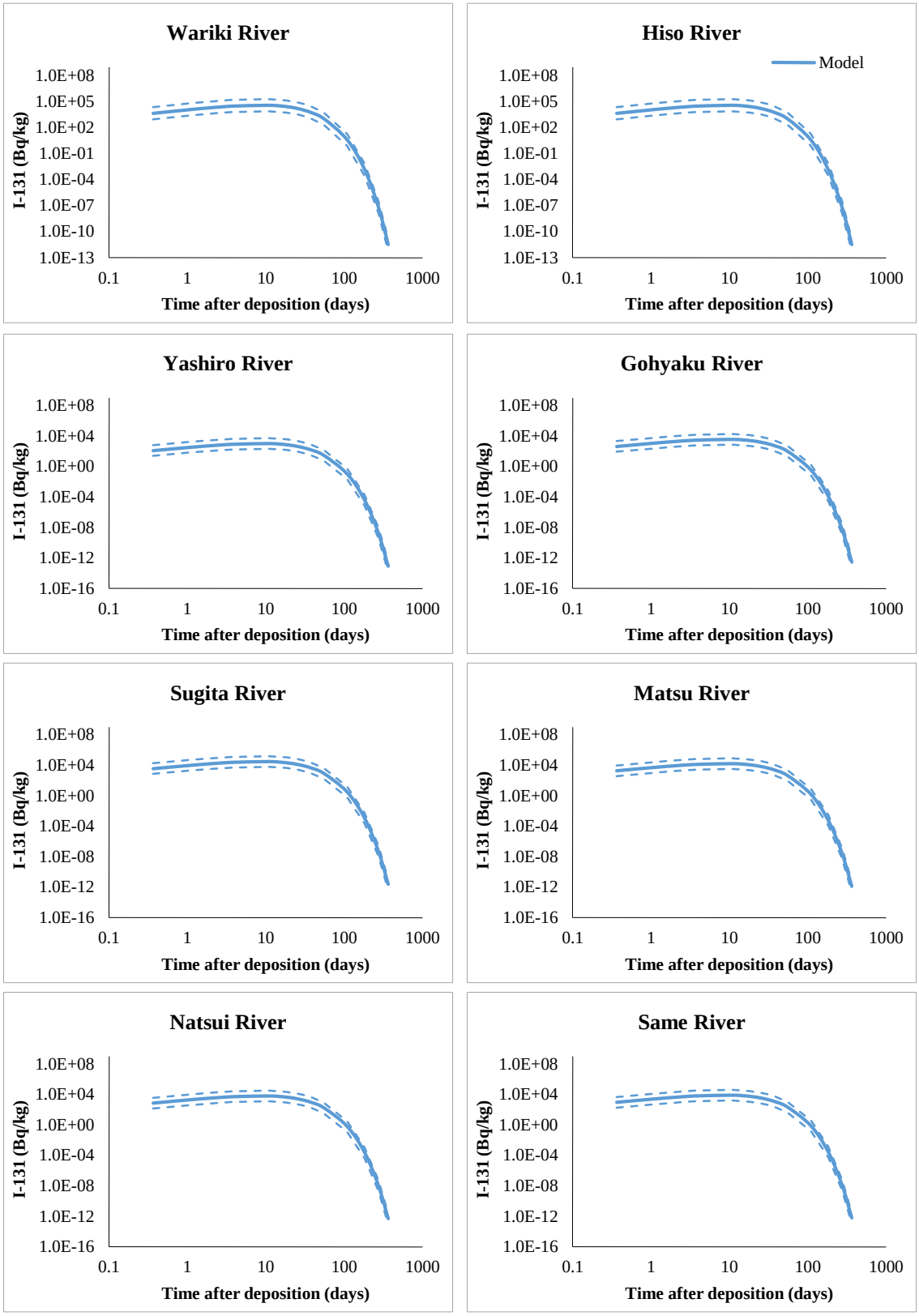

Figure D-3 Predictions of concentration (Bq kg^{-1}) of ^{131}I in both predatory and non-predatory fish at all eight rivers around Fukushima I NPSs.

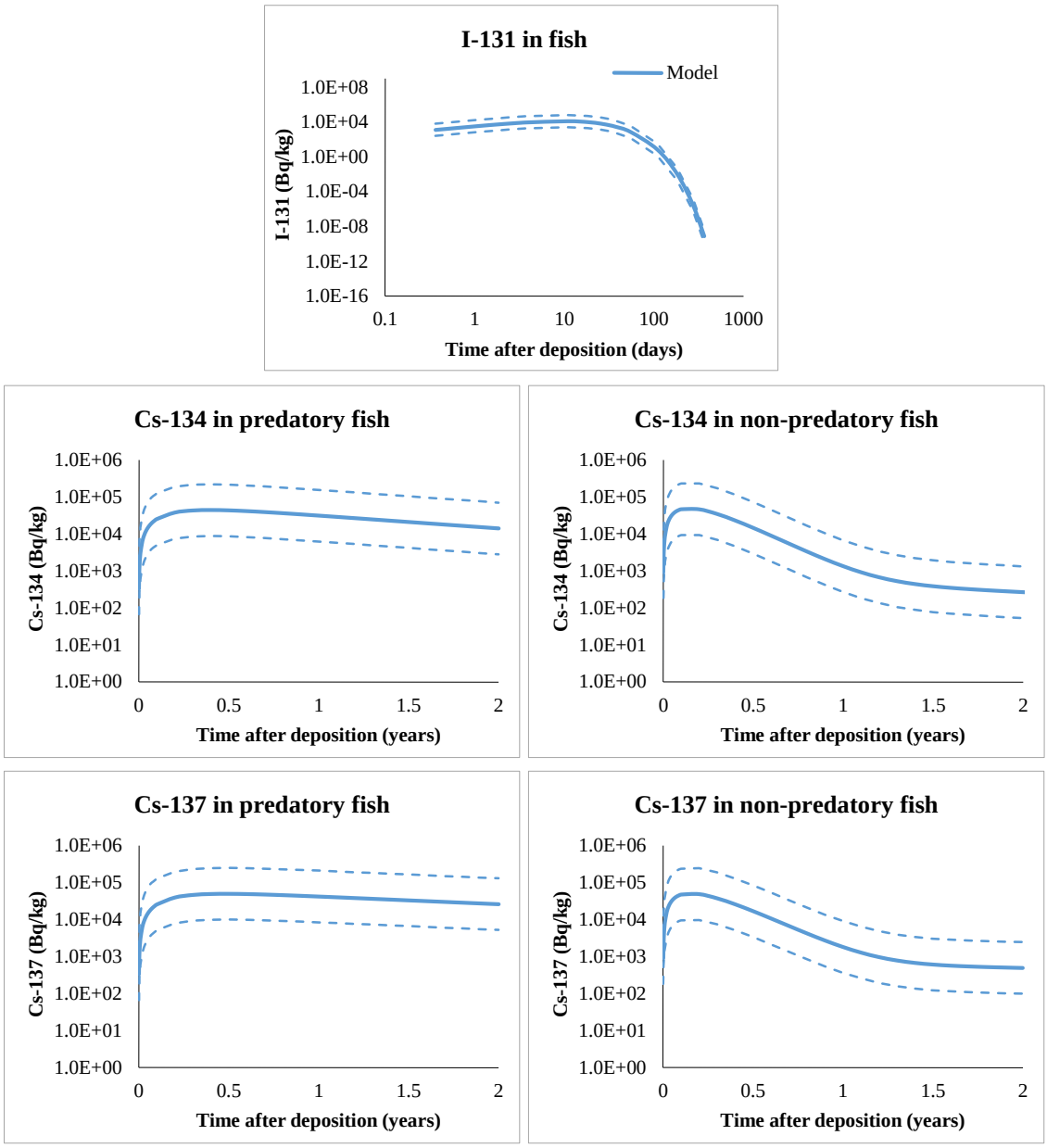

Figure D-4 Results of radioactivity concentration (Bq kg^{-1}) in fish at Iitate Lake.

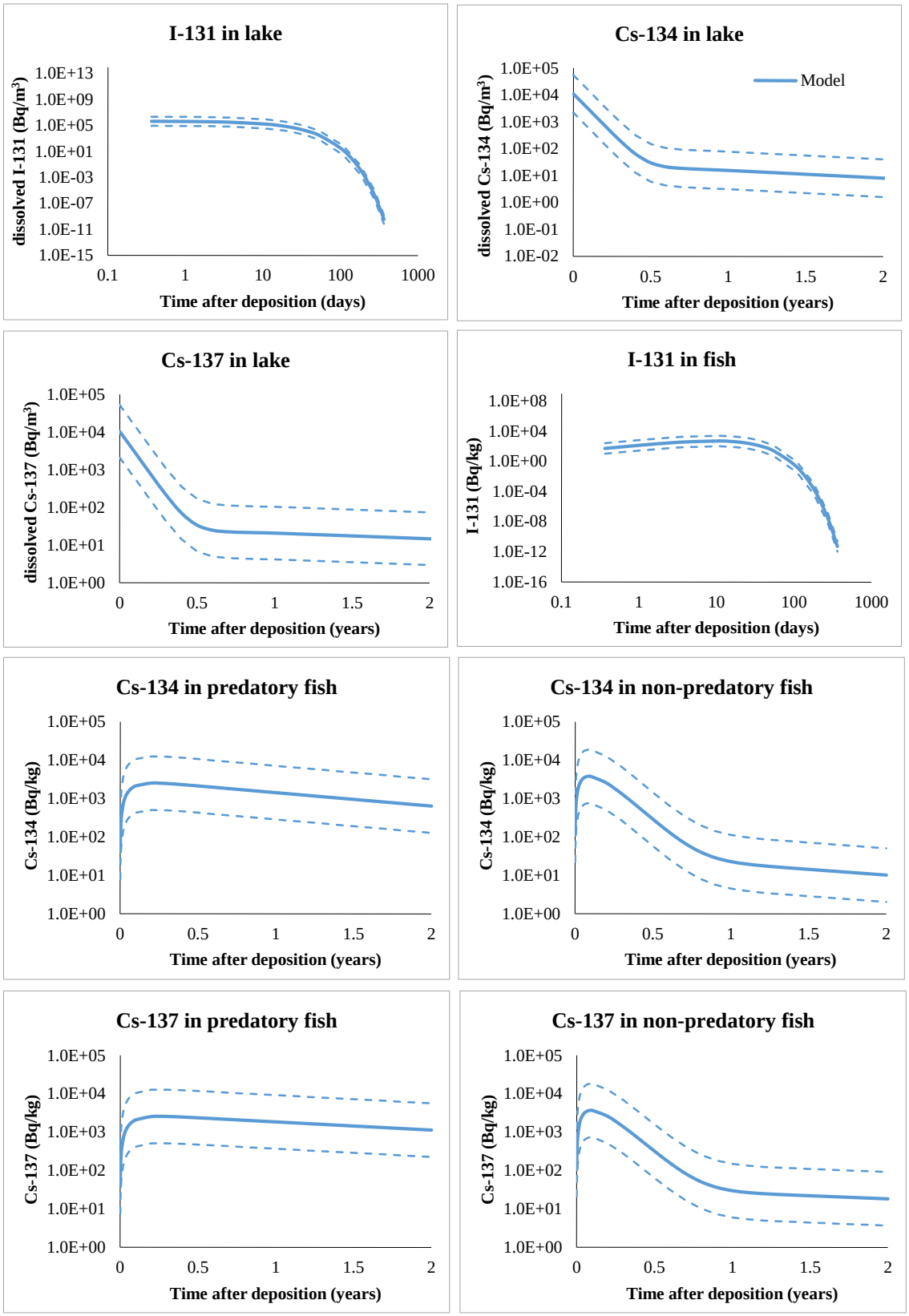

Figure D-5 Results of the model of radioactivity concentration (Bq kg^{-1}) in water and fish at Teganuma Lake.

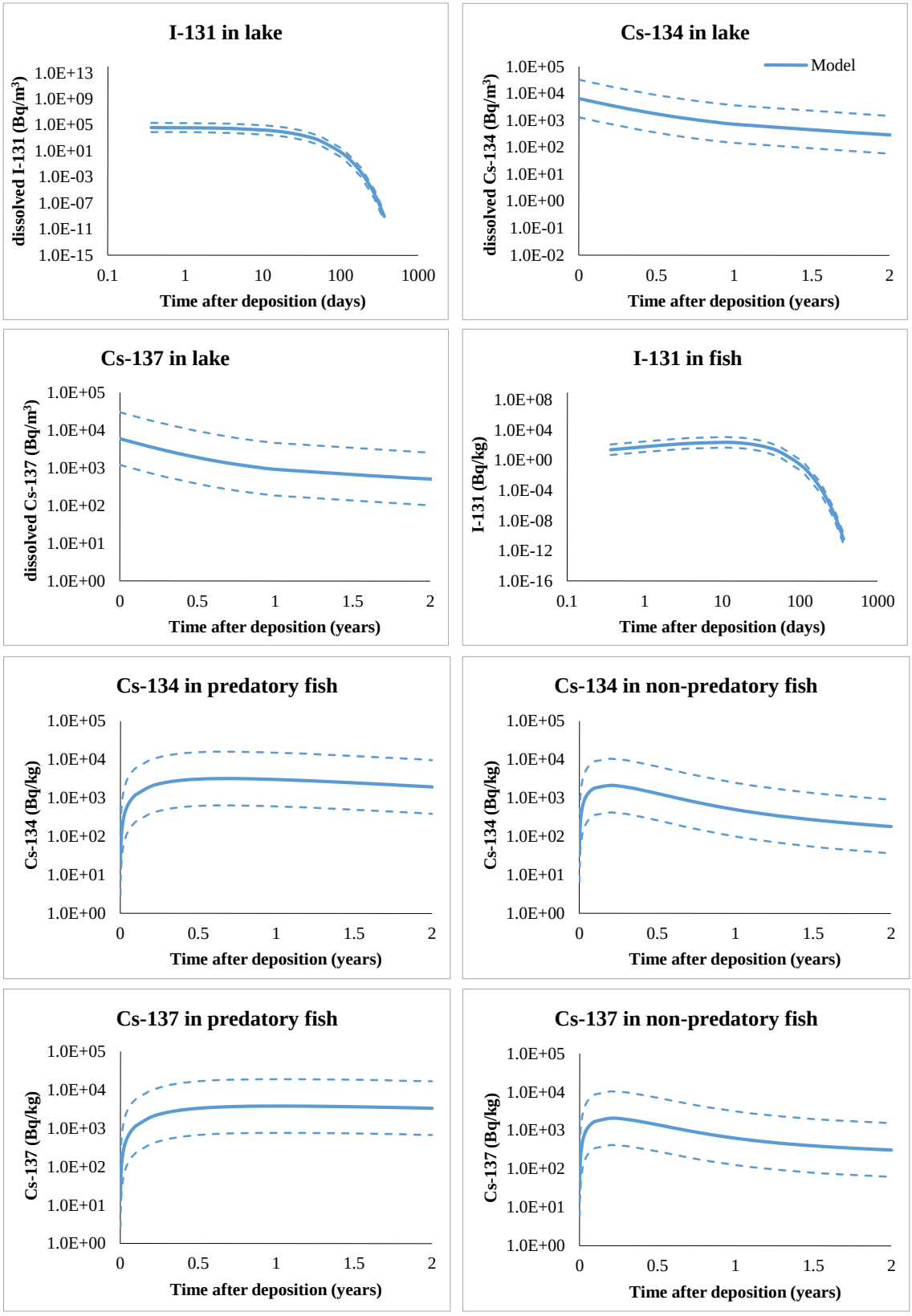

Figure D-6 Results of the model of radioactivity concentrations (Bq kg^{-1}) in water and fish at Kasumigaura Lake.

Appendix E Equilibrium of the short half-life nuclides

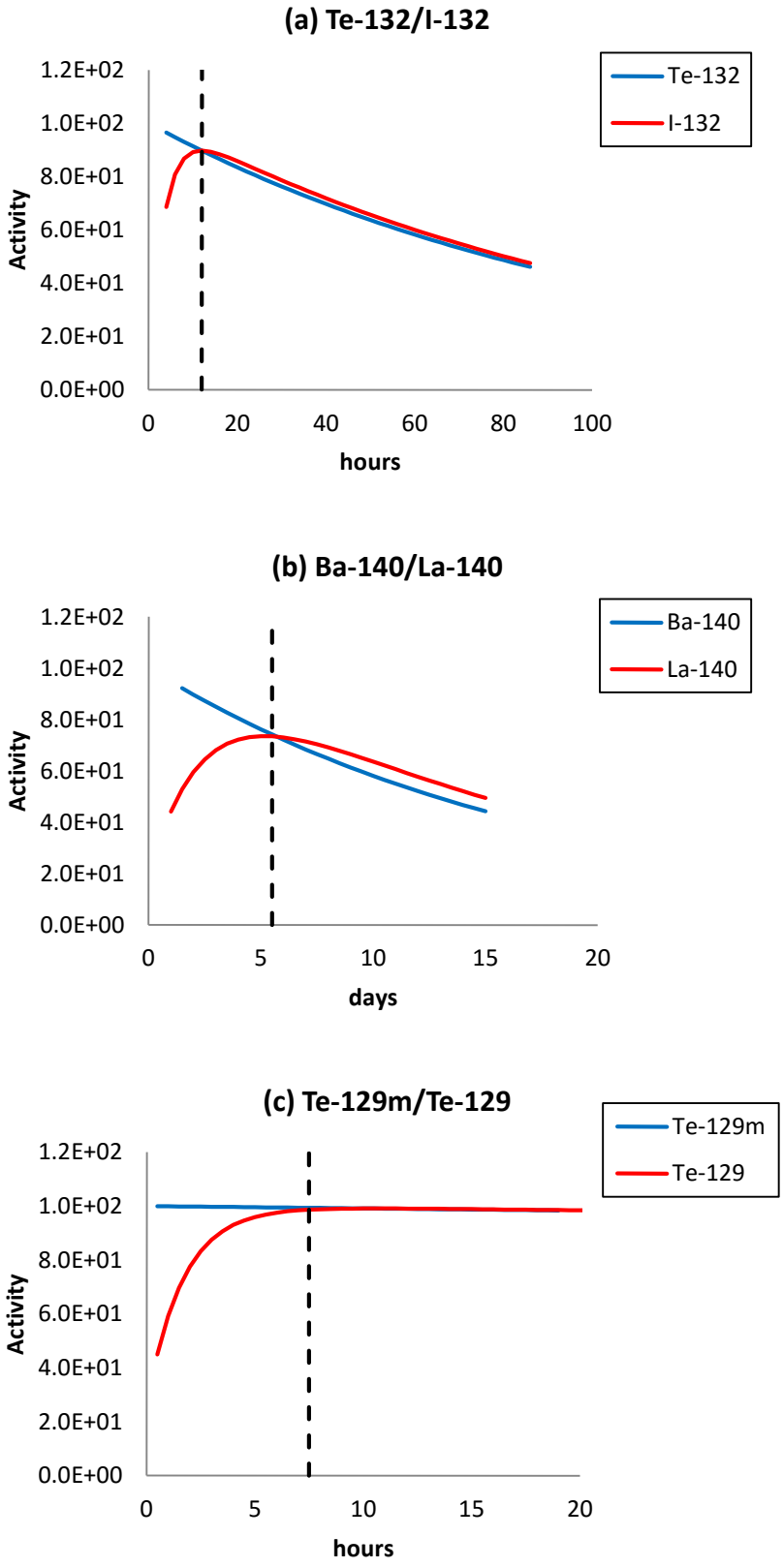

Figure E-1 Estimating the duration time to reach the equilibrium of the short half-life nuclides.

Appendix F Journal Publication

SCIENTIFIC REPORTS

OPEN

SUBJECT AREAS:
ATMOSPHERIC CHEMISTRY
ENVIRONMENTAL SCIENCES
BIOGEOCHEMISTRY
APPLIED PHYSICS

Received
10 May 2013

Accepted
12 August 2013

Published
10 September 2013

Correspondence and requests for materials should be addressed to J.T.S. (jim.smith@port.ac.uk)

*Current address: ZNF, University of Hamburg, Beim Schlump 83, 20144 Hamburg, Germany.

Worldwide isotope ratios of the Fukushima release and early-phase external dose reconstruction

Kittisak Chaisan[1], Jim T. Smith[1], Peter Bossew[2], Gerald Kirchner[2]* & Gennady V. Laptev[3]

[1]School of Earth and Environmental Sciences, University of Portsmouth, Portsmouth, PO1 3QL, UK, [2]German Federal Office for Radiation Protection, Köpenicker Allee 120-130, 10318 Berlin, Germany, [3]Ukrainian Institute of Hydrometeorology, Nauka Ave. 37, Kiev, 252028, Ukraine.

Measurements of radionuclides (RNs) in air made worldwide following the Fukushima accident are quantitatively compared with air and soil measurements made in Japan. Isotopic ratios RN:^{137}Cs of ^{131}I, ^{132}Te, ^{134,136}Cs, are correlated with distance from release. It is shown, for the first time, that both within Japan and globally, ratios RN:^{137}Cs in air were relatively constant for primarily particle associated radionuclides (^{134,136}Cs; ^{132}Te) but that ^{131}I shows much lower local (<80 km) isotope ratios in soils relative to ^{137}Cs. Derived isotope ratios are used to reconstruct external dose rate during the early phase post-accident. Model "blind" tests show more than 95% of predictions within a factor of two of measurements from 15 sites to the north, northwest and west of the power station. It is demonstrated that generic isotope ratios provide a sound basis for reconstruction of early-phase external dose rates in these most contaminated areas.

Following the accident at the Fukushima Dai-ichi (I) Nuclear Power Station (NPS), many measurements were made worldwide of radioisotopes in air. In Japan, the Japanese Ministry of Education, Culture, Sports, Science and Technology (MEXT) established daily measurement of gamma dose rate and deposited activity at a number of sites around the Fukushima I NPS, and within the highly contaminated area to the north and west (W, NW, N) of the plant. There were, however, relatively few sites where gamma-ray dose and deposited radioactivity monitoring were available to evaluate early-phase external dose rates, particularly in the Fukushima Prefecture[1]. ("Early-phase" is here defined as within the first 30 days following the accident, before external dose was dominated by relatively long-lived ^{134,137}Cs.) Since external dose rates declined rapidly due to decay of short-lived radionuclides[2], and external dose rates in other countries could not be measured directly, models are required for reconstruction of early-phase dose rates. This is of particular importance for the highly contaminated region to the northwest of Fukushima I NPS, some parts of which were still inhabited during the weeks after the accident[3].

This study represents the first systematic review of available air and soil monitoring data both in the highly contaminated areas of Japan and worldwide. Potential isotopic fractionation is evaluated over the long distances (from 10's of km to thousands) travelled, as was observed for a number of radionuclides after Chernobyl[4]. The study of the variation in isotope ratio with distance provides supporting evidence for a model to reconstruct early-phase external dose rates. Since there are relatively few measurements of early-phase dose rates, radionuclide depth profiles and isotopic composition, it is necessary to parameterise models for external dose rate based on generalized radionuclide isotope ratios. The model presented here, for the first time, generalises external dose models[5,6] to sites at which dose rate, isotopic composition and depth-distribution in soils data are not available. It is noted that, whilst isotope ratios of primarily particulate bound radionuclides were relatively even in the area to the north and west (W, NW, N) of Fukushima prefecture (formed largely by the 15 March release and rapid washout in rainfall), fallout to the south and southwest was also influenced by the March 21–23 rainfall event and characterized by more variable isotope ratios[7]. We will here focus on the area to the north, northwest and west for which external dose rate data are available for model testing and calibration, though in principle the approach could be used for other areas.

Results

Mean isotope ratios. The change in radionuclide (RN) ratios RN:^{137}Cs in air (particulate phase) and soil with distance from the Fukushima I NPS are shown in Figure 1 and Table 1. As shown in Table 1, ^{131}I/^{137}Cs isotope

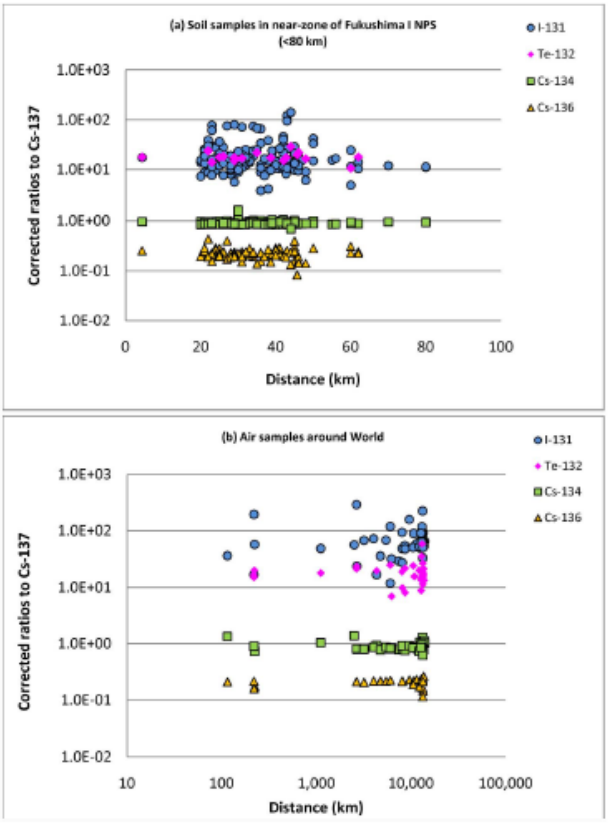

Figure 1 | Average corrected ratios to ^{137}Cs of ^{131}I, ^{134,136}Cs and ^{132}Te in (a) soils and (b) air particulates (data for gaseous-phase ^{131}I are shown in Figure 3). Many of the I-131 measurements in air taken in the vicinity of Fukushima NPS were excluded from (b) as sampling did not begin until some days after the radionuclide release.

Table 1 | Average corrected mean ratios to ^{137}Cs from release of Fukushima (±2 S.E., based on variation of means between sites)

Radioisotope	Soil samples in near-zone (<80 km)	Air samples in near-zone (<80 km) Particulate	Air samples in Japan (80–2,000 km) Particulate	Air samples in Pacific Ocean and US (2,000–12,000 km) Particulate	Air samples in EU (>12,000 km) Particulate
^{131}I	22.5 ± 3.7 Sites – 145 Samples – 1,844	31.8 ± 12.9 * Sites – 22 Samples – 90	70.9 ± 63.5 Sites – 5 Samples – 234	69.5 ± 26.9 Sites – 20 Samples – 457	77.1 ± 16.6 Sites – 22 Samples – 196
^{132}Te	18.3 ± 1.7 Sites – 20 Samples – 20	No data	17.5 ± 2.1 Sites – 5 Samples – 226	17.1 ± 4.2 Sites – 21 Samples – 455	22.0 ± 6.0 Sites – 22 Samples – 196
^{134}Cs	0.90 ± 0.01 Sites – 146 Samples – 1,866	1.03 ± 0.10 Sites – 17 Samples – 68	0.99 ± 0.21 Sites – 5 Samples – 217	0.87 ± 0.06 Sites – 20 Samples – 420	0.91 ± 0.07 Sites – 22 Samples – 193
^{136}Cs	0.22 ± 0.01 Sites – 88 Samples – 297	No data	0.19 ± 0.03 Sites – 4 Samples – 105	0.22 ± 0.04 Sites – 11 Samples – 184	0.20 ± 0.03 Sites – 9 Samples – 27

*Note that these measurements began 4–5 days after the passage of the initial plumes so, because the ^{131}I/^{137}Cs ratio varied with release time, cannot be directly compared with other data and are not included in Figure 1.

ratios in soil deposits in the area within 80 km of Fukushima I NPS (mean ratio $^{131}I/^{137}Cs$ = 22.5) were low compared to those in air particulates worldwide (ratio ca. 70–80). The measurements in soil in the key region to the NW of Fukushima I NPS (Figure 2) show a highly significant inverse correlation between the ^{131}I:^{137}Cs ratio and the ^{137}Cs activity concentration (Spearman's correlation coefficient −0.54; N = 89; $p < 0.001$). The best fit equation (using the Akaike Information Criterion[8]) to these data was of the form

$$^{131}I : {}^{137}Cs \text{ ratio} = a(C_{137Cs})^b + c \quad (1)$$

as shown in Figure 2 in comparison with a standard power law fit (i.e. excluding the intercept c).

Parameter values for the fitted equations are shown in Figure 2. [Model fits were carried out on log-transformed data of the concentration of each isotope in soil (C_{131I} vs C_{137Cs}) then back-transformed and expressed as a ratio ^{131}I:^{137}Cs for presentation of results.] Note that Equation (1) is only applicable in the high fallout areas (>*ca.* 300 Bq kg^{-1} ^{137}Cs) to the north, northwest and west of Fukushima I NPS. For lower C_{Cs137} fallout areas, a generic value of 76 could be used (the value of the ratio at 300 Bq kg^{-1} of ^{137}Cs). The value of 300 Bq kg^{-1} is the lower bound of available ^{131}I:^{137}Cs measurements in soil (see fig. 2). The choice of this lower bound value (^{131}I:^{137}Cs ratio = 76 at 300 Bq kg^{-1} ^{137}Cs) is supported by the far field particulate air monitoring data in Japan, Europe and North America (ratio = 70–80, Table 1). Given efficient washout of the particulate form of ^{131}I the far-field air particulate ratio is likely to be more accurate, though the higher gaseous phase ratio (discussed below) could be used if conservative estimates of dose are required. It is noted that fallout to the south and southwest of Fukushima I NPS was also influenced by the March 21 rainfall event and characterized by different isotope ratios[7]; more site-specific ratios may be required for these areas.

Measurements of gaseous and particulate ^{131}I in Japan in the early stages of the accident (15/16 March) were only available at two sites: Nuclear Science Research Institute, Tokai-mura[9] and the High Energy Linear Accelerator Research Centre, Tsukuba[10] (respectively, 120 and 160 km south of Fukushima I NPS). Measurements from other sites worldwide began later, but due to longer travel times, captured the peak air concentrations from the early stages of the accident. Figure 3 shows the available mean ^{131}I:^{137}Cs ratios of both gaseous and particulate phase ^{131}I as a function of distance.

External dose model. Equation (2) (*Methods* section, below) was used to quantify the time change in external dose rate at each of six sites to the north and west (W, NW, N) of Fukushima I NPS (for map see Supplementary Fig. S1). The measured radiocaesium activity concentration in soil at each site was used as the independent, the measured dose rate as the dependent variable in a linear regression model (Eq. 2, *Methods* section). Activity concentrations of other radioisotopes were estimated using the generic mean RN:^{137}Cs ratios in Table 2. For ^{131}I, the relation between ^{131}I:^{137}Cs ratio and measured ^{137}Cs activity concentration was used (Eq. 1; Figure 2). For other radionuclides, mean isotope ratios measured in soil within 80 km were used (longer-range isotope ratios were observed to be similar). Model fits to measured external gamma dose rate are shown in Figure 4 for the six sites for which "good" time-series of dose rate were available; "good" means that the investigated period is exhaustively covered by a high number of observations.

Given that only one site-specific input parameter (^{137}Cs activity concentration) and one fitting parameter (A, a measure of absorption of gamma rays in the soil) are used in the model, the fits show good agreement with observations. This confirms the accuracy of the derived mean isotope ratios. A slight tendency to under-predict dose rates in the period from 20–80 days is likely due to differences in absorption in soil at different sites, and (relatively small) local variation in isotope ratios. The model sensitivity to uncertainty in ^{131}I:^{137}Cs ratio, and in the value of A is evaluated in Figures 5 and 6.

In Fig. 5, the data are shown together with the model using the mean value of A, the mean radionuclide ratios (Table 2) (bold line), and the model with the mean ^{131}I:^{137}Cs ratio r (Eq. 1 parameterized as in Table 2) replaced by $r \pm 2\sigma(R)$ (dotted curves). Sigma (σ) represents the standard deviation in the residuals of the fit of Eq. 1 to observed data (std. deviation of $r_{measured}/r_{modelled}$ where r is the $^{131}I/^{137}Cs$ ratio: these were normally distributed; Kolmogorov-Smirnov test in IBM SPSS Statistics 20). In Fig. 6, the data are again shown with the model, using the mean value of A and the mean radionuclide ratios (Table 2) (bold line), and the model with the minimum and maximum observed A values (6.0–14.2) × 10^{-5}) instead (dotted lines).

Blind testing of the model. The external dose model was blind tested by comparing predictions of the change in external gamma dose rate with time against measurements at a further fifteen sites. Figure 7 plots model blind predicted dose rates against those measured at four of the fifteen test sites (see Supplementary Figure S4 for the remainder). Figure 8 compares model predictions against data

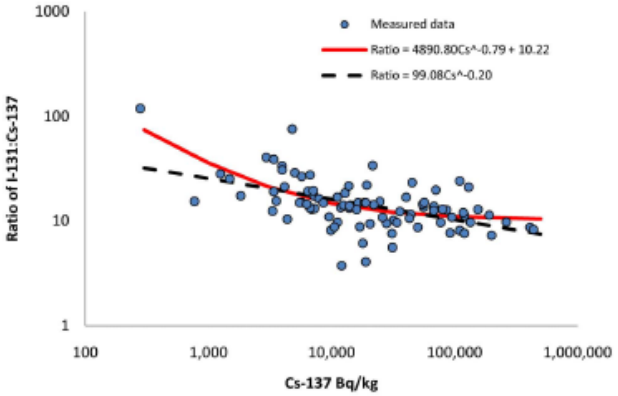

Figure 2 | Scatter plot of ratio of I-131 to Cs-137 against activity of Cs-137 in soil around Fukushima I NPS. In areas of very high radiocaesium fallout, the ratio $^{131}I/^{137}Cs$ is much lower than in areas of lower radiocaesium fallout.

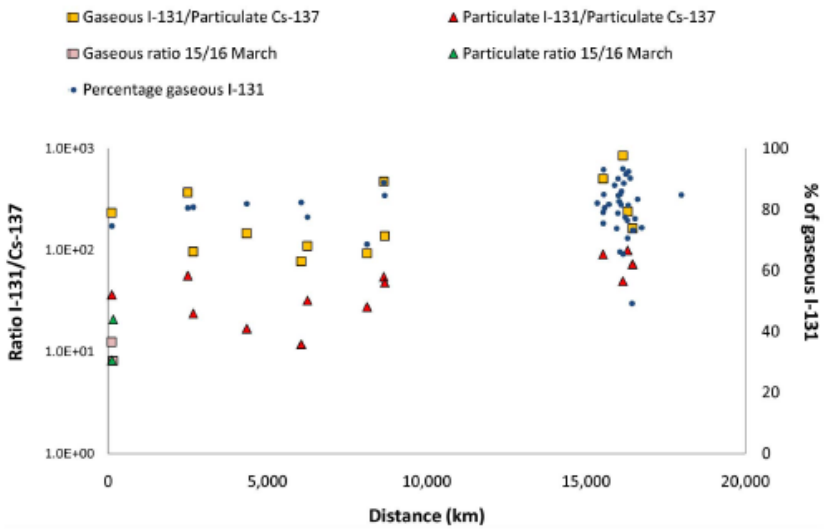

Figure 3 | Ratios of particulate and gaseous ^{131}I to particulate ^{137}Cs with distance from Fukushima I NPS. At two sites 120 and 160 km to the south of the accident site, lower ^{131}I:^{137}Cs ratios were observed in both phases on 15 March.

from six calibration sites plus the fifteen test sites. Ninety-five percent of measured values are within a factor of two of predictions.

The pattern of data in Figure 8 (b) appears "stepwise" because of short term variability in the measurements at a given site (likely due primarily to soil moisture content and measurement uncertainty). The model does not (and does not aim to) reproduce this variability. This results, for longer (>30 days) time periods, in variation in the measured value with little variation in the model prediction for a given site, giving the apparent "stepwise" pattern. The uncertainty in the measurement of external dose rate is expected to be small in comparison with uncertainties introduced by varying isotope ratios at individual sites (particularly ^{131}I:^{137}Cs ratio) and varying early-phase depth distributions.

Discussion

As was observed after Chernobyl[11], ratios of the radiocaesium isotopes (^{134}Cs:^{137}Cs; ^{136}Cs:^{137}Cs) show low variability and are relatively constant with distance (as observed in Japan[7]). It should be noted, however, that there appears to be a slightly higher ^{134}Cs/^{137}Cs ratio in air within 80 km of Fukushima I NPS than >80 km (Table 1), potentially due to differences between release events: ^{134}Cs:^{137}Cs ratios may vary according to the source of contamination depending on fuel age in a given reactor[12]. A shift of this isotope ratio had been noted in Europe and attributed to the small fraction of ^{137}Cs released during the Chernobyl accident or nuclear weapons test fallout still present in the atmosphere[12]. However, radiocaesium concentrations in Japan were too high to be significantly influenced by atmospheric ^{137}Cs from these sources. The mean ^{132}Te:^{137}Cs ratio shows relatively little difference between air concentrations and soil deposits, and no evidence of fractionation with distance (though there is significant variability in values from different sites). This is likely because both are mainly transported as fine particulates. The slight variations in ratios of primarily particulate-bound radionuclides would not significantly affect external dose rate predictions.

In contrast to the primarily particulate-borne radionuclides, the (particulate) ^{131}I:^{137}Cs ratios in air are significantly more variable, and are much higher, on average, than those measured in soil near to the Fukushima I NPS. Apparently lower ratios in air are observed within 80 km of the Fukushima I NPS (Table 1) compared to those measured in the U.S. and Europe. These data, however, must be interpreted with caution since significant air monitoring in the Fukushima area only began 4–5 days after passage of the initial

Table 2 | Summary of the parameter values used in the predictive model*

Radioelements	Decay constant (d^{-1})	Emitted gamma energy (MeV/nt)	Ratio to ^{137}Cs	A
^{131}I	8.64E-02	0.3828	$R_{1311} = 4.89 \times 10^3 \times C_{137Cs}{}^{-0.76} + 10.22$	$A = 9.17 \times 10^{-5}$
^{132}Te	2.16E-01	0.2344	18.30	
^{132}I	2.16E-01+	2.2645		
^{134}Cs	9.20E-04	1.5551	0.90	
^{136}Cs	5.27E-02	2.1283	0.22	
^{137}Cs	6.29E-05	0.5963	1.00	

*R_{1311} is the ratio of ^{131}I:^{137}Cs and C_{137Cs} is the mean activity concentration of ^{137}Cs (Bq/kg) in soil. The relationship for R_{1311} is only valid in areas of relatively high fallout (C_{137Cs} > 300 Bq kg^{-1}). For areas of lower fallout, a value of R_{1311} = 76 should be used.
†^{132}I is in secular equilibrium with ^{132}Te hence follows the ^{132}Te decay curve.

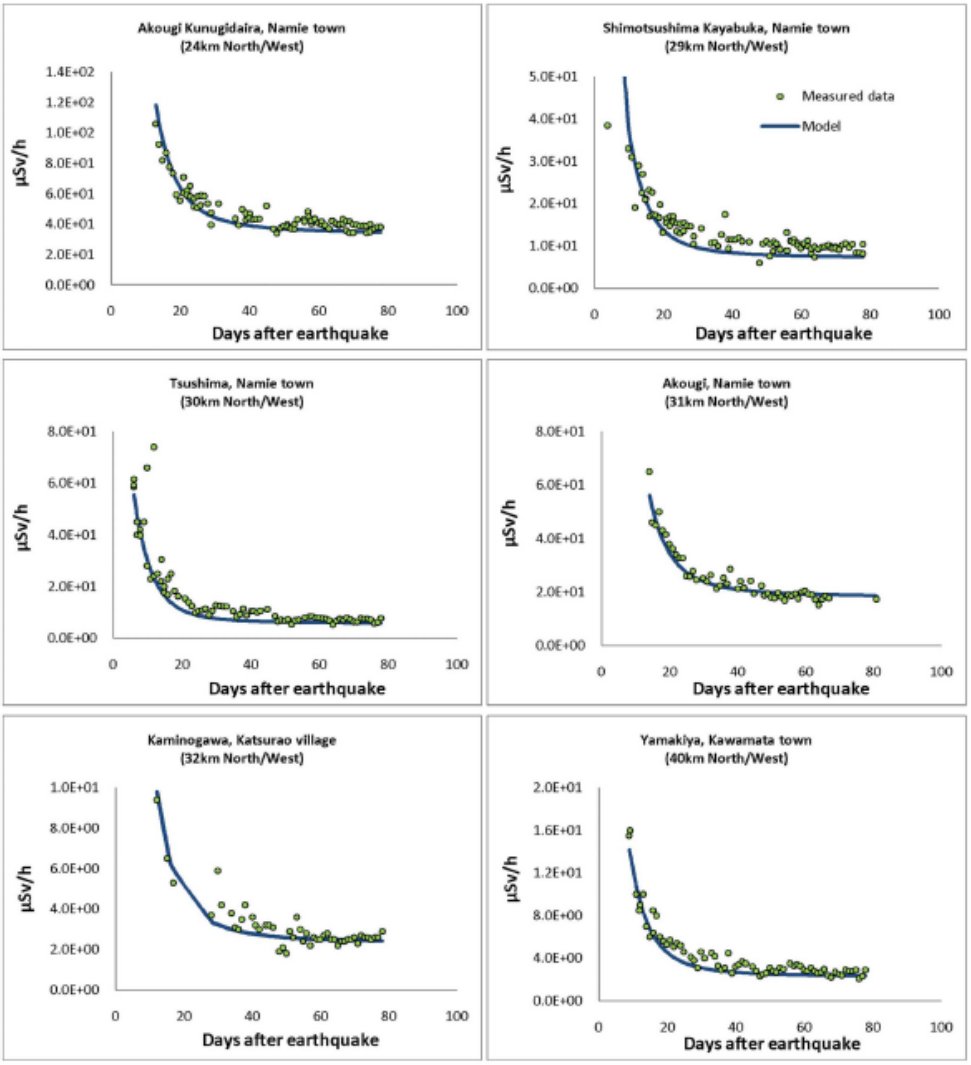

Figure 4 | Model fits to measured gamma dose rates obtained using generic isotope ratios for radiocaesium isotopes and ^{132}Te, and using a regression Equation (Eq. 1) for ^{131}I; the *A* parameter is fitted to the data using SAS (SAS Institute Inc.).

contamination plumes. Thus much of the local (<80 km) ^{131}I/^{137}Cs air monitoring data are not shown in Figure 1b.

The limited data for two Japanese sites on 15 March (peak release period) suggests lower ^{131}I:^{137}Cs ratios in both particulate and gaseous phases at this time, as illustrated in Figure 3 (mean of two sites: 14.6 for particulate ^{131}I:^{137}Cs and 10.3 gaseous ^{131}I:particulate ^{137}Cs), and much lower fraction of ^{131}I in the gaseous phase. The observed low ratios of ^{131}I relative to ^{137}Cs in soil deposits in areas of high fallout (Fig. 2) are consistent with these limited data in air in Japan on 15th March (Fig. 3) and with the expected ratio in the source term at this time[13]. Thus, the constant in the regression equation (Eq. 1, Fig. 2: c = 10.2 with 95% confidence interval 7.7–12.8) for the iodine ratio in soil is similar to the limited measurements in air in Japan on 15th/16th March. This likely reflects the fact that the contamination plume to the northwest of Fukushima INPS was formed from deposition with low ^{131}I:^{137}Cs isotope ratio from the peak release on 15th March. Rain

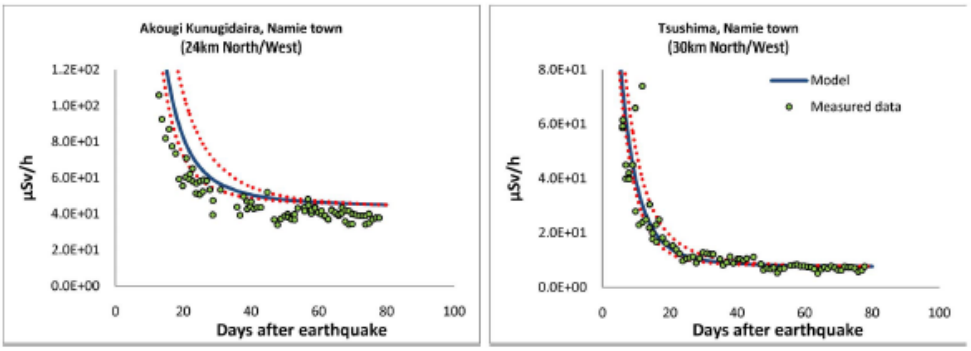

Figure 5 | Model results using a generic mean *A* value and isotope ratios (bold lines) with ±2σ uncertainty in estimation of I-131/Cs-137 ratio (dotted lines) compared with the measurement data at two of the six calibration sites. The values of *A* and isotope ratios were the generic values from Table 2: not fitted to the data. The graphs for the other four sites are shown in Supplementary Information Figure S2.

was observed in the Fukushima prefecture during the night from 17:00 on March 15 to 04:00 on March 16[7]: this time corresponded with significant emissions.

The relatively low ^{131}I:^{137}Cs isotope ratios observed in the areas of high fallout and in the 15th March air monitoring data in Japan (Figs. 2 and 3) are not seen in the measurements in other countries. The ^{131}I:^{137}Cs ratios in both phases at longer distances were much higher, even in the peak corresponding to the early (12–15 March) releases from Fukushima. Mean values were 73.1 (N = 48 range 12–290) for ^{131}I:^{137}Cs particulate and 269 (N = 13 range 78–853) for the ratio of gaseous ^{131}I to particulate ^{137}Cs. The much higher ^{131}I:^{137}Cs isotope ratios observed at long distances suggest highly efficient deposition of the 15th March release (characterised by low I/Cs ratios[13]) in the area to the northwest of Fukushima I NPS.

There is no clear evidence of a significant change in ^{131}I:^{137}Cs ratio over long distances in either airborne particulate or gaseous phases (Fig. 3). But there appears to be a (non-significant) trend of increasing ratio with distance potentially implying more efficient deposition of ^{137}Cs. This appears to be in contrast to observations following the Chernobyl accident[4] which showed generally *decreasing* ^{131}I:^{137}Cs ratio with distance due to greater dry deposition of gaseous and particulate ^{131}I. It should be noted, however, that this observation was based on relatively few data and, in the Chernobyl near-zone, radiocaesium deposition rates may have exceeded ^{131}I due to fallout of larger airborne particulates including fuel particles[14].

Mean fractions of gaseous phase ^{131}I were relatively constant with distance (Fig. 3), with mean gaseous fraction 80.4% ((standard error (S.E.) 1.3%; range 49.2–93.4%). The consistency of gaseous fractions of ^{131}I over long distances implies relatively little transfer from gaseous to particulate form. As discussed by Masson et al.[15], "^{131}I [from Fukushima] remains mainly in its gaseous form during transport. Thus, the transfer from gaseous to particulate form, if it exists, was not sufficient within the two-week interval to counterbalance the decrease of particulate ^{131}I due to its deposition, mainly by rain."

The external dose model shows good agreement with data from the fifteen blind test sites (Figures 7, 8 and Supplementary Fig. S4), implying that the model and parameter values are generally applicable to other sites in areas to the north, northwest and west of Fukushima I NPS. Given the consistency of isotope ratios at greater distances (and good agreement between "low fallout" $^{131}I/^{137}Cs$ ratio of 76 and the mean of 70–80 observed in the long distance data in Table 1), the model could be used to estimate the very much lower external dose rates in other countries.

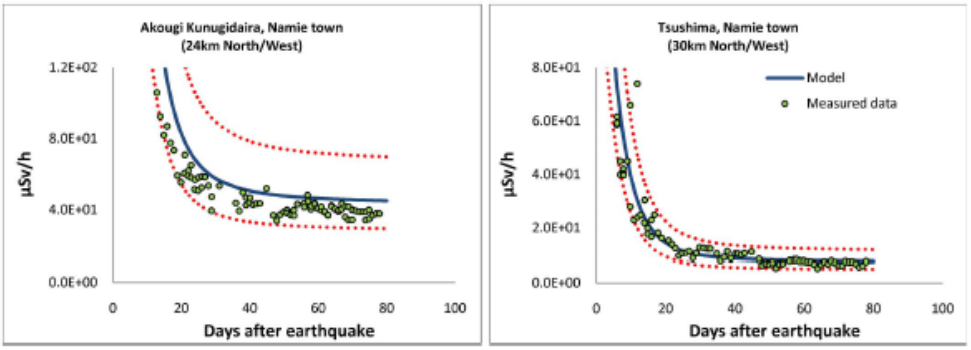

Figure 6 | Model results using generic *A* value and isotope ratios (Table 2) (bold lines) with ±2σ uncertainty in estimates of the A-parameter (dotted lines) compared with the measurement data at two calibration sites. The graphs for the other four sites are shown in Supplementary Information, Figure S3. The values of *A* and isotope ratios were the generic values from Table 2: not fitted to the data.

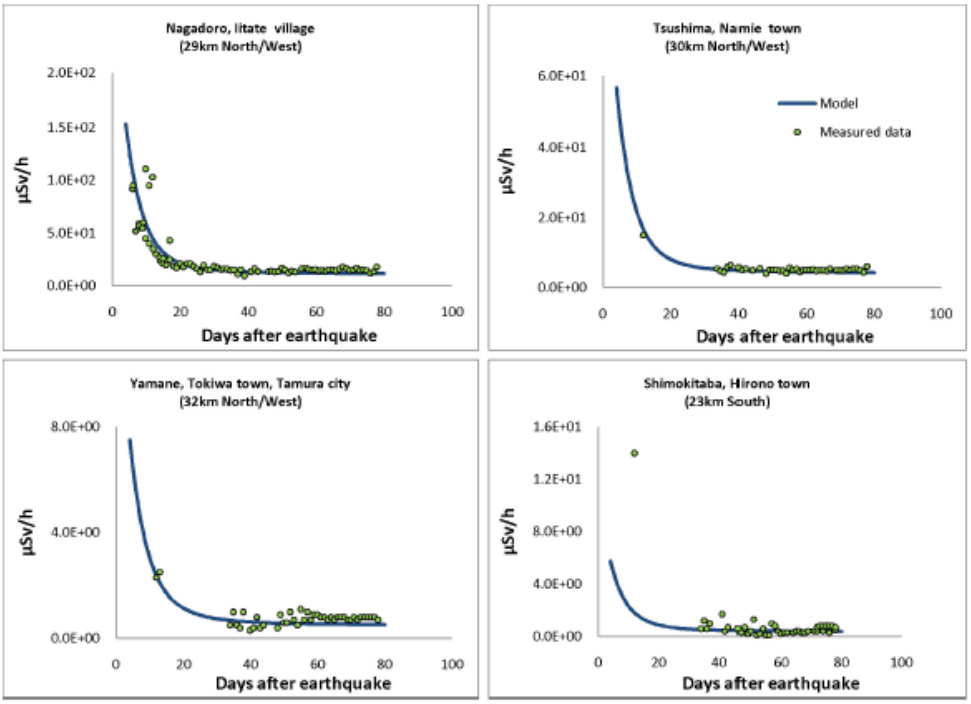

Figure 7 | Blind prediction of external gamma dose vs days since the earthquake using only measured Cs-137 concentration at each of four sites as an input variable. The graphs illustrate the good fit in regions to the North and West, but, as expected, relatively poorer fit at the one site to the south. For blind predictions at all 15 test sites, see Supplementary Information Figure S4.

The fitted values of the *A* parameter (primarily a measure of absorption of gamma rays in soil) at the six calibration sites were in a relatively narrow range ($(6.0–14.2) \times 10^{-5}$) with mean 9.2×10^{-5}. This relatively narrow range gives confidence that values of this unknown parameter can be extrapolated to reconstruct external dose rates at other sites, on the basis only of the measured ^{137}Cs activity concentration. It also implies that, in the early phase, soil self-shielding was broadly similar across the different sites.

The results of the model sensitivity analysis (Figures 5, 6 and Supplementary Figures S2, S3) are consistent with the factor of two uncertainty range of model predictions in blind testing, implying that the value of the *A* parameter, representing to a large extent soil shielding, and of the ^{131}I:^{137}Cs ratio, are the greatest source of model uncertainty. Under conditions of high rainfall, radiocaesium can penetrate relatively deeply into the soil profile[16], however in most areas affected by Chernobyl[14], and at Fukushima[17], the majority of radioactivity remained near the soil surface, limiting gamma-ray absorption within the soil. Over years to decades after fallout, gamma dose rates will decline due to radioactive decay and further slow penetration of radiocaesium into the soil profile[14,16].

In summary, uncertainty in model predictions results from: attenuation and shift of the energy spectrum by penetration of fallout into the soil; geometry of the dose rate monitors (i.e. response to given contamination); uncertainty of the I/Cs ratio, and possibly different fallout episodes with different radionuclide ratios. Nevertheless, the model shows good agreement with measured dose rates against test data, providing strong evidence for the ability of such models to extrapolate dose rates at sites for which early phase dose rates and isotopic compositon are not available. In principle, the model could be applied to other areas of Japan, outside the areas to the north and northwest considered here, by adapting in particular to take account of the important second deposition event (21 March) to the south and southwest.

Methods

Isotope ratios and key radionuclides. Measurements of radionuclides in air and soil worldwide were collated[9,9,10,18–20]. In addition, we use measurements at fourteen sites in Europe summarised in Masson et al.[18], Bossew et al.[37] and one site in Ukraine (this study, see Supplementary Table S1). Most of the available measured data are of the relatively long-lived isotopes of radiocaesium (^{134}Cs, ^{137}Cs), so ratios of all radionuclides to ^{137}Cs were determined. In total, we collected 1866 measurements from 147 soil sampling sites and 1112 measurements from 114 air sampling stations. All ratios were corrected to 11 March 2011 at 14:46 when the earthquake occurred and the reactors of Fukushima I NPS were shutdown, so the generation of fission products was effectively stopped. The total gamma decay energies of all radionuclides and their decay products were determined from ICRP Publication 107[38] along with their decay constants. These data were then analysed (on the basis of emission energies, half-life and information on contamination levels) to determine eight radionuclides (Supplementary Table S2) which could potentially have made a significant contribution to external gamma-ray dose rate in the weeks and months after the accident. In the first days after the accident, external dose was dominated by ^{132}Te and ^{132}I, followed by ^{131}I for a period of several weeks, after which the radiocaesium isotopes (^{134,136,137}Cs) were dominant.

Note that the contribution of ^{132}I is due to ingrowth from ^{132}Te; the direct release from the reactor does not significantly contribute due to its short half-life (2.295 h). ^{129m}Te and ^{129}Te were also found around Fukushima I NPS[7], and are included in

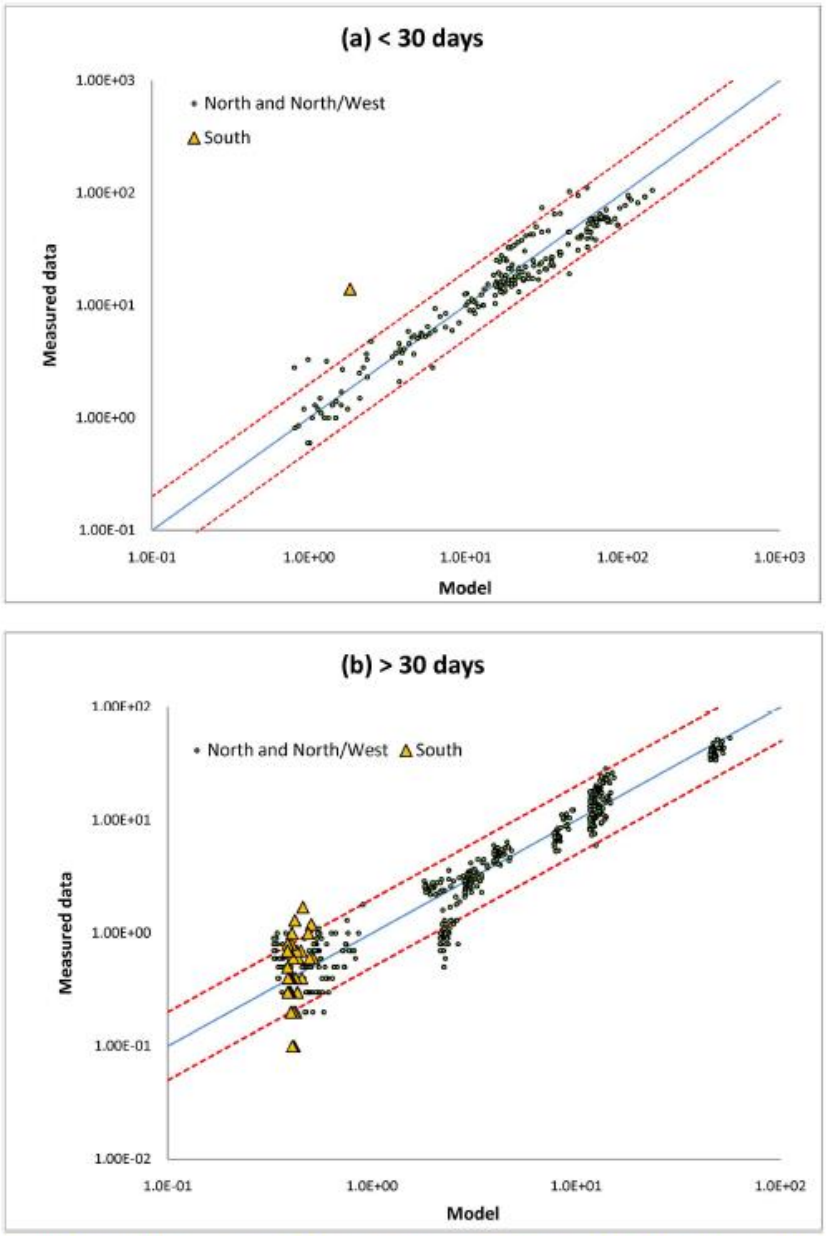

Figure 8 | Comparison of predicted dose rates (uSv/h) and measured data from (a) first measurement up to 30 days and (b) more than 30 days after the accident when the gamma dose rate were dominated by short-lived (^{132}Te/^{132}I and ^{131}I) and long-lived (^{134,137}Cs) radionuclides respectively. Dotted lines show a factor of two over- and under-estimation of model predictions. As expected, model predictions at a site to the south of the NPS are poorer than those to the north and northwest due to the March 21 fallout event to the south.

Table S2 for completeness, but these nuclides have only a minor effect on gamma-ray dose rate because of their low emitted gamma energy at 0.0376 and 0.0625 MeV for ^{129m}Te and ^{129}Te respectively. In addition, Tagami[39] show very low activity concentrations of other radioelements including ^{95}Nb, ^{110m}Ag and ^{140}Ba + ^{140}La, all of which can be ignored for evaluating gamma dose in this model.

Model. In the initial period, before significant penetration of radionuclides into the soil[36,37], the external gamma-ray dose rate is determined primarily by level of radioisotope deposition and decay energy. We therefore estimate the external gamma dose rate, D (μSv h^{-1}), at 1 m above the soil surface by:

$$D(t) = A.C_{137Cs}.\sum_i E_i.R_i e^{-\lambda_i t} \qquad (2)$$

Where E_i is total gamma decay energy of each nuclide (MeV) (see Supplementary Table S2), C_{137Cs} (Bq kg^{-1}) is the mean activity concentration of ^{137}Cs in the surface 5 cm of soil, R_i is ratio of deposition of each nuclide to ^{137}Cs, λ_i is the decay constant of each nuclide (d^{-1}), and t (d) is time after the earthquake. A [μSv hr^{-1} MeV^{-1} kg Bq^{-1}] is an empirically-determined constant to convert gamma decay energy to gamma dose, being dependent on absorption in soil and air. Since, in the early phase, the majority of radioactivity is on or close to the soil surface, the model neglects energy-dependence of absorption, but the A parameter accounts for potentially different distributions of radionuclides with depth at different sites.

Using mean ratios of each radionuclide to ^{137}Cs, Equation (2) was fitted to measurements of changes in external gamma-ray dose rate with time at six sites at a distance 24–40 km from Fukushima I NPS. Model fits were carried out in SAS (PROC Nlin; SAS Institute Inc.) to determine the value of the one unknown parameter, A. The model was then "blind" tested against data from a further fifteen sites for which (more limited) dose rate measurements were available.

1. Hirose, K. Fukushima Dai-ichi nuclear power plant accident: summary of regional radioactive deposition monitoring results. *Journal of Environmental Radioactivity* **111**, 13–17.
2. Hosoda, M. *et al.* The time variation of dose rate artificially increased by the Fukushima nuclear crisis. *Sci. Rep.* **1**, 87, dx.doi.org/10.1038/srep00087 (2011).
3. Tokonami, S. *et al.* Thyroid doses for evacuees from the Fukushima nuclear accident. *Sci. Rep.* **2**, 507 dx.doi.org/10.1038/srep00507 (2012).
4. Mück, K. *et al.* A Consistent Radionuclide Vector After the Chernobyl Accident. *Health Physics* **82**, 141–156 (2002).
5. Endo, S. *et al.* Measurement of soil contamination by radionuclides due to the Fukushima Dai-ichi Nuclear Power Plant accident and associated estimated cumulative external dose estimation. *Journal of Environmental Radioactivity* **111**, 18–27 (2012).
6. Beck, H. L. Exposure Rate Conversion Factors for Radionuclides Deposited on the Ground. (U.S. Department of Commerce, Springfield, 1980).
7. Kinoshita, N. *et al.* Assessment of individual radionuclide distributions from the Fukushima nuclear accident covering central-east Japan. *Proceedings of the National Academy of Sciences* **108**, 19526–19529 (2011).
8. Bergman, R. N., Ider, Y. Z., Bowden, C. R. & Cobelli, C. Quantitative estimation of insulin sensitivity. *American Journal of Physiology - Endocrinology And Metabolism* **236**, E667–677 (1979).
9. JAEA. Emergency Monitoring of Environmental Radiation and Atmospheric Radionuclides at Nuclear Science Research Institute, JAEA Following the Accident of Fukushima Daiichi Nuclear Power Plant. A. <http://jolissrch-inter.tokai-sc.jaea.go.jp/pdfdata/JAEA-Data-Code-2012-010.pdf> (accessed 07 March 13).
10. KEK. *Measurement result of airborne nuclide and air radiation level in Tsukuba area* <http://legacy.kek.jp/quake/radmonitor/GeMonitor-e.html> (accessed 04 May 2011).
11. Mück, K. *et al.* A Consistent Radionuclide Vector After the Chernobyl Accident. *Health Physics* **82** (2002).
12. Kirchner, G., Bossew, P. & De Cort, M. Radioactivity from Fukushima Dai-ichi in air over Europe; part 2: what can it tell us about the accident? *Journal of Environmental Radioactivity* **114**, 35–40 (2012).
13. Chino, M. *et al.* Preliminary Estimation of Release Amounts of ^{131}I and ^{137}Cs Accidentally Discharged from the Fukushima Daiichi Nuclear Power Plant into the Atmosphere. *Journal of Nuclear Science and Technology* **48**, 1129–1134 (2011).
14. Smith, J. T. & Beresford, N. A. *Chernobyl – Catastrophe and Consequences.* (Springer-Praxis, 2005).
15. Masson, O. *et al.* Tracking of Airborne Radionuclides from the Damaged Fukushima Dai-Ichi Nuclear Reactors by European Networks. *Environmental Science & Technology* **45**, 7670–7677 (2011).
16. Bunzl, K. *et al.* Cs-137 mobility in soils and its long-term effect on the external radiation exposure. *Radiation and Environmental Biophysics* **36**, 31–37 (1997).
17. Kato, H., Onda, Y. & Teramage, M. Depth distribution of ^{137}Cs, ^{134}Cs, and ^{131}I in soil profile after Fukushima Dai-ichi Nuclear Power Plant Accident. *Journal of Environmental Radioactivity* **111**, 59–64 (2012).
18. Bieringer, S. P. *et al.* Analysis of data from sensitive US monitoring stations for the
19. Carvalho, F. P., Reis, M. C., Oliveira, J. M., Malta, M. & Silva, L. Radioactivity from Fukushima nuclear accident detected in Lisbon, Portugal. *Journal of Environmental Radioactivity* **114**, 152–156 (2012).
20. EPA. Japanese Nuclear Emergency: Radiation Monitoring. (2011). <http://epa.gov/japan2011/rert/radnet-sampling-data.html#air> (accessed 19 March 2013).
21. Gudelis, A. *et al.* Radionuclides in the ground-level atmosphere in Vilnius, Lithuania, in March 2011, detected by gamma-ray spectrometry. *Journal of Environmental Radioactivity* **109**, 13–18 (2012).
22. HPA. *Update on the Fukushima Incident 14 July 2011,* <http://www.hpa.org.uk/web/HPAweb&HPAwebStandard/HPAweb_C/1309968917992> (accessed 21 August 2012).
23. Imanaka, T. *et al.* Early Radiation Survey of Iitate Village, Which Was Heavily Contaminated by the Fukushima Daiichi Accident, Conducted on 28 and 29 March 2011. *Health Physics* **102**, 680–686 (2012).
24. Kanai, Y. Monitoring of aerosols in Tsukuba after Fukushima Nuclear Power Plant incident in 2011. *Journal of Environmental Radioactivity* **111**, 33–37 (2012).
25. Leon, J. D. *et al.* Arrival time and magnitude of airborne fission products from the Fukushima, Japan, reactor incident as measured in Seattle, WA, USA. *Journal of Environmental Radioactivity* **102**, 1032–1038 (2011).
26. Loaiza, P. *et al.* Air radioactivity levels following the Fukushima reactor accident measured at the laboratoire Souterrain de Modane, France. *Journal of Environmental Radioactivity* **114**, 66–70 (2012).
27. MacMullin, S. *et al.* Measurement of airborne fission products in Chapel Hill, NC, USA from the Fukushima Dai-ichi reactor accident. *Journal of Environmental Radioactivity* **112**, 165–170 (2012).
28. Perrot, F. *et al.* Evidence of ^{131}I and ^{134,137}Cs activities in Bordeaux, France due to the Fukushima nuclear accident. *Journal of Environmental Radioactivity* **114**, 54–60 (2012).
29. Pham, M. K. *et al.* Detection of Fukushima Daiichi nuclear power plant accident radioactive traces in Monaco. *Journal of Environmental Radioactivity* **114**, 131–137 (2012).
30. Piñero García, F. & Ferro García, M. A. Traces of fission products in southeast Spain after the Fukushima nuclear accident. *Journal of Environmental Radioactivity* **114**, 146–151 (2012).
31. RIKEN. *Report on the γ-ray measurement after the accident of Fukushima 1 Nuclear Power Station,* <http://www.radiochem.org/kinkyu/49.pdf> (accessed 05 May 2011).
32. Stoehlker, U., Nikkinen, M. & Gheddou, A. Detection of radionuclides emitted during the Fukushima nuclear accident with the CTBT radionuclide network. *Monitoring Research Review: Ground-Based Nuclear Explosion Monitoring Technologies*, 715-724 (2011).
33. UCB. *Air Sampling Results* <http://www.nucberkeley.edu/UCBAirSampling/AirSamplingResults> (21 August 2012).
34. MEXT. *Readings of dust sampling (All Results for May 2011)* <http://www.mext.go.jp/component/english/__icsFiles/afieldfile/2011/06/15/1306621_053110.pdf> (accessed 21 August 2012).
35. MEXT. *Readings of soil monitoring (All Results for May 2011),* <http://www.mext.go.jp/component/english/__icsFiles/afieldfile/2011/06/15/1306622_053110.pdf> (accessed 10 July 2011).
36. MEXT. *Readings of environmental monitoring sample (All Results for May 2011),* <http://www.mext.go.jp/component/english/__icsFiles/afieldfile/2011/06/15/1306623_053110.pdf> (accessed 10 July 2011).
37. Bossew, P. *et al.* Radioactivity from Fukushima Dai-ichi in air over Europe; part 1: spatio-temporal analysis. *Journal of Environmental Radioactivity* **114**, 22–40 (2012).
38. ICRP. Nuclear Decay Data for Dosimetric Calculations. ICRP Publication 107. (International Commission on Radiological Protection, 2008).
39. Tagami, K. *et al.* Specific activity and activity ratios of radionuclides in soil collected about 20 km from the Fukushima Daiichi Nuclear Power Plant: Radionuclide release to the south and southwest. *Science of the Total Environment* **409**, 4885–4888 (2011).

Acknowledgements

This study would not have been possible without the open disclosure by Japanese authorities, and scientists around the world, of environmental measurements following the Fukushima accident. The authors are also grateful to the UK Health Protection Agency's Centre for Radiation, Chemical and Environmental Hazards for discussions about this work. We would also like to thank Dr Yutaka Kameda of the Chiba Institute of Technology for help in obtaining information from a Japanese source. We would further like to thank the anonymous reviewers, whose comments substantially improved the manuscript.

Author contributions

K.C. and U.S. wrote the main manuscript text, with contributions from P.B. and G.K. K.C.

Additional information

Supplementary information accompanies this paper at http://www.nature.com/scientificreports

Competing financial interests: The authors declare no competing financial interests.

How to cite this article: Chaiann, K., Smith, J.T., Bossew, P., Kirchner, G. & Laptev, G.V. Worldwide isotope ratios of the Fukushima release and early-phase external dose reconstruction. *Sci. Rep.* 3, 2520; DOI:10.1038/srep02520 (2013).

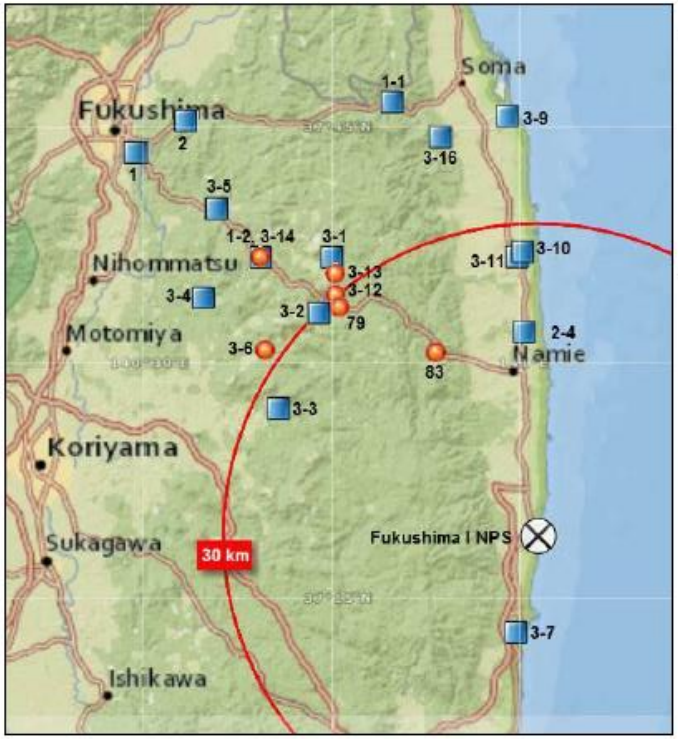

Code	Direction	Distance (km)	City	Start time of gamma dose measurement
6 sites for calibration				
79	North/West	29	Shimotsushima Kayabuka, Namie town	20/03/2011 13:55
83	North/West	24	Akougi Kunugidaira, Namie town	24/03/2011 09:46
3-6	North/West	32	Kaminogawa, Katsurao village	23/03/2011 14:00
3-12	North/West	30	Tsushima, Namie town	25/03/2011 14:13
3-13	North/West	31	Akougi, Namie town	25/03/2011 14:30
3-14	North/West	40	Yamakiya, Kawamata town	20/03/2011 11:20
15 sites for model blind testing				
3-1	North/West	29	Nagadoro, Iitate village	23/03/2011 11:10
3-9	North	42	Nakano, Soma city	25/03/2011 11:24
3-11	North	32	Kashima ward, Minami Soma city	25/03/2011 12:33
3-4	North/West	43	Ota, Nihonmatsu city	23/03/2011 11:08
3-5	North/West	47	Kawamata town	23/03/2011 10:30
3-16	North	45	Yamakami, Soma city	28/03/2011 16:18
1	North/West	62	Sugitsuma town, Fukushima city	14/04/2011 18:08
2	North/West	56	Onami Takinoiri, Fukushima city	31/03/2011 10:20
1-1	North/West	46	Sasu Nameri, Iitate village	31/03/2011 11:19
1-2	North/West	40	Yamakiya, Kawamata town	03/04/2011 09:52
2-4	North	24	Takami town, Haramachi ward, Minami Soma city	03/04/2011 11:57
3-10	North	32	Kashima ward, Minami Soma city	25/03/2011 12:18
3-2	North/West	30	Tsushima, Namie town	23/03/2011 13:17
3-3	North/West	32	Yamane, Tokiwa town, Tamura city	23/03/2011 12:50
3-7	South	23	Shimokitaba, Hirono town	23/03/2011 13:00

Fig. S1. The map generated by ESRI's ArcGIS explorer (ESRI, http://www.esri.com/Software/arcgis/explorer) illustrates the positions of 6 sites for model calibration (red circles) and 15 sites for model blind testing (blue squares) and the table shows details of these sites

Model sensitivity to uncertainty in $^{131}I/^{137}Cs$ ratio.

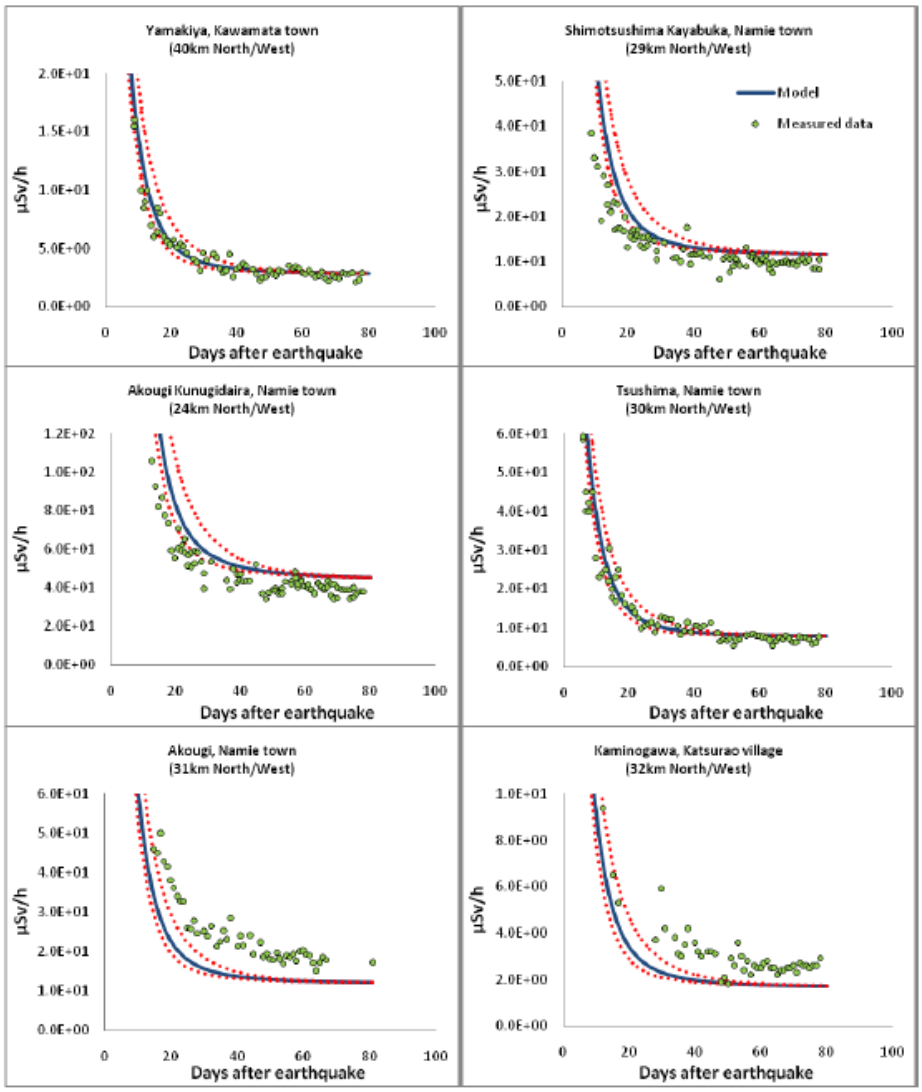

Fig. S2. Model results with ±2σ uncertainty in estimation of I-131/Cs-137 ratio, compared with the measurement data at all six calibration sites.

Model sensitivity to uncertainty in A value

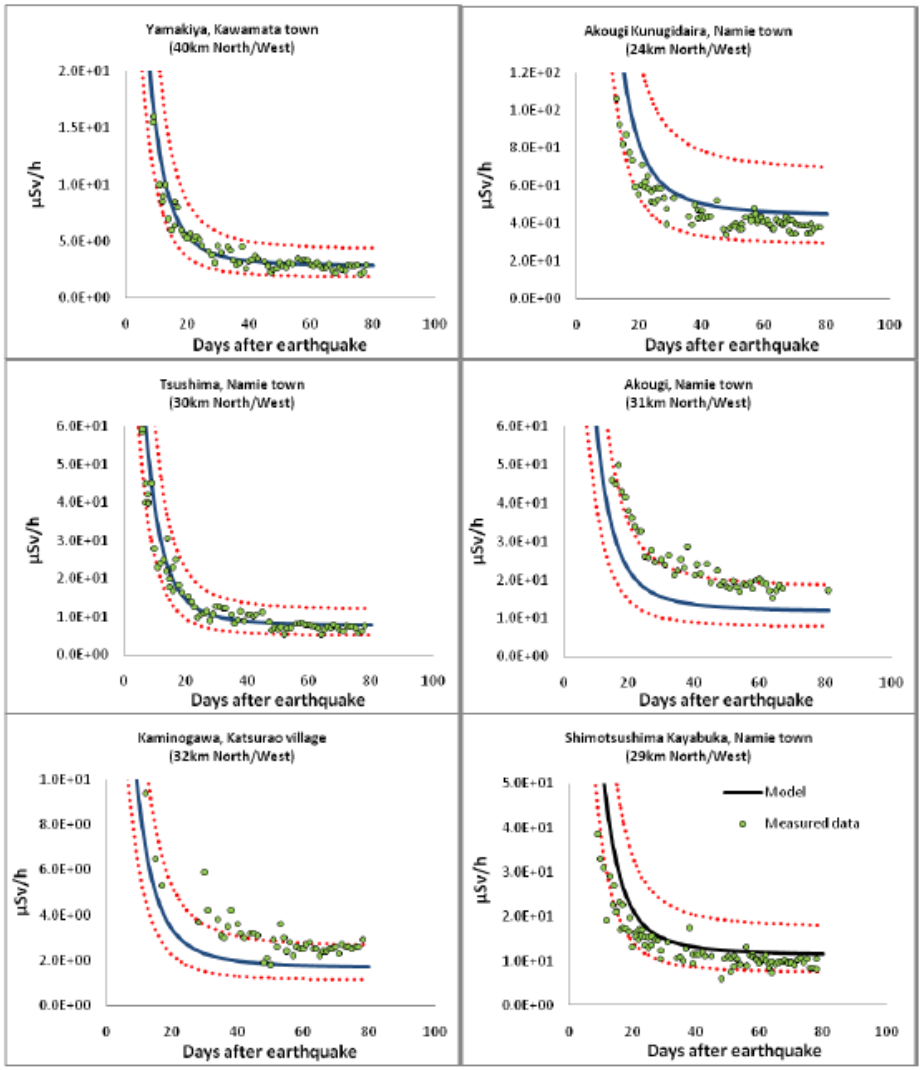

Fig. S3. Model results with uncertainty in estimation of A-parameter compared with the measurement data at all six calibration sites.

Model blind predictions at 15 sites.

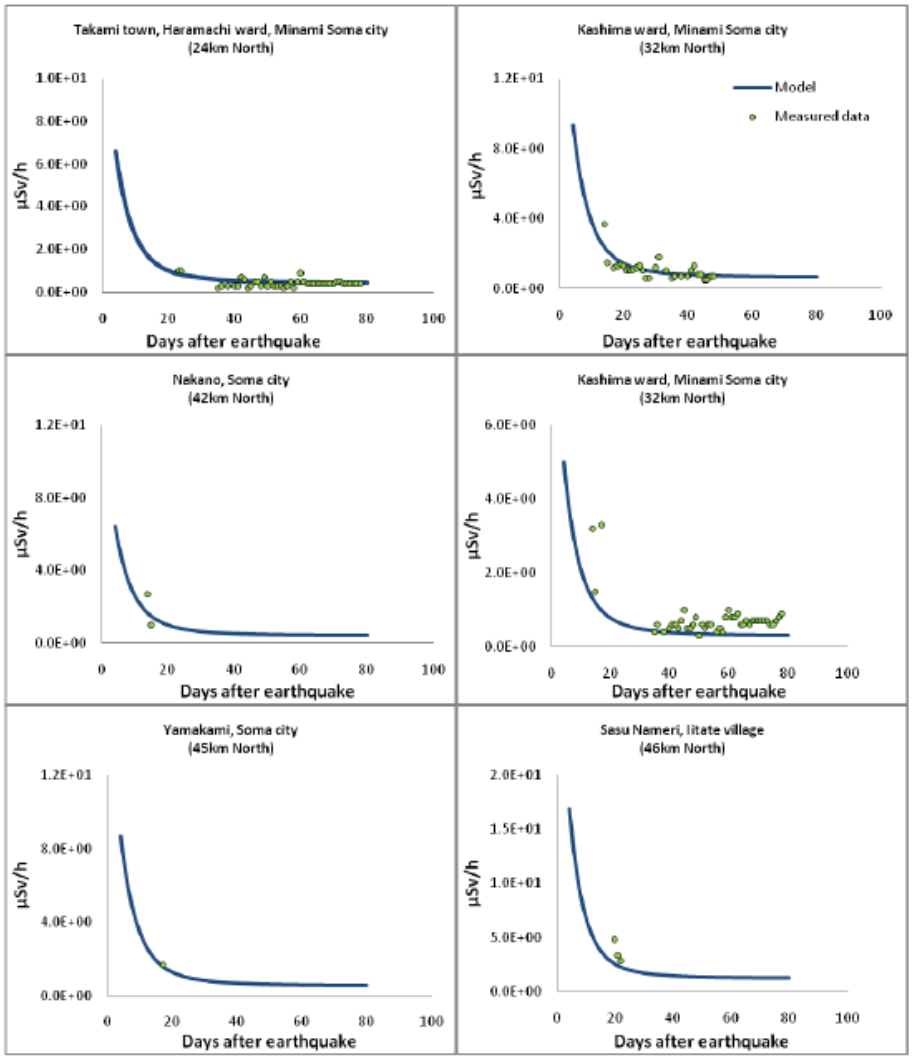

Fig. S4. Blind predictions of external gamma dose using only measured Cs-137 concentration in soil at each site.

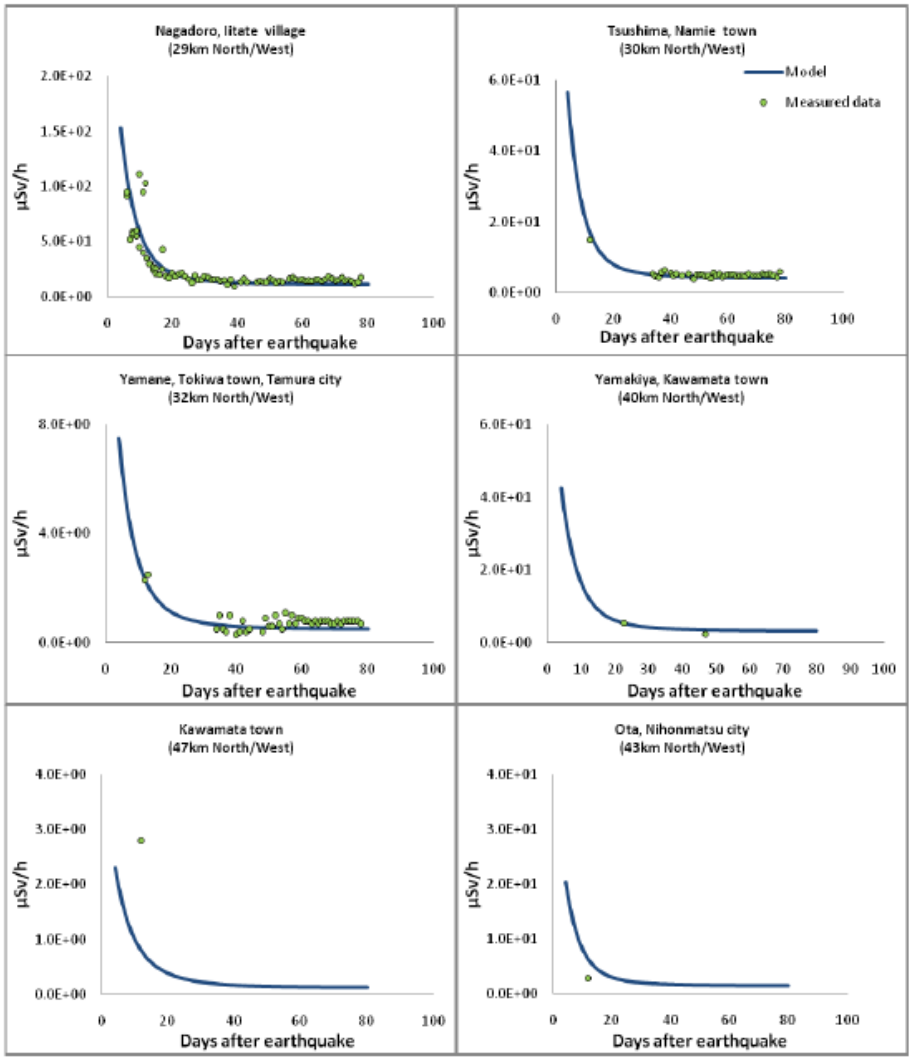

Fig. S4 (continued). Blind predictions of external gamma dose using only measured Cs-137 concentration in soil at each site.

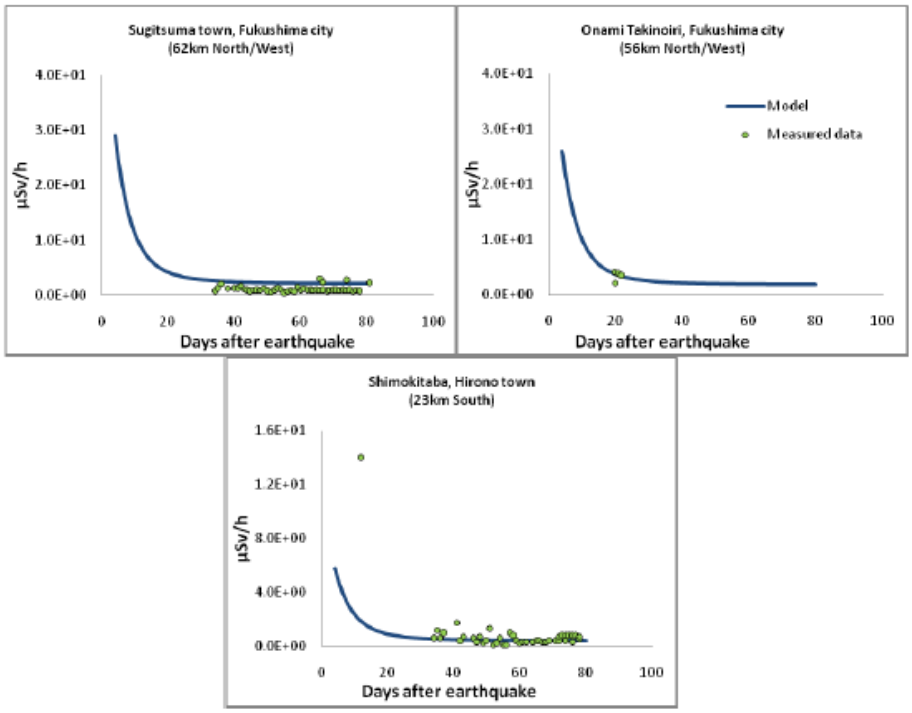

Fig. S4 (continued). Blind predictions of external gamma dose using only measured Cs-137 concentration in soil at each site.

Table S1: Particulate air sampling measurements in Ukraine conducted by Ukrainian Institute of Hydrometeorology.

Site	Mid time of Exposure (UTC time)	Radionuclide activity concentration (Bq/m^3)				
		I-131	Cs-134	Cs-136	Cs-137	Te-132
Rivnenska NPP, Kiev, Ukraine	24/03/2011 00:00	3.76E-04	2.21E-05	-	2.77E-05	2.21E-05
	26/03/2011 00:00	6.59E-04	2.44E-05	-	3.25E-05	-
	27/03/2011 00:00	2.27E-04	3.67E-05	-	4.40E-05	-
	28/03/2011 12:00	6.22E-04	1.08E-05	-	2.16E-05	3.24E-05
	30/03/2011 00:00	6.32E-03	5.37E-04	-	4.16E-04	1.07E-04
	31/03/2011 00:00	3.63E-03	4.56E-04	-	3.20E-04	6.13E-05
	01/04/2011 00:00	1.93E-03	2.68E-04	-	2.03E-04	-
	02/04/2011 00:00	1.60E-03	3.97E-04	-	3.41E-04	9.75E-05
	03/04/2011 12:00	4.08E-03	1.23E-03	-	1.11E-03	1.02E-04
	05/04/2011 00:00	2.54E-03	5.80E-04	-	5.12E-04	-
	06/04/2011 00:00	1.52E-03	5.30E-04	-	4.17E-04	-
	07/04/2011 00:47	5.87E-04	1.13E-04	-	1.13E-04	-
	08/04/2011 02:35	2.41E-04	3.16E-05	-	3.80E-05	-
	10/04/2011 00:40	1.34E-04	2.23E-05	-	2.23E-05	-
	11/04/2011 22:37	1.97E-04	5.09E-05	-	6.36E-05	-
	13/04/2011 23:02	1.06E-04	2.53E-05	-	2.07E-05	-
	16/04/2011 23:27	9.80E-05	2.00E-05	-	2.45E-05	-
	20/04/2011 12:15	7.01E-05	1.88E-05	-	2.56E-05	-
	24/04/2011 12:50	4.05E-05	1.52E-05	-	1.35E-05	-
Average corrected ratio to Cs-137 at 11/03/2012 14:46	***Mean (± 2 S.E.)***	***6.54E+01 1.48E+01***	***1.03E+00 1.16E-01***	-	***1.00E+00*** -	***2.43E+01 1.57E+01***

Table S2 The half-life and emitted energy (the sum of gamma-ray energies weighted by emission probability) per nuclear transformation (nt) from ICRP[38].

Nuclide	Half-life	Total emitted gamma energy (MeV/nt)
^{129m}Te	33.6 d	0.0376
^{129}Te	69.6 m	0.0625
^{131}I	8.02070 d	0.3828
^{132}Te	3.204 d	0.2344
^{132}I	2.295 h	2.2645
^{134}Cs	2.0648 y	1.5551
^{136}Cs	13.16 d	2.1283
^{137}Cs	30.1671 y	0.5963$^{\Delta}$

Table S3 Average percentage of gaseous I-131 and corrected ratio of particulate and gaseous of I-131 to particulate Cs-137 ± S.E., in air sampling around the world. From references 9, 10, 15, 18-22, 25-30, 32, 33, 37.

Site	Average percentage of I-131(g)	Average corrected ratio* of	
		I-131(p)/Cs-137(p)	I-131(g)/Cs-137(p)
Fukushima MP-1, Japan	59.42	87.52±18.63	106.16±20.27
High Energy Accelerator Reserch Organization, Tsukuba, Ibaraki, Japan	28.59	20.85±13.01	8.17±4.92
the Nuclear Science Research Institute, Tokai-mura, Ibaraki, Japan	74.67	36.55±6.97	233.79±59.44
Saipan, CNMI, US	80.50	56.4±0.00	371.7±0.00
Guam, US	80.81	23.87±8.59	96.93±21.69
Dutch Harbor, AK, US	81.93	16.95±6.50	147.14±102.74
Oahu, HI, US	82.31	11.90±2.65	77.98±35.41
Juneau, AK, US	77.57	32.12±5.56	110.13±10.99
Boise, ID, US	68.63	27.74±6.87	93.62±47.89
Anaheim, CA, US	88.86	54.86±22.91	473.57±238.82
San Bernardino, CA, US	84.67	47.87±52.19	138.05±52.87
Cherbourg, France	82.11	-	-
Saclay, France	79.17	91.22±28.82	505.92±434.44
Orsay, France	75.50	-	-
Guipavas, France	93.10	-	-
Brest, France	85.02	-	-
Mol, Belgium	80.55	-	-
Helsinki, Finland	81.73	-	-
Fessenheim, France	88.00	-	-
Le Péage-de-Roussillon, France	73.84	-	-
Romans-sur-Isère, France	78.86	-	-
Valence, France	90.10	-	-
Grenoble, France	84.69	-	-
Montélimar, France	82.70	-	-
Santander, Spain	66.15	-	-
Bilbao, Spain	85.06	-	-
Avignon, France	81.64	-	-
Oviedo, Spain	86.05	-	-
Cadarache, France	93.40	91.22±28.82	853.10±11.66
Milan, Italy	65.48	-	-
Puigcerdà, Spain	88.63	-	-
Piacenza, Italy	77.60	-	-
Gerona, Spain	91.64	-	-
Ascó, Spain	76.43	-	-
Linz, France	70.60	99.87±20.00	240.37±40.00
Vandellòs, Spain	81.48	-	-
Calafat, Spain	92.54	-	-
Madrid, Spain	90.29	-	-
Ljubljana, Slovenia	49.20	-	-
Vienna, Austria	73.28	72.92±23.67	164.45±70.18
Valencia, Spain	73.28	-	-
Cáceres, Spain	77.03	-	-
Badajoz, Spain	83.46	-	-
Granada, Spain	74.09	-	-
San Cristóbal de La Laguna, Spain	84.86	-	-

*Note that all ratios are corrected back to 11/03/2011 14:46

FORM UPR16

Research Ethics Review Checklist

University of Portsmouth

Please complete and return the form to Research Section, Quality Management Division, Academic Registry, University House, with your thesis, prior to examination

Postgraduate Research Student (PGRS) Information			**Student ID:**	**504280**
Candidate Name:	**Kittisak Chaisan**			
Department:	**SEES**	**First Supervisor:**	**Prof. Jim Smith**	
Start Date: (or progression date for Prof Doc students)	**15th June 2010**			

Study Mode and Route:	Part-time ❑	MPhil ❑	Integrated Doctorate (NewRoute) ❑
	Full-time ☑	MD ❑	Prof Doc (PD) ❑
		PhD ☑	

Title of Thesis:	**Modelling the environmental transfers of radioactivity following the Fukushima accident**
Thesis Word Count: (excluding ancillary data)	**39,296 words**

If you are unsure about any of the following, please contact the local representative on your Faculty Ethics Committee for advice. Please note that it is your responsibility to follow the University's Ethics Policy and any relevant University, academic or professional guidelines in the conduct of your study

Although the Ethics Committee may have given your study a favourable opinion, the final responsibility for the ethical conduct of this work lies with the researcher(s).

UKRIO Finished Research Checklist:
(If you would like to know more about the checklist, please see your Faculty or Departmental Ethics Committee rep or see the online version of the full checklist at: http://www.ukrio.org/what-we-do/code-of-practice-for-research/)

a) Have all of your research and findings been reported accurately, honestly and within a reasonable time frame?	**YES**
b) Have all contributions to knowledge been acknowledged?	**YES**
c) Have you complied with all agreements relating to intellectual property, publication and authorship?	**YES**
d) Has your research data been retained in a secure and accessible form and will it remain so for the required duration?	**YES**
e) Does your research comply with all legal, ethical, and contractual requirements?	**YES**

Candidate Statement:	
I have considered the ethical dimensions of the above named research project, and have successfully obtained the necessary ethical approval(s)	
Ethical review number(s) from Faculty Ethics Committee (or from NRES/SCREC):	
Signed: *(Student)* 	**Date:** 11 November 2015
If you have *not* submitted your work for ethical review, and/or you have answered 'No' to one or more of questions a) to e), please explain why this is so:	
Project is compliant with UKRIO checklist.	
Signed: *(Student)* 	**Date:** 11 November 2015